HIV-ASSOCIATED IMMUNE ACTIVATION AND PERSISTENT INFLAMMATION

EDITED BY: Martin Hoenigl, Sara Gianella and Harald H. Kessler
PUBLISHED IN: Frontiers in Immunology

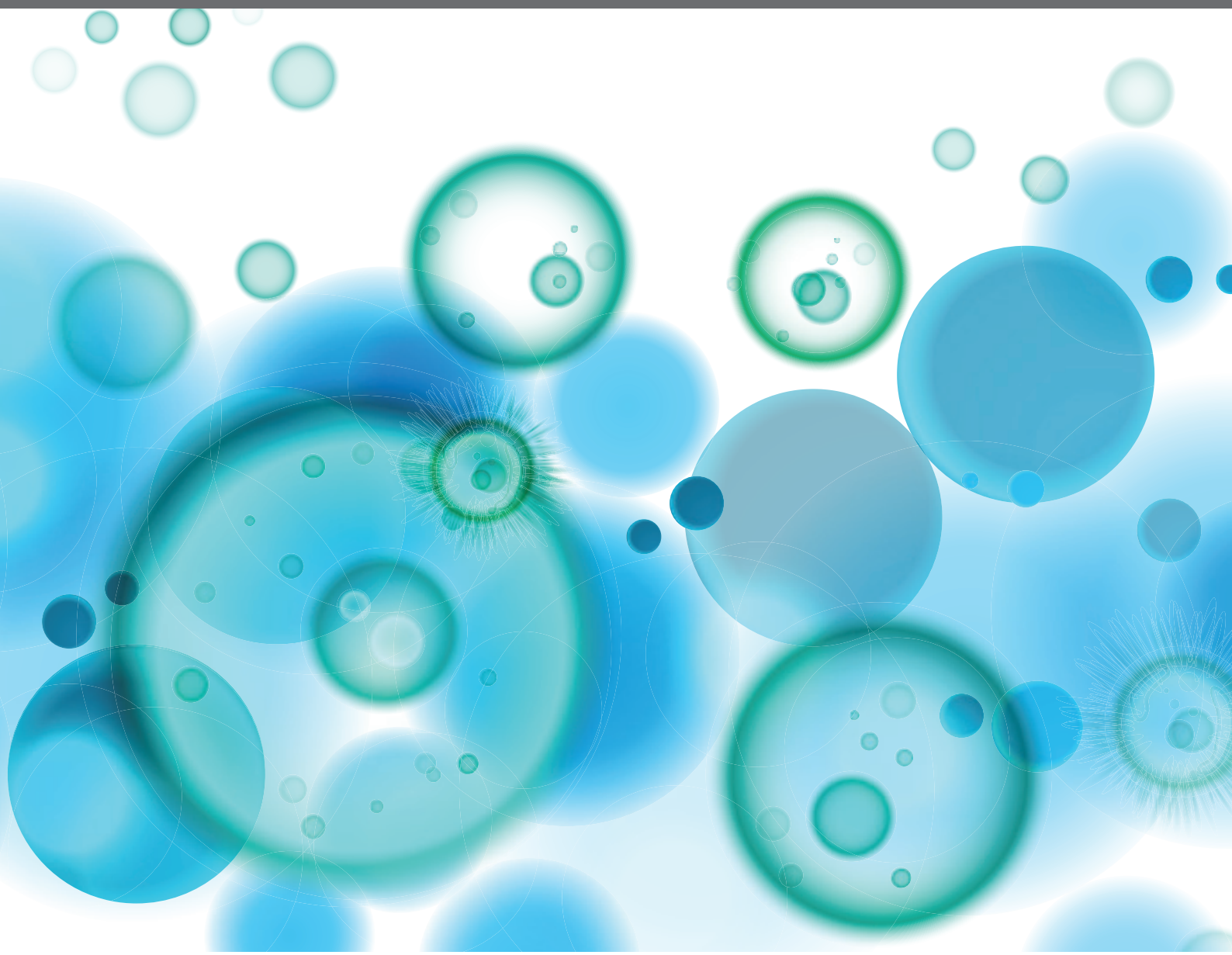

frontiers Research Topics

ISSN 1664-8714
ISBN 978-2-88963-438-5
DOI 10.3389/978-2-88963-438-5

About Frontiers

Frontiers is more than just an open-access publisher of scholarly articles: it is a pioneering approach to the world of academia, radically improving the way scholarly research is managed. The grand vision of Frontiers is a world where all people have an equal opportunity to seek, share and generate knowledge. Frontiers provides immediate and permanent online open access to all its publications, but this alone is not enough to realize our grand goals.

Frontiers Journal Series

The Frontiers Journal Series is a multi-tier and interdisciplinary set of open-access, online journals, promising a paradigm shift from the current review, selection and dissemination processes in academic publishing. All Frontiers journals are driven by researchers for researchers; therefore, they constitute a service to the scholarly community. At the same time, the Frontiers Journal Series operates on a revolutionary invention, the tiered publishing system, initially addressing specific communities of scholars, and gradually climbing up to broader public understanding, thus serving the interests of the lay society, too.

Dedication to Quality

Each Frontiers article is a landmark of the highest quality, thanks to genuinely collaborative interactions between authors and review editors, who include some of the world's best academicians. Research must be certified by peers before entering a stream of knowledge that may eventually reach the public - and shape society; therefore, Frontiers only applies the most rigorous and unbiased reviews.
Frontiers revolutionizes research publishing by freely delivering the most outstanding research, evaluated with no bias from both the academic and social point of view. By applying the most advanced information technologies, Frontiers is catapulting scholarly publishing into a new generation.

What are Frontiers Research Topics?

Frontiers Research Topics are very popular trademarks of the Frontiers Journals Series: they are collections of at least ten articles, all centered on a particular subject. With their unique mix of varied contributions from Original Research to Review Articles, Frontiers Research Topics unify the most influential researchers, the latest key findings and historical advances in a hot research area! Find out more on how to host your own Frontiers Research Topic or contribute to one as an author by contacting the Frontiers Editorial Office: researchtopics@frontiersin.org

HIV-ASSOCIATED IMMUNE ACTIVATION AND PERSISTENT INFLAMMATION

Topic Editors:
Martin Hoenigl, Medical University of Graz, Austria
Sara Gianella, University of California, United States
Harald H. Kessler, Medical University of Graz, Austria

Citation: Hoenigl, M., Gianella, S., Kessler, H. H., eds. (2020). HIV-Associated Immune Activation and Persistent Inflammation. Lausanne: Frontiers Media SA. doi: 10.3389/978-2-88963-438-5

Table of Contents

frontiers in Immunology

EDITORIAL
published: 18 December 2019
doi: 10.3389/fimmu.2019.02858

Editorial: HIV-Associated Immune Activation and Persistent Inflammation

Martin Hoenigl[1,2]*, *Harald H. Kessler*[3] *and Sara Gianella*[1]*

[1] Division of Infectious Diseases and Global Public Health, University of California, San Diego, San Diego, CA, United States, [2] Section of Infectious Diseases and Tropical Medicine, Medical University of Graz, Graz, Austria, [3] Research Unit Molecular Diagnostics, Diagnostic and Research Center for Molecular Biomedicine, Medical University of Graz, Graz, Austria

Keywords: non-AIDS events, microbial translocation, fungal translocation, beta-D-glucan, CXCL12, LPS, dysbiosis

Editorial on the Research Topic

HIV-Associated Immune Activation and Persistent Inflammation

While modern antiretroviral therapy (ART) improves health, prolongs survival, and reduces HIV transmission, successfully treated HIV infection remains associated with persistent inflammation and immune dysfunction (1–3). Persistent systemic inflammation is a major contributing factor to HIV-associated morbidity, including neurocognitive impairment (Yu et al.) and non-AIDS events, which result in devastating outcomes and loss of quality of life during aging with HIV infection (4, 5).

The current Research Topic includes in total 11 high-quality manuscripts, ranging from host-response activation during HIV infection (Tjitro et al.), the role of toll-like receptor (TLR)-10 ligand during HIV replication (Henrick et al.), microRNA-19b as a regulator of $CD8^+$ T cell functions during HIV infection (Yin et al.), to potentiating the immune response via PD1 checkpoint inhibition (Filaci et al.).

While it is known that HIV infection is characterized by a dramatic depletion of $CD4^+$ T cells, a study comparing people with HIV (PWH) with age-matched uninfected controls identified specifically gamma delta (γδ)-T cells as an inflammatory driver in ART-suppressed PWH and provided evidence of distinct "inflamm-aging" processes with and without active HIV replication (Belkina et al.). Depletion of $CD4^+$ T cells together with impaired polarization of Th17 cells in the gastrointestinal tract and a massive expansion of activated $CD8^+$ T cells causes $CD8^+$ T cell-mediated enteropathy (6). In another study of this Research Topic authors also reported dysbiosis and translocation of microbial products in the study participants, which persisted despite long term ART mediated viral suppression (Rhoades et al.). Specifically, the gut microbiome of long term suppressed PWH was enriched in bacterial taxa typically found in the oral cavity suggestive of loss of compartmentalization, while levels of beneficial butyrate producing taxa were reduced. Additionally, prevalence of *Prevotella* negatively correlated with $CD4^+$ T-cells numbers, indicating that despite long-term adherence and undetectable viral loads, HIV infection results in significant shifts in gut microbial communities (Rhoades et al.).

Bacteria and fungi are the two most abundant populations of the gut microbiome. While bacterial translocation has been a focus of HIV research for a number of years, fungal translocation recently came into focus as a driver of immune activation, persistent inflammation, and non-AIDS events (7–12). A review included in this supplement evaluated recent literature to untangle the respective roles of circulating lipopolysaccharide (LPS) and (1–>3)-B-D-Glucan (BDG), which are major components of bacterial and fungal cell walls respectively and established biomarker

OPEN ACCESS

Edited and reviewed by:
Francesca Chiodi,
Karolinska Institutet (KI), Sweden

***Correspondence:**
Martin Hoenigl
mhoenigl@ucsd.edu
Sara Gianella
gianella@ucsd.edu

Specialty section:
This article was submitted to Viral Immunology, a section of the journal Frontiers in Immunology

Received: *07 November 2019*
Accepted: *21 November 2019*
Published: *18 December 2019*

Citation:
Hoenigl M, Kessler HH and Gianella S (2019) Editorial: HIV-Associated Immune Activation and Persistent Inflammation. Front. Immunol. 10:2858. doi: 10.3389/fimmu.2019.02858

of bacterial and fungal translocation (Ramendra et al.). While LPS is a well-known inducer of innate immune activation, BDG is emerging as a significant source of monocyte and natural killer (NK) cell activation that contributes to immune dysfunction, and both may serve as biomarkers of disease progression and immune activation during ART (Ramendra et al.). Further studies are needed to enhance our understanding of the consequences of elevated LPS and BDG on immune activation, which may inform novel therapeutic strategies against the occurrence of AIDS and non-AIDS events.

Another proposed marker of systemic immune activation during early and chronic HIV infection is plasma CXCL13, which is preferentially secreted by Follicular Helper T cells to attract B cells to germinal centers (Mehraj et al.). A study included in this supplement found that in 114 PWH plasma CXCL13 levels correlated with BDG levels, were higher in those with CMV infection and increased with HIV disease progression (Mehraj et al.). In contrast, early initiation of ART reduced plasma CXCL13 and B cell activation but without normalization. Future studies are needed to compare CXCL13 with more established biomarkers such as soluble urokinase plasminogen activator receptor (suPAR), or sTNFrI, and sTNFrII (2, 4) for prediction of the development of non-AIDS events.

Another study included in this supplement elucidated the role of the immunomodulatory carbohydrate-binding protein Galectin-9 in HIV transcription and in maintaining chronic immune activation during ART-suppressed HIV infection (Colomb et al.). Interactions between cell-surface glycans and glycan-binding proteins (lectins) are key regulators of immunological functions and are involved in several cellular processes. Galectins are a class of lectins that play critical roles in T cell function, and Galectin-9 specifically has recently been recognized to play an essential role in regulating both adaptive and innate defense mechanisms (Colomb et al.). Interestingly, the study found that uncoupling Galectin-9-mediated viral reactivation from undesirable pro-inflammatory effects, using rapamycin, may increase the potential utility of recombinant Galectin-9 within the reversal of HIV latency eradication framework (Colomb et al.).

Finally, this Research Topic includes a paper reporting on a randomized, placebo-controlled, double-blinded trial of the TLR-3 agonist Poly-ICLC in aviremic, ART-treated PWH (Saxena et al.). Poly-ICLC can activate immune cells and induce HIV replication in pre-clinical experiments, but this study for the first time investigated its effect in disrupting HIV latency *in vivo* while simultaneously enhancing innate immune responses. The study found that poly-ICLC was overall safe and well-tolerated (Saxena et al.). Transcriptional analyses revealed upregulation of innate immune pathways in peripheral blood mononuclear cells (PBMCs) following Poly-ICLC treatment, including strong interferon signaling accompanied by transient increases in circulating Interferon gamma-induced protein (IP)-10 (CXCL10) levels (Saxena et al.). These responses generally peaked by 24–48 h after the first injection and returned to baseline by day 8. Overall, $CD4^+$ T cell number and phenotype were unchanged, plasma viral control was maintained and no significant effect on HIV reservoirs was observed (Saxena et al.). These finding suggest that Poly-ICLC may be used for inducing transient innate immune responses in treated PWH indicating promise as an adjuvant for HIV therapeutic vaccines (Saxena et al.).

Collectively, the studies described in original research and review articles in this topic describe recent advances and provide optimism for the future of treating HIV-associated inflammation. We hope these articles will stimulate further research with the ultimate goal of improving outcomes for patients with HIV infection.

AUTHOR CONTRIBUTIONS

All authors listed have made a substantial, direct and intellectual contribution to the work, and approved it for publication.

FUNDING

This work was supported by funds from the National Institutes of Health: AI036214, DA026306, AI064086, MH081482, MH113477, MH062512, and AI106039; and HNRP developmental grant PST-HN68. The funders had no role in study design, data collection and analysis, decision to publish, or preparation of the manuscript.

REFERENCES

1. Deeks SG, Verdin E, McCune JM. Immunosenescence and HIV. *Curr Opin Immunol.* (2012) 24:501–6. doi: 10.1016/j.coi.2012.05.004
2. Tenorio AR, Zheng Y, Bosch RJ, Krishnan S, Rodriguez B, Hunt PW, et al. Soluble markers of inflammation and coagulation but not T-cell activation predict non-AIDS-defining morbid events during suppressive antiretroviral treatment. *J Infect Dis.* (2014) 210:1248–59. doi: 10.1093/infdis/jiu254
3. Hoenigl M, Chaillon A, Little SJ. CD4/CD8 cell ratio in acute HIV Infection and the impact of early antiretroviral therapy. *Clin Infect Dis.* (2016) 63:425–6. doi: 10.1093/cid/ciw293
4. Hoenigl M, Moser C, Funderburg N, Bosch R, Kantor A, Zhang Y, et al. Soluble Urokinase Plasminogen Activator Receptor (suPAR) is predictive of Non-AIDS Events during Antiretroviral Therapy-mediated Viral Suppression. *Clin Infect Dis.* (2019) 69:676–86. doi: 10.1093/cid/ciy966
5. Kay A, Moser C, McKhann A, Vargas M, Porrachia M, Gianella S, et al. Soluble suppression of tumorigenicity 2 levels are not predictive of non-AIDS events during antiretroviral therapy-mediated viral suppression. *Aids.* (2019) 33:1397–9. doi: 10.1097/qad.0000000000002228
6. Arnoczy GS, Ferrari G, Goonetilleke N, Corrah T, Li H, Kuruc J, et al. Massive CD8 T cell response to primary HIV infection in the setting of severe clinical presentation. *AIDS Res Hum Retroviruses.* (2012) 28:789–92. doi: 10.1089/AID.2011.0145
7. Hoenigl M, Perez-Santiago J, Nakazawa M, de Oliveira MF, Zhang Y, Finkelman MA, et al. (1 → 3)-β-D-Glucan: a biomarker for microbial translocation in individuals with acute or early HIV infection? *Front Immunol.* (2016) 7:404. doi: 10.3389/fimmu.2016.00404
8. Farhour Z, Mehraj V, Chen J, Ramendra R, Lu H, Routy JP. Use of (1 → 3)-β-D-glucan for diagnosis and management of invasive mycoses in HIV-infected patients. *Mycoses.* (2018) 61:718–22. doi: 10.1111/myc.12797
9. Gianella S, Letendre SL, Iudicello J, Franklin D, Gaufin T, Zhang Y, et al. Plasma (1 → 3)-β-D-glucan and suPAR levels correlate with neurocognitive performance in people living with HIV on antiretroviral therapy: a CHARTER

analysis. *J Neurovirol.* (2019). doi: 10.1007/s13365-019-00775-6. [Epub ahead of print].
10. Hoenigl M. Fungal translocation: a driving force behind the occurrence of non-AIDS events? *Clin Infect Dis.* (2019). doi: 10.1093/cid/ciz215. [Epub ahead of print].
11. Mehraj V, Ramendra R, Isnard S, Dupuy FP, Ponte R, Chen J, et al. Circulating (1 → 3)-β-D-Glucan is associated with immune activation during HIV infection. *Clin Infect Dis.* (2019). doi: 10.1093/cid/ciz212. [Epub ahead of print].
12. Hoenigl M, de Oliveira MF, Perez-Santiago J, Zhang Y, Morris S, McCutchan AJ, et al. (1 → 3)-β-D-Glucan Levels Correlate With Neurocognitive Functioning in HIV-Infected Persons on suppressive antiretroviral therapy: a cohort study. *Medicine.* (2016) 95:e3162. doi: 10.1097/MD.0000000000003162

Conflict of Interest: MH received research funding from Gilead that was not related to this Research Topic.

The remaining authors declare that the research was conducted in the absence of any commercial or financial relationships that could be construed as a potential conflict of interest.

frontiers in Immunology

PERSPECTIVE
published: 23 October 2018
doi: 10.3389/fimmu.2018.02447

Rationale for an Association Between PD1 Checkpoint Inhibition and Therapeutic Vaccination Against HIV

Gilberto Filaci[1,2]*, *Daniela Fenoglio*[1,2], *Lucia Taramasso*[3], *Francesco Indiveri*[1] and *Antonio Di Biagio*[3]

[1] Centre of Excellence for Biomedical Research and Department of Internal Medicine, University of Genoa, Genoa, Italy, [2] Biotherapy Unit, Ospedale Policlinico San Martino, Genoa, Italy, [3] Infectious Disease Unit, Ospedale Policlinico San Martino, Genoa, Italy

The pathogenesis of HIV immunodeficiency is mainly dependent on the cytopatic effects exerted by the virus against infected CD4+ T cells. However, CD4+ T cell loss cannot be the only pathogenic factor since severe opportunistic infections may develop in HIV infected patients with normal CD4+ T cell counts and since the recent START study indicated that absolute CD4+ T cell counts are not predictive for AIDS and non-AIDS events. Recently our group demonstrated that CD8+CD28-CD127lowCD39+ regulatory T lymphocytes, previously found highly concentrated within tumor microenvironment, circulate with elevated frequency in the peripheral blood of HIV infected patients. Here, we show that these cells, that at least in part are HIV specific, express the PD1 immune checkpoint. Based on these evidences and considerations, in this Perspective article we speculate on the opportunity to treat HIV infected patients with anti-PD1 immune checkpoint inhibitors as a way to counteract the T regulatory cell compartment and to unleash virus-specific immune responses. In order to potentiate the immune responses against HIV we also propose the potential utility to associate immune checkpoint inhibition with HIV-specific therapeutic vaccination, reminiscent of what currently applied in oncologic protocols. We suggest that such an innovative strategy could permit drug-sparing regimens and, perhaps, lead to eradication of the infection in some patients.

Keywords: HIV, Treg, immune checkpoints, HIV vaccine, PD1

OPEN ACCESS

Edited by:
Martin Hoenigl,
University of California, San Diego, United States

Reviewed by:
Johannes S. Gach,
University of California, Irvine, United States
Said Dermime,
National Center for Cancer Care and Research, Qatar

***Correspondence:**
Gilberto Filaci
gfilaci@unige.it

Specialty section:
This article was submitted to Vaccines and Molecular Therapeutics, a section of the journal Frontiers in Immunology

Received: *18 June 2018*
Accepted: *03 October 2018*
Published: *23 October 2018*

Citation:
Filaci G, Fenoglio D, Taramasso L, Indiveri F and Di Biagio A (2018) Rationale for an Association Between PD1 Checkpoint Inhibition and Therapeutic Vaccination Against HIV. Front. Immunol. 9:2447. doi: 10.3389/fimmu.2018.02447

The pathogenesis of HIV immunodeficiency is dependent on the cytopatic effects exerted by the virus against infected CD4+ T cells and to subsequent CD4+ T cell loss (1, 2). Some aspects of the disease remain unexplained as the case of HIV infected patients with normal CD4+ T cell counts after anti-retroviral therapy (ART) initiation who develop severe opportunistic infections (3, 4), or that of HIV infected patients with reduced CD4+ T cell counts who do not show immunodeficiency manifestations (5). Accordingly, the results of the recent START study indicated that absolute CD4+ T cell counts are not predictive for AIDS and non-AIDS events since these events may occur in ART treated patients with absolute CD4 counts >500 cells/μl (6). Searching for other pathogenic mechanisms, we focused our attention on regulatory T lymphocytes (Treg). The role of these cells in HIV immunodeficiency pathogenesis is still unclear since studies on alterations of CD4+ Treg in HIV infected patients led to controversial results (7–17). Hence, we took into consideration a different subset of Treg constituted by CD8+ Treg (18). CD8+ Treg, in particular those expressing the CD8+CD28-CD127lowCD39+ phenotype, are regulatory T lymphocytes

found highly concentrated within tumor microenvironment, where they can exert remarkable immunosuppressive activity due to their capacity to target T cell proliferation and cytotoxicity (19–21). We investigated on the presence of these cells in the circulation of HIV-infected patients, and on possible correlations between their frequency and markers of disease activity. The results of this study demonstrated that HIV-infected patients have elevated circulating levels of functional CD8+CD28-CD127lowCD39+ Treg, the majority of which is antigen-specific for HIV proteins. This observation is remarkable since these cells are virtually absent from the circulation of healthy subjects (19, 21). In HIV patients, their frequency post-ART correlates with HIV-RNA, CD4+ T cell count, and immune activation markers, suggesting their pathogenic involvement in AIDS or non-AIDS related complications. Moreover, their increase after initiation of ART heralds a lack of virological or clinical response (i.e., appearance of co-morbidity): hence their monitoring is clinically relevant (22).

Further studies from our group show that CD8+CD28-CD127lowCD39+ Treg stably and consistently express PD1 (**Figure 1** and **Supplemental Material**). PD1 is a member of immune checkpoints (23–26). These are

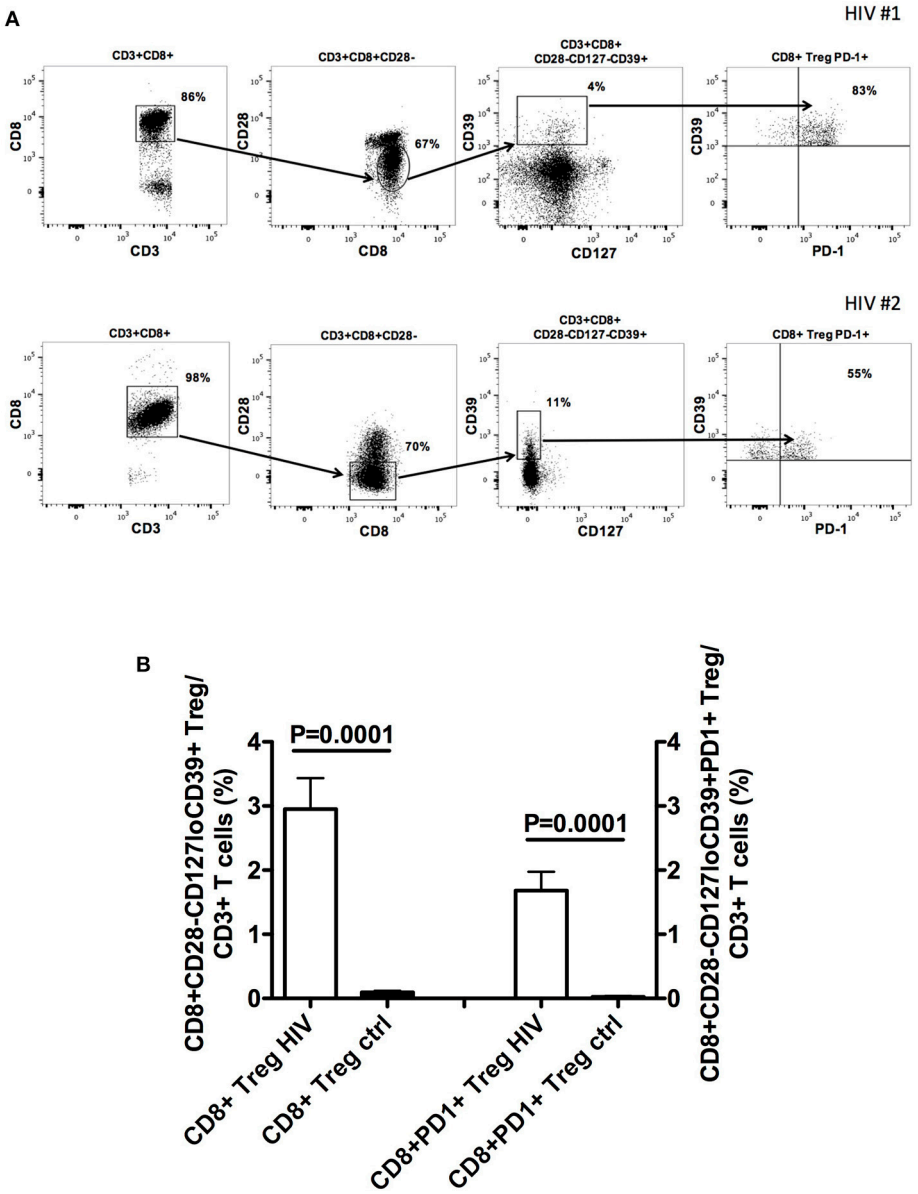

FIGURE 1 | CD8+CD28−CD127loCD39+PD1+ Treg frequency in the peripheral blood of naïve HIV-infected patients. **(A)** The gating strategy for the analysis of CD8+CD28−CD127loCD39+PD1+ Treg frequency in the circulation of two representative naïve HIV-infected patients is shown. **(B)** Comparison between the mean frequency of CD8+CD28−CD127loCD39+ Treg as well as that of CD8+CD28−CD127loCD39+PD1+ Treg in the circulation of 22 naïve HIV-infected patients and those of 22 healthy controls. Detailed information on patient population and methods is provided in the **Supplementary File**—Patients and Methods.

molecules expressed by immune cells in order to control the immune responses. In particular, PD1 is mainly expressed by T lymphocytes at advanced stage of maturation, i.e., effector memory and terminally-differentiated effector memory cells. Hence, it is involved in the control of the effector phase of the immune response. Indeed, PD1+ T cells are present within tumor infiltrating lymphocytes, suggesting that PD1 expression contributes to tumor immune evasion (24, 27). In HIV-infected patients CD4+PD1+ T cells constitute the major HIV cell reservoir (28, 29). Interestingly, PD1+ T cell frequency is elevated in HIV-infected patients and reduces after beginning of the treatment, a behavior reminiscent of what occurs to circulating CD8+CD28-CD127loCD39+ Treg frequency (30, 31). In HIV-infected patients, the presence of increased frequency of PD1+ T cells, including abnormally expanded CD8+CD28-CD127loCD39+PD1+ Treg, could be involved in generating immunodeficiency and hampering anti-virus immune responses. Hence, the fact that expansion of CD8+ Treg and of PD1+ T lymphocytes co-exist in both tumors and HIV infection envisages a pathogenic crossing between the two pathologic conditions. This suggests that targeting PD1+ T cells through a specific checkpoint inhibitor could be a useful therapeutic strategy for HIV infection borrowed from anti-cancer protocols, based that recent trials support the safety of this approach (32, 33). The potential efficacy of this strategy is further supported by previous studies in which a PD1 inhibitor was administered to non-human primates. In these studies, anti-PD1 treatment of uninfected animals co-immunized with a SIV-gag adenovirus vector vaccine enhanced the frequency of gag-specific T cells (34), while treatment of SIV infected macaques increased SIV-specific immune response, decreased viral load and prolonged survival (35). Accordingly, administration of anti-PD-L1 monoclonal antibodies to ART-treated SIV infected macaques allowed the maintenance of a lower viral load after ART suspension than in non-administered animals (36).

However, in the majority of cancer patients the activity of the sole checkpoint inhibitor is not sufficient to provide a robust therapeutic effect. Hence, association of checkpoint inhibitors with therapeutic vaccination is currently proposed as optimal way for inducing/reinforcing anti-tumor immune responses in the absence of abnormal and detrimental regulatory mechanisms (37, 38). Interestingly, the development of a vaccine against HIV has been recently evoked as urgent medical need, notwithstanding the efficacy of ART. In fact, HIV pandemia is so wide (more than 36 million infected people, about 1.8 million people newly infected each year) that the costs for life-long ART are huge for government health care systems. Hence, therapeutic vaccination has been proposed as a preferential therapeutic tool for corroborating ART activity possibly through the eradication of HIV-1 latent reservoirs (39, 40). Indeed, an optimal vaccine against HIV should elicit both virus-specific cytotoxic CD8+ T cells and neutralizing antibodies in order to kill virus-infected cells, that constitute the viral reservoir, and to avoid spreading of infection by viral particles released by already infected cells. Among HIV antigens, gag has been considered a useful immunogen for vaccine preparation since the presence of elevated titers of antibodies against gag, but not against other HIV antigens, correlated with reduced viremia in HIV infected patients (41). Disappointingly, all vaccination trials so far performed in prophylactic or therapeutic settings, including those using gag as immunogen, did not achieve brilliant clinical results (42). Now, the finding of an abnormal expansion of CD8+CD28-CD127loCD39+PD1+ Treg in these patients suggests that such defective activity of HIV vaccines could have a bi-faceted origin, related to inner deficiency of vaccine immunogenicity and/or to the generalized immunosuppressive effect exerted by CD8+ Treg. Accordingly, a DNA vaccine based on a chimeric gene product fusing PD1 and gag moieties induced high frequency of gag-specific cytotoxic CD8+ T cells associated with high titers of virus-specific antibodies, conferring remarkable protection against mucosal challenge with vaccinia gag viruses in experimental animals (43).

These considerations may constitute a robust rationale for a combination therapy associating anti-PD1 checkpoint inhibition and therapeutic vaccination in ART treated HIV-infected patients. Our hypothesis is that early co-administration of ART, checkpoint inhibition, and vaccination in recently HIV-infected patients could allow to take advantage of the synergic effect of the three-faceted approach when the HIV latent reservoir is not yet consolidated. We expect that such an innovative strategy could lead to the onset of HIV specific immune responses more effective than those spontaneously developed in the absence of Treg inhibition, since unleashed by the regulatory control of PD1+ Treg. Hopefully, this strategy could permit drug-sparing regimens and, perhaps, lead to eradicate the infection in some patients.

ETHICS STATEMENT

The study was carried out in compliance with the Helsinki Declaration and was approved by the Ethics Committee of the San Martino Hospital in Genoa, Italy (P.R.251REG2014). All enrolled patients provided written informed consent.

AUTHOR CONTRIBUTIONS

GF, FI, and AD wrote the manuscript; DF performed the phenotypic analyses; LT enrolled and clinically managed the patients.

SUPPLEMENTARY MATERIAL

The Supplementary Material for this article can be found online at: https://www.frontiersin.org/articles/10.3389/fimmu.2018.02447/full#supplementary-material

REFERENCES

1. Phetsouphanh C, Xu Y, Zaunders J. CD4 T cells mediate both positive and negative regulation of the immune response to HIV infection: complex role of T follicular helper cells and regulatory T cells in pathogenesis. *Front Immunol*. (2015) 5:681. doi: 10.3389/fimmu.2014.00681
2. Haase AT. Population biology of HIV-1 infection: viral and $CD4^+$ T cell demographics and dynamics in lymphatic tissues. *Annu Rev Immunol*. (1999) 17:625–56. doi: 10.1146/annurev.immunol.17.1.625
3. Rey D, de Mautort E, Saussine C, Hansmann Y, Waller J, Herbrecht R, et al. Isolated renal Aspergillus abscess in an AIDS patient with a normal $CD4^+$ cell count on highly active antiretroviral therapy. *Eur J Clin Microbiol Infect Dis*. (1999) 18:137–41. doi: 10.1007/s100960050242
4. Mori S, Polatino S, Estrada-Y-Martin RM. Pneumocystis-associated organizing pneumonia as a manifestation of immune reconstitution inflammatory syndrome in an HIV-infected individual with a normal $CD4^+$ T-cell count following antiretroviral therapy. *Int J STD AIDS* (2009) 20:662–5. doi: 10.1258/ijsa.2008.008428
5. Mandalia S, Westrop SJ, Beck EJ, Nelson M, Gazzard BG, Imami N. Are long-term non-progressors very slow progressors? Insights from the Chelsea and Westminster HIV cohort, 1988–2010. *PLoS ONE* (2012) 7:e29844. doi: 10.1371/journal.pone.0029844
6. INSIGHT START Study Group, Lundgren JD, Babiker AG, Gordin F, Emery S, Grund B, et al. Initiation of antiretroviral therapy in early asymptomatic HIV infection. *N Engl J Med*. (2015) 373:795–807. doi: 10.1056/NEJMoa1506816
7. Chevalier MF, Weiss L. The split personality of regulatory T cells in HIV infection. *Blood* (2013) 121:29–37. doi: 10.1182/blood-2012-07-409755
8. Veiga-Parga T, Sehrawat S, Rouse BT. Role of regulatory T cells during virus infection. *Immunol Rev*. (2013) 255:182–96. doi: 10.1111/imr.12085
9. Weiss L, Donkova-Petrini V, Caccavelli L, Balbo M, Carbonneil C, Levy Y. Human immunodeficiency virus-driven expansion of $CD4^+CD25^+$ regulatory T cells, which suppress HIV-specific CD4 T-cell responses in HIV-infected patients. *Blood* (2004) 104:3249–56. doi: 10.1182/blood-2004-01-0365
10. Kinter AL, Horak R, Sion M, Riggin L, McNally J, Lin Y, et al. $CD25^+$ regulatory T cells isolated from HIV-infected individuals suppress the cytolytic and nonlytic antiviral activity of HIV-specific $CD8^+$ T cells *in vitro*. *AIDS Res Hum Retroviruses* (2007) 23:438–50. doi: 10.1089/aid.2006.0162
11. Jiao Y, Fu J, Xing S, Fu B, Zhang Z, Shi M, et al. The decrease of regulatory T cells correlates with excessive activation and apoptosis of $CD8^+$ T cells in HIV-1-infected typical progressors, but not in long-term non-progressors. *Immunology* (2009) 128:e366–75. doi: 10.1111/j.1365-2567.2008.02978.x
12. Eggena MP, Barugahare B, Jones N, Okello M, Mutalya S, Kityo C, et al. Depletion of regulatory T cells in HIV infection is associated with immune activation. *J Immunol*. (2005) 174:4407–14. doi: 10.4049/jimmunol.174.7.4407
13. Oswald-Richter K, Grill SM, Shariat N, Leelawong M, Sundrud MS, Haas DW, et al. HIV infection of naturally occurring and genetically reprogrammed human regulatory T-cells. *PLoS Biol*. (2004) 2:E198. doi: 10.1371/journal.pbio.0020198
14. Angin M, Sharma S, King M, Murooka TT, Ghebremichael M, Mempel TR, et al. HIV-1 infection impairs regulatory T-cell suppressive capacity on a per-cell basis. *J Infect Dis*. (2014) 210:899–903. doi: 10.1093/infdis/jiu188
15. Schulze Zur Wiesch J, Thomssen A, Hartjen P, Tóth I, Lehmann C, Meyer-Olson D, et al. Comprehensive analysis of frequency and phenotype of T regulatory cells in HIV infection: CD39 expression of $FoxP3^+$ T regulatory cells correlates with progressive disease. *J Virol*. (2011) 85:1287–97. doi: 10.1128/JVI.01758-10
16. Ndhlovu LC, Loo CP, Spotts G, Nixon DF, Hecht FM. FOXP3 expressing CD127lo $CD4^+$ T cells inversely correlate with $CD38^+$ $CD8^+$ T cell activation levels in primary HIV-1 infection. *J Leukoc Biol*. (2008) 83:254–62. doi: 10.1189/jlb.0507281
17. Whiteside TL. Clinical impact of regulatory T cells (Treg) in cancer and HIV. *Cancer Microenviron*. (2015) 8:201–7. doi: 10.1007/s12307-014-0159-1
18. Filaci G, Fenoglio D, Indiveri F. $CD8^+$ T regulatory/suppressor cells and their relationships with autoreactivity and autoimmunity. *Autoimmunity* (2011) 44:51–7. doi: 10.3109/08916931003782171
19. Filaci G, Fenoglio D, Fravega M, Ansaldo G, Borgonovo G, Traverso P, et al. $CD8^+$ $CD28^-$ T regulatory lymphocytes inhibiting T cell proliferative and cytotoxic functions infiltrate human cancers. *J Immunol*. (2007) 179:4323–34. doi: 10.4049/jimmunol.179.7.4323
20. Filaci G, Fravega M, Negrini S, Procopio F, Fenoglio D, Rizzi M, et al. Nonantigen specific $CD8^+$ T suppressor lymphocytes originate from $CD8^+CD28^-$ T cells and inhibit both T-cell proliferation and CTL function. *Hum Immunol*. (2004) 65:142–56. doi: 10.1016/j.humimm.2003.12.001
21. Parodi A, Battaglia F, Kalli F, Ferrera F, Conteduca G, Tardito S, et al. CD39 is highly involved in mediating the suppression activity of tumor-infiltrating $CD8^+$ T regulatory lymphocytes. *Cancer Immunol Immunother*. (2013) 62:851–62. doi: 10.1007/s00262-013-1392-z
22. Fenoglio D, Dentone C, Signori A, Di Biagio A, Parodi A, Kalli F, et al. $CD8^+CD28^-CD127loCD39^+$ regulatory T-cell expansion: a new possible pathogenic mechanism for HIV infection? *J Allergy Clin Immunol*. (2018) 141:2220–2233.e4. doi: 10.1016/j.jaci.2017.08.021
23. Pardoll DM. The blockade of immune checkpoints in cancer immunotherapy. *Nat Rev Cancer* (2012) 12:252–64. doi: 10.1038/nrc3239
24. Kyi C, Postow MA. Checkpoint blocking antibodies in cancer immunotherapy. *FEBS Lett*. (2014) 588:368–76. doi: 10.1016/j.febslet.2013.10.015
25. Naidoo J, Page DB, Wolchok JD. Immune modulation for cancer therapy. *Br J Cancer* (2014) 111:2214–9. doi: 10.1038/bjc.2014.348
26. Klocke K, Sakaguchi S, Holmdahl R, Wing K. Induction of autoimmune disease by deletion of CTLA-4 in mice in adulthood. *Proc Natl Acad Sci USA*. (2016) 113:E2383–92. doi: 10.1073/pnas.1603892113
27. Khagi Y, Kurzrock R, Patel SP. Next generation predictive biomarkers for immune checkpoint inhibition. *Cancer Metastasis Rev*. (2017) 36:179–90. doi: 10.1007/s10555-016-9652-y
28. Perreau M, Savoye AL, De Crignis E, Corpataux JM, Cubas R, Haddad EK, et al. Follicular helper T cells serve as the major CD4 T cell compartment for HIV-1 infection, replication, and production. *J Exp Med*. (2013) 210:143–56. doi: 10.1084/jem.20121932
29. Banga R, Procopio FA, Noto A, Pollakis G, Cavassini M, Ohmiti K, et al. $PD\text{-}1^+$ and follicular helper T cells are responsible for persistent HIV-1 transcription in treated aviremic individuals. *Nat Med*. (2016) 22:754–61. doi: 10.1038/nm.4113
30. Yamamoto T, Price DA, Casazza JP, Ferrari G, Nason M, Chattopadhyay PK, et al. Surface expression patterns of negative regulatory molecules identify determinants of virus-specific $CD8^+$ T-cell exhaustion in HIV infection. *Blood* (2011) 117:4805–15. doi: 10.1182/blood-2010-11-317297
31. Cockerham LR, Jain V, Sinclair E, Glidden DV, Hartogenesis W, Hunt PW, et al. Programmed death-1 expression on CD4+ and CD8+ T cells in treated and untreated HIV disease. *AIDS* (2014) 28:1749–58. doi: 10.1097/QAD.0000000000000314
32. Gay CL, Bosch RJ, Ritz J, Hataye JM, Aga E, Tressler RL, et al. Clinical trial of the anti-PD-L1 antibody BMS-936559 in HIV-1 infected participants on suppressive antiretroviral therapy. *J Infect Dis*. (2017) 215:1725–33. doi: 10.1093/infdis/jix191
33. Ostios-Garcia L, Faig J, Leonardi GC, Adeni AE, Subegdjo SJ, Lydon CA, et al. Safety and efficacy of PD-1 inhibitors among HIV-positive patients with non-small-cell lung cancer. *J Thorac Oncol*. (2018) 13:1037–42. doi: 10.1016/j.jtho.2018.03.031
34. Finnefrock AC, Tang A, Li F, Freed DC, Feng M, Cox KS, et al. PD-1 blockade in rhesus macaques: impact on chronic infection and prophylactic vaccination. *J Immunol*. (2009) 182:980–7. doi: 10.4049/jimmunol.182.2.980
35. Velu V, Titanji K, Zhu B, Husain S, Pladevega A, Lai L, et al. Enhancing SIV-specific immunity *in vivo* by PD-1 blockade. *Nature* (2009) 458:206–10. doi: 10.1038/nature07662
36. Gill AL, Green SA, Abdullah S, Le Saout C, Pittaluga S, Chen H, et al. Programed death-1/programed death-ligand 1 expression in lymph nodes of HIV infected patients: results of a pilot safety study in rhesus macaques using anti-programed death-ligand 1 (Avelumab). *AIDS* (2016) 30:2487–93. doi: 10.1097/QAD.0000000000001217
37. Koster BD, de Gruijl TD, van den Eertwegh AJ. Recent developments and future challenges in immune checkpoint inhibitory cancer treatment. *Curr Opin Oncol*. (2015) 27:482–8. doi: 10.1097/CCO.0000000000000221

38. Zanetti M. A second chance for telomerase reverse transcriptase in anticancer immunotherapy. *Nat Rev Clin Oncol*. (2017) 14:115–28. doi: 10.1038/nrclinonc.2016.67
39. Fauci AS. An HIV vaccine is essential for ending the HIV/AIDS pandemic. *JAMA* (2017) 318:1535–6. doi: 10.1001/jama.2017.13505
40. Perreau M, Banga R, Pantaleo G. Targeted immune interventions for an HIV-1 cure. *Trends Mol Med*. (2017) 23:945–61. doi: 10.1016/j.molmed.2017.08.006
41. Kiepiela P, Ngumbela K, Thobakgale C, Ramduth D, Honeyborne I, Moodley E, et al. $CD8^+$ T-cell responses to different HIV proteins have discordant associations with viral load. *Nat Med*. (2007) 13:46–53. doi: 10.1038/nm1520
42. Pantaleo G, Levy Y. Therapeutic vaccines and immunological intervention in HIV infection: a paradigm change. *Curr Opin HIV AIDS* (2016) 11:576–84. doi: 10.1097/COH.0000000000000324
43. Zhou J, Cheung AK, Tan Z, Wang H, Yu W, Du Y, et al. PD1-based DNA vaccine amplifies HIV-1 GAG-specific $CD8^+$ T cells in mice. *J Clin Invest*. (2013) 123:2629–42. doi: 10.1172/JCI64704

Conflict of Interest Statement: The authors declare that the research was conducted in the absence of any commercial or financial relationships that could be construed as a potential conflict of interest.

frontiers in Immunology

ORIGINAL RESEARCH
published: 05 December 2018
doi: 10.3389/fimmu.2018.02783

Multivariate Computational Analysis of Gamma Delta T Cell Inhibitory Receptor Signatures Reveals the Divergence of Healthy and ART-Suppressed HIV+ Aging

Anna C. Belkina[1,2], Alina Starchenko[3], Katherine A. Drake[4], Elizabeth A. Proctor[3], Riley M. F. Pihl[1], Alex Olson[5], Douglas A. Lauffenburger[3], Nina Lin[5†] and Jennifer E. Snyder-Cappione[1,6†]*

[1] Flow Cytometry Core Facility, Boston University School of Medicine, Boston, MA, United States, [2] Department of Pathology and Laboratory Medicine, Boston University School of Medicine, Boston, MA, United States, [3] Department of Biological Engineering, Massachusetts Institute of Technology, Cambridge, MA, United States, [4] Cytobank, Inc., Santa Clara, CA, United States, [5] Department of Medicine, Boston University School of Medicine, Boston, MA, United States, [6] Department of Microbiology, Boston University School of Medicine, Boston, MA, United States

Even with effective viral control, HIV-infected individuals are at a higher risk for morbidities associated with older age than the general population, and these serious non-AIDS events (SNAEs) track with plasma inflammatory and coagulation markers. The cell subsets driving inflammation in aviremic HIV infection are not yet elucidated. Also, whether ART-suppressed HIV infection causes premature induction of the inflammatory events found in uninfected elderly or if a novel inflammatory network ensues when HIV and older age co-exist is unclear. In this study we measured combinational expression of five inhibitory receptors (IRs) on seven immune cell subsets and 16 plasma markers from peripheral blood mononuclear cells (PBMC) and plasma samples, respectively, from a HIV and Aging cohort comprised of ART-suppressed HIV-infected and uninfected controls stratified by age ($\leq$35 or $\geq$50 years old). For data analysis, multiple multivariate computational algorithms [cluster identification, characterization, and regression (CITRUS), partial least squares regression (PLSR), and partial least squares-discriminant analysis (PLS-DA)] were used to determine if immune parameter disparities can distinguish the subject groups and to investigate if there is a cross-impact of aviremic HIV and age on immune signatures. IR expression on gamma delta ($\gamma\delta$) T cells exclusively separated HIV+ subjects from controls in CITRUS analyses and secretion of inflammatory cytokines and cytotoxic mediators from $\gamma\delta$ T cells tracked with TIGIT expression among HIV+ subjects. Also, plasma markers predicted the percentages of TIGIT+ $\gamma\delta$ T cells in subjects with and without HIV in PSLR models, and a PLS-DA model

OPEN ACCESS

Edited by:
Sara Gianella Weibel, University of California, San Diego, United States

Reviewed by:
Jennifer Ann Juno, The University of Melbourne, Australia
Natalia Soriano-Sarabia, University of North Carolina at Chapel Hill, United States

***Correspondence:**
Jennifer E. Snyder-Cappione
cappione@bu.edu

† These authors have contributed equally to this work

Specialty section:
This article was submitted to Viral Immunology, a section of the journal Frontiers in Immunology

Received: *07 September 2018*
Accepted: *12 November 2018*
Published: *05 December 2018*

Citation:
Belkina AC, Starchenko A, Drake KA, Proctor EA, Pihl RMF, Olson A, Lauffenburger DA, Lin N and Snyder-Cappione JE (2018) Multivariate Computational Analysis of Gamma Delta T Cell Inhibitory Receptor Signatures Reveals the Divergence of Healthy and ART-Suppressed HIV+ Aging. Front. Immunol. 9:2783. doi: 10.3389/fimmu.2018.02783

of γδ T cell IR signatures and plasma markers significantly stratified all four of the subject groups (uninfected younger, uninfected older, HIV+ younger, and HIV+ older). These data implicate γδ T cells as an inflammatory driver in ART-suppressed HIV infection and provide evidence of distinct "inflamm-aging" processes with and without ART-suppressed HIV infection.

Keywords: γδ T cell, TIGIT, HIV, aging, inflammation, citrus, immune exhaustion, checkpoint inhibition

INTRODUCTION

Although anti-retroviral therapy (ART) has dramatically reduced the rates of HIV-associated morbidity and mortality, HIV+ individuals have a shorter lifespan than uninfected counterparts (1–3) due in part to the onset and progression of co-morbidities associated with older age, including cardiovascular disease, stroke, neurocognitive impairment, diabetes mellitus, impaired renal function, non-AIDS malignancies, and osteoporosis (4–6). These conditions, sometimes referred to as serious non-AIDS events (SNAEs), afflict older HIV+ individuals more frequently than both younger counterparts (4, 6) and the uninfected elderly (6) and SNAE disease onset is reported to occur at younger ages in aviremic HIV+ individuals as compared with uninfected controls (5, 7), with the latter observations supporting the concept of HIV+ persons undergoing early or accelerated aging (8). Mortality and age-associated co-morbidities among HIV+ individuals track with plasma inflammatory and coagulation markers, such as C-reactive protein (CRP), IL-6, D-dimer, and fibrinogen (9–14), similar to the general population (15–21). These findings strongly implicate the general inflammation associated with aging, sometimes referred to as "inflamm-aging" (22, 23), as an integral link to SNAE occurrence in aviremic HIV infection.

Gamma delta (γδ) T cells are a unique T cell lineage that is typically <10% of T cells in the circulation yet are present in considerably higher proportions in the intestinal epithelium (24–27). With a limited T cell receptor repertoire and evidence indicating that a predominant mode of cell activation is in response to non-peptidic ligands, cytokines, and signaling via NKG2D and similar receptors (28–35), γδ T cells are implicated as early responders in immune responses and/or as innate-adaptive bridging cells, responding to innate signals to then direct the development of the adaptive immune response via secretion of cytokines and other factors. As a population, γδ T cells can exert inflammatory/cytotoxic (36, 37) or immuno-regulatory effector functions (38, 39), are integral to the control of infections (40, 41), and can exhibit potent anti-tumor activity (42–44). The role of γδ T cells in HIV viral pathogenesis is unclear to date; shifts in γδ T cell subsets defined by T cell receptor usage (Vδ1 and Vδ2) occur early in infection (45) due to a substantial loss of the Vγ2-Jγ1.2/Vδ2+ subset that is not always recovered with viral suppression (46). However, functional differences between γδ T cell subsets that differ in γ and δ chain usage are not well-established and therefore the significance of this subset shift in relation to disease pathogenesis is uncertain. Also, circulating γδ T cells serve as a reservoir for latent HIV infection (47) and thus may have relevance in cure strategies. To date, the role of γδ T cells in the inflammation observed in aviremic HIV infection is unknown.

To understand the cellular network that drives the onset and progression of age-associated morbidities in both ART-suppressed (aviremic) HIV and healthy aging, we conducted a study that measured a large number of immune parameters from a well-characterized HIV and Aging cohort, comprised of both ART-suppressed HIV+ and age-matched uninfected controls with similar exposures and demographics, stratified by age in younger and older groups. Our results from multivariate computational analyses of high parameter single cell cytometry, plasma markers, and *ex vivo* culture supernatant cytokine data identify γδ T cells as a putative key player in the immune cell network driving "inflamm-aging" in aviremic HIV infection. Also, our bioinformatic analyses revealed an novel combined impact of both virally suppressed HIV and aging on immune networks, thereby indicating that aviremic HIV+ persons do not simply prematurely age but undergo a novel inflammatory course when these two conditions collide.

RESULTS

Inhibitory Receptor (IR) Expression on γδ T Cells Distinguishes ART-Suppressed HIV+ Subjects From Uninfected Controls

Expression of IRs has been linked to altered functionality of immune cells (48–51). While increased IR expression on T cell populations has been reported with aging in mice and humans (52–56), and separately with HIV infection (49, 57–59), a more comprehensive investigation of IR signatures on circulating immune cells from matched younger and older subjects with and without ART-suppressed HIV infection had not been performed to our knowledge. Therefore, in this study we analyzed PBMC from our HIV and Aging Cohort, comprised of ART-suppressed HIV+ younger (≤35 yo), and older (≥50 yo) subjects age-matched with uninfected counterparts (**Table 1**). We measured five inhibitory receptors (PD-1, TIGIT, TIM-3, CD160, LAG-3) on seven immune cell subsets [CD4+ T, CD8+ T, T regulatory (Treg), $CD56^{bright}$ and $CD56^{dim}$ natural killer (NK), gamma delta T (γδ T), and invariant natural killer T (iNKT) cells] using the 16-color flow cytometry panel we developed and previously described (60). Using the CITRUS algorithm (61) we determined whether IR expression on any of the immune subsets (**Supplementary Figure 1**) could be used to distinguish ART-suppressed HIV+ subjects from uninfected controls. Using 10-fold cross-validation (CV) to select the model with the minimum number of features necessary to predict these two groups, only

TABLE 1 | Cohort characteristics.

	Uninfected controls		ART-suppressed HIV+[a]			
	Younger (≤35)	Older (≥50)	Younger (≤35)		Older (≥50)	
n	21	21	22		28	
Age (mean,range)	27 (22–35)	58 (50–72)	28 (22–33)		58 (50–76)	
Sex (%M/F)	100/0	100/0	100/0		86/14	
Ethnicity (C/B/A/O)[b]	15/3/3/0	11/6/3/2	17/3/1/0		18/10/0/0	
CD4 count (cells/mm^3, mean, range)[c]			611 (89–1,362)		719 (246–1,216)	
ART duration (years)			**Mean**	***n***	**Mean**	***n***
0–5	–	–	2.2	19	2.9	17
5–10	–	–	6.2	3	6.8	6
>10	–	–	–	0	16.5	5
Nadir CD4 count (cells/mm^3)			**Mean**	***n***	**Mean**	***n***
0–250	–	–	159	6	133	9
251–500	–	–	339	11	311	12
>501	–	–	649	5	680	6

[a] *Undetectable HIV-1 viral loads for ≥ 6months;* [b] *Caucasian/Black/Asian/other;* [c] *Values within 1 year of enrollment.*

TIGIT expression in four cellular clusters comprised of γδ T cells (**Figure 1A**, clusters 1–4 in red circles), was necessary to differentiate the two subject groups with 88.6% CV accuracy (**Supplementary Figure 1**). In all four clusters, TIGIT expression was higher in the ART-suppressed HIV+ subjects compared to the uninfected controls (**Figure 1B**). Expression of other surface antigens on the cells in clusters 1–4 was similar for CD4 and CD127 (all negative), CD56 (all clusters intermediate) and varied for other antigens, such as CD8 (low in cluster 1, intermediate in clusters 2–4), CD16 (intermediate in clusters 1, 2, and 4, and low in cluster 3), and CD3 (all four clusters positive, with cluster 3 intermediate) (**Figure 1C**). Next, a false discovery rate (FDR) threshold of 1% was used to identify all clusters that were significantly different between the two subject groups using IR expression differences. Using this method, seven clusters were significant and they all contained γδ T cells (**Figure 1D**); all seven clusters differed in TIGIT expression between the HIV+ subjects and uninfected controls, one (cluster 3) differed in CD160 expression, and one (cluster 4) differed in TIM-3 expression between the two subject groups. Six of the seven TIGIT expression clusters contain only or predominantly γδ T cells (**Supplementary Figure 1**, **Figure 1F**), with one cluster (cluster 5) containing both NK and γδ T cells; however, it is likely that γδ T cells are the sole driver of this finding given the γδ T predominance in all other clusters. Similar to the 10-fold CV results (**Figure 1B**), the expression of the defining IR for clusters 3–7 was consistently higher in the HIV+ subject group compared to uninfected controls (**Figure 1E**). Further phenotypic analysis of the three additional clusters that emerged from the FDR-constrained analysis (clusters 5, 6, and 7) show the presence of NK cells in cluster 5 (CD3-, CD16/56+), while clusters 6 and 7 are predominantly CD16-, CD56-, CD4-, CD8-, and γδ TcR^{lo} (**Figure 1F**). Together, these data demonstrate that the IR expression on circulating γδ T cells distinguishes ART-suppressed HIV+ subjects from uninfected controls. Also, the γδ T cell subsets that predict these two subject groups are diverse, including populations that differ in CD8, CD16, CD56, and CD127 expression.

γδ T Cell IR Expression Increases With Age and HIV Infection

We next investigated γδ T cells in more detail by performing traditional expert-driven gating and analysis. We first determined the frequencies and absolute counts of γδ T cells (gating strategy shown in **Supplementary Figure 2A**) and found overall similar γδ T cell levels within the HIV+ and uninfected control groups (**Supplementary Figures 2B–E**). We next measured Vδ1+ and Vδ2+ γδ T cell frequencies from a subset of samples and found an inversion of the Vδ1:Vδ2 ratio in the HIV+ subjects compared to the uninfected group, confirming that the findings in our cohort are consistent with previous reports (45, 62) (**Supplementary Figures 2F–I**). Next, we compared the percentages of IR+ γδ T cells between the ART-suppressed HIV+ and control groups and found that the HIV+ subjects expressed significantly higher frequencies of TIGIT+, CD160+, and TIM-3+ cells than age-matched controls (**Figure 2A**). As TIM-3 and LAG-3 are not bimodally expressed, setting flow cytometry gates to determine the percentage of positive cells is difficult; therefore, we also calculated the median expression of each IR and found significantly higher levels of TIM-3 but not LAG-3 on the γδ T cells from the HIV+ subjects compared with controls (**Figure 2B**). As expression of more than one IR on individual γδ T cells could reflect distinct states of activation or an advanced stage of immune exhaustion (63), we compared the expression of ≥2, ≥3, or ≥4 IRs per γδ T cell between our HIV+ and uninfected control subjects and found significantly higher levels in the HIV+ subjects for all comparisons (**Figure 2C**). To control for bias due to manual gating, γδ T cell events were extracted from the flow cytometry data using SPADE clustering

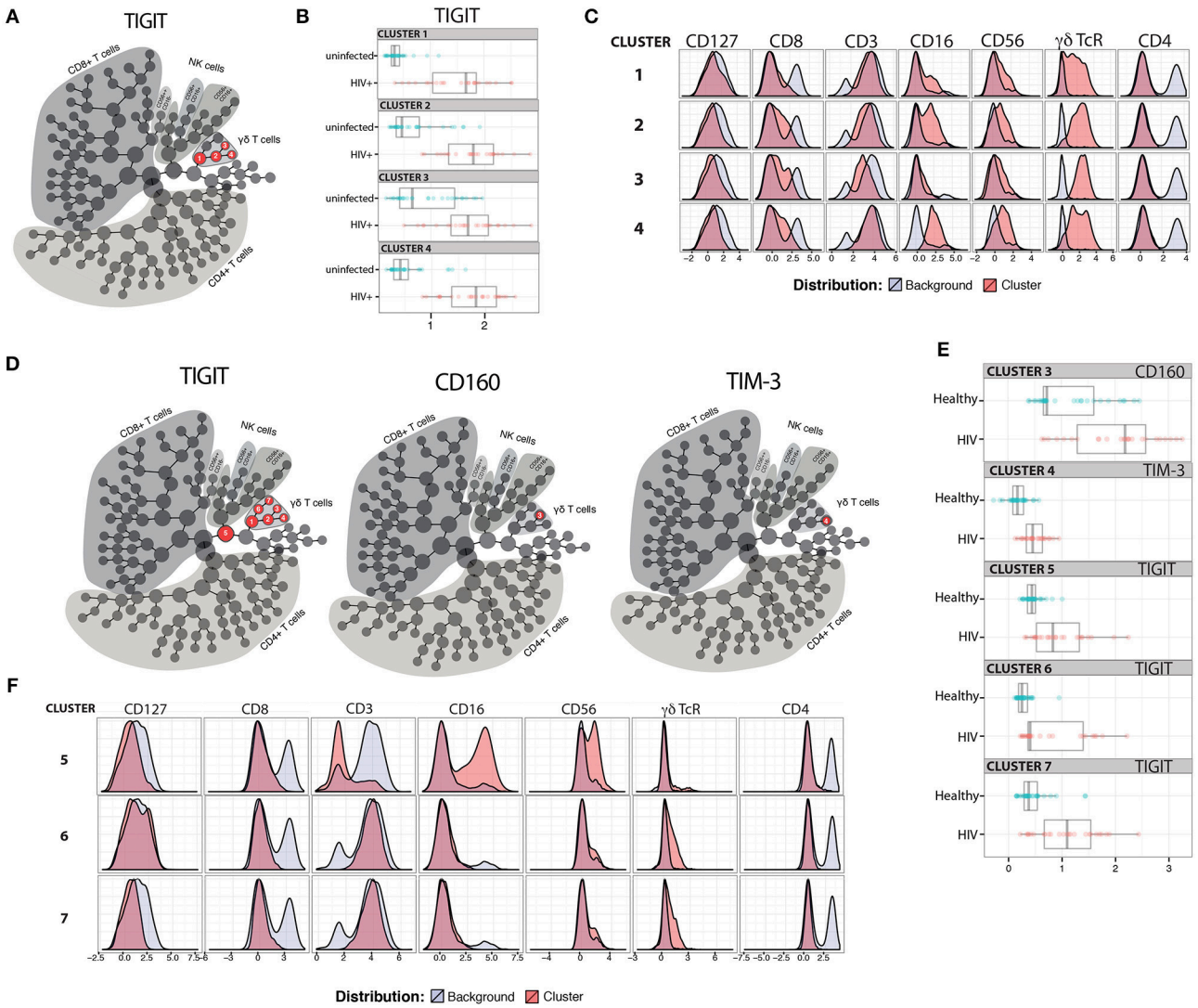

FIGURE 1 | TIGIT, CD160, and TIM-3 on γδ T cells distinguish ART-suppressed HIV+ subjects from uninfected controls. CITRUS analysis of a 16-parameter flow cytometry dataset from PBMC of ART-suppressed HIV+ subjects and uninfected controls. **(A)** Model selected by minimum cross-validated error rate yielded four clusters necessary to differentiate the groups, numbered 1–4 and highlighted in red. **(B)** TIGIT expression of cells in clusters 1–4 in the ART-suppressed HIV+ (red) and uninfected control (blue) groups, log-transformed Mean Fluorescence Intensity (MFI) is shown, and each dot represents one subject, **(C)** expression of other measured antigens on cells from clusters 1–4 as compared to all other (background) cells; **(D)** Model constrained to include all significant clusters below a FDR threshold of 1% reveals seven clusters with significantly different expression of TIGIT, CD160, and/or TIM-3 between the groups, **(E)** log-transformed MFI of CD160, TIM-3, and TIGIT expression per subject for clusters 3, 4, and 5–7, respectively, and **(F)** expression of other measured antigens on cells from clusters 5, 6, and 7. All scales in **(B,C,E,F)** are log-transformed. CITRUS clustering data per lineage channel are shown in **Supplementary Figure 1**.

(64) and γδ T cell IR median expression was assessed (LAG-3 not shown due to negligible results), confirming our manual gating findings (data not shown) and allowing visualization of IR expression from individual subjects (**Figure 2D**). Overall patterns indicate higher IR expression of the ART-suppressed HIV+ subjects compared with controls and also seemingly independent regulation of each of the four IRs within individual subjects. Next, subjects were further stratified into the younger and older groups as defined in **Table 1** and the percentages of IR+ γδ T cells were compared (**Figure 2E**). TIGIT+ γδ T cells were significantly higher in: (1) older vs. younger uninfected subjects, (2) HIV+ younger vs. uninfected younger subjects, (3) HIV+ older vs. uninfected older subjects, and (4) HIV older vs. uninfected younger subjects (**Figure 2E**). Analysis of the other IRs did not result in significant differences between the groups, with the exception of TIM-3 expression of the uninfected younger vs. HIV+ younger subjects (**Figure 2E**). Comparison of multi-IR expression with subjects stratified by both age and HIV status shows higher percentages of ≥2IR per cell with advancing age and with HIV infection. Notably, for all analyses in **Figures 2E,F**, no significant differences were found between the HIV+ younger and HIV+ older groups, indicating a lack of

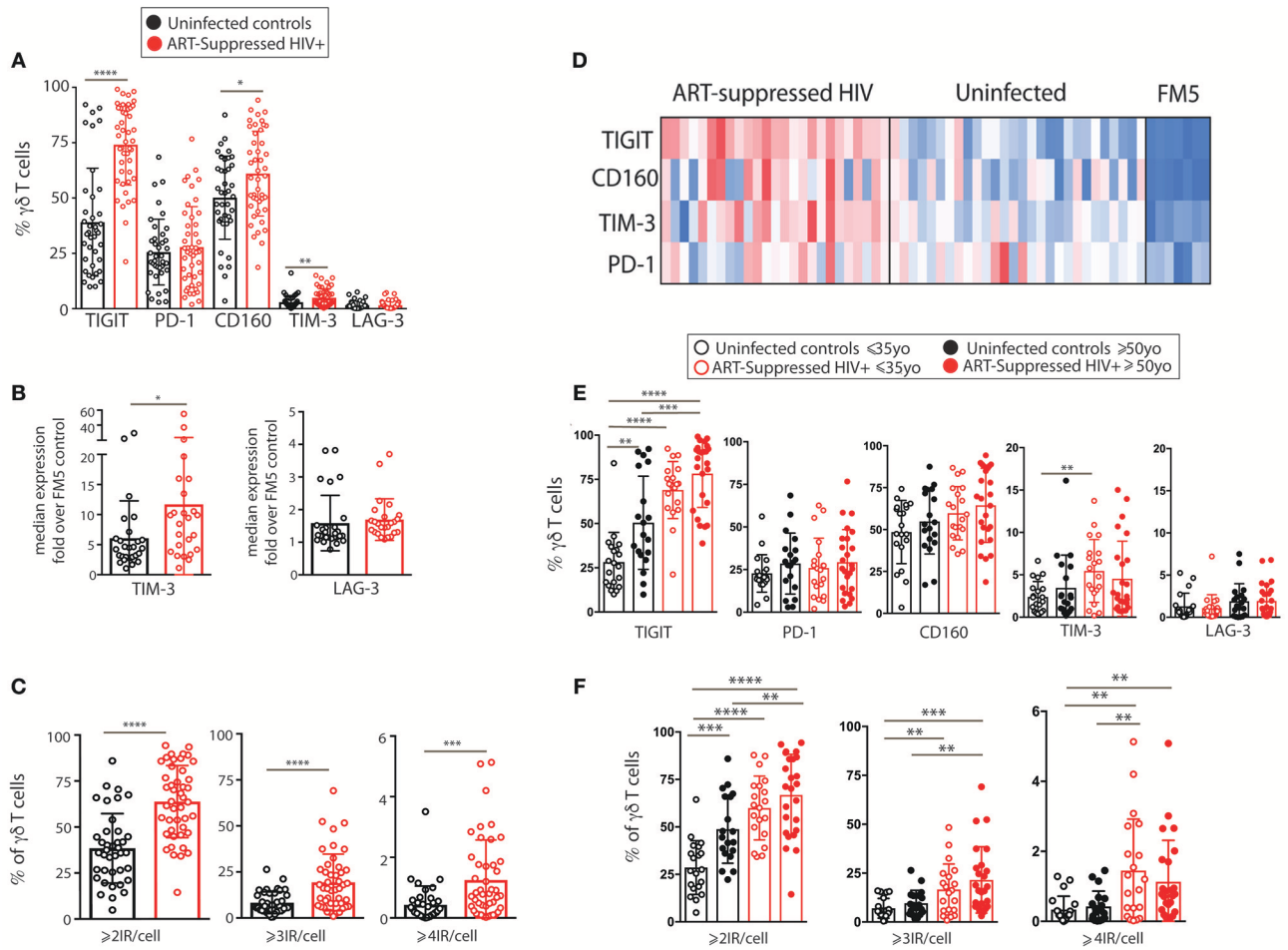

FIGURE 2 | IR expression on γδ T cells from ART-suppressed HIV+ subjects and uninfected controls stratified into younger and older groups. **(A)** The total percentages of IR+ γδ T cells in ART-suppressed HIV+ subjects and uninfected control groups; **(B)** the average fluorescence intensity of γδ T cell TIM-3 and LAG-3 expression for HIV+ and uninfected subjects, determined by median intensity divided by FM5 control results; **(C)** the percentage of γδ T cells expressing ≥2, ≥3, or ≥4 IRs, in any combination, of CD160, TIGIT, TIM-3, LAG-3, and PD-1 in HIV+ subjects and controls, **(D)** median intensity of IR expression on SPADE-identified γδ T cells per individual (one subject per column), including FM5 uninfected control samples from each batch run; **(E)** total percentages of IR+ γδ T cells and **(F)** percentages of γδ T cells expressing ≥2, ≥3, or ≥4 IRs, in any combination, of TIGIT, PD-1, CD160, TIM-3, and LAG-3, with subjects stratified by both HIV status and age. For **(A–C)**, two-tailed *t*-tests were performed for each comparison. For graphs with multiple comparisons **(E,F)** only significant results after Bonferroni correction ($p < 0.008$) are shown. *$p > 0.05$, **$p > 0.01$, ***$p > 0.001$, ****$p > 0.0001$.

a definitive additive or multiplicative effect of both age and HIV on γδ T cell IR expression found with univariate analysis. Also, HIV infection and not aging appears to drive γδ T cells to express ≥3 or ≥4 IR per cell (**Figure 2F**). Taken together, these results suggest that healthy aging and HIV infection independently drive TIGIT and multi-IR expression on γδ T cells, that IR expression does not change significantly as aviremic HIV+ individuals age, and HIV and not aging drives γδ T cells to a ≥3 or ≥4 IR per cell phenotype.

γδ T Cells Expressing Distinct Combinations of PD-1, TIGIT, and CD160 Vary With Aging and Aviremic HIV Infection

We next investigated how the combinational expression of PD-1, TIGIT, and CD160 on γδ T cells differed with healthy aging and ART-suppressed HIV infection. Due to the non-bimodal expression of TIM-3 and LAG-3 on the γδ T cells in our cohort, it was not possible to accurately define positive and negative cells for the multi-expression analysis shown in **Figure 3**. First, the percentage of γδ T cells expressing each of the eight possible combinations of these three IRs were compared across the four subject groups using beta regression of abundance on HIV status and age and correcting for multiple hypotheses testing with a family-wise error rate of 0.05. Both aging and HIV infection were significantly associated with lower percentages of PD-1- TIGIT- CD160- ("triple negative") and PD-1- TIGIT- CD160+ ("CD160 only") cells. HIV infection was also associated with a lower percentage of PD-1+ TIGIT- CD160- ("PD-1 only") cells and a higher percentage of three populations: PD-1- TIGIT+ CD160- ("TIGIT+ only"), PD1-, TIGIT+ CD160+ ("TIGIT and CD160 double positive") and

PD-1+ TIGIT+ CD160+ ("triple positive") cells (**Figure 3A**). Similar to the results for HIV infection, there were higher average frequencies of TIGIT only and TIGIT and CD160 double positive cells in older compared with younger uninfected subjects (albeit not statistically significant). To further assess the potential relationships between γδ T cells bearing different IR combinations, Pearson correlation coefficients were generated for the percentages of all eight possible IR combinations with one another in a pair-wise manner separately for the uninfected controls (**Figure 3B**) and ART-suppressed HIV+ subjects (**Figure 3C**). Within the uninfected group, strong inverse correlations were found that agree with the results in **Figure 3A**, specifically, the triple negative and CD160 only populations with the TIGIT single positive and the TIGIT CD160 double positive cells (**Figure 3B**, asterisks). Within the HIV+ group, there were also strong inverse correlations of the triple negative/CD160 only populations, in this case with the TIGIT CD160 double positive cells as well as the triple positive cells (**Figure 3C**, asterisks). These data suggest that both aging and HIV infection skew the circulating γδ T cell compartment from predominantly triple negative and CD160 only expressing cells to TIGIT only and CD160 TIGIT double positive cells (**Figure 3D**). The triple positive γδ T cell population, while inversely associated with no IR expressing cells in both uninfected controls and HIV+ subjects, is higher in frequency only of the HIV+ subjects compared with controls, and not between the uninfected younger and older groups. Taken together, these data suggest that the triple negative and CD160 only γδ T cell populations are a resting/precursor population to the subsets expressing TIGIT alone, TIGIT with CD160, and TIGIT, CD160, and PD-1, and such IR expression is suggestive of an activated or exhausted state (63, 65).

Spontaneous Secretion of Inflammatory Cytokines and Cytotoxic Mediators From γδ T Cells Differentially Tracks With TIGIT Expression During Aging +/- Aviremic HIV Infection

As an indirect measurement of the potential *in vivo* functional activity of the γδ T cells, cells were sorted and cultured overnight without stimulation and the secretion of 33 analytes was measured in the supernatants. The spontaneous release of sCD137, a marker of cell activation that correlates with circulating C-reactive protein (CRP) in plasma (66) and is positively associated with both acute coronary syndromes (66) and stroke (67), was significantly higher from the γδ T cells of HIV+ older subjects compared with the other three groups (**Figure 4A**, results from the other detected analytes are shown in **Supplementary Figure 4**). As each sample stained with the 16-color panel was run through the FACSARIA cell sorter, the percentages of TIGIT+ γδ T cells were determined and the γδ T cells were sorted for cell culture simultaneously. Ten analytes significantly correlated with percentages of defined IR-expressing γδ T cell subsets (**Figure 3D**) from either the HIV+ and/or the uninfected subject group (**Figure 4B**). Of the HIV+ data, 14 of the 15 significant results included negative correlations with "resting" and positive correlations with "activated/exhausted" populations as defined in **Figure 3D**; this suggests progression from a resting to an activated state with HIV infection. Next, we used linear regression to relate levels of eleven analytes detected in the supernatants of a substantial percentage (≥45%) of the subjects with the percentage of TIGIT+ γδ T cells (eight are shown in **Figure 4C**, three in **Supplementary Figure 4**). Of the analytes that were produced by <45% of the subjects, the average number of subjects whose γδ T cells produced the cytokine was only nine per cent. Therefore, we set 45% as the cutoff of "positive" responses by the cohort. All data where a detectable amount of analyte was found from at least one subject is included in **Supplementary Figure 4B**). Overall, of γδ T cells from the uninfected controls, the TIGIT+ percentages did not associate with cytokine release (**Figures 4B,C**), with the exception of MIP1-β, which showed a negative correlation. Conversely, the percentage of TIGIT+ γδ T cells from the ART-suppressed HIV+ subjects positively and significantly correlated with the secretion of five analytes: sCD137, Granzyme A, Granzyme B, MIP1-β, and CCL20/MIP3-α and showed a positive trend for others such as perforin, TNF-α, and IFN-γ (**Figures 4B,C**). Also, there is a notable trend of lower analyte release of γδ T cells from the older compared with younger uninfected subjects, and a converse trend of increased analyte secretion with older age within the HIV+ subject group. These data suggest unlike the uninfected controls, the γδ T cells from ART-suppressed HIV+ subjects are activated, secreting inflammatory factors *in vivo,* and possibly contributing to the inflammatory milieu linked to SNAEs in this population, and that TIGIT expression marks inflammatory activity of γδ T cells from aviremic HIV+ subjects. To further explore the relationships between TIGIT expression and *ex vivo* analyte production by γδ T cells in the HIV+ subjects vs. controls, two partial least square regression (PLSR) models (one for uninfected controls, one for HIV+ subjects) were generated to specifically ask if cytokine measurements in the supernatants can predict the percentage of TIGIT+ cells in the PBMC samples. In PLSR modeling, linear combinations of analytes are used to predict the variance in the dependent variables (68, 69), in this case the percentage of TIGIT+ cells. PLSR analysis is more potent than simple regression analyses when the behavior of multiple analytes of interest is known to be interdependent, since it enables determination of the combinations of analytes that maximally correlate with TIGIT expression. Analyte measurements were compressed in low-dimensional latent variable (LV) space; notably, the younger and older subjects separated into distinct groups for each model without the models being trained on age parameter (**Figures 4D,E** left panels). Both models significantly linked spontaneous analyte production with TIGIT expression by γδ T cells. VIP (variable importance of projection) calculation was then used to assess the importance of each analyte variable with values >1 considered influential above average in the model. Notably, the VIP (statistically significant) analytes within each model were different (**Figures 4D,E** right panels, light blue bars), confirming that there are distinct associations between TIGIT expression and the cytokines produced from γδ T cells of both HIV+ subjects and uninfected controls. These findings indicate that relationships between γδ T cell TIGIT expression

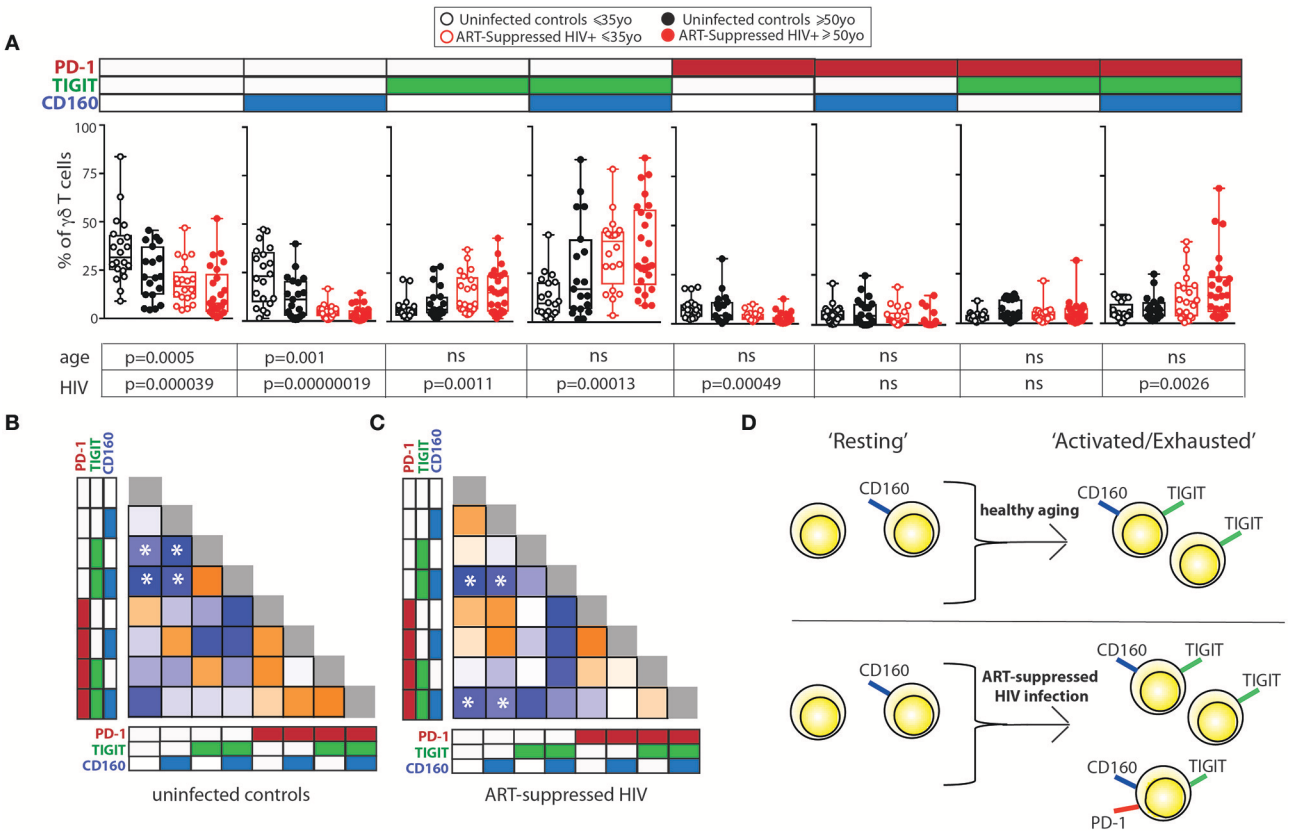

FIGURE 3 | Inhibitory receptor signatures of γδ T cells vary with aging, ART-suppressed HIV infection. **(A)** γδ T cell IR signature analysis of TIGIT, CD160, and PD-1 comparing younger and older subjects and ART-suppressed HIV+ and matched uninfected control groups. Positivity of PD-1, TIGIT, and CD160 is noted above each graph, with the white and colored boxes representing negative and positive expression, respectively. Abundance for each subset of γδ T cells expressing specific IRs was compared across the four groups using beta regression of abundance on HIV status and age group. Significance of age and HIV infection was determined after correcting for multiple hypotheses testing as described in the Materials and Methods section. **(B)** Correlation analysis of the abundances of each IR expressing subset of γδ T cells in uninfected controls and **(C)** ART-suppressed HIV+ subjects. Heatmaps are colored based on strength of the Pearson correlation coefficient between each IR subset (orange: positive, blue: negative). Both age groups are included in each heatmap. The Pearson correlation coefficients and *p*-values for these analyses are shown in **Supplementary Figure 3**. Asterisks indicate biologically interesting correlations used to inform **(D)** diagram depicting the hypothesized differential progression of IR expression due to healthy aging vs. ART-suppressed HIV infection.

and spontaneous cytokine release change with both normal aging and aging with aviremic HIV infection.

Plasma Markers of Inflammation and Coagulation Differentially Track With TIGIT Expression During Aging With and Without ART-Suppressed HIV Infection

We measured the concentrations of 16 analytes in plasma, many of which are well-defined markers of inflammation and have been strongly associated with the onset of co-morbid conditions and/or mortality in HIV-infected populations (10, 13, 70–73) as well as with disease in normal aging (15–21). We found significantly higher levels of sCD14, alpha-2 macroglobulin (A2M), fibrinogen, serum amyloid P (SAP), adipsin, and von Willebrand factor (vWF) in the plasma from HIV+ subjects compared to uninfected controls (**Supplementary Figure 5A**). When the subjects were further stratified by age, we found significant differences among subject groups for D-dimer, C-reactive protein (CRP), fibrinogen, SAP, adipsin, and vWF (**Supplementary Figure 5B**) that seem to be driven by age in uninfected subjects or by HIV infection, with no significant differences found between HIV+ younger and HIV+ older subjects. To determine if there are associations between IR expressing γδ T cell subsets and plasma marker levels, we performed linear regression analysis of the plasma marker data against the percentages of our "resting" or "activated/exhausted" γδ subsets (as defined in **Figure 3D**). Of the 16 analytes measured, nine were significantly associated with one or more γδ T cell IR-defined subset(s) in the uninfected controls and/or the ART-suppressed HIV+ groups (**Figure 5A**). For both the HIV+ and uninfected subject groups, there was a predominant trend of negative association with the "resting" and positive association with the "activated/exhausted" γδ T cell populations with plasma markers (**Figures 5A–E**). Also, it is notable that the younger and older age groups are clearly separated in these analyses among the

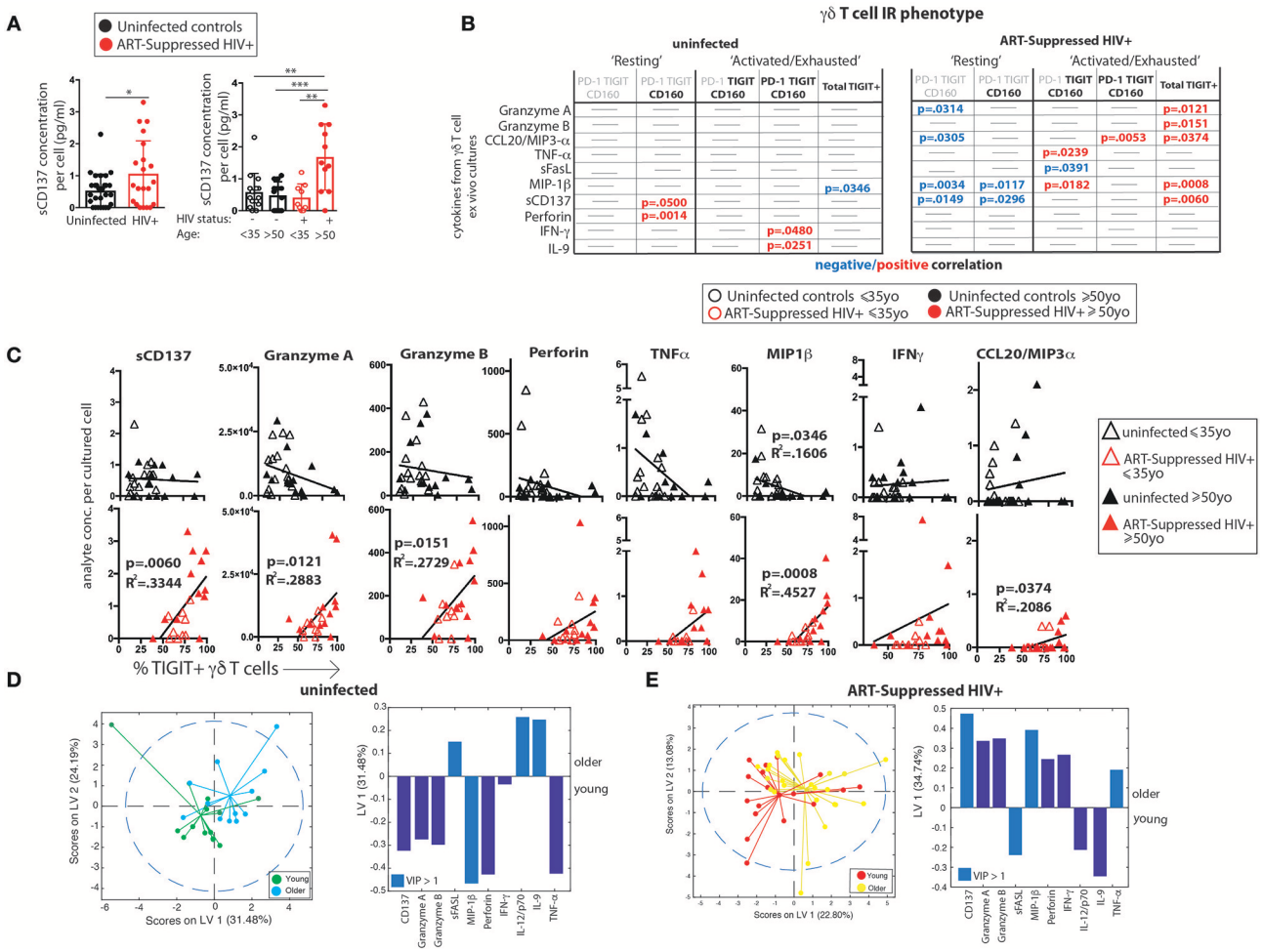

FIGURE 4 | γδ T cell *ex vivo* spontaneous cytokine secretion profiles reveal differential associations with IR expression and age in ART-suppressed HIV infection and uninfected controls. **(A)** sCD137 (pg) secreted per cultured γδ T cell from all HIV+ subjects compared with uninfected controls, and with data also stratified into younger and older sub-groups. **(B)** Tables showing the linear regression analysis results for the 10 analytes that significantly correlated with an IR signature-expressing γδ T cell subset in either subject group as defined in **Figure 3D**. Positive and negative expression of each IR is depicted with black bold and gray lettering, respectively, at the top of each table. **(C)** Linear regression plots of the percentage of TIGIT+ γδ T cells and cytokine concentration (average per cell) for uninfected controls and ART-suppressed HIV+ subjects for the 8 analytes that highlight the opposite trends between the subject groups (results from the other 3 analytes with >45% subject cells responding are shown in **Supplementary Figure 3**). Subjects within the younger and older groups are noted with open and solid triangles, respectively. Units for secreted analytes are as follows: sCD137, Granzyme A, Granzyme B, perforin, MIP-1β; pg/cell; TNF-α, IFN-γ, CCL20/MIP-3 α; pg × 10^4/cell. Scores plot and LV1 derived from a PLSR model of supernatant cytokines regressed against the percentage of TIGIT+ γδ T cells for each donor for uninfected controls **(D)** and ART-suppressed HIV+ subjects **(E)**. Dotted lines in **(D)** and **(E)** show the 95% confidence interval. *$p > 0.05$, **$p > 0.01$, ***$p > 0.001$, ****$p > 0.0001$.

controls but not the HIV-infected subjects (**Figures 5B–E**). These results indicate that TIGIT and multi-IR expression on γδ T cells is linked with the elevated general inflammation found in both healthy aging and ART-suppressed HIV infection, and that HIV appears to generate a new inflammatory status as defined by these plasma markers that is independent of aging. Next, we asked how the concentrations of plasma markers were connected to the percentage of TIGIT+ γδ T cells by training two orthogonalized PLSR models using plasma marker levels to predict the percentage of TIGIT positive cells in the uninfected and HIV+ subject groups (**Figures 5F,G**). We note that the models have differing contributions attributed to each marker (as determined by loadings on LV1), and that different markers emerged as the most important to the correlation of inflammatory state to percent TIGIT positive cells (as determined by VIP score); together, these results indicate that the connections between TIGIT+ γδ T cells and the immune network driving systemic inflammation are fundamentally different between aviremic HIV infection and healthy aging. Notably, this conclusion is based on the multivariate analysis of cytokine profiles that allow analysis of the co-varying multifactorial nature of the data that is characteristic of biological systems (74). Also, similar to the results in **Figures 4D,E**, subjects in the younger and older sub-groups for both uninfected and HIV+ subjects separated without age being added to either model; this indicates that the multivariate analyses (**Figures 5F,G**) reveal age-induced changes

in the inflammatory network of ART-suppressed HIV+ subjects that are not apparent in the univariate (linear regression) dataset (**Figures 5A–E**, **Supplementary Figure 5B**). Overall, our data show that γδ T cells are integral components of distinct inflammatory processes that occur during aging both with and without ART-suppressed HIV infection.

Partial Least Squares Determinant Analysis (PLS-DA) Reveals That γδ IR Signatures Selectively Distinguish the Younger and Older Subject Groups Within Both the Uninfected Control and ART Suppressed HIV+ Subject Groups

To further confirm that the aging process is distinct in uninfected controls and aviremic HIV+ subjects, we used the percentages of γδ T cells expressing all possible combinations of the IRs PD-1, CD160, TIGIT, and TIM-3 and the 16 plasma marker datasets to train a PLS-DA model that determined if a combination of these variables can separate subjects into four groups based on age and HIV status. In the input data, PLS-DA finds which measurements from each subject would "fit" that subject into its clinical group and verifies if such classification is statistically significant. The chosen biological measurements were sufficient to significantly differentiate all four groups in our dataset (**Figure 6A**). In these models, LV1 separated mostly based on HIV status, while LV2 captured the remaining variance attributed mainly to age group. Notably, we trained an alternative model with CD8+ T cell IR signatures used in place of the γδ T cell data and the groups did not separate with significance (data not shown). This analysis indicates that γδ T cells are integral to the inflammatory networks underlying the divergent processes of healthy aging and aging with ART-suppressed HIV infection and we propose that IR expression marks different functional and/or activation/exhaustion states of the γδ T cells in these conditions.

DISCUSSION

In this study, we present evidence that γδ T cells are linked to and may help instigate and perpetuate the elevated inflammation found in aviremic HIV+ individuals, and our multivariate analyses indicate that a distinct inflammatory course occurs during ART-suppressed HIV+ aging. Currently, more than 50% of the HIV-infected population in the U.S. is older than 50 years (75) and the world population over the ages of 65 and 80 is predicted to double and nearly quadruple, respectively, by 2050 (76). Elucidating the cell populations and precise immune networks that drive "inflamm-aging" both with and without HIV infection is a preeminent global health priority.

There are multiple proposed triggers of the aberrant inflammation found in HIV+ persons with successful viral suppression, including the latent HIV viral reservoir itself (77), co-infections such as cytomegalovirus (CMV) (78), and translocation of microbial products across the epithelial barrier of the gastrointestinal tract into the systemic circulation (79). There is a reported connection between harboring latent HIV and IR expression on T cells: CD4+ T cells from virally suppressed HIV+ subjects that express at least one of the IRs TIGIT, PD-1, or LAG-3 contained the majority, on average, of CD4+ T cells with inducible HIV genomes, with multi-IR+ CD4+ T cells particularly enriched for integrated HIV DNA (80); also, TIGIT+ CD4+ T cell frequencies positively correlate with CD4+ T cell HIV DNA content (49), and TIGIT transcription is elevated in cells bearing replication competent latent HIV (81). Our recent studies indicate that sensing of HIV viral intron-containing RNA by infected macrophages leads to type I interferon secretion and induction of IRs on co-cultured T cells (82). Circulating γδ T cells are known to harbor latent virus at a high frequency (47), therefore it is worth investigating if IR+ γδ T cells, particularly TIGIT+ and multi-IR+ subsets, are selectively harboring inducible HIV genomes. Further studies investigating the mechanistic relationship(s) between intracellular HIV, γδ T cell IR expression, and the secretion of inflammatory cytokines and cytotoxic mediators could lead to novel targets for selective therapeutic γδ T cell ablation to help purge the latent HIV pool and reduce general inflammation.

The integrity of the gastrointestinal epithelial barrier is compromised in HIV and SIV infection (79, 83) and does not sufficiently recover with effective ART (84). This "gut leakiness" is connected to the movement of microbial products such as LPS into the systemic circulation and this likely contributes to general inflammation (85). γδ T cells are a predominant immune cell subset in intestinal epithelia (24, 25), and the majority of human mucosal intraepithelial lymphocytes (IELs) are Vδ1+ T cells (86, 87), the subset found to predominate the circulation of aviremic HIV+ subjects but not uninfected controls in this study (**Supplementary Figures 2G–I**) and others (45, 62). Measuring the IR signatures and resident memory markers on Vδ1+ and Vδ2+ γδ T cell subsets from our HIV and Aging cohort is an important next step to help elucidate if the IR differences noted between subject groups are impacted by Vδ1+ and Vδ2+ subset shifts in the circulation and if such shifts indicate emigration from the GI tract. Also, murine intestinal γδ T cells described as "activated yet resting" expressed very high levels of mRNA for Granzymes A and B (88). In light of our functional results showing that spontaneous production of cytolytic machinery tracked with TIGIT expression in HIV+ subjects, this is further evidence that the circulating TIGIT+ γδ T cells, activated and armed with cytolytic machinery, are from the GI tract. It should be noted that cytokine production in response to *in vitro* stimulation was not performed, due to the challenges of stimulating purified γδ T cell cultures efficiently. Functional profiles post-*ex vivo* re-stimulation would provide additional information about the γδ T cells activation/exhaustion status, as rested and not exhausted cells would likely produce higher numbers of analytes and at higher amounts than cells in an activated or exhausted state. Immune cell composition in the blood has reflected what is found in the GALT in aviremic HIV+ subjects (89). Future work examining mucosal resident γδ T cells in SIV-infected animals and HIV+ individuals could provide new insight into how immune

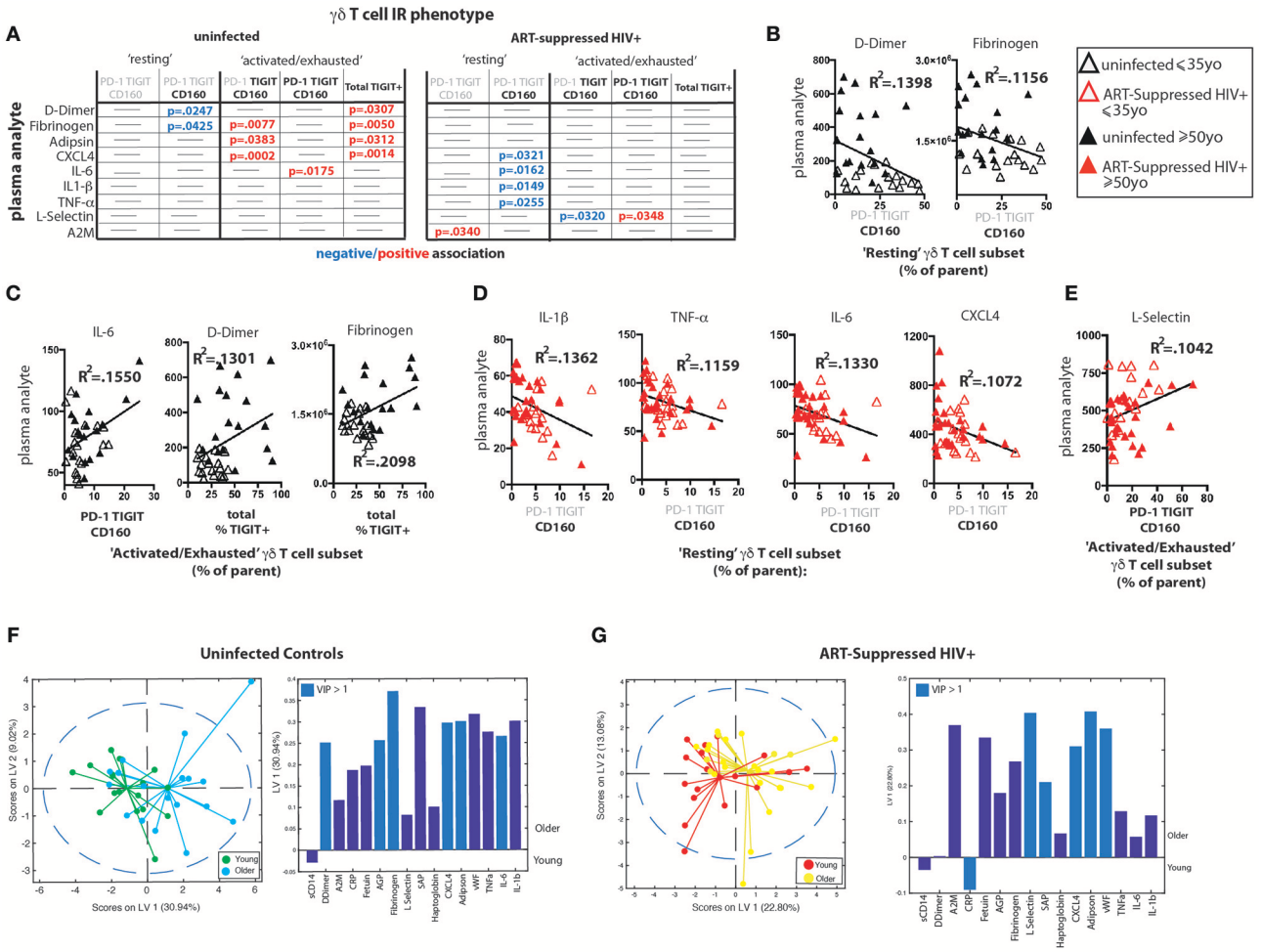

FIGURE 5 | γδ T cell IR signatures correlate with inflammatory plasma markers in both healthy aging and ART-suppressed HIV infection. Sixteen plasma analytes were measured and linear regression analysis was performed with the percentages of IR expressing γδ T cell subsets defined in **Figure 3D** (positive and negative expression of each IR is depicted with black bold and gray lettering, respectively, at the top of each table) and total percent TIGIT+; all statistically significant results ($p < 0.05$) are shown in the tables in **(A)** for uninfected controls and ART-suppressed HIV+ subjects. Examples of correlation plots with a fitted linear regression line comparing "Resting" or "Activated/Exhausted" γδ T cell subsets from uninfected controls with plasma inflammatory/coagulation markers **(B,C)** and analogous graphs for the ART-suppressed HIV+ subjects **(D,E)**. Subjects within the younger and older groups are noted with open and solid triangles, respectively, in **(B–E)**. Units for plasma analytes are as follows: D-Dimer, fibrinogen, CXCL4, L-selectin; ng/ml; IL-6, IL-1β, TNF-α; pg/ml. Scores plot and loadings on LV1 derived from a PLSR model of plasma markers vs. the percentage of TIGIT+ γδ T cells for uninfected controls **(F)** and ART-suppressed HIV+ subjects **(G)**.

changes in the gut direct general inflammation in aviremic HIV infection.

Unlike traditional (adaptive) T cells, a principal means of γδ T cell activation is via cytokine and NK receptors (34), mechanisms easily triggered by activated monocyte/macrophage populations, an immune cell subset strongly linked to inflammation in aviremic HIV+ infection. Markers of monocyte/macrophage activation in the circulation, such as sCD14, sCD163, and tissue factor (TF), have been linked with mortality, atherosclerosis, and other markers of inflammation and coagulation (90–92). Furthermore, TF-expressing monocytes, present with successful HIV viral suppression, produce multiple inflammatory cytokines upon exposure to LPS and induce a coagulation cascade and treatment of SIV-infected macaques with an anti-coagulant that blocks the TF pathway led to a decrease in circulating D-dimer levels as well as markers of immune activation (93). The effect of TF+ monocytes on γδ T cells is unknown to date. It is of interest to investigate the potential cross-activation of monocytes/macrophages and γδ T cells in aviremic HIV infection.

Inhibitory receptors, such as PD-1, TIM-3, and TIGIT, negatively regulate T cell activation and are believed to be critical for limiting immunopathology during immune responses. Expression of IRs is often associated with diminished functional capacity, frequently called immune exhaustion, in HIV, aging and other chronic diseases (50, 53, 59). TIGIT (T cell immunoreceptor with immunoglobulin and ITIM domains) is a more recently described inhibitory receptor that is a member of the

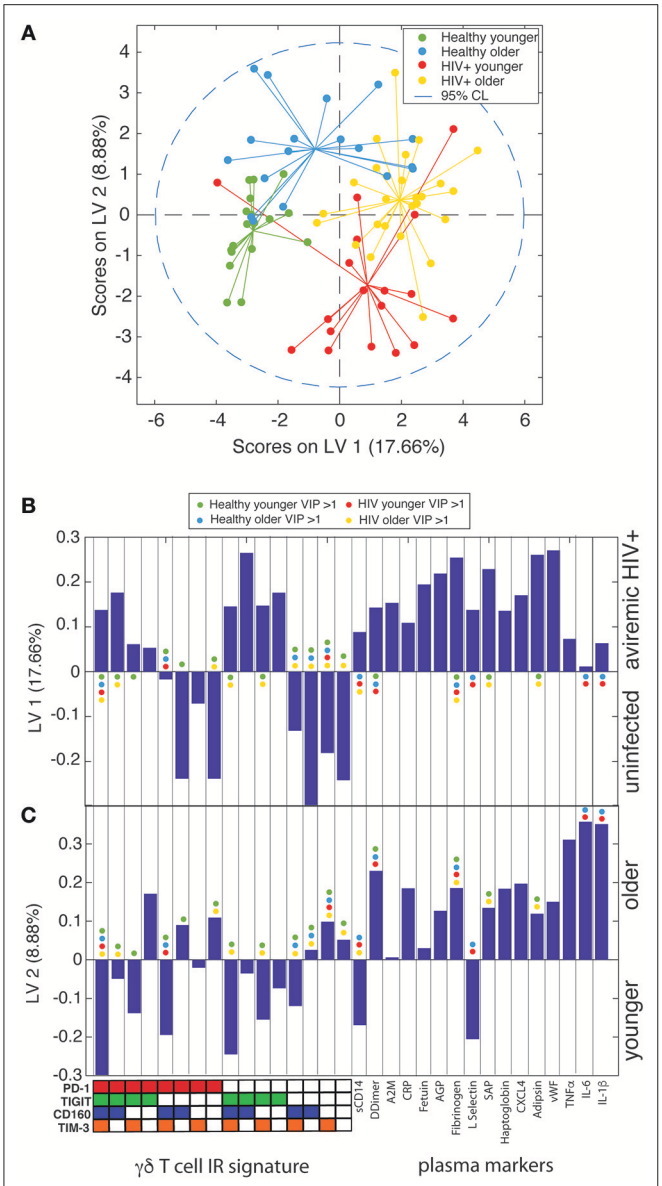

FIGURE 6 | γδ T cell IR signatures and plasma inflammatory cytokines define the divergent aging processes in ART-suppressed HIV+ individuals and uninfected controls. **(A)** A two-dimensional PLS-DA model constructed using the percentages of all possible combinations of the IRs PD-1, TIGIT, CD160, and TIM-3 and 16 markers of inflammation and coagulation in plasma. Each data point represents scores generated by the model, composed of all measurements for a given subject mapped onto the two-dimensional latent variable space. The percentages on the axes show the percent variance in the dataset captured by a particular LV. Dotted line shows the 95% confidence interval. **(B)** Bar plot showing the loadings on LV1 of all parameters used to train the PLS-DA model, which included all possible combinations of the IRs PD-1, TIGIT, CD160, and TIM-3 and the concentrations of all 16 plasma markers measured. LV1 is the latent variable that separated the scores predominantly based on presence or absence of HIV infection. The Y-axis quantifies the positive or negative contribution of a particular parameter to the indicated LV. **(C)** Bar plot as in **(B)**, showing the loadings on LV2, the latent variable that separates the scores affected by patient age, of all parameters used to train the model. The colored dots in **(B,C)** mark the parameters (IR signatures of γδ T cells and plasma markers) with a VIP score >1 (statistically significant) for each subject group in the model.

CD28 family of signaling molecules (94). It is expressed on NK cells, CD8+ T cells, and CD4+ T cells (94), is induced upon activation in multiple immune cell subsets (95–97), and its expression marks exhausted CD8+ T cells in HIV and SIV infection (49). Publications investigating IR expression on γδ T cells are scarce to date and include a report of PD-1 expression on $\gamma\delta^{lo}$ T cells in mouse skin (98) another of TIGIT expression on γδ T cells in the epidermis of stem cell transplant recipients (99), and a recent study reporting higher percentages of IR+ γδ T cells with Plasmodium vivax infection (100). γδ T cells are also implicated as pro-tumorigenic with the PD-1:PDL-1 pathway one proposed mechanism of action (101). Here, TIGIT expression tracked with *ex vivo* secretion of inflammatory cytokines and cytotoxic mediators without re-stimulation from the γδ T cells of aviremic HIV+ subjects. These findings suggest that TIGIT+ γδ T cells are activated in ART-suppressed HIV+ subjects and secrete inflammatory mediators *in vivo*. This association was not found in the uninfected control subjects (**Figure 4**). However, it is important to note that while the percentage of TIGIT+ γδ T cells sorted into the individual culture wells significantly correlates with the amount of inflammatory analyte measured, the functional profiles of actual TIGIT+ vs. TIGIT- γδ T cells were not directly measured in this study. From these results it can be concluded that the same immune cell subset with an identical IR signature may have different functionality in different disease states or other conditions. Therefore, we contend that IR expression analysis should be consistently paired with functional readouts to determine the true status of a given immune cell population. As IRs have been referred to as "exhaustion markers" (102, 103) our data support arguments by others to not limit IR definitions in this manner (65).

It has been postulated that multi-IR expression by individual T cells reflects more advanced immune exhaustion (104) in agreement with reports of T cells in virally infected mice (63, 105). In our study, the percentages of γδ T cells expressing ≥2IR per cell were higher with both healthy aging and HIV infection, yet the ≥3IR and ≥4IR per cell levels were elevated only with HIV infection (**Figures 2C,F**) possibly suggesting a more progressed immune exhaustion status of these cells. However, our measurements of analyte secretion indicate that the HIV+ subjects' γδ T cells expressing IRs are activated and not exhausted (**Figure 4B**). When we performed more detailed IR signature analysis to parse out potential lineage trajectories of γδ T cell subsets bearing combinations of PD-1, TIGIT, and CD160 in ART-suppressed HIV infection and/or aging, interesting findings emerged; firstly, our results show that a substantial proportion of the circulating γδ T cell compartment in healthy younger subjects express CD160 (**Figure 3A**) that is not elevated with HIV- or age-associated activation or exhaustion (**Figures 3A–C**). CD160 recognizes class 1a and 1b molecules (106) and serves as a co-receptor for activation of γδ T cells (107) yet its expression has been linked to immune exhaustion on CD8+ T cells in HIV and other chronic diseases (108, 109). These results underscore the importance of evaluating IR expression in a cell type and disease-specific manner. Also, our data indicate that TIGIT and PD-1 are up-regulated on what we cautiously define as "activated/exhausted" cell subsets,

and the PD-1+ TIGIT+ CD160+ (triple positive) T cells are elevated with aviremic HIV infection and not healthy aging, suggesting that HIV drives further progression of γδ T cell populations along activation/exhaustion routes. Taken together, our data suggest that multi-IR expression per cell may not always signify advanced immune exhaustion and that combinational IR signature analysis could provide new insight into the progression of changes in immune cell functional activity and capacity (activation vs. exhaustion) in chronic conditions. Future work measuring the functional profiles of sorted γδ T populations with distinct IR signatures from our cohort will help elucidate how functions change with IR expression during aging with and without aviremic HIV infection.

There is debate in the literature as to whether aviremic HIV infection leads to a distinct inflammatory signature that exists regardless of age (110–112). If so, we would expect similarities in immune signatures between the younger HIV+ and healthy older subjects, as well as between the HIV+ younger and HIV+ older individuals. Our univariate analyses agree with this concept, for comparisons of γδ T cell IR expression, spontaneous *ex vivo* cytokine production, and γδ T cell links with and the total levels of inflammatory plasma analytes are not significantly different between HIV+ younger and older subject groups (**Figures 2E,F**, **3A**, **4C**, **5D,E**, and **Supplementary Figure 5B**). Therefore, this data suggests that aviremic HIV infection and aging are not impacting immune cell phenotypes in an additive or multiplicative manner, consistent with a report of CD8+ T cells (113). However, γδ T cell secretion of sCD137 is significantly higher from the cells from the HIV older group compared to all other three subject groups (HIV younger, uninfected younger, and uninfected older) (**Figure 4A**), indicating a synergistic impact of age and HIV on the activation of γδ T cells. sCD137 is a pro-inflammatory molecule that can be produced as an alternatively spliced variant or by proteolytic cleavage of CD137 (4-1BB) (114), a member of TNF superfamily, and a marker associated with multiple inflammatory diseases. sCD137 plasma levels positively associate with acute coronary syndromes (66) and atherothrombotic stroke (67), and we hypothesize that *in vivo*, γδ T cells produce sCD137 which is also known to trigger pro-inflammatory networks that involve macrophages and DCs (115) Also, our multivariate PSLR results (**Figures 4D,E**, and **Figures 5F,G**) show that the relationships between γδ IR signatures and both the cytokines they produce and plasma markers with which they co-vary are different in the younger vs. older subjects in both the uninfected control and HIV+ groups, since the younger and older subjects separated in all four PLSR models without age being added as a variable. These results show that there are distinct aging courses in relation to immune network changes with and without HIV infection. Finally and perhaps most importantly, in our PLS-DA model all four subject groups separated with significance (**Figure 6**) demonstrating separate aging processes with and without HIV infection. Our multivariate results underscore the importance of performing this type of analyses to gain novel insights into immune networks in relation to inflammation and other states.

Altogether, our findings indicate that γδ T cells are a possible source of inflammation in aviremic HIV infection and potentially other inflammatory diseases. IR expression on circulating γδ T cells, and TIGIT in particular, should be investigated for biomarker utility to effectively diagnose, predict, and/or treat both general inflammation and propensity to age-associated morbidities and mortality with and without HIV infection.

MATERIALS AND METHODS

Participants

The subjects were part of the HIV and aging cohort which enrolled HIV+ subjects with ART effective viral suppression (undetectable HIV-1 RNA <50 copies/ml) for a minimum of 6 months and were age-stratified into≤35 years and ≥50 years age groups from the infectious disease clinics at Brigham and Women's Hospital, Beth Israel Deaconess Hospital, Massachusetts General Hospital, and Boston Medical Center, all located in Boston, MA. Study protocols were approved by the institutional review boards at each institution and all subjects provided written informed consent. The committee that approved the research protocol was the Boston University Institutional Review Board, IRB# H-33095. Uninfected controls were recruited from the same clinics in Boston and had similar demographic and socioeconomic status as HIV+ subjects. HIV negative status was verified with both a negative HIV antibody test and HIV-1 viral load test. Exclusion criteria included active hepatitis B or C, recent active infection within past 6 months, recent immunomodulatory therapy, and receipt of an HIV vaccine. HIV+ subjects in different age groups are matched by duration of ART (**Table 1**). Detailed information about the study subject characteristics can be found in **Table 1** and **Supplemental Table 2**. All subjects were recruited with detailed clinical history and socio-demographic data, and information of other common confounders, such as gender, co-infections, and other pro-inflammatory exposures (i.e., STDs, obesity, and drug/tobacco use).

Peripheral Blood Processing

Peripheral blood mononuclear cells (PBMC) were isolated from blood originally drawn into EDTA tubes by Ficoll-Hypaque and cryopreserved in liquid nitrogen until use. Plasma was acquired from whole blood and stored at −80°C until use. All paired plasma and PBMC samples used in this study are from the same blood draw.

Flow Cytometry Panels and Reagents

Two flow cytometry panels were used in the study. Panel 1 was a modified version of the previously published panel (60) where 3 markers were moved to different detection channels and one replaced. Panel 2 was a modification of Panel 1 constructed to allow detection of γδ T cell Vδ1 and Vδ2 subsets. All reagents used in both panels are listed in **Supplementary Table 1**. Buffers and blocking reagents were used as described (60). All fluorescent reagents were titrated and Fluorescence Minus One (FMO) controls were performed to verify the validity of the modified panels. Ultracomp capture beads (Thermo Fisher) were used

to establish the compensation matrix. Ultra Rainbow Beads (Spherotech) were used to establish target values for running the instrument. CS&T beads (BD) were used for daily QC of the instruments.

Flow Cytometry Protocol

1×10^7 PBMC per donor were thawed and immediately stained with a 16-color antibody/reagent cocktail developed for the BUMC FACSARIA (BD Biosciences) cell sorter as previously described (60). Briefly, cells were washed, stained with live/dead reagent (Biolegend's Zombie NIR) in DPBS for 20 min, washed again with FACS buffer (DPBS/0.5% BSA/2 mM EDTA), and pre-blocked with human Fc-blocking reagent (Biolegend) for 10 min. The antibody cocktail was prepared by combining antibody stocks with BD Brilliant Buffer and adding the master mixes to the pre-blocked cells that were then incubated for 20 min at room temperature. After staining, cells were washed twice with FACS buffer (PBS 0.5% BSA 2 mM EDTA), resuspended in FACS buffer and run on the BUMC FACSARIA cell sorter (BD Biosciences). Samples were divided into 11 different runs and a mix of subjects from the four groups (uninfected younger, uninfected older, ART Suppressed HIV+ younger, ART-suppressed HIV+ older) were included in each run to control for potential alterations in machine performance and batch effects. For each run, a mixture containing 5% of each individual sample was prepared and stained with the reagent mix that did not include IR-specific fluorescent antibodies (Fluorescence Minus Five, or FM5). For Panel 2, anti-Vδ2-biotin and anti-Vδ1-PE added were added to cells for 20 min then cells were washed prior to the addition of other reagents that were then added and incubated for 20 min. For each batch run, Ultracomp capture beads (Thermo Fisher) were stained with same reagents and acquired prior to the samples. PDGFRα-APC antibody (Biolegend) was used for the APC single stain.

γδ T cell cultures: During data acquisition and sample running on the BD FACSARIA, γδ T cells (LIVE/DEAD–, CD14–, CD19–, CD3+, γδTCR+) were sorted into tubes and cultured in 25 μl of RPMI1640 10% FBS/1% pen-strep in half-area 96-well flat-bottom plates (Greiner) for 20 h. The number of cells cultured per well-varied from 2,000 to 26,000, with a comparable range in numbers across each of the four subject groups. At the end of the culture period, supernatants were frozen into multiple aliquots and later thawed to perform analyte measurements.

Milliplex Bead Assays of Culture Supernatants

Supernatant samples were thawed, centrifuged for 30 seconds to remove debris, and added to a 384-well plate for analyte measurement via use of the Milliplex human Th17 25-plex kit (Millipore Sigma) and a modified Milliplex human CD8 9-plex kit (Millipore Sigma). Antibodies and magnetic beads were diluted 1:1 with assay buffer and utilized at half-volume to adjust the manufacturer's protocol to the 384-well plate format. Plates were washed in between incubations using a BioTek 406 Touch plate washer (BioTek) and read using the Luminex FlexMap 3D system (Luminex). Observed concentration values were adjusted to cell counts per well.

Milliplex and ELISA Assays of Plasma Samples

Frozen plasma samples were thawed and analyzed using (1) the 11-plex Human Cardiovascular Disease (Acute Phase) Milliplex kit (MilliporeSigma, HCVD3MAG-67K), (2) a custom 3-plex Milliplex kit for TNF-α, IL-6, and IL-1β (HCYTOMAG-3K) sCD14 and D-dimer ELISA kits (from RD Systems and Abcam, respectively). For (1), samples were pre-diluted 1:40,000 and the kit was run according to manufacturer's instructions and similar to the culture supernatants described above.

Flow Cytometry Data Analysis

Data were recorded with BD FACSDIVA 6.1.2 and automatically compensated with compensation matrix recorded within the sample files according to FCS 3.0 standards. Manual gating (expert-guided analysis) was performed in FlowJo v.10.2-10.3 (FlowJo, Inc) while blinded to sample identifier. Inhibitory receptor (IR) gating was guided using the FM5 sample from each run as described above. Numeric values from FlowJo data analysis were exported to Prism 7.0 (Graphpad) for statistical analysis. Flow cytometry data files were also uploaded to Cytobank, a cloud-based computational platform, and arcsin-transformed. Doublets, dead cells, debris, CD14+ cells, and CD19+ cells were excluded by manual gating and remaining live single non-CD14, non-CD19 events (downsampled to 10,000 events/subject) were input into the CITRUS algorithm (61). After hierarchical clustering based on lineage markers (CD3, CD4, CD8, γδ TCR, CD127, CD16, CD56) shown in **Supplementary Figure 1**, median fluorescence of TIGIT, TIM-3, PD-1, CD160, and LAG-3 expression was measured and a supervised comparison between HIV- and HIV+ individuals was carried out and assessed via Nearest Shrunken Centroid (PAMR) association modeling (**Supplementary Figure 1**). Additionally, live, single, non-CD14, non-CD19 events were input to the SPADE clustering algorithm, and the nodes containing cells with higher γδ TCR expression were exported from each sample file and used for IR median fluorescence intensity representation (**Figure 2D**). Beta regression of abundance on HIV status and age group was performed in **Figure 3A**. To correct for multiple hypothesis testing, a significance threshold was set for each regression term using a family-wise error rate of 0.05. The significance threshold was established in the following manner. First, 100 permuted abundance datasets were created by randomly resampling without replacement the abundance of each of the eight IR subsets within each subject, so that the inter-dependency of the IR subset abundances for an individual was maintained. Then, for each of the 100 permuted abundances, the beta regression for each IR subset was performed and the minimum p-value across all IR subsets was recorded for each model term. Finally, the 5th percentile of this distribution of minimum p-values was set as the significance threshold for each model term (HIV threshold: 0.0047; age group threshold: 0.0068).

PLS Analysis

Partial least squares discriminant analysis (PLSDA) and partial least squares regression (PLSR) were performed using the

MATLAB PLS Toolbox (Eigenvector Research, Inc.). Data were normalized along each X and Y parameter by Z-score before application of the algorithm. Cross-validation was performed with one-third of the relevant dataset. The number of latent variables (LVs) was chosen so as to minimize cumulative error over all predictions. We orthogonally rotated the models so that maximal separation was achieved across LV1 where noted. We calculated model confidence by randomly permuting Y 100 times and rebuilding the model to form a distribution of error for these randomly generated models. We compared our model to this distribution with the Mann–Whitney *U*-test to determine the significance of our model. The importance of each parameter to the overall model prediction was quantified using variable importance in projection (VIP) score. A VIP score >1 (above average contribution) was considered important for model performance and prediction.

DATA AVAILABILITY

The raw data supporting the conclusions of this manuscript will be made available by the authors, without undue reservation, to any qualified researcher.

ETHICS STATEMENT

The study protocol was approved by the Boston University School of Medicine, Partners Healthcare, and Beth Israel Deaconess Medical Center institutional review boards. All participants provided written informed consent to participate in the study.

AUTHOR CONTRIBUTIONS

AB, AO, NL, and JS-C conceived and designed the experiments. KD, DL, NL, and JS-C contributed to reagents, materials, and funding. AB, RP, and JS-C performed experiments. AB, AS, KD, EP, RP, and JS-C analyzed data and JS-C wrote the manuscript. All authors read and approved the final version of the manuscript.

FUNDING

This work was supported by the National Institute of Health (R01-DK108056, R01 DA041748-01, R01 AG060890-01, 1UL1TR001430), the National Institute Of General Medical Sciences (R44GM117914), and the Army Institute for Collaborative Biotechnologies (W911NF-09-0001).

ACKNOWLEDGMENTS

We thank Drs. Jeffrey Browning, Amedeo Cappione, Andrew Henderson, and Barbara Nikolajczyk for their critical reading of the manuscript, Drs. Suryaram Gummuluru and Manish Sagar for their helpful discussions regarding data interpretation, and Dr. Barbara Nikolajczyk and Dr. Madhur Agrawal for their assistance with the multiplex assays. All flow cytometry data were collected at the Boston University School of Medicine Flow Cytometry Core Facility.

SUPPLEMENTARY MATERIAL

The Supplementary Material for this article can be found online at: https://www.frontiersin.org/articles/10.3389/fimmu.2018.02783/full#supplementary-material

REFERENCES

1. Wada N, Jacobson LP, Cohen M, French A, Phair J, Muñoz A. Cause-specific life expectancies after 35 years of age for human immunodeficiency syndrome-infected and human immunodeficiency syndrome-negative individuals followed simultaneously in long-term cohort studies, 1984-2008. *Am J Epidemiol.* (2013) 177:116–25. doi: 10.1093/aje/kws321
2. Marcus JL, Chao CR, Leyden WA, Xu L, Quesenberry CP, Klein DB, et al. Narrowing the gap in life expectancy between HIV-infected and HIV-uninfected individuals with access to care. *J Acquir Immune Defic Syndr.* (2016) 73:39–46. doi: 10.1097/QAI.0000000000001014
3. Antiretroviral Therapy Cohort Collaboration. Life expectancy of individuals on combination antiretroviral therapy in high-income countries: a collaborative analysis of 14 cohort studies. *Lancet* (2008) 372:293–9. doi: 10.1016/S0140-6736(08)61113-7
4. Hasse B, Ledergerber B, Furrer H, Battegay M, Hirschel B, Cavassini M, et al. Morbidity and aging in HIV-infected persons: the Swiss HIV cohort study. *Clin Infect Dis.* (2011) 53:1130–9. doi: 10.1093/cid/cir626
5. Schouten J, Wit FW, Stolte IG, Kootstra NA, van der Valk M, Geerlings SE, et al. Cross-sectional comparison of the prevalence of age-associated comorbidities and their risk factors between HIV-infected and uninfected individuals: the AGEhIV cohort study. *Clin Infect Dis.* (2014) 59:1787–97. doi: 10.1093/cid/ciu701
6. Rodriguez-Penney AT, Iudicello JE, Riggs PK, Doyle K, Ellis RJ, Letendre SL, et al. Co-morbidities in persons infected with HIV: increased burden with older age and negative effects on health-related quality of life. *AIDS Patient Care STDS* (2013) 27:5–16. doi: 10.1089/apc.2012.0329
7. Guaraldi G, Orlando G, Zona S, Menozzi M, Carli F, Garlassi E, et al. Premature age-related comorbidities among HIV-infected persons compared with the general population. *Clin Infect Dis.* (2011) 53:1120–6. doi: 10.1093/cid/cir627
8. Capeau J. Premature aging and premature age-related comorbidities in HIV-infected patients: facts and hypotheses. *Clin Infect Dis.* (2011) 53:1127–9. doi: 10.1093/cid/cir628
9. So-Armah KA, Tate JP, Chang CH, Butt AA, Gerschenson M, Gibert CL, et al. Do biomarkers of inflammation, monocyte activation, and altered coagulation explain excess mortality between HIV infected and uninfected people? *J Acquir Immune Defic Syndr.* (2016) 72:206–213. doi: 10.1097/QAI.0000000000000954
10. Kuller LH, Tracy R, Belloso W, De Wit S, Drummond F, Lane HC, et al. Inflammatory and coagulation biomarkers and mortality in patients with HIV infection. *PLoS Med.* (2008) 5:e203. doi: 10.1371/journal.pmed.0050203
11. Duprez DA, Neuhaus J, Kuller LH, Tracy R, Belloso W, De Wit S, et al. Inflammation, coagulation and cardiovascular disease in HIV-infected individuals. *PLoS ONE* (2012) 7:e44454. doi: 10.1371/journal.pone.0044454
12. Montoya JL, Iudicello J, Oppenheim HA, Fazeli PL, Potter M, Ma Q, et al. Coagulation imbalance and neurocognitive functioning in older HIV-positive adults on suppressive antiretroviral therapy. *AIDS* (2017) 31:787–95. doi: 10.1097/QAD.0000000000001404
13. Tenorio AR, Zheng Y, Bosch RJ, Krishnan S, Rodriguez B, Hunt PW, et al. Soluble markers of inflammation and coagulation but not T-cell activation

predict non-AIDS-defining morbid events during suppressive antiretroviral treatment. *J Infect Dis.* (2014) 210:1248–59. doi: 10.1093/infdis/jiu254
14. Hart BB, Nordell AD, Okulicz JF, Palfreeman A, Horban A, Kedem E, et al. Inflammation-related morbidity and mortality among HIV-positive adults: how extensive is it? *J Acquir Immune Defic Syndr.* (2018) 77:1–7. doi: 10.1097/QAI.0000000000001554
15. Folsom AR, Alonso A, George KM, Roetker NS, Tang W, Cushman M. Prospective study of plasma D-dimer and incident venous thromboembolism: the atherosclerosis risk in communities (ARIC) study. *Thromb Res.* (2015) 136:781–5. doi: 10.1016/j.thromres.2015.08.013
16. Folsom AR, Delaney JA, Lutsey PL, Zakai NA, Jenny NS, Polak JF, et al. Associations of factor VIIIc, D-dimer, and plasmin-antiplasmin with incident cardiovascular disease and all-cause mortality. *Am J Hematol.* (2009) 84:349–53. doi: 10.1002/ajh.21429
17. Folsom AR, Gottesman RF, Appiah D, Shahar E, Mosley TH. Plasma d-Dimer and incident ischemic stroke and coronary heart disease: the atherosclerosis risk in communities study. *Stroke* (2016) 47:18–23. doi: 10.1161/STROKEAHA.115.011035
18. Danesh J, Kaptoge S, Mann AG, Sarwar N, Wood A, Angleman SB, et al. Long-term interleukin-6 levels and subsequent risk of coronary heart disease: two new prospective studies and a systematic review. *PLoS Med.* (2008) 5:e78. doi: 10.1371/journal.pmed.0050078
19. Ridker PM, Rifai N, Stampfer MJ, Hennekens CH. Plasma concentration of interleukin-6 and the risk of future myocardial infarction among apparently healthy men. *Circulation* (2000) 101:1767–72. doi: 10.1161/01.CIR.101.15.1767
20. Stack AG, Donigiewicz U, Abdalla AA, Weiland A, Casserly LF, Cronin CJ, et al. Plasma fibrinogen associates independently with total and cardiovascular mortality among subjects with normal and reduced kidney function in the general population. *QJM* (2014) 107:701–13. doi: 10.1093/qjmed/hcu057
21. Kuller LH, Tracy RP, Shaten J, Meilahn EN. Relation of C-reactive protein and coronary heart disease in the MRFIT nested case-control study. Multiple risk factor intervention trial. *Am J Epidemiol.* (1996) 144:537–47. doi: 10.1093/oxfordjournals.aje.a008963
22. Nasi M, De Biasi S, Gibellini L, Bianchini E, Pecorini S, Bacca V, et al. Ageing and inflammation in patients with HIV infection. *Clin Exp Immunol.* (2017) 187:44–52. doi: 10.1111/cei.12814
23. Franceschi C. Inflammaging as a major characteristic of old people: can it be prevented or cured? *Nutr Rev.* (2007) 65(12 Pt 2):S173–6.
24. Goodman T, Lefrançois L. Expression of the gamma-delta T-cell receptor on intestinal CD8+ intraepithelial lymphocytes. *Nature* (1988) 333:855–8. doi: 10.1038/333855a0
25. Bonneville M, Janeway CA, Ito K, Haser W, Ishida I, Nakanishi N, et al. Intestinal intraepithelial lymphocytes are a distinct set of gamma delta T cells. *Nature* (1988) 336:479–81. doi: 10.1038/336479a0
26. Kyes S, Carew E, Carding SR, Janeway CA, Hayday A. Diversity in T-cell receptor gamma gene usage in intestinal epithelium. *Proc Natl Acad Sci USA.* (1989) 86:5527–31. doi: 10.1073/pnas.86.14.5527
27. Bucy RP, Chen CL, Cooper MD. Tissue localization and CD8 accessory molecule expression of T gamma delta cells in humans. *J Immunol.* (1989) 142:3045–9.
28. Constant P, Davodeau F, Peyrat MA, Poquet Y, Puzo G, Bonneville M, et al. Stimulation of human gamma delta T cells by nonpeptidic mycobacterial ligands. *Science* (1994) 264:267–70. doi: 10.1126/science.8146660
29. Girardi M, Oppenheim DE, Steele CR, Lewis JM, Glusac E, Filler R, et al. Regulation of cutaneous malignancy by gammadelta T cells. *Science* (2001) 294:605–9. doi: 10.1126/science.1063916
30. Hintz M, Reichenberg A, Altincicek B, Bahr U, Gschwind RM, Kollas AK, et al. Identification of (E)-4-hydroxy-3-methyl-but-2-enyl pyrophosphate as a major activator for human gammadelta T cells in Escherichia coli. *FEBS Lett.* (2001) 509:317–22. doi: 10.1016/S0014-5793(01)03191-X
31. Martin B, Hirota K, Cua DJ, Stockinger B, Veldhoen M. Interleukin-17-producing gammadelta T cells selectively expand in response to pathogen products and environmental signals. *Immunity* (2009) 31:321–30. doi: 10.1016/j.immuni.2009.06.020
32. Qin G, Mao H, Zheng J, Sia SF, Liu Y, Chan PL, et al. Phosphoantigen-expanded human gammadelta T cells display potent cytotoxicity against monocyte-derived macrophages infected with human and avian influenza viruses. *J Infect Dis.* (2009) 200:858–65. doi: 10.1086/605413
33. Shibata K, Yamada H, Hara H, Kishihara K, Yoshikai Y. Resident Vdelta1+ gammadelta T cells control early infiltration of neutrophils after *Escherichia coli* infection via IL-17 production. *J Immunol.* (2007) 178:4466–72. doi: 10.4049/jimmunol.178.7.4466
34. Silva-Santos B, Strid J. Working in "NK Mode": Natural killer group 2 member D and natural cytotoxicity receptors in stress-surveillance by gammadelta T cells. *Front Immunol.* (2018) 9:851. doi: 10.3389/fimmu.2018.00851
35. Tanaka Y, Morita CT, Tanaka Y, Nieves E, Brenner MB, Bloom BR. Natural and synthetic non-peptide antigens recognized by human gamma delta T cells. *Nature* (1995) 375:155–8. doi: 10.1038/375155a0
36. Biswas P, Ferrarini M, Mantelli B, Fortis C, Poli G, Lazzarin A, et al. Double-edged effect of Vgamma9/Vdelta2 T lymphocytes on viral expression in an *in vitro* model of HIV-1/mycobacteria co-infection. *Eur J Immunol.* (2003) 33:252–63. doi: 10.1002/immu.200390028
37. Wallace M, Gan YH, Pauza CD, Malkovsky M. Antiviral activity of primate gamma delta T lymphocytes isolated by magnetic cell sorting. *J Med Primatol.* (1994) 23:131–5. doi: 10.1111/j.1600-0684.1994.tb00113.x
38. Ye J, Ma C, Hsueh EC, Eickhoff CS, Zhang Y, Varvares MA, et al. Tumor-derived gammadelta regulatory T cells suppress innate and adaptive immunity through the induction of immunosenescence. *J Immunol.* (2013) 190:2403–14. doi: 10.4049/jimmunol.1202369
39. Ye J, Ma C, Wang F, Hsueh EC, Toth K, Huang Y, et al. Specific recruitment of gammadelta regulatory T cells in human breast cancer. *Cancer Res.* (2013) 73:6137–48. doi: 10.1158/0008-5472.CAN-13-0348
40. Qaqish A, Huang D, Chen CY, Zhang Z, Wang R, Li S, et al. Adoptive transfer of phosphoantigen-specific gammadelta T Cell Subset Attenuates Mycobacterium tuberculosis Infection in Nonhuman Primates. *J Immunol.* (2017) 198:4753–63. doi: 10.4049/jimmunol.1602019
41. Dillen CA, Pinsker BL, Marusina AI, Merleev AA, Farber ON, Liu H, et al. Clonally expanded gammadelta T cells protect against Staphylococcus aureus skin reinfection. *J Clin Invest.* (2018) 128:1026–42. doi: 10.1172/JCI96481
42. Cordova A, Toia F, La Mendola C, Orlando V, Meraviglia S, Rinaldi G, et al. Characterization of human gammadelta T lymphocytes infiltrating primary malignant melanomas. *PLoS ONE* (2012) 7:e49878. doi: 10.1371/journal.pone.0049878
43. Zocchi MR, Ferrarini M, Rugarli C. Selective lysis of the autologous tumor by delta TCS1+ gamma/delta+ tumor-infiltrating lymphocytes from human lung carcinomas. *Eur J Immunol.* (1990) 20:2685–9. doi: 10.1002/eji.1830201224
44. Meraviglia S, Lo Presti E, Tosolini M, La Mendola C, Orlando V, Todaro M, et al. Distinctive features of tumor-infiltrating gammadelta T lymphocytes in human colorectal cancer. *Oncoimmunology* (2017) 6:e1347742. doi: 10.1080/2162402X.2017.1347742
45. Autran B, Triebel F, Katlama C, Rozenbaum W, Hercend T, Debre P. T cell receptor gamma/delta+ lymphocyte subsets during HIV infection. *Clin Exp Immunol.* (1989) 75:206–10.
46. Bordon J, Evans PS, Propp N, Davis CE, Redfield RR, Pauza CD. Association between longer duration of HIV-suppressive therapy and partial recovery of the V gamma 2 T cell receptor repertoire. *J Infect Dis.* (2004) 189:1482–6. doi: 10.1086/382961
47. Soriano-Sarabia N, Archin NM, Bateson R, Dahl NP, Crooks AM, Kuruc JD, et al. Peripheral Vgamma9Vdelta2 T cells are a novel reservoir of latent HIV infection. *PLoS Pathog.* (2015) 11:e1005201. doi: 10.1371/journal.ppat.1005201
48. Snyder-Cappione JE, Nixon DF, Chi JC, Nguyen ML, Kirby CK, Milush JM, et al. Invariant natural killer T (iNKT) cell exhaustion in sarcoidosis. *Eur J Immunol.* (2013) 43:2194–205. doi: 10.1002/eji.201243185
49. Chew GM, Fujita T, Webb GM, Burwitz BJ, Wu HL, Reed JS, et al. TIGIT marks exhausted T cells, correlates with disease progression, and serves as a target for immune restoration in HIV and SIV Infection. *PLoS Pathog.* (2016) 12:e1005349. doi: 10.1371/journal.ppat.1005349

50. Wherry EJ, Ha SJ, Kaech SM, Haining WN, Sarkar S, Kalia V, et al. Molecular signature of CD8+ T cell exhaustion during chronic viral infection. *Immunity* (2007) 27:670–84. doi: 10.1016/j.immuni.2007.09.006
51. Horne-Debets JM, Faleiro R, Karunarathne DS, Liu XQ, Lineburg KE, Poh CM, et al. PD-1 dependent exhaustion of CD8+ T cells drives chronic malaria. *Cell Rep.* (2013) 5:1204–13. doi: 10.1016/j.celrep.2013.11.002
52. Channappanavar R, Twardy BS, Krishna P, Suvas S. Advancing age leads to predominance of inhibitory receptor expressing CD4 T cells. *Mech Ageing Dev.* (2009) 130:709–12. doi: 10.1016/j.mad.2009.08.006
53. Decman V, Laidlaw BJ, Doering TA, Leng J, Ertl HC, Goldstein DR, et al. Defective CD8 T cell responses in aged mice are due to quantitative and qualitative changes in virus-specific precursors. *J Immunol.* (2012) 188:1933–41. doi: 10.4049/jimmunol.1101098
54. Lee KA, Shin KS, Kim GY, Song YC, Bae EA, Kim IK, et al. Characterization of age-associated exhausted CD8(+) T cells defined by increased expression of Tim-3 and PD-1. *Aging Cell* (2016) 15:291–300. doi: 10.1111/acel.12435
55. Shimada Y, Hayashi M, Nagasaka Y, Ohno-Iwashita Y, Inomata M. Age-associated up-regulation of a negative co-stimulatory receptor PD-1 in mouse CD4+ T cells. *Exp Gerontol.* (2009) 44:517–22. doi: 10.1016/j.exger.2009.05.003
56. Song Y, Wang B, Song R, Hao Y, Wang D, Li Y, et al. T-cell Immunoglobulin and ITIM Domain Contributes to CD8(+) T-cell Immunosenescence. *Aging Cell* (2018) 17:e12716. doi: 10.1111/acel.12716
57. Jones RB, Ndhlovu LC, Barbour JD, Sheth PM, Jha AR, Long BR, et al. Tim-3 expression defines a novel population of dysfunctional T cells with highly elevated frequencies in progressive HIV-1 infection. *J Exp Med.* (2008) 205:2763–79. doi: 10.1084/jem.20081398
58. Trautmann L, Janbazian L, Chomont N, Said EA, Gimmig S, Bessette B, et al. Upregulation of PD-1 expression on HIV-specific CD8+ T cells leads to reversible immune dysfunction. *Nat Med.* (2006) 12:1198–202. doi: 10.1038/nm1482
59. Day CL, Kaufmann DE, Kiepiela P, Brown JA, Moodley ES, Reddy S, et al. PD-1 expression on HIV-specific T cells is associated with T-cell exhaustion and disease progression. *Nature* (2006) 443:350–4. doi: 10.1038/nature05115
60. Belkina AC, Snyder-Cappione JE. OMIP-037: 16-color panel to measure inhibitory receptor signatures from mulitple immune cell subsets. *Cytometry A* (2016) 91:175–9. doi: 10.1002/cyto.a.22983
61. Bruggner RV, Bodenmiller B, Dill DL, Tibshirani RJ, Nolan GP. Automated identification of stratifying signatures in cellular subpopulations. *Proc Natl Acad Sci USA.* (2014) 111:E2770–7. doi: 10.1073/pnas.1408792111
62. De Paoli P, Gennari D, Martelli P, Basaglia G, Crovatto M, Battistin S, et al. A subset of gamma delta lymphocytes is increased during HIV-1 infection. *Clin Exp Immunol.* (1991) 83:187–91. doi: 10.1111/j.1365-2249.1991.tb05612.x
63. Blackburn SD, Shin H, Haining WN, Zou T, Workman CJ, Polley A, et al. Coregulation of CD8+ T cell exhaustion by multiple inhibitory receptors during chronic viral infection. *Nat Immunol.* (2009) 10:29–37. doi: 10.1038/ni.1679
64. Qiu P, Simonds EF, Bendall SC, Gibbs KD, Bruggner, RV, Linderman MD, et al. Extracting a cellular hierarchy from high-dimensional cytometry data with SPADE. *Nat Biotechnol.* (2011) 29:886–91. doi: 10.1038/nbt.1991
65. Fuertes Marraco SA, Neubert NJ, Verdeil G, Speiser DE. Inhibitory receptors beyond T cell exhaustion. *Front Immunol.* (2015) 6:310. doi: 10.3389/fimmu.2015.00310
66. Dongming L, Zuxun L, Liangjie X, Biao W, Ping Y. Enhanced levels of soluble and membrane-bound CD137 levels in patients with acute coronary syndromes. *Clin Chim Acta* (2010) 411:406–10. doi: 10.1016/j.cca.2009.12.011
67. He Y, Ao DH, Li XQ, Zhong SS, A R, Wang YY, et al. Increased Soluble CD137 Levels and CD4+ T-cell-associated expression of CD137 in acute atherothrombotic stroke. *Clin Transl Sci.* (2018). 11:428–34. doi: 10.1111/cts.12553
68. Lau KS, Juchheim AM, Cavaliere KR, Philips SR, Lauffenburger DA, Haigis KM. *In vivo* systems analysis identifies spatial and temporal aspects of the modulation of TNF-alpha-induced apoptosis and proliferation by MAPKs. *Sci Signal.* (2011) 4:ra16. doi: 10.1126/scisignal.2001338
69. Simmons RP, Scully EP, Groden EE, Arnold KB, Chang JJ, Lane K, et al. HIV-1 infection induces strong production of IP-10 through TLR7/9-dependent pathways. *AIDS* (2013) 27:2505–17. doi: 10.1097/01.aids.0000432455.06476.bc
70. Tien PC, Choi AI, Zolopa AR, Benson C, Tracy R, Scherzer R, et al. Inflammation and mortality in HIV-infected adults: analysis of the FRAM study cohort. *J Acquir Immune Defic Syndr.* (2010) 55:316–22. doi: 10.1097/QAI.0b013e3181e66216
71. Triant VA, Meigs JB, Grinspoon, SK. Association of C-reactive protein and HIV infection with acute myocardial infarction. *J Acquir Immune Defic Syndr.* (2009) 51:268–73. doi: 10.1097/QAI.0b013e3181a9992c
72. Ford ES, Greenwald JH, Richterman AG, Rupert A, Dutcher L, Badralmaa Y, et al. Traditional risk factors and D-dimer predict incident cardiovascular disease events in chronic HIV infection. *AIDS* (2010) 24:1509–17. doi: 10.1097/QAD.0b013e32833ad914
73. Nordell AD, McKenna M, Borges ÁH, Duprez D, Neuhaus J, Neaton JD, et al. Severity of cardiovascular disease outcomes among patients with HIV is related to markers of inflammation and coagulation. *J Am Heart Assoc.* (2014) 3:e000844. doi: 10.1161/JAHA.114.000844
74. Benedict KF, Lauffenburger DA. Insights into proteomic immune cell signaling and communication via data-driven modeling. *Curr Top Microbiol Immunol.* (2013) 363:201–33. doi: 10.1007/82_2012_249
75. Effros RB, Fletcher CV, Gebo K, Halter JB, Hazzard WR, Horne FM, et al. Aging and infectious diseases: workshop on HIV infection and aging: what is known and future research directions. *Clin Infect Dis.* (2008) 47:542–53. doi: 10.1086/590150
76. He W, Goodkind D, Kowal P. *An Aging World: 2015.* United States Census Bureau (2016).
77. Hatano H. Immune activation and HIV persistence: considerations for novel therapeutic interventions. *Curr Opin HIV AIDS* (2013) 8:211–6. doi: 10.1097/COH.0b013e32835f9788
78. Hunt PW, Martin JN, Sinclair E, Epling L, Teague J, Jacobson MA, et al. Valganciclovir reduces T cell activation in HIV-infected individuals with incomplete CD4+ T cell recovery on antiretroviral therapy. *J Infect Dis.* (2011) 203:1474–83. doi: 10.1093/infdis/jir060
79. Brenchley JM, Price DA, Schacker TW, Asher TE, Silvestri G, Rao S, et al. Microbial translocation is a cause of systemic immune activation in chronic HIV infection. *Nat Med.* (2006) 12:1365–71. doi: 10.1038/nm1511
80. Fromentin R, Bakeman W, Lawani MB, Khoury G, Hartogensis W, DaFonseca S, et al. CD4+ T cells expressing PD-1, TIGIT and LAG-3 contribute to HIV persistence during ART. *PLoS Pathog.* (2016) 12:e1005761. doi: 10.1371/journal.ppat.1005761
81. Cohn LB, da Silva IT, Valieris R, Huang AS, Lorenzi JCC, Cohen YZ, et al. Clonal CD4(+) T cells in the HIV-1 latent reservoir display a distinct gene profile upon reactivation. *Nat Med.* (2018) 24:604–9. doi: 10.1038/s41591-018-0017-7
82. Akiyama H, Miller CM, Ettinger CR, Belkina AC, Snyder-Cappione JE, Gummuluru S. HIV-1 intron-containing RNA expression induces innate immune activation and T cell dysfunction. *Nat Commun.* (2018) 9:3450. doi: 10.1038/s41467-018-05899-7
83. George MD, Reay E, Sankaran S, Dandekar S. Early antiretroviral therapy for simian immunodeficiency virus infection leads to mucosal CD4+ T-cell restoration and enhanced gene expression regulating mucosal repair and regeneration. *J Virol.* (2005) 79:2709–19. doi: 10.1128/JVI.79.5.2709-2719.2005
84. Wojcik-Cichy K, Piekarska A, Jablonowska, E. Intestinal barrier impairment and immune activation in HIV-infected advanced late presenters are not dependent on CD4 Recovery. *Arch Immunol Ther Exp.* (2018) 66:321–7. doi: 10.1007/s00005-018-0508-8
85. Ortiz AM, Brenchley JM. Microbial translocation: translating simian immunodeficiency virus to HIV. *Curr Opin HIV AIDS* (2018) 13:15–21. doi: 10.1097/COH.0000000000000424
86. Bucht A, Söderström K, Esin S, Grunewald J, Hagelberg S, Magnusson I, et al. Analysis of gamma delta V region usage in normal and diseased human intestinal biopsies and peripheral blood by polymerase chain reaction (PCR) and flow cytometry. *Clin Exp Immunol.* (1995) 99:57–64. doi: 10.1111/j.1365-2249.1995.tb03472.x
87. Holtmeier W, Chowers Y, Lumeng A, Morzycka-Wroblewska E, Kagnoff MF. The delta T cell receptor repertoire in human colon and peripheral blood is

oligoclonal irrespective of V region usage. *J Clin Invest.* (1995) 96:1108–17. doi: 10.1172/JCI118097
88. Shires J, Theodoridis E, Hayday AC. Biological insights into TCRgammadelta+ and TCRalphabeta+ intraepithelial lymphocytes provided by serial analysis of gene expression (SAGE). *Immunity* (2001) 15:419–34.
89. Serrano-Villar S, Sainz T, Lee SA, Hunt PW, Sinclair E, Shacklett BL, et al. HIV-infected individuals with low CD4/CD8 ratio despite effective antiretroviral therapy exhibit altered T cell subsets, heightened CD8+ T cell activation, and increased risk of non-AIDS morbidity and mortality. *PLoS Pathog.* (2014) 10:e1004078. doi: 10.1371/journal.ppat.1004078
90. Wilson EM, Singh A, Hullsiek KH, Gibson D, Henry WK, Lichtenstein K, et al. Monocyte-activation phenotypes are associated with biomarkers of inflammation and coagulation in chronic HIV infection. *J Infect Dis.* (2014) 210:1396–406. doi: 10.1093/infdis/jiu275
91. Sandler NG, Wand H, Roque A, Law M, Nason MC, Nixon DE, et al. Plasma levels of soluble CD14 independently predict mortality in HIV infection. *J Infect Dis.* (2011) 203:780–90. doi: 10.1093/infdis/jiq118
92. McKibben RA, Margolick JB, Grinspoon S, Li X, Palella FJ, Kingsley LA, et al. Elevated levels of monocyte activation markers are associated with subclinical atherosclerosis in men with and those without HIV infection. *J Infect Dis.* (2015) 211:1219–28. doi: 10.1093/infdis/jiu594
93. Schechter ME, Andrade BB, He T, Richter GH, Tosh KW, Policicchio BB, et al. Inflammatory monocytes expressing tissue factor drive SIV and HIV coagulopathy. *Sci Transl Med.* (2017) 9:eaam5441. doi: 10.1126/scitranslmed.aam5441
94. Yu X, Harden K, Gonzalez LC, Francesco M, Chiang E, Irving B, et al. The surface protein TIGIT suppresses T cell activation by promoting the generation of mature immunoregulatory dendritic cells. *Nat Immunol.* (2009) 10:48–57. doi: 10.1038/ni.1674
95. Stengel KF, Harden-Bowles K, Yu X, Rouge L, Yin J, Comps-Agrar L, et al. Structure of TIGIT immunoreceptor bound to poliovirus receptor reveals a cell-cell adhesion and signaling mechanism that requires cis-trans receptor clustering. *Proc Natl Acad Sci USA.* (2012) 109:5399–404. doi: 10.1073/pnas.1120606109
96. Joller N, Hafler JP, Brynedal B, Kassam N, Spoerl S, Levin SD, et al. Cutting edge: TIGIT has T cell-intrinsic inhibitory functions. *J Immunol.* (2011) 186:1338–42. doi: 10.4049/jimmunol.1003081
97. Stanietsky N, Simic H, Arapovic J, Toporik A, Levy O, Novik A, et al. The interaction of TIGIT with PVR and PVRL2 inhibits human NK cell cytotoxicity. *Proc Natl Acad Sci USA.* (2009) 106:17858–63. doi: 10.1073/pnas.0903474106
98. Imai Y, Ayithan N, Wu X, Yuan Y, Wang L, Hwang ST. Cutting Edge: PD-1 Regulates Imiquimod-Induced Psoriasiform Dermatitis through Inhibition of IL−17A Expression by Innate gammadelta-Low T Cells. *J Immunol.* (2015) 195:421–5. doi: 10.4049/jimmunol.1500448
99. de Witte MA, Sarhan D, Davis Z, Felices M, Vallera DA, Hinderlie P, et al. Early Reconstitution of NK and gammadelta T Cells and Its Implication for the Design of Post-Transplant Immunotherapy. *Biol Blood Marrow Transplant.* (2018) 24:1152–62. doi: 10.1016/j.bbmt.2018.02.023
100. Gogoi D, Biswas D, Borkakoty B, Mahanta J. Exposure to Plasmodium vivax is associated with the increased expression of exhaustion markers on gammadelta T lymphocytes. *Parasite Immunol.* 2018:e12594. doi: 10.1111/pim.12594
101. Fleming C, Morrissey S, Cai Y, Yan J. gammadelta T Cells: unexpected regulators of cancer development and progression. *Trends Cancer* (2017) 3:561–570. doi: 10.1016/j.trecan.2017.06.003
102. Henao-Tamayo M, Irwin SM, Shang S, Ordway D, Orme IM. T lymphocyte surface expression of exhaustion markers as biomarkers of the efficacy of chemotherapy for tuberculosis. *Tuberculosis* (2011) 91:308–13. doi: 10.1016/j.tube.2011.04.001
103. Shin EC, Park SH, Nascimbeni M, Major M, Caggiari L, de Re V, et al. The frequency of CD127(+) hepatitis C virus (HCV)-specific T cells but not the expression of exhaustion markers predicts the outcome of acute HCV infection. *J Virol.* (2013) 87:4772–7. doi: 10.1128/JVI.03122-12
104. Wherry EJ. T cell exhaustion. *Nat Immunol.* (2011) 12:492–9.
105. Jin HT, Anderson AC, Tan WG, West EE, Ha SJ, Araki K, et al. Cooperation of Tim-3 and PD-1 in CD8 T-cell exhaustion during chronic viral infection. *Proc Natl Acad Sci USA.* (2010) 107:14733–8. doi: 10.1073/pnas.1009731107
106. Le Bouteiller P, Tabiasco J, Polgar B, Kozma N, Giustiniani J, Siewiera J, et al. CD160: a unique activating NK cell receptor. *Immunol Lett.* (2011) 138:93–6. doi: 10.1016/j.imlet.2011.02.003
107. Nikolova M, Marie-Cardine A, Boumsell L, Bensussan A. BY55/CD160 acts as a co-receptor in TCR signal transduction of a human circulating cytotoxic effector T lymphocyte subset lacking CD28 expression. *Int Immunol.* (2002) 14:445–51. doi: 10.1093/intimm/14.5.445
108. Wentink MWJ, Mueller YM, Dalm VASH, Driessen GJ, van Hagen PM, van Montfrans JM, et al. Exhaustion of the CD8(+) T cell compartment in patients with mutations in phosphoinositide 3-kinase delta. *Front Immunol.* (2018) 9:446. doi: 10.3389/fimmu.2018.00446
109. Peretz Y, He Z, Shi Y, Yassine-Diab B, Goulet JP, Bordi R, et al. CD160 and PD-1 co-expression on HIV-specific CD8 T cells defines a subset with advanced dysfunction. *PLoS Pathog.* (2012) 8:e1002840. doi: 10.1371/journal.ppat.1002840
110. Althoff KN, McGinnis KA, Wyatt CM, Freiberg MS, Gilbert C, Oursler KK, et al. Comparison of risk and age at diagnosis of myocardial infarction, end-stage renal disease, and non-AIDS-defining cancer in HIV-infected versus uninfected adults. *Clin Infect Dis.* (2015) 60:627–38. doi: 10.1093/cid/ciu869
111. Scully E, Lockhart A, Huang L, Robles Y, Becerril C, Romero-Tejeda M, et al. Elevated levels of microbial translocation markers and CCL2 among older HIV-1-infected men. *J Infect Dis.* (2015) 213:771–5. doi: 10.1093/infdis/jiv501
112. Shiels MS, Althoff KN, Pfeiffer RM, Achenbach CJ, Abraham AG, Castilho J, et al. HIV infection, immunosuppression, and age at diagnosis of non-AIDS-defining cancers. *Clin Infect Dis.* (2017) 64:468–75. doi: 10.1093/cid/ciw764
113. Remacha AF, Cadafalch J, Sardà P, Barceló M, Fuster M. HIV and age do not synergistically affect age-related T-cell markers. *J Acquir Immune Defic Syndr.* (2018) 77:337–44. doi: 10.1097/QAI.0000000000001595
114. Setareh M, Schwarz H, Lotz M. A mRNA variant encoding a soluble form of 4-1BB, a member of the murine NGF/TNF receptor family. *Gene* (1995) 164:311–5.
115. Croft M. The role of TNF superfamily members in T-cell function and diseases. *Nat Rev Immunol.* (2009) 9:271–85. doi: 10.1038/nri2526

Conflict of Interest Statement: KD was an employee of Cytobank, Inc.

The remaining authors declare that the research was conducted in the absence of any commercial or financial relationships that could be construed as a potential conflict of interest.

frontiers in Immunology

ORIGINAL RESEARCH
published: 11 January 2019
doi: 10.3389/fimmu.2018.03140

Elevated Expression of miR-19b Enhances CD8$^+$ T Cell Function by Targeting PTEN in HIV Infected Long Term Non-progressors With Sustained Viral Suppression

Lin-Bo Yin[1,2,3,4], *Cheng-Bo Song*[1,2,3,4], *Jie-Fu Zheng*[1,2,3,4], *Ya-Jing Fu*[1,2,3,4], *Shi Qian*[1,2,3,4], *Yong-Jun Jiang*[1,2,3,4], *Jun-Jie Xu*[1,2,3,4], *Hai-Bo Ding*[1,2,3,4], *Hong Shang*[1,2,3,4]* and *Zi-Ning Zhang*[1,2,3,4]*

[1] NHC Key Laboratory of AIDS Immunology (China Medical University), Department of Laboratory Medicine, The First Affiliated Hospital of China Medical University, Shenyang, China, [2] Key Laboratory of AIDS Immunology of Liaoning Province, The First Affiliated Hospital of China Medical University, Shenyang, China, [3] Key Laboratory of AIDS Immunology, Chinese Academy of Medical Sciences, Shenyang, China, [4] Collaborative Innovation Center for Diagnosis and Treatment of Infectious Diseases, Hangzhou, China

OPEN ACCESS

Edited by:
Sara Gianella Weibel,
University of California, San Diego,
United States

Reviewed by:
Maria Paximadis,
National Institute of Communicable Diseases (NICD), South Africa
Lishomwa Ndhlovu,
University of Hawaii at Manoa,
United States

***Correspondence:**
Hong Shang
hongshang100@hotmail.com
Zi-Ning Zhang
zi_ning101@hotmail.com

Specialty section:
This article was submitted to Viral Immunology, a section of the journal Frontiers in Immunology

Received: 04 July 2018
Accepted: 19 December 2018
Published: 11 January 2019

Citation:
Yin L-B, Song C-B, Zheng J-F, Fu Y-J, Qian S, Jiang Y-J, Xu J-J, Ding H-B, Shang H and Zhang Z-N (2019) Elevated Expression of miR-19b Enhances CD8$^+$ T Cell Function by Targeting PTEN in HIV Infected Long Term Non-progressors With Sustained Viral Suppression. Front. Immunol. 9:3140. doi: 10.3389/fimmu.2018.03140

Human immunodeficiency virus (HIV)-infected long-term non-progressors (LTNPs) are of particular importance because of their unique disease progression characteristics. Defined by the maintenance of normal CD4$^+$T cells after more than 8 years of infection, these LTNPs are heterogeneous. Some LTNPs exhibit ongoing viral production, while others do not and are able to control viral production. The underlying basis for this heterogeneity has not been clearly elucidated. In this study, the miRNA expression profiles of LTNPs were assessed. The levels of microRNA-19b (miR-19b) were found to be significantly increased in peripheral blood mononuclear cells of LTNPs with lower rather than higher viral load. We made clear that miR-19b may regulate CD8$^+$T cell functions in HIV infection, which has not been addressed before. Overexpression of miR-19b promoted CD8$^+$T cell proliferation, as well as interferon-γ and granzyme B expression, while inhibiting CD8$^+$T cells apoptosis induced by anti-CD3/CD28 stimulation. The target of miR-19b was found to be the "phosphatase and tensin homolog", which regulates CD8$^+$T cells function during HIV infections. Furthermore, we found that miR-19b can directly inhibit viral production in *in-vitro* HIV infected T cells. These results highlight the importance of miR-19b to control viral levels, which facilitate an understanding of human immunodeficiency virus pathogenesis and provide potential targets for improved immune intervention.

Keywords: CD8$^+$T cells, long-term non-progressors, microRNA-19b, phosphatase and tensin homolog, HIV

INTRODUCTION

Human immunodeficiency virus (HIV) infected patients with atypical disease progression are of particular importance because they can provide important information regarding HIV pathogenesis and therapy. The first evidence of long-term non-progressors (LTNPs) was reported in 1993, showing that 15% of individuals infected with HIV maintain a CD4 count >500 cells/μl (1, 2).

In 2005, study showed that ∼1/300 HIV-infected patients had undetectable plasma HIV RNA loads without antiretroviral therapy (ART) (3). Described as "Elite Controllers" (ECs) in 2007, these patients maintained HIV RNA levels below 50 copies/ml for at least 1 year in the absence of ART (4–8). Although there is overlap between LTNPs and ECs, they are not identical. Most ECs exhibit minimal reductions in $CD4^+$ T cells over time, although reductions are observed in some ECs. Furthermore, some LTNPs have ongoing viral production, while others do not (3, 5, 7, 9–11). Transcriptomic analysis showed that ECs with higher $CD4^+$T cell numbers were indistinguishable from HIV-1-negative individuals. In contrast, ECs with lower $CD4^+$ T cell numbers were similar to ART-treated patients, but different from HIV-1-negative individuals (12). Alterations in T cell homeostasis predict the loss of immunological control in ECs (13)4. However, viral control differs among LTNPs and the reason for this difference is currently unknown. LTNPs maintaining high viral loads are prone to long-term disease progression, with reduced life expectancy compared to HIV negative individuals (14, 15). Analysis of the underlying reason for the differing levels of viral control in LTNPs may facilitate an understanding of HIV pathogenesis and may provide for new approaches to immune intervention.

The level of virus control is affected by immunologic and virologic factors. MicroRNAs (miRNAs) may be a potential mechanistic factor involved in this process. It has been shown that miRNAs play important roles in the regulation of immune responses and viral production. In HIV infection, miRNAs can directly modulate viral production by targeting the HIV-1 genome or by indirectly modulating cellular genes that influence viral propagation (16–20). Dramatic advances have been made in understanding how miRNAs regulate the development and function of immune cells (21, 22), including $CD8^+$T cells which are key players in the antiviral immune response (23, 24). It is established that miRNAs modulate the expression of numerous regulatory proteins required for the development, differentiation, and function of $CD8^+$T cells (25). Studies have shown that, in HIV infection, miRNAs modulate the expression of key markers associated with T cell exhaustion or dysfunction, such as interleukin 10 and B lymphocyte-induced maturation protein-1 (26). We postulated that differential miRNA profiles may contribute to the divergent control of viral load in LTNPs by affecting viral production and/or $CD8^+$T cell function. Although previous studies have identified miRNA profiles in HIV-infected ECs and LTNPs (16, 27–30), the role of miRNAs in the differential control of viral load in LTNPs has not been addressed.

In this study, miRNA expression profiles of LTNPs were assessed. The expression of miR-19b was found to be significantly increased in the peripheral blood mononuclear cells (PBMCs) of LTNPs with low (LTNP-Ls) compared to high levels (LTNP-Hs) of virus production. In addition, miR-19b promoted proliferation, and expression of interferon gamma (IFN-γ) and granzyme B, while inhibiting $CD8^+$T apoptosis induced by anti-CD3/CD28 stimulation. The phosphatase and tensin homolog (PTEN) is a target of miR-19b regulating $CD8^+$T cell function in HIV infection. Furthermore, we found that miR-19b directly inhibits viral production in HIV-infected T cells *in vitro*. Our results revealed a previously unknown mechanism of sustained viral control by miR-19b in a subtype of LTNPs, suggesting that miR-19b may be a novel target for immune intervention in HIV infection.

MATERIALS AND METHODS

Study Population

In total, samples obtained from 27 LTNPs, six typical progressors (TPs), and four healthy controls (HCs) were analyzed. The LTNPs were HIV positive patients who maintained normal $CD4^+$ T cell counts (CD4 >500 cells/μl) for >10 years (mean ± SD: 14.72 ± 1.79 years at the time of sample collection) without receiving ART (**Supplemental Table 1**). The TPs were ART naive HIV positive patients who progressed to CD4 counts <500 cells/μl at 2.53 ± 0.95 years (**Supplemental Table 2**). The initial 347-miRNA array was performed in a training cohort, including nine LTNPs (age, mean ± SD: 41 ± 6 years; gender, eight males and one female), six TPs (age, mean ± SD: 30 ± 15 years; gender, six males) and four HCs (age, mean ± SD: 37 ± 6 years; gender, four males). From the training cohort, miRNAs differentially expressed in LTNPs with differing viral loads were detected in a subsequent validation group that included 18 LTNPs. Ethical approval was obtained from the First Hospital of China Medical University, Shenyang, China and written informed consent was provided by all participants.

miRNA Array Analysis

Quantitative real-time polymerase chain reaction (qRT-PCR)-based high-throughput miRNA profiling was performed at QuantoBio Biotechnology Co. Ltd. (Beijing, China). Briefly, total RNA extracted from peripheral blood mononuclear cells (PBMCs) was isolated using TRIzol® (Invitrogen, Carlsbad, USA). *Escherichia coli* poly (A) polymerase was used to add adenines to the 3′ end of RNA molecules lacking a poly (A) tail. After oligo dT annealing, a universal tag was attached to the 3′ end of cDNAs during cDNA synthesis using retrotranscriptase Superscript III (Invitrogen). With this universal tag, a SYBR®-based qRT-PCR was performed using miRNA-specific forward primers and a reverse universal primer mix. Of note, U1 and U6 were used in the training cohort for normalization. The variation of change in the threshold cycle (CT, target-CT, and control) was evaluated and used as a relative qualitative value.

RT-PCR Quantification of miRNA and mRNA

We extracted miRNAs from cells using the miRNeasy Micro kit (Qiagen, Hilden, Germany). The RNA was reverse transcribed using a Primpscript® RT reagent kit (TAKARA, Dalian, China) according to the instructions provided by the manufacturer. Subsequently, RT-PCR was performed using a SYBR® Premix Ex Taq™ II (TAKARA). The levels of miRNA were normalized to the U6 small nucleolar RNA and quantified through the relative quantification method ($2^{-\Delta\Delta Ct}$), as previously described (31). Cellular total mRNA was isolated using the RNeasy Micro kit (Qiagen). The cDNA was generated using the Primpscript® RT reagent kit (TAKARA). The levels of mRNA

were quantified through the SYBR® Premix Ex Taq™ II (TAKARA), normalized to GAPDH transcripts, and expressed using the relative quantification method ($2^{-\Delta\Delta Ct}$). All primer sequences for the quantification of miRNA and mRNA are listed in **Supplemental Table 3**.

Isolation of Cells

PBMCs were obtained by Ficoll–Hypaque density gradient centrifugation. If indicated, $CD8^+$ or $CD4^+$ T cells were further purified from isolated PBMCs by negative selection with magnetic beads using a $CD8^+$ or $CD4^+$ T cell Enrichment Kit (Cell purity >95%, Stem Cell Technologies, Vancouver, Canada). The following antibodies were used for immunostaining to isolate cell subtypes: FITC-CD3, APC-cy7-CD8, APC-CD4, PE-cy7-CD14 and 7-AAD (Biolegend, San Diego, CA, USA). $CD4^+$ T cells ($CD3^+CD4^+$), $CD8^+$ T cells ($CD3^+CD8^+$), and monocytes ($CD3^-CD14^+$) were selected from 7-AAD-negative live PBMCs using a FACSAria™ flow cytometer (BD Biosciences, Franklin Lake, NJ, USA).

Cell Culture

The Jurkat human leukemia T cells, Clone-X cells, and primary cells were maintained in RPMI1640 media (HyClone, Logan, UT, USA) supplemented with 10% fetal bovine serum and 1% penicillin-streptomycin. The 293T cells were maintained in DMEM media (HyClone) supplemented with 10% fetal bovine serum and 1% penicillin-streptomycin.

Transfection

Transfection of miRNAs to cell lines was achieved using Lipofectamine® 2000 (Invitrogen). Briefly, 20 μM miR-19b mimics or controls (GenePharma, Shanghai, China) were transfected to 293T cells, Jurkat cells, or Clone-X cells according to the protocol provided by the manufacturer. In primary cells, Lipofectamine® RNAiMAX (Invitrogen) was used for the transfection according to the protocol provided by the manufacturer. Briefly, 20 μM miR-19b mimics, inhibitors (GenePharma), or controls were transfected to isolated $CD8^+$T or $CD4^+$T cell-depleted PBMCs. In addition, isolated primary $CD4^+$ T cells from healthy controls were transfected with 20 μM miR-19b mimics or controls. The forced reduction of phosphatase and tensin homolog (PTEN) was achieved by introducing 20 μM PTEN siRNA (Invitrogen) to isolated $CD8^+$T cells. The siRNA control used in this experiment was non-specific Stealth RNAi® Negative Control Duplexes. The sequences of the mimics and inhibitors are listed in **Supplemental Table 3**.

Proliferation Assays

After transfection (24 h), Jurkat cells and primary $CD8^+$T cells were labeled with Cell Trace™ Violet (Thermo Fisher Scientific, Waltham, USA) for 15 min at 37°C according to the instructions provided by the manufacturer, washed with complete medium, and cultured (1×10^6 cells/ml). Primary $CD8^+$T cells were cultured in the presence of anti-CD3/CD28 (3 μg/ml; Gibco, New York, NY, USA). After incubation for 5 days, the dividing cells were analyzed using a BD LSR II flow cytometer and the FlowJo software.

Detection of Apoptosis

After transfection (72 h), Jurkat cells were stained with PE-conjugated anti-Annexin V and 7-AAD (Biolegend). After transfection (24 h), primary $CD8^+$T cells were stimulated using anti-CD3/CD28 (3 μg/ml). After stimulation (48 h), $CD8^+$T cells were stained with PE-cy7-conjugated anti-CD3, APC-cy7-conjugated anti-CD8, PE-conjugated anti-Annexin V, and 7-AAD (Biolegend). The cells were analyzed using a BD LSR II flow cytometer and the FlowJo software.

Cell Cycle Assay

Cell cycle phases were determined using the BD Cycletest™ Plus DNA Reagent Kit (BD Biosciences) according to the instructions provided by the manufacturer. In brief, Jurkat cells were cultured for 72 h after transfection. After transfection (24 h), primary $CD8^+$T cells were cultured for 48 h under stimulation using anti-CD3/CD28 (3 μg/ml). The distribution of DNA content was determined using a BD LSR II flow cytometer and analyzed using the FlowJo software.

Intracellular Staining of IFN-γ and Granzyme B

After transfection (24 h), primary $CD8^+$T cells were stimulated using anti-CD3/CD28 (3 μg/ml) for 24 h. The protein transport inhibitor (GolgiStop; 1 μl/ml, BD Biosciences) was added to the culture for the last 6 h. The cells were stained with PE-cy7-conjugated anti-CD3 and APC-cy7-conjugated anti-CD8 (Biolegend). Subsequently, intracellular staining was performed by incubating the cells in 1X Perm/Wash Buffer for 15 min in the dark, followed by incubation with APC-conjugated anti-IFN-γ and FITC-conjugated anti-granzyme B for 30 min at 4°C. After staining, the cells were fixed in 1% formaldehyde. The intracellular expression of IFN-γ and granzyme B was determined using a BD LSR II flow cytometer and data were analyzed using the FlowJo software.

IFN-γ ELISpot Assay

$CD4^+$ T cells were depleted from PBMCs using anti-CD4 MAb-coated magnetic beads (Biolegend) as described in the instructions provided by the manufacturer. The Human IFN-γ ELISpot Kit (Mabtech, Nacka, Sweden) was used to detect the secretion of IFN-γ according to the instruction manual. After transfection (24 h), 2×10^5 $CD4^+$ T cell-depleted PBMCs were added per well (in duplicates) in a volume of 200 μl. The HIV-1 gag peptide pools (10 μg/ml, Sigma) were added for 20 h. Anti-CD3/CD28 (3 μg/ml) were used as a positive control, and negative controls consisted of cells without stimuli. The number of IFN-γ-secreting cells was calculated by subtracting the negative control (medium only) values. A positive response was defined as >50 spot-forming units/10^6 PBMC.

In-vitro Infection

Viral particles were produced by transfecting 293T cells with HIV-1 pNL4-3 plasmids and vesicular stomatitis virus glycoprotein (VSV-G) plasmids. Transfection of miR-19b mimics, pNL4-3 plasmids, and VSV-G plasmids into 293T cells was performed to detect the effects of miR-19 on HIV

production. The levels of p24 in the supernatants were measured by ELISA (Biomedical Engineering Center of Hebei Medical University, Hebei, China) 2 days later. For the infection of Clone-X cells, the cells were transfected with miR-19b mimics for 24 h and subsequently infected with VSV-G pseudotyped HIV-1 (NL4-3) virus. GFP^+ cells were detected by flow cytometry 48 h after infection.

Replication-competent HIV-1 isolate was used to test the effects of miR-19b in primary $CD4^+$ T cells. Isolated primary $CD4^+$ T cells from healthy controls were transfected with miR-19b mimics or controls. After transfection (24 h), the cells were stimulated using anti-CD3/CD28 (3 μg/ml). A cryopreserved primary HIV-1 isolate—obtained by a co-culture using mixed PBMCs from an HIV-1-infected patient and a healthy donor—was thawed and added to the cells. The supernatant was collected after 3 days of infection and the levels of p24 in the supernatants were measured by ELISA.

Statistical Analysis

Principal component analysis (PCA) was used (Origin 9.1 software) to analyze the distribution of miRNAs in HIV-infected patients with differing disease progression. The non-parametric Mann–Whitney test was used to determine differences between LTNPs with a relatively high viral load (>1,000 copies/ml) (LTNP-Hs) and LTNPs with relative control of viral load (<1,000 copies/ml) (LTNP-Ls). A paired *t*-test was used to analyze differences in $CD8^+$T cell function between groups. Data analysis was performed using the SPSS 21.0 and GraphPad Prism Version 5.0 software packages. A $P < 0.05$ was considered statistically significant.

RESULTS

miRNA Profiles Distinguish LTNPs With Different Virus Levels

A training cohort was formed including nine LTNPs, six TPs, and four HCs to identify the miRNA profiles of LTNPs. Using qRT-PCR-based arrays, the expression levels of 347 miRNAs were quantified. Based on an unsupervised PCA of all array data, the six TPs, nine LTNPs and four HCs were segregated into two groups (**Figure 1A**). All the HCs were clustered in one group. Most of the TPs were clustered in the other group, except one TP with a relatively low viral load (<1,000 copies/ml), indicating that HIV infection alters miRNAs. This finding was consistent with those reported in previous studies (30, 32, 33). Interestingly, the nine LTNPs were divided into two groups, one of which was very close to the TPs (Group A, $n = 6$) and another that was intertwined with the HCs (Group B, $n = 3$) (**Figure 1A**). We subsequently sought to identify differences between the two groups of LTNPs. By comparison of clinical characteristics (i.e., age, number of $CD4^+$T cells, and viral loads), we found that viral load was the only significantly different parameter between the two groups of LTNPs ($P = 0.024$, **Figure 1B**). Six LTNPs in Group A, whose miRNA profiles were similar to those of TPs, had a relatively high level of viral load (>1,000 copies/ml, hereinafter referred to as "LTNP-Hs"). Three LTNPs in Group B, whose miRNA profiles were similar to those of HCs, had relative control of viral load (VL < 1,000 copies/ml, hereinafter referred to as "LTNP-Ls," **Supplemental Table 1**). The results of the unsupervised PCA suggest that the expression of miRNAs can distinguish LTNP-Hs and LTNP-Ls, and may account for the differing viral loads observed in LTNPs.

Expression of miR-19b Is High in LTNP-Ls in Comparison With That in LTNP-Hs

Subsequently, the differential expression of miRNAs in LTNP-Hs and LTNP-Ls was assessed. The miRNAs were determined to be significantly differentially expressed in LTNP-Hs and LTNP-Ls with a Benjamini–Hochberg false discovery rate-adjusted $P < 0.05$. We found that 78 miRNAs were differentially expressed with >2-fold change between the three LTNP-Ls and six LTNP-Hs in the training cohort (adj. $P < 0.05$, **Supplemental Table 4**). Among those, 55 miRNAs were upregulated and 23 were downregulated in LTNP-Ls compared with that in LTNP-Hs. Using an unsupervised clustering method, 78 miRNAs accurately distinguished and clustered LTNP-Hs and LTNP-Ls (**Figure 2A**). A total of 75 miRNAs with differential expression levels between LTNP-Hs or LTNP-Ls and HCs or TPs ($P < 0.05$) were excluded to identify miRNAs that can uniquely differentiate LTNP-Hs from LTNP-Ls (**Figure 2B; Supplemental Table 4**). This exclusion was carried out because these miRNAs may reflect differences caused by HIV infection or the stages of infection. Only three miRNAs which were differentially expressed between LTNP-Hs and LTNP-Ls in the training cohort were selected, including miR-15a ($P = 0.024$), miR-19b ($P = 0.048$), and miR-33 ($P = 0.024$, **Figure 2C**).

The expression levels of these three miRNAs were assessed in a subsequent validation group, including ten LTNP-Hs and eight LTNP-Ls (**Supplemental Table 1**). In the validation cohort, only miR-19b was verified to be highly expressed in LTNP-Ls compared with LTNP-Hs ($P = 0.034$, **Figures 2D–F**). Subsequently, $CD8^+$, $CD4^+$ T cells, and monocytes from LTNPs were sorted to identify the cell subtypes in which the expression of miR-19b was altered. We found that the expression of miR-19b decreased in $CD4^+$T cells and $CD8^+$ T cells in LTNP-Hs ($n = 10$) compared with that observed in LTNP-Ls ($n = 9$) ($P = 0.041$, **Figure 2G**; $P = 0.028$, **Figure 2H**). There were no differences observed in the expression of miR-19b in monocytes between the two groups (data not shown).

miR-19b Promotes Proliferation and Expression IFN-γ, and Inhibits the Apoptosis of Primary $CD8^+$T Cells

As the most important immune effector cell population, $CD8^+$T cells play a key role in anti-HIV immune responses. We hypothesized that miR-19b may contribute to the control of the virus in LTNP-Ls by regulating $CD8^+$T cell function. This was the first study addressing this question. Initially, we overexpressed miR-19b in Jurkat cells by transfection with miRNA mimics to investigate the effect of miR-19b on lymphocyte proliferation and apoptosis. After transfection (48 h), miR-19b was highly expressed (**Supplemental Figure 1**). After 5 days, the proliferation of miR-19b-overexpressing cells

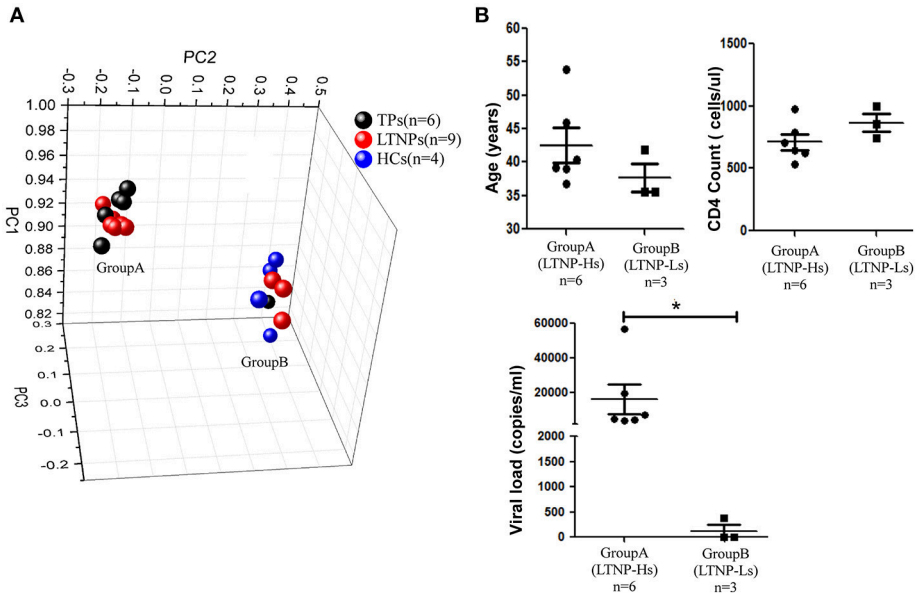

FIGURE 1 | miRNA profiles distinguish LTNPs with different levels of virus. **(A)** Principal component analysis (PCA) plot of miRNA expression data from LTNPs, TPs, and HCs in the training cohort. Nine LTNPs were divided into two groups, one of which was very close to the TPs (Group A, $n = 6$) and another that was intertwined with the HCs (Group B, $n = 3$). **(B)** Comparison of age, CD4 counts, and viral load between Group A and Group B of LTNPs. $^{*}P < 0.05$.

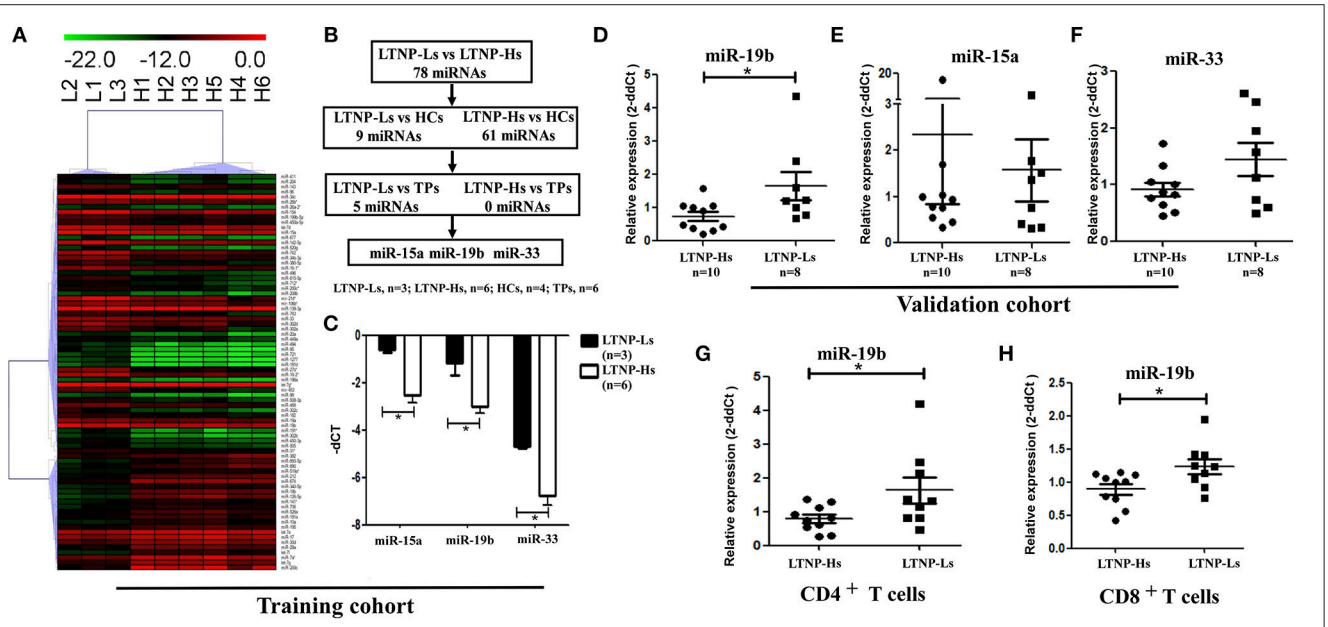

FIGURE 2 | Expression of miR-19b is high in LTNP-Ls compared with that observed in LTNP-Hs. **(A)** Heatmap demonstrating 78 miRNAs differentially expressed between LTNP-Hs ($n = 6$) and LTNP-Ls ($n = 3$) in the training cohort (Benjamini–Hochberg false discovery rate-adjusted $P < 0.05$ and fold change >2). Hierarchical clustering of change in the threshold cycle (ΔCT) was performed using the complete linkage method and Pearson correlation coefficient. **(B)** The protocol for the selection of candidate miRNA from the training cohort. Among the 78 miRNAs differentially expressed between LTNP-Hs ($n = 6$) and LTNP-Ls ($n = 3$), 70 miRNAs differentially expressed between LTNPs and HCs ($P < 0.05$) were excluded. Subsequently, five differentially expressed miRNAs between LTNPs and TPs were excluded. Three candidate miRNAs, namely miR-15a, miR-19b, and miR-33 were selected. **(C)** Comparison of the three candidate miRNAs between LTNP-Ls ($n = 3$) and LTNP-Hs ($n = 6$) in the training cohort. **(D,F)** Relative expression of miR-19b **(D)**, miR-15a **(E)** and miR-33 **(F)** in PBMCs obtained from LTNP-Ls ($n = 8$) and LTNP-Hs ($n = 10$) in the subsequent validation group. **(G,H)** $CD4^+$ and $CD8^+$T cells from LTNPs were sorted through flow cytometry. The expression of miR19b in $CD4^+$ **(G)** and $CD8^+$ T **(H)** cells was compared between LTNP-Ls ($n = 9$, one from training cohort, eight from validation cohort) and LTNP-Hs ($n = 10$, two from training cohort, eight from validation cohort) using qRT-PCR. $^{*}P < 0.05$.

was significantly increased compared with that observed in the control group, suggesting that miR-19b promotes cell proliferation ($P = 0.013$, **Figure 3A**). Overexpression of miR-19b significantly accelerated the cell cycle ($P = 0.033$, **Figure 3B**). Furthermore, the percentage of Annexin V^+ 7-AAD^- apoptotic cells was lower following the overexpression of miR-19b ($P = 0.005$, **Figure 3C**). These data indicate that miR-19b promotes proliferation and inhibits apoptosis of T cell lines.

We subsequently assessed the role of miR-19b in regulating the function of primary $CD8^+$T cells by transfection of miR-19b mimics into $CD8^+$T cells obtained from HCs. We found that overexpression of miR-19b significantly promoted the proliferation of $CD8^+$T cells after anti-CD3/CD28 stimulation ($P = 0.010$, **Figure 3D**). Similarly, forced expression of miR-19b significantly inhibited apoptosis of $CD8^+$T cells after stimulation of the anti-CD3/CD28 ($P = 0.009$, **Figure 3E**). $CD8^+$T cells were sorted using magnetic beads to study the effect of miR-19b on the cytotoxic function of $CD8^+$T cells. Overexpression of miR-19b in $CD8^+$T cells significantly increased the intracellular levels of IFN-γ and granzyme B after stimulation of the anti-CD3/CD28 ($P = 0.006$, **Figure 3F**; $P = 0.002$, **Figure 3G**, respectively). These results demonstrate that miR-19b promotes cell proliferation, and the expression of IFN-γ and granzyme B in $CD8^+$T cells. Moreover, it inhibits the apoptosis of $CD8^+$T cells after stimulation of the anti-CD3/CD28.

miR-19b Regulates $CD8^+$ T Cell Function via Expression of PTEN

Cell signaling pathways involving miR-19b target genes were assessed through a bioinformatics analysis (http://diana.imis.athena-innovation.gr/) to further explore the molecular mechanistic basis of miR-19b regulation (**Figure 4A**). The FOXO signaling pathway plays critical roles in cell cycle regulation and is the main cell signaling pathway in which miR-19b target genes are involved. Through the detection of several key molecules in the FOXO pathway using qRT-PCR, we found that overexpression of miR-19b in Jurkat cells significantly reduced the expression level of PTEN ($P < 0.001$, **Figure 4B**). The direct regulation of PTEN by miR-19b was demonstrated using a Luciferase reporter assay, qRT-PCR, and western blotting (34–38). Considering that PTEN is closely associated with cell proliferation and cell cycle (39), we sought to determine the effect of miR19b on the function of $CD8^+$T cells by regulating the expression of the target gene PTEN.

We reduced the expression of PTEN in primary HCs $CD8^+$T cells using specific siRNAs (**Supplemental Figure 1**). Cell proliferation was promoted and apoptosis was inhibited via the knockdown of PTEN in comparison with the negative control group ($P = 0.040$ **Figure 4C**; $P = 0.047$, **Figure 4D**, respectively). Moreover, the secretion of granzyme B by $CD8^+$ T cells was significantly increased ($P = 0.006$, **Figure 4E**) and that of IFN-γ showed an increasing trend ($P = 0.094$, **Figure 4F**) after stimulation of the anti-CD3/CD28, in response to the suppression of PTEN. These findings demonstrate that inhibition of PTEN, which is a potential target of miR-19b, exerts similar effects on $CD8^+$T cell function to those observed following the overexpression of miR-19b.

miR-19b Regulates the Function of $CD8^+$ T Cells From HIV-Infected Patients

The function of miR-19b in $CD8^+$T cells from 7 HIV-infected patients (**Supplemental Table 5**) was also studied. Primary $CD8^+$T cells from HIV-infected patients were sorted. Following the overexpression of miR-19b (**Supplemental Figure 1**), $CD8^+$T cells showed a significant increase in proliferation ($P = 0.010$), and secretion of IFN-γ ($P = 0.010$) and granzyme B ($P = 0.003$) after stimulation of the anti-CD3/CD28 (**Figure 5A**). Apoptosis of $CD8^+$T cells was significantly reduced in comparison with the controls ($P = 0.040$, **Figure 5A**). Furthermore, the expression of miR-19b was inhibited by transfection of miR-19b inhibitors into $CD8^+$ T cells from HIV patients (**Supplemental Figure 1**). Contrary to the miRNA overexpression results, the proliferation of $CD8^+$ T cells was reduced ($P = 0.043$, **Figure 5B**), the secretions of IFN-γ ($P = 0.023$) and granzyme B ($P = 0.049$) were reduced, and the apoptosis of $CD8^+$T cells was increased ($P = 0.035$, **Figure 5B**).

Subsequently, the expression of PTEN in primary $CD8^+$T cells was inhibited using siRNA to verify that PTEN was a miR-19b target gene involved in the regulation of $CD8^+$T cell function in HIV infection. Consistent with the findings reported in healthy patients, inhibition of PTEN resulted in an increase in proliferation ($P = 0.005$) and secretion of IFN-γ ($P < 0.001$) and granzyme B ($P = 0.012$), as well as a decrease in $CD8^+$T cell apoptosis ($P = 0.006$) in HIV-infected patients (**Figure 5C**). Furthermore, siRNA was used to suppress the expression of PTEN in miR-19b-low-expressing $CD8^+$ T cells to verify that miR-19b affects $CD8^+$ T cell function through regulation of PTEN. Following the downregulation of PTEN, there was no statistical difference detected in proliferation, expression of IFN-γ and granzyme B, or apoptosis compared with controls. These data suggest that downregulation of PTEN antagonizes the effect of miR-19b inhibitors on the function of $CD8^+$T cells in HIV patients (**Figures 5D–G**).

An IFN-γ ELISPOT assay was performed to further confirm the effect of miR-19b on HIV specific $CD8^+$T cells. We found that overexpression of miR-19b significantly increased the secretion of IFN-γ by gag peptide-stimulated $CD8^+$T cells ($P = 0.041$). Of note, the secretion of IFN-γ was significantly reduced in response to suppression of the expression of miR-19b by inhibitors ($P = 0.020$, **Figure 5H**). These data suggested that miR-19b augments the function of HIV specific $CD8^+$T cells.

miR-19b Inhibits Viral Replication in *in-vitro* HIV-Infected T Cells

Lastly, we hypothesized that miR-19b may play a role in the direct inhibition of HIV replication, besides its regulation of $CD8^+$T cells. The levels of miR-19b in the plasma have been reported to be associated with $CD4^+$ T cell counts, indicating that miR-19b may be a biomarker for the monitoring of the HIV immune status (40). However, its direct effects on HIV viral production

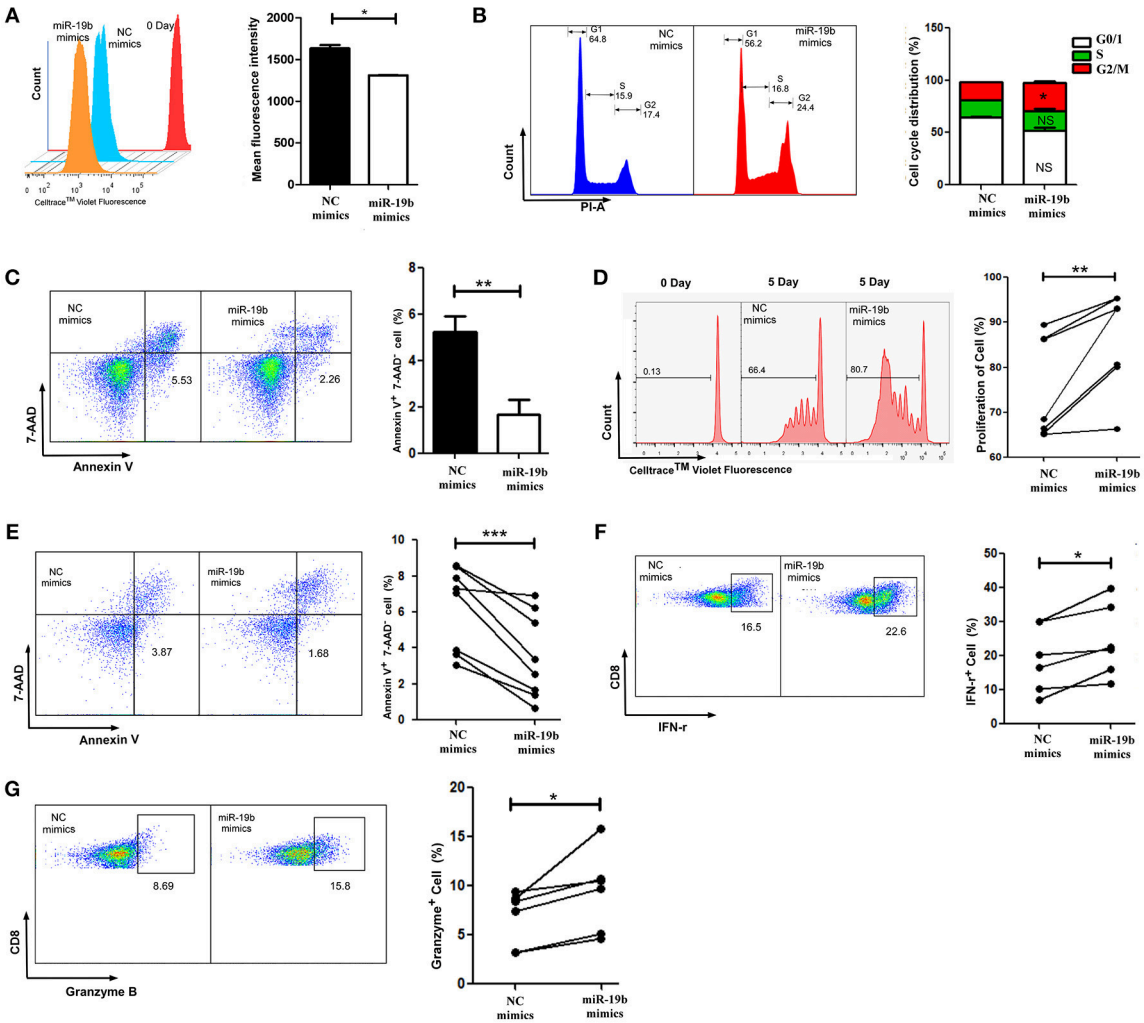

FIGURE 3 | Overexpression of miR-19b regulates the function of $CD8^+$ T cells from healthy controls. Jurkat cells were transfected with miR-19b mimics using Lipofectamine® 2000. **(A)** After transfection (24 h), Jurkat cells were labeled with Cell Trace™ Violet. After incubation for 5 days, the dividing cells were analyzed. **(B)** After transfection (72 h), the cell cycle of Jurkat cells was determined. **(C)** After transfection (72 h), Jurkat cells were stained with Annexin V and 7-AAD and the apoptosis of the cells was determined. **(D–G)** $CD8^+$ T cells from healthy controls were sorted and transfected with miR-19b mimics or controls using Lipofectamine® RNAiMAX. **(D)** After transfection (24 h), $CD8^+$T cells were labeled with Cell Trace™ Violet and stimulated with anti-CD3/CD28 (3 μg/ml) for 5 days, the proliferation of $CD8^+$T cells was determined. **(E)** After transfection (24 h), $CD8^+$T cells were stimulated using anti-CD3/CD28 (3 μg/ml) for 48 h and the rate of apoptosis were determined. **(F,G)** After transfection (24 h), $CD8^+$ T cells were stimulated using anti-CD3/CD28 (3 μg/ml) for 24 h and expression of intracellular IFN-γ **(F)** and granzyme B **(G)** was determined. In each part, representative flow cytometry data and comparisons of the parameters between miR-19b-overexpressing cells and controls are shown. $n = 7$ for each group in **(D)**, $n = 8$ for each group in **(E)**, $n = 6$ for each group in **(F,G)**. $^*P < 0.05$. $^{**}P < 0.01$, $^{***}P < 0.001$, respectively.

have not been reported. We found that overexpression of miR-19b by mimics reduced the production of HIV. Following the co-transfection of miR-19b mimics and the pNL4-3 plasmid into 293T cells, the expression level of P24 in supernatants was lower than that in the control group after 48 h of culture ($P = 0.040$, **Figure 6A**). Furthermore, Clone-X cells were infected with the same titer of HIV pseudovirus, the percentage of HIV-positive cells overexpressing miR-19b was lower compared with that in the control group ($P = 0.007$, **Figure 6B**). Finally, we infected primary $CD4^+$ T cells from normal controls using replication-competent HIV-1 virus isolates and found that overexpression of miR-19b inhibited the production of HIV ($P = 0.001$, **Figure 6C**). These data demonstrated that, besides its role in the regulation of $CD8^+$T cells, miR-19b inhibits viral production, leading to lower viral levels.

DISCUSSION

LTNPs are defined by the maintenance of normal $CD4^+$T cells counts for more than 8 years after infection. However, LTNPs exhibit heterogeneity in their viral loads. LTNPs maintaining high viral loads are prone to long-term progression, with reduced overall life expectancy vs. healthy individuals. However, the factors involved in the differential control of viral levels in LTNPs

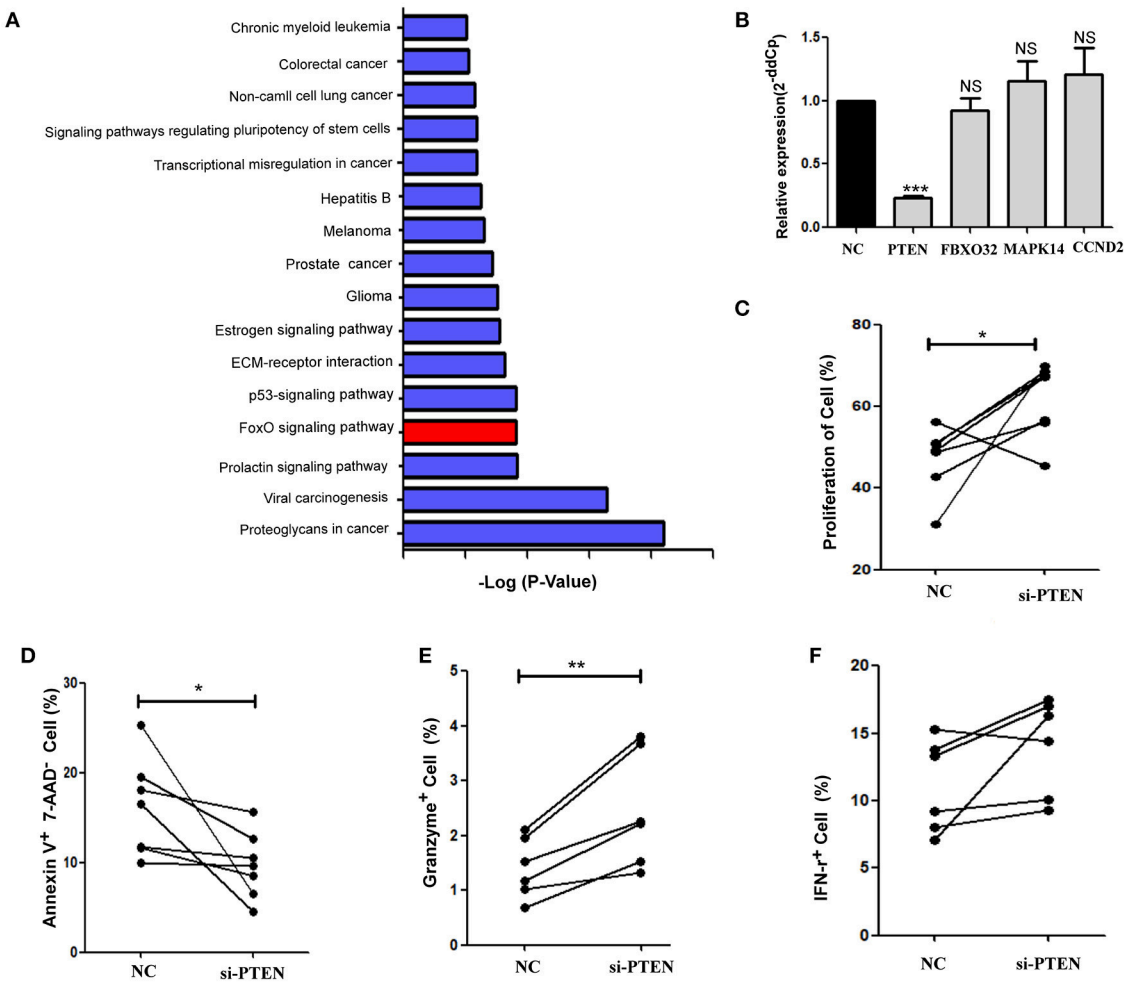

FIGURE 4 | PTEN is a potential target of miR-19b. **(A)** Cell signaling pathways involving miR-19b target genes were assessed through a bioinformatics analysis (http://diana.imis.athena-innovation.gr/). The FOXO signaling pathway (Red) is a major cellular signaling pathway playing a key role in cell cycle regulation. **(B)** The expression of miR-19b was enhanced by mimics in Jurkat cells. Four genes in the FOXO pathway were detected through qRT-PCR. **(C–F)** The expression of PTEN was inhibited by introducing 20 μM PTEN siRNA to isolated $CD8^+$T cells. **(C)** After transfection (24 h), $CD8^+$T cells were labeled with Cell Trace™ Violet and stimulated using anti-CD3/CD28 (3 μg/ml) for 5 days. The proliferation of $CD8^+$T cells was determined. **(D)** After transfection (24 h), $CD8^+$ T cells were stimulated using anti-CD3/CD28 (3 μg/ml) for 48 h and the rate of apoptosis of $CD8^+$ T cells was determined. **(E,F)** After transfection (24 h), $CD8^+$ T cells were stimulated using anti-CD3/CD28 (3 μg/ml) for 24 h and the intracellular expression of IFN-γ **(E)** and granzyme B **(F)** was determined. $n = 6$ for each group in **(C)**, $n = 7$ for each group in **(D)**, $n = 6$ for each group in **(E,F)**. $^*P < 0.05$. $^{**}P < 0.01$. $^{***}P < 0.001$, respectively.

have not been identified. In this study, we found that miR-19b is highly expressed in LTNP-Ls vs. LTNP-Hs. It was shown that miR-19b influences the low viral load of LTNP-Ls by promoting the function of $CD8^+$T cells in HIV infection and directly inhibiting viral production of HIV.

Factors contributing to the different levels of $CD4^+$T cells in ECs have already been studied (12, 13). However, thus far, the underlying mechanistic basis for the differing levels of viral control in LTNPs has not been investigated. Considering the important role of miRNAs in regulating immune responses and viral replication, we performed a miRNA profiling analysis of HIV-infected individuals. The miRNA profiles distinguished LTNPs with differing viral loads. LTNPs whose miRNA profiles were similar to those of TPs exhibited a relatively high viral load. In contrast, LTNPs with miRNA profiles similar to those of HCs showed relatively well-controlled viral loads. Based on the results of the miRNA array analysis and subsequent validation, miR-19b was verified to be highly expressed in LTNP-Ls compared with LTNP-Hs. In HIV infection, plasma miR-19b was associated with $CD4^+$ T cell counts and may be a useful biomarker for monitoring the HIV immune status (40). Our study showed that the expression of miR-19b is significantly different between LTNP-Hs and LTNP-Ls. We speculated that miR-19b contributes to the control of viral load in LTNP-Ls by affecting viral production and/or regulating immune cell function.

$CD8^+$T cells play a crucial role in the control of HIV replication by direct cytolysis of infected cells and production

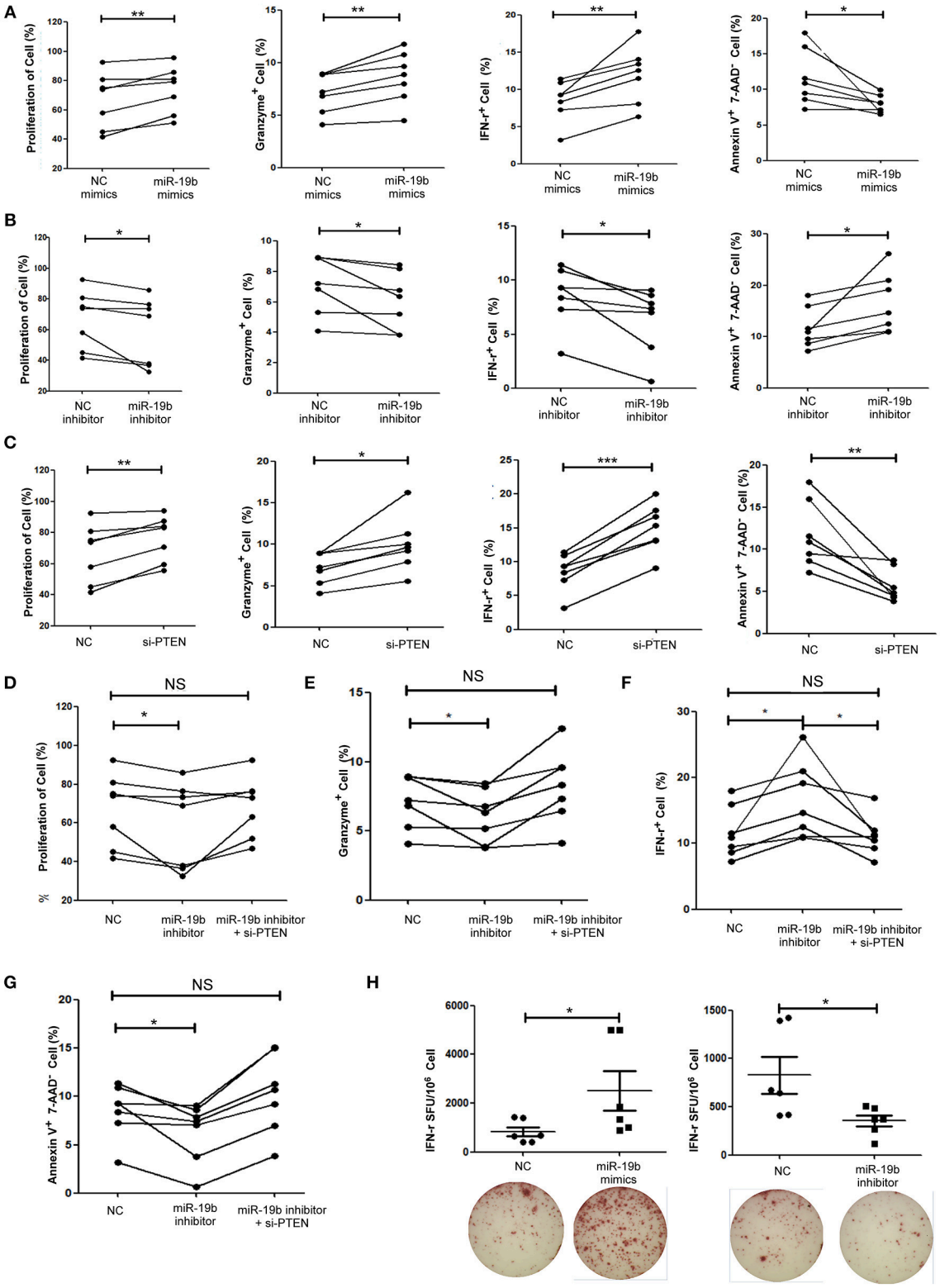

FIGURE 5 | miR-19b regulates CD8$^+$T cell function in HIV-infected patients. CD8$^+$ T cells from HIV-infected treatment-naive patients were sorted. **(A)** CD8$^+$ T cells were transfected with miR-19b mimics using Lipofectamine® RNAiMAX. After transfection (24 h), CD8$^+$ T cells were stimulated using anti-CD3/CD28 (3 μg/ml). Proliferation (day 5), intracellular expression of IFN-γ and granzyme B (day 1), and apoptosis (day 2) were compared between miR-19b-overexpressing CD8$^+$ T

(Continued)

FIGURE 5 | cells and controls. **(B)** $CD8^+$ T cells were transfected with miR-19b inhibitors using Lipofectamine® RNAiMAX. After transfection (24 h), $CD8^+$ T cells were stimulated using anti-CD3/CD28 (3 μg/ml). Proliferation (day 5), intracellular expression of IFN-γ and granzyme B (day 1), and apoptosis (day 2) were compared between miR-19b-overexpressing $CD8^+$T cells and controls. **(C)** The expression of PTEN was inhibited by introducing 20 μM PTEN siRNA to isolated $CD8^+$ T cells. Proliferation (day 5), intracellular expression of IFN-γ and granzyme B (day 1), and apoptosis (day 2) were compared between PTEN-inhibited $CD8^+$ T cells and controls. **(D–G)** $CD8^+$ T cells were transfected with a miR-19b inhibitor and PTEN siRNAs simultaneously. After transfection (24 h), $CD8^+$ T cells were stimulated using anti-CD3/CD28 (3 μg/ml). Proliferation **(D)**, apoptosis **(G)**, and intracellular expression of granzyme B **(E)** and IFN-γ **(F)** were compared. **(H)** $CD4^+$ T cells were depleted from PBMCs and transfected with miR-19b mimics or inhibitors. An IFN-γ ELISPOT assay was performed 24 h after transfection. Spot-forming units were compared between miR-19b-overexpressing/inhibited cells and controls. $n = 7$ for each group in **(A–G)**, $n = 6$ for each group in **(H)**. $^*P < 0.05$. $^{**}P < 0.01$. $^{***}P < 0.001$, respectively.

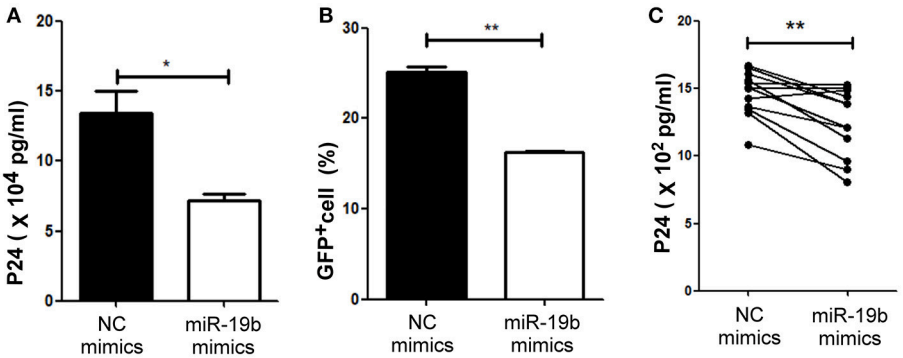

FIGURE 6 | miR-19b inhibits viral replication in *in-vitro* HIV-infected T cells. **(A)** Mimics of miR-19b and the pseudoviral plasmid NL4-3 were co-transfected into 293T cells and the level of P24 in the supernatants was measured through ELISA. **(B)** Clone-X cells were transfected with miR-19b mimics for 24 h and subsequently infected with vesicular stomatitis virus glycoprotein (VSV-G) pseudotyped HIV-1 (NL4-3) virus. GFP^+ cells were detected through flow cytometry 48 h after infection. **(C)** Primary $CD4^+$ T cells isolated from healthy controls were transfected with miR-19b mimics or controls. After transfection (24 h), the cells were stimulated using anti-CD3/CD28 (3 μg/ml). A cryopreserved primary HIV-1 isolate was added to the cells and the levels of p24 in the supernatants were measured after 3 days of infection through ELISA. $n = 12$ for each group in **(C)** $^*P < 0.05$. $^{**}P < 0.01$.

of secreted factors (41, 42). We assessed the role of miR-19b in maintaining low levels of virus through the regulation of $CD8^+$T cell function. Studies based on a lymphocytic choriomeningitis virus mouse model showed that knockout of the entire miR-17-92 cluster (miR-17, miR-18a, miR-19a, miR-20a, miR-19b, and miR-92a) impairs effector $CD8^+$ T cell proliferation. In contrast, overexpression of the entire cluster promotes effector $CD8^+$ T cell expansion and skews the differentiation of effector $CD8^+$T cells to terminal effector cells (43, 44). The function of miR-19b in human primary $CD8^+$T cells has not been determined. In this study, the data revealed the pro-proliferative and anti-apoptotic role of miR-19b in $CD8^+$T cells from both HCs and HIV-infected patients. These findings are consistent with data reported in mice (43, 44). In addition, we found that miR-19b significantly enhances the antiviral responses of $CD8^+$T cells (i.e., secretion of IFN-γ and granzyme B after stimulation of the anti-CD3/CD28). It is evident that miR-19b plays an important role in the regulation of $CD8^+$T cell responses against HIV. Through a bioinformatics analysis, we analyzed the cell signaling pathways involving miR-19b target genes and assessed the effect of PTEN downregulation on the function of miR-19b in $CD8^+$T cells. Previous studies have shown that miR-19b downregulates the expression of the target gene PTEN. However, the involvement of PTEN in the regulation of $CD8^+$T cell functions by miR-19b in HIV infection had not been investigated. This study confirmed that downregulation of PTEN antagonizes the effect of miR-19b inhibition on the function of $CD8^+$T cells in HIV patients, suggesting that PTEN is one of the targets of miR-19b in $CD8^+$T cells. Our results indicate that miR-19b influences the low viral loads in LTNP-Ls through the regulation of $CD8^+$T cells in HIV infection. Furthermore, we found that miR-19b directly inhibits viral production in *in-vitro* HIV-infected T cell lines and primary $CD4^+$T cells. Previous studies have shown that miR-19b inhibits the replication of hepatitis B virus (45, 46). However, its effect on the viral production of HIV has not been reported. Our study demonstrated that miR-19b inhibits the production of HIV in T cells. Previous study showed that overexpressing PTEN enhanced HIV-1 expression by inhibiting PI3K (47). We found that miR-19b was increased in LTNPs with sustained viral control. Because overexpression of miR-19b inhibits PTEN expression, we postulated that PTEN might be involved in the viral control by miR-19b in LNTP-Ls. Our study emphasized the need to further examine the mechanism of direct inhibition of HIV in detail. We found that the expression of miR-19b was decreased in sorted $CD8^+$T cells and $CD4^+$T cells in LTNP-Hs compared with that in LTNP-Ls. The current data highlighted the importance of miR-19b in HIV infection, promoting $CD8^+$T cell function and inhibiting viral production. These results provide potential targets for improved immune intervention.

In summary, this study provided the first comprehensive overview of the expression of miRNA in LTNP-Hs and LTNP-Ls. The investigation identified miR-19b as a highly expressed miRNA in LTNP-Ls, contributing to low viral load in LTNPs through promotion of $CD8^+$T cell function and inhibition of viral production. This study provides useful information for the exploration of new intervention paths in HIV infection.

AUTHOR CONTRIBUTIONS

HS, Z-NZ, and L-BY conceived and designed the experiments. L-BY performed the experiments. L-BY analyzed the data. C-BS, J-FZ, Y-JF, SQ, Y-JJ, J-JX, and H-BD contributed reagents, materials, and analysis tools. L-BY and Z-NZ wrote the article.

FUNDING

This study was supported by grants from the National Natural Science Foundation of China (81871708), Mega-Projects of National Science Research for the 12th Five-Year Plan (2012ZX10001-006) and the Mega-Projects of National Science Research for the 13th Five-Year Plan (2017ZX10201101). The authors wish to express their gratitude for the generosity of patients who participated in this study.

SUPPLEMENTARY MATERIAL

The Supplementary Material for this article can be found online at: https://www.frontiersin.org/articles/10.3389/fimmu.2018.03140/full#supplementary-material

REFERENCES

1. Sheppard HW, Lang W, Ascher MS, Vittinghoff E, Winkelstein W. The characterization of non-progressors: long-term HIV-1 infection with stable $CD4^+$ T-cell levels. *Aids* (1993) 7:1159–66.
2. Pantaleo G, Fauci AS. New concepts in the immunopathogenesis of HIV infection. *Annu Rev Immunol.* (1995) 13:487–512. doi: 10.1146/annurev.iy.13.040195.002415
3. Lambotte O, Boufassa F, Madec Y, Nguyen A, Goujard C, Meyer L, et al. HIV controllers: a homogeneous group of HIV-1-infected patients with spontaneous control of viral replication. *Clin Infect Dis.* (2005) 41:1053–6. doi: 10.1086/433188
4. Grabar S, Selinger-Leneman H, Abgrall S, Pialoux G, Weiss L, Costagliola D. Prevalence and comparative characteristics of long-term nonprogressors and HIV controller patients in the French Hospital Database on HIV. *Aids* (2009) 23:1163–9. doi: 10.1097/QAD.0b013e32832b44c8
5. Lambotte O, Delfraissy JF. HIV controllers: a homogeneous group of HIV-1 infected patients with a spontaneous control of viral replication. *Pathol Biol (Paris)* (2006) 54:566–71. doi: 10.1016/j.patbio.2006.07.035
6. O'Connell KA, Bailey JR, Blankson JN. Elucidating the elite: mechanisms of control in HIV-1 infection. *Trends Pharmacol Sci.* (2009) 30:631–7. doi: 10.1016/j.tips.2009.09.005
7. Deeks SG, Walker BD. Human immunodeficiency virus controllers: mechanisms of durable virus control in the absence of antiretroviral therapy. *Immunity* (2007) 27:406–16. doi: 10.1016/j.immuni.2007.08.010
8. Okulicz JF, Lambotte O. Epidemiology and clinical characteristics of elite controllers. *Curr Opin HIV AIDS* (2011) 6:163–8. doi: 10.1097/COH.0b013e328344f35e
9. Walker BD. Elite control of HIV Infection: implications for vaccines and treatment. *Top HIV Med.* (2007)15:134–6.
10. Saez-Cirion A, Pancino G, Sinet M, Venet A, Lambotte O. HIV controllers: how do they tame the virus? *Trends Immunol.* (2007) 28:532–40. doi: 10.1016/j.it.2007.09.002
11. Autran B, Descours B, Avettand-Fenoel V, Rouzioux C. Elite controllers as a model of functional cure. *Curr Opin HIV AIDS* (2011) 6:181–7. doi: 10.1097/COH.0b013e328345a328
12. Vigneault F, Woods M, Buzon MJ, Li C, Pereyra F, Crosby SD, et al. Transcriptional profiling of CD4 T cells identifies distinct subgroups of HIV-1 elite controllers. *J Virol.* (2011) 85:3015–9. doi: 10.1128/JVI.01846-10
13. Benito JM, Ortiz MC, Leon A, Sarabia LA, Ligos JM, Montoya M, et al. Class-modeling analysis reveals T-cell homeostasis disturbances involved in loss of immune control in elite controllers. *BMC Med.* (2018) 16:30. doi: 10.1186/s12916-018-1026-6
14. Grabar S, Selinger-Leneman H, Abgrall S, Pialoux G, Weiss L, Costagliola D. Loss of long-term non-progressor and HIV controller status over time in the French Hospital Database on HIV–ANRS CO4. *PLoS ONE* (2017) 12:e0184441. doi: 10.1371/journal.pone.0184441
15. van der Helm JJ, Geskus R, Lodi S, Meyer L, Schuitemaker H, Gunsenheimer-Bartmeyer B, et al. Characterisation of long-term non-progression of HIV-1 infection after seroconversion: a cohort study. *Lancet HIV* (2014) 1:e41–8. doi: 10.1016/s2352-3018(14)70016-5
16. Witwer KW, Watson AK, Blankson JN, Clements JE. Relationships of PBMC microRNA expression, plasma viral load, and $CD4^+$ T-cell count in HIV-1-infected elite suppressors and viremic patients. *Retrovirology* (2012) 9:5. doi: 10.1186/1742-4690-9-5
17. Huang J, Wang F, Argyris E, Chen K, Liang Z, Tian H, et al. Cellular microRNAs contribute to HIV-1 latency in resting primary $CD4^+$ T lymphocytes. *Nat Med.* (2007) 13:1241–7. doi: 10.1038/nm1639
18. Wang X, Ye L, Hou W, Zhou Y, Wang YJ, Metzger DS, et al. Cellular microRNA expression correlates with susceptibility of monocytes/macrophages to HIV-1 infection. *Blood* (2009) 113:671–4. doi: 10.1182/blood-2008-09-175000
19. Ahluwalia JK, Khan SZ, Soni K, Rawat P, Gupta A, Hariharan M, et al. Human cellular microRNA hsa-miR-29a interferes with viral nef protein expression and HIV-1 replication. *Retrovirology* (2008) 5:117. doi: 10.1186/1742-4690-5-117
20. Triboulet R, Mari B, Lin YL, Chable-Bessia C, Bennasser Y, Lebrigand K, et al. Suppression of microRNA-silencing pathway by HIV-1 during virus replication. *Science* (2007) 315:1579–82. doi: 10.1126/science.1136319
21. Mehta A, Baltimore D. MicroRNAs as regulatory elements in immune system logic. *Nat Rev Immunol.* (2016) 16:279–94. doi: 10.1038/nri.2016.40
22. O'Connell RM, Rao DS, Chaudhuri AA, Baltimore D. Physiological and pathological roles for microRNAs in the immune system. *Nat Rev Immunol.* (2010) 10:111–22. doi: 10.1038/nri2708
23. Kuerten S, Nowacki TM, Kleen TO, Asaad RJ, Lehmann PV, Tary-Lehmann M. Dissociated production of perforin, granzyme B, and IFN-gamma by HIV-specific CD8(+) cells in HIV infection. *AIDS Res Hum Retroviruses* (2008) 24:62–71. doi: 10.1089/aid.2007.0125
24. Nasi A, Chiodi F. Mechanisms regulating expansion of $CD8^+$ T cells during HIV-1 infection. *J Intern Med.* (2018) 283:257–67. doi: 10.1111/joim.12722
25. Liang Y, Pan HF, Ye DQ. microRNAs function in $CD8^+$T cell biology. *J Leukoc Biol.* (2015) 97:487–97. doi: 10.1189/jlb.1RU0814-369R
26. Swaminathan S, Kelleher AD. microRNA modulation of key targets associated with T cell exhaustion in HIV-1 infection. *Curr Opin HIV AIDS* (2014) 9:464–71. doi: 10.1097/COH.0000000000000089
27. Zwolińska K. Host genetic factors associated with susceptibility to HIV infection and progression of infection. *Postepy Hig Med Dosw.* (2009) 63:73–91.
28. Dey R, Soni K, Saravanan S, Balakrishnan P, Kumar V, Boobalan J, et al. Anti-HIV microRNA expression in a novel Indian cohort. *Sci Rep.* (2016) 6:28279. doi: 10.1038/srep28279
29. Reynoso R, Laufer N, Hackl M, Skalicky S, Monteforte R, Turk G, et al. MicroRNAs differentially present in the plasma of HIV elite controllers reduce HIV infection *in vitro*. *Sci Rep.* (2014) 4:05915. doi: 10.1038/srep05915

30. Egaña-Gorroño L, Escribà T, Boulanger N, Guardo AC, León A, Bargalló ME, et al. Differential MicroRNA expression profile between stimulated PBMCs from HIV-1 infected elite controllers and viremic progressors. *PLoS ONE* (2014) 9:e0106360. doi: 10.1371/journal.pone.0106360
31. Schmittgen TD, Livak KJ. Analyzing real-time PCR data by the comparative CT method. *Nat Protoc.* (2008) 3:1101–8. doi: 10.1038/nprot.2008.73
32. Zhu LY, Qiu C, Lv JX, Xu JQ. HIV-1 infection changes miRNA expression profile in the whole blood. *Bing Du Xue Bao* (2013) 29:323–9. doi: 10.13242/j.cnki.bingduxuebao.002394
33. Gupta A, Nagilla P, Le HS, Bunney C, Zych C, Thalamuthu A, et al. Comparative expression profile of miRNA and mRNA in primary peripheral blood mononuclear cells infected with human immunodeficiency virus (HIV-1). *PLoS ONE* (2011) 6:e22730. doi: 10.1371/journal.pone.0022730
34. Jia Z, Wang K, Zhang A, Wang G, Kang C, Han L, et al. miR-19a and miR-19b overexpression in gliomas. *Pathol Oncol Res.* (2013) 19:847–53. doi: 10.1007/s12253-013-9653-x
35. Wang F, Li T, Zhang B, Li H, Wu Q, Yang L, et al. MicroRNA-19a/b regulates multidrug resistance in human gastric cancer cells by targeting PTEN. *Biochem Biophys Res Commun.* (2013) 434:688–94. doi: 10.1016/j.bbrc.2013.04.010
36. Ventura W, Koide K, Hori K, Yotsumoto J, Sekizawa A, Saito H, et al. Placental expression of microRNA-17 and−19b is down-regulated in early pregnancy loss. *Eur J Obstet Gynecol Reprod Biol.* (2013) 169:28–32. doi: 10.1016/j.ejogrb.2013.01.025
37. Riley KJ, Rabinowitz GS, Yario TA, Luna JM, Darnell RB, Steitz JA. EBV and human microRNAs co-target oncogenic and apoptotic viral and human genes during latency. *EMBO J.* (2012) 31:2207–21. doi: 10.1038/emboj.2012.63
38. Mavrakis KJ, Wolfe AL, Oricchio E, Palomero T, de Keersmaecker K, McJunkin K, et al. Genome-wide RNA-mediated interference screen identifies miR-19 targets in Notch-induced T-cell acute lymphoblastic leukaemia. *Nat Cell Biol.* (2010) 12:372–9. doi: 10.1038/ncb2037
39. Groszer M, Erickson R, Scripture-Adams DD, Lesche R, Trumpp A, Zack JA, et al. Negative regulation of neural stem/progenitor cell proliferation by the Pten tumor suppressor gene *in vivo*. *Science* (2001) 294:2186–9. doi: 10.1126/science.1065518
40. Qi Y, Hu H, Guo H, Xu P, Shi Z, Huan X, et al. MicroRNA profiling in plasma of HIV-1 infected patients: potential markers of infection and immune status. *J Pub Health Emerg.* (2017) 1:65. doi: 10.21037/jphe.2017.05.11
41. Walker BD, Chakrabarti S, Moss B, Paradis TJ, Flynn T, Durno AG, et al. HIV-specific cytotoxic T lymphocytes in seropositive individuals. *Nature* (1987) 328:345–8. doi: 10.1038/328345a0
42. Levy JA. The search for the $CD8^+$ cell anti-HIV factor (CAF). *Trends Immunol.* (2003) 24:628–32. doi: 10.1016/j.it.2003.10.005
43. Wu T, Wieland A, Araki K, Davis CW, Ye L, Hale JS, et al. Temporal expression of microRNA cluster miR-17-92 regulates effector and memory $CD8^+$ T-cell differentiation. *Proc Natl Acad Sci USA*. (2012) 109:9965–70. doi: 10.1073/pnas.1207327109
44. Khan AA, Penny LA, Yuzefpolskiy Y, Sarkar S, Kalia V. MicroRNA-17–92 regulates effector and memory CD8 T-cell fates by modulating proliferation in response to infections. *Blood* (2013) 121:4473–83. doi: 10.1182/blood-2012-06-435412
45. Jung YJ, Kim JW, Park SJ, Min BY, Jang ES, Kim NY, et al. c-Myc-mediated overexpression of miR-17-92 suppresses replication of hepatitis B virus in human hepatoma cells. *J Med Virol.* (2013) 85:969–78. doi: 10.1002/jmv.23534
46. Ji F, Yang B, Peng X, Ding H, You H, Tien P. Circulating microRNAs in hepatitis B virus-infected patients. *J Viral Hepat.* (2011) 18:e242–51. doi: 10.1111/j.1365-2893.2011.01443.x
47. Cook JA, August A, Henderson AJ. Recruitment of phosphatidylinositol 3-kinase to CD28 inhibits HIV transcription by a Tat-dependent mechanism. *J Immunol.* (2002) 169:254–60. doi: 10.4049/jimmunol.169.1.254

Conflict of Interest Statement: The authors declare that the research was conducted in the absence of any commercial or financial relationships that could be construed as a potential conflict of interest.

frontiers in Immunology

ORIGINAL RESEARCH
published: 04 February 2019
doi: 10.3389/fimmu.2018.03110

Modeling the Function of TATA Box Binding Protein in Transcriptional Changes Induced by HIV-1 Tat in Innate Immune Cells and the Effect of Methamphetamine Exposure

*Ryan Tjitro[1], Lee A. Campbell[2], Liana Basova[1,3], Jessica Johnson[1], Julia A. Najera[1], Alexander Lindsey[3] and Maria Cecilia Garibaldi Marcondes[1,3]**

[1] Department of Neurosciences, The Scripps Research Institute, La Jolla, CA, United States, [2] LAC Intramural Research Program, National Institute on Drug Abuse, Baltimore, MD, United States, [3] San Diego Biomedical Research Institute, San Diego, CA, United States

OPEN ACCESS

Edited by:
Sara Gianella Weibel,
University of California, San Diego,
United States

Reviewed by:
Mudit Tyagi,
Thomas Jefferson University,
United States
Nazira El-Hage,
Florida International University,
United States

***Correspondence:**
Maria Cecilia Garibaldi Marcondes
cmarcondes@SDBRI.org

Specialty section:
This article was submitted to Viral Immunology, a section of the journal Frontiers in Immunology

Received: 08 August 2018
Accepted: 17 December 2018
Published: 04 February 2019

Citation:
Tjitro R, Campbell LA, Basova L, Johnson J, Najera JA, Lindsey A and Marcondes MC (2019) Modeling the Function of TATA Box Binding Protein in Transcriptional Changes Induced by HIV-1 Tat in Innate Immune Cells and the Effect of Methamphetamine Exposure. Front. Immunol. 9:3110. doi: 10.3389/fimmu.2018.03110

Innate immune cells are targets of HIV-1 infection in the Central Nervous System (CNS), generating neurological deficits. Infected individuals with substance use disorders as co-morbidities, are more likely to have aggravated neurological disorders, higher CNS viral load and inflammation. Methamphetamine (Meth) is an addictive stimulant drug, commonly among HIV+ individuals. The molecular basis of HIV direct effects and its interactions with Meth in host response, at the gene promoter level, are not well understood. The main HIV-1 peptide acting on transcription is the transactivator of transcription (Tat), which promotes replication by recruiting a Tata-box binding protein (TBP) to the virus long-terminal repeat (LTR). We tested the hypothesis that Tat can stimulate host gene expression through its ability to increase TBP, and thus promoting its binding to promoters that bear Tata-box binding motifs. Genes with Tata-box domains are mainly inducible, early response, and involved in inflammation, regulation and metabolism, relevant in HIV pathogenesis. We also tested whether Tat and Meth interact to trigger the expression of Tata-box bearing genes. The THP1 macrophage cell line is a well characterized innate immune cell system for studying signal transduction in inflammation. These cells are responsive to Tat, as well as to Meth, by recruiting RNA Polymerase (RNA Pol) to inflammatory gene promoters, within 15 min of stimulation (1). THP-1 cells, including their genetically engineered derivatives, represent valuable tools for investigating monocyte structure and function in both health and disease, as a consistent system (2). When differentiated, they mimic several aspects of the response of macrophages, and innate immune cells that are the main HIV-1 targets within the Central Nervous System (CNS). THP1 cells have been used to characterize the impact of Meth and resulting neurotransmitters on HIV entry (1), mimicking the CNS micro-environment. Integrative consensus sequence analysis in genes with enriched RNA Pol, revealed that TBP was a major transcription factor in Tat stimulation, while the co-incubation with Meth shifted usage to a distinct and diversified pattern. For validating these findings, we engineered a THP1 clone to be deficient in the expression of all major

TBP splice variants, and tested its response to Tat stimulation, in the presence or absence of Meth. Transcriptional patterns in TBP-sufficient and deficient clones confirmed TBP as a dominant transcription factor in Tat stimulation, capable of inducing genes with no constitutive expression. However, in the presence of Meth, TBP was no longer necessary to activate the same genes, suggesting promoter plasticity. These findings demonstrate TBP as mechanism of host-response activation by HIV-1 Tat, and suggest that promoter plasticity is a challenge imposed by co-morbid factors such as stimulant drug addiction. This may be one mechanism responsible for limited efficacy of therapeutic approaches in HIV+ Meth abusers.

Keywords: HIV, Tat, Methamphetamine, TATA-box, TATA-box binding peptide, Crispr/Cas9, macrophages, inflammation

INTRODUCTION

The infection with the Human Immunodeficiency Virus (HIV) triggers inflammatory pathogeneses in several tissues (3), including in the Central Nervous System (CNS) (4). Inflammation in the brain and cognitive deficits can be significantly aggravated upon the co-morbid use of addictive substances, such as Methamphetamine (Meth), which impair the success of antiretroviral therapies and increase viral load specifically in the brain (5, 6). The Meth-induced aggravation of HIV—induced CNS deficits, inflammatory response, and brain viral load, have been replicated in non-human primate models of neuroHIV (5, 7, 8). Of the HIV-1 peptides, the trans-activator of transcription (Tat) is the only one that is secreted across the plasma membrane (9–12), affecting neighboring cell types. *In vivo*, HIV-Tat is linked to impaired learning and memory, and gray matter deficits (13, 14), suggesting its involvement in HIV-associated neurological disorders (HAND). In a mouse model of neuroHIV, the induction of Tat in CNS glial cells enhances behaviors associated with Meth exposure, while contributing to changes in microglial activation and in the expression of neurotransmitter receptors (15).

In the brain, innate immune cells, microglia and macrophages, are targets of HIV infection. The main role of the HIV Tat peptide is maintaining viral transcription by activating the viral promoter, located within the 5′ long terminal repeat (LTR) of the integrated viral genome. In that process, the virus gains the ability to hijack the host cell RNA polymerase II (RNA Pol II) machinery for initiating viral transcription. In previous experiments, we observed that the SIV infection in rhesus macaques, which is a model of neuroHIV, causes a strong upregulation of TATA-box binding peptide (TBP) and components of the transcription initiation complex in brain microglia, suggesting that a mechanism of gene transcription that involves TATA box may be stimulated by the infection.

HIV-1 proviral transcription starts with the binding of cellular factors, such as NF-κB and Sp1, as well as the TATA box binding protein (TBP), which is a key component for recruiting RNA Pol II to the LTR. This complex allows the production of viral transcripts, which are then spliced and translated. Epigenetic and other limiting host factors, as well as the level of cellular activation, can potentially regulate such process. Tat binds to the trans-activator response (TAR) element hairpin at the 5′ end of viral RNA transcripts (16–19), and to the apical loop, to which the transcriptional elongation factor pTEFb binds in a Tat-dependent manner (20, 21). Upon TAR binding, the kinase component of pTEFb, cyclin-dependent kinase 9 (CDK9), can phosphorylate the C-terminal domain of RNA Pol II (21, 22). The pTEFb also directs the recruitment of TATA box binding protein (TBP) to the LTR, stimulating the assembly of new transcription complexes (23). Core promoter elements participate in the initiation factor TFIID complex, where TBP works as an anchor for TBP-associated factors (TAFs) 4–12 (24). The TFIID complex then makes contact with acidic activator proteins such as Sp1 and the initiator, while TBP recognizes the TATA box. Thus, TBP is a key element in the ability of Tat to recruit the host transcriptional machinery in favor of viral transcription.

The activation of the LTR-directed gene expression by Tat has been observed in CNS-derived cells, and in astrocytic glial cell lines (25). Importantly, it has been demonstrated that this can happen in the absence of a TAR element (25), suggesting that alternative mechanisms may exist. Importantly, HIV Tat can strongly upregulate inflammatory cytokines in the brain, *per se* mimicking aspects of the inflammatory outcomes observed in HIV infection (26, 27). In addition, it has been demonstrated that the ability of Tat to initiate transcription of heterologous genes through the TATA-box element can happen in the absence of any HIV-1 sequence, through mechanisms that are similar to DNA sequence-specific transcription factors (28, 29). This suggests that HIV-1 Tat may have the ability to enhance genes that present a TATA-box promoter element. While the HIV Tat peptide *per se* has the ability to stimulate a diversity of genes, both *in vivo* (15, 26, 27, 30), and *in vitro* (31–37), the contribution of the TATA-box promoter element to upregulated heterologous transcripts has not been examined.

The TATA box is the most well-studied core promoter element. The canonical TATA-box sequence, TATAAAA, may be variable in natural promoters (38, 39). Methodologies to estimate the frequency of TATA box-containing promoters also vary. As a result, there is a wide-range of estimates of how many genes have a Tata-box promoter motif [revised by (40)]. It is most accepted that the TATA-containing promoters make up only 10–16% of the genes read by RNA Pol II, of which only 30% contain the canonical TATA box (41). Systematic analysis of genes that

bear this promoter element has pointed to specific biological processes, associated to organogenesis and morphogenesis, with an impact in early development, but also has found a second largest contribution to responses to stimulus and to stress, as well as to defense, supporting the role of TATA-box mediated transcription in the elevation of early-response, immune and inflammatory genes. TATA-less promoters, on the other hand, tend to be involved in basic biological maintenance processes, or be constitutively expressed (40, 42).

Here, we have examined the hypothesis that the HIV-1 Tat protein has the property of increasing inflammatory cytokines in innate immune cells through favoring a TATA box-supported mechanism, and that this mechanism may be enhanced by Meth exposure. Using the THP1 innate immune cell line system, we show evidence that the TATA box-binding transcription factor TBP is increased by HIV-1 Tat, along with the recruitment of RNA PolII to promoters of genes that bear the TATA-box promoter. We also show that this effect is enhanced when HIV-1 Tat is combined with Meth.

The lack of TAR in host gene promoters argues against a direct interaction between TBP and Tat. Yet, binding of HIV Tat to the host chromatin has been described in T cells (43), where it functions through master transcriptional regulators bound at promoters and enhancers, rather than through cellular "TAR-like" motifs, to both activate and repress gene sets sharing common functional annotations (44). The functional interaction between HIV-1 Tat and TBP has been proposed in different models (29, 45, 46). In our system, we have not tested whether Tat plays a role at bridging TBP and its binding motifs, or whether Tat just activates TBP as major transcription factor in the innate immune environment. However, we have found evidence that Tat is able to translocate to the nucleus soon after cell exposure.

We have developed a strategy to test the hypothesis of TBP as a major transcription factor in the activation of TATA-box-bearing inflammatory genes by HIV Tat *in vitro*, by engineering a THP1 cell line with impaired transcription of TBP dominant splice variants. As a result, we produced a human innate immune cell line with a deficient expression of TBP protein. In that cell line, we have found that TBP was critical for the upregulation of genes stimulated by HIV Tat, including inflammatory molecules. Yet, in the presence of Meth, alternative transcriptional factors positively enhanced a significant fraction of genes with TATA box motifs, bypassing the TBP disruption.

Our findings demonstrate that TBP is indeed a critical transcription factor in Tat-induced host responses that can result in pathogenesis, but co-morbidities such as the stimulant drug Meth, can increase the transcriptional complexity and promoter plasticity, downgrading the central role of TBP in inflammation.

MATERIALS AND METHODS

THP1 Cell Culture

THP-1 cells were obtained from ATCC (TIB-202). They were maintained in RPMI 1640 containing 2 mM glutamine; 10 mM HEPES; 1 mM sodium pyruvate; 4.5 g/L glucose; 1.5 g/L sodium bicarbonate; 0.05 mM beta2 mercaptoethanol, as well as 10% heat inactivated fetal bovine serum (Hyclone), and 100 ug/ml Pen/Strep.

In vitro Treatments With HIV-1 Tat and With Meth

For treatments, the THP1 cells were plated at 2×10^6 cells/well in 12 well plates, containing 2 ml per well. The HIV-1 IIIB Tat Recombinant Protein (MW: 14,000) was obtained from the NIH AIDS Reagent Program. The doses used were 1–100 ng/ml for Western Blots, and 10 ng/ml for all the other assays. Meth was used at 60 μM, following previously optimized protocols, and for mimicking abuse concentrations in plasma (47). The cells were treated with either Vehicle, HIV-1 Tat, Meth, or HIV-1 Tat and Meth. The concentrations of Tat in culture were 1, 10, and 100 ng/ml. The concentrations of Meth were 30 μM, 60 μM (shown in Figures), and 120 μM, which produced similar results regarding the lack of TBP induction. The cells were then harvested 15 min after exposure for ChIP assays, and 2 h for Western blots, RNA-seq and validations. These time points were selected following a time-course that demonstrated that epigenetic events that result directly from Tat and/or Meth, and not from factors produced by the cells as a result from the stimulation, are detectable in 15 min. Yet, a 2 h period is necessary for confirming productive events at the transcriptional and protein level. All experiments were performed at least 3 times, in triplicate, otherwise stated in the figure legend.

Western Blots

The cells treated as described were centrifuged at 2,500 g for 5 min, and the pellets were washed twice in PBS, and in 0.5% Triton X buffer, for isolation of nuclear fraction, before being resuspended in RIPA buffer (Thermofisher), added 1 mini tablet Complete (Roche protease inhibitors) for protein extraction. Western blots for detection of TBP and TAF9 were performed by loading 20 μg of whole cell lysates and 5 μl of PageRuler Plus Prestained Protein Ladder (Thermofisher) per well, onto a Mini-Protean TGX 4–20% pre-cast gel (Biorad). Proteins were transferred to a nitrocellulose membrane using a G2 Blotter, and blocked with 5% Casein in TBST for 1 h at room temperature. The N-terminus of the TATA binding protein (TBP) was detected at 36–38 kD using a TBP monoclonal antibody (1TBP18/ MA1-189) at a dilution of 1:1,000. TATA box associated factor 9 (TAF9) was detected at ∼20 kD using a polyclonal antibody (PA5-40919), at 1:1,000. Both antibodies were incubated overnight at 4oC on a rocking platform, followed by a Goat anti-Mouse IgG (H+L) HRP conjugate (Cell Signaling) for 1 h at room temperature. Chemiluminescent detection was performed using SuperSignal Pico substrate (Thermofisher).

TBP and Tat Nuclear Translocation

The THP1 cells were brought to the concentration of 10^6/ml and stimulated with 50 nM of phorbol-12-myristate-13-acetate (PMA) for 24 h for differentiation, prior to the stimulation with Meth (30 or 60 μM), and/or HIV Tat (10 ng/ml). The cells were fixed with 4% paraformaldehyde, 5, 15, 30, and 60 min following stimulation, and then were washed with PBS. The wells were then treated with PBS containing 0.1% Triton

X-100 for 20 min at room temperature, rinsed 3 times with PBS, and then blocked with 5 g/l Casein (Sigma Aldrich) in PBS, containing 0.5 g/l Thimerosal (Sigma Aldrich) for 1 h at room temperature. The primary antibody against TBP was a rabbit polyclonal (HPA049805, Sigma Aldrich), and the antibody anti-Tat peptide was obtained through the NIH AIDS Reagent Program, Division of AIDS, NIAID, NIH: Anti-HIV-1 Tat Monoclonal (15.1) from NIAID, DAIDS (cat# 1974). Both antibodies were diluted in blocking solution, and then placed overnight, at 4°C, with gentle rotation. Then cells were rinsed 3 times for 10 min with 1% blocking solution in PBS, containing 0.1% Triton-X, followed by incubation with a secondary AlexaFluor 647-labeled anti-rabbit or anti-mouse IgG (Thermo Fisher Scientific), for 2 h at room temperature, in the dark. After rinsing, 4′, 6-Diamidino-2-Phenylindole, Dihydrochloride (DAPI) was diluted to 300 ng/ml in 1% blocking solution for 2 min, in the dark. Cells were rinsed and maintained in PBS, and observed in a Nikon A1R laser-scanning confocal mounted onto a Nikon inverted Ti-E scope (Nikon, Melville, NY), and with a 20x PlanApo objective, 0.8NA (Nikon) and Images were acquired using a NIS-Elements C software (Nikon). Fluorescence intensity was normalized against background (secondary antibody only). Image analysis was performed in Fiji/ImageJ (National Institute of Health, USA). For that, tiff image files from separate channels were opened, transformed into 32-bit images, and manually thresholded to identify DAPI nuclei, and stained cells. A binary mask was obtained from the negative thresholded DAPI image and subtrated from the total transcription factor stained area. The translocation index was calculated as percentage of the total transcription factor stained measurement values that is co-localized within the nuclear area, and derived from the difference between total and nuclear staining. The colocalization was further confirmed in calculated images where 32-bit thresholded channels were averaged.

Fixation for Chromatin Immunoprecipitation

The cells were fixed with a 1.1% Formaldehyde (Sigma Aldrich F-8775), and molecular grade 0.01 M NaCl, 0.1 mM EDTA pH 8, 50 mM HEPES pH 7.9, in H_2O. The plate was then agitated on a titer plate shaker for exactly 15 min at room temperature. The fixation was then interrupted with 125 mM Glycine (Sigma Aldrich G-7403). The samples were let set at room temperature for 5 min. After the glycine incubation, the cells were transferred to conical 15 ml tubes and kept on ice for the remainder of the procedure. The tubes were centrifuge at 800 × g at 4°C for 10 min, the supernatants were removed and the cells were resuspended in 10 ml ice-cold PBS-Igepal (PBS containing 0.5% Igepal CA-630 (Sigma Aldrich I-8896) per tube, by pipetting up and down. The tubes were centrifuged again as before, and pellets were again resuspended in 10 ml PBS-Igepal. Then, 100 µl from a PMSF stock (100 mM in ethanol) was added to each tube for a final concentration of 1 mM. The tubes were centrifuged a third time to pellet the cells, and the supernatant was completely removed from cell pellets. The pellets were snap-frozen on dry ice and store at −80°C, until further procedures. The pellets were sonicated and the DNA sheared to an average length of 300–500 bp. Genomic DNA (input) was prepared by treating aliquots of chromatin with RNase, proteinase K, and heat (65°C) to reverse cross-linking, followed by phenol and chloroform extractions and ethanol precipitation. Pellets were resuspended in 10 mM Tris, 1 mM EDTA, and the resulting DNA was quantified on a Nanodrop spectrophotometer (Thermo Fisher Scientific, Chicago, IL). Results were used to calculate the total chromatin yield.

Chromatin Immunoprecipitation (ChIP) of RNA Pol II

RNA Pol II ChIP reactions were performed using 30 µg of human THP1 cell chromatin and 4 µg of antibody anti-RNA Pol II (Abcam, ab5095). Positive control primers (b-Actin and GAPDH) as well as negative control primer pairs were used to amplify regions in a gene desert on chromosome 12 and 4 (Untr12, Untr4) by qRT-PCR. Signals for RNA Pol II were strong, with enrichments of the best positive control signal over background up to 99-fold. For the library generation and sequencing, 50-nt sequence reads identified using Illumina's Hi-Seq, were mapped to the genome using the BWA algorithm with default settings. Alignment information to Human Hg19 for each read was stored in BAM format. Only reads that passed the purity filter, aligned with no more than 2 mismatches, and mapped uniquely to the genome were used in the subsequent analysis. Duplicate reads were removed. Since the 5′-ends of the aligned reads (= "tags") represent the end of ChIP/IP-fragments, the tags were extended *in silico* (using Active Motif software) at their 3′- ends to a length of 150–250 bp. To estimate the density, the genome was divided into 32-nt bins and the number of fragments in each bin was determined, to provide a "signal map"; histograms of fragment densities were stored in both a BAR file, for viewing in Integrated Genome Browser (IGB), and bigWig file, uploaded to the UCSC Genome Browser. BAR/bigWig files also provide the peak metrics in the Active Motif analysis program as described below. Intervals, describing genomic regions with local enrichments in tag numbers, were defined by the chromosome number, a start and end coordinates. SICER (48) was used to study RNA polymerase II binding to extended regions in the genome, by looking for significant enrichments in the ChIP/IP data file when compared to the Input data file (random background), and also for examining transcription factor binding sites using TRANSFAC Match weight matrix (49, 50). Peaks and false positives were estimated by thresholding of the BAR files. In the default analysis, the tag number of all samples is reduced (by random sampling) to the number of tags present in the smallest sample. Only Input/IgG control peaks that overlapped with Intervals in the ChIP/IP data were used in the analysis. After defining the Intervals and Active Regions, their genomic locations, their proximities to gene annotations, and other genomic features, were determined.

ChIP Analysis

Genes with RNA Pol II peaks found within 10 kb of start/end were compared in the ChIP samples. Overlap between the samples was high (70–90% in pairwise comparisons), reflecting

the fact that the majority of gene transcription does not change. There were 4,865 active genomic regions that presented overlapping intervals from all conditions. Active regions were identified for the comparison of all samples, and the peak metrics was used in combination with the present/absent peak call information to find genomic regions with RNA Pol II occupancy patterns of interest. Ratios of treated samples compared to their respective controls were used to average signal values (>1.5-fold change) and to perform transcription factor and pathway analysis using TRANSFAC, iRegulon and Genemania in Cytoscape, and iPathwayGuide. Regions of Pol II enrichment in ChIP-Seq data often did not correlate perfectly with the gene annotations. Typically, a stronger peak was seen at the transcription start site (TSS/promoter), and high enrichments were often seen extending into downstream regions. Therefore, the average fragment densities for 25,143 human genes (from TSS to termination site) and the corresponding promoters (from −1,000 to +1,000 nt relative to TSS) were determined. The values between different gene promoters were comparable because they were based on a 2,000 bp segment. Peak values that were found in gene bodies were corrected by length. **Table 1** shows the total number of reads sequenced and their alignment to the human genome (hg19). For the analysis, the data files were normalized to the same number of unique alignments without duplicate reads, which was 16 million. Intervals were determined using the SICER algorithm at a cutoff of FDR1E-10 and a Gap parameter of 600 bp (which merges peaks located within 600 bp of each other). Gene intervals (peaks) were determined using the SICER algorithm at a cutoff of FDR1E-10 and a Gap parameter of 600 bp (which merges peaks located within 600 bp of each other into a single "island"). The number of intervals identified ranged from 9,775 in Meth-treated cells to 14,124 in cells treated with both Meth and Tat, within 10 kb of start/end. The overlap between the samples was high (70–90% in pairwise comparisons), reflecting the fact that the majority of gene transcription does not change. At 4,865 genomic regions, all conditions showed overlapping intervals. Because RNA Pol II- enriched regions are not typical bell- shaped, symmetrical peaks, average signal values were used in the analysis, and for estimating the ratios between each treatment condition and controls, and in additional pairwise comparisons. Regions of RNA Pol II enrichment in ChIP-Seq data did not correlate perfectly with the gene annotations, but as expected, stronger peaks were typically seen at the transcription start site (TSS/promoter), and high enrichments are often seen extending into the downstream region. Thus, the tag densities/signal metrics relative to the known gene annotation were examined. In this analysis, the average fragment densities for 25,143 human genes (from TSS to termination site) and the corresponding 25,143 human promoters (from −1,000 to +1,000, relative to TSS) were determined. The values between different gene promoters were comparable since they were based on a 2,000 bp segment.

Production of TBP-Knock Out THP1 Clone by CRISPR/Cas9

A template for disruption of the TBP gene (ENST00000412512, NM001172085) was established following described methods (51–54), and based on the conserved protein coding sequence in 8 detected splice variants (ENST00000423353.1, 703 bp). Primers for detection of human TBP and GAPDH by SyBrGreen qRT-PCR were purchased from Qiagen (Germantown, MD). A guide sequence was designed in http://crispr.mit.edu/guides, by introducing the FASTA sequence of the TBP coding region onto the target human genome (h19). Twenty-six high score guide sequences targeting exon 1 coding region mapped to the correct transcript, from which one was selected for oligo synthesis (sgTBP#1.1 AGCCTGCCACCTTACGCTCA), by Integrated DNA Technologies (San Diego, CA). For nickase Cas9, gRNA left GATAGGGATTCCGGGAGTCA, and gRNA right CCAATGATGCCTTATGGCAC were selected. Using the protein coding sequence data from ENSEMBLE and the designed gRNAs from the CRISPR database, the guide binding pattern was mapped out, identifying 5 out of 7 total wild-type gRNA targets transcripts, and 6 out of 7 nickase gRNA targets, with 0 off targets. The gRNAs and the Cas 9 protein were put into a plasmid for expression, using a GFP tag for assessing efficiency and selecting positively transfected cells by flow cytometry. For that, we used the CRISPR/Cas9 gesicle technology (55), with Guide-It CRISPR/Cas9 gesicle system (Clontech, Mountain View, CA). First, the oligos were annealed and cloned into pGuide-it-sgRNA1 vector, following manufacturer's protocols. Positive colonies were picked and expanded in LB, and plasmid DNA was isoladed using NucleoBond Xtra Midi (Clontech), and sequencing analysis was performed by Eton Bioscience Inc (San Diego, CA), using provided Guide-it sequencing primer 1. The gesicle-producing 293T cell line (Clontech) was expanded in DMEM with high glucose (4.5 g/l) (Genesee, San Diego, CA), 4 mM L-glutamine, and sodium bicarbonate, 10% fetal bovine serum Hyclone (GE Healthcare Lifesciences, Pittsburgh, PA), and 1% Penicilin/Streptomycin (Genesee), and split using Trypsine-EDTA (Sigma-Aldrich). These cells were seeded in 10-cm tissue culture dishes treated with poly-L-Lysine (Corning).

TABLE 1 | Number of sequenced reads and their alignment to the human genome (hg19).

	Control	Meth	Tat	Meth + Tat	Pooled Input
Total number of reads	35,582,719	36,449,122	23,742,921	40,019,315	35,838,803
Total number of alignments	32,594,991	34,255,959	21,211,764	36,906,854	34,240,934
Unique alignments (-q 25)	27,536,469	28,943,392	17,774,903	31,197,538	28,385,207
Unique alignments (without duplicate reads)	22,337,553	24,631,143	15,956,453	27,319,946	25,642,285
Normalized	15,956,453	15,956,453	15,956,453	15,956,453	15,956,453

Then 10 μg of plasmids encoding for sgRNA mixed to a plasmid containing Cherry picker red fluorescence, and the Cas9 enzyme were applied to the 293T cells, following manufacture's protocols. The A/C heterodimerizer ligand was added to the cultures for driving active loading of the Cas9/sgRNA complex into gesicles. A similar procedure, using Cas9 without the sgRNA was performed for producing "empty" gesicles, used for control conditions. Seventy-two hours after that, transfected cells were visualized due to Cherry picker red fluorescence. The cell media was harvested, and centrifuged overnight at 8,000 × g in a Beckman J2-HS centrifuge, with a JS 7.5 swinging rotor, and the pellet was concentrated to ∼100 μl final volume in PBS. The gesicles were placed at 4°C on a rocking platform for 2 h, and stored in aliquots at −80°C until ready for treating THP1 cells. The cells were resuspended in protamine medium (containing 8 μg/ml protamine sulfate, Sigma), plated at 2×10^5 cells/ well in 500 μl, in 24 well plates, and 30 μl of gesicles were added. The plates were centrifuged at 1,150 × g for 30 min at room temperature. The plates were incubated at 37°C overnight, and then positively transfected cells were visualized under a fluorescence-microscope for detection of intracellular red fluorescence signal originated from the Cherry Picker reporter on the gesicle surface. The Cherry Picker-positive cells from each positive well were washed in HBSS without phenol red, containing 10% fetal bovine serum, 1% penicillin/streptomycin, and resuspended in this buffer for sorting using a BD FACSJazz (BD Biosciences, San Diego, CA). Sorted positive cells were expanded into clones (1A, 1B, 2A, 2B, 2C, and 8), for at least 7 days before testing the TBP mutation. The detection of the TBP mutation was tested using DNA hybridization with Guide-It Resolvase (Clontech), on the gel-purified TBP band, amplified from QIAmp-extracted genomic DNA (Qiagen), and following manufacturers' protocols. The TBP gene was amplified with primers 5′ GAGTTCCAGCGCAAGGGTT forward, and 5′ TTTTGCAGCTGCGGTACAAT, using Phusion High Fidelity DNA Polymerase (New England Biolabs, Ipswich, MA), following manufacture's protocol, to generate two fragments, one 63 bp and one 465 bp, visualized on 2% agarose gel. Clone 2A presented efficient TBP mutagenesis and was used for the comparison with control clone C, which was generated as above, but with empty gesicles. Clone 1A had poor mutagenesis, and was used in some experiments as a control in addition to clone C. The TBP gene disruption was further tested at the mRNA level, which was extracted from cell pellets using RNeasy Mini kit (Qiagen), and reverse-transcribed with Superscript II (Thermo Fisher). The presence or absence of the TBP transcript confirmed the efficacy of CRISPR/Cas9 to disrupt the TBP gene (**Figure 4**).

Treatment of TBP-Mutant Clone 2A and TBP-Sufficient Clone C

The TBP-deficient clone 2A and control clone C were expanded in RMPI 1640, containing 10% fetal bovine serum (Hyclone), 1% penicillin/streptomycin, and 25 mM HEPES (Invitrogen). The cells were plated in 24-well plates at 2×10^6 cell/ml, and then stimulated with 10 ng/ml of HIV-1 IIIB Tat Recombinant Protein (NIH AIDS Reagent Program), 30 or 60 μM of Meth, or both HIV-1 Tat and Meth together. The cells were then harvested 2 h after stimulation, and RNA-seq was performed.

RNA-Seq Protocol

RNA was isolated from TBP-deficient THP1 clone 2A, and TBP-sufficient control clone C using the RNeasy Mini Kit (Qiagen) with on-column DNAse I treatment. quantified using Qubit 2.0 Fluorometer (Life Technologies, Carlsbad, CA, USA). The eluted RNA had a 260/280 of greater than 1.8. RNA integrity was checked with Agilent TapeStation (Agilent Technologies, Palo Alto, CA, USA). RNA samples were quantified using Qubit 2.0 Fluorometer (Life Technologies, Carlsbad, CA, USA) and RNA integrity was checked with Agilent TapeStation (Agilent Technologies, Palo Alto, CA, USA). RNA library preparation, sequencing reaction, and bioinformatics analysis were conducted at GENEWIZ, LLC. (South Plainfield, NJ, USA). RNA sequencing library preparations used the NEBNext Ultra RNA Library Prep Kit for Illumina by following manufacturer's recommendations (NEB, Ipswich, MA, USA). Briefly, mRNA was first enriched with Oligod(T) beads. Enriched mRNAs were fragmented for 15 min at 94°C. First strand and second strand cDNA were subsequently synthesized. cDNA fragments were end repaired and adenylated at 3′ends, and universal adapter was ligated to cDNA fragments, followed by index addition and library enrichment with limited cycle PCR. The sequencing libraries were validated on the Agilent TapeStation (Agilent Technologies, Palo Alto, CA, USA), and quantified by using Qubit 2.0 Fluorometer (Invitrogen, Carlsbad, CA) as well as by quantitative PCR (Applied Biosystems, Carlsbad, CA, USA). The sequencing libraries were clustered on one lane of a flowcell. After clustering, the flow-cell was loaded on the Illumina HiSeq instrument according to manufacturer's instructions. The samples were sequenced using a 2 × 150 Paired End (PE) configuration. Image analysis and base calling were conducted by the HiSeq Control Software (HCS). Raw sequence data (.bcl files) generated from Illumina HiSeq was converted into fastq files and de-multiplexed using Illumina's bcl2fastq 2.17 software. One mismatch was allowed for index sequence identification. After investigating the quality of the raw data, sequence reads were trimmed to remove possible adapter sequences and nucleotides with poor quality using Trim Sequences Module in CLC Genomics Workbench 9.0.1. The trimmed reads were mapped to the Homo sapiens GRCh38 reference genome available on ENSEMBL using the RNA-Seq Analysis Module in CLC Genomics Workbench 9.0.1. BAM files, Unique gene hit counts and Unique transcript hit counts were generated as a result of this step. After extraction of gene and transcript hit counts, the hit counts tables were used for downstream differential expression analysis. Using Kal's test, a comparison of gene expression between the groups of samples was performed. The Kal's test was used to generate p-values and Log2 fold changes. Genes and transcripts with adjusted p-values < 0.05 and absolute log2 fold changes > 1 were called as differentially expressed genes and transcripts, respectively, for each comparison. A gene ontology analysis was performed on the statistically significant set of genes by implementing the Hyoergeometric tests in CLC Genomics Workbench 9.0.1. The goa human GO list

was used to cluster the set of genes based on their biological process and determine their statistical significance. Sequencing performance was assessed for total number of aligned reads, total number of uniquely aligned reads, and genes detected. All gene counts were then imported into the R/Bioconductor package EdgeR and TMM normalization size factors were calculated to adjust for samples for differences in library size, and then imported into R/Bioconductor package Limma. Performance of the samples was assessed with a Spearman correlation matrix. Weighted likelihoods based on the observed mean-variance relationship of every gene and sample were calculated with the voom WithQualityWeights function and gene performance was assessed with plots of residual standard deviation of every gene to their average log-count with a robustly fitted trend line of the residuals. Generalized linear models were created to test for gene level differential expression, and the results were displayed with FDR p-values $\leq$ 0.05 and log 2-fold-changes greater than an absolute value of 2, in each given comparison.

Expression Data Analysis

Using the Cytoscape interface platform, Mentha and Biogrid were used for building a network, using transformed fold change and FDR corrected p-values as attributes to visualize the effects of TBP deficiency in changes caused by 2 h of stimulation with HIV Tat, in the presence or absence of Meth. BinGO was used to estimate pathways affected in cells that were engineered to lack TBP expression, following stimulation.

RESULTS

TBP Is Activated and Translocated by HIV-1 Tat in Human THP1 Macrophages

In order to test the hypothesis that the HIV-1 Tat may utilize a TATA-box mediated mechanism, which may be involved in the ability of that protein to activate transcription of inflammatory genes that have a TATA-box promoter domain, we used a human macrophage cell line, THP1. These cells can activate the TBP protein when treated with 10 and 100 ng of the HIV-1 Tat peptide for 2 h, but not with 1 ng (**Figure 1**). Meth alone did not activate TBP at any concentration, but when combined with Tat, there was a detectable increase (**Figure 1**). The optimal concentration of Tat for activation of TBP was 10 ng/ml, which was the concentration maintained throughout the experiments. Other components of the TFIID complex, such as TAF9, were increased by Tat, with or without Meth, but not by Meth alone (**Figure 1**).

We tested the ability of Tat and Meth to translocate TBP by immunocytochemistry, using image analysis strategies illustrated in **Figures 2A,B**, and described in Methods. Representative original images are in of **Supplementary Figure 1**. The treatment of THP1 cells with Tat was able to translocate TBP into the nucleus, detectable since 5 min following the exposure (**Figure 2C**), and maintained TBP translocation throughout the analysis period, with a peak at 15 min (**Figure 2D**). On the other hand, Tat together with Meth induced a stronger translocation at 5 min, but that was gradually decreased. Meth alone also induced TBP translocation at 5 min, but this was quickly decreased and returned to baseline levels at 60 min (**Figures 2E,F**).

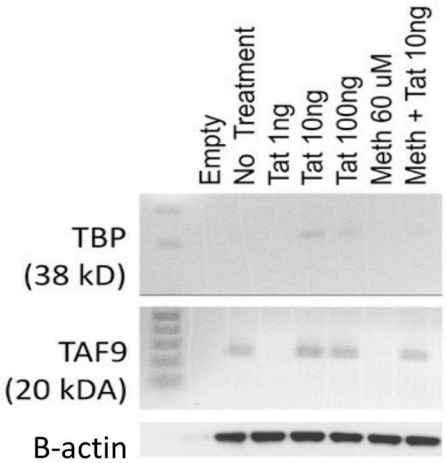

FIGURE 1 | Levels of TBP and TAF9 in the nuclear fraction of THP1 cells stimulated with HIV-1 Tat and with Meth. THP1 cells were incubated with different concentrations of HIV-1 Tat peptide (1, 10, and 100 ng/ml), and with Meth (60 μM). Protein was extracted from nuclear pellets 2 h after stimulation.

We have also tested whether Tat is able to translocate to the nucleus. **Figure 3A** shows that Tat enters the cellular nucleus soon after exposure and over time. The acute translocation of Tat was enhanced by Meth at 5 min, but this was followed by a gradual extinction effect. **Figures 3B,C** show the channel average overlap confirming the entry of Tat (black) into the nuclear structure (gray).

RNA Pol II Recruitment to Promoters Containing the TATA-Box Element Is Increased by HIV-1 Tat, and Further Enhanced by Meth

In order to examine the effects of Tat, and of the interactions with Meth on early transcriptional modifications in innate immune cells, we have used ChIP-seq to estimate changes in RNA Pol II recruitment to gene promoter regions, and to determine commonalities in transcription factor regulation. For that, THP1 macrophages were stimulated with 10 ng/ml of HIV Tat and/or 60 μM of Meth. The cell pellets were examined 15 min after stimulation, for identification of changes that are immediately due, and specific to, the provided stimuli, rather than due to secondary autocrine cytokine stimulation.

The examination of active promoter regions revealed that the majority of the differences in RNA Pol II signal enrichment between conditions were not above 2-fold, except for cells treated with Meth, which showed strongest signals (**Supplementary Materials**—Active Regions).

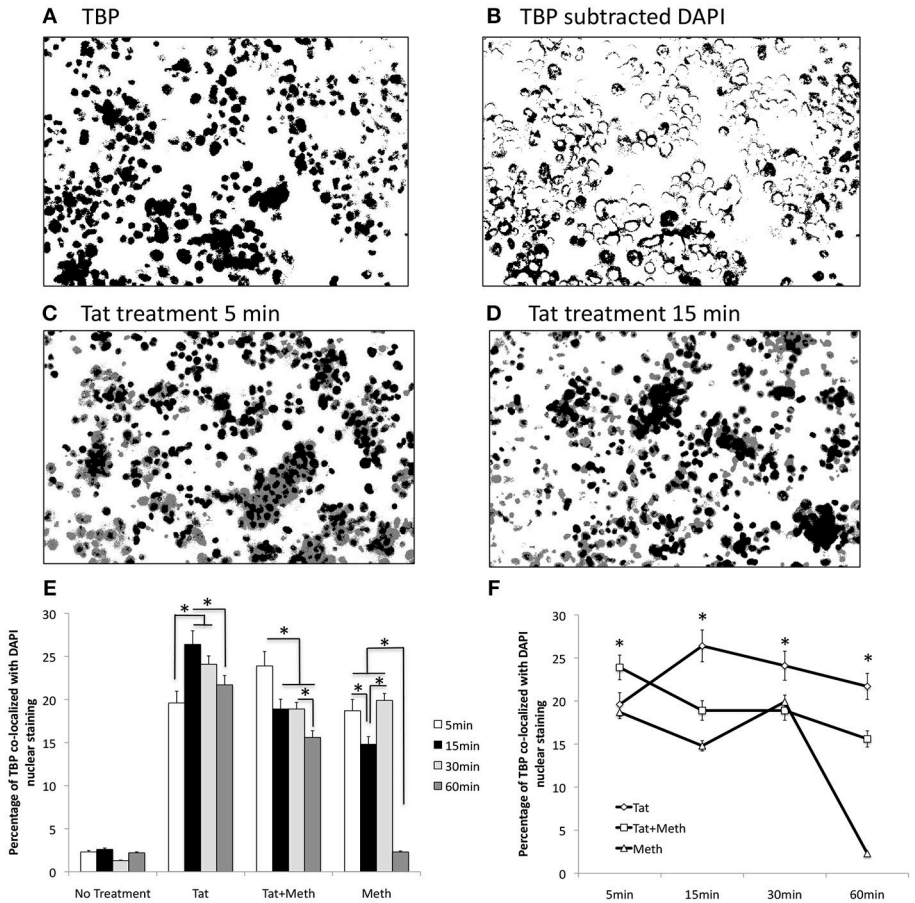

FIGURE 2 | TBP translocation patterns by Tat and by Meth. Translocation was estimated by immunocytochemistry on differentiated THP1 cells that were treated with HIV-1 Tat (10 ng/ml), and/or Meth (60 μM), over 5, 15, 30, and 60 min. Acquired images of cells stained with anti-TBP (rabbit polyclonal), and anti-rabbit AlexaFluor 647, and counterstained with DAPI are in **Supplementary Materials**. The images were digitalized as described in Methods. DAPI staining was converted into a binary mask and subtracted from the total TBP staining **(A)**, to produce an image of cytoplasmatic staining **(B)**. The average of overlapped binary masks confirmed the co-localization of TBP and DAPI upon Tat stimulation at 5 min **(C)**, and with a peak at 15 min **(D)**. After measurements, the translocation index was calculated as the percentage of the total staining that was co-localized with DAPI. **(E)** Bar graph showing translocation indexes for baseline untreated cells, and cells treated with all stimulants over time. **(F)** Line graph for visualization of the effect of time on TBP translocation with the different stimuli. The assays were performed in triplicate, and in three independent experiments. Results represent the average and standard deviation of 3 experiments performed in duplicate. *$p < 0.05$ in two-way ANOVA, followed by Bonferroni's test.

Visualization of Changes in RNA Pol II Recruitment Patterns

Using Cytoscape interface platform, Mentha and Biogrid interactomes were imported from the Proteomics Standard Initiative Common QUery InterfaCe (PSICQUIC) (www.bioconductor.org). These two databases were used for building a network from RNA Pol II recruitment data, ratio between experimental and controls' peaks signal average, and FDR-corrected *p*-values as node attributes, for visualizing changes.

The network was filtered for eliminating genes that were not represented in our data set. Gene networks were 63.73% due to co-expression, followed by 15.84% due to physical interactions. The organic layouts were restricted to selected default pathway database attributes (combined Wu-Stein-2010, PathwayCommons NCI Nature, IMID, Reactome and Cell_Map), which connected 5.27% of the genes (**Figure 4**). The application of attributes and visualization in Cytoscape suggested that Meth had a stronger effect on RNA Pol II recruitment when compared to HIV-1 Tat (**Figure 4**). Pathway perturbation and over-representation analysis by iPathwayGuide, showed that RNA Pol II recruitment was disturbed by Tat, mainly on genes involved in metabolism, activation and response to stimulus, such as cell adhesion molecules ($p = 0.023$), fatty acid elongation ($p = 0.024$), sulfur-relay system ($p = 0.026$), hematopoietic lineage ($p = 0.034$), Notch-signaling pathway ($p = 0.04$), purine metabolism ($p = 0.043$), systemic lupus erythematous ($p = 0.046$), and tryptophan metabolism ($p = 0.049$). Meth promoted RNA Pol recruitment to genes involved in metabolic pathways, such as fatty acid elongation ($p = 0.007$), glycan degradation ($p = 0.007$), DNA replication ($p = 0.022$), endocrine and other factor-regulated calcium reabsorption ($p = 0.028$), ribosome biogenesis ($p = 0.039$), NOD-like

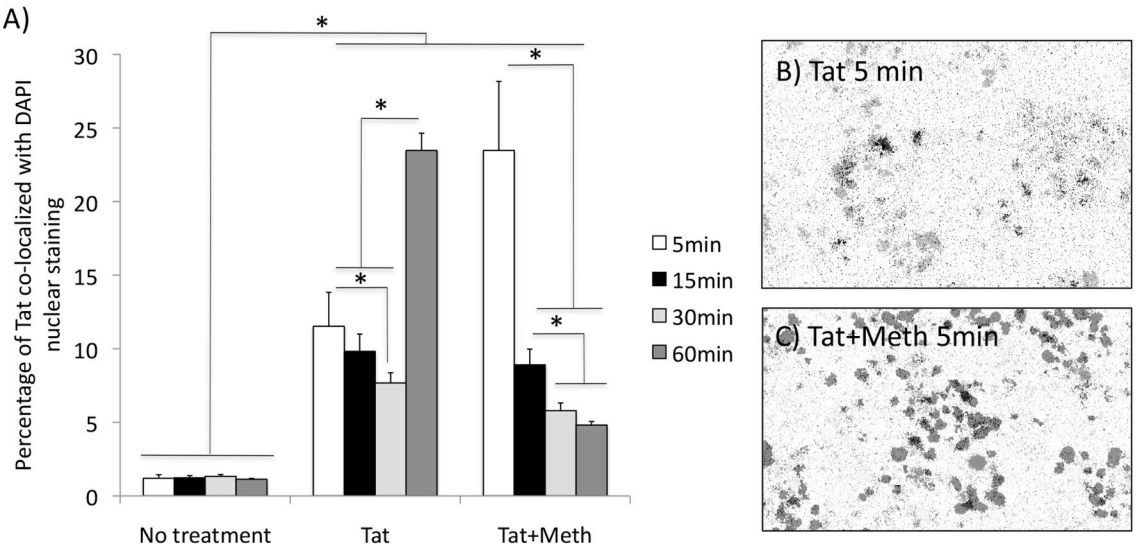

FIGURE 3 | Tat translocation patterns in the presence of Meth. Translocation was estimated by immunocytochemistry on differentiated THP1 cells that were treated with HIV-1 Tat (10 ng/ml), or Tat together with Meth (60 μM), over 5, 15, 30, and 60 min. The cells were stained with anti-Tat (Monoclonal 15.1), and anti-mouse AlexaFluor 647, and counterstained with DAPI. The images were digitalized as described in Methods. DAPI staining was converted into a binary mask and subtracted from the total Tat staining. **(A)** Measurements were used for calculating the percentage of the total Tat staining that was co-localized to DAPI. Results represent the average standard deviation of 3 experiments performed in duplicate. **(B)** Representative image of the averaged overlapped binary masks, which confirmed the co-localization of Tat and DAPI upon Tat stimulation at 5 min), and **(C)** enhancement by Meth simultaneous stimulation. *$p < 0.05$ 2-way ANOVA, followed by Bonferroni's *post hoc* test.

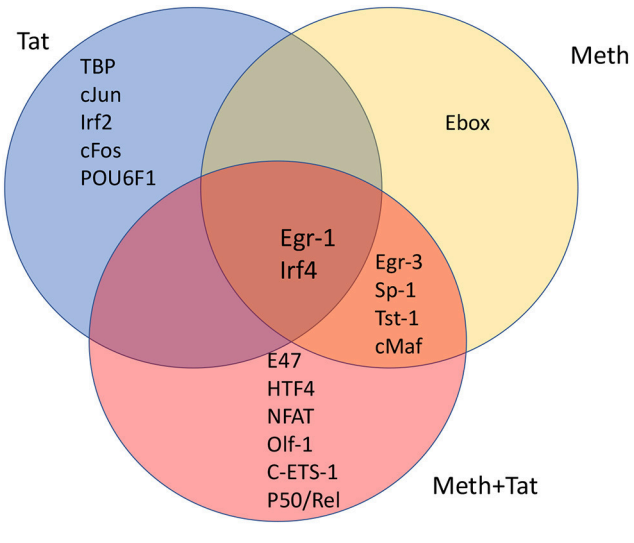

FIGURE 4 | Venn's diagram showing transcription factors with frequent binding motifs among genes with significant changes in RNA Pol II recruitment, immediately following the stimulation of THP1 cells with HIV-1 Tat, Meth, or both together. Matrices for transcription factor binding motifs were generated from ChIP-seq data. For that, SICER raw data in BED format was loaded into TRANSFAC, and the Match-algorithm, was applied as binding factor identifier. Transcription factors with highest frequency of binding motifs in gene promoters affected by HIV-1 Tat, Meth, or both together were estimated. The transcription factors listed in each segment of the Venn's diagram are all significantly increased in comparison to control conditions, and are ranked in order according to frequency matrices, from highest on top to lowest at the bottom of the segregated lists.

receptor signaling pathway ($p = 0.048$) and synaptic vesicle ($p = 0.048$).

We investigated whether promoters where RNA Pol II recruitment was changed by HIV-1 Tat, or Meth, or by both factors together, displayed critical promoter sequence commonalities, based on alignment and frequency of transcription factor binding motifs. This was examined using a combination of strategies, aiming at identifying common transcription master regulators potentially orchestrating the observed effects. First, SICER BED files were analyzed using MATCH tool algorithm (50) with h19 genome as a template, and using a library of mononucleotide weight matrices from TRANSFAC database (Wolfenbuttel, Germany). This tool created nucleotide matrices that calculated frequency of promoter binding motifs among genes exhibiting significant changes in RNA Pol II recruitment. **Figure 4** shows the identified condition-specific transcription factors, in order of importance, in a Venn diagram. The attributed matrix score identified TBP (V$TATA_01, V$TATA_C, VTBP_Q6, VTBP_01, V$TBP_06), as the main transcription factor regulating changes upon HIV-1 Tat exposure, as determined by a consensus sequence matrix (**Table 2**). TBP was followed by other exclusive factors, cJun, Irf2, cFos and POU6F1, which were also statistically significant, but occurred at lower frequency when compared to TBP. Meth stimulation drastically shifted RNA Pol recruitment patterns to genes with high frequency of Egr-3, Sp-1, Tst-1, cMaf, and Ebox binding motifs. Of these, the Ebox (CACGTG/CAGCTG) binding motif aligned exclusively in Meth alone, while the other factors were common to Meth+Tat stimulation. E47, HTF4,

TABLE 2 | TATA box promoter element matrices obtained from THP1 cells stimulated with Tat or with Meth+Tat.

Reverse Consensus	A	C	G	T	Complement Consensus	A	C	G	T
(A) Tat stimulation									
T	4	9	2	29	N	15	10	15	4
T	3	11	1	29	G	8	6	27	3
T	11	2	1	30	N	8	7	21	8
T	2	4	0	38	N	6	13	18	7
A	25	8	0	11	T	5	4	11	24
T	1	5	0	38	A	38	0	5	1
A	24	11	4	5	T	11	0	8	25
N	7	18	13	6	A	38	0	4	2
N	8	21	7	8	A	30	1	2	11
C	3	27	6	8	A	29	1	11	3
N	4	15	10	15	A	29	2	9	4
(B) Meth+Tat stimulation									
T	1	1	1	20	N	5	5	8	2
T	0	0	0	20	T	3	2	3	12
T	0	0	0	20	A	18	0	0	2
A	15	2	1	2	T	2	1	2	15
T	2	0	0	18	A	20	0	0	0
A	12	3	2	3	A	20	0	0	0
N	2	8	5	5	A	17	1	1	1

The frequency of nucleotides matching the TATA box promoter element was calculated on complementary and reverse genomic sequences, using TRANSFAC.

NFAT, Olf-1, cETS-1, and p50/Rel were the transcription factors exclusively associated to Meth+Tat stimulation.

The finding that TBP binding motifs were the most frequent in genes affected by Tat alone is in agreement with the initial finding of increase of TBP at the protein level. It suggests a key role for the TATA-box promoter element in innate immune responses to HIV. **Table 2** shows the frequency of nucleotides comprising the TATA box element matrix compiled from individual genomic sites upon HIV-1 Tat stimulation, in the absence or presence of Meth. The matrices estimating the frequency of nucleotides at the correct positions, suggest that upon Tat stimulation 31.5% of the genes showing enriched RNA Pol recruitment have the TATA box promoter element sequence. In contrast, in Meth+Tat stimulated cells, the average was decreased to 12%. In those cells stimulated with both Meth and Tat, the predominant transcription factor sequence domain (30.6%) identified by TRANSFAC was Egr-1 (GCGCATGCG), followed by Egr-3 (GTGGGT/C), and Sp-1 (GGGGCGGGG), all classified as C2H2 zink finger proteins.

Interestingly, many genes affected by Tat alone and by Meth+Tat were the same. Yet, estimated master regulators differed in those conditions, with Egr-1 and Irf4 in common. These two factors were also identified in genes affected by Meth alone, in addition to Egr-3, Sp-1, Tst-1, and cMaf, which were shared with Meth+Tat. On the other hand, Tat alone and Meth+Tat had no common regulators (**Figure 4**).

The prediction of TBP as a master regulator of changes caused by Tat stimulation was further examined in iRegulon within the Cytoscape platform, using a targeted approach. This method identified all the genes displaying a TATA box element within ± 500 bp from the transcription starting site within the dataset. A table with predicted TBP-controlled genes and attributes was generated, and then utilized to produce a network in Genemania, for comparative analysis and visualization of critical differences between Tat and Meth stimulation (**Figure 5**). Overall, in Tat – stimulated THP1 cells there was a significantly higher number of genes with decreased RNA Pol II recruitment, while in Meth-stimulated cells, more genes were increased. However, upon the generation of a sub-network through targeting TBP and its first neighbors linked through physical interactions, most genes associated with that transcription factor had increased recruitment of RNA Pol II with all treatments (**Figure 6**).

The predicted significance of TBP as a transcription factor in Tat stimulated cells but not in Meth, or Meth+Tat, was challenged by the similarities in RNA Pol II recruitment found in all three conditions. Thus, we developed a strategy to test whether TBP is indeed important for the changes caused by HIV Tat, as well as by Meth, and their interactions. Our strategy consisted on impairing the expression of the TBP gene, using CRISPR/Cas9 guides delivered into THP1 cells by using exosomic gesicles. The efficient transfection of guide sequences was monitored using mCherryPicker reporter (**Figure 7A**). One representative high efficiency clone (2A), was compared to a low efficiency clone (1A) and to a control clone (C) that was treated with empty gesicles. Cells that were positive to mCherryPicker, indicating efficient delivery of guide sequences were sorted using flow cytometry procedures, and placed in culture for expansion and testings (**Figure 7B**). The disruption of the TBP gene was confirmed using Resolvase and visualized in a 2% gel (**Figure 7C**). The significantly decreased baseline expression of the TBP gene was confirmed using qRT-PCR (**Figure 7D**).

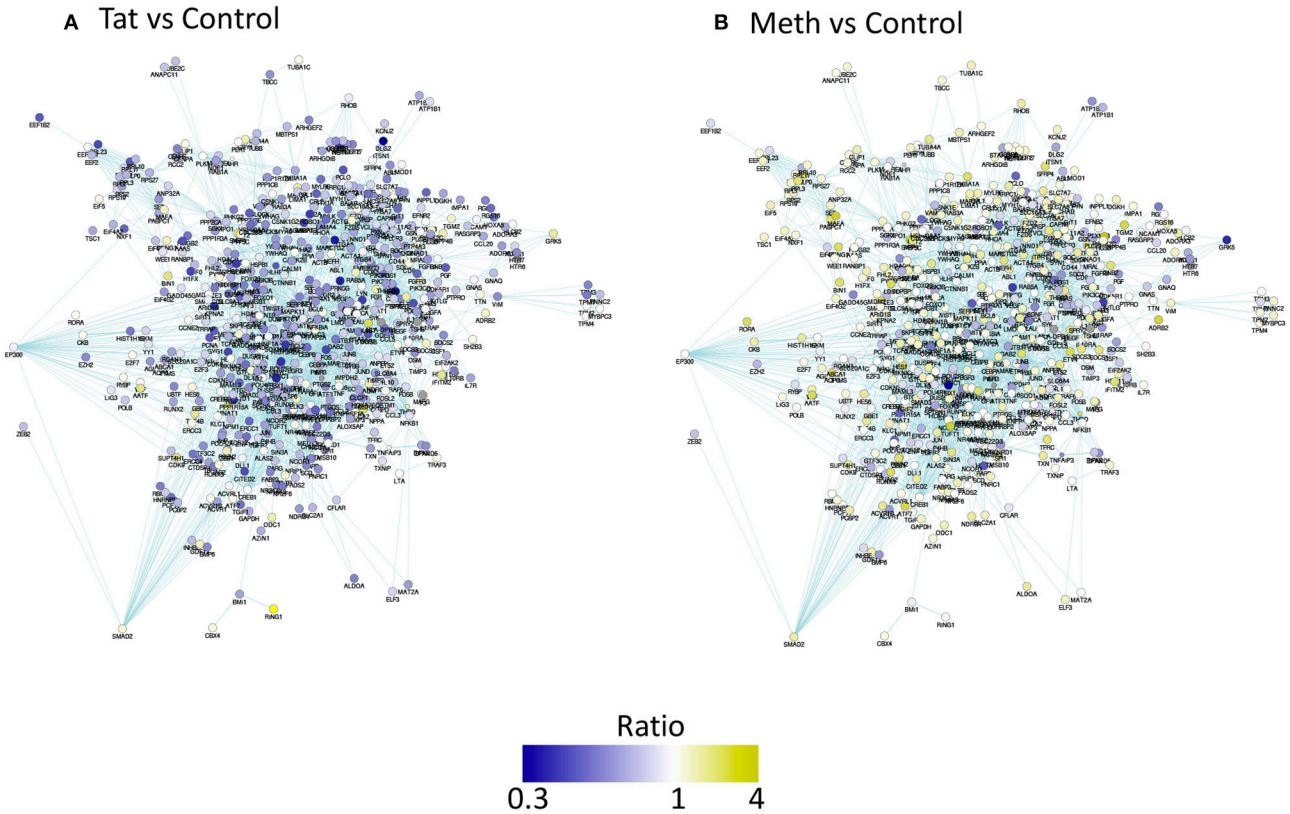

FIGURE 5 | Pathway-based network association of genes with promoter activity changes due to HIV-1 Tat or Meth, compared to vehicle treatment. Ratio between RNA Pol normalized peak values between treated conditions and controls were used for designing a color-coded visualization. Genes were filtered to display only significantly decreased (blue), and increased (yellow) RNA Pol II recruitment patterns. **(A)** Visual representation of ratio of Tat over Control and **(B)** Meth over Control.

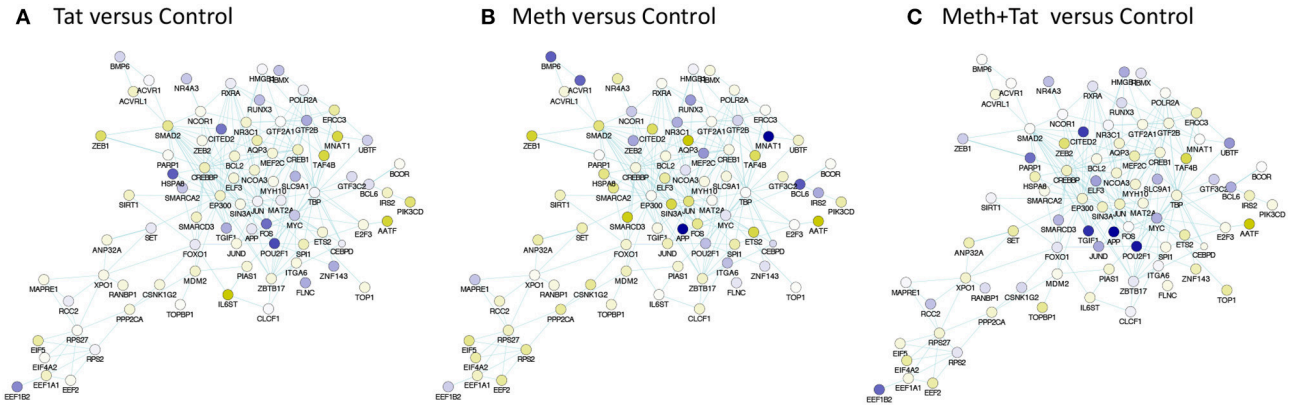

FIGURE 6 | TBP-centered genomic neighborhood derived from pathway-based network association of genes with RNA Pol recruitment patterns affected by HIV-1 Tat or Meth. A sub-network was generated from the pathway-based association study through targeting and selecting the TBP gene and its first neighbors, through physical interaction edges. Colors designate significantly decreased (blue), and increased (yellow) RNA Pol II recruitment patterns, based on the ratio between **(A)** Tat over Control, **(B)** Meth over Control, and **(C)** Meth+Tat over Control.

The confirmation of the disruption in TBP expression included the examination of potentially remaining splice variants (**Table 3**), where we observed only residual expression of TBP_4, but complete clearance of TBP_7 splice variant.

In order to estimate the impact of TBP depletion on the response to HIV-1 Tat, alone and in the context of Meth exposure, a TBP-regulated gene network was identified in the RNA Pol II gene list, with Biogrid Homo sapiens 3.4 gene

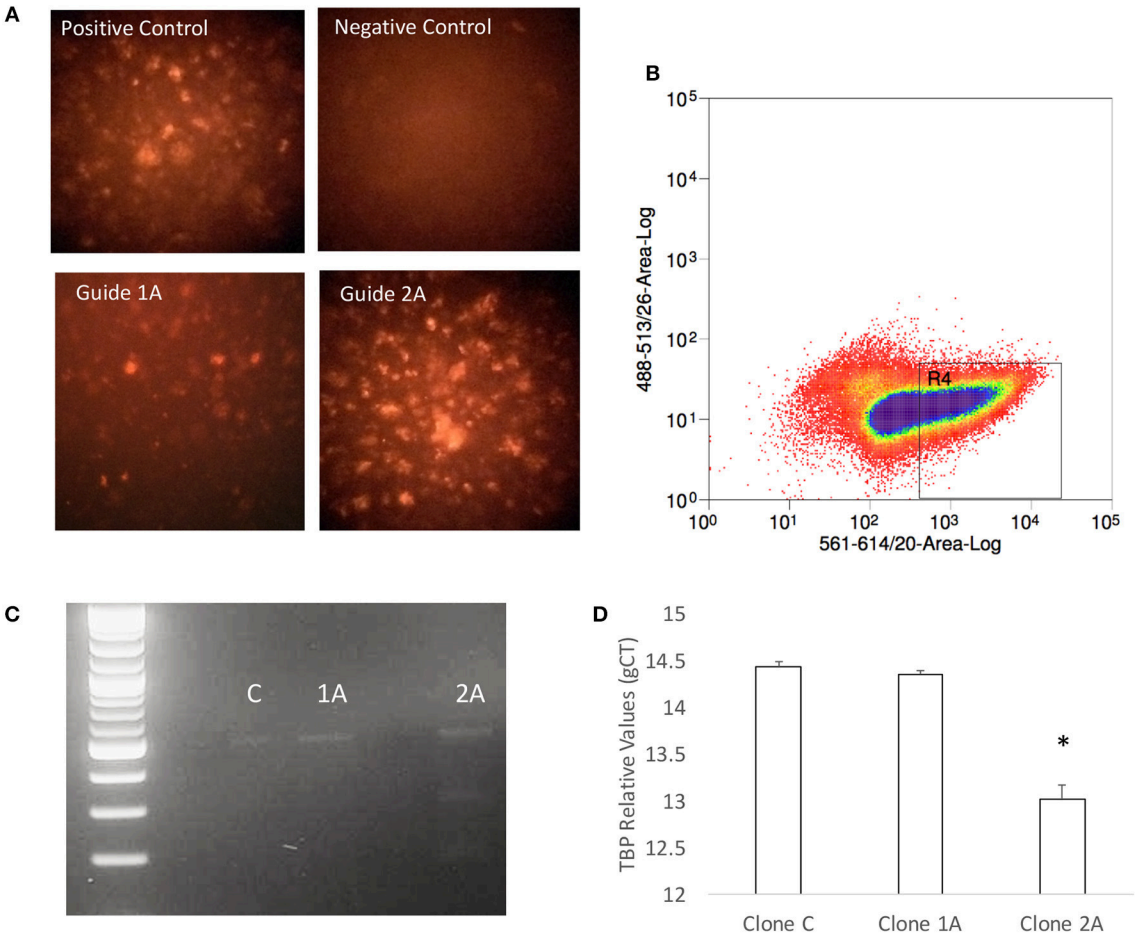

FIGURE 7 | Generation of a TBP-deficient THP1 clone. **(A)** Seventy-two hours after exposure to gesicles containing the TBP guide sequence and Cas9, positively transfected cells were visualized under a fluorescence-microscope for detection of intracellular red fluorescence signal originated from the Cherry Picker reporter on the gesicles' surface. Positive control provided by the manufacturer was compared with a negative control performed with empty gesicles, and two clones that received the guide sequence. Clone 1A showed low efficiency, and clone 2A was highly positive. **(B)** The Cherry Picker-positive cells were gated based on fluorescence intensity, and sorted using a BD FACSJazz (BD Biosciences, San Diego, CA). **(C)** The TBP mutation was confirmed in clone 2A using DNA hybridization with Guide-It Resolvase on a gel-purified genomic TBP sequence, and with **(D)** qRT-PCR. Results are the average ± standard error of 2 experiments performed in triplicate.

network. We then used iRegulon (56) in Cytoscape environment, to reverse-engineer the TBP transcriptional regulatory network through the detection of enriched TATA box motifs and their optimal sets of targets in the RNA Pol II data, pooled from all experimental conditions performed in TBP-sufficient clones (**Figure 8** and **Supplementary Table 1**). The resulting TBP targetome contained 1,811 genes identified in THP1 cells. The expression levels of these genes was estimated by RNA seq performed in the control THP1 clones (C), and in the clone that was depleted of TBP gene expression using Crispr/Cas9, upon the stimulation with HIV-1 Tat, or with Tat plus Meth. **Figure 8A** shows that control C clones stimulated with Tat had a global upregulation of the genes in that network (gene nodes with yellow color), suggesting a significant effect orchestrated through TBP. In **Figure 8B**, the TBP targetome gene network in the TBP-deficient clone 2A that has either similar (white nodes) or lower baseline expression (blue nodes) when compared to control clone C. Interestingly, the genes in the TBP targetome were significantly suppressed in Tat-stimulated TBP-deficient clone 2A compared to clone C, as revealed by the higher number and intensity of blue colored nodes in the network, and confirming that these genes, under Tat stimulation, were predominantly transcribed via Tata box promoter element, and in a TBP-dependent manner (**Figure 8C**). However, when Tat was incubated together with Meth, the genes in the TBP targetome were upregulated even in clone 2A, bypassing the TBP deficiency, as shown by the higher number of yellow colored nodes, and suggesting that in the context of Meth exposure, a diversification of transcriptional factors plays a role in activating the same promoters (**Figure 8D**), as a potential mechanism of exacerbated consequences in HIV and drug abuse.

In order to further estimate the impact of TBP in Tat stimulation and the effect of Meth, global changes in the TBP targetome genes were calculated by the sum of fold changes in all 1811 genes, in clones C and 2A, upon Tat, plus and minus Meth stimulation (**Figure 9**). The strategy showns that Tat globally

TABLE 3 | TBP splice variant reads in Control and 2A clones.

Feature ID	Transcript ID	Experiment - Range	C clone (unique transcript reads)	2A clone (unique transcript reads)	Kahl's *Z*-test *p* value
TBP_1	ENST00000421512	1	33	0	0.000703333
TBP_2	ENST00000446829	0	0	0	1
TBP_3	ENST00000616883	12	12	1	0.001138457
TBP_4	ENST00000230354	76	361	24	0.01604091
TBP_5	ENST00000423353	0	0	0	1
TBP_6	ENST00000540980	0	0	0	1
TBP_7	ENST00000392092	143	489	0	0.000164347

The potential of residual TBP expression through alternative splice was estimated in the Control and 2A clones using RNA seq. The number of reads in both clones and p values are reported.

TABLE 4 | KEGG pathway analysis of genes that failed to upregulate in response to Tat in TBP-deficient 2A clones.

Genes Pathway	*p* value	Benjamini
Proteoglycans in cancer	0.00043	0.067
Hedgehog signaling pathway	0.00076	0.059
Axon guidance	0.001	0.052
Signaling pathways regulating pluripotency of stem cells	0.0018	0.07
Central carbon metabolism in cancer	0.0038	0.11
FoxO signaling pathway	0.0052	0.13
Transcriptional misregulation in cancer	0.0067	0.14
HTLV-I infection	0.01	0.18
Basal cell carcinoma	0.012	0.2
Tight junction	0.026	0.34
Wnt signaling pathway	0.026	0.34
Pathways in cancer	0.027	0.32
Hippo signaling pathway	0.039	0.41
Mineral absorption	0.043	0.42
AMPK signaling pathway	0.046	0.42
Notch signaling pathway	0.048	0.41
Progesterone-mediated oocyte maturation	0.05	0.4

increased TATA-box bearing genes by an average of 8.6%, in the control clone (CT/CPhi), but failed to do it so in the clone 2A (2AT/2APhi). However, Tat in combination with Meth increased the same genes in the TBP-defficient clone 2A by an average of 29% (2AMT/2APhi).

These findings may have profound implications to the character of the inflammatory pathogenesis in HIV-infected Meth abusers. A prediction of the involvement of TBP-regulated genes in molecular pathways was examined using BinGO (57, 58) (**Figure 10** and **Supplementary Table 2**). TBP-regulated genes are predominantly involved in immune and inflammatory pathways, but also in epigenetic, regulatory and metabolic pathways. In **Figure 10**, large circles report overrepresentation, and orange color report higher perturbation, to allow the visualization of stronger effects on innate immune and epigenetic function, as well as regulation (adjusted $p = 0.00136$, $p = 0.000601$, respectively). Within the whole TBP targetome, genes that failed to be upregulated in clone 2A upon Tat stimulation were functionally associated to the nucleus, DNA-binding, transcription, nucleotide binding, developmental protein and cytoskeleton (Benjamini $p < 0.01$), but genes involved in tyrosine-protein kinase, Wnt-signaling, ATP binding, methylation and tight junction were also represented (Benjamini $p < 0.05$). Main identified TBP-controlled pathways using this strategy were assessed in KEGG, and are shown in **Table 4**.

Genes that play a role in inflammatory pathology, and that have been described to have an involvement in HIV pathogenesis, in the brain and elsewhere, were selected for a closer validation of the role of TBP in Tat stimulation, and of the ability of Meth as a co-morbidity to enhance those same genes through other transcription factors. A detailed examination of genes that have a TATA box promoter element and their changes in response to Tat in the TBP-sufficient (C) and deficient (2A) clones reveals two classes of genes, which seem to segregate based on their expression levels in unstimulated controls (**Figure 11**). The genes in **Figure 11A**, which are not detectable in the unstimulated clone C or clone 2A, are highly induced by Tat in clone C, but not in clone 2A, suggesting that the transcription of these genes upon HIV-1 Tat stimulation is primarily triggered via the TATA box promoter domain, under TBP control. On the other hand, the stimulation with Tat in the presence of Meth, or Meth alone, was able to increase these transcripts in both clones, and bypassing the TBP deficiency in clone 2A, confirming a diversification of transcription factor usage by the drug, alone or in the context of HIV Tat. Examples include genes involved in blood brain barrier permeability, inflammation and immune regulation, neuroprotection and metabolic outcomes, such as CD163, Claudins 5 and 9 (CLDN5 and CLDN9), FoxP3, Brain-derived neurotrophic factor (BDNF), Insulin growth factor 1 Receptor (IGF1R), Retinoic acid receptor alpha (RARA), and the important kinase CDK9. The genes in **Figure 10B** also present TATA box promoter element, and were detected in the TBP targetome, but differed from the genes represented in **Figure 11A** by being constitutively expressed in unstimulated cells, regardless of the TBP expression. Interestingly, these genes were not responsive to Tat, or to Meth. This was the case for instance of CXCL2, Tumor necrosis factor receptor superfamily member 25 (TNFRsF25), and the T-box 2 transcription factor (TBX2).

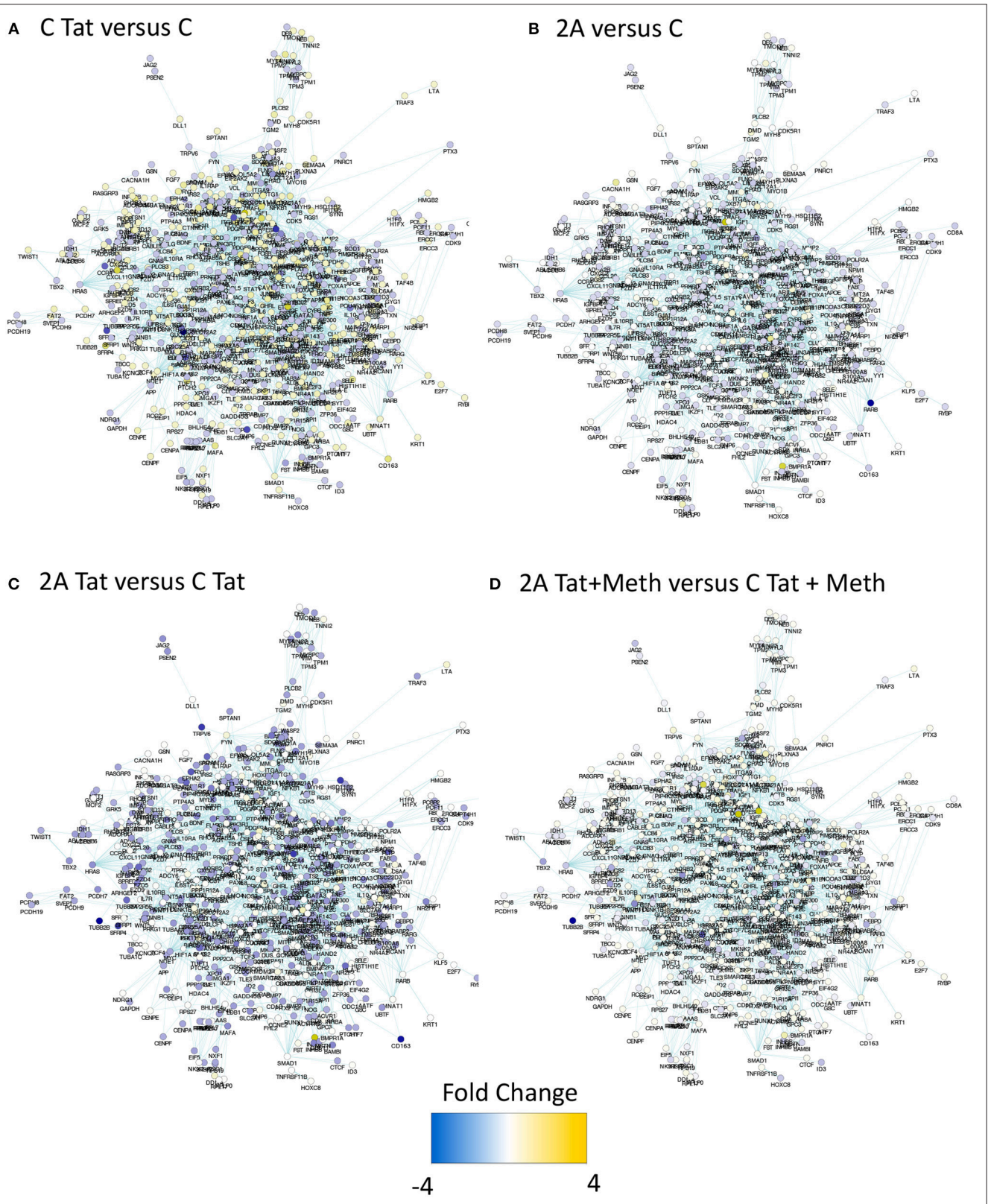

FIGURE 8 | Impact of TBP deficiency on the expression of genes in the TBP targetome following stimulation with Tat, in the presence and in the absence of Meth. The genes that contain Tata box promoter elements and their relationship was estimated in Homo sapiens 3.4 Biogrid default network using iRegulon, with TBP as a factor, and filtered to contain genes that were significantly represented in THP1 cells based on RNA Pol II recruitment capacity at any given experimental condition.

(Continued)

FIGURE 8 | The produced mega-network containing 1811 genes was denominated TBP targetome, and used to determine the effect of TBP depletion on Tat stimulation, alone or in the context of Meth. For that, RNA seq was performed in the control clone C and in the TBP-deficient clone 2A, stimulated with 10 μg/ml of HIV Tat, alone or together with 60 μM of Meth. The expression changes were estimated 24 h after stimulation. Yellow tones represent upregulation, and blue tones represent downregulation. **(A)** Clone C treated with Tat was compared to clone C treated with vehicle, showing that the majority of the genes in this network are yellow, indicating that Tat upregulates genes with a TBP binding domain. **(B)** Vehicle-treated clones 2A and C were compared, showing little or no change in color, indicating that they do not differ at baseline. **(C)** Clone 2A stimulated with Tat was compared to clone C stimulated with Tat, showing that most genes are in blue nodes indicating that clone 2A had a lower expression than clone C, upon Tat stimulation. **(D)** Clone 2A treated with Tat+Meth was compared with clone C also treateated with Tat+Meth, where nodes with no color change or yellow indicate that in the presence of Meth, the TBP deficient clone 2A either does not differ from clone C or further increases the expression of genes with a TBP binding promoter domain.

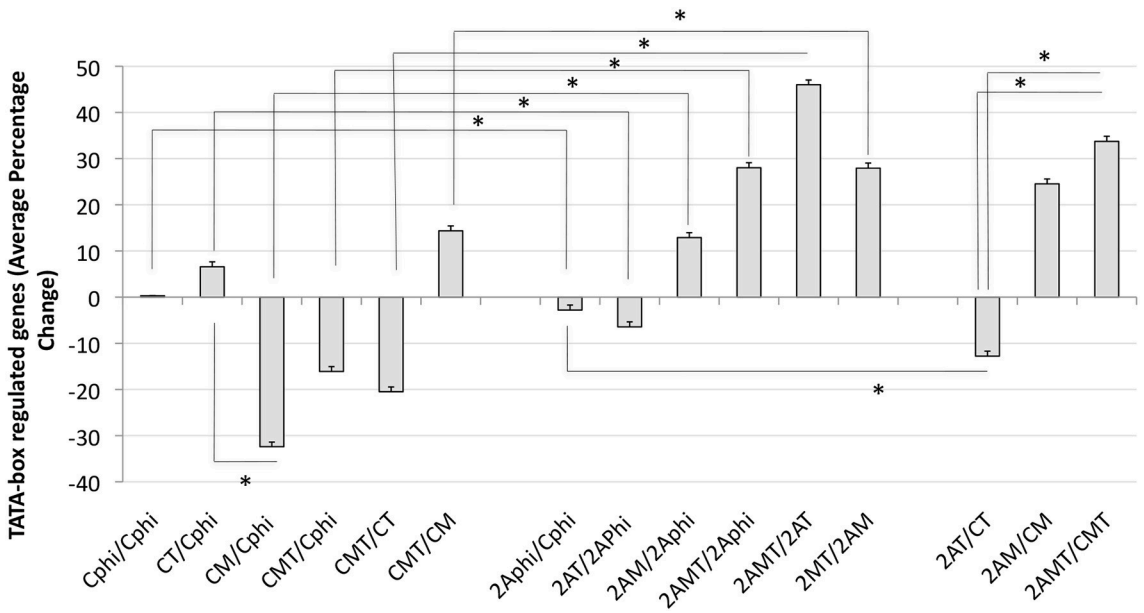

FIGURE 9 | Global changes in the TBP targetome in TBP-sufficient and –deficient monocyte clones after Tat stimulation with or without Meth. The sum of all fold changes in genes that have a Tata box promoter element upon designated stimulations. C is Control clone and 2A is the TBP-defficient clone. T refers to Tat stimulation, M to Meth stimulation, and MT is their combination. Phi refers to control function. Results represent the average ± standard deviation of expression of 1,811 genes included in the TBP megatargetome identified in iRegulon. *$p < 0.05$ in assigned comparisons, using ANOVA and Bonferroni's *post hoc* test.

Overall, our results indicate that the HIV-1 Tat peptide acts through the usage of TBP as a transcription factor that engages in the Tata-box binding motif in the promoter of promptly inducible genes, which are expressed at low or undetectable levels in unstimulated resting states. These genes include a large collection of inflammatory genes, regulatory elements and metabolic components. In the presence of Meth, which is a common comorbidity of HIV infection, a larger number of transcription factors may increase the probability of transcription, and increase the number of transcribed early response genes, explaining the exacerbation of pathogenic hallmarks, particularly in the brain of HIV+ drug users.

DISCUSSION

The role of the Tata-box promoter domain in HIV transcription has been suggested (23). In addition, single nucleotide polymorphisms in its sequence located in the long-terminal repeat (LTR) in the viral transcription complex, which confers a low affinity to TBP, the Tata-box binding transcription factor, results in significantly slower replication (59). The main HIV-1 peptide that is responsible for the transactivation of viral transcription, Tat, performs its task by directly inducing and recruiting TBP to the LTR, via its ability to directly interact with the cellular cofactor positive transcription elongation factor b (P-TEFb), which bridges TBP binding to the promoter without the need of other TBP-associated factors (23). While this is a mechanism that is relevant to promote viral replication, here we investigated the hypothesis that HIV-1 Tat is able to activate transcription of thousands of host genes through a TBP-dependent strategy, producing hyper-inflammatory phenotypes that are further beneficial to the viral propagation.

By engineering a macrophage cell line that is deficient on the expression of dominant TBP splice variants, we demonstrated that transcriptional changes induced by the incubation with HIV-1 Tat favor inducible genes that have the Tata-box promoter sequence in their promoters. We also showed that such effect is achieved through the dominant usage of TBP as a transcription factor. Other transcription factors that may be triggered, cJun, interferon regulatory factor 2 (IRF2), cFos and POU6F1, also

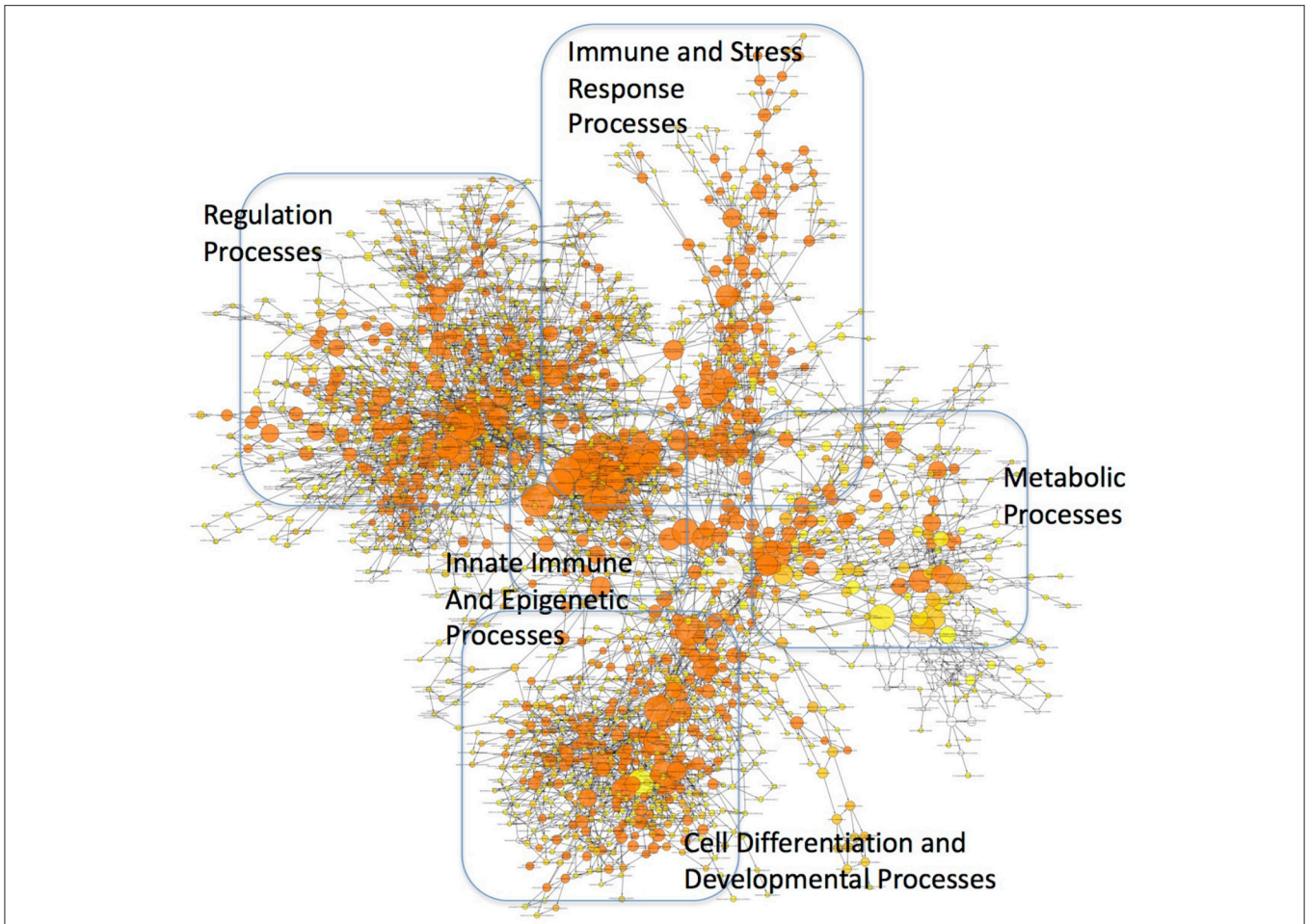

FIGURE 10 | Mapping of functional categories identified in genes of the TBP targetome. Gene Ontology (GO) analysis was performed using BinGO. The circles' size show overrepresentation, and colors report perturbation, orange being high, and yellow, low.

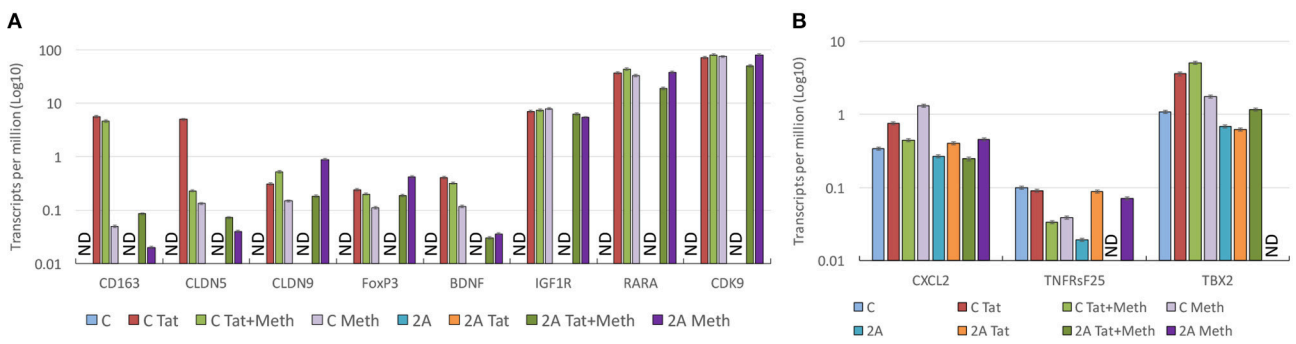

FIGURE 11 | Effect of TBP transcription factor in the upregulation of gene transcripts in response to Tat and Meth. Gene transcript counts are represented in log10 of transcripts per million (TPM). The axis in log allows the appreciation of genes that are increased with different intensities for comparison of their behaviors in response to stimulation. **(A)** Representative TBP targets illustrating the changes in genes that are undetectable in unstimulated cells and responsive to Tat and/or Meth. **(B)** Representative hits illustrating the behavior of genes that are constitutively transcribed in unstimulated cells, and not responsive to Tat and/or Meth. ND, Not detectable.

appear to be triggered, as their binding motifs are identified in the promoters of genes with increased RNA Pol recruitment, and can be controlling different sets of genes. These findings may have important implications for understanding mechanisms of pathogenesis in HIV infection, and potentially for therapy. We also showed that the exposure of macrophages to a stimulant drug, Meth, together with HIV-1 Tat, is able to activate the same gene promoters, which is revealed by the efficient recruitment of RNA Pol. However, this happens through a distinctive and more diversified usage of transcriptional factors. The absence of TAF9 in Meth-stimulated cells, and the results of the analysis of consensus promoter sequences in TBP-sufficient cells stimulated with Tat plus Meth, support that an alternative to TBP is triggered by Meth, it can potentially co-exist with TBP in the context of HIV-1 Tat, but ultimately support promoter activation through different motifs. This may suggest that co-morbidities represent a factor of complexity in therapies that target transcriptional machineries.

We have shown that TBP and Tat are translocated within 5 min into the cell nucleus, when in the presence of Meth, which may have important implications to the viral transcription. However, we did not test the effects of TBP disruption on viral transcription or replication, but exclusively on the effects of Tat as a factor that enhances transcription of host genes. The identification of TBP as a the most frequently aligned promoter motif in genes with RNA Pol efficiently recruited, suggested that TBP played an important role. Yet, it does not explain the basis for the interaction between Tat and TBP. Further experiments are necessary to establish the molecular basis for that interaction in the context of absence of TAR, or on the effects over the LTR. Although TBP was the most frequent transcription factor motif, other transcription motifs were also significant, such as cJun/cFos, IRF2, and POU6F1. In other systems, Sp-1 has been suggested as a Tat molecular partner, bridged by Cyclin T1/CDK9 complexes, which can promote transcription of the virus in a TAR-independent fashion (60–62), and likely also of host gene promoters. Sp-1 did not appear as a binding motif in Tat-enhanced promoters, but it was one of the factors associated with Meth-induced activation. Thus, in the presence of Meth, or in the absence of TBP, transcription factor redundancy and promoter plasticity may perpetuate and broaden gene transcription, including of HIV.

Two transcription factors appeared to be common between HIV-1 Tat and Meth, which were Egr-1, and IRF4. Further studies are necessary to examine which common genes can be controlled by these transcription factors, to estimate their value as targets of intervention. In the non-human primate model of neuroHIV, we have previously demonstrated that a decrease in Egr-1 expression in neurons is associated with neurological deficits in the context of inflammation (63). Its role in cell transcriptional regulation has been described (64). IRF4, on the other hand, is a positive regulator of inflammation (65, 66), converge as a common epigenetic switch.

Our results suggest that the occurrence of additional cellular stimulus in HIV-1 may deviate transcription factor usage, by promoting diversity. However, a role for TBP inhibitors should not be ruled out as a strategy to ameliorate stimulant drug users. For instance, it has been suggested that although the Tata-box promoter domain sequences are selectively used by TBP *in vivo*, the binding can be modulated by TBP inhibitors such as TBA-associated factor 1 (TAF1) (67–69). In addition, Tat in combination with Meth enhanced the acute translocation of Tat into the cellular nucleus, which may have implications to the viral transcription, not examined here.

Overall, we have found a key role for TBP in the induction of genes containing the TATA-box core promoter element by the HIV Tat peptide, characterized by early response, inflammatory and metabolic genes. We have also determined the effect of the interactions between Tat and Meth, a common co-morbidity of HIV infection, on diversifying the collection of transcription factors able to redundantly act on the activation of promoters, RNA Pol recruitment and ultimately transcription of genes with important implications in inflammatory pathology. Our findings help explain aggravated phenotypes associated to inflammation and to metabolic disorders that are commonly observed in HIV+ individuals with substance use disorders, but also suggest that in these individuals, targeting elements of the transcriptional machinery posits the risk of failure, while dealing with additional molecular complexities.

AUTHOR CONTRIBUTIONS

RT performed the Crispr/Cas9 disruption of TBP expression, tested and selected the positive clones, and performed all the *in vitro* stimulations. JAN performed the fixation of cells for RNA Pol ChIP assay. AL performed THP1-deficient cells PCRs. LAC provided guidance for the design and execution of Crispr/Cas9-based TBP disruption, reviewed all the results, helped in the analysis, and in the writing of the manuscript. JJ tested all the primers for PCR validation. LB participated in the experimental design, performed all TBP-sufficient cell cultures and stimulation experiments, fixations for ChIP assays, performed PCRs, and helped in writing the manuscript. MM developed the concept, designed the study, obtained funding, supervised experiments, menthored students, revised all results, performed all systems biology-based approaches, revised statistical results, and wrote the manuscript.

FUNDING

This work was entirely funded by the NIH R01 DA036164 grant to MM. RT was funded by the NIDA Summer Research Internship supplemented to the NIH parent grant. LAC was supported by the Intramural Research Program at the National Institute on Drug Abuse. JJ was funded by the TSRI Summer Undergrad Research Fellowship (SURF) program.

ACKNOWLEDGMENTS

We want to thank Drs. Paul Labhart and Madeleine Lisa Craske (Active Motif Inc., Carlsbad, CA), for technical support and help with troubleshooting. We thank Daniel Ryan (SDBRI) and Nikki

Bortell for critically reviewing the manuscript, Christine Auciello and Fazila Kiyam for administrative support.

SUPPLEMENTARY MATERIAL

The Supplementary Material for this article can be found online at: https://www.frontiersin.org/articles/10.3389/fimmu.2018.03110/full#supplementary-material

Supplementary Table 1 | TBP megatargetome-RNA Pol ChIP average peak values in genes that have a TATA-box binding motif in the core promoter element. Cross linking for RNA Pol II ChIP was performed 15 min after stimulation with HIV Tat (10 ng/ml), Meth (60 μM), or Tat+Meth, for determination of gene intervals, and average peak ratios.

Supplementary Table 2 | The effect of TBP disruption in the response to Tat and/or Meth. RNA-seq was performed in TBP-defficient clone 2A and compared to TBP-sufficient clone C. T = Tat stimulation, M = Meth stimulation, MT = Meth+Tat. Gene IDs, Transcript ID, chromosomes and gene intervals are provided. This experiment was performed in triplicate.

Supplementary Figure S1 | TBP nuclear translocation. The PMA-differentiated THP1 cells were stimulated with Meth (60 μM), and/or HIV Tat (10 ng/ml) for examination of TBP nuclear translocation 5, 15, 30, and 60 min following stimulation, by immunocytochemistry. TBP was stained in red, and nuclei were visualized with DAPI (blue). Confocal images were used for the determination of a translocation index, as the percentage of total TBP staining that was co-localized with DAPI. Representative images of **(A)** Controls and Tat stimulation, **(B)** Tat+Meth stimulation. This experiment was performed three times in triplicate.

REFERENCES

1. Basova L, Najera JA, Bortell N, Wang D, Moya R, Lindsey A, et al. Dopamine and its receptors play a role in the modulation of CCR5 expression in innate immune cells following exposure to Methamphetamine: implications to HIV infection. *PLoS ONE* (2018) 13:e0199861. doi: 10.1371/journal.pone.0199861
2. Bosshart H, Heinzelmann M. THP-1 cells as a model for human monocytes. *Ann Transl Med*. (2016) 4:438. doi: 10.21037/atm.2016.08.53
3. Fauci AS. Host factors and the pathogenesis of HIV-induced disease. *Nature* (1996) 384:529–34. doi: 10.1038/384529a0
4. Lindl KA, Marks DR, Kolson DL, Jordan-Sciutto KL. HIV-associated neurocognitive disorder: pathogenesis and therapeutic opportunities. *J Neuroimmune Pharmacol*. (2010) 5:294–309. doi: 10.1007/s11481-010-9205-z
5. Marcondes MC, Flynn C, Watry DD, Zandonatti M, Fox HS. Methamphetamine increases brain viral load and activates natural killer cells in simian immunodeficiency virus-infected monkeys. *Am J Pathol*. (2010) 177:355–61. doi: 10.2353/ajpath.2010.090953
6. Nath A, Maragos WF, Avison MJ, Schmitt FA, Berger JR. Acceleration of HIV dementia with methamphetamine and cocaine. *J Neurovirol*. (2001) 7:66–71. doi: 10.1080/13550280130006973 7
7. Najera JA, Bustamante EA, Bortell N, Morsey B, Fox HS, Ravasi T, et al. Methamphetamine abuse affects gene expression in brain-derived microglia of SIV-infected macaques to enhance inflammation and promote virus targets. *BMC Immunol*. (2016) 17:7. doi: 10.1186/s12865-016-0145-0
8. Bortell N, Morsey B, Basova L, Fox HS, Marcondes MC. Phenotypic changes in the brain of SIV-infected macaques exposed to methamphetamine parallel macrophage activation patterns induced by the common gamma-chain cytokine system. *Front Microbiol*. (2015) 6:900. doi: 10.3389/fmicb.2015.00900
9. Debaisieux S, Rayne F, Yezid H, Beaumelle B. The ins and outs of HIV-1 Tat. *Traffic* (2012) 13:355–63. doi: 10.1111/j.1600-0854.2011.01286.x
10. Rayne F, Debaisieux S, Bonhoure A, Beaumelle B. HIV-1 Tat is unconventionally secreted through the plasma membrane. *Cell Biol Int*. (2010) 34:409–13. doi: 10.1042/CBI20090376
11. Rayne F, Debaisieux S, Tu A, Chopard C, Tryoen-Toth P, Beaumelle B. Detecting HIV-1 Tat in cell culture supernatants by ELISA or Western Blot. *Methods Mol Biol*. (2016) 1354:329–42. doi: 10.1007/978-1-4939-3046-3_22
12. Vendeville, Rayne F, Bonhoure A, Bettache N, Montcourrier P, Beaumelle B. HIV-1 Tat enters T cells using coated pits before translocating from acidified endosomes and eliciting biological responses. *Mol Biol Cell* (2004) 15:2347–60. doi: 10.1091/mbc.e03-12-0921
13. Carey AN, Liu X, Mintzopoulos D, Paris JJ, Muschamp JW, McLaughlin JP, et al. Conditional Tat protein expression in the GT-tg bigenic mouse brain induces gray matter density reductions. *Prog Neuro Psychopharmacol Biol Psychiatry* (2013) 43:49–54. doi: 10.1016/j.pnpbp.2012.12.018
14. Carey AN, Sypek EI, Singh HD, Kaufman MJ, McLaughlin JP. Expression of HIV-Tat protein is associated with learning and memory deficits in the mouse. *Behav Brain Res*. (2012) 229:48–56. doi: 10.1016/j.bbr.2011.12.019
15. Kesby JP, Najera JA, Romoli B, Fang Y, Basova L, Birmingham A, et al. HIV-1 TAT protein enhances sensitization to methamphetamine by affecting dopaminergic function. *Brain Behav Immun*. (2017) 65:210–21. doi: 10.1016/j.bbi.2017.05.004
16. Bannwarth S, Gatignol A. HIV-1 TAR RNA: the target of molecular interactions between the virus and its host. *Curr HIV Res*. (2005) 3:61–71. doi: 10.2174/1570162052772924
17. Brady J, Kashanchi F. Tat gets the "green" light on transcription initiation. *Retrovirology* (2005) 2:69. doi: 10.1186/1742-4690-2-69
18. Davidson A, Leeper TC, Athanassiou Z, Patora-Komisarska K, Karn J, Robinson JA, et al. Simultaneous recognition of HIV-1 TAR RNA bulge and loop sequences by cyclic peptide mimics of Tat protein. *Proc Natl Acad Sci USA*. (2009) 106:11931–6. doi: 10.1073/pnas.0900629106
19. Naryshkin NA, Gait MJ, Ivanovskaya MG. RNA recognition and regulation of HIV-1 gene expression by viral factor Tat. *Biochemistry* (1998) 63:489–503.
20. Richter, Ping YH, Rana TM. TAR RNA loop: a scaffold for the assembly of a regulatory switch in HIV replication. *Proc Natl Acad Sci USA*. (2002) 99:7928–33. doi: 10.1073/pnas.122119999
21. Wei P, Garber ME, Fang SM, Fischer WH, Jones KA. A novel CDK9-associated C-type cyclin interacts directly with HIV-1 Tat and mediates its high-affinity, loop-specific binding to TAR RNA. *Cell* (1998) 92:451–62. doi: 10.1016/S0092-8674(00)80939-3
22. Bieniasz PD, Grdina TA, Bogerd HP, Cullen BR. Recruitment of cyclin T1/P-TEFb to an HIV type 1 long terminal repeat promoter proximal RNA target is both necessary and sufficient for full activation of transcription. *Proc Natl Acad Sci USA*. (1999) 96:7791–6. doi: 10.1073/pnas.96.14.7791
23. Raha T, Cheng SW, Green MR. HIV-1 Tat stimulates transcription complex assembly through recruitment of TBP in the absence of TAFs. *PLoS Biol*. (2005) 3:e44. doi: 10.1371/journal.pbio.0030044
24. Verrijzer CP, Yokomori K, Chen JL, Tjian R. Drosophila TAFII150: similarity to yeast gene TSM-1 and specific binding to core promoter DNA. *Science* (1994) 264:933–41. doi: 10.1126/science.8178153
25. Kim YS, Panganiban AT. Examination of TAR-independent Trans activation by human immunodeficiency virus type 1 Tat in human glial cells. *J Neurosci Res*. (1996) 43:652–66. doi: 10.1002/(SICI)1097-4547(19960315)43:6<652::AID-JNR2>3.0.CO;2-D
26. Pu H, Tian J, Flora G, Lee YW, Nath A, Hennig B, et al. HIV-1 Tat protein upregulates inflammatory mediators and induces monocyte invasion into the brain. *Mol Cell Neurosci*. (2003) 24:224–37. doi: 10.1016/S1044-7431(03)00171-4
27. Toborek M, Lee YW, Pu H, Malecki A, Flora G, Garrido R, et al. HIV-Tat protein induces oxidative and inflammatory pathways in brain endothelium. *J Neurochem*. (2003) 84:169–79. doi: 10.1046/j.1471-4159.2003.01543.x
28. Roebuck KA, Rabbi MF, Kagnoff MF. HIV-1 Tat protein can transactivate a heterologous TATAA element independent of viral promoter sequences and the trans-activation response element. *AIDS* (1997) 11:139–46. doi: 10.1097/00002030-199702000-00002

29. Veschambre P, Simard P, Jalinot P. Evidence for functional interaction between the HIV-1 Tat transactivator and the TATA box binding protein in vivo. *J Mol Biol*. (1995) 250:169–80. doi: 10.1006/jmbi.1995.0368
30. Andras IE, Pu H, Deli MA, Nath A, Hennig B, Toborek M. HIV-1 Tat protein alters tight junction protein expression and distribution in cultured brain endothelial cells. *J Neurosci Res*. (2003) 74:255–65. doi: 10.1002/jnr.10762
31. Ben Haij N, Planes R, Leghmari K, Serrero M, Delobel P, Izopet J, et al. HIV-1 Tat protein induces production of proinflammatory cytokines by human dendritic cells and monocytes/macrophages through engagement of TLR4-MD2-CD14 complex and activation of NF-kappaB pathway. *PLoS ONE* (2015) 10:e0129425. doi: 10.1371/journal.pone.0129425
32. Ben Haij N, Leghmari K, Planes R, Thieblemont N, Bahraoui E. HIV-1 Tat protein binds to TLR4-MD2 and signals to induce TNF-alpha and IL-10. *Retrovirology* (2013) 10:123. doi: 10.1186/1742-4690-10-123
33. Leghmari K, Bennasser Y, Bahraoui E. HIV-1 Tat protein induces IL-10 production in monocytes by classical and alternative NF-kappaB pathways. *Eur J Cell Biol*. (2008) 87:947–62. doi: 10.1016/j.ejcb.2008.06.005
34. Contreras X, Bennasser Y, Bahraoui E. IL-10 production induced by HIV-1 Tat stimulation of human monocytes is dependent on the activation of PKC beta(II) and delta isozymes. *Microbes Infect*. (2004) 6:1182–90. doi: 10.1016/j.micinf.2004.06.008
35. Bennasser Y, Badou A, Tkaczuk J, Bahraoui E. Signaling pathways triggered by HIV-1 Tat in human monocytes to induce TNF-alpha. *Virology* (2002) 303:174–80. doi: 10.1006/viro.2002.1676
36. Bennasser Y, Contreras X, Moreau M, Le Clerc C, Badou A, Bahraoui E. HIV-1 Tat protein induces IL-10 production by human monocytes: implications of the PKC and calcium pathway. *J Soc Biol*. (2001) 195:319–26. doi: 10.1051/jbio/2001195030319
37. Vives E, Charneau P, van Rietschoten J, Rochat H, Bahraoui E. Effects of the Tat basic domain on human immunodeficiency virus type 1 transactivation, using chemically synthesized Tat protein and Tat peptides. *J Virol*. (1994) 68:3343–53.
38. Hahn S, Buratowski S, Sharp PA, Guarente L, Isolation of the gene encoding the yeast TATA binding protein TFIID: a gene identical to the SPT15 suppressor of Ty element insertions. *Cell* (1989) 58:1173–81. doi: 10.1016/0092-8674(89)90515-1
39. Hahn S, Buratowski S, Sharp PA, Guarente L. Yeast TATA-binding protein TFIID binds to TATA elements with both consensus and nonconsensus DNA sequences. *Proc Natl Acad Sci US A*. (1989) 86:5718–22. doi: 10.1073/pnas.86.15.5718
40. Yang C, Bolotin E, Jiang T, Sladek FM, Martinez E. Prevalence of the initiator over the TATA box in human and yeast genes and identification of DNA motifs enriched in human TATA-less core promoters. *Gene* (2007) 389:52–65. doi: 10.1016/j.gene.2006.09.029
41. Suzuki Y, Tsunoda T, Sese J, Taira H, Mizushima-Sugano J, Hata H, et al. Identification and characterization of the potential promoter regions of 1031 kinds of human genes. *Genome Res*. (2001) 11:677–84. doi: 10.1101/gr.GR-1640R
42. Tullai JW, Schaffer ME, Mullenbrock S, Sholder G, Kasif S, Cooper GM. Immediate-early and delayed primary response genes are distinct in function and genomic architecture. *J Biol Chem*. (2007) 282:23981–95. doi: 10.1074/jbc.M702044200
43. Marban C, Su T, Ferrari R, Li B, Vatakis D, Pellegrini M, et al. Genome-wide binding map of the HIV-1 Tat protein to the human genome. *PLoS ONE* (2011) 6:e26894. doi: 10.1371/journal.pone.0026894
44. Reeder JE, Kwak YT, McNamara RP, Forst CV, D'Orso I. HIV Tat controls RNA Polymerase II and the epigenetic landscape to transcriptionally reprogram target immune cells. *Elife* (2015) 4:e08955. doi: 10.7554/eLife.08955
45. Kashanchi F, Piras G, Radonovich MF, Duvall JF, Fattaey A, Chiang CM, et al. Direct interaction of human TFIID with the HIV-1 transactivator tat. *Nature* (1994) 367:295–9. doi: 10.1038/367295a0
46. Majello B, Napolitano G, Lania L. Recruitment of the TATA-binding protein to the HIV-1 promoter is a limiting step for Tat transactivation. *AIDS* (1998) 12:1957–64. doi: 10.1097/00002030-199815000-00006
47. Wilson JM, Kalasinsky KS, Levey AI, Bergeron C, Reiber G, Anthony RM, et al. Striatal dopamine nerve terminal markers in human, chronic methamphetamine users. *Nat Med*. (1996) 2:699–703. doi: 10.1038/nm0696-699
48. Xu S, Grullon S, Ge K, Peng W. Spatial clustering for identification of ChIP-enriched regions (SICER) to map regions of histone methylation patterns in embryonic stem cells. *Methods Mol Biol*. (2014) 1150:97–111. doi: 10.1007/978-1-4939-0512-6_5
49. Chekmenev DS, Haid C, Kel AE. P-Match: transcription factor binding site search by combining patterns and weight matrices. *Nucleic Acids Res*. (2005) 33:W432–7. doi: 10.1093/nar/gki441
50. Kel AE, Gossling E, Reuter I, Cheremushkin E, Kel-Margoulis OV, Wingender E. MATCH: A tool for searching transcription factor binding sites in DNA sequences. *Nucleic Acids Res*. (2003) 31:3576–9. doi: 10.1093/nar/gkg585
51. Zuris JA, Thompson DB, Shu Y, Guilinger JP, Bessen JL, Hu JH, et al. Cationic lipid-mediated delivery of proteins enables efficient protein-based genome editing *in vitro* and *in vivo*. *Nat Biotechnol*. (2015) 33:73–80. doi: 10.1038/nbt.3081
52. Fu Y, Foden JA, Khayter C, Maeder ML, Reyon D, Joung JK, et al. High-frequency off-target mutagenesis induced by CRISPR-Cas nucleases in human cells. *Nat Biotechnol*. (2013) 31:822–6. doi: 10.1038/nbt.2623
53. Lin S, Staahl BT, Alla RK, Doudna JA. Enhanced homology-directed human genome engineering by controlled timing of CRISPR/Cas9 delivery. *Elife* (2014) 3:e04766. doi: 10.7554/eLife.04766
54. Mali P, Aach J, Stranges PB, Esvelt KM, Moosburner M, Kosuri S, et al. CAS9 transcriptional activators for target specificity screening and paired nickases for cooperative genome engineering. *Nat Biotechnol*. (2013) 31:833–8. doi: 10.1038/nbt.2675
55. Hsu PD, Scott DA, Weinstein JA, Ran FA, Konermann S, Agarwala V, et al. DNA targeting specificity of RNA-guided Cas9 nucleases. *Nat Biotechnol*. (2013) 31:827–32. doi: 10.1038/nbt.2647
56. Janky R, Verfaillie A, Imrichova H, Van de Sande B, Standaert L, Christiaens V, et al. iRegulon: from a gene list to a gene regulatory network using large motif and track collections. *PLoS Comput Biol*. (2014) 10:e1003731. doi: 10.1371/journal.pcbi.1003731
57. Blake JA, Harris MA. The Gene Ontology (GO) project: structured vocabularies for molecular biology and their application to genome and expression analysis. *Curr Protoc Bioinformatics* (2002) Chapter 7:Unit 7.2. doi: 10.1002/0471250953.bi0702s23
58. Harris MA, Clark J, Ireland A, Lomax J, Ashburner M, Foulger R, et al. The Gene Ontology (GO) database and informatics resource. *Nucleic Acids Res*. (2004) 32:D258–61. doi: 10.1093/nar/gkh036
59. Suslov VV, Ponomarenko PM, Efimov VM, Savinkova LK, Ponomarenko MP, Kolchanov NA. SNPs in the HIV-1 TATA box and the AIDS pandemic. *J Bioinform Comput Biol*. (2010) 8:607–25. doi: 10.1142/S0219720010004677
60. Berkhout B, Gatignol A, Rabson AB, Jeang KT. TAR-independent activation of the HIV-1 LTR: evidence that tat requires specific regions of the promoter. *Cell* (1990) 62:757–67. doi: 10.1016/0092-8674(90)90120-4
61. Loregian A, Bortolozzo K, Boso S, Sapino B, Betti M, Biasolo MA, et al. The Sp1 transcription factor does not directly interact with the HIV-1 Tat protein. *J Cell Physiol*. (2003) 196:251–7. doi: 10.1002/jcp.10271
62. Loregian A, Bortolozzo K, Boso S, Caputo A, Palu G. Interaction of Sp1 transcription factor with HIV-1 Tat protein: looking for cellular partners. *FEBS Lett*. (2003) 543:l61–5. doi: 10.1016/S0014-5793(03)00399-5
63. Gersten M, Alirezaei M, Marcondes MC, Flynn C, Ravasi T, Ideker T, et al. An integrated systems analysis implicates EGR1 downregulation in simian immunodeficiency virus encephalitis-induced neural dysfunction. *J Neurosci*. (2009) 29:12467–76. doi: 10.1523/JNEUROSCI.3180-09.2009
64. Sarkar R, Verma SC. Egr-1 regulates RTA transcription through a cooperative involvement of transcriptional regulators. *Oncotarget* (2017) 8:91425–44. doi: 10.18632/oncotarget.20648
65. Achuthan A, Cook AD, Lee MC, Saleh R, Khiew HW, Chang MW, et al. Granulocyte macrophage colony-stimulating factor induces CCL17 production via IRF4 to mediate inflammation. *J Clin Invest*. (2016) 126:3453–66. doi: 10.1172/JCI87828
66. Lech M, Weidenbusch M, Kulkarni OP, Ryu M, Darisipudi MN, Susanti HE, et al. IRF4 deficiency abrogates lupus nephritis despite enhancing

systemic cytokine production. *J Am Soc Nephrol*. (2011) 22:1443–52. doi: 10.1681/ASN.2010121260

67. Basehoar AD, Zanton SJ, Pugh BF. Identification and distinct regulation of yeast TATA box-containing genes. *Cell* (2004) 116:699–709. doi: 10.1016/S0092-8674(04)00205-3
68. Chitikila, Huisinga KL, Irvin JD, Basehoar AD, Pugh BF. Interplay of TBP inhibitors in global transcriptional control. Mol *Cell* (2002) 10:871–82. doi: 10.1016/S1097-2765(02)00683-4
69. Jackson-Fisher AJ, Chitikila C, Mitra M, Pugh BF. A role for TBP dimerization in preventing unregulated gene expression. *Mol Cell* (1999) 3:717–27. doi: 10.1016/S1097-2765(01)80004-6

Conflict of Interest Statement: The authors declare that the research was conducted in the absence of any commercial or financial relationships that could be construed as a potential conflict of interest.

frontiers in Immunology

ORIGINAL RESEARCH
published: 20 February 2019
doi: 10.3389/fimmu.2019.00267

Galectin-9 Mediates HIV Transcription by Inducing TCR-Dependent ERK Signaling

*Florent Colomb[1], Leila B. Giron[1], Thomas A. Premeaux[2], Brooks I. Mitchell[2], Toshiro Niki[3,4], Emmanouil Papasavvas[1], Luis J. Montaner[1], Lishomwa C. Ndhlovu[2] and Mohamed Abdel-Mohsen[1]**

[1] Vaccine and Immunotherapy Center, The Wistar Institute, Philadelphia, PA, United States, [2] Department of Tropical Medicine, Hawaii Center for AIDS, John A. Burns School of Medicine, University of Hawaii, Honolulu, HI, United States, [3] GalPharma Co., Ltd., Takamatsu-shi, Takamatsu, Japan, [4] Department of Immunology and Immunopathology, Kagawa University, Takamatsu, Japan

Endogenous plasma levels of the immunomodulatory carbohydrate-binding protein galectin-9 (Gal-9) are elevated during HIV infection and remain elevated after antiretroviral therapy (ART) suppression. We recently reported that Gal-9 regulates HIV transcription and potently reactivates latent HIV. However, the signaling mechanisms underlying Gal-9-mediated viral transcription remain unclear. Given that galectins are known to modulate T cell receptor (TCR)-signaling, we hypothesized that Gal-9 modulates HIV transcriptional activity, at least in part, through inducing TCR signaling pathways. Gal-9 induced T cell receptor ζ chain (CD3ζ) phosphorylation (11.2 to 32.1%; $P = 0.008$) in the J-Lat HIV latency model. Lck inhibition reduced Gal-9-mediated viral reactivation in the J-Lat HIV latency model (16.8–0.9%; $P < 0.0001$) and reduced both Gal-9-mediated $CD4^+$ T cell activation (10.3 to 1.65% CD69 and CD25 co-expression; $P = 0.0006$), and IL-2/TNFα secretion ($P < 0.004$) in primary $CD4^+$ T cells from HIV-infected individuals on suppressive ART. Using phospho-kinase antibody arrays, we found that Gal-9 increased the phosphorylation of the TCR-downstream signaling molecules ERK1/2 (26.7-fold) and CREB (6.6-fold). ERK and CREB inhibitors significantly reduced Gal-9-mediated viral reactivation (16.8 to 2.6 or 12.6%, respectively; $P < 0.0007$). Given that the immunosuppressive rapamycin uncouples HIV latency reversal from cytokine-associated toxicity, we also investigated whether rapamycin could uncouple Gal-9-mediated latency reactivation from its concurrent pro-inflammatory cytokine production. Rapamycin reduced Gal-9-mediated secretion of IL-2 (4.4-fold, $P = 0.001$) and TNF (4-fold, $P = 0.02$) without impacting viral reactivation (16.8% compared to 16.1%; $P = 0.2$). In conclusion, Gal-9 modulates HIV transcription by activating the TCR-downstream ERK and CREB signaling pathways in an Lck-dependent manner. Our findings could have implications for understanding the role of endogenous galectin interactions in modulating TCR signaling and maintaining chronic immune activation during ART-suppressed HIV infection. In addition, uncoupling Gal-9-mediated viral reactivation from undesirable pro-inflammatory effects, using rapamycin, may increase the potential utility of recombinant Gal-9 within the reversal of HIV latency eradication framework.

Keywords: HIV, lectins, galectin-9, T cell receptor, TCR signaling, rapamycin, HIV latency, HIV persistence

OPEN ACCESS

Edited by:
Sara Gianella Weibel, University of California, San Diego, United States

Reviewed by:
Pierre Busson, Centre National de la Recherche Scientifique (CNRS), France
Yvonne Rosenstein, Universidad Nacional Autónoma de México, Mexico

***Correspondence:**
Mohamed Abdel-Mohsen
mmohsen@wistar.org

Specialty section:
This article was submitted to Viral Immunology, a section of the journal Frontiers in Immunology

Received: *13 November 2018*
Accepted: *31 January 2019*
Published: *20 February 2019*

Citation:
Colomb F, Giron LB, Premeaux TA, Mitchell BI, Niki T, Papasavvas E, Montaner LJ, Ndhlovu LC and Abdel-Mohsen M (2019) Galectin-9 Mediates HIV Transcription by Inducing TCR-Dependent ERK Signaling. Front. Immunol. 10:267. doi: 10.3389/fimmu.2019.00267

INTRODUCTION

Antiretroviral therapy (ART) effectively suppresses HIV replication but does not achieve viral eradication due to the persistence of latently-infected, long-lived $CD4^+$ T cells (1, 2). This persistent infection leads to continued immune activation, chronic inflammation, and ongoing damage to multiple organ systems (3, 4). Many studies indicate that HIV persistence is regulated, at least in part, by the immune system (5–8). Thus, understanding the host immune factors driving and maintaining HIV persistence is needed to develop new strategies to cure HIV and/or prevent the development of HIV-associated co-morbidities, which remain prevalent despite suppressive therapy.

One key regulator of immunological functions, and several cellular processes, is interactions between cell-surface glycans and glycan-binding proteins (lectins) (9–12). One class of lectins that play critical roles in T cell function are galectins, a family of β-galactoside-binding, soluble lectins (13–17). Among galectins, galectin-9 (Gal-9) has recently been recognized to play an essential role in regulating both adaptive and innate defense mechanisms and thus may be involved in HIV pathogenesis (18–20). Our prior work showed that endogenous secretion of Gal-9 is rapidly increased after HIV infection, and that elevated levels of Gal-9 do not return to normal after suppressive ART (20). More recently, we reported that the endogenous levels of Gal-9 are associated with HIV transcription *in vivo,* in plasma of HIV-infected, ART-suppressed individuals (8). We also demonstrated that treating $CD4^+$ T cells with recombinant Gal-9 (rGal-9) induces HIV transcription and reverses HIV latency *in vitro* and *ex vivo* (8). However, the signaling pathways by which Gal-9 modulates HIV transcriptional activity remain unclear.

The goal of this work was to identify the signaling mechanisms underlying Gal-9-mediated HIV transcription. We hypothesized that Gal-9 modulates HIV transcriptional activity through T cell receptor (TCR) signaling transduction, based on results in non-HIV contexts showing that galectins, including Gal-9, modulate TCR-signaling (21–23), and that Gal-9 interacts with various cell-surface proteins known to induce TCR signaling, including CD44 (24) and 41-BB (25–27). We show that Gal-9 modulates HIV transcription through activating the TCR-downstream ERK and CREB signaling pathways in a lymphocyte-specific protein tyrosine kinase (Lck)-dependent manner. This signaling pathway also induces an undesirable, pro-inflammatory response, namely secretion of IL-2 and TNF-α, and activating $CD4^+$ T cells. This pro-inflammatory response can be inhibited using the mTOR pathway inhibitor, rapamycin, without impacting Gal-9-mediated viral reactivation. Our results could have implications for understanding the role of endogenous galectin-9 in modulating TCR signaling *in vivo* and maintaining chronic immune activation during ART-suppressed HIV infection. In addition, uncoupling Gal-9-mediated viral reactivation from undesirable pro-inflammatory effects, using rapamycin, may increase the potential utility of rGal-9 within the reversal of HIV latency eradication framework.

MATERIALS AND METHODS

Cell Lines

As a model of HIV latency, we used "J-Lat" cells, which harbor latent, transcriptionally competent HIV provirus that encodes green fluorescent protein (GFP) as an indicator of viral reactivation (28, 29). We have shown in our previous work (8) that this latency model mimics the impact of Gal-9 on HIV transcription *ex vivo* using $CD4^+$ T cells from HIV-infected ART-suppressed individuals. Therefore, it can be used to investigate the signaling mechanisms underlying Gal-9-mediated viral transcription. J-Lat 5A8 clone was kindly provided by Dr. Warner Greene (The Gladstone Institute of Virology and Immunology). J-Lat 15.4 (catalog number 9850), 10.6 (catalog number 9849), and Jurkat E6-1 (catalog number 177) clones were provided by the NIH AIDS Reagent Program (Germantown, MD). J.CaM1.6 clone, a derivative mutant of Jurkat cells, which is deficient in Lck activity (30), was purchased from American Type Culture Collection (ATCC; Manassas, VA; catalog number CRL-2063). Cell lines were maintained in Roswell Park Memorial Institute (RPMI) medium with L-glutamine (Corning Cellgro, Tewksbury, MA, United States), supplemented with 10% Fetal Bovine Serum (Gibco, Thermo Fisher Scientific, Waltham, MA, United States), and 1% Penicillin/Streptomycin (Thermo Fisher Scientific, Waltham, MA, United States).

Primary Cells

Cryopreserved peripheral blood mononuclear cells (PBMCs) were retrospectively collected from five HIV-infected individuals on suppressive ART, enrolled in the Philadelphia FIGHT cohort. Research protocols were approved by Wistar Institute and Philadelphia FIGHT Committees on Human Research. Written informed consent was obtained for all participants, and all data and specimens were coded to protect confidentiality. Subject characteristics are documented in **Supplementary Table 1**.

Reagents

A stable form of recombinant galectin-9 was obtained through our collaborators at GalPharma Co., Ltd. (Kagawa, Japan). A natural form of recombinant galectin-9 was purchased from R&D Systems (Minneapolis, MN; catalog # 2045-GA-050). Lck inhibitor A770041 was purchased from Axon Med Chem (Reston, VA). ERK inhibitor LY3214996 was purchased from Selleck Chemicals (Houston, TX). CREB inhibitor 666-15 and InSolution Rapamycin were purchased from Millipore Sigma (Burlington, MA). SMARTpool Accell Lck siRNA was purchased from Dharmacon (Lafayette, CO; cat # E-003151-00-0005) and Silencer™ Select Negative Control No. 1 siRNA was purchased from Thermo Fisher (Waltham, MA; cat# 4390843). ImmunoCult Human CD3/CD28 T Cell Activator was purchased from STEMCELL (Vancouver, BC, Canada).

Phosphorylated CD3ζ-Chain Quantification

J-Lat 5A8, Jurkat, or J.CaM1.6 cells were cultured at 1×10^6 cells/ml and treated with stable form of rGal-9 (200 nM), natural form of rGal-9 (200 nM), or an equivalent volume of phosphate buffered saline (PBS), in the presence of Lck inhibitor (1 μM)

or an equivalent volume of dimethyl sulfoxide (DMSO). After 15 min, cells were collected, washed twice in ice-cold PBS, fixed, and permeabilized using the BD Cytofix/Cytoperm kit according to the manufacturer's instructions. Fixed cells were stained with PE anti-CD247 (TCRζ, CD3ζ) antibody (Clone 6B10.2, Biolegend), washed, and analyzed for PE fluorescence using LSR II flow cytometer and FACSDiva software (Becton Dickinson, Mountain View, CA, United States). Data were analyzed using FlowJo (TreeStar Inc., Ashland, OR, United States).

Human Phospho-Kinase Antibody Array

Proteome profiler human phospho-kinase arrays were purchased from R&D Systems, Inc. (Minneapolis, MN, United States). Ten million J-Lat 5A8 cells were treated for 30 min with 200 nM rGal-9 or an equivalent volume of PBS. Cells were washed twice in cold PBS and processed according to the manufacturer's instructions. Briefly, the cells were lysed for 30 min on a rotating shaker at 4°C. Lysates were centrifuged at 14,000 g for 5 min, and supernatants were incubated on the array membrane overnight on an orbital shaker at 4°C. Membranes were washed three times and incubated for 2 h at room temperature with anti-horseradish peroxidase antibody. After another three washes, membranes were incubated for 1 min with Chemi Reagent. Membrane images were captured using ImageQuant LAS 4010 (GE Healthcare Bio-Sciences, Pittsburg, PA, United States) and densitometry analysis was performed with Image Studio Lite Version 5.2 (LI-COR Biotechnology, Lincoln, NE, United States).

Measurement of HIV Latency Reversal

J-Lat 5A8, 10.6, and 15.4 cells were pre-incubated for 1 h with 1 μM for Lck inhibitor, 1 μM for ERK1/2 inhibitor, 1 μM for CREB inhibitor, 5 μM for rapamycin, or an equivalent volume of PBS. Cells were then treated with rGal-9 (multiple concentrations), 25 μl of ImmunoCult human CD3/CD28 T Cell Activator, or an equivalent volume of PBS, for 24 h. Mean fluorescence intensity of HIV-encoded GFP expression was assessed using LSR II flow cytometer and FACSDiva software. Data were analyzed with FlowJo.

Lck Silencing Using Small Interfering RNA (siRNA)

J-Lat 5A8 were resuspended in Nucleofector solution (Lonza) at 1×10^6 cells/100 μL, in the presence of 1.5 μM of Silencer™ Select (non-target) negative control No. 1 siRNA (Thermo Fisher, Cat# 4390843) or SMARTpool Accell Lck siRNA (Dharmacon, Cat # E-003151-00-0005). Cells were nucleofected using Amaxa Nucleofector4D (Lonza), according to manufacturer protocol for Jurkat clone E6.1 nucleofection. Cells were then plated in 1 ml of RPMI supplemented with 10% FBS. After 48 h, cells were resuspended in fresh medium at 1×10^6 cells/ml, plated in 96-well plates, and treated with rGal-9 (200 nM), or an equivalent volume of PBS, for 24 h. Mean fluorescence intensity of HIV-encoded GFP expression was assessed using LSR II flow cytometer and FACSDiva software. Data were analyzed with FlowJo.

Isolation and Treatment of Primary $CD4^+$ T Cells

CD4+ T cells were enriched from the cryopreserved PBMCs by negative selection using the EasySep Human $CD4^+$ T Cell Enrichment Kit (Stemcell Technologies), according to the manufacturer's instructions. Primary $CD4^+$ T cells were maintained in RPMI with L-glutamine supplemented with 20% FBS. Primary $CD4^+$ T cells were pre-incubated with 1 μM for Lck inhibitor or 5 μM for rapamycin. Cells were then treated with 500 nM of rGal-9, ImmunoCult human CD3/CD28 T Cell Activator, or an equivalent volume of PBS, for 24 h. Cells were centrifuged for 5 min at 250 g, and cells and supernatants were collected separately.

Measurement of $CD4^+$ T Cells Viability and Activation

The surface expression of CD69 and CD25 markers of T-cell activation were measured using flow cytometry. Cells were stained with Zombie Aqua Fixable Viability Kit (Biolegend) and then stained with the following fluorescently-conjugated monoclonal antibodies: APC mouse anti-human CD3 (Clone UCHT1, Biolegend), V450 mouse anti-human CD4 (Clone RPA-T4, Biolegend), PE mouse anti-human CD69 (Clone FN50, Biolegend), PerCP-Cy5.5 mouse anti-human CD25 (Clone M-A251, Biolegend). Apoptosis was determined using Propidium iodide and Annexin V Pacific blue (Biolegend). anti-CD95 (1 ug/ml; clone E0S9.1; Biolegend) stimulation for 6 h was used as positive control for apoptosis. Cells were analyzed using LSR II flow cytometer and FACSDiva software. Data were analyzed with FlowJo software.

Measurement of TNF-α and IL-2 Levels Using ELISA

Supernatants from J-Lat 5A8 and primary $CD4^+$ T cells cultures treated or not with rGal-9, αCD3/αCD28, and inhibitors were collected. Levels of TNFα and IL-2 cytokines were quantified using human TNF and IL-2 DuoSet Elisa kits (R&D Systems, Inc., Minneapolis, MN) according to the manufacturer's instructions. Optical density was measured at 450 and 540 nm using Versa Max microplate reader. Data were analyzed using GraphPad Prism.

Measurement of Cytokine Secretion Using Multiplex Luminex

Isolated $CD4^+$ T cells from three HIV-infected ART-suppressed individuals were treated with 200 nM Gal-9, 500 nM Gal-9, or 0.5% DMSO as control for 4 h, 24 h, or 3 days. Culture supernatants were collected after 3 days and were processed according to recommended manufacture procedure with a Milliplex MAP Human High Sensitivity T Cell Panel (EMD Millipore, Billerica, Massachusetts) for GM-CSF, TNF-α, IL-13, IL-12 (p70), IL-10, IL-8, IL-7, IL-6, IL-5, IL-4, IL-2, IL-1b, and IFN-γ. Samples were acquired on a Luminex 200 (EMD Millipore). Samples were run in duplicate. The intra-assay CV% for analytes measured was <7%. The inter-assay CV% was <11%.

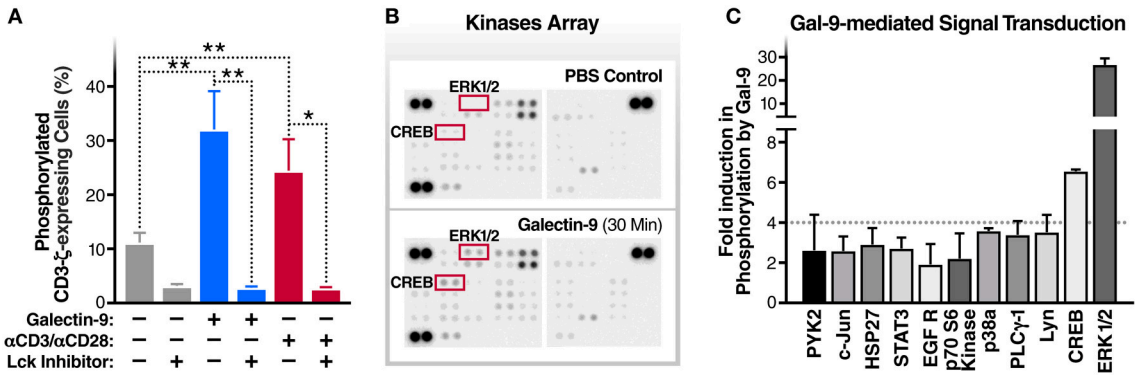

FIGURE 1 | Gal-9 induces the phosphorylation of TCR complex CD3ζ chain, ERK, and CREB. **(A)** J-Lat 5A8 cells were treated with Gal-9 (200 nM, blue bars) or αCD3/αCD28 antibodies (red bars) for 15 min in the presence or absence of Lck inhibitor (1 μM) and stained with PE-conjugated anti-phospho-CD3ζ antibody. Cell staining/phosphorylation was quantified by flow cytometry. Mean ± SD is displayed, and statistical comparisons were performed using two-tailed unpaired *t*-tests. $^{*}p < 0.05$, and $^{**}p < 0.01$. **(B,C)** J-Lat 5A8 cells were treated with Gal-9 (200 nM) or an equivalent volume of PBS for 30 min and analyzed using Proteome Profiler Human Phospho-Kinase Array Kit. **(B)** Array images were captured using ImageQuant™ LAS 4,000 and **(C)** phosphorylation signal intensity was analyzed by pixel density quantification using Image Studio Lite.

Statistical Analysis

Two-tailed paired and unpaired *t*-tests were used for comparisons. All statistical analyses were conducted using GraphPad Prism release 7.0 (GraphPad Software, San Diego, CA, United States) and statistical significance was set at a *p*-value of 0.05.

RESULTS

Gal-9 Induces Lck-Dependent T Cell Receptor ζ Chain (CD3ζ) Phosphorylation

The T cell receptor ζ chain (CD3ζ) is the principal signal transduction component of TCR signaling (31–33). Lck activity is required for the phosphorylation of signaling motifs in CD3-ζ and this phosphorylation is the initial step in the TCR signaling cascade (34, 35). To begin to test our hypothesis that Gal-9-mediates HIV transcriptional activity by activating TCR signaling, we examined the impact of rGal-9 on the phosphorylation of CD3ζ in the J-Lat 5A8 latency model. rGal-9 significantly induced the percentage of cells expressing phosphorylated CD3ζ [from 11.2 ± 1.8% to 32.1 ± 7.0% (mean ± SD); $P = 0.0076$] (**Figure 1A**). This induction was completely inhibited by preincubation with an Lck inhibitor (from 32.1 ± 7.0% to 2.8 ± 0.2%; $P = 0.002$) (**Figure 1A**). To confirm that Gal-9-mediated CD3ζ phosphorylation is Lck-dependent, we used the J.CaM1.6 clone (a derivative mutant of Jurkat cells, which is deficient in Lck activity). rGal-9 induced CD3ζ phosphorylation in wild type Jurkat cells [from 8.2 ± 2.2% to 44.4 ± 6.2% (mean ± SD); $P = 0.0007$], but had no effect on J.CaM1.6 (from 2.1 ± 0.6% to 1.6 ± 0.02%; $P = 0.23$) (**Supplementary Figure 1**). Confirming dose-dependent relationship, we found that rGal-9 is able to phosphorylate CD3ζ starting from 25 nM in the J-Lat 5A8 HIV latency model (**Supplementary Figure 2**). These data demonstrate that Gal-9 induces TCR-signaling in HIV latently-infected cells through Lck-mediated CD3ζ phosphorylation.

Gal-9 Induces Phosphorylation of ERK and CREB Signaling Molecules

To identify components of the TCR signaling cascade that are induced by Gal-9 downstream of CD3ζ phosphorylation, we used Proteome Profiler Human Phospho-Kinase arrays to assess the phosphorylation levels of 43 kinases and related transcription factors. rGal-9 treatment of J-Lat 5A8 cells induced the phosphorylation of several downstream effectors of TCR signaling, including ERK1/2 (26.7-fold) and CREB (6.6-fold) (**Figures 1B,C**). These data demonstrate that Gal-9-mediated induction of CD3ζ phosphorylation results in activation of ERK1/2 and CREB signaling pathways.

Gal-9 Modulates HIV Transcription Through Activating the TCR Downstream Signaling, ERK and CREB, in an Lck Dependent Manner

To evaluate whether TCR/Lck-dependent ERK1/2-CREB phosphorylation modulate the reactivation of latent HIV by Gal-9, we assessed the impact of Lck, ERK, and CREB inhibitors on rGal-9-mediated HIV latency reactivation in three J-Lat HIV latency model clones, 5A8, 10.6, and 15.4. Lck inhibition strongly reduced rGal-9-mediated HIV latency reactivation in the J-Lat 5A8 clone [from 16.8 ± 0.7% to 0.9 ± 0.03% (mean ± SD); $P < 0.0001$], the J-Lat 10.6 clone (from 41.9 ± 4.9% to 9.9 ± 0.44%; $P = 0.0004$), and the J-Lat 15.4 clone (from 2.5 ± 0.64% to 0.1 ± 0.06%; $P = 0.0027$). ERK inhibition showed a similar strong reduction of rGal-9-mediated HIV latency reactivation in the J-Lat 5A8 clone [from 16.8 ± 0.7% to 2.6 ± 0.3% (mean ± SD); $P < 0.0001$], the J-Lat 10.6 clone (from 41.9 ± 4.9% to 21.23 ± 1.29%; $P = 0.002$), and the J-Lat 15.4 clone (from 2.5 ± 0.64% to 0.1 ± 0.1%; $P = 0.0029$). Last, CREB inhibition showed a modest, yet significant, reduction in rGal-9-mediated HIV latency reactivation in the J-Lat 5A8 clone [from 16.8 ± 0.7% to 12.6 ± 0.3% (mean ± SD); $P =$

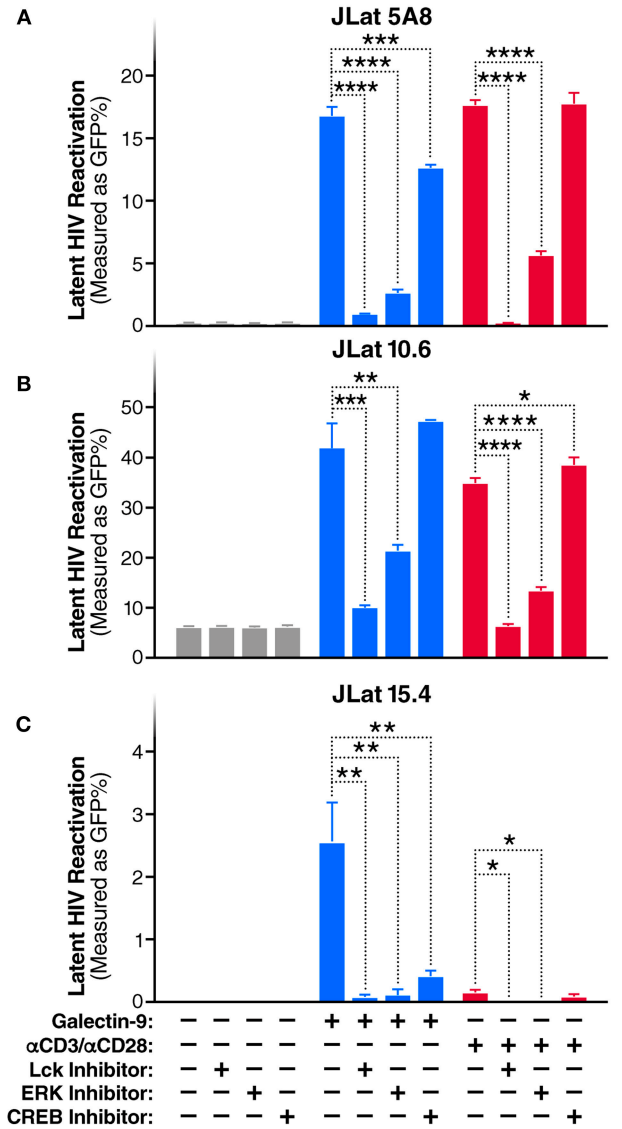

FIGURE 2 | Gal-9 induces HIV transcription through TCR-dependent ERK/CREB signaling. Levels of latent HIV reactivation in three J-Lat clones 24 h after *in vitro* stimulation with Gal-9 (200 nM) in the presence or absence of 1 μM of Lck inhibitor, ERK inhibitor, or CREB inhibitor. HIV-encoded GFP expression was detected by flow cytometry. **(A)** J-Lat 5A8, **(B)** J-Lat 10.6, **(C) J**-Lat 15.4 cells. αCD3 /αCD28 antibodies (red bars) were used as a positive control. Mean ± SD is displayed, and statistical comparisons were performed using two-tailed unpaired *t*-tests. *$p < 0.05$; **$p < 0.01$, ***$p < 0.001$, and ****$p < 0.0001$.

0.0007], and the J-Lat 15.4 clone (from 2.5 ± 0.64% to 0.4 ± 0.1%; $P = 0.0047$) (**Figures 2A–C**). As expected, Lck/ERK/CREB inhibition had a similar impact on αCD3/αCD28-mediated HIV latency reactivation (**Figures 2A–C**). To confirm the role of Lck in Gal-9-mediated HIV latency reactivation, we used siRNA to silence Lck in the J-Lat 5A8 HIV latency model. Lck siRNA significantly reduced Gal-9-mediated HIV latency reactivation compared to non-target siRNA control [from 13.4 ± 0.3% to 6.8 ± 0.2% (mean ± SD); $P < 0.0001$] (**Supplementary Figure 3**). Confirming a dose-dependent relationship, we found that rGal-9 is able to reactivate a fraction of latent HIV at 10 nM in the J-Lat 5A8 HIV latency model (**Supplementary Figure 4**). Together, these data indicate that Gal-9 modulates HIV transcriptional activity through induction of TCR/Lck-mediated ERK1/2 signaling and to a lesser extent CREB signaling.

Throughout this study, we are using a stable form of galectin-9 (8, 22, 26, 36–39). To confirm that the natural form of Gal-9 functions in a similar way as the stable form in phosphorylating CD3ζ and reactivating HIV latency, we repeated some of the above experiments using a natural form of recombinant Gal-9 (R&D systems). The natural form of recombinant Gal-9 induced CD3ζ phosphorylation [from 8.2 ± 2.2% to 44.4 ± 6.2% (mean ± SD); $P = 0.0007$], and HIV latency reactivation [from 0.1 ± 00.6% to 20.2 ± 0.8% (mean ± SD); $P < 0.0001$] in the J-Lat 5A8 HIV latency model, and these effects were significantly inhibited by Lck inhibitor (**Supplementary Figures 5A,B**).

Gal-9-Mediated CD4$^+$ T Cell Activation Is Lck-Dependent

Next, to determine whether Gal-9-mediated T cell activation is dependent on the same mechanism as Gal-9-mediated viral activation, we examined the impact of Lck inhibition of Gal-9-mediated CD4$^+$ T cell activation in primary cells from HIV-infected ART-suppressed individuals. Cell viability was determined using Zombie Aqua Fixable Viability and apoptosis was determined using Propidium iodide and Annexin V staining (**Supplementary Figure 6**). T cell activation was measured by co-expression of the T cell-surface activation markers CD69 and CD25. rGal-9 induced CD4$^+$ T cell activation [from 0.14 ± 0.03% to 10.34 ± 1.1% (mean ± SEM)]. This effect was significantly reduced by Lck inhibition (from 10.34 ± 1.1% to 1.65 ± 0.5%; $P = 0.0006$) (**Figure 3**). Lck inhibition did not fully inhibit Gal-9-mediated T cell activation, suggesting that while TCR signaling plays a major role in Gal-9-mediated T cell activation, other signaling pathways may contribute to this effect.

Gal-9 Induces IL2 and TNF-α Secretion by Inducing Lck-Dependent ERK and CREB Signaling

Given that Gal-9 induces TCR signaling and activates T cells, we posited that the Gal-9-mediated reactivation of HIV latency would be accompanied by secretion of pro-inflammatory cytokines. Indeed, rGal-9 treatment of J-Lat 5A8 cells was associated with a significant induction of IL2 [from < 15.6 pg/ml to 375.6 ± 28.1 pg/ml (mean ± SD)] and TNFα (from <15.6 pg/ml to 208.8 ± 9.7 pg/ml). This effect was significantly reduced by inhibiting Lck, ERK, or CREB activity ($P < 0.001$; **Figures 4A,B**). Similar results were obtained using primary CD4$^+$ T cells from HIV-infected, ART-suppressed individuals: rGal-9 significantly induced the production of IL2 (from < 15.6 pg/ml to 700.2 ± 93.1 pg/ml (mean ± SEM)] and TNFα (from <15.6 pg/ml to 1372.68 ± 240.75 pg/ml); Lck inhibition significantly reduced IL2 (from 700.2 ± 93.1 pg/ml to 47.9 ± 47.9

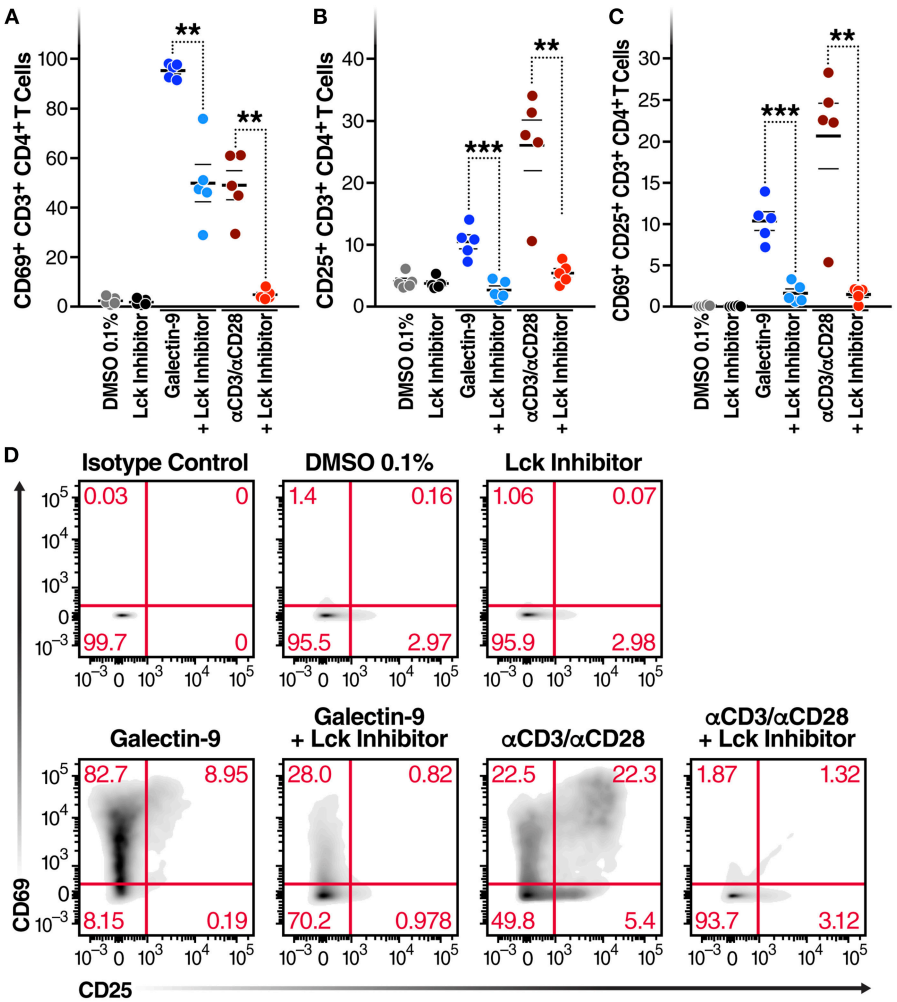

FIGURE 3 | Gal-9-mediated CD4$^+$ T cell activation is Lck-dependent. CD4$^+$ T cells isolated from 5 HIV-infected ART-suppressed individuals were treated for 24 h with Gal-9 (500 nM) or the equivalent volume of PBS (Control) in the presence of 1 μM of Lck inhibitor or the equivalent volume of DMSO. Cells were analyzed by flow cytometry for expression of CD69 and CD25 activation markers. **(A)** % of CD4$^+$ T cells expressing CD69, **(B)** % of CD4+ T cells expressing CD25, **(C)** % of CD4$^+$ T cells co-expressing CD69 and CD25. **(D)** A representative flow cytometry plot of one individual. αCD3/αCD28 antibodies were used as a positive control. Mean ± SEM is displayed, and statistical comparisons were performed using two-tailed paired *t*-tests. $^{**}p < 0.01$, and $^{***}p < 0.001$.

pg/ml; $P = 0.0006$) and TNFα secretion (from 1372.68 ± 240.75 pg/ml to 37.8 ± 37.8 pg/ml; $P = 0.0035$) (**Figures 4C,D**). Further, we examined the impact of rGal-9 on the secretion of a panel of pro and anti-inflammatory cytokines. **Supplementary Figure 7** shows that rGal-9 induces the secretion of several pro- and anti- inflammatory cytokines. Together the data in **Figures 3**, **4** demonstrate that Gal-9-mediated T cell activation and pro-inflammatory cytokine secretion are dependent on the same mechanism that induces HIV transcriptional activity, namely Lck-mediated induction of the TCR downstream ERK/CREB signaling. These undesirable, pro-inflammatory effects of Gal-9 limit its potential to be used as an HIV latency reversal agent. Thus, we asked whether it would be possible to separate the desirable (HIV latency reversal) from the undesirable (T cell activation and cytokine secretion) effects of Gal-9.

Rapamycin Reduces Gal-9-Mediated Cytokine-Secretion Without Impacting the Ability of Gal-9 to Reactivate HIV

A recent study demonstrated that the immunosuppressive mTOR inhibitor rapamycin can uncouple HIV latency reversal from cytokine-associated toxicity (40). Furthermore, it has been shown that rapamycin can inhibit the proinflammatory effects of Gal-9 (41). We, therefore, investigated whether rapamycin could uncouple Gal-9-mediated latency reactivation from its concurrent effect on pro-inflammatory cytokine production. Co-treatment with rapamycin (5 μM) did not reduce the ability of Gal-9 to reactivate latent HIV (5 μM) [16.8 ± 0.7% compared to 16.1 ± 0.3% (mean ± SD); $P = 0.2$] (**Figure 5A**). However, rapamycin did significantly reduce Gal-9-mediated secretion of IL-2 [from 375.6 ± 28.13 pg/ml to 194.8 ± 12.43 pg/ml

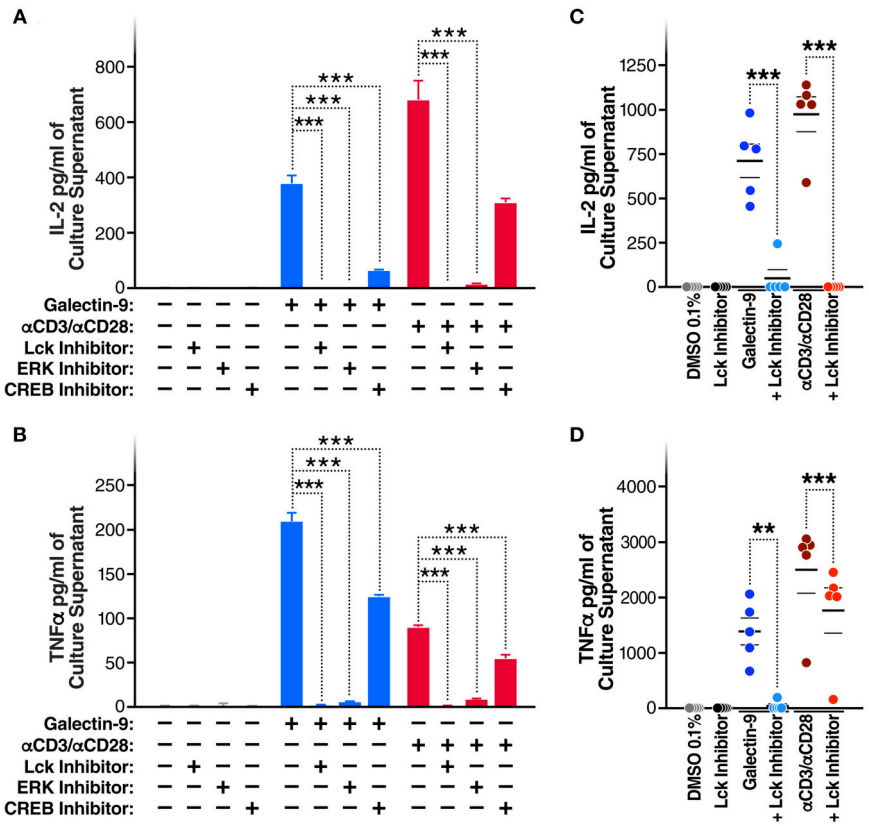

FIGURE 4 | Gal-9 induces IL2 and TNF-α secretion by the same mechanism as viral reactivation. **(A)** IL2 and **(B)** TNF-α concentrations quantified by ELISA, in J-LAT 5A8 cell culture supernatants, after 24 h of Gal-9 treatment (200 mM) in presence or absence of 1 μM of Lck inhibitor, ERK inhibitor, or CREB inhibitor. Mean ± SD is displayed, and statistical comparisons were performed using two-tailed unpaired *t*-tests. ***$p < 0.001$. **(C)** IL2 and **(D)** TNF concentrations quantified by ELISA, in supernatants from $CD4^+$ T cells from five HIV-infected, ART-suppressed individuals, after 24 h treatment with Gal-9 (500 nM) or the equivalent volume of PBS (Control) in the presence of 1 μM of Lck inhibitor or the equivalent volume of DMSO. αCD3/αCD28 antibodies were used as a positive control. Mean ± SEM is displayed, and statistical comparisons were performed using two-tailed paired *t*-tests. **$p < 0.01$, and ***$p < 0.001$.

(mean ± SD); $P < 0.001$] and TNF (from 208.8 ± 9.7 pg/ml to 107.2 ± 5 pg/ml; $P < 0.001$) in the J-Lat 5A8 latency model (**Figures 5B,C**). Similarly, Rapamycin reduced Gal-9-mediated secretion of IL-2 [from 700.23 ± 91.1 pg/ml to 160.36 ± 105.9 pg/ml (mean ± SEM); $P = 0.0006$] and TNF (from 1372.68 ± 240.75 pg/ml to 340.13 ± 120.6 pg/ml; $P = 0.0015$) in primary $CD4^+$ T cells from HIV-infected individuals on suppressive ART (**Figures 5D,E**). These data demonstrate that mTOR signaling inhibition may be used to uncouple Gal-9-mediated viral reactivation from undesirable pro-inflammatory effects.

DISCUSSION

Gal-9 promotes HIV transcription by a previously unidentified mechanism (8). Given that Gal-9 is known to cross-link several surface proteins, some of which are involved in TCR signaling and that Gal-9 can induce TCR signaling (22), we hypothesized that Gal-9 promotes HIV transcriptional activity through TCR signaling transduction. In this study, we demonstrate that Gal-9 modulates HIV transcription through activating the TCR-downstream ERK and CREB signaling pathways, in an Lck-dependent manner. We also show that this same signaling pathway that induces HIV transcription also induces an undesirable pro-inflammatory response, namely secretion of IL-2 and TNFα as a consequence of T cell activation. These undesirable, Gal-9-mediated pro-inflammatory responses can be inhibited using the mTOR pathway inhibitor, rapamycin, without blunting Gal-9-mediated viral reactivation.

Gal-9 has several effects on T cells during HIV infection. It renders $CD4^+$ T cells less susceptible to HIV infection via induction of the host restriction factor cyclin-dependent kinase inhibitor 1 (p 21) (42). It can also increase HIV entry by inducing the $CD4^+$ T cell-surface concentration of protein disulfide isomerase (PDI) (43). We have previously shown that the endogenous levels of Gal-9 are induced after HIV infection and that these levels do not return to normal levels after ART suppression (20). We also found a positive correlation between endogenous levels of Gal-9 and levels of HIV transcription in $CD4^+$ T cells during ART suppression (8). The impact of this chronically elevated levels of Gal-9 on immune functions during ART-suppressed HIV infection is not

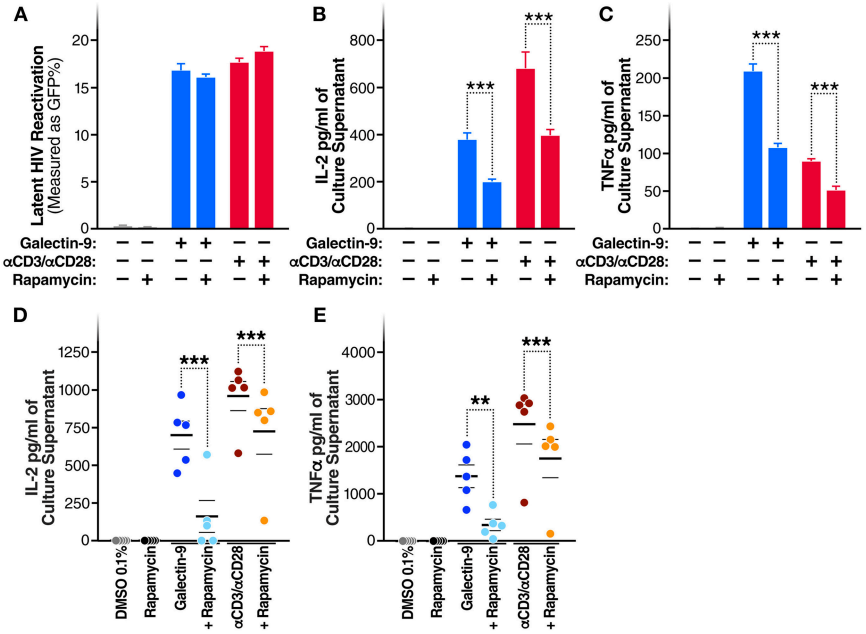

FIGURE 5 | Rapamycin reduces Gal-9-mediated cytokine-secretion without impacting the ability of Gal-9 to reactivate HIV. **(A)** Viral reactivation in J-Lat 5A8 cells by Gal-9 (200 nM) in the presence or absence of 5 μM of rapamycin. Concentration of **(B)** IL2, and **(C)** TNF-α quantified by ELISA in cell culture supernatants. Mean ± SD is displayed, and statistical comparisons were performed using two-tailed unpaired *t*-tests. ***$p < 0.001$. Concentration of IL2 **(D)** and TNF-α **(E)** secretion quantified by ELISA in culture supernatants of $CD4^+$ T cells isolated from five HIV+ ART-suppressed individuals after 24 h of Gal-9 stimulation (500 mM) in the presence of absence of 5 μM rapamycin. Mean ± SEM are displayed, and statistical comparisons were performed using two-tailed paired *t*-tests. **$p < 0.01$, and ***$p < 0.001$.

clear. Our current study demonstrates that Gal-9 induces Lck-dependent ERK/CREB signaling in HIV-infected latently infected cells, which may explain the correlation between Gal-9 and HIV transcriptional activity *in vivo*. However, this induction of TCR signaling by Gal-9 raises an important question of whether elevated endogenous Gal-9 levels contribute to the state of chronic inflammation and chronic immune activation during suppressive ART. Elevated T cell activation persists during suppressive ART (44) and is associated with the development of HIV-associated co-morbidities and premature mortality (44–47); it may also contribute to HIV persistence (48–51). This chronic immune activation involves multifactorial mechanisms (52–59), and the persistent induction of TCR signaling by the elevated levels of endogenous Gal-9 may be playing an important, unrecognized, role in sustaining it. Interventions that target Gal-9 may prove useful in inhibiting chronic immune activation, which might ultimately reduce the development of HIV-associated co-morbidities and levels of HIV persistence during suppressive ART.

Gal-9 is a multifaceted lectin, with opposing roles in modulating innate and adaptive immune responses. Gal-9 was mainly described to exhibit immunosuppressive activities (24, 60–67). Gal-9 can also increase the function of regulatory T cells (T-regs) through interaction with CD44 (24) and may impair Natural Killer cells (NK) cytotoxicity and cytokine production through a Tim-3 independent mechanism (68). Along the same line, two recent studies demonstrated that Gal-9 suppresses B cell receptor signaling and B cell activation through interaction with CD45 and IgM-BCR complex (69, 70). However, other studies showed that Gal-9 exhibits immunopotentiating activity in the setting of immunosuppression (71) and induces TCR signaling (22), similar to our current study. Also, the endogenous levels of Gal-9 are induced during many inflammatory conditions (66, 72–74). Together, it is likely that Gal-9 effects are context-dependent and cell-type-dependent. The effect of Gal-9 on cell-mediated immunity in different subsets of T cells and other immune cells, during ART-suppressed HIV infection, warrants a broader investigation. Clarifying the signaling pathways induced or inhibited by Gal-9 in different cell-population, during HIV infection, may provide insights that may lead to the development of novel therapies to improve immune functionality, and reduce inflammation-associated co-morbidities, in the setting of viral suppression by ART.

The ability of Gal-9 to potently induce latent HIV transcription suggested that it could be considered within the "shock and kill" HIV eradication framework (8). However, the adverse Gal-9-mediated induction of pro-inflammatory cytokines, by the same pathway, limits the potential use of Gal-9 as a shock and kill agent. The recent study by Martin et al. (40) raised the possibility of using rapamycin, an immunosuppressive agent that does not affect TCR signaling, to prevent the adverse effects of T cell activation without impacting HIV transcription. Unlike several immunosuppressive agents that impact TCR signaling, rapamycin suppresses IL-2 downstream signaling (75, 76). Our data show that rapamycin is able to inhibit the pro-inflammatory impact of Gal-9 without affecting its ability to reactivate latent infection. That is in agreement with a previous study that used rapamycin to inhibit the proinflammatory effects of galectin-9 on dendritic cells and promote allograft tolerance in mice (41). Uncoupling Gal-9-mediated viral reactivation from

undesirable pro-inflammatory effects, using rapamycin, may increase the potential utility of recombinant Gal-9 within the "reversal of HIV latency" eradication framework.

In summary, we identified TCR/Lck-dependent ERK1/2-CREB as the signaling pathways underlying Gal-9 modulation of HIV transcriptional activity. We also found that rapamycin can uncouple the Gal-9 impact on HIV transcription from the undesirable, pro-inflammatory secretions associated with inducing TCR signaling. Our data highlight the further investigations needed to comprehensively understand the immunologic consequences of Gal-9 *in vivo*, during ART-suppressed HIV infection. Our findings could have implications for understanding the role of endogenous galectin interactions in modulating TCR signaling and maintaining chronic immune activation, that persists during ART-suppressed HIV infection. Finally, uncoupling Gal-9-mediated viral reactivation from undesirable pro-inflammatory effects, using rapamycin, may increase the potential utility of recombinant Gal-9 within the reversal of HIV latency eradication framework.

AUTHOR CONTRIBUTIONS

FC, LG, TP, BM, EP, LM, LN, and MA-M designed and carried out experiments. EP and LM selected study subjects and provided samples. TN contributed reagents. FC, LG, TP, EP, TN, LM, LN, and MA-M analyzed and interpreted data. FC and MA-M wrote the manuscript, and all authors edited it.

FUNDING

This work was supported by NIH (R21 AI129636, R21 NS106970, and P30CA010815-49S2), W.W. Smith Charitable Trust (grant # A1701), Campbell Foundation award, Penn Center for AIDS Research (P30 AI 045008), and The Foundation for AIDS Research (amfAR) Impact Grant # 109840-65-RGRL. Additional support was provided by the NIH-funded BEAT-HIV Martin Delaney Collaboratory to cure HIV-1 infection (1UM1Al126620) and the Philadelphia Foundation.

ACKNOWLEDGMENTS

We would like to thank Rachel E. Locke, Ph.D. for providing comments and editing.

SUPPLEMENTARY MATERIAL

The Supplementary Material for this article can be found online at: https://www.frontiersin.org/articles/10.3389/fimmu.2019.00267/full#supplementary-material

Supplementary Figure 1 | Gal-9-mediated CD3ζ phosphorylation is Lck-dependent. Jurkat E6-1 and J.CaM1.6 (a derivative mutant of Jurkat cells, which are deficient in Lck activity) cells were treated with Gal-9 (200 nM), or an equivalent volume of PBS, for 15 min and stained with PE-conjugated anti-phospho-CD3ζ antibody. Cell staining/phosphorylation was quantified by flow cytometry. Mean ± SD is displayed, and statistical comparisons were performed using two-tailed unpaired *t*-tests. ***$p < 0.001$.

Supplementary Figure 2 | Low concentrations of Gal-9 induce CD3ζ phosphorylation. J-Lat 5A8 cells were treated with escalating doses of Gal-9 (0–200 nM) for 15 min and stained with PE-conjugated anti-phospho-CD3ζ antibody. Cell staining/phosphorylation was quantified by flow cytometry. Mean ± SD is displayed, and statistical comparisons were performed using two-tailed unpaired *t*-tests comparing each concentration to the 0 nM control. *$p < 0.05$, and **$p < 0.01$.

Supplementary Figure 3 | Gal-9-mediated HIV latency reactivation is Lck-dependent. J-Lat 5A8 were transfected with Lck siRNA or non-target siRNA control using Amaxa Nucleofector4D. After 48 h, cells were treated with rGal-9 (200 nM), or an equivalent volume of PBS, for 24 h. HIV-encoded GFP expression was detected by flow cytometry. Mean ± SD is displayed, and statistical comparisons were performed using two-tailed unpaired *t*-tests. ***$p < 0.001$, and ****$p < 0.0001$.

Supplementary Figure 4 | Low concentrations of Gal-9 reactivate latent HIV in the J-Lat HIV latency model. J-Lat 5A8 cells were treated with escalating doses of Gal-9 (0–200 nM) for 24 h. HIV-encoded GFP expression was detected by flow cytometry. Mean ± SD is displayed, and statistical comparisons were performed using two-tailed unpaired *t*-tests comparing each concentration to the 0 nM control. *$p < 0.05$, ***$p < 0.001$, and ****$p < 0.0001$.

Supplementary Figure 5 | The natural form of Gal-9 phosphorylates CD3ζ and reactivates latent HIV in Lck dependent. **(A)** J-Lat 5A8 cells were treated with the natural form of Gal-9 (200 nM) or an equivalent volume of PBS for 15 min and stained with PE-conjugated anti-phospho-CD3ζ antibody. Cell staining/phosphorylation was quantified by flow cytometry. **(B)** J-Lat 5A8 cells were treated with the natural form of Gal-9 (200 nM) or an equavelent volume of PBS for 24 h. HIV-encoded GFP expression was detected by flow cytometry. Mean ± SD is displayed, and statistical comparisons were performed using two-tailed unpaired *t*-tests. ****$p < 0.0001$.

Supplementary Figure 6 | Impact of Gal-9 on CD4+ T cell viability and apoptosis. **(A)** $CD4^+$ T cells isolated from 5 HIV-infected ART-suppressed individuals were treated for 24 h with Gal-9 (500 nM) or DMSO Control in the presence of 1 μM of Lck inhibitor or the equivalent volume of DMSO. Cell viability was determined using Zombie Aqua Fixable Viability staining. **(B)** A representative flow cytometry plot from one individual. **(C)** $CD4^+$ T cells isolated from one HIV-infected ART-suppressed individual were treated for 24 h with Gal-9 (500 nM) or DMSO Control. Apoptosis was determined using Propidium iodide and Annexin V Pacific blue (Biolegend). anti-CD95 (1 ug/ml) stimulation for 6 h was used as positive control. Experiment was performed in duplicates. Mean ± SD is displayed **(D)** A representative flow cytometry plot of one replicate.

Supplementary Figure 7 | Gal-9 induces the secretion of several pro- and anti-inflammatory cytokines. $CD4^+$ T cells isolated from 3 HIV-infected ART-suppressed individuals were treated for 24 h with Gal-9 (200 nM), rGal-9 (500 nM), or DMSO Control for 4 h, 24 h, or 3 days. Culture supernatants were collected on day 3 and levels the 13 indicated pro- and anti-inflammatory cytokines were determined using Luminex assay.

Supplementary Table 1 | Subject characteristics.

REFERENCES

1. Finzi D, Hermankova M, Pierson T, Carruth LM, Buck C, Chaisson RE, et al. Identification of a reservoir for HIV-1 in patients on highly active antiretroviral therapy. *Science* (1997) 278:1295–300. doi: 10.1126/science.278.5341.1295
2. Wong JK, Hezareh M, Gunthard HF, Havlir DV, Ignacio CC, Spina CA, et al. Recovery of replication-competent HIV despite prolonged suppression of plasma viremia. *Science* (1997) 278:1291–5. doi: 10.1126/science.278.5341.1291
3. Rodger AJ, Lodwick R, Schechter M, Deeks S, Amin J, Gilson R, et al. Mortality in well controlled HIV in the continuous antiretroviral therapy arms of the

SMART and ESPRIT trials compared with the general population. *AIDS* (2013) 27:973–9. doi: 10.1097/QAD.0b013e32835cae9c
4. Wandeler G, Johnson LF, Egger M. Trends in life expectancy of HIV-positive adults on antiretroviral therapy across the globe: comparisons with general population. *Curr Opin HIV AIDS* (2016) 11:492–500. doi: 10.1097/COH.0000000000000298
5. Shan L, Deng K, Shroff NS, Durand CM, Rabi SA, Yang HC, et al. Stimulation of HIV-1-specific cytolytic T lymphocytes facilitates elimination of latent viral reservoir after virus reactivation. *Immunity* (2012) 36:491–501. doi: 10.1016/j.immuni.2012.01.014
6. Graf EH, Pace MJ, Peterson BA, Lynch LJ, Chukwulebe SB, Mexas AM, et al. Gag-positive reservoir cells are susceptible to HIV-specific cytotoxic T lymphocyte mediated clearance. *PLoS ONE* (2013) 8:e71879. doi: 10.1371/annotation/3aa92c3d-b6dd-4c6e-8cee-9587ce80a9c9
7. Abdel-Mohsen M, Wang C, Strain MC, Lada SM, Deng X, Cockerham LR, et al. Select host restriction factors are associated with HIV persistence during antiretroviral therapy. *AIDS* (2015) 29:411–20. doi: 10.1097/QAD.0000000000000572
8. Abdel-Mohsen M, Chavez L, Tandon R, Chew GM, Deng X, Danesh A, et al. Human galectin-9 is a potent mediator of HIV transcription and reactivation. *PLoS Pathog.* (2016) 12:e1005677. doi: 10.1371/journal.ppat.1005677
9. Barrera C, Espejo R, Reyes VE. Differential glycosylation of MHC class II molecules on gastric epithelial cells: implications in local immune responses. *Hum Immunol.* (2002) 63:384–93. doi: 10.1016/S0198-8859(02)00386-5
10. Dwek RA, Butters TD, Platt FM, Zitzmann N. Targeting glycosylation as a therapeutic approach. *Nat Rev Drug Discov.* (2002) 1:65–75. doi: 10.1038/nrd708
11. De Freitas Junior JC, Silva Bdu R, De Souza WF, De Araujo WM, Abdelhay ES, Morgado-Diaz JA. Inhibition of N-linked glycosylation by tunicamycin induces E-cadherin-mediated cell-cell adhesion and inhibits cell proliferation in undifferentiated human colon cancer cells. *Cancer Chemother Pharmacol.* (2011) 68:227–38. doi: 10.1007/s00280-010-1477-8
12. Walt D, Aoki-Kinoshita KF, Bendiak B, Bertozzi CR, Boons GJ, Darvill A, et al. *Transforming Glycoscience*: *A Roadmap for the Future.* Washington, DC: Nacional Academies Press (2012).
13. Barondes SH, Cooper DN, Gitt MA, Leffler H. Galectins. Structure and function of a large family of animal lectins *J Biol Chem.* (1994) 269:20807–10.
14. Zhuo Y, Bellis SL. Emerging role of alpha2,6-sialic acid as a negative regulator of galectin binding and function. *J Biol Chem.* (2011) 286:5935–41. doi: 10.1074/jbc.R110.191429
15. Gordon-Alonso M, Hirsch T, Wildmann C, Van Der Bruggen P. Galectin-3 captures interferon-gamma in the tumor matrix reducing chemokine gradient production and T-cell tumor infiltration. *Nat Commun.* (2017) 8:793. doi: 10.1038/s41467-017-00925-6
16. Mendez-Huergo SP, Blidner AG, Rabinovich GA. Galectins: emerging regulatory checkpoints linking tumor immunity and angiogenesis. *Curr Opin Immunol.* (2017) 45:8–15. doi: 10.1016/j.coi.2016.12.003
17. Smith LK, Boukhaled GM, Condotta SA, Mazouz S, Guthmiller JJ, Vijay R, et al. Interleukin-10 directly inhibits CD8(+) T cell function by enhancing N-glycan branching to decrease antigen sensitivity. *Immunity* (2018) 48:299–312 e295. doi: 10.1016/j.immuni.2018.01.006
18. Sehrawat S, Reddy PB, Rajasagi N, Suryawanshi A, Hirashima M, Rouse BT. Galectin-9/TIM-3 interaction regulates virus-specific primary and memory CD8 T cell response. *PLoS Pathog.* (2010) 6:e1000882. doi: 10.1371/journal.ppat.1000882
19. Jost S, Moreno-Nieves UY, Garcia-Beltran WF, Rands K, Reardon J, Toth I, et al. Dysregulated Tim-3 expression on natural killer cells is associated with increased Galectin-9 levels in HIV-1 infection. *Retrovirology* (2013) 10:74. doi: 10.1186/1742-4690-10-74
20. Tandon R, Chew GM, Byron MM, Borrow P, Niki T, Hirashima M, et al. Galectin-9 is rapidly released during acute HIV-1 infection and remains sustained at high levels despite viral suppression even in elite controllers. *AIDS Res Hum Retroviruses* (2014) 30:654–64. doi: 10.1089/aid.2014.0004
21. Chen HY, Fermin A, Vardhana S, Weng IC, Lo KF, Chang EY, et al. Galectin-3 negatively regulates TCR-mediated CD4+ T-cell activation at the immunological synapse. *Proc Natl Acad Sci USA.* (2009) 106:14496–501. doi: 10.1073/pnas.0903497106
22. Lhuillier C, Barjon C, Niki T, Gelin A, Praz F, Morales O, et al. Impact of exogenous galectin-9 on Human T Cells: contribution of the t cell receptor complex to antigen-independent activation but not to apoptosis induction. *J Biol Chem.* (2015) 290:16797–811. doi: 10.1074/jbc.M115.661272
23. Gordon-Alonso M, Bruger AM, Van Der Bruggen P. Extracellular galectins as controllers of cytokines in hematological cancer. *Blood* (2018) 132:484–91. doi: 10.1182/blood-2018-04-846014
24. Wu C, Thalhamer T, Franca RF, Xiao S, Wang C, Hotta C, et al. Galectin-9-CD44 interaction enhances stability and function of adaptive regulatory T cells. *Immunity* (2014) 41:270–82. doi: 10.1016/j.immuni.2014.06.011
25. Nam KO, Kang H, Shin SM, Cho KH, Kwon B, Kwon BS, et al. Cross-linking of 4-1BB activates TCR-signaling pathways in CD8+ T lymphocytes. *J Immunol.* (2005) 174:1898–905. doi: 10.4049/jimmunol.174.4.1898
26. Madireddi S, Eun SY, Lee SW, Nemcovicova I, Mehta AK, Zajonc DM, et al. Galectin-9 controls the therapeutic activity of 4-1BB-targeting antibodies. *J Exp Med.* (2014) 211:1433–48. doi: 10.1084/jem.20132687
27. Bitra A, Doukov T, Wang J, Picarda G, Benedict CA, Croft M, et al. Crystal structure of murine 4-1BB and its interaction with 4-1BBL support a role for galectin-9 in 4-1BB signaling. *J Biol Chem.* (2018) 293:1317–29. doi: 10.1074/jbc.M117.814905
28. Jordan A, Bisgrove D, Verdin E. HIV reproducibly establishes a latent infection after acute infection of T cells *in vitro*. *EMBO J.* (2003) 22:1868–77. doi: 10.1093/emboj/cdg188
29. Chavez L, Kauder S, Verdin E. *In vivo, in vitro*, and *in silico* analysis of methylation of the HIV-1 provirus. *Methods* (2011) 53:47–53. doi: 10.1016/j.ymeth.2010.05.009
30. Jiang Y, Cheng H. Evidence of LAT as a dual substrate for Lck and Syk in T lymphocytes. *Leuk Res.* (2007) 31:541–5. doi: 10.1016/j.leukres.2006.07.010
31. Minami Y, Weissman AM, Samelson LE, Klausner RD. Building a multichain receptor: synthesis, degradation, and assembly of the T-cell antigen receptor. *Proc Natl Acad Sci USA.* (1987) 84:2688–92. doi: 10.1073/pnas.84.9.2688
32. Weissman AM, Ross P, Luong ET, Garcia-Morales P, Jelachich ML, Biddison WE, et al. Tyrosine phosphorylation of the human T cell antigen receptor zeta-chain: activation via CD3 but not CD2. *J Immunol.* (1988) 141:3532–6.
33. Irving BA, Weiss A. The cytoplasmic domain of the T cell receptor zeta chain is sufficient to couple to receptor-associated signal transduction pathways. *Cell* (1991) 64:891–901. doi: 10.1016/0092-8674(91)90314-O
34. Iwashima M, Irving BA, Van Oers NS, Chan AC, Weiss A. Sequential interactions of the TCR with two distinct cytoplasmic tyrosine kinases. *Science* (1994) 263:1136–9. doi: 10.1126/science.7509083
35. Thome M, Duplay P, Guttinger M, Acuto O. Syk and ZAP-70 mediate recruitment of p56lck/CD4 to the activated T cell receptor/CD3/zeta complex. *J Exp Med.* (1995) 181:1997–2006. doi: 10.1084/jem.181.6.1997
36. Mishra R, Grzybek M, Niki T, Hirashima M, Simons K. Galectin-9 trafficking regulates apical-basal polarity in Madin-Darby canine kidney epithelial cells. *Proc Natl Acad Sci USA.* (2010) 107:17633–8. doi: 10.1073/pnas.1012424107
37. Gleason MK, Lenvik TR, Mccullar V, Felices M, O'brien MS, Cooley SA, et al. Tim-3 is an inducible human natural killer cell receptor that enhances interferon gamma production in response to galectin-9. *Blood* (2012) 119:3064–72. doi: 10.1182/blood-2011-06-360321
38. Wiersma VR, De Bruyn M, Wei Y, Van Ginkel RJ, Hirashima M, Niki T, et al. The epithelial polarity regulator LGALS9/galectin-9 induces fatal frustrated autophagy in KRAS mutant colon carcinoma that depends on elevated basal autophagic flux. *Autophagy* (2015) 11:1373–88. doi: 10.1080/15548627.2015.1063767
39. Madireddi S, Eun SY, Mehta AK, Birta A, Zajonc DM, Niki T, et al. Regulatory T cell-mediated suppression of inflammation induced by DR3 signaling is dependent on galectin-9. *J Immunol.* (2017) 199:2721–8. doi: 10.4049/jimmunol.1700575
40. Martin AR, Pollack RA, Capoferri A, Ambinder RF, Durand CM, Siliciano RF. Rapamycin-mediated mTOR inhibition uncouples HIV-1 latency reversal from cytokine-associated toxicity. *J Clin Invest.* (2017) 127:651–6. doi: 10.1172/JCI89552
41. Cai L, Zhou H, Fang Z, Yuan J, Niki T, Hirashima M, et al. Galectin-9 in combination with rapamycin induces cardiac allograft tolerance in mice. *Transplantation* (2013) 96:379–86. doi: 10.1097/TP.0b013e31829b07b5

42. Elahi S, Niki T, Hirashima M, Horton H. Galectin-9 binding to Tim-3 renders activated human CD4+ T cells less susceptible to HIV-1 infection. *Blood* (2012) 119:4192–204. doi: 10.1182/blood-2011-11-389585
43. Schaefer K, Webb NE, Pang M, Hernandez-Davies JE, Lee KP, Gonzalez P, et al. Galectin-9 binds to O-glycans on protein disulfide isomerase. *Glycobiology* (2017) 27:878–87. doi: 10.1093/glycob/cwx065
44. Hunt PW, Martin JN, Sinclair E, Bredt B, Hagos E, Lampiris H, et al. T cell activation is associated with lower CD4+ T cell gains in human immunodeficiency virus-infected patients with sustained viral suppression during antiretroviral therapy. *J Infect Dis.* (2003) 187:1534–43. doi: 10.1086/374786
45. Hunt PW, Cao HL, Muzoora C, Ssewanyana I, Bennett J, Emenyonu N, et al. Impact of CD8+ T-cell activation on CD4+ T-cell recovery and mortality in HIV-infected Ugandans initiating antiretroviral therapy. *AIDS* (2011) 25:2123–31. doi: 10.1097/QAD.0b013e32834c4ac1
46. Kaplan RC, Sinclair E, Landay AL, Lurain N, Sharrett AR, Gange SJ, et al. T cell activation and senescence predict subclinical carotid artery disease in HIV-infected women. *J Infect Dis.* (2011a) 203:452–63. doi: 10.1093/infdis/jiq071
47. Kaplan RC, Sinclair E, Landay AL, Lurain N, Sharrett AR, Gange SJ, et al. T cell activation predicts carotid artery stiffness among HIV-infected women. *Atherosclerosis* (2011b) 217:207–13. doi: 10.1016/j.atherosclerosis.2011.03.011
48. Chun TW, Justement JS, Pandya P, Hallahan CW, Mclaughlin M, Liu S, et al. Relationship between the size of the human immunodeficiency virus type 1 (HIV-1) reservoir in peripheral blood CD4+ T cells and CD4+:CD8+ T cell ratios in aviremic HIV-1-infected individuals receiving long-term highly active antiretroviral therapy. *J Infect Dis.* (2002) 185:1672–6. doi: 10.1086/340521
49. Chomont N, El-Far M, Ancuta P, Trautmann L, Procopio FA, Yassine-Diab B, et al. HIV reservoir size and persistence are driven by T cell survival and homeostatic proliferation. *Nat Med.* (2009) 15:893–900. doi: 10.1038/nm.1972
50. Hatano H, Jain V, Hunt PW, Lee TH, Sinclair E, Do TD, et al. Cell-based measures of viral persistence are associated with immune activation and programmed cell death protein 1 (PD-1)-expressing CD4+ T cells. *J Infect Dis.* (2013) 208:50–6. doi: 10.1093/infdis/jis630
51. Khoury G, Fromentin R, Solomon A, Hartogensis W, Killian M, Hoh R, et al. Human immunodeficiency virus persistence and T-cell activation in blood, rectal, and lymph node tissue in human immunodeficiency virus-infected individuals receiving suppressive antiretroviral therapy. *J Infect Dis.* (2017) 215:911–9. doi: 10.1093/infdis/jix039
52. Schacker TW, Nguyen PL, Beilman GJ, Wolinsky S, Larson M, Reilly C, et al. Collagen deposition in HIV-1 infected lymphatic tissues and T cell homeostasis. *J Clin Invest.* (2002) 110:1133–9. doi: 10.1172/JCI0216413
53. Naeger DM, Martin JN, Sinclair E, Hunt PW, Bangsberg DR, Hecht F, et al. Cytomegalovirus-specific T cells persist at very high levels during long-term antiretroviral treatment of HIV disease. *PLoS ONE* (2010) 5:e8886. doi: 10.1371/journal.pone.0008886
54. Nixon DE, Landay AL. Biomarkers of immune dysfunction in HIV. *Curr Opin HIV AIDS* (2010) 5:498–503. doi: 10.1097/COH.0b013e32833ed6f4
55. Kamat A, Misra V, Cassol E, Ancuta P, Yan Z, Li C, et al. A plasma biomarker signature of immune activation in HIV patients on antiretroviral therapy. *PLoS ONE* (2012) 7:e30881. doi: 10.1371/journal.pone.0030881
56. Weber R, Ruppik M, Rickenbach M, Spoerri A, Furrer H, Battegay M, et al. Decreasing mortality and changing patterns of causes of death in the Swiss HIV Cohort Study. *HIV Med.* (2013) 14:195–207. doi: 10.1111/j.1468-1293.2012.01051.x
57. Borges AH, O'connor JL, Phillips AN, Ronsholt FF, Pett S, Vjecha MJ, et al. Factors associated with plasma IL-6 levels during HIV infection. *J Infect Dis.* (2015) 212:585–95. doi: 10.1093/infdis/jiv123
58. Freiberg MS, Bebu I, Tracy R, So-Armah K, Okulicz J, Ganesan A, et al. D-Dimer levels before HIV seroconversion remain elevated even after viral suppression and are associated with an increased risk of non-AIDS events. *PLoS ONE* (2016) 11:e0152588. doi: 10.1371/journal.pone.0152588
59. So-Armah KA, Tate JP, Chang CH, Butt AA, Gerschenson M, Gibert CL, et al. Do biomarkers of inflammation, monocyte activation, and altered coagulation explain excess mortality between HIV infected and uninfected people? *J Acquir Immune Defic Syndr.* (2016) 72:206–13. doi: 10.1097/QAI.0000000000000954
60. Zhu C, Anderson AC, Schubart A, Xiong H, Imitola J, Khoury SJ, et al. The Tim-3 ligand galectin-9 negatively regulates T helper type 1 immunity. *Nat Immunol.* (2005) 6:1245–52. doi: 10.1038/ni1271
61. Wang F, He W, Zhou H, Yuan J, Wu K, Xu L, et al. The Tim-3 ligand galectin-9 negatively regulates CD8+ alloreactive T cell and prolongs survival of skin graft. *Cell Immunol.* (2007) 250:68–74. doi: 10.1016/j.cellimm.2008.01.006
62. Seki M, Oomizu S, Sakata KM, Sakata A, Arikawa T, Watanabe K, et al. Galectin-9 suppresses the generation of Th17, promotes the induction of regulatory T cells, and regulates experimental autoimmune arthritis. *Clin Immunol.* (2008) 127:78–88. doi: 10.1016/j.clim.2008.01.006
63. Lv K, Zhang Y, Zhang M, Zhong M, Suo Q. Galectin-9 promotes TGF-beta1-dependent induction of regulatory T cells via the TGF-beta/Smad signaling pathway. *Mol Med Rep.* (2013) 7:205–10. doi: 10.3892/mmr.2012.1125
64. Ungerer C, Quade-Lyssy P, Radeke HH, Henschler R, Konigs C, Kohl U, et al. Galectin-9 is a suppressor of T and B cells and predicts the immune modulatory potential of mesenchymal stromal cell preparations. *Stem Cells Dev.* (2014) 23:755–66. doi: 10.1089/scd.2013.0335
65. Kim SN, Lee HJ, Jeon MS, Yi T, Song SU. Galectin-9 is involved in immunosuppression mediated by human bone marrow-derived clonal mesenchymal stem cells. *Immune Netw.* (2015) 15:241–51. doi: 10.4110/in.2015.15.5.241
66. Yang S, Wang J, Chen F, Liu G, Weng Z, Chen J. Elevated galectin-9 suppresses Th1 effector function and induces apoptosis of activated CD4(+) T cells in osteoarthritis. *Inflammation* (2017) 40:1062–71. doi: 10.1007/s10753-017-0549-x
67. Panda SK, Facchinetti V, Voynova E, Hanabuchi S, Karnell JL, Hanna RN, et al. Galectin-9 inhibits TLR7-mediated autoimmunity in murine lupus models. *J Clin Invest.* (2018) 128:1873–87. doi: 10.1172/JCI97333
68. Golden-Mason L, Mcmahan RH, Strong M, Reisdorph R, Mahaffey S, Palmer BE, et al. Galectin-9 functionally impairs natural killer cells in humans and mice. *J Virol.* (2013) 87:4835–45. doi: 10.1128/JVI.01085-12
69. Cao A, Alluqmani N, Buhari FHM, Wasim L, Smith LK, Quaile AT, et al. Galectin-9 binds IgM-BCR to regulate B cell signaling. *Nat Commun.* (2018) 9:3288. doi: 10.1038/s41467-018-05771-8
70. Giovannone N, Liang J, Antonopoulos A, Geddes Sweeney J, King SL, Pochebit SM, et al. Galectin-9 suppresses B cell receptor signaling and is regulated by I-branching of N-glycans. *Nat Commun.* (2018) 9:3287. doi: 10.1038/s41467-018-05770-9
71. Nagahara K, Arikawa T, Oomizu S, Kontani K, Nobumoto A, Tateno H, et al. Galectin-9 increases Tim-3+ dendritic cells and CD8+ T cells and enhances antitumor immunity via galectin-9-Tim-3 interactions. *J Immunol.* (2008) 181:7660–9. doi: 10.4049/jimmunol.181.11.7660
72. He XW, Li WL, Li C, Liu P, Shen YG, Zhu M, et al. Serum levels of galectin-1, galectin-3, and galectin-9 are associated with large artery atherosclerotic stroke. *Sci Rep.* (2017) 7:40994. doi: 10.1038/srep40994
73. Liu Y, Liu Z, Fu Q, Wang Z, Fu H, Liu W, et al. Galectin-9 as a prognostic and predictive biomarker in bladder urothelial carcinoma. *Urol Oncol.* (2017) 35:349–55. doi: 10.1016/j.urolonc.2017.02.008
74. Enninga EAL, Harrington SM, Creedon DJ, Ruano R, Markovic SN, et al. and Dronca RS. Immune checkpoint molecules soluble program death ligand 1 and galectin-9 are increased in pregnancy. *Am J Reprod Immunol.* (2018) 79:e12795. doi: 10.1111/aji.12795
75. Sehgal SN. Rapamune (RAPA, rapamycin, sirolimus): mechanism of action immunosuppressive effect results from blockade of signal transduction and inhibition of cell cycle progression. *Clin Biochem.* (1998) 31:335–40. doi: 10.1016/S0009-9120(98)00045-9
76. Powell JD, Pollizzi KN, Heikamp EB, Horton MR. Regulation of immune responses by mTOR. *Annu Rev Immunol.* (2012) 30:39–68. doi: 10.1146/annurev-immunol-020711-075024

Conflict of Interest Statement: The authors declare that the research was conducted in the absence of any commercial or financial relationships that could be construed as a potential conflict of interest.

frontiers in Immunology

ORIGINAL RESEARCH
published: 21 February 2019
doi: 10.3389/fimmu.2019.00289

CXCL13 as a Biomarker of Immune Activation During Early and Chronic HIV Infection

Vikram Mehraj[1,2,3†], Rayoun Ramendra[1,2,4†], Stéphane Isnard[1,2], Franck P. Dupuy[1,2], Bertrand Lebouché[1,2,5], Cecilia Costiniuk[1,2], Réjean Thomas[6], Jason Szabo[1,7], Jean-Guy Baril[7], Benoit Trottier[7], Pierre Coté[7], Roger LeBlanc[8], Madéleine Durand[3], Carl Chartrand-Lefebvre[3], Ido Kema[9], Yonglong Zhang[10], Malcolm Finkelman[10], Cécile Tremblay[3,11] and Jean-Pierre Routy[1,2,12] for the Montreal Primary HIV-infection, Canadian HIV infected Slow Progressors, and Canadian HIV and Aging Cohort Study Groups*

[1] Chronic Viral Illness Service, McGill University Health Centre, Montreal, QC, Canada, [2] Infectious Diseases and Immunity in Global Health Program, Research Institute, McGill University Health Centre, Montreal, QC, Canada, [3] University of Montreal Hospital Health Centre (CRCHUM), Montreal, QC, Canada, [4] Department of Microbiology and Immunology, McGill University, Montreal, QC, Canada, [5] Department of Family Medicine, McGill University, Montreal, QC, Canada, [6] Clinique Médicale l'Actuel, Montreal, QC, Canada, [7] Clinique Médicale Quartier Latin, Montreal, QC, Canada, [8] Clinique Médicale OPUS, Montreal, QC, Canada, [9] Department of Laboratory Medicine, University Medical Center, University of Groningen, Groningen, Netherlands, [10] Associates of CapeCod Inc., Falmouth, MA, United States, [11] Département de Microbiologie, Infectiologie et Immunologie, Université de Montréal, Montreal, QC, Canada, [12] Hematology Clinic, McGill University Health Centre, Montreal, QC, Canada

OPEN ACCESS

Edited by:
Sara Gianella Weibel, University of California, San Diego, United States

Reviewed by:
Nicholas Funderburg, The Ohio State University, United States
Mirko Paiardini, Emory University School of Medicine, United States

***Correspondence:**
Jean-Pierre Routy
jean-pierre.routy@mcgill.ca

† These authors have contributed equally to this work

Specialty section:
This article was submitted to Viral Immunology, a section of the journal Frontiers in Immunology

Received: *23 December 2018*
Accepted: *04 February 2019*
Published: *21 February 2019*

Citation:
Mehraj V, Ramendra R, Isnard S, Dupuy FP, Lebouché B, Costiniuk C, Thomas R, Szabo J, Baril J-G, Trottier B, Coté P, LeBlanc R, Durand M, Chartrand-Lefebvre C, Kema I, Zhang Y, Finkelman M, Tremblay C and Routy J-P (2019) CXCL13 as a Biomarker of Immune Activation During Early and Chronic HIV Infection. Front. Immunol. 10:289. doi: 10.3389/fimmu.2019.00289

Background: CXCL13 is preferentially secreted by Follicular Helper T cells (T_{FH}) to attract B cells to germinal centers. Plasma levels of CXCL13 have been reported to be elevated during chronic HIV-infection, however there is limited data on such elevation during early phases of infection and on the effect of ART. Moreover, the contribution of CXCL13 to disease progression and systemic immune activation have been partially defined. Herein, we assessed the relationship between plasma levels of CXCL13 and systemic immune activation.

Methods: Study samples were collected in 114 people living with HIV (PLWH) who were in early (EHI) or chronic (CHI) HIV infection and 35 elite controllers (EC) compared to 17 uninfected controls (UC). A subgroup of 11 EHI who initiated ART and 14 who did not were followed prospectively. Plasma levels of CXCL13 were correlated with CD4 T cell count, CD4/CD8 ratio, plasma viral load (VL), markers of microbial translocation [LPS, sCD14, and (1→3)-β-D-Glucan], markers of B cell activation (total IgG, IgM, IgA, and IgG1-4), and inflammatory/activation markers like IL-6, IL-8, IL-1β, TNF-α, IDO-1 activity, and frequency of $CD38^+HLA\text{-}DR^+$ T cells on $CD4^+$ and $CD8^+$ T cells.

Results: Plasma levels of CXCL13 were elevated in EHI (127.9 ± 64.9 pg/mL) and CHI (229.4 ± 28.5 pg/mL) compared to EC (71.3 ± 20.11 pg/mL), and UC (33.4 ± 14.9 pg/mL). Longitudinal analysis demonstrated that CXCL13 remains significantly elevated after 14 months without ART ($p < 0.001$) and was reduced without normalization after 24 months on ART ($p = 0.002$). Correlations were observed with VL, CD4 T cell count, CD4/CD8 ratio, LPS, sCD14, (1→3)-β-D-Glucan, total IgG, TNF-α, Kynurenine/Tryptophan ratio, and frequency of CD38+HLA-DR+ CD4 and CD8 T cells. In addition, CMV+ PLWH presented with higher levels of plasma CXCL13 than CMV- PLWH ($p = 0.005$).

Conclusion: Plasma CXCL13 levels increased with HIV disease progression. Early initiation of ART reduces plasma CXCL13 and B cell activation without normalization. CXCL13 represents a novel marker of systemic immune activation during early and chronic HIV infection and may be used to predict the development of non-AIDS events.

Keywords: CXCL13, humoral immune response, microbial translocation, inflammation, immune activation, CMV

INTRODUCTION

Despite the success of antiretroviral therapy (ART), people living with HIV (PLWH) still suffer from chronic immune activation and the development of non-AIDS events (1). Progressive CD4 T cell decline, elevated CD8 T cell counts, early damage to the intestinal mucosa, microbial translocation, CMV co-infection, and persistence of HIV in cellular reservoirs all contribute to systemic immune activation (2–6). Chronic immune activation and inflammation among PLWH on ART have been linked with increased risk for mortality and development of non-AIDS events such as cardiovascular dysfunction, renal failure, hepatic steatosis, neurocognitive degeneration, accelerated aging, and cancer (7, 8). Therefore, therapeutic strategies are needed to tackle residual immune activation to improve the quality of life of PLWH.

Apart from the virus itself or its proteins, factors contributing to immune activation among PLWH include elevated circulation of microbial products leaking from the gut and CMV infection (9, 10). It has been reported that epithelial gut damage, leading to microbial translocation, precedes systemic immune activation in a SIV-infected rhesus macaque model of the disease (11). Circulation of gram-negative bacterial cell wall antigen, lipopolysaccharide (LPS), and major component of fungal cell walls, (1→3)-β-D-Glucan (βDG), have been reported to be elevated in the plasma of PLWH (12–16). These markers of microbial translocation have been previously associated with activated CD4 and CD8 T cells, indoleamine 2,3-dioxygenase 1 (IDO-1) activity, and plasma levels of inflammatory cytokines. Thus, the optimal marker of systemic immune activation in PLWH should account for the contribution of circulating microbial products LPS and βDG.

Several cellular and soluble markers of immune activation/inflammation have been identified (17). Frequencies of HLA-DR and CD38 expressing CD4 and CD8 T cells are used to measure lymphoid cell activation (18). Inflammatory myeloid cells including monocytes, macrophages, and dendritic cells (DC) are reported to induce IDO-1 enzyme activity upon antigen stimulation (19). IDO-1 converts essential amino acid tryptophan into immune suppressive kynurenines. Frequency of activated CD4 and CD8 T cells as well as IDO-1 activity of myeloid cells have been associated with the degree of epithelial gut damage, microbial translocation, and size of HIV reservoir (1, 20–22). Plasma level markers of inflammation/immune activation include marker of monocyte activation soluble CD14 (sCD14) as well as inflammatory cytokines such as IL-6, IL-1β, IL-8, and TNF-α which are secreted by activated immune cells (23–25). While there are several validated markers of immune activation/inflammation in PLWH, there is currently no single marker that can account for both lymphoid and myeloid cell activation during early and chronic stages of HIV infection.

B cells play a crucial role in mounting an antiviral humoral immune response. Upon maturation in germinal centers (GCs), they are mainly localized in secondary lymphoid tissues where they present antigens, secrete cytokines, and produce antigen-specific antibodies (26). PLWH have been reported to have humoral immune dysfunction that is regulated by GCs, which have been linked to HIV-associated immune activation (27–29). Both structural and functional impairment of lymph node GCs lead to B cell dysfunction. Subsequent B cell activation results in hypergammaglobulinemia, impaired antibody response, and loss of B cell memory (27). B cell activation and trafficking to lymph node GCs is controlled by secretion of chemokine CXCL13 [(C-X-C motif) ligand 13] that is recognized by leukocytes, which express CXCR5. As such, CXCL13 is considered as a marker of GC activity as it is secreted by follicular DC and helper T (T_{FH}) cells. Furthermore, myeloid cells such as macrophages have also been reported to secrete CXCL13 upon activation (30). It has been previously reported that PLWH have elevated plasma levels of CXCL13 during chronic infection (31). However, plasma levels of CXCL13 during early infection, the effect of ART on CXCL13 secretion, and the contribution of CXCL13 to HIV disease progression and systemic immune activation are poorly understood. Herein, we assessed the validity of plasma levels of CXCL13 as a biomarker of systemic immune activation in a well-defined cohort of early and chronic, untreated and treated PLWH.

METHODS

Study Design and Population

114 adult PLWH were cross-sectionally grouped into those in early HIV-infection (EHI) ($n = 37$), defined as being within 6 months of the estimated date of infection, and those with chronic HIV-infection (CHI) who were either untreated ($n = 13$) or ART treated ($n = 64$). EHI participants were enrolled from the Montreal Primary HIV Infection Study (32); while CHI participants were enrolled from the Chronic Viral Illness Service at the McGill University Health Centre and Canadian HIV and Aging Cohort Study (33). In addition, 35 elite controllers (EC)s, defined as PLWH who control plasma viral loads below 50 copies per mL and maintain CD4 T-cell counts above 500 cells per mm^3 in the absence of ART were included from the Canadian Cohort of HIV-infected Slow Progressors (34). Within the EHI group, 24 participants were prospectively followed-up for about 2 years. During the follow-up, 10 EHI participants were on ART for at

least 1 year while the remaining participants were ART naïve during the time of longitudinal assessment. A group of 17 HIV-uninfected controls (UC) were assessed for comparison with EHI and CHI groups.

Laboratory Measurements

Participants were diagnosed with HIV by measuring plasma HIV-1 p24 antigen/antibody and were further confirmed by Western blot as previously reported (32, 35). HIV viral load (VL) in plasma was quantified by the Abbott RealTime HIV-1 assay (Abbott Laboratories, Abbott Park, Illinois, U.S.A). Assessment of CD4 and CD8 T cell counts was done by 4-color flow cytometry. For further research measurements blood samples of study participants were collected to isolate plasma and peripheral blood mononuclear cells (PBMC) samples and stored at −80°C and in liquid nitrogen, respectively. All participants were fasting at the time of blood collection.

Quantification of Plasma Levels of CXCL13

Plasma CXCL13 levels were measured in duplicate by using the Human CXCL13/BLC/BCA-1 Quantikine ELISA Kit (R&D Systems, Minneapolis, MN), a 4.5-h solid phase enzyme linked immunosorbent assay (ELISA).

Quantification of Markers of B-Cell Activity (Total IgG, IgM, IgA, IgG1-4, BAFF, sCD40L)

Total IgG, IgM, and IgA were measured using the Olympus AU5800 (Beckman Coulter). Further subclasses of IgG (IgG1, IgG2, IgG3, and IgG4) were measured by using ELISA kits (eBiosciences, Saint Laurent, QC, Canada) as per manufacturer's instructions. B cell activating factor (BAFF) and soluble CD40L (sCD40L) were measured in duplicate using an ELISA (R&D Systems, Minneapolis, MN, USA).

Quantification of Markers of Epithelial Gut Damage and Microbial Translocation

Intestinal-fatty acid binding protein (I-FABP) was measured using an ELISA kit (Hycult Biotech, Uden, Netherlands). Soluble suppressor of tumorigenicity 2 (sST2) was measured by ELISA as described before (21). LPS was measured using a human lipopolysaccharide ELISA kit (Cusabio, Wuhan, China). sCD14 was measured by immunoassay (Quantikine, R&D Systems, Minneapolis, MN, USA). (1→3)-β-D-Glucan (βDG) was measured by the Fungitell® Limulus Amebocyte Lysate assay (Associates of Cape Cod, Inc., East Falmouth, MA, USA). All the analytes were measured in duplicate as per manufacturer's instructions.

Multiplex Quantification of Soluble Inflammatory Markers

Plasma levels of IL-1β, Tumor Necrosis Factor α (TNF-α), IL-6, and IL-8 were measured in duplicate using the Meso Scale Discovery (MSD) U-Plex Pro-Inflammatory Combo 4 kit (MSD, Rockville, Maryland, USA).

Measurement of Kynurenine and Tryptophan Plasma Levels

Kynurenine and Tryptophan were measured using an automated on-line solid-phase extraction-liquid chromatographic-tandem mass spectrometric method (36, 37). Ratio of kynurenine to tryptophan was calculated as a measure of IDO-1 enzyme activity.

Flow Cytometry Analyses

Frozen PBMC samples were rapidly thawed and stained for 20 min at 4°C using fluorochrome conjugated antibody panels from BD Biosciences (Mississauga, ON, Canada) or BioLegend (San Diego, CA, USA) using anti-CD56-FITC, anti-CD11c BV711, anti-CD3 PE-Dazzle594, anti-CD4 BUV395, anti-CD8 BUV737, anti-CD38 BV605, anti-HLADR APC-Cy7. Cells were then washed and fixed in 2% paraformaldehyde before acquisition. CD38 and HLA-DR expression were analyzed on CD4 and CD8 T cells. Dead cells were excluded as Live/dead positive (ThermoFisher, Saint Laurent QC, Canada). Fluorescence minus one color controls were used to discriminate auto-fluorescence from positive signals. BD Fortessa X20 flow cytometer was used for FACS and the data was analyzed using FlowJo 10.0.7 (FLOWJO, LLC, Ashland, OR, USA).

In vitro Stimulations

One million PBMC from uninfected donors were stimulated for 18 h in 1 mL complete medium [RPMI (Wisent) + 10% FBS (Wisent) + 1% Penicillin/Streptomycin (ThermoFisher)] with 1 μg/ml of LPS (Sigma), βDG (Sigma) or both. Supernatants were collected and CXCL13 was measured as previously described.

Statistical Analyses

Descriptive and inferential analyses were conducted using SPSS 24.0 (Chicago, IL, USA) and GraphPad Prism 6.0 (La Jolla, CA, USA). Data were summarized using means and standard deviations calculated for the variables with normal distribution and using median with interquartile range (IQR) calculated for variables with a non-normal distribution. Percentages were calculated for categorical variables. Subsequently, both parametric and non-parametric tests including student t, chi-square, Mann-Whitney *U*, χ^2, and ANOVA with LSD test were used for comparisons. Paired *t*-test was used for before-after comparisons. Pearson correlation test was conducted to assess association between two quantitative variables. Statistical significance was determined at $p < 0.05$. Multivariate linear regression analysis was conducted to determine the independent association of CXCL13 with HIV-infection adjusting for the confounding factors such as age, sex, CD4 T cell count and inflammatory markers.

RESULTS

Clinical Characteristics of Study Participants

Eighty one percent of the participating PLWH were male and the median (IQR) age was 47 (37–51). CD4 T-cell count was lower in untreated EHI and CHI vs. controls, which increased amongst

TABLE 1 | Descriptive characteristics of study participants ($n = 166$).

Characteristics	EHI ($n = 37$)	CHI ART– ($n = 13$)	CHI ART+ ($n = 64$)	EC ($n = 35$)	UC ($n = 17$)
Age in years					
Median (IQR)	34 (28–44)	43 (33–51)	50 (55–61)	45 (39–50)	41 (35–49)
Sex					
Male, *n* (%)	36 (97.3)	8 (38.5)	58 (90.6)	21 (60.0)	11 (64.7)
Female, *n* (%)	1 (2.7)	5 (61.5)	6 (9.4)	14 (40.0)	6 (35.3)
CD4 T cells/μL					
Median (IQR)	480 (368–650)	81 (14–319)	605 (412–700)	650 (552–823)	866 (566–1,022)
CD8 T cells/μL					
Median (IQR)	810 (630–1,030)	1,030 (267–1,232)	746 (554–1,001)	690 (409–968)	408 (281–689)
CD4/CD8					
Median (IQR)	0.6 (0.4–0.9)	0.1 (0.1–0.4)	0.8 (0.5–1.1)	1.1 (0.8–1.4)	1.7 (1.2–3.0)
VL (log_{10} copies/mL)					
Median (IQR)	4.4 (3.7–5.0)	5.1 (4.6–5.3)	<1.7	<1.7	NA

EHI, early HIV infection; ART, antiretroviral therapy; CHI, chronic HIV infection; EC, elite controllers; UC, uninfected controls; NA, not applicable.

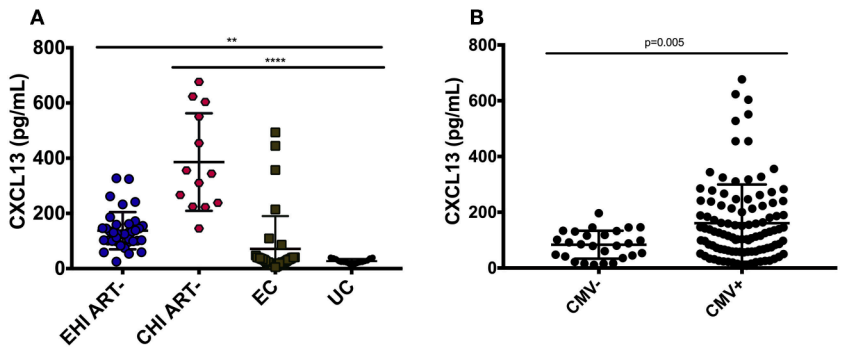

FIGURE 1 | Plasma levels of CXCL13 over the course of HIV-infection. **(A)** Circulating CXCL13 during early and chronic infection compared to elite controllers and uninfected controls. EHI ART– ($n = 37$), CHI ART– ($n = 13$), EC ($n = 35$), UC ($n = 17$). **(B)** Comparison of plasma levels of CXCL13 in CMV+ and CMV– HIV-infected progressors with similar CD4 T cell count. EHI, early HIV infection; CHI, chronic HIV infection; EC, elite controllers; UC, uninfected controls; ART, antiretroviral therapy. $^{**}p < 0.01$; $^{****}p < 0.0001$.

those receiving antiretroviral therapy (ART). In contrast, CD8 T-cell count among untreated PLWH was higher than those receiving ART. Untreated EHI and CHI groups had a median log_{10} plasma viral loads of 4.4 (3.7–5.0) and 5.1 (4.6–5.3) copies per mL, respectively. All the participants on ART and all ECs had plasma viral loads <50 copies/mL (**Table 1**).

Elevation of Plasma CXCL13 Levels During Early and Chronic HIV Infection and Impact of Antiretroviral Therapy

Plasma levels of CXCL13 were significantly elevated in ART-naive EHI (137.3 ± 67.4 pg/mL) and ART-naive CHI (385.91 ± 76.8 pg/mL) compared to EC (71.3119.0 pg/mL) and UC (33.414.9 pg/mL) (**Figure 1A**). EC had lower levels of plasma CXCL13 than EHI and CHI but still had nearly two-fold more CXCL13 than UC. However, this difference was not statistically significant. This is likely because EC are known to have a comparatively preserved immune system compared to progressors (38). We observed PLWH with CMV co-infection to have higher plasma levels of CXCL13 than PLWH without CMV co-infection ($p = 0.005$) (**Figure 1B**). Of note, CMV co-infection has been reported to be linked to HIV-associated immune activation (39). In cross-sectional analysis, both EHI and CHI groups on ART compared to their untreated counterparts showed a significant decrease in their CXCL13 levels without normalization. Longitudinal analysis of the EHI participants that remained without ART for a median of 24 months demonstrated that their plasma CXCL13 levels increased from 133.2 ± 17.3 to 260.5 ± 30.4 pg/mL ($p < 0.001$). On the other hand, EHI participants who received ART for a median of 24 months showed a decrease in their CXCL13 levels without normalization (81.6 ± 10.3 pg/mL, $p = 0.002$) (**Figure 2**). It is important to note that while there is an overall trend of reduced plasma levels of CXCL13 after 24 months of ART, such reduction is pronounced in two participants.

These results suggest that plasma levels of CXCL13 progressively increases with HIV disease progression and is

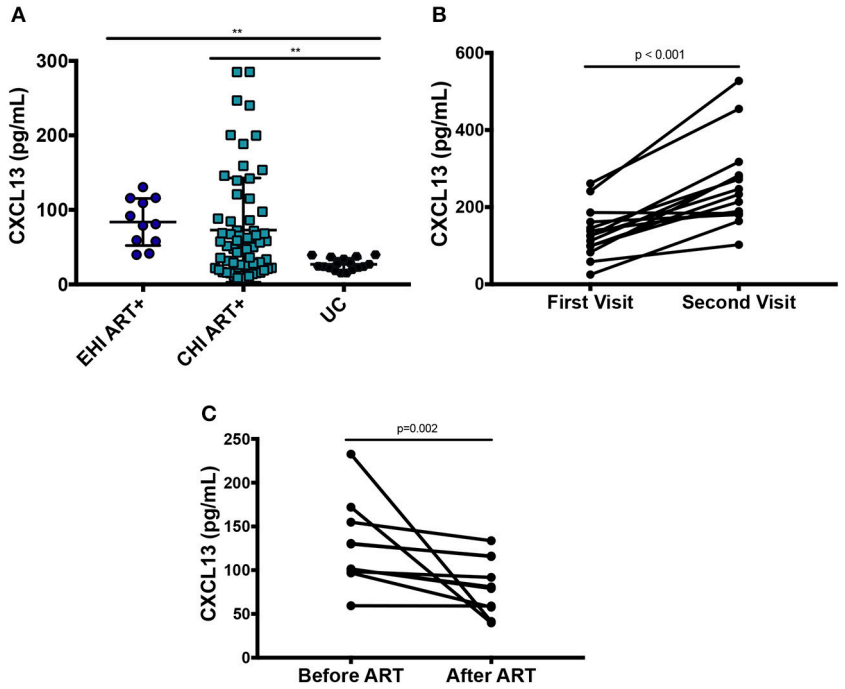

FIGURE 2 | Effect of ART on plasma levels of CXCL13. **(A)** Cross-sectional analysis on the effect of ART on plasma levels of CXCL13 (EHI ART+ $n = 11$; CHI ART+ $n = 64$; UC $n = 17$). **(B)** Longitudinal analysis on the change of plasma levels of CXCL13 over 24 months in PLWH without ART ($n = 14$). **(C)** Longitudinal analysis on the change of plasma levels of CXCL13 in PLWH after 24 months on ART ($n = 10$). EHI, early HIV infection; CHI, chronic HIV infection; UC, uninfected controls; ART, antiretroviral therapy. $^{**}p < 0.01$.

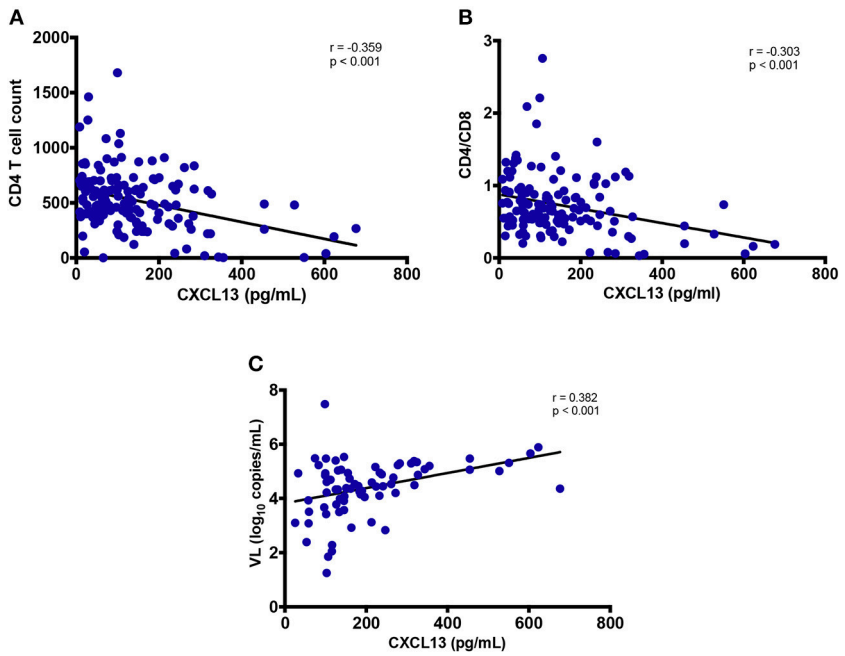

FIGURE 3 | Association of plasma levels of CXCL13 with markers of HIV disease progression. **(A)** Plasma levels of CXCL13 are correlated with CD4 T cell count in HIV-infected progressors ($n = 144$). **(B)** Plasma levels of CXCL13 are correlated with CD4/CD8 T cell ratio in HIV-infected progressors ($n = 144$). **(C)** Plasma levels of CXCL13 are correlated with plasma viral load in untreated PLWH ($n = 72$).

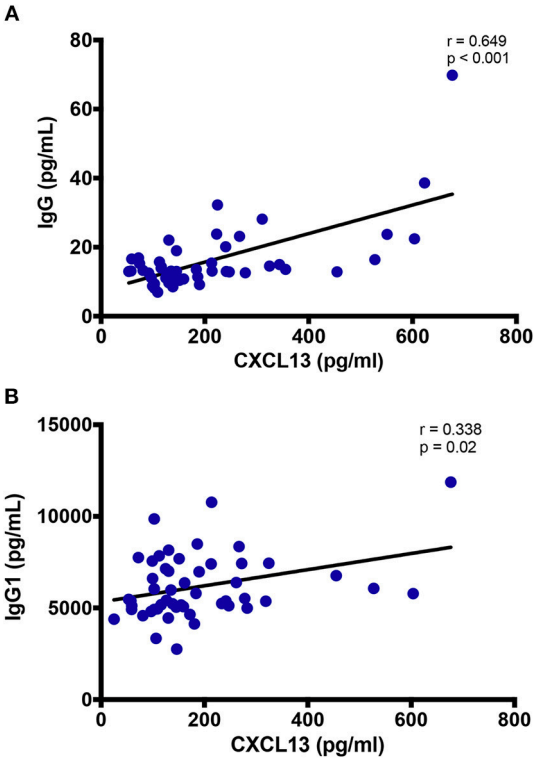

FIGURE 4 | Plasma levels of CXCL13 are associated with immunoglobulin production. **(A)** Plasma levels of CXCL13 are correlated with plasma levels of non-specific IgG in a subset of EHI and CHI PLWH, including participants on and off ART ($n = 49$). **(B)** Plasma levels of CXCL13 are correlated with plasma levels of non-specific IgG1 in a subset of EHI and CHI PLWH, including participants on and off ART ($n = 51$).

decreased without normalization upon initiation of ART. This is in line with previous findings that ART results in a decrease without normalization of systemic immune activation (40). Multivariate analysis confirmed that elevated CXCL13 levels among PLWH were independent of the effect of age, sex, HIV viral load, CD4 T cell count, and inflammatory markers.

Correlation of Plasma CXCL13 Levels With CD4 and CD8 T-Cell Counts, CD4/CD8 T Cell Ratio and Plasma Viral Load

Among PLWH, CXCL13 levels correlated negatively with both CD4 T-cell count ($r = -0.359$; $p < 0.001$) and CD4/CD8 T cell ratio ($r = -0.303$; $p < 0.001$) but not with CD8 T-cell count ($r = 0.107$; $p = 0.232$, data not shown). Elevated CXCL13 levels among untreated participants (both EHI and CHI) positively correlated with viral load ($r = 0.382$; $p < 0.001$) (**Figures 3A–C**) (41).

Correlation of Plasma CXCL13 Levels With B-Cell Activation Markers

CXCL13 levels correlated with total IgG ($r = 0.649$; $p < 0.001$), and IgG1 ($r = 0.338$; $p = 0.02$) in circulation (**Figures 4A,B**), while no correlation was observed with IgG2, IgG3, nor IgG4 (data not shown). Similarly, despite a positive trend, the correlation of plasma CXCL13 was not significant with plasma BAFF and sCD40L levels, two other indicators of B-cell activity (data not shown). These results highlight the distinctive contribution of CXCL13 in B-cell activation and humoral immune response.

Correlation of Plasma CXCL13 Levels With Soluble Markers of Gut Damage and/or Microbial Translocation

Plasma CXCL13 did not correlate with marker of epithelial gut damage, I-FABP (data not shown). We also assessed sST2 as an emerging marker of gut damage (21). CXCL13 levels did not show any correlation with sST2 (data not shown). However, plasma levels of gram-negative bacterial cell wall endotoxin LPS and monocyte activation marker sCD14 positively correlated with systemic CXCL13 levels ($r = 0.332$; $p < 0.001$ and $r = 0.322$; $p = 0.005$, respectively) (**Figures 5A,B**). Both LPS and sCD14 are considered as markers of bacterial translocation. In addition, we also measured fungal translocation using a major fungal cell wall polysaccharide antigen, βDG (42). Plasma levels of βDG correlated significantly with plasma CXCL13 ($r = 0.257$; $p = 0.03$) (**Figure 5C**). Of note, βDG has been used as a diagnostic marker for invasive fungal infections and its role is emerging in HIV-associated fungal translocation as we and others have previously reported (13, 15, 43). *In vitro*, both LPS and βDG induced CXCL13 secretion by PBMC from uninfected donors. Combination of both LPS and βDG did not show an additive effect on CXCL13 secretion compared to LPS or βDG alone (data not shown).

Correlation of Plasma CXCL13 Levels With Soluble Markers of Inflammation and/or Immune Activation

Plasma TNF-α levels were observed to have a significant positive correlation with circulating CXCL13 levels ($r = 0.316$; $p < 0.001$, **Figure 6A**), while no correlation of CXCL13 was observed with other inflammatory markers IL-1β, IL-6, and IL-8 (data not shown). We also quantified plasma Tryptophan and Kynurenine levels to measure IDO-1 enzyme activity as a marker of myeloid cell inflammation and/or immune activation. Plasma CXCL13 levels had a significant positive correlation with plasma kynurenine ($r = 0.569$; $p < 0.001$, **Figure 6B**). We computed ratio of kynurenine to tryptophan as a measure of IDO-1 enzyme activity. This ratio further significantly correlated ($r = 0.653$; $p < 0.001$, **Figure 6C**) with plasma CXCL13 levels. Taken together, these results portray the involvement of CXCL13 in HIV-associated myeloid cell activation and inflammation.

Correlation of Plasma CXCL13 Levels With Lymphocyte Activation Markers

We analyzed PBMC by FACS for whom samples were available. Frequency of $CD38^+HLA\text{-}DR^+$ CD4 T cells ($r = 0.561$; $p = 0.04$, **Figure 6D**) and frequency of $CD38^+HLA\text{-}DR^+$ CD8 T cells ($r = 0.527$; $p = 0.02$, **Figure 6E**) correlated with plasma levels of CXCL13. These findings highlight CXCL13 as a plasma level biomarker of lymphoid cell activation.

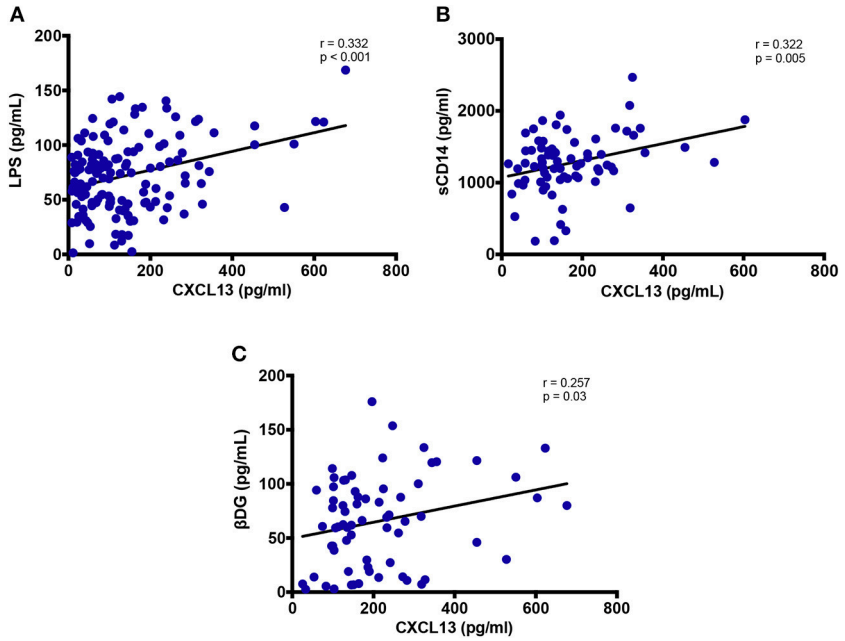

FIGURE 5 | Plasma levels of CXCL13 are associated with markers of microbial translocation. **(A)** Plasma levels of CXCL13 are correlated with plasma levels of LPS ($n = 144$). **(B)** Plasma levels of CXCL13 are correlated with plasma levels of soluble CD14 (sCD14), in a subset of EHI and CHI PLWH, including those on and off ART ($n = 74$). **(C)** Plasma levels of CXCL13 are correlated with plasma levels of (1→3)-β-D-Glucan (βDG), in a subset of EHI and CHI PLWH, including those on and off ART ($n = 68$).

DISCUSSION

We report significant elevation of plasma CXCL13 levels during early and chronic HIV infection that reduced without normalization in PLWH receiving antiretroviral therapy. To our knowledge, this is the first observation reporting a correlation of CXCL13 levels with markers of microbial translocation, inflammatory cytokines, IDO-1 enzyme activity and markers of myeloid and lymphoid cell activation in PLWH. In addition, we also showed a significant correlation of plasma CXCL13 levels with markers of B cell activation in the context of HIV infection. Interestingly, plasma levels of CXCL13 were also associated with CMV co-infection which was reported to be a contributor to HIV-associated systemic inflammation (39). Immune activation is considered as a major factor contributing to the size of HIV reservoirs and development of non-AIDS events despite long-term ART (1, 4, 7). Therefore, therapeutic strategies targeting immune activation remains a priority for curing HIV infection.

Our results are in line with the first report of elevated CXCL13 levels in PLWH. Widney et al. observed a positive correlation of plasma CXCL13 with inflammatory markers and with CD4 T cell count in chronically infected patients (31). In contrast, we observed a negative correlation of CXCL13 with CD4 T cell counts and CD4/CD8 T cell ratio. Progressive decline in the CD4 T cell numbers and CD4/CD8 T cell ratio is a hallmark of HIV-infection (44, 45). Therefore, their negative correlation with CXCL13 levels explains a role of the later in HIV-disease progression via immune activation. Furthermore, in untreated participants, we observed a correlation of plasma CXCL13 with viral load. In untreated participants, the associations of plasma CXCL13 with CD4 T cell count, CD4/CD8 ratio, LPS, sCD14, βDG, and IDO-1 metabolism were independent of HIV viral load.

Moreover, Widney et al. did not observe an association of CXCL13 levels and immunoglobulins. On the other hand, we found a correlation of CXCL13 with IgG and more specifically with its predominant subclass IgG1. This observation shows concordance of plasma CXCL13 levels with B cell activation, which is mediated via CXCR5 expression (46).

Chronic immune activation and inflammation are understood to be the driving factors of HIV disease progression and a significant underlying cause of non-AIDS events in PLWH on long-term ART. As such, it is of clinical interest to validate a biomarker that can monitor myeloid and lymphoid cell activation/inflammation in early and chronic stages of infection in both progressors and non-progressors. In these lines, T_{FH} cells are reported to secrete CXCL13 (47). Cohen et al. have shown that HIV-1 ssRNA induces the production of CXCL13 by DC (48). Furthermore, Carlsen et al. showed that LPS stimulates macrophages to produce CXCL13 *in vitro* (30). We show plasma levels of CXCL13, measured by ELISA, to be a valid marker of HIV disease progression (CD4 T cell count and plasma viral load), microbial translocation (circulation of LPS and βDG), myeloid cell activation (IDO-1 activity and plasma sCD14 levels), lymphoid cell activation (frequency of CD38+ HLA-DR+ CD4 and CD8 T cells), and general inflammation (plasma levels of TNF-α). Thus, we propose plasma levels of CXCL13 as a marker of systemic myeloid and lymphoid cell

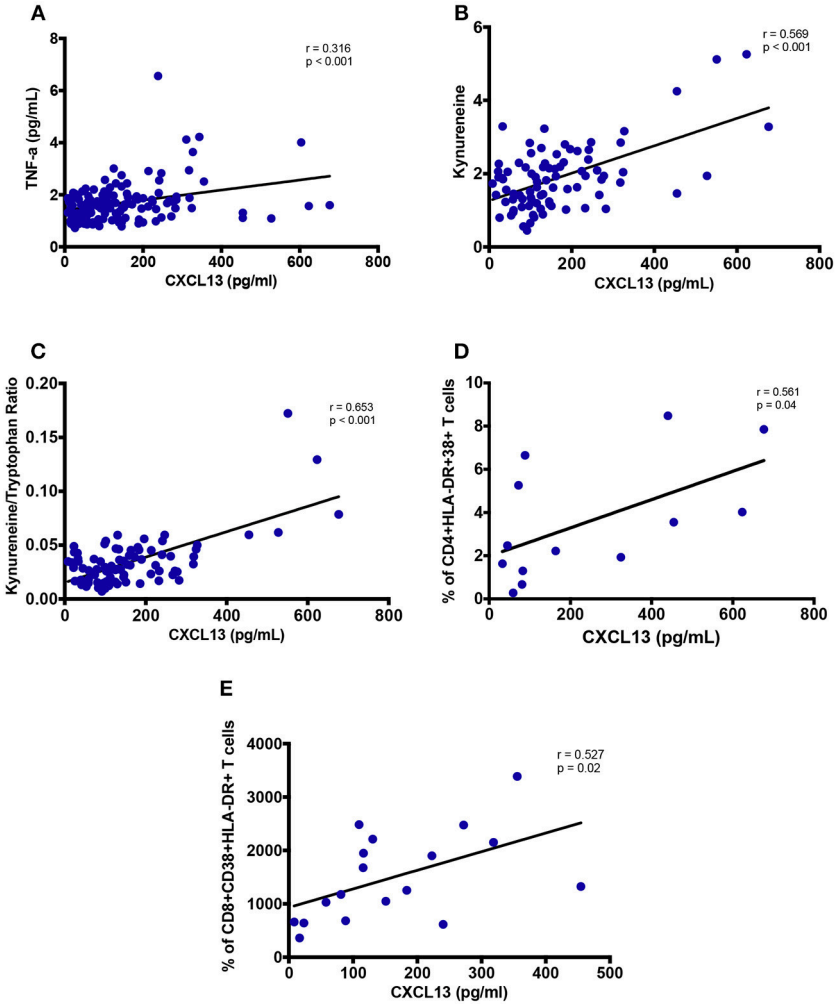

FIGURE 6 | Plasma levels of CXCL13 are associated with markers of myeloid and lymphoid activation. **(A)** Plasma levels of CXCL13 are correlated with plasma levels of TNF-α ($n = 139$). **(B)** Plasma levels of CXCL13 are correlated with plasma levels of Kynurenine, in a subset of PLWH in early and chronic stages of infection, including those on and off ART ($n = 84$). **(C)** Plasma levels of CXCL13 are correlated with IDO-1 metabolism (Kynurenine/Tryptophan), in a subset of EHI and CHI participants including those on and off ART ($n = 84$). **(D)** Plasma levels of CXCL13 are correlated with frequency of HLA-DR$^+$CD38$^+$ CD4 T cells, in a random subset of PLWH from early and chronic HIV-infection ($n = 13$). **(E)** Plasma levels of CXCL13 are correlated with frequency of HLA-DR+CD38+ CD8 T cells, in a random subset of PLWH from early and chronic HIV-infection ($n = 18$).

activation and inflammation in PLWH. Future studies should investigate the contribution of CXCL13 to the development of non-AIDS events and assess if plasma levels of CXCL13 can be used as a prognostic marker for the development of certain non-AIDS events including lymphoma.

T_{FH} cells in GCs and follicular DC in B cell follicles are major producers of CXCL13 owing to their expression of CXCL13 receptor CXCR5 (41, 46, 49). CXCL13 overexpression has been associated with immune activation in chronic conditions such as infection with HIV and systemic sclerosis (31, 50). Havenar-Daughton et al. studied a large longitudinal cohort of PLWH and reported a significant elevation of plasma CXCL13 with the generation of broad neutralizing antibodies (bnAbs) against HIV (41). They further correlated plasma CXCL13 levels with the magnitude of Ab responses and the frequency of T_{FH}-like cells expressing ICOS in the blood of individuals' post-vaccination. Similarly, we observed an association of plasma CXCL13 with Abs such as total IgG and its subtype IgG1 in PLWH. Taken together, such findings display CXCL13 not only as another marker but also as an indicator of GC activity, which is influenced by non-specific and specific stimuli, inflammation, and vaccine response.

Our study has certain limitations that need to be considered while interpreting these findings. Causality cannot be determined as an inherent bias in observational studies like ours despite being conducted on well-defined clinical cohorts. Therefore, this study could not rule out the possibility that the dysfunction caused by chronic immune activation contributes to an increase in plasma CXCL13. Furthermore, limited sample availability did not allow us to assess whether plasma levels

of CXCL13 is a marker of immune activation in known HIV reservoirs such as the gut (51). Our multivariate model did not account for potential confounding factors such as risk behaviors, economic status, smoking, alcohol, and drug abuse. Future studies should consider these limitations to further highlight the role of CXCL13 as a biomarker of immune activation among PLWH. Nevertheless, our study represents a novel and comprehensive assessment of plasma CXCL3 in the context of immune activation among PLWH with early HIV infection, before initiation of ART and while being on ART.

CONCLUSION

Globally, our results suggest that elevated plasma levels of CXCL13 in PLWH are partially restored on ART and remains associated with markers of microbial translocation and systemic immune activation. Elevated CXCL13 levels can be used to monitor HIV disease progression and inflammation. Furthermore, it has potential to be used to predict the development of non-AIDS events and residual immune activation after long-term ART.

ETHICS STATEMENT

The study was conducted in accordance with the principles of the declaration of Helsinki and all study participants provided written informed consent for study enrollment. Ethical approval was obtained from the MUHC research ethics board and by each participating medical center.

AUTHOR CONTRIBUTIONS

VM and RR performed the experiments, analyzed the data, wrote the first draft, and revised the final draft of the manuscript. SI, FD, IK, YZ, and MF contributed to the experiments, data analysis, and critical review of the manuscript. J-PR designed the study, contributed to data analysis, and critically reviewed the first and final draft of the manuscript. BL, CC, RT, JS, J-GB, BT, PC, RL, MD, CC-L, CT, and J-PR all contributed to recruitment and follow up of study participants and critically reviewed the manuscript. All authors have read and approved the contents of this manuscript.

FUNDING

This study was financed by the Fonds de la Recherche Québec-Santé (FRQ-S): Réseau SIDA/Maladies infectieuses and Thérapie cellulaire; the Canadian Institutes of Health Research (CIHR; grants MOP 103230 and 154051); the Vaccines & Immunotherapies Core of the CIHR Canadian HIV Trials Network (CTN; grant CTN 257); the Canadian Foundation for AIDS Research (CANFAR; grant 02-512); and the Canadian HIV Cure Enterprise Team Grant (HIG-133050) awarded by the CIHR in partnership with CANFAR. RR is an undergraduate student supported by the H. Grenville Smith Studentship, SI is a post-doctoral fellow supported by the William Turner research fellowship, MD is supported by a salary award from the Fonds de recherche du Québec—Santé, J-PR is the holder of the Louis Lowenstein Chair in Hematology and Oncology, McGill University and William Turner award holder from the McGill University Health Centre.

ACKNOWLEDGMENTS

We thank Angie Massicotte, Josée Girouard, and Danica Albert for study coordination and assistance as well as Mario Legault and Stéphanie Matte for coordinating the Montreal Primary HIV Infection Study, the Canadian HIV and aging cohort study and the Canadian Cohort of HIV-infected Slow Progressors. We are highly grateful to the study participants for their contribution.

REFERENCES

1. Paiardini M, Muller-Trutwin M. HIV-associated chronic immune activation. *Immunol Rev.* (2013) 254:78–101. doi: 10.1111/imr.12079
2. Sousa AE, Carneiro J, Meier-Schellersheim M, Grossman Z, Victorino RM. CD4 T cell depletion is linked directly to immune activation in the pathogenesis of HIV-1 and HIV-2 but only indirectly to the viral load. *J Immunol.* (2002) 169:3400–6. doi: 10.4049/jimmunol.169.6.3400
3. Cao W, Mehraj V, Kaufmann DE, Li T, Routy JP. Elevation and persistence of CD8 T-cells in HIV infection: the Achilles heel in the ART era. *J Int AIDS Soc.* (2016) 19:20697. doi: 10.7448/IAS.19.1.20697
4. Klatt NR, Chomont N, Douek DC, Deeks SG. Immune activation and HIV persistence: implications for curative approaches to HIV infection. *Immunol Rev.* (2013) 254:326–42. doi: 10.1111/imr.12065
5. Brenchley JM, Price DA, Schacker TW, Asher TE, Silvestri G, Rao S, et al. Microbial translocation is a cause of systemic immune activation in chronic HIV infection. *Nat Med.* (2006) 12:1365–71. doi: 10.1038/nm1511
6. Gianella S, Chaillon A, Mutlu EA, Engen PA, Voigt RM, Keshavarzian A, et al. Effect of cytomegalovirus and Epstein-Barr virus replication on intestinal mucosal gene expression and microbiome composition of HIV-infected and uninfected individuals. *AIDS* (2017) 31:2059–67. doi: 10.1097/QAD.0000000000001579
7. Brites-Alves C, Luz E, Netto EM, Ferreira T, Diaz RS, Pedroso C, et al. Immune activation, proinflammatory cytokines, and conventional risks for cardiovascular disease in HIV patients: a case-control study in Bahia, Brazil. *Front Immunol.* (2018) 9:1469. doi: 10.3389/fimmu.2018.01469
8. Nasi M, De Biasi S, Gibellini L, Bianchini E, Pecorini S, Bacca V, et al. Ageing and inflammation in patients with HIV infection. *Clin Exp Immunol.* (2017) 187:44–52. doi: 10.1111/cei.12814
9. Klatt NR, Funderburg NT, Brenchley JM. Microbial translocation, immune activation, and HIV disease. *Trends Microbiol.* (2013) 21:6–13. doi: 10.1016/j.tim.2012.09.001
10. Maidji E, Somsouk M, Rivera JM, Hunt PW, Stoddart CA. Replication of CMV in the gut of HIV-infected individuals and epithelial barrier dysfunction. *PLoS Pathog.* (2017) 13:e1006202. doi: 10.1371/journal.ppat.1006202
11. Hensley-McBain T, Berard AR, Manuzak JA, Miller CJ, Zevin AS, Polacino P, et al. Intestinal damage precedes mucosal immune dysfunction in SIV infection. *Mucosal Immunol.* (2018) 11:1429–40. doi: 10.1038/s41385-018-0032-5

12. Ancuta P, Kamat A, Kunstman KJ, Kim EY, Autissier P, Wurcel A, et al. Microbial translocation is associated with increased monocyte activation and dementia in AIDS patients. *PLoS ONE* (2008) 3:e2516. doi: 10.1371/journal.pone.0002516
13. Hoenigl M, Perez-Santiago J, Nakazawa M, de Oliveira MF, Zhang Y, Finkelman MA, et al. (1→3)-β-d-Glucan: a biomarker for microbial translocation in individuals with acute or early HIV infection? *Front Immunol.* (2016) 7:404. doi: 10.3389/fimmu.2016.00404
14. Morris A, Hillenbrand M, Finkelman M, George MP, Singh V, Kessinger C, et al. Serum (1→3)-β-D-glucan levels in HIV-infected individuals are associated with immunosuppression, inflammation, and cardiopulmonary function. *J Acquir Immune Defic Syndr.* (2012) 61:462–8. doi: 10.1097/QAI.0b013e318271799b
15. Mehraj V, Ramendra R, Costiniuk C, Lebouché B, Ponte R, Thomas R, et al. Circulating (1→3)-β-d-glucan as a marker of microbial translocation in HIV infection. In: *The Annual Conference on Retroviruses and Opportunistic Infections CROI 2018*, Poster 254. Boston, MA (2018).
16. Hoenigl M, Moser C, Funderburg N, Bosch R, Kantor A, Zhang Y, et al. Soluble Urokinase Plasminogen Activator Receptor (suPAR) is predictive of non-AIDS events during antiretroviral therapy-mediated viral suppression. *Clin Infect Dis*. (2018). doi: 10.1093/cid/ciy966. [Epub ahead of print].
17. Siewe B, Landay A. Cellular and soluble immune activation markers in HIV-infected subjects. In: Hope TJ, Stevenson M, Richman D, editors. *Encyclopedia of AIDS*. New York, NY: Springer (2014). p. 1–8.
18. Kestens L, Vanham G, Vereecken C, Vandenbruaene M, Vercauteren G, Colebunders RL, et al. Selective increase of activation antigens HLA-DR and CD38 on CD4+ CD45RO+ T lymphocytes during HIV-1 infection. *Clin Exp Immunol.* (1994) 95:436–41. doi: 10.1111/j.1365-2249.1994.tb07015.x
19. Mehraj V, Routy JP. Tryptophan catabolism in chronic viral infections: handling uninvited guests. *Int J Tryptophan Res.* (2015) 8:41–8. doi: 10.4137/IJTR.S26862
20. Cockerham LR, Siliciano JD, Sinclair E, O'Doherty U, Palmer S, Yukl SA, et al. CD4+ and CD8+ T cell activation are associated with HIV DNA in resting CD4+ T cells. *PLoS ONE* (2014) 9:e110731. doi: 10.1371/journal.pone.0110731
21. Mehraj V, Jenabian MA, Ponte R, Lebouche B, Costiniuk C, Thomas R, et al. The plasma levels of soluble ST2 as a marker of gut mucosal damage in early HIV infection. *AIDS* (2016) 30:1617–27. doi: 10.1097/QAD.0000000000001105
22. Chen J, Xun J, Yang J, Ji Y, Liu L, Qi T, et al. Plasma indoleamine 2,3-dioxygenase activity is associated with the size of HIV reservoir in patients receiving antiretroviral therapy. *Clin Infect Dis.* (2018) ciy676. doi: 10.1093/cid/ciy676. [Epub ahead of print].
23. Feghali CA, Wright TM. Cytokines in acute and chronic inflammation. *Front Biosci.* (1997) 2:d12–26. doi: 10.2741/A171
24. Esser R, von Briesen H, Brugger M, Ceska M, Glienke W, Muller S, et al. Secretory repertoire of HIV-infected human monocytes/macrophages. *Pathobiology* (1991) 59:219–22. doi: 10.1159/000163649
25. Scherberich JE, Nockher WA. Blood monocyte phenotypes and soluble endotoxin receptor CD14 in systemic inflammatory diseases and patients with chronic renal failure. *Nephrol Dial Transplant.* (2000) 15:574–8. doi: 10.1093/ndt/15.5.574
26. Moir S, Buckner CM, Ho J, Wang W, Chen J, Waldner AJ, et al. B cells in early and chronic HIV infection: evidence for preservation of immune function associated with early initiation of antiretroviral therapy. *Blood* (2010) 116:5571–9. doi: 10.1182/blood-2010-05-285528
27. Moir S, Fauci AS. B cells in HIV infection and disease. *Nat Rev Immunol.* (2009) 9:235–45. doi: 10.1038/nri2524
28. Velu V, Mylvaganam G, Ibegbu C, Amara RR. Tfh1 cells in germinal centers during chronic HIV/SIV infection. *Front Immunol.* (2018) 9:1272. doi: 10.3389/fimmu.2018.01272
29. Pallikkuth S, de Armas L, Rinaldi S, Pahwa S. T follicular helper cells and B cell dysfunction in aging and HIV-1 infection. *Front Immunol.* (2017) 8:1380. doi: 10.3389/fimmu.2017.01380
30. Carlsen HS, Baekkevold ES, Morton HC, Haraldsen G, Brandtzaeg P. Monocyte-like and mature macrophages produce CXCL13 (B cell-attracting chemokine 1) in inflammatory lesions with lymphoid neogenesis. *Blood* (2004) 104:3021–7. doi: 10.1182/blood-2004-02-0701
31. Widney DP, Breen EC, Boscardin WJ, Kitchen SG, Alcantar JM, Smith JB, et al. Serum levels of the homeostatic B cell chemokine, CXCL13, are elevated during HIV infection. *J Interferon Cytokine Res*. (2005) 25:702–6. doi: 10.1089/jir.2005.25.702
32. Mehraj V, Cox J, Lebouche B, Costiniuk C, Cao W, Li T, et al. Socio-economic status and time trends associated with early ART initiation following primary HIV infection in Montreal, Canada: 1996 to 2015. *J Int AIDS Soc.* (2018) 21:e25034. doi: 10.1002/jia2.25034
33. Durand M, Chartrand-Lefebvre C, Baril JG, Trottier S, Trottier B, Harris M, et al. The Canadian HIV and aging cohort study - determinants of increased risk of cardio-vascular diseases in HIV-infected individuals: rationale and study protocol. *BMC Infect Dis*. (2017) 17:611. doi: 10.1186/s12879-017-2692-2
34. El-Far M, Kouassi P, Sylla M, Zhang Y, Fouda A, Fabre T, et al. Proinflammatory isoforms of IL-32 as novel and robust biomarkers for control failure in HIV-infected slow progressors. *Sci Rep*. (2016) 6:22902. doi: 10.1038/srep22902
35. Cao W, Mehraj V, Trottier B, Baril JG, Leblanc R, Lebouche B, et al. Early initiation rather than prolonged duration of antiretroviral therapy in HIV infection contributes to the normalization of CD8 T-cell counts. *Clin Infect Dis.* (2016) 62:250–7. doi: 10.1093/cid/civ809
36. Jenabian MA, El-Far M, Vyboh K, Kema I, Costiniuk CT, Thomas R, et al. Immunosuppressive tryptophan catabolism and gut mucosal dysfunction following early HIV infection. *J Infect Dis.* (2015) 212:355–66. doi: 10.1093/infdis/jiv037
37. Jenabian MA, Patel M, Kema I, Kanagaratham C, Radzioch D, Thebault P, et al. Distinct tryptophan catabolism and Th17/Treg balance in HIV progressors and elite controllers. *PLoS ONE* (2013) 8:e78146. doi: 10.1371/journal.pone.0078146
38. Zaunders J, van Bockel D. Innate and adaptive immunity in long-term non-progression in HIV disease. *Front Immunol.* (2013) 4:95. doi: 10.3389/fimmu.2013.00095
39. Lurain NS, Hanson BA, Hotton AL, Weber KM, Cohen MH, Landay AL. The association of human cytomegalovirus with biomarkers of inflammation and immune activation in HIV-1-infected women. *AIDS Res Hum Retroviruses* (2016) 32:134–43. doi: 10.1089/aid.2015.0169
40. Chen J, Ramendra R, Lu H, Routy JP. The early bird gets the worm: benefits and future directions with early antiretroviral therapy initiation in primary HIV infection. *Fut. Virol.* (2018) 13, 779–786. doi: 10.2217/fvl-2018-0110
41. Havenar-Daughton C, Lindqvist M, Heit A, Wu JE, Reiss SM, Kendric K, et al. CXCL13 is a plasma biomarker of germinal center activity. *Proc Natl Acad Sci USA*. (2016) 113:2702–7. doi: 10.1073/pnas.1520112113
42. Camilli G, Tabouret G, Quintin J. The complexity of fungal beta-Glucan in health and disease: effects on the mononuclear phagocyte system. *Front Immunol.* (2018) 9:673. doi: 10.3389/fimmu.2018.00673
43. Farhour Z, Mehraj V, Chen J, Ramendra R, Lu H, Routy JP. Use of (1→3)-β-d-glucan for diagnosis and management of invasive mycoses in HIV-infected patients. *Mycoses* (2018) 61:718–22. doi: 10.1111/myc.12797
44. Lu W, Mehraj V, Vyboh K, Cao W, Li T, Routy JP. CD4:CD8 ratio as a frontier marker for clinical outcome, immune dysfunction and viral reservoir size in virologically suppressed HIV-positive patients. *J Int AIDS Soc.* (2015) 18:20052. doi: 10.7448/IAS.18.1.20052
45. Vidya Vijayan KK, Karthigeyan KP, Tripathi SP, Hanna LE. Pathophysiology of CD4+ T-cell depletion in HIV-1 and HIV-2 infections. *Front Immunol.* (2017) 8:580. doi: 10.3389/fimmu.2017.00580
46. Rasheed AU, Rahn HP, Sallusto F, Lipp M, Muller G. Follicular B helper T cell activity is confined to CXCR5(hi)ICOS(hi) CD4 T cells and is independent of CD57 expression. *Eur J Immunol.* (2006) 36:1892–903. doi: 10.1002/eji.200636136
47. Gu-Trantien C, Migliori E, Buisseret L, de Wind A, Brohee S, Garaud S, et al. CXCL13-producing TFH cells link immune suppression and

adaptive memory in human breast cancer. *JCI Insight*. (2017) 2:91487. doi: 10.1172/jci.insight.91487
48. Cohen KW, Dugast AS, Alter G, McElrath MJ, Stamatatos L. HIV-1 single-stranded RNA induces CXCL13 secretion in human monocytes via TLR7 activation and plasmacytoid dendritic cell-derived type I IFN. *J Immunol.* (2015) 194:2769–75. doi: 10.4049/jimmunol.1400952
49. Wang X, Cho B, Suzuki K, Xu Y, Green JA, An J, et al. Follicular dendritic cells help establish follicle identity and promote B cell retention in germinal centers. *J Exp Med*. (2011) 208:2497–510. doi: 10.1084/jem.20111449
50. Taniguchi T, Miyagawa T, Toyama S, Yamashita T, Nakamura K, Saigusa R, et al. CXCL13 produced by macrophages due to Fli1 deficiency may contribute to the development of tissue fibrosis, vasculopathy and immune activation in systemic sclerosis. *Exp Dermatol.* (2018) 27:1030–7. doi: 10.1111/exd.13724
51. Mehraj V, Ghali P, Ramendra R, Costiniuk C, Lebouche B, Ponte R, et al. The evaluation of risk-benefit ratio for gut tissue sampling in HIV cure research. *J Virus Erad*. (2017) 3:212–7.

Conflict of Interest Statement: MF and YZ are employees of Associates of Cape Cod, Inc., the manufacturers of Fungitell, the (1→3)-β-D-glucan *in vitro* diagnostic kit.

The remaining authors declare that the research was conducted in the absence of any commercial or financial relationships that could be construed as a potential conflict of interest.

frontiers in Immunology

ORIGINAL RESEARCH
published: 12 March 2019
doi: 10.3389/fimmu.2019.00463

Altered Immunity and Microbial Dysbiosis in Aged Individuals With Long-Term Controlled HIV Infection

*Nicholas Rhoades[1], Norma Mendoza[1], Allen Jankeel[1], Suhas Sureshchandra[1], Alexander D. Alvarez[1], Brianna Doratt[1], Omeid Heidari[2], Rod Hagan[3], Brandon Brown[4], Steven Scheibel[3], Theodore Marbley[3], Jeff Taylor[5] and Ilhem Messaoudi[1]**

[1] Molecular Biology and Biochemistry, University of California Irvine, Irvine, CA, United States, [2] School of Nursing, John Hopkins University, Baltimore, MD, United States, [3] Stonewall Medical Center, Borrego Health, Cathedral City, CA, United States, [4] School of Medicine, University of California, Riverside, Riverside, CA, United States, [5] HIV+ Aging-Palm Springs, Palm Springs, CA, United States

The introduction of highly active antiretroviral therapy (HAART) resulted in a significant increase in life expectancy for HIV patients. Indeed, in 2015, 45% of the HIV+ individuals in the United States were ≥55 years of age. Despite improvements in diagnosis and treatment of HIV infection, geriatric HIV+ patients suffer from higher incidence of comorbidities compared to age-matched HIV- individuals. Both chronic inflammation and dysbiosis of the gut microbiome are believed to be major contributors to this phenomenon, however carefully controlled studies investigating the impact of long-term (>10 years) controlled HIV (LTC-HIV) infection are lacking. To address this question, we profiled circulating immune cells, immune mediators, and the gut microbiome from elderly (≥55 years old) LTC-HIV+ and HIV- gay men living in the Palm Springs area. LTC-HIV+ individuals had lower frequency of circulating monocytes and CD4+ T-cells, and increased frequency CD8+ T-cells. Moreover, levels of systemic INFγ and several growth factors were increased while levels of IL-2 and several chemokines were reduced. Upon stimulation, immune cells from LTC-HIV+ individuals produced higher levels of pro-inflammatory cytokines. Last but not least, the gut microbiome of LTC-HIV+ individuals was enriched in bacterial taxa typically found in the oral cavity suggestive of loss of compartmentalization, while levels of beneficial butyrate producing taxa were reduced. Additionally, prevalence of *Prevotella* negatively correlated with CD4+ T-cells numbers in LTC-HIV+ individuals. These results indicate that despite long-term adherence and undetectable viral loads, LTC-HIV infection results in significant shifts in immune cell frequencies and gut microbial communities.

Keywords: HIV, HAART, aging, dysbiosis, inflammation

OPEN ACCESS

Edited by:
Martin Hoenigl, University of California, San Diego, United States

Reviewed by:
Cristian Apetrei, University of Pittsburgh, United States
Seema N. Desai, Rush University Medical Center, United States

***Correspondence:**
Ilhem Messaoudi
imessaou@uci.edu

Specialty section:
This article was submitted to Viral Immunology, a section of the journal Frontiers in Immunology

Received: *30 November 2018*
Accepted: *20 February 2019*
Published: *12 March 2019*

Citation:
Rhoades N, Mendoza N, Jankeel A, Sureshchandra S, Alvarez AD, Doratt B, Heidari O, Hagan R, Brown B, Scheibel S, Marbley T, Taylor J and Messaoudi I (2019) Altered Immunity and Microbial Dysbiosis in Aged Individuals With Long-Term Controlled HIV Infection. Front. Immunol. 10:463. doi: 10.3389/fimmu.2019.00463

INTRODUCTION

Advances in the diagnosis and treatment of HIV infection has transformed what used to be a fatal diagnosis into a long-term chronic disease with individuals living up to 50 years after diagnosis (1, 2). In the United States, 450,000 of those living with HIV are ≥50 years of age, and this number is expected to grow over the coming decade (3). Highly active anti-retroviral

therapy (HAART) must be taken continuously to maintain viral loads below detection (4, 5). However, low levels of viral replication can be detected in virtually all patients receiving HAART (6). Moreover, mortality rates among individuals living with long-term controlled HIV infection (LTC-HIV) remains higher than those seen in age-matched HIV- individuals due to HIV-associated non-AIDS (HANA) co-morbidities (7–9). HANA co-morbidities include neurocognitive disorders, cardiovascular disease, cancer, liver cirrhosis, kidney, and lung disease (10–16). The average number of comorbid conditions is higher in older HIV+ patients compared to age-matched HIV- subjects, indicative of accelerated aging (10, 17). The mechanisms underlying this increase in comorbidities and resulting mortality remain unclear. Consequently, very few interventions are available to counteract these adverse outcomes.

Some of these comorbidities could be explained by the high rates of co-infection among LTC-HIV patients, notably with Hepatitis C (18, 19). Moreover, HAART toxicity itself increases the risk of cardiovascular disease and metabolic dysfunction via mitochondrial dysfunction, but this does not fully explain the increase in neurocognitive disorders (20–23). Another potential factor is the increased systemic inflammation reported in LTC-HIV infection (24–27). While the initiation of HAART has been shown to reduce immune activation, the levels remain higher than those observed in HIV- individuals even after 2 years of treatment (28–31). The sources of this systemic inflammation are poorly understood. Some studies have suggested an association between shifts in the gut microbiome and systemic inflammation (32, 33). HIV-induced loss of Th17 CD4+ T cells in the gut is thought to disrupt the microbial community and impair the gut barrier resulting in the translocation of microbial products (34, 35). Indeed, increased levels of sCD14, LPS, IgM, iFABP, and endotoxin-bound IgM have been reported in HIV+ individuals at various stages of infection (36, 37). Some studies have reported an increase in the abundance of *Prevotella* in untreated, and HAART treated HIV+ individuals while others reported no changes (33, 38). Furthermore, disruption in tryptophan metabolism, reduction in short chain fatty acid (SCFA) production, and an increase in trimethylamine-n-oxide (TMAO) production have all been linked to increased HANA co-morbidities (39–41).

Our understanding of the role of circulating immune cells in the development and exacerbation of systemic inflammation also remains incomplete. While many have reported some recovery of CD4+ T cells upon initiation of HAART, this finding has only has been explored through the first 5 years of treatment (42–44). An increase in terminally differentiated T cells has also been listed as a potential source of aberrant immune activation (45). CD4+ T cells are not the only immune cells affected by HIV infection. Monocytes in particular are activated directly during initial infection by circulating viral proteins such as gp120 and Nef (45) and indirectly at later stages due to an increase in bacterial products such as LPS in circulation (46–48). Activated monocytes can release multiple immune mediators such as TNFα, IL-1β, IL-6 that can contribute to systemic inflammation (49). Natural Killer (NK) cells also play an important role in controlling HIV through the production of INFγ which suppresses infection, but can also contribute to excessive inflammation (50). HAART has been shown to restore NK populations over the first couple of years of treatment, but the durability of this recovery is not well-understood (51).

The lack of clear understanding of the impact of LTC-HIV infection on immune status, systemic inflammation, and microbiome communities is likely due to the paucity of well-controlled studies. Researchers often compare HIV+ and HIV- groups of differing socioeconomic status, sexual orientation, and geographic location. These factors can affect immunological status and the gut microbiome. To address this limitation, we obtained blood and rectal swabs from older (≥55 years of age) LTC-HIV+ gay men (>10 years post-infection) and HIV- participants residing in the Palm Springs area. Our analysis shows that despite adherence to HAART treatment, HIV status is associated with a reduction in circulating CD4+ T-cells and monocytes, an increase in CD8+ T-cells, and greater activation/differentiation of NK cells. We also detected signs of heightened systemic inflammation and induced inflammatory response to polyclonal stimulation. Surprisingly, we detected a limited number of shifts in the gut microbial community with an increase in Fusobacteria, Bifidobacteriales, and Lactobacillales in LTC-HIV+ men. *Prevotella* was negatively correlated with CD4+ T-cell count in LTC-HIV+ but not HIV- individuals. Together these data suggest that significant differences in immunological and microbial communities persist in LTC-HIV infection.

METHODS

Study Population and Sample Collection

The Institutional Review Board of the University of California, Riverside reviewed and approved this study, and the University of California, Irvine obtained a reliance registry.

A total of 105 men ≥55 years of age (HIV- $n = 47$, LTC-HIV+ $n = 58$) were recruited from Palm Springs, CA. All LTC-HIV+ individuals have been on HAART therapy for >10 years with undetectable viral loads. Median CD4+ cell counts in the LTC-HIV cohort were 689 cells/mm^3 with only two individuals having CD4+ T cell count <200 cells/mm^3 while CD4+ cell counts in the HIV- cohort were 1198 cells/mm^3. Each participant submitted a blood sample, a rectal swab, and completed a paper demographics/co-morbidities survey (**Table 1**). Complete blood cell counts (CBC) were determined using a hematology analyzer (Beckman Coulter). Peripheral blood mononuclear cells (PBMC) and plasma were obtained by standard density gradient centrifugation over the blood separation polymer Ficoll (GE Healthcare Life Sciences, Pittsburg, PA, United States). PBMC were frozen in 10% DMSO/FBS and stored in liquid nitrogen while plasma was stored at 80°C until analysis.

Flow Cytometry

1–2 × 10^6 PBMC were stained using antibodies against: CD4, CD8b, CD95, CD28, CCR7, CD20, CD27, IgD, PD-1, KLRG1, and Ki-67 to delineate naïve and memory T and B cell populations, as well as measure activation and proliferation (**Supplementary Figure 1**). A second tube of 1–2 × 10^6 PBMC was stained using antibodies against: CD3, CD20,

TABLE 1 | Demographics and co-morbidities.

	Total *n* [*S.D.*](%)	LTC-HIV + *n* [*S.D.*](%)	HIV – *n* [*S.D.*](%)	*p*
DEMOGRAPHICS				
Age	64 [6.8]	65.7 [7.3]	62.7 [6.03]	0.02*
Race				0.82
Non-hispanic white	90 (84.6)	49 (84.5)	41 (87.2)	
Other	15 (15.5)	9 (15.5)	6 (12.8)	
Education				0.299
High school	8 (8.3)	7 (12.5)	1 (2.4)	
Some college	32 (33.3)	21 (37.5)	11 (26.8)	
Four-year university	25 (24.0)	13 (23.2)	12 (29.3)	
Graduate school	32 (33.3)	15 (26.8)	17 (41.4)	
Relationship status				0.10
Single	43 (41.7)	29 (49.2)	14 (31.8)	
In a relationship	18 (17.5)	10 (16.9)	8 (18.2)	
Engaged	2 (1.9)	1 (1.7)	1 (2.3)	
Married	34 (33.0)	14 (23.7)	20 (45.5)	
Widowed	6 (5.8)	5 (8.5)	1 (2.3)	
On disability	28 (28.28)	25 (43.86)	3 (7.14)	0.001***
COMORBIDITIES				
Depression	27 (25.96)	21 (35.59)	6 (13.33)	0.013*
Arthritis	30 (28.85)	17 (28.81)	13 (28.89)	1.000
Hepatitis	8 (7.69)	8 (13.56)	0 (0)	0.009***
Neuropathy	33 (31.73)	24 (40.68)	9 (20)	0.033*
Hypertension	38 (36.54)	18 (30.51)	20 (44.44)	0.156
Dermatitis	12 (11.54)	10 (16.95)	2 (4.44)	0.064
Herpes	13 (12.50)	8 (13.56)	5 (11.11)	0.773
Vision loss	17 (16.35)	9 (15.25)	8 (17.78)	0.792
Diabetes	13 (12.5)	8 (13.56)	5 (11.11)	0.773
Hearing loss	25 (24.04)	11 (18.64)	14 (31.11)	0.168
Respiratory problems	6 (5.78)	3 (5.08)	3 (6.67)	1.000
Heart condition	11 (10.58)	4 (6.78)	7 (15.56)	0.201
Broken bones	1 (0.96)	0 (0)	1 (2.22)	0.433

*Chi-squared or Fisher's exact tests were conducted to determine significant differences between the two *p < 0.05, ***p < 0.001.*

HLA-DR, CD14, CD11c, CD123, CD56, CD16, granzymeB, and CD57 to delineate monocytes, myeloid dendritic cells (mDC), plasmacytoid dendritic cells (pDC), and natural killer (NK) cell subsets, respectively (**Supplementary Figure 2**). All flow cytometry samples were acquired with Attune NxT (Life Technologies, Carlsbad, CA, United States) and analyzed using FlowJo (TreeStar, Ashland, OR, United States).

PBMC Stimulation

5×10^5 PBMC were incubated for 16 h in the absence (unstimulated) or presence (stimulated) of 5 ng/ml PMA and 1 μg/ml Ionomycin at 37°C in a humidified incubator (5% CO_2). At the end of the incubation, cells were spun down for 5 min at 2,000 rpm. Supernatants were collected to measure production of immune mediators and cell pellets were used for RNA extraction.

Analysis of Immune Mediator Production

Plasma levels of immune mediators were assessed using a human 45-plex assay (Thermo Fisher Scientific, Waltham, MA, United States). Immune mediators produced by PBMC in response to PMA/ionomycin stimulation were measured using Magnetic 33-plex assay (R&D Systems, Minneapolis, MN, United States). All samples were analyzed using a MAGPIX instrument (Luminex, Austin, TX, United States).

RNAseq Library Prep

Total RNA was isolated from PBMC pellets obtained from control and stimulated wells using the Qiagen mRNAeasy kit (Qiagen, Valencia, CA, United States). RNA concentration and integrity was verified using Agilent 2,100 Bioanalyzer. Total RNA was depleted of ribosomal fraction using Ribo-Gone rRNA removal kit. Libraries were then constructed using SMARTer Stranded RNA-Seq Kit (Clontech, Mountain View, CA, United States). Following assessment of size, quality, and concentrations, libraries were multiplexed and subject to sequencing (75 bp single end) on the NextSeq platform (Illumina, San Diego, CA, United States).

RNAseq Data Analysis

Quality control of raw reads was performed retaining bases with quality scores of 20 and reads at least 50 base pair long. Reads were aligned to human genome (hg38) using splice aware aligner TopHat as previously described (52) using annotations available from Ensembl (GRCh38.85) database. Quantification and statistical validation of differentially expressed genes (DEGs) was performed using edgeR (https://bioconductor.org/packages/release/bioc/html/edgeR.html), with candidate genes defined by at least two-fold change in expression with multiple hypothesis corrected (Benjamini-Hochberg procedure) FDR <0.05. Functional enrichment of DEGs was performed using open source functional enrichment tool Metascape (53) and disease associations analyzed using MetaCore™. Heatmaps were generated in R. Gene expression data have been deposited in NCBI's Sequence Read Archive BioProject (PRJNA518909).

16S rRNA Gene Library Construction and Sequencing

Total DNA was extracted from rectal swabs using the PowerSoil DNA Isolation Kit (MO BIO Laboratories, Carlsbad, CA, USA), and a 30-s bead-beating step using a Mini-Beadbeater-16 (BioSpec Products, Bartlesville, OK, USA). This genomic DNA was used as the template to amplify the hypervariable V4 region of the 16S rRNA gene using PCR primers (515F/806R with the reverse primers including a 12-bp barcode) and reactions containing: 50 mM Tris (pH 8.3), 500 μg/ml bovine serum albumin (BSA), 2.5 mM MgCl2, 250 μM of each deoxynucleotide triphosphate (dNTP), 400 nM of each primer, 5 μl of DNA template, and 0.25 units of JumpStart Taq DNA polymerase (Sigma-Aldrich, St Louis, MO, USA). Thermal cycling parameters were 94°C for 5 min; 35 cycles of 94°C for 20 s, 50°C for 20 s, 72°C for 30 s, followed by 72°C for 5 min. PCR products were purified using a MinElute 96 UF PCR Purification

Kit (Qiagen, Valencia, CA, USA). Libraries were sequenced (1 × 300 bases) using an Illumina MiSeq.

16S rRNA Gene Sequence Processing

Raw FASTQ sequence files of 16S rRNA genes were processed with the UPARSE pipeline (54). We used a custom Python script to demultiplex and prepare sequence files for clustering. Sequences were then filtered at a maxee value of 1.0 (allowing only one nucleotide per sequence to be incorrect) to remove low-quality sequences. The remaining sequences were dereplicated and singletons were removed. Operational taxonomic units (OTUs) were assigned with UPARSE at a 97% sequence identity threshold. Taxonomy was assigned to sequences for each OTU using the Ribosomal Database Project (RDP) classifier with a confidence threshold of 0.5 against the Greengenes 13_8 database using Quantitative Insights Into Microbial Ecology (QIIME) version 1.9.1 (55). To eliminate any bias due to sequencing depth, all samples were rarefied to 13,000 sequences per sample before calculating diversity metrics. 16S amplicon sequencing data have been deposited in NCBI's Sequence Read Archive BioProject (PRJNA518910).

RESULTS

Long-Term HIV Infection Is Associated With Significant Shifts in Circulating Immune Cell Populations.

It has been well-established that HIV infection is associated with alterations of lymphocyte subsets both in circulation and lymphoid tissues (56). This can be partially remediated using HAART (57), but the long-term outcomes of HAART (>10 years) on immune cell frequencies has not been addressed. To this end, we compared frequencies of circulating lymphocyte and myeloid populations within peripheral blood mononuclear cells (PBMC) between HIV- and LTC-HIV+ older men (≥55 years of age). As previously reported, our CBC data showed a reduced number of total lymphocytes in the blood with LTC-HIV infection (**Supplementary Figure 3C**) with no additional changes in total leukocytes, granulocytes or monocyte numbers (**Supplementary Figures 3A,B,D**). Since CBC data is based on cell size and granularity rather than specific cell markers, we next investigated the impact of LTC-HIV infection on circulating immune population via flow cytometry.

Total T and B cell numbers (CD3+ and CD19+, respectively) did not differ significantly between the two groups (**Figures 1A,B**). However, a significant reduction in the number of CD4+ helper T cells was detected in LTC-HIV+ individuals (**Figure 1C**). Conversely, the number of circulating CD8+ cytotoxic T cells was increased in the LTC-HIV+ group (**Figure 1D**). We next determined the effect of LTC-HIV infection on the relative frequencies of naïve, transitional effector memory (TEMRA), central memory (TCM), and effector memory (TEM) (**Supplementary Figure 1**). This analysis showed that the frequency of CD4+TCM cells was significantly reduced, while the frequency of CD4+TEM cells was significantly increased (**Figure 1E**). No changes in frequency of naïve and memory CD8+ T cell subsets were detected (**Figure 1F**). Moreover, no changes in the frequency of naïve and memory B cell subsets were noted (**Supplementary Figures 3E–G**). In terms of homeostatic proliferation, we detected an increase in the TEM CD8+ cells subset but none of the other subsets (**Supplementary Figures 4A–D**). No differences in homeostatic proliferation of CD4+ subsets were detected (**Supplementary Figures 4E–H**). Interestingly, we found no differences in T cell activation measured via KLRG1 expression levels, or exhaustion measured via PD-1 expression levels, in either CD4+ (**Supplementary Figures 5A,B**) or CD8+ (**Supplementary Figures 5C,D**) T cell subsets.

We next characterized the frequency of circulating innate immune cells. No significant differences were seen in the abundance of total dendritic cells (DC) or in the relative frequencies of myeloid DC (mDC) and plasmacytoid DC (pDC) with LTC-HIV infection (**Figures 2A–C**). In contrast, the number of circulating monocytes was reduced in LTC-HIV+ individuals (**Figure 2D**), with no differences observed within monocyte subsets (**Figures 2E,F**). Lastly, no differences were detected in natural killer (NK) cell frequencies (**Figure 2G**). However, the relative abundances of activated CD57+ and cytotoxic CD16+GrzmB+ NK cells were higher in LTC-HIV+ group (**Figures 2H,I**).

Long-Term HIV Infection Leads to a Heightened Pro-Inflammatory Response at Baseline and After Stimulation

To explore the impact of LTC-HIV on systemic inflammatory markers, we measured plasma levels of cytokines, chemokines, and growth factors using Luminex technology. This analysis revealed significantly higher levels of the pro-inflammatory cytokine INFγ as well as growth factors BDNF, SCF, and VEGF (**Figure 3A**). On the other hand, levels of anti-inflammatory cytokines IL-1RA, T cell cytokine IL-2, eosinophil maturation factor IL-5, inhibitory cytokine LIF, growth factor SDF1a, as well as chemo-attractants MCP-1, MIP-1b, and IL-8 were reduced in LTC-HIV+ individuals (**Figure 3A**).

To further explore the effect of LTC-HIV infection on immune mediator production, we stimulated a subset of PBMC samples (HIV- $n = 9$, LTC-HIV $n = 11$) with PMA/ionomycin for 16 h and measured the production of cytokines, chemokines, and growth factors via Luminex technology. Samples from LTC-HIV patients generated a more pronounced and variable response to stimulation (**Figure 3B**). After correcting for baseline spontaneous production, 21 of 33 measured analytes were produced in higher amounts in response to stimulation by samples from the LTC-HIV+ group compared to the HIV- group. These included the pro-inflammatory cytokines IL-6, TNFα, INFγ as well as anti-inflammatory cytokine IL-10 (**Figure 3C**).

We next interrogated whether the increased response of LTC-HIV PBMCs to PMA/ionomycin was mirrored by an increased transcriptional response using RNA sequencing (RNA-Seq). Principal component analysis (PCA) shows that the samples clustered based on group and treatment (**Figure 4A**). At baseline,

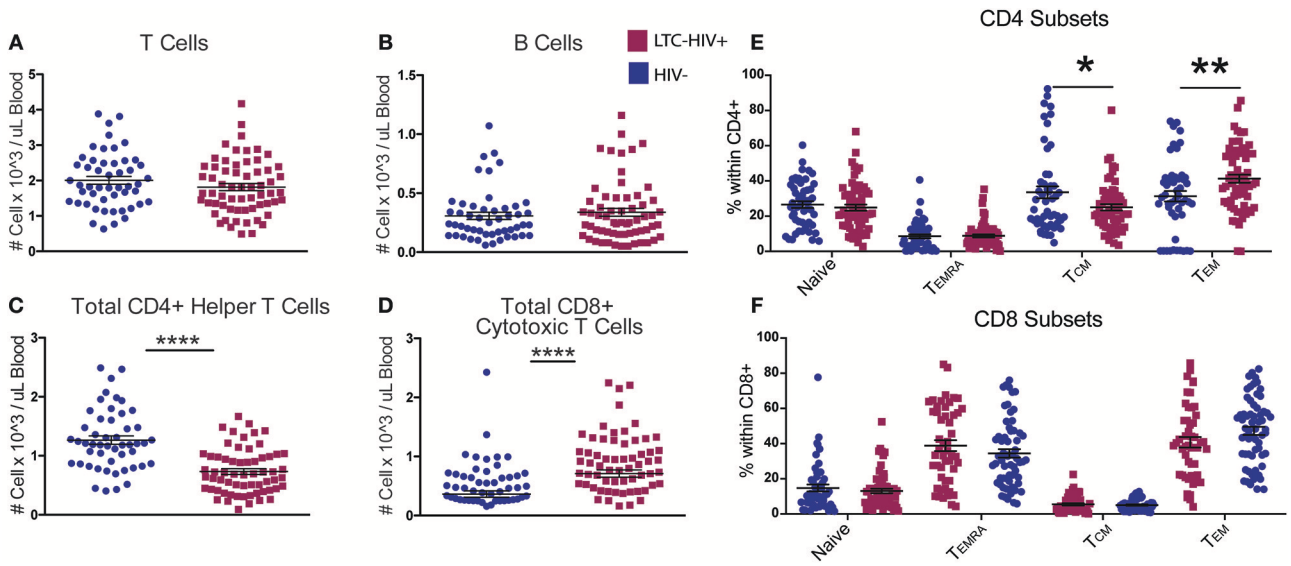

FIGURE 1 | LTC-HIV results in alterations in T but not B cell subsets. **(A)** Numbers of circulating CD3+ T cells **(B)** CD20+ B cells **(C)** CD3+CD4+ helper T cells, and **(D)** CD3+CD8+ cytotoxic T cells. **(E,F)** Relative frequencies of CD4+ **(E)** and CD8+ **(F)** T cell subsets **(E)**. Each point represents a study subject. Horizontal bars and whiskers indicate the mean ± SEM. Significance was determined using an unpaired *t*-test. $^{*}p < 0.05$, $^{**}p < 0.01$, $^{****}p < 0.0001$.

we identified only 11 protein coding differentially expressed genes (DEGs) all of which were down-regulated in LTC-HIV samples (*TNFRSF1B, IL7R, ARHGDIB, RPS27, PPBP, CTSL, HIST1H2BJ, TNKS2, TTC37, SEC24B,* and *EEF1A1).* Following PMA/ionomycin stimulation, a larger number of DEGs were detected in the HIV- group (334) compared to the LTC-HIV+ group (183), with 85 DEGs detected in both groups (**Figure 4A**). To better understand the biological significance of these changes, we carried out an initial functional enrichment using Metascape (53). DEGs detected in the samples from the HIV- group enriched to gene ontology (GO) terms associated with host defense including "cell chemotaxis," "response to TNF," and "leukocyte degranulation" (**Figure 4B**). On the other hand, DEGs detected in the LTC-HIV+ group enriched to GO terms associated with metabolic processes (**Figure 4B**). DEGs detected in both groups enriched to GO terms associated with signaling (**Figure 4B**).

Additional functional enrichment using Metacore™ showed that the 85 common DEGs enriched to GO terms such as "response to LPS" and "response to molecule of bacterial origin" characteristic of a response to antigenic stimulation (**Table 2**). Several of 32 genes that were downregulated upon stimulation in both groups were important for cell adhesion, and proliferation such as: *IL-24, ZNF740, MAP3K3, THBS1,* and *THBS4* (**Figure 4C**). Some of the 53 genes that were upregulated in both groups include genes important for myeloid activation and interferon regulation such as: *CD300LB, TNFAIP8L1, MMP1, SLC35F5,* and *IRF4* (**Figure 4C**).

In line with the output of Metascape, functional enrichment using Metacore™ showed that DEGs that were only detected in PBMCs from HIV- individuals enriched to GO terms such as "inflammatory response," and "response to cytokines" (**Table 2**). Some of the notable DEGs that were only significantly up-regulated in PBMCs from HIV- individuals included: *CXCL9, TNFSF8, NFKBIE, CXCR3*, and *STAT4* (**Figure 4D**). Downregulated DEGs that enriched to the same GO terms included: *LYZ, CCL2*, and *CD14* (**Figure 4D**). Similar to the Metascape output, DEGs that were only detected in PBMC from the LTC-HIV+ group enriched to GO terms associated with signaling (**Table 2**). Genes that were uniquely up-regulated in PBMCs from LTC-HIV+ individuals included: *HIF1A, DHE3,* and solute carrier gene *SLC3A2* which are unique to CD8+ T cells as well as *CXCR5, IL17C*, and *TRPA1* (**Figure 4E**).

To elucidate the source of the DEGs detected, we used the Immunological Genome Project Consortium database (ImmGen), which delineates gene expression patterns across different leukocyte subsets (58). This analysis revealed that DEGs detected only in LTC-HIV+ samples are predicted to be expressed by DCs, monocytes, macrophages, and to a lesser extent T cells and B cells (**Supplementary Figure 6A**). DEGs detected only in the HIV- samples were mostly expressed by monocytes/macrophages and DCs (**Supplementary Figure 6B**), while common DEGs exhibited broad distribution (**Supplementary Figure 6C**). To gain a better understanding of alterations in immune cells frequencies following stimulation, we employed Immquant, which uses the digital cell quantification algorithm (59) to predict changes in immune cell subsets based on total transcriptional profiles using the IRIS database (60). This analysis predicted that the transcriptional changes observed were associated with a significant increase of stimulated Th1 CD4+ T cells in both LTC-HIV+ and HIV- individuals upon PMA stimulation (**Supplementary Figure 6D**). Additionally, transcriptional changes in LTC-HIV+ individuals were associated with an

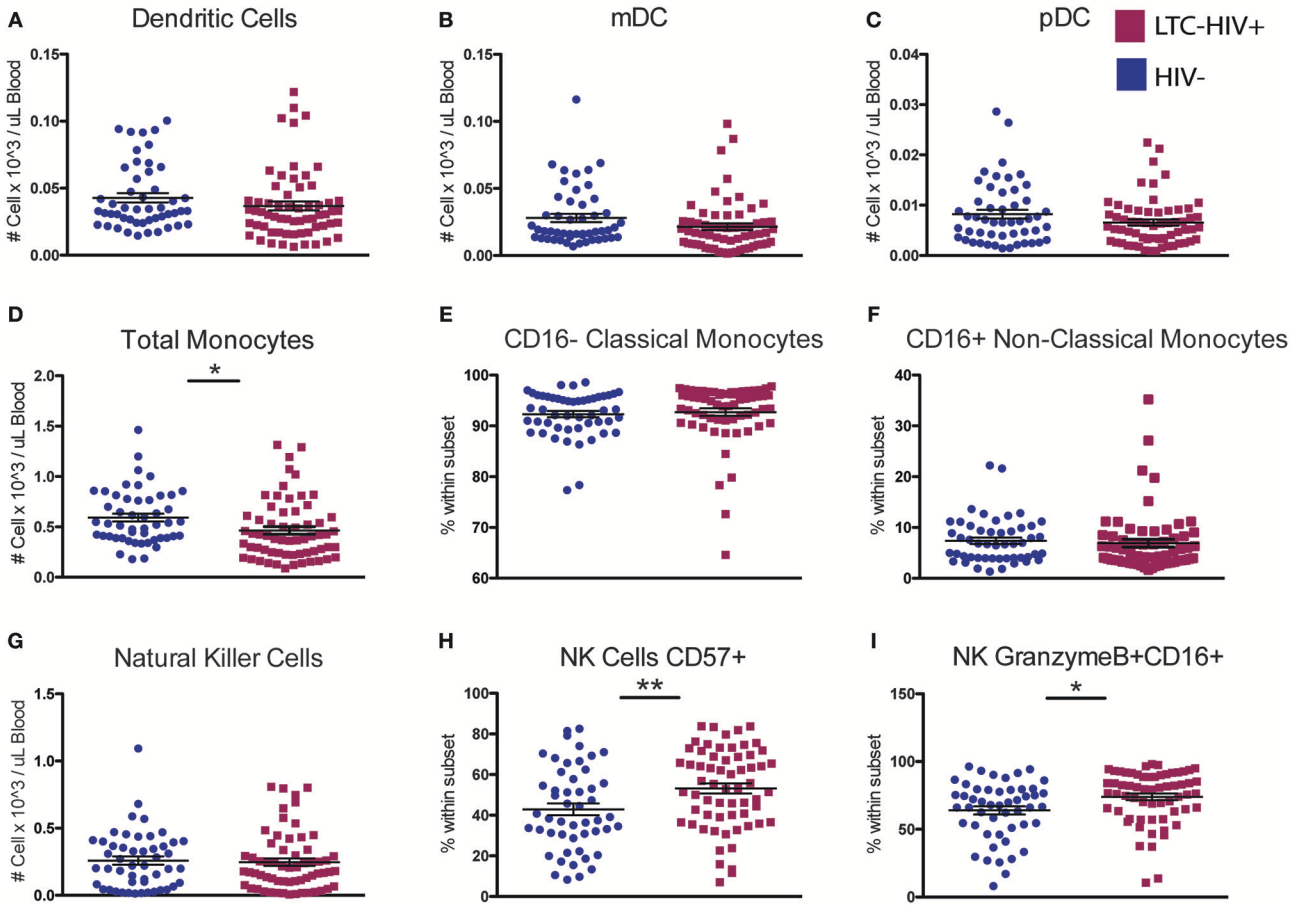

FIGURE 2 | A reduction in circulating monocytes and increase in NK cell activation seen with LTC-HIV infection. **(A)** Number of total circulating dendritic cells (DC) **(B)** myeloid DCs, and **(C)** plasmacytoid (DC). **(D)** Number of total circulating CD14+ monocytes and **(E)** relative abundance of CD16- Classical monocytes, and **(F)** CD16+ non-classical monocytes. **(G)** Number of total circulating CD56+ natural killer (NK) cells and **(H)** relative frequency of CD57+ NK cells and **(I)** granzymeB+CD16+ cytotoxic NK cells. Horizontal bar and whisker indicate the mean ± SEM. Significance was determined using an unpaired *t*-test. $^{*}p < 0.05$, $^{**}p < 0.01$.

increase in stimulated Th2 CD4+ T cells and LPS stimulated DCs upon PMA stimulation (**Supplementary Figure 6D**).

Long-Term HIV Infection Leads to Dysbiosis

Several studies have suggested that HIV infection results in increased gut permeability and translocation of microbial products into circulation (46, 47, 61, 62). To determine if those changes were evident in an older population with LTC-HIV infection, we evaluated several markers of barrier function. Analysis of circulating levels of sCD14, fatty acid binding protein (iFABP), IgM-bound endotoxin and Limulus amebocyte lysate (LAL) did not reveal significant differences between the two group (**Supplementary Figures 7A–D**).

Next, we investigated whether LTC-HIV infection is associated with alterations in the gut microbiome using 16S amplicon sequencing. The overall taxonomic landscape of the gut microbiome was not significantly different as measured by alpha- and beta-diversity (**Figure 5A**, **Supplementary Figures 7E–G**). Specifically, principal coordinate analysis (PCoA) of unweighted UniFrac distance showed significant overlap in the overall gut microbiome communities of HIV- and LTC-HIV+ individuals (**Supplementary Figure 7E**). Both groups also had similar numbers of observed species and Pielou evenness (**Supplementary Figures 7F,G**).

At the phyla level, microbiomes from both groups were dominated by Firmicutes and Bacteroidetes with smaller contributions from Actinobacteria and Proteobacteria (**Figure 5A**). Fusobacteria was the fourth most abundant phyla across all samples and significantly enriched in LTC-HIV+ individuals (**Figure 5B**). Clostridiales and Bacteroidales were the most abundant bacterial orders and *Prevotella* was the most abundant genus across both groups (**Figure 5A**). Ten genera were differentially abundant between LTC-HIV+ and HIV- individuals. The gut microbiomes of LTC-HIV+ individuals were enriched in; *Garnerella*, *Snethia*, *Fusobacterium*, *Lactobacillus*, and *Helicobater* (**Figure 5B**). While the gut microbiomes of HIV- individuals had a significantly higher relative abundance of; *Oxalobacter*, *Streptococcus*, *Enhydrobacter*, *Eggerthella*, and *Clostridiaceae* 02d06 (**Figure 5B**).

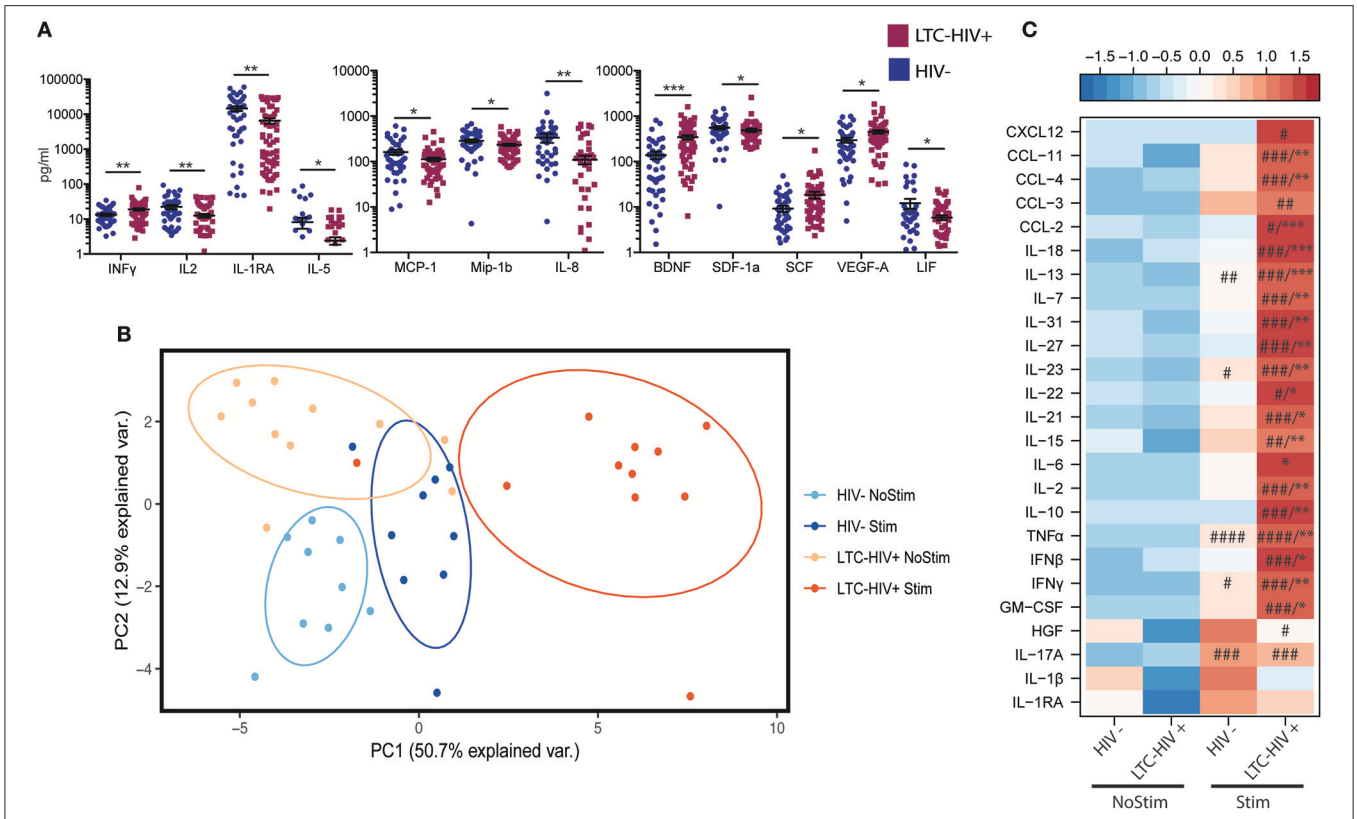

FIGURE 3 | Change in circulating and production of immune mediators following stimulation. **(A)** Serum level of immune mediators measured using a multiplexed ELISA assay. Horizontal bar and whiskers indicate the mean ± SEM. Significance was determined using an unpaired *t*-test. $^{*}p < 0.05$, $^{**}p < 0.01$, $^{***}p < 0.001$ **(B)** Principal component analysis of immune mediators released by PBMC's from HIV- and LTC-HIV+ individuals in the absence and presence of PMA/ionomycin. **(C)** Heat map of differentially abundant immune mediators produced by PBMCs upon stimulation (all immune mediators statistically significant via 1-way ANOVA, Significant Tukeys *post-hoc* comparison of stimulated samples vs. corresponding baseline samples) #$p < 0.05$, ##$p < 0.01$, ###$p < 0.001$, ####$p < 0.0001$. Unpaired *T*-tests of absolute change followed by Welch's correction [Stimulation—baseline] in immune mediator production $^{*}p < 0.05$, $^{**}p < 0.01$, $^{***}p < 0.001$.

To further explore the relationship between the microbial communities of the gut microbiome and LTC-HIV, we stratified our LTC-HIV+ individuals into quartiles based on the CD4+ T cell numbers and compared the microbial communities of individuals in the highest and lowest quartile. This analysis revealed seven differentially abundant genera between the highest and lowest CD4+ T cell quartiles (**Figure 5C**). Of note, *Prevotella* was significantly more abundant in individuals with a low CD4+ individuals (**Figure 5C**) and negatively correlated with CD4+ T cell count across all LTC-HIV+ individuals (**Figure 5D**), a pattern not seen in HIV- individuals (**Figure 5E**).

DISCUSSION

The advent and rapid adoption of HAART treatment in the U.S. has turned HIV infection into a chronic disease. Indeed, the average life expectancy of individuals diagnosed with HIV at age 20 has risen from 32 in the late 1980's to 71 in 2018 (63). Consequently, the majority of HIV+ individuals in the U.S. are expected to be older than 50 years of age by 2020 (64). However, HAART treatment is associated with significant adverse outcomes, and individuals who have received long-term HAART are experiencing a higher incidence of several morbidities compared to age-matched HIV- individuals (17). These HANA co-morbidities include cardiovascular disease, neurocognitive disorders, osteoporosis, cancer, liver cirrhosis, kidney, and lung disease (10–16). The mechanisms underlying this increased susceptibility are poorly understood due to the lack of carefully controlled studies on older HIV+ individuals who have been on HAART for >5 years. In this study, we addressed this question using samples collected from a large cohort of LTC-HIV+ gay men who have received HAART treatment for at least 10 years. Importantly, the control population was matched with the LTC-HIV+ cohort for age, sexual preference, location, and socioeconomic status. This experimental set up allowed us to determine the effects of LTC-HIV infection on immunological and microbial shifts that can be subsequently targeted for intervention to reduce HANA co-morbidities.

HAART treatment within the first 3 years results in a rebound in CD4 T cell count that is strongly linked to the CD4 count at the time of treatment initiation (42–44, 57). However, our data showed a significant reduction in total circulating CD4+ T cells. Thirty-six of the fifty-seven participants in this study were initially infected with HIV in the 1980's well before the introduction of HAART. Consequently, 28 of these individuals did not have access to therapy for ∼10 years prior to starting

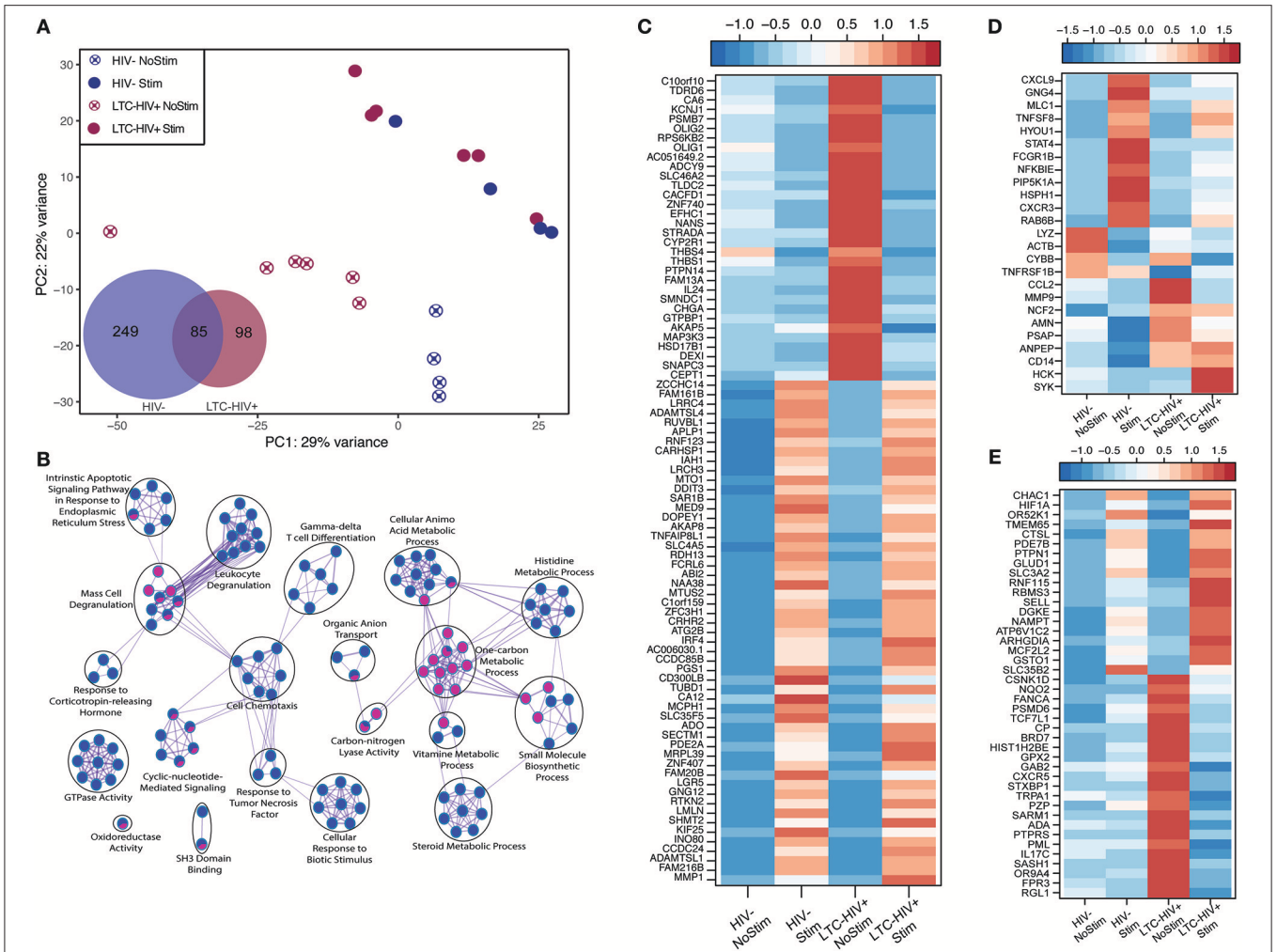

FIGURE 4 | LTC-HIV infection alters PBMC transcriptional response to PMA/Ionomycin. **(A)** Principal component analysis of unstimulated and PMA/ionomycin stimulated PBMCs from HIV- and LTC-HIV and Venn diagram of stimulation DEGs showing unique and common protein coding genes. **(B)** Network visualization using Cytoscape of functional enrichment output of DEGs detected in PBMC from LTC-HIV+ and HIV- subjects following PMA stimulation obtained using Metascape. The size of node represents the number of DEGs associated with each gene ontology (GO) term and the pie chart filling represents relative proportion of each group's DEGs that enriched to that GO term. Heat maps of select DEGs for Common **(C)**, HIV- **(D)**, and LTC-HIV+ **(E)**.

this treatment and likely began with very low CD4+ counts. Unfortunately we did not have access to the nadir CD4+ counts for our study population, which were shown to be predictive of CD4+ levels during HAART treatment (42, 65, 66). Levels of IL-2, a cytokine critical for T cell survival were also reduced and could partially explain the reduced CD4+ T cell numbers we observed in LTC-HIV+ individuals (67). Both aging and long-term HIV infection have been associated with an accumulation of terminally differentiated T cells (68, 69). In line with these earlier studies, we found a greater shift toward terminally differentially CD4+ T cells in this group indicative of accelerated differentiation of memory T cells.

CD8+ T cells play an important role in the control of HIV infection and their numbers become elevated rapidly upon HIV infection and persist after initiation of HAART (70, 71). Although the numbers of CD8+ T cells were significantly higher in LTC-HIV+ individuals, no differences were observed in the relative abundance of naïve and memory subsets. We did however detect a significant increase in homeostatic proliferation within the CD8+ T cell EM subset, suggestive of accelerated conversion to memory T cells. Additionally, a large percentage of circulating NK cells showed higher activation with LTC-HIV infection. Collectively, this increased differentiation/proliferation of circulating lymphocytes could contribute to heightened systemic inflammation in LTC-HIV infection. Analysis of circulating immune mediators showed increased serum levels of the antiviral cytokine INFγ. This is in line with previous studies that reported increased levels of INFγ, but not IL-6 and TNFα in HAART treated HIV patients (49). The source of INFγ could be the activated NK cells, CD8+ T cells, or TEM CD4+ T cells, but testing this hypothesis will require additional studies such as single cell RNA sequencing.

The effect of LTC-HIV infection on the innate arm of the immune system is not well-understood. Acute HIV

infection is associated with a dramatic increase in inflammatory (non-classical CD16+) monocytes (28). This population has been shown to remain elevated throughout the first year of HAART treatment (72). In contrast, we observed a reduction in total circulating monocytes, and no differences in the relative proportions of CD16+ and CD16- monocytes. Monocytes are susceptible to HIV infection and can serve as a reservoir for latent HIV (48). The reduction in circulating monocyte numbers could potentially be due to low levels of viral reactivation (73), or alternatively mediated by lower levels circulating chemokines MCP-1, MIP-1b, and IL-8. Further analysis of the functional capacity (e.g., phagocytosis and wound healing) of monocytes is needed to assess their contribution to the development of HANA co-morbidities.

We also observed a substantial increase in circulating BDNF, and VEGF-A in the serum of LTC-HIV. Both of these factors have been previously linked to HIV associated neurological disorders including depression (74, 75). HIV protein gp120 has been shown to both increase the production and negatively alter neuronal processing of BDNF (76, 77). It is possible that the buildup of circulating BDNF is a compensatory mechanism due to decreased bioavailability of BDNF in the brain. The continuation of this process despite low viral load seen in LTC-HIV could explain the higher incidence of depression and neuropathy that we and others have observed (78–80). We also detected a reduction in the anti-inflammatory cytokine IL-1RA, which could indicate a higher level of systemic inflammation. These changes are consistent with, but are not as pronounced as what has been reported in HIV+ patients on HAART for a shorter duration

TABLE 2 | Functional enrichment of DEGs detected in response to PMA stimulation.

	No of genes	FDR *p*-value
COMMON DEGs		
Regulation of purine nucleotide metabolic process	12	1.517E-05
Response to lipopolysaccharide	10	1.565E-02
Response to molecule of bacterial origin	10	1.888E-02
Regulation of phosphorus metabolic process	21	2.026E-02
DEGs DETECTED IN LTC-HIV SAMPLES ONLY		
Regulation of signaling	46	1.711E-03
Neutrophil homeostasis	23	2.506E-03
Regulation of communication	44	2.506E-03
Regulation of blood circulation	11	2.574E-03
DEGs DETECTED IN HIV- SAMPLES ONLY		
Intracellular signal transduction	63	1.190E-06
Cell chemotaxis	19	1.335E-06
Response to cytokine	52	1.740E-06
Inflammatory response	32	2.492E-06

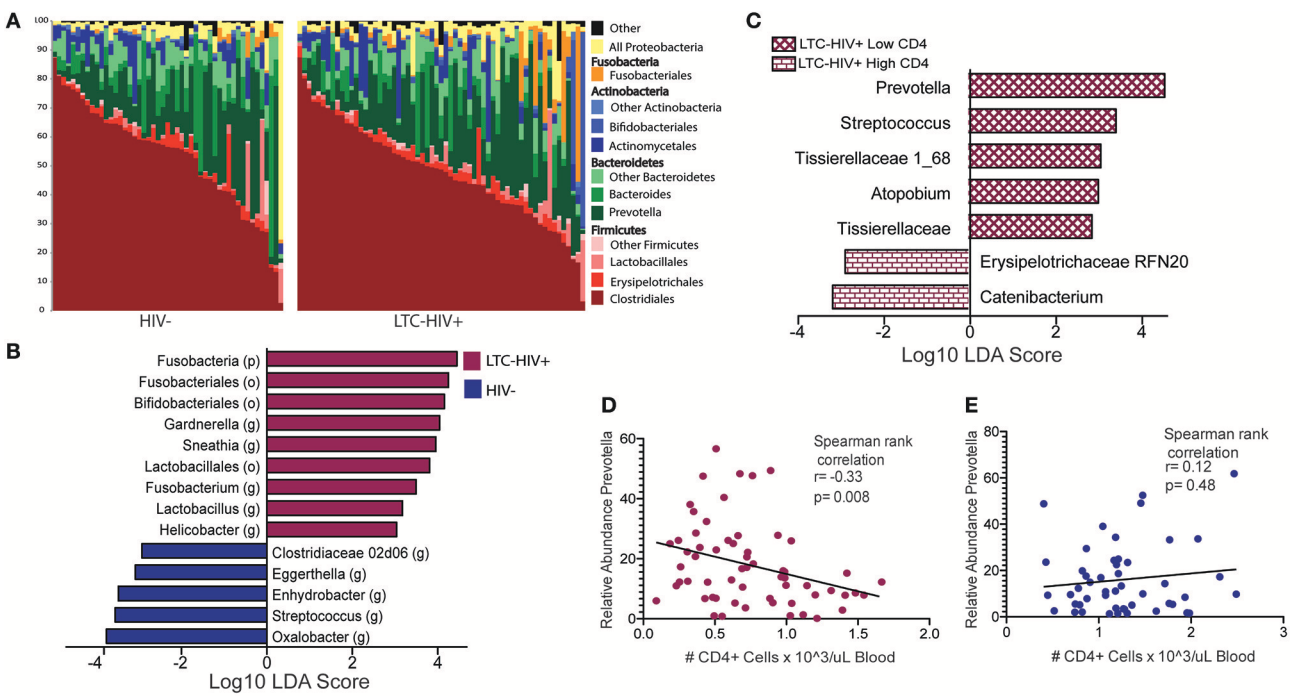

FIGURE 5 | Taxonomic differences in the gut microbiome of LTC-HIV **(A)** Stack bar plot illustrating the abundance of bacterial orders and phyla in HIV- and LTC-HIV+ individuals. **(B)** Differentially abundant bacterial taxa between LTC-HIV+/HIV- determined using LEfSE (Log_{10} LDA score >2) at the Phyla, Order and Genus level. **(C)** Differentially abundant genera between LTC-HIV+ High CD4+ and LTC-HIV+ Low CD4+ individuals (Log_{10} LDA score > 2). **(D)** Spearman rank correlation between CD4+ T cell abundance and relative abundance of *Prevotella* in LTC-HIV+ individuals. **(E)** Spearman rank correlation between CD4+ T cell abundance and relative abundance of *Prevotella* in HIV- individuals.

(81) or during acute infection prior to the initiation of HAART treatment (82).

Upon polyclonal activation of PBMC we observed a significantly heightened inflammatory response by PBMCs from LTC-HIV individuals. While our study design does not allow us to decisively identify the source of these immune mediators, these data clearly indicate functional abnormalities in circulating immune populations. HIV infection has been shown to alter the epigenetic landscape of both T-cells and monocytes during acute and HAART controlled infections (83–85). Future studies should investigate the link between these epigenetic changes and aberrant inflammatory and anti-microbial responses. Interestingly, our transcriptional analysis showed a smaller number of DEGs in PBMC from LTC-HIV+ subjects despite a greater production of immune mediators. Moreover, while DEGs detected in PBMC from HIV- subjects enriched to GO terms associated with leukocyte activation, those detected in LTC-HIV+ samples enriched to GO terms associated with signaling. One possible explanation is that the response to stimulation peaked earlier in the LTC-HIV+ samples. While the luminex data captures accumulation of immune mediators, RNA-Seq only provides a snap shot of the specific time point selected. Future studies can address this question through a kinetic analysis.

Dysbiosis in the gut microbiome during HIV infection has been implicated as a source of aberrant immune activation and inflammation in acute infection and chronic HIV (32, 33, 86). The host immune system tightly regulates the large reservoir of microbes in the human gut; and loss of key immune cells due to HIV infection (87) can result in changes in composition of microbial communities and their compartmentalization. However, data on HIV-associated shifts in the gut microbiome have been inconsistent likely due to the lack of studies that appropriately controlled for race/ethnicity, diet, sanitary conditions, sexual habits, and socioeconomic status. In contrast, our samples were collected from a cohort of gay, mostly Caucasian, men living in a single geographic location of similar age and socioeconomic status. Analysis of the gut microbial community revealed largely comparable communities with only 10 differentially abundant genera. Fusobacteria, Lactobacillus, and multiple Bifidobacteriales genera were all enriched in LTC-HIV+ individuals. Since these genera primarily colonize the mouth, their presence in the gut microbial communities could signal de-compartmentalization has previously been shown to result in local immune activation (88). Additionally, identical strains of *Fusobacterium* have been found in the oral cavities, and tumors of patients with colorectal cancers (89).

Previous studies reported an increased abundance of the bacterial genus *Prevotella* in LTC-HIV+ individuals; however, many of these studies did not control for sexual orientation, and geographic location, which can influence abundance of *Prevotella* (90, 91). Although we did not find a difference in the abundance of *Prevotella* based on HIV status, we observed a negative correlation between CD4+ T cell counts and *Prevotella* abundance. *Prevotella* has previously been linked to high circulating levels of trimethylamine-N-oxide (TMAO) a compound strongly associated with cardiovascular disease (92). Future metabolomics, and transcriptomic studies will be needed to determine if this higher abundance of *Prevotella* leads to more inflammatory microbial products and if this activity varies in LTC-HIV vs. age matched controls. Abundance of other bacterial genera such as *Streptococcus* and *Atopbium* was also negatively correlated with CD4+ T cell counts and are both commonly found in the oral cavity (93). On the other hand, abundance of the short chain fatty acid (SCFA)-producing Clostridia *Catenibacterium* was higher in LTC-HIV+ individuals in the highest CD4+ T cell quartile. SCFAs produced by gut microbes play an important role in maintaining gut homeostasis and local immune function (94–96). While the abundances of these taxa were too sparse to obtain meaningful correlations with CD4+ T cell counts, this could indicate a greater capacity for beneficial SCFA production in LTC-HIV+ patients with a higher CD4+ count.

In summary, this study provides novel insight into the impact of LTC-HIV infection on systemic immunity and microbial gut communities in older patient populations ($\geq$55 years). A little over half of the subjects in our study were initially infected prior to the advent of HAART. This delay may have interfered with the restorative effect of HAART as shown by a lower abundance of CD4+ T cells and monocytes when compared to age-matched HIV- individuals; immune dysregulation, as evidenced by differences in circulating immune mediators and a more pronounced response to stimulation in LTC-HIV; and taxonomic shifts in the gut microbiome indicative of loss of compartmentalization. Taken together these data provide a more complete picture of the immune and microbial landscape of LTC-HIV infection in an aging population, thereby providing potential avenues for intervention and prevention of HANA co-morbidities.

DATA AVAILABILITY

The datasets generated for this study can be found in SRA, PRJNA518909, PRJNA518910.

AUTHOR CONTRIBUTIONS

IM, JT, TM, StS, RH, and BB contributed conception and design of the study. NM, AJ, SuS, AA, BD, and NR generated and analyzed data. OH and NR performed the statistical analysis. NR and IM wrote the first draft of the manuscript. All authors contributed to manuscript revision, read, and approved the submitted version.

FUNDING

University of California Riverside collaborative seed grant. NR was supported by National Institutes of Health (GM055246).

SUPPLEMENTARY MATERIAL

The Supplementary Material for this article can be found online at: https://www.frontiersin.org/articles/10.3389/fimmu.2019.00463/full#supplementary-material

REFERENCES

1. Siddiqi AE, Hall HI, Hu X, Song R. Population-based estimates of life expectancy after HIV diagnosis: United States 2008-2011. *J Acquir Immune Defic Syndr*. (2016) 72:230–6. doi: 10.1097/QAI.0000000000000960
2. Harrison KM, Song R, Zhang X. Life expectancy after HIV diagnosis based on national HIV surveillance data from 25 states, United States. *J Acquir Immune Defic Syndr*. (2010) 53:124–30. doi: 10.1097/QAI.0b013e3181b563e7
3. Center for Disease Control and Prevention. Estimated HIV Incidence and Prevalence in the United States, 2010–2015. (2018). Available online at: http://www.cdc.gov/hiv/library/reports/hiv-surveillance.html
4. Le T, Farrar J, Shikuma C. Rebound of plasma viremia following cessation of antiretroviral therapy despite profoundly low levels of HIV reservoir: implications for eradication. *AIDS*. (2011) 25:871–2; author reply 872–3. doi: 10.1097/QAD.0b013e32834490b1
5. Maldarelli F, Palmer S, King MS, Wiegand A, Polis MA, Mican J, et al. ART suppresses plasma HIV-1 RNA to a stable set point predicted by pretherapy viremia. *PLoS Pathog*. (2007) 3:e46. doi: 10.1371/journal.ppat.0030046
6. Martinez-Picado J, Deeks SG. Persistent HIV-1 replication during antiretroviral therapy. *Curr Opin HIV AIDS*. (2016) 11:417–23. doi: 10.1097/COH.0000000000000287
7. de Coninck Z, Hussain-Alkhateeb L, Bratt G, Ekström AM, Gisslén M, Petzold M, et al. Non-AIDS mortality is higher among successfully treated people living with HIV compared with matched HIV-negative control persons: a 15-year follow-up cohort study in Sweden. *AIDS Patient Care STDS*. (2018) 32:297–305. doi: 10.1089/apc.2018.0015
8. Engsig FN, Zangerle R, Katsarou O, Dabis F, Reiss P, Gill J, et al. Long-term mortality in HIV-positive individuals virally suppressed for >3 years with incomplete CD4 recovery. *Clin Infect Dis*. (2014) 58:1312–21. doi: 10.1093/cid/ciu038
9. Marin B, Thiébaut R, Bucher HC, Rondeau V, Costagliola D, Dorrucci M, et al. Non-AIDS-defining deaths and immunodeficiency in the era of combination antiretroviral therapy. *AIDS*. (2009) 23:1743–53. doi: 10.1097/QAD.0b013e32832e9b78
10. Knobel H, Domingo P, Suarez-Lozano I, Gutierrez F, Estrada V, Palacios R, et al. Rate of cardiovascular, renal and bone disease and their major risks factors in HIV-infected individuals on antiretroviral therapy in Spain. (2018) *Enferm Infecc Microbiol Clin*. doi: 10.1016/j.eimc.2018.09.015
11. Rogalska-Płonska M, Rogalski P, Leszczyszyn-Pynka M, Stempkowska J, Kocbach P, Kowalczuk-Kot A, et al. Hypertension, dyslipidaemia, and cardiovascular risk in HIV-infected adults in Poland. *Kardiol Pol*. (2017) 75:1324–31. doi: 10.5603/KP.a2017.0148
12. Friis-Møller N, Weber R, Reiss P, Thiébaut R, Kirk O, d'Arminio Monforte A, et al. Cardiovascular disease risk factors in HIV patients–association with antiretroviral therapy. Results from the DAD study. *AIDS*. (2003) 17:1179–93. doi: 10.1097/00002030-200305230-00010
13. Clifford GM, Polesel J, Rickenbach M, Dal Maso L, Keiser O, Kofler A, et al. Cancer risk in the Swiss HIV Cohort Study: associations with immunodeficiency, smoking, and highly active antiretroviral therapy. *J Natl Cancer Inst*. (2005) 97:425–32. doi: 10.1093/jnci/dji072
14. Cohen RA, Gullett JM, Porges EC, Woods AJ, Lamb DG, Bryant VE, et al. Age effects on HIV-associated neurocognitive function. (2018) *Alcohol Clin Exp Res*. 32:519–28. doi: 10.1111/acer.13915
15. Chan P, Brew BJ. HIV associated neurocognitive disorders in the modern antiviral treatment era: prevalence, characteristics, biomarkers, and effects of treatment. *Curr HIV/AIDS Rep*. (2014) 11:317–24. doi: 10.1007/s11904-014-0221-0
16. Thio CL, Seaberg EC, Skolasky R, Phair J, Visscher B, Muñoz A, et al. HIV-1, hepatitis B virus, and risk of liver-related mortality in the Multicenter Cohort Study (MACS). *Lancet*. (2002) 360:1921–6. doi: 10.1016/S0140-6736(02)11913-1
17. Guaraldi G, Orlando G, Zona S, Menozzi M, Carli F, Garlassi E, et al. Premature age-related comorbidities among HIV-infected persons compared with the general population. *Clin Infect Dis*. (2011) 53:1120–6. doi: 10.1093/cid/cir627
18. Sterling RK, Lissen E, Clumeck N, Sola R, Correa MC, Montaner J, et al. Development of a simple noninvasive index to predict significant fibrosis in patients with HIV/HCV coinfection. *Hepatology*. (2006) 43:1317–25. doi: 10.1002/hep.21178
19. Matthews GV, Dore GJ. HIV and hepatitis C coinfection. *J Gastroenterol Hepatol*. (2008) 23:1000–8. doi: 10.1111/j.1440-1746.2008.05489.x
20. Parsons TD, Tucker KA, Hall CD, Robertson WT, Eron JJ, Fried MW, et al. Neurocognitive functioning and HAART in HIV and hepatitis C virus co-infection. *AIDS*. (2006) 20:1591–5. doi: 10.1097/01.aids.0000238404.16121.47
21. Ganta KK, Mandal A, Chaubey B. Depolarization of mitochondrial membrane potential is the initial event in non-nucleoside reverse transcriptase inhibitor efavirenz induced cytotoxicity. *Cell Biol Toxicol*. (2017) 33:69–82. doi: 10.1007/s10565-016-9362-9
22. Nomura R, Sato T, Sato Y, Medin JA, Kushimoto S, Yanagisawa T. Azidothymidine-triphosphate impairs mitochondrial dynamics by disrupting the quality control system. *Redox Biol*. (2017) 13:407–17. doi: 10.1016/j.redox.2017.06.011
23. Foli Y, Ghebremichael M, Li M, Paintsil E. Upregulation of apoptosis pathway genes in peripheral blood mononuclear cells of HIV-infected individuals with antiretroviral therapy-associated mitochondrial toxicity. *Antimicrob Agents Chemother*. (2017) 61:e00522-17. doi: 10.1128/AAC.00522-17
24. Heron SE, Elahi S. HIV Infection and compromised mucosal immunity: oral manifestations and systemic inflammation. *Front Immunol*. (2017) 8:241. doi: 10.3389/fimmu.2017.00241
25. Erlandson KM, Ng DK, Jacobson LP, Margolick JB, Dobs AS, Palella FJ Jr, et al. Inflammation, immune activation, immunosenescence, and hormonal biomarkers in the frailty-related phenotype of men with or at risk for HIV infection. *J Infect Dis*. (2017) 215:228–37. doi: 10.1093/infdis/jiw523
26. Fukui SM, Piggott DA, Erlandson KM. Inflammation strikes again: frailty and HIV. *Curr HIV/AIDS Rep*. (2018) 15:20–9. doi: 10.1007/s11904-018-0372-5
27. Montoya JL, Campbell LM, Paolillo EW, Ellis RJ, Letendre SL, Jeste DV, et al. Inflammation relates to poorer complex motor performance among adults living with HIV on suppressive antiretroviral therapy. *J Acquir Immune Defic Syndr*. (2018) 80:15–23. doi: 10.1097/QAI.0000000000001881
28. Han J, Wang B, Han N, Zhao Y, Song C, Feng X, et al. CD14(high)CD16(+) rather than CD14(low)CD16(+) monocytes correlate with disease progression in chronic HIV-infected patients. *J Acquir Immune Defic Syndr*. (2009) 52:553–9. doi: 10.1097/QAI.0b013e3181c1d4fe
29. Sereti I, Krebs SJ, Phanuphak N, Fletcher JL, Slike B, Pinyakorn S, et al. Persistent, albeit reduced, chronic inflammation in persons starting antiretroviral therapy in acute HIV infection. *Clin Infect Dis*. (2017) 64:124–31. doi: 10.1093/cid/ciw683
30. Lichtfuss GF, Cheng WJ, Farsakoglu Y, Paukovics G, Rajasuriar R, Velayudham P, et al. Virologically suppressed HIV patients show activation of NK cells and persistent innate immune activation. *J Immunol*. (2012) 189:1491–9. doi: 10.4049/jimmunol.1200458
31. Rajasuriar R, Wright E, Lewin SR. Impact of antiretroviral therapy (ART) timing on chronic immune activation/inflammation and end-organ damage. *Curr Opin HIV AIDS*. (2015) 10:35–42. doi: 10.1097/COH.0000000000000118
32. Gootenberg DB, Paer JM, Luevano JM, Kwon DS. HIV-associated changes in the enteric microbial community: potential role in loss of homeostasis and development of systemic inflammation. *Curr Opin Infect Dis*. (2017) 30:31–43. doi: 10.1097/QCO.0000000000000341
33. Monaco CL, Gootenberg DB, Zhao G, Handley SA, Ghebremichael MS, Lim ES, et al. Altered virome and bacterial microbiome in human immunodeficiency virus-associated acquired immunodeficiency syndrome. *Cell Host Microbe*. (2016) 19:311–322. doi: 10.1016/j.chom.2016.02.011
34. Prendergast A, Prado JG, Kang YH, Chen F, Riddell LA, Luzzi G, et al. HIV-1 infection is characterized by profound depletion of CD161+ Th17 cells and gradual decline in regulatory T cells. *AIDS*. (2010) 24:491–502. doi: 10.1097/QAD.0b013e3283344895
35. Mudd JC, Brenchley JM. Gut mucosal barrier dysfunction, microbial dysbiosis, and their role in HIV-1 disease progression. *J Infect Dis*. (2016) 214 (Suppl. 2):S58–66. doi: 10.1093/infdis/jiw258
36. Sandler NG, Wand H, Roque A, Law M, Nason MC, Nixon DE, et al. Plasma levels of soluble CD14 independently predict mortality in HIV infection. *J Infect Dis*. (2011) 203:780–90. doi: 10.1093/infdis/jiq118
37. Hunt PW, Sinclair E, Rodriguez B, Shive C, Clagett B, Funderburg N, et al. Gut epithelial barrier dysfunction and innate immune activation

predict mortality in treated HIV infection. *J Infect Dis.* (2014) 210:1228–38. doi: 10.1093/infdis/jiu238
38. Dubourg G, Lagier JC, Hüe S, Surenaud M, Bachar D, Robert C, et al. Gut microbiota associated with HIV infection is significantly enriched in bacteria tolerant to oxygen. *BMJ Open Gastroenterol.* (2016) 3:e000080. doi: 10.1136/bmjgast-2016-000080
39. Missailidis C, Neogi U, Stenvinkel P, Trøseid M, Nowak P, Bergman P. The microbial metabolite trimethylamine-N-oxide in association with inflammation and microbial dysregulation in three HIV cohorts at various disease stages. *AIDS.* (2018) 32:1589–98. doi: 10.1097/QAD.0000000000001813
40. Keegan MR, Chittiprol S, Letendre SL, Winston A, Fuchs D, Boasso A, et al. Tryptophan metabolism and its relationship with depression and cognitive impairment among HIV-infected individuals. *Int J Tryptophan Res.* (2016) 9:79–88. doi: 10.4137/IJTR.S36464
41. Das B, Dobrowolski C, Shahir AM, Feng Z, Yu X, Sha J, et al. Short chain fatty acids potently induce latent HIV-1 in T-cells by activating P-TEFb and multiple histone modifications. *Virology.* (2015) 474:65–81. doi: 10.1016/j.virol.2014.10.033
42. Clouse K, Pettifor A, Maskew M, Bassett J, Van Rie A, Gay C, et al. Initiating antiretroviral therapy when presenting with higher CD4 cell counts results in reduced loss to follow-up in a resource-limited setting. *AIDS.* (2013) 27:645–50. doi: 10.1097/QAD.0b013e32835c12f9
43. Collazos J, Knobel H, Casado JL, Grupo Español para el Estudio Multifactorial de la Adherencia. CD4 count and viral load time-courses in patients treated with highly active antiretroviral therapy and association with the CDC staging system. *HIV Med.* (2006) 7:504–13. doi: 10.1111/j.1468-1293.2006.00405.x
44. Chaisson RE, Keruly JC, Moore RD. Association of initial CD4 cell count and viral load with response to highly active antiretroviral therapy. *JAMA.* (2000) 284:3128–9. doi: 10.1001/jama.284.24.3123
45. Appay V, Sauce D. Immune activation and inflammation in HIV-1 infection: causes and consequences. *J Pathol.* (2008) 214:231–41. doi: 10.1002/path.2276
46. Ancuta P, Kamat A, Kunstman KJ, Kim EY, Autissier P, Wurcel A, et al. Microbial translocation is associated with increased monocyte activation and dementia in AIDS patients. *PLoS ONE.* (2008) 3:e2516. doi: 10.1371/journal.pone.0002516
47. Brenchley JM, Price DA, Schacker TW, Asher TE, Silvestri G, Rao S, et al. Microbial translocation is a cause of systemic immune activation in chronic HIV infection. *Nat Med.* (2006) 12:1365–71. doi: 10.1038/nm1511
48. Campbell JH, Hearps AC, Martin GE, Williams KC, Crowe SM. The importance of monocytes and macrophages in HIV pathogenesis, treatment, and cure. *AIDS.* (2014) 28:2175–87. doi: 10.1097/QAD.0000000000000408
49. Amirayan-Chevillard N, Tissot-Dupont H, Capo C, Brunet C, Dignat-George F, Obadia Y, et al. Impact of highly active anti-retroviral therapy (HAART) on cytokine production and monocyte subsets in HIV-infected patients. *Clin Exp Immunol.* (2000) 120:107–112. doi: 10.1046/j.1365-2249.2000.01201.x
50. Terunuma H, Deng X, Dewan Z, Fujimoto S, Yamamoto N. Potential role of NK cells in the induction of immune responses: implications for NK cell-based immunotherapy for cancers and viral infections. *Int Rev Immunol.* (2008) 27:93–110. doi: 10.1080/08830180801911743
51. Luo Z, Li Z, Martin L, Hu Z, Wu H, Wan Z, et al. Increased natural killer cell activation in HIV-infected immunologic non-responders correlates with CD4+ T cell recovery after antiretroviral therapy and viral suppression. *PLoS ONE.* (2017) 12:e0167640. doi: 10.1371/journal.pone.0167640
52. Trapnell C, Pachter L, Salzberg SL. TopHat: discovering splice junctions with RNA-Seq. *Bioinformatics.* (2009) 25:1105–11. doi: 10.1093/bioinformatics/btp120
53. Tripathi S, Pohl MO, Zhou Y, Rodriguez-Frandsen A, Wang G, Stein DA, et al. Meta- and orthogonal integration of influenza "OMICs" data defines a role for UBR4 in virus budding. *Cell Host Microbe.* (2015) 18:723–35. doi: 10.1016/j.chom.2015.11.002
54. Edgar RC. UPARSE: highly accurate OTU sequences from microbial amplicon reads. *Nat Methods.* (2013) 10:996–8. doi: 10.1038/nmeth.2604
55. Caporaso JG, Kuczynski J, Stombaugh J, Bittinger K, Bushman FD, Costello EK, et al. QIIME allows analysis of high-throughput community sequencing data. *Nat Methods.* (2010) 7:335–6. doi: 10.1038/nmeth.f.303
56. Wei X, Ghosh SK, Taylor ME, Johnson VA, Emini EA, Deutsch P, et al. Viral dynamics in human immunodeficiency virus type 1 infection. *Nature.* (1995) 373:117–22. doi: 10.1038/373117a0
57. Li TS, Tubiana R, Katlama C, Calvez V, Ait Mohand H, Autran B. Long-lasting recovery in CD4 T-cell function and viral-load reduction after highly active antiretroviral therapy in advanced HIV-1 disease. *Lancet.* (1998) 351:1682–6. doi: 10.1016/S0140-6736(97)10291-4
58. Heng TS, Painter MW, Immunological Genome Project Consortium. Immunological genome project, the immunological genome project: networks of gene expression in immune cells. *Nat Immunol.* (2008) 9:1091–4. doi: 10.1038/ni1008-1091
59. Frishberg A, Brodt A, Steuerman Y, Gat-Viks I. ImmQuant: a user-friendly tool for inferring immune cell-type composition from gene-expression data. *Bioinformatics.* (2016) 32:3842–3. doi: 10.1093/bioinformatics/btw535
60. Abbas AR, Baldwin D, Ma Y, Ouyang W, Gurney A, Martin F, et al. Immune response *in silico* (IRIS): immune-specific genes identified from a compendium of microarray expression data. *Genes Immun.* (2005) 6:319–31. doi: 10.1038/sj.gene.6364173
61. Dinh DM, Volpe GE, Duffalo C, Bhalchandra S, Tai AK, Kane AV, et al. Intestinal microbiota, microbial translocation, and systemic inflammation in chronic HIV infection. *J Infect Dis.* (2015) 211:19–27. doi: 10.1093/infdis/jiu409
62. Li SK, Leung RK, Guo HX, Wei JF, Wang JH, Kwong KT, et al. Detection and identification of plasma bacterial and viral elements in HIV/AIDS patients in comparison to healthy adults. *Clin Microbiol Infect.* (2012) 18:1126–33. doi: 10.1111/j.1469-0691.2011.03690.x
63. Center for Disease Control and Prevention. Today's HIV/AIDS Epidemic. (2018). Available online at: https://www.cdc.gov/nchhstp/newsroom/docs/factsheets/todaysepidemic-508.pdf
64. Center for Disease Control and Prevention. HIV Among People Aged 50 and Older. (2016). Available online at: https://www.cdc.gov/hiv/group/age/olderamericans/index.html
65. Grimsrud A, Cornell M, Schomaker M, Fox MP, Orrell C, Prozesky H, et al. CD4 count at antiretroviral therapy initiation and the risk of loss to follow-up: results from a multicentre cohort study. *J Epidemiol Commun Health.* (2016) 70:549–55. doi: 10.1136/jech-2015-206629
66. Mberi MN, Kuonza LR, Dube NM, Nattey C, Manda S, Summers R. Determinants of loss to follow-up in patients on antiretroviral treatment, South Africa, 2004-2012: a cohort study. *BMC Health Serv Res.* (2015) 15:259. doi: 10.1186/s12913-015-0912-2
67. Onwumeh J, Okwundu CI, Kredo T. Interleukin-2 as an adjunct to antiretroviral therapy for HIV-positive adults. *Cochrane Database Syst Rev.* (2017) 5:CD009818. doi: 10.1002/14651858.CD009818.pub2
68. Appay V, Zaunders JJ, Papagno L, Sutton J, Jaramillo A, Waters A, et al. Characterization of CD4(+) CTLs *ex vivo*. *J Immunol.* (2002) 168:5954–8. doi: 10.4049/jimmunol.168.11.5954
69. Salam N, Rane S, Das R, Faulkner M, Gund R, Kandpal U, et al. T cell ageing: effects of age on development, survival & function. *Indian J Med Res.* (2013) 138:595–608.
70. Cao W, Mehraj V, Kaufmann DE, Li T, Routy JP. Elevation and persistence of CD8 T-cells in HIV infection: the Achilles heel in the ART era. *J Int AIDS Soc.* (2016) 19:20697. doi: 10.7448/IAS.19.1.20697
71. Mudd JC, Lederman MM. CD8 T cell persistence in treated HIV infection. *Curr Opin HIV AIDS.* (2014) 9:500–5. doi: 10.1097/COH.0000000000000086
72. Tippett E, Cheng WJ, Westhorpe C, Cameron PU, Brew BJ, Lewin SR, et al. Differential expression of CD163 on monocyte subsets in healthy and HIV-1 infected individuals. *PLoS ONE.* (2011) 6:e19968. doi: 10.1371/journal.pone.0019968
73. Palmer S, Maldarelli F, Wiegand A, Bernstein B, Hanna GJ, Brun SC, et al. Low-level viremia persists for at least 7 years in patients on suppressive antiretroviral therapy. *Proc Natl Acad Sci USA.* (2008) 105:3879–84. doi: 10.1073/pnas.0800050105
74. Sporer B, Koedel U, Paul R, Eberle J, Arendt G, Pfister HW. Vascular endothelial growth factor (VEGF) is increased in serum, but not in cerebrospinal fluid in HIV associated CNS diseases. *J Neurol Neurosurg Psychiatry.* (2004) 75:298–300. doi: 10.1136/jnnp.2003.016287

75. Del Guerra FB, Fonseca JL, Figueiredo VM, Ziff EB. Konkiewitz EC. Human immunodeficiency virus-associated depression: contributions of immuno-inflammatory, monoaminergic, neurodegenerative, and neurotrophic pathways. *J Neurovirol*. (2013) 19:314–27. doi: 10.1007/s13365-013-0177-7
76. Bachis A, Avdoshina V, Zecca L, Parsadanian M, Mocchetti I. Human immunodeficiency virus type 1 alters brain-derived neurotrophic factor processing in neurons. *J Neurosci*. (2012) 32:9477–84. doi: 10.1523/JNEUROSCI.0865-12.2012
77. Wang Y, Liao J, Tang SJ, Shu J, Zhang W. HIV-1 gp120 upregulates brain-derived neurotrophic factor (BDNF) expression in BV2 cells via the Wnt/beta-catenin signaling pathway. *J Mol Neurosci*. (2017) 62:199–208. doi: 10.1007/s12031-017-0931-z
78. Schütz SG, Robinson-Papp J. HIV-related neuropathy: current perspectives. *HIV AIDS*. (2013) 5:243–51. doi: 10.2147/HIV.S36674
79. Simioni S, Cavassini M, Annoni JM, Rimbault Abraham A, Bourquin I, Schiffer V, et al. Cognitive dysfunction in HIV patients despite long-standing suppression of viremia. *AIDS*. (2010) 24:1243–50. doi: 10.1097/QAD.0b013e3283354a7b
80. Abas M, Ali GC, Nakimuli-Mpungu E, Chibanda D. Depression in people living with HIV in sub-Saharan Africa: time to act. *Trop Med Int Health*. (2014) 19:1392–6. doi: 10.1111/tmi.12382
81. Keating SM, Golub ET, Nowicki M, Young M, Anastos K, Crystal H, et al. The effect of HIV infection and HAART on inflammatory biomarkers in a population-based cohort of women. *AIDS*. (2011) 25:1823–32. doi: 10.1097/QAD.0b013e3283489d1f
82. Haissman JM, Vestergaard LS, Sembuche S, Erikstrup C, Mmbando B, Mtullu S, et al. Plasma cytokine levels in Tanzanian HIV-1-infected adults and the effect of antiretroviral treatment. *J Acquir Immune Defic Syndr*. (2009) 52:493–7. doi: 10.1097/QAI.0b013e3181b627dc
83. Espíndola MS, Soares LS, Galvão-Lima LJ, Zambuzi FA, Cacemiro MC, Brauer VS, et al. Epigenetic alterations are associated with monocyte immune dysfunctions in HIV-1 infection. *Sci Rep*. (2018) 8:5505. doi: 10.1038/s41598-018-23841-1
84. Horvath S, Stein DJ, Phillips N, Heany SJ, Kobor MS, Lin DTS, et al. Perinatally acquired HIV infection accelerates epigenetic aging in South African adolescents. *AIDS*. (2018) 32:1465–74. doi: 10.1097/QAD.0000000000001854
85. Horvath S, Levine AJ. HIV-1 Infection accelerates age according to the epigenetic clock. *J Infect Dis*. (2015) 212:1563–73. doi: 10.1093/infdis/jiv277
86. Vujkovic-Cvijin I, Dunham RM, Iwai S, Maher MC, Albright RG, Broadhurst MJ, et al. Dysbiosis of the gut microbiota is associated with HIV disease progression and tryptophan catabolism. *Sci Transl Med*. (2013) 5:193ra191. doi: 10.1126/scitranslmed.3006438
87. Brenchley JM, Schacker TW, Ruff LE, Price DA, Taylor JH, Beilman GJ, et al. CD4+ T cell depletion during all stages of HIV disease occurs predominantly in the gastrointestinal tract. *J Exp Med*. (2004) 200:749–59. doi: 10.1084/jem.20040874
88. Atarashi K, Suda W, Luo C, Kawaguchi T, Motoo I, Narushima S, et al. Ectopic colonization of oral bacteria in the intestine drives TH1 cell induction and inflammation. *Science*. (2017) 358:359–65. doi: 10.1126/science.aan4526
89. Komiya Y, Shimomura Y, Higurashi T, Sugi Y, Arimoto J, Umezawa S, et al. Patients with colorectal cancer have identical strains of Fusobacterium nucleatum in their colorectal cancer and oral cavity. *Gut*. (2018) doi: 10.1136/gutjnl-2018-316661 [Epub ahead of print]
90. Noguera-Julian M, Rocafort M, Guillén Y, Rivera J, Casadellà M, Nowak P, et al. Gut microbiota linked to sexual preference and HIV infection. *EBioMedicine*. (2016) 5:135–46. doi: 10.1016/j.ebiom.2016.01.032
91. De Filippo C, Di Paola M, Ramazzotti M, Albanese D, Pieraccini G, Banci E, et al. Diet, environments, and gut microbiota. a preliminary investigation in children living in rural and urban burkina faso and Italy. *Front Microbiol*. (2017) 8:1979. doi: 10.3389/fmicb.2017.01979
92. Koeth RA, Wang Z, Levison BS, Buffa JA, Org E, Sheehy BT, et al. Intestinal microbiota metabolism of L-carnitine, a nutrient in red meat, promotes atherosclerosis. *Nat Med*. (2013) 19:576–85. doi: 10.1038/nm.3145
93. Paster BJ, Olsen I, Aas JA, Dewhirst FE. The breadth of bacterial diversity in the human periodontal pocket and other oral sites. *Periodontol 2000*. (2006) 42:80–7. doi: 10.1111/j.1600-0757.2006.00174.x
94. Kau AL, Ahern PP, Griffin NW, Goodman AL, Gordon JI. Human nutrition, the gut microbiome and the immune system. *Nature*. (2011) 474:327–36. doi: 10.1038/nature10213
95. Liu J, Kandasamy S, Zhang J, Kirby CW, Karakach T, Hafting J, et al. Prebiotic effects of diet supplemented with the cultivated red seaweed Chondrus crispus or with fructo-oligo-saccharide on host immunity, colonic microbiota and gut microbial metabolites. *BMC Complement Altern Med*. (2015) 15:279. doi: 10.1186/s12906-015-0802-5
96. Rooks MG, Garrett WS. Gut microbiota, metabolites and host immunity. *Nat Rev Immunol*. (2016) 16:341–52. doi: 10.1038/nri.2016.42

Conflict of Interest Statement: The authors declare that the research was conducted in the absence of any commercial or financial relationships that could be construed as a potential conflict of interest.

frontiers in Immunology

ORIGINAL RESEARCH
published: 15 March 2019
doi: 10.3389/fimmu.2019.00482

TLR10 Senses HIV-1 Proteins and Significantly Enhances HIV-1 Infection

Bethany M. Henrick[1,2], Xiao-Dan Yao[3], Muhammad Atif Zahoor[3], Alash'le Abimiku[4], Sophia Osawe[4] and Kenneth L. Rosenthal[3] for the InFANT Study Team*

[1] *Evolve Biosystems, Davis, CA, United States,* [2] *Department of Food Science and Technology, University of Nebraska, Lincoln, NE, United States,* [3] *Department of Pathology and Molecular Medicine, McMaster University, Hamilton, ON, Canada,* [4] *Institue of Human Virology-Nigeria, Abuja, Nigeria*

Toll-like receptors (TLRs) play a crucial role in innate immunity and provide a first line of host defense against invading pathogens. Of the identified human TLRs, TLR10 remains an orphan receptor whose ligands and functions are poorly understood. In the present study, we sought to evaluate the level of TLR10 expression in breast milk (BM) and explore its potential function in the context of HIV-1 infection. We evaluated HIV-1-infected (Nigerian: $n = 40$) and uninfected (Nigerian: $n = 27$; Canadian: $n = 15$) BM samples for TLR expression (i.e., TLR10, TLR2, and TLR1) and report here that HIV-1-infected BM from Nigerian women showed significantly higher levels of TLR10, TLR1, and TLR2 expression. Moreover, the level of TLR10 expression in HIV-1-infected BM was upregulated by over 100-fold compared to that from uninfected control women. *In vitro* studies using TZMbl cells demonstrated that TLR10 overexpression contributes to higher HIV-1 infection and proviral DNA integration. Conversely, TLR10 inhibition significantly decreased HIV-1 infection. Notably, HIV-1 gp41 was recognized as a TLR10 ligand, leading to the induction of IL-8 and NF-κBα activation. The identification of a TLR10 ligand and its involvement in HIV-1 infection enhances our current understanding of HIV-1 replication and may assist in the development of improved future therapeutic strategies.

Keywords: human breast milk, HIV-1, gp41, p17, p24, TLR10, IL-8, NF-κBα

OPEN ACCESS

Edited by:
Sara Gianella Weibel, University of California, San Diego, United States

Reviewed by:
Barbara Louise Lohman-Payne, University of Rhode Island, United States
Anna-Lena Spetz, Stockholm University, Sweden

****Correspondence:***
Kenneth L. Rosenthal
rosenthl@mcmaster.ca

Specialty section:
This article was submitted to Viral Immunology, a section of the journal Frontiers in Immunology

Received: *31 October 2018*
Accepted: *22 February 2019*
Published: *15 March 2019*

Citation:
Henrick BM, Yao X-D, Zahoor MA, Abimiku A, Osawe S and Rosenthal KL (2019) TLR10 Senses HIV-1 Proteins and Significantly Enhances HIV-1 Infection. Front. Immunol. 10:482. doi: 10.3389/fimmu.2019.00482

INTRODUCTION

Toll-like receptors (TLRs) are the most well-known and researched family of pattern recognition receptors (PRRs) that recognize conserved regions of pathogen-associated molecular patterns (PAMPs) and endogenous danger-associated molecular patterns (DAMPs) responsible for driving cellular activation central to innate immunity. To date, 10 TLRs have been identified in humans, with TLR10 being the only remaining family member without a clearly defined ligand (1, 2); however, a number of ligands, including synthesized TLR2 ligands (i.e., Pam3CSK4 and $PamCysPamSK_4$), have been identified as potential TLR10 PAMPs through computational protein modeling (3).

Once believed to be only preferentially expressed on various types of immune cells (4), TLR10 has now been identified in multiple mucosal sites, including the small intestine, fallopian tubes, eye, and stomach (5–8). Interestingly, many of these sites are also highly affected during acute viral

infections, including HIV-1; therefore, identifying ligands for TLR10 and defining the mechanisms of host defense following viral infection is of particular interest for the development of novel vaccines and drug therapies.

Immune activation is critical to HIV-1 infection and pathogenesis, leading to increased proinflammatory cytokine production, T cell exhaustion, and the eventual development of opportunistic infections (9); however, our understanding of immunopathogenesis remains incomplete. Historically, research has focused on HIV-1-specific adaptive immune responses, whereas the role of innate immunity has been largely overlooked, despite the fact that it provides the first line of defense and shapes subsequent adaptive responses. Although the identification of HIV-1 PAMPs recognized by PRRs remain poorly elucidated, data indicate that peripheral blood mononuclear cells (PBMCs) and plasmacytoid dendritic cells (pDCs) derived from HIV-1 infected individuals have increased levels of TLR2, TLR3, TLR4, TLR6, TLR7, and TLR8 mRNA at various stages of disease progression (10, 11). In addition, our laboratory has previously investigated the genital epithelium of Kenyan commercial sex workers and found significant modification in TLR expression, which correlates with resistance to HIV-1 (12). Furthermore, we were the first to demonstrate that soluble TLR2 (sTLR2), which is highly prevalent in human breast milk (BM) (13) serves as an innate antiviral factor in BM and significantly inhibits HIV-1 infection and integration *in vitro* (14, 15). We further reported a significant increase in TLR2 expression in BM cells, and that the overexpression of TLR2 in reporter cells greatly enhanced HIV-1 infection *in vitro* (15). We further identified HIV-1-specific structural proteins, p17, p24, and gp41, which serve as PAMPs, leading to significantly increased immunopathogenesis and infection *in vitro* (16).

Given that TLR10 is a homolog of both TLR2 and TLR1, we hypothesized that TLR10 is involved in sensing specific HIV-1 structural proteins, which leads to increased cellular activation and HIV-1 infection. In this study, we report highly significantly increased TLR10 and TLR1 expression in HIV-1-infected human primary BM cells. Additionally, for the first time, TLR10 was found to be involved in innate immune sensing and cellular activation induced by HIV-1, leading to increased infection *in vitro*. Taken together, we provide clear evidence that specific HIV-1 structural proteins trigger TLR10-dependent cellular activation. These findings indicate that TLR10 and its heterodimers, TLR1 and TLR2, play a central role in the innate immune response to HIV-1 infection by sensing viral proteins, leading to increased immunopathogenesis.

RESULTS

Healthy Human BM Derived Macrophages and Mammary Epithelial Cells Express TLR10, TLR2, and TLR1

Depending on the stage of lactation, the predominant cell types in BM consist of a variety of leukocytes in colostrum (4×10^6 cells/mL) and mature BM (10^5-10^6 cells/mL), as well as mammary epithelial cells (MECs) (16–18). The majority of leukocytes present in BM display an activated phenotype (19) and are comprised primarily of macrophages (55–60%) and neutrophils (30–40%), with the remaining 5–10% composed of lymphocytes (∼65% CD8+ T cells, 15% CD4+ T cells, and 20% B cells) (18). Macrophages and MECs are thought to facilitate mother-to-child transmission (MTCT) of HIV-1, and both cell types express several canonical HIV-1 receptors, (e.g., CD4 and CCR5), readily endocytose cell-free HIV-1, and can function as a viral reservoir (20). To explore how TLR expression is linked to HIV-1 infection, we first analyzed the phenotype of the macrophages and MECs present in HIV-1 uninfected human BM using flow cytometry. We found that the majority of cells that were CD14+ and CD45+ (>10%) expressed TLR1 (3.03%), TLR2 (58.6%), and TLR10 (99.3%). Similarly, MUC1+ (75.4%) MECs also expressed TLR1, TLR2, and TLR10 exhibiting 3.67, 69.1, and 0.39%, respectively (**Figure 1**). Based on our flow cytometry data our findings suggest that BM derived macrophages predominantly express TLR10 which implies that these cells may play an important role in innate immunity against invading pathogens in suckling infants.

TLR10 and TLR1 Are Highly Expressed in HIV-1 Infected Human Primary BM Cells

The biological relevance of primary BM cells in HIV MTCT remains unclear. BM derived TLRs such as TLR2, TLR3, and TLR5 along with other bioactive molecules are known to play an important role in intestinal protection, inflammatory responses and even microbial recognition (21). Indeed, it has been suggested that certain cytokines such as interferon gamma secreted by primary BM cells reduce the rate of BM transmission of HIV-1 in breastfeeding infants (22, 23); therefore, we next sought to determine the level of TLR10 and TLR1 expression in BM collected from HIV-1 infected women from Nigeria and compared to HIV-1 uninfected women. Both HIV-1 infected as well as uninfected control women were recruited from Plateau State, Nigeria and a series of BM samples from first week to 52 weeks postpartum were collected and shipped to Canada. All HIV-1 positive women were on antiretroviral therapy (ART) and receiving antiretroviral drugs according to the regimen set by Nigerian Government and world Health Organization (WHO) as described (24) We evaluated HIV-1-infected (Nigerian: $n = 40$) and uninfected (Nigerian: $n = 27$; Canadian: $n = 15$) BM samples for the expression of TLR10 and TLR1. Our results clearly demonstrated a highly significant increase in the expression of both TLR1 and TLR10 cDNA in HIV-1-infected compared to uninfected primary BM cells from the same geographical location (**Figure 2**; $P = 0.0006$ and $P < 0.0001$, respectively). Specifically, TLR10 expression was ∼100-fold higher in HIV-1 infected vs. HIV-1 uninfected primary BM cells. In addition to HIV-1 infected and uninfected women from Nigeria, we also collected BM samples from uninfected healthy women from Hamilton region, Ontario, Canada and compared their TLR1 and TLR10 expression levels with uninfected healthy control women from Nigeria. Interestingly, it was found that TLR1 and TLR10 expression on Nigerian HIV-1 uninfected primary BM cells was significantly lower compared to that on Canadian HIV-1

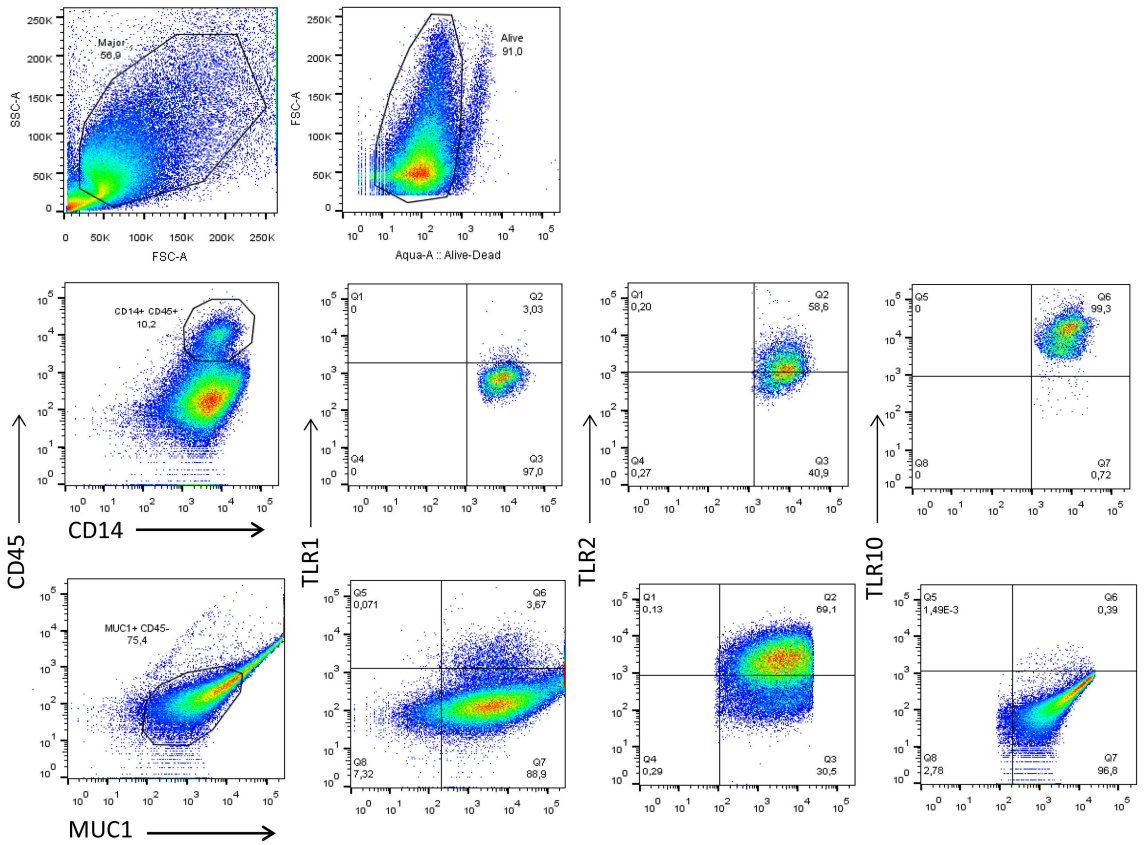

FIGURE 1 | Flow cytometry analyses of TLR1, TLR2, and TLR10 expression in the two major types of primary BM cells obtained from HIV-1 uninfected women at 3 months post-partum. Leucocytes were gated with CD45-PerCP-Cy5.5 and CD14-V450 whereas the epithelial cells were gated with MUC1-PE-Cy7 and CD45-. The antibodies TLR1-APC TLR2-APC and TLR10-PE were separately used to detect TLR1, TLR2, and TLR10 in $CD14^{+}$-$CD45^{+}$-$MUC1^{-}$ and $MUC1^{+}$-$CD45^{-}$ cell types to differentiate the two major constituents of BM. Representative images are shown with TLR1, TLR2, and TLR10 expression depicted as percentages on right corner of each image.

uninfected primary BM cells thus highlighting the demographic differences. Taken together, these results show that TLRs are highly expressed on primary BM cells, and this expression may be closely associated with an individual's HIV-1 infection and innate immune status.

The Level of TLR10 Expression Significantly Alters HIV-1 Infection and Integration

Since the extracellular expression of TLR10, TLR1, and TLR2 are innate immune molecules involved in pathogen signaling and are highly expressed on cells in BM (**Figures 1**, **2**) and PBMCs (1, 25) we decided to utilize human mammary epithelial (Michigan Cancer Foundation-10A; MCF-10A) cells and macrophage cell lines (human acute monocytic leukemia; THP-1) for further downstream experiments. MCF-10A is a human non-tumorigenic epithelial cell line with no signs of terminal differentiation and has been used in our previous studies (15). THP-1 is an immortalized monocyte-like cell line derived from the peripheral blood of a childhood case of acute monocytic leukemia (26, 27) and has been utilized previously (28). First we determined whether the expression levels could influence HIV-1 infection *in vitro*. For this purpose, HIV-1 reporter TZMbl cells (29) were transiently transfected alone or in combination with plasmids overexpressing TLR10 and the heterodimers, TLR2 and TLR1 (**Figure 3A**), followed by HIV-1 infection and measurement of luciferase activity. The results showed a significantly increased rate of HIV-1 infection in TZMbl cells overexpressing TLR10 and heterodimers TLR1 or TLR2 compared to the empty vector alone, uninfected control or a T20 control (Enfuvirtide; HIV-1 fusion inhibitor) (30, 31) (**Figure 3A**; $P < 0.05$). In addition, HIV-1 infection was significantly elevated in TZMbl cells, which were either co-transfected with TLR1/10 or TLR2/10 compared to the control (**Figure 3A**; $P < 0.05$).

Next, we determined the extent of HIV-1 infection in TLR10 and TLR2 stable reporter cell lines. TZMbl-T2 and TZMbl-T10 displayed significantly higher levels of proviral DNA compared to TZMbl cells, which served as a control (**Figure 3B**; $P < 0.05$). Furthermore, stable TZMbl-T2 transiently over-expressing

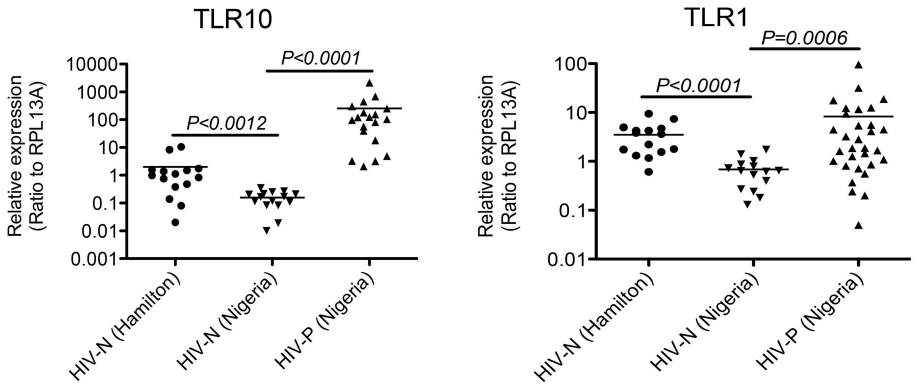

FIGURE 2 | Significantly elevated expression level of TLR1 and TLR10 in HIV-1 infected human primary BM cells. Expression of TLR1 and TLR10 as measured by qRT-PCR with the mRNA extracted from primary BM cells collected from HIV-1 negative Hamilton, Canada women (HIV-N Hamilton) and Nigerian HIV-1 negative (HIV-N) and HIV-1 positive (HIV-P) women. TLR1 expression is shown on right ($p = 0.0006$) whereas TLR10 expression is shown on left ($p < 0.0001$).

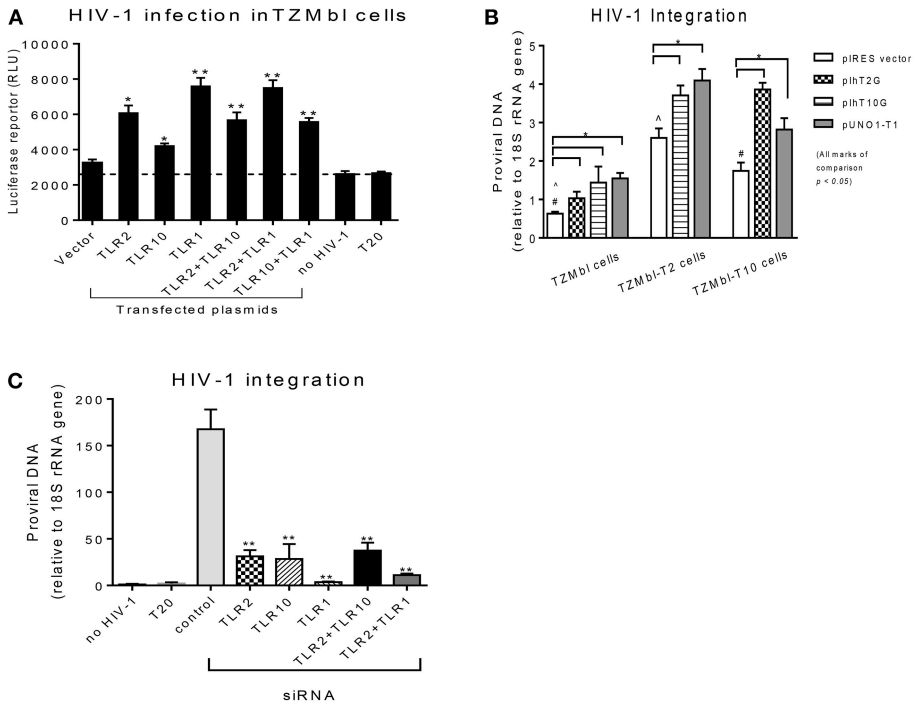

FIGURE 3 | Overexpression or siRNA mediated knockdown of TLR10 significantly alters HIV-1 infection and integration **(A)** HIV-1 infection was significantly enhanced in HIV-1 reporter TZMbl cells transiently overexpressing TLR10 alone and co-transfected with TLR2 or TLR1 expression plasmids by measuring luciferase activity in relative light units (RLU). **(B)** HIV-1 integration was significantly increased in stable TZMbl reporter cells overexpressing TLR10, TLR2, and TLR1. TZMbl, TLR2- stable, and TLR10-stable cells were used for co-transfection with plasmids: empty vector, TLR2, TLR10, and TLR1 vector, TLR10 and TLR1 vector, and TLR2 and TLR1 vector. Proviral DNA (DNA pol) was detected by PCR and normalized to the 18S rRNA gene. **(C)** Proviral DNA was obviously decreased in macrophages with TLR10 knocked down prior to HIV-1 infection. T20: Enfuvirtide, an HIV-1 fusion inhibitor used as a negative control. Data set is representative of three different experiments completed in triplicate (Statistic marks in the plots: $*p < 0.05$, $**p < 0.01$ for Mann Whitney *t*-tests, each group compared to the vector group in A and B, or to the control group in C; pair comparison ∧, # in B, respectively).

TLR10 or TLR1 also enhanced HIV-1 pol gene expression. Similarly, stable TZMbl-T10 cells transiently over-expressing TLR2 or TLR1 also enhanced proviral pol DNA at 8 h post-infection compared with the empty vector-transient stable cells (**Figure 3B**; $P < 0.05$).

In order to observe the HIV-1 infection in susceptible cells, macrophages were differentiated from THP-1 cells to determine whether siRNA-mediated knockdown of TLR1, 2 and/or 10 for 2 days prior to CCR5-tropic HIV-1 (BAL strain) exposure for 7 days would affect the HIV-1 infection rate. THP-1 cells were

first transfected with siRNAs targeting TRL1, TLR2, or TLR10, and their knockdown was confirmed by Western blot. TLR1 and TLR2 knockdown was complete compared to TLR10 where it was partial (**Supplementary Figure 1**). After the confirmation of the siRNA-mediated knockdown, HIV-1 integration was determined by PCR, which showed significantly decreased proviral DNA production in the cells that received siRNAs against TLR1, TLR2, TLR10, or combinations of TLR2 with TRL10 or TLR1 compared to the control siRNA (**Figure 3C**). In addition, since we observed incomplete TLR10 knockdown in THP-1 cells, it is likely that upon complete knockdown of TLR10, HIV-1 integration and proviral DNA production will be impacted. Together, these data indicate that the expression of TLR1, 2 and TLR10 alone or in combination significantly enhances HIV-1 infection and integration *in vitro*. Moreover, based on TLR10 and TLR2 co-transfection or co-depletion through siRNA and effect on HIV-1 infection or integration, TLR10 appears to play a role in HIV-1 infection and integration independent of TLR2 since no additive effect of TLR10 and TLR2 was observed (**Figures 3B,C**). Therefore, it is highly likely that TLR2 and TLR10 are independently involved in the regulation of HIV-1 infection in a non-heterodimeric form.

Expression of TLR10, TLR1, and TLR2 Is Up-Regulated by PAMPs and HIV-1

We next determined whether the expression of TLR1, 2, or 10 changes in response to various TLR ligands. MCF-10A, THP-1, and primary BM cells were stimulated with TLR ligands of interest at the following doses: 100 ng/mL Pam3Cys-Ser-(Lys)4 (Pam3CSK4); 10 ng/mL lipopolysaccharide (LPS), ssRNA40 1 μg/mL, and cell-free HIV-1 overnight. Total RNA was isolated from the cells and qRT-PCR was performed. Data showed that compared to medium control, MCF-10A cells exposed to the TLR2/1 ligand, Pam3CSK4, significantly increased the level of TLR1, 2, and 10 expression (**Figure 4A**). Similarly, exposure to TLR4 ligand, LPS, significantly increased TLR1 and 2 expression (**Figure 4A**). In contrast, although ssRNA40 showed a significant increase in TLR1 and TLR10, but had no significant effect on TLR2 expression (**Figure 4A**). Conversely, HIV-1 exposure significantly increased the level of TLR10 expression on MCF-10A cells (**Figure 4A**) despite the fact that HIV-1 does not productively infect this cell type (20). In THP-1 cells, Pam3CSK4 exposure significantly increased the level of TLR2 and 10 expression, whereas LPS exposure resulted in an increase in TLR1 and 2 expression (**Figure 4B**). Following exposure to ssRNA40, the expression of TLR1, 2, and 10 was significantly increased. Similarly, HIV-1 exposure significantly increased the level of TLR1, 2, and 10 expression in THP-1 cells (**Figure 4B**). Primary BM cells exposed to specific PAMPs also exhibited significantly increased levels of TLR1 and TLR2 expression following exposure to Pam3CSK4 and LPS (**Figure 4C**). Elevated TLR2 expression was also observed after exposure to ssRNA40 and cell-free HIV-1 (**Figure 4C**). Most importantly, the data indicated that TLR10 was significantly elevated after exposure to ssRNA40 and HIV-1 (**Figure 4C**). Taken together, these data indicate that specific HIV-1 PAMPs, as well as cell-free HIV-1, significantly increase TLR10, TLR1, and TLR2 expression in primary BM cells.

HIV-1 Proteins Regulate TLR Expression Levels and Induce IL-8 Secretion

HIV-1 structural proteins and glycoproteins have been detected in BM (15) and have been shown to exert immunological effects typical of a proinflammatory response (32–37). Based on our recent findings that HIV-1 structural proteins bind to TLR2 (16), we hypothesized that HIV-1 components may contact the cell surface and trigger TLR10 signaling. Therefore, we next investigated whether specific HIV-1 structural proteins increased cellular activation in primary BM cells. To characterize which HIV-1 structural proteins were involved in this process, we used purified p17 (200 ng/mL), p24 (200 ng/mL), gp41 (1 μg/mL), and gp120 (1 μg/mL) to treat MCF-10A and THP-1 cells and detected the cellular responses. The results demonstrated that the expression of TLR10 and TLR2 mRNA was significantly altered following exposure to gp41 alone compared to untreated medium, as well as Pam3CSK4, which served as a positive control in MCF-10A cells (**Figure 5A**). IL-8 production increased in a dose-dependent manner in the supernatants of MCF-10A cell cultures containing gp41 and Pam3CSK4 (**Figure 5B**). However, TLR10 was significantly highly expressed in THP-1 cells in the presence of gp41 as well as p17 (**Figure 5C**). TLR2 and TLR1 were obviously increased in the presence of gp41, p17, and p24. In the THP-1 cell culture, IL-8 was also correspondingly produced with increases in the amount of Pam3CSK4 and structural proteins, except gp120 (**Figure 5D**). Together, this data indicates that HIV-1 gp41 is able to induce the innate immune response and alters the level of TLR10 expression, similar to TLR2 (16) and is not cell-type-sensitive.

Furthermore, we confirmed our observations by transfecting THP-1 cells with siRNA specific to target genes (**Figure 6A**). Compared to the cells treated with the control siRNA, TLR10 siRNA suppressed more than 3-fold of IL-8 production in the cells treated with HIV-1 PAMPs. Treatment with TLR2 siRNA decreased IL-8 production by ∼2-fold. The combination of TLR10 and TLR2 siRNAs decreased IL-8 production more than 2-fold. In addition, we used antibodies to neutralize TLR10, TLR2, and TLR1 in gp41 and p17-treated THP-1 cells. As shown in **Figure 6B**, treatment with anti-TLR10 and TLR1 antibodies significantly reduced IL-8 production in gp41- and p17-treated cells, respectively. Anti-TLR2 antibodies exhibited a similar trend but without a statistical difference. Since the primary focus of this study was TLR10-related events, we only used anti-TLR10 antibodies to treat MCF-10A cells in the neutralization experiments. The results revealed that gp41-induced IL-8 production was also significantly decreased in the presence of the anti-TLR10 antibody (**Figure 6C**). Similarly, primary BM cells were incubated with the anti-TLR10 antibody before treatment with HIV-1 proteins. The data revealed that gp41-induced IL-8 production was also significantly decreased in the presence of TLR10 antibodies in primary BM cells

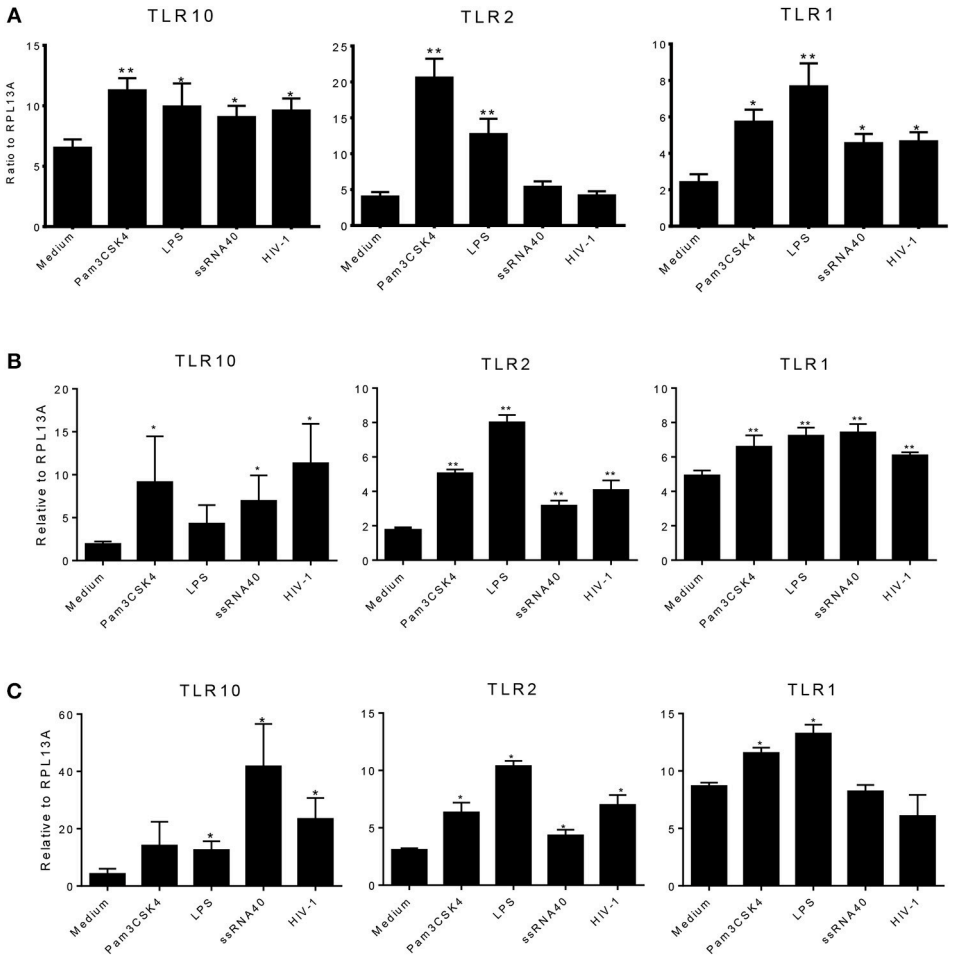

FIGURE 4 | Effects of PAMPs and HIV-1 on the level of TLR expression in cell cultures. **(A)** qRT-PCR of TLR10, TLR2, and TLR1 mRNA from MCF-10A cells treated with TLR2 PAMP Pam3CSK4, TLR4 PAMP LPS, TLR7/TLR8 PAMP ssRNA40, and cell-free HIV-1 BAL. **(B)** q-RT-PCR in THP-1 cells. **(C)** qRT-PCR in primary BM cells. Data set is representative of three different experiments completed in triplicate. Statistic marks: $*p < 0.05$, $**p < 0.01$ for the Mann-Whitney *t*-tests, each group compared to medium-treated group (Medium).

(**Figure 6D**). These results suggest that HIV-1 gp41 is capable of upregulating both TLR2 (15) and TLR10 in all cells under our experimental conditions.

HIV-1 Proteins Induce TLR10, TLR2, and TLR1 Signaling Through the Activation of NF-κBα

TLR2 and TLR1-mediated signaling pathways have been well-studied. We have recently discovered that the HIV-1 structural proteins p17, p24, and gp41 directly interact with TLR2, inducing NF-κBα activation. We then asked whether these structural proteins also induce NF-κBα activation via their PAMP effects on TLR10. Cells were treated with Pam3CSK4, p17, p24, and gp41, followed by a Western blot of the lysates with anti-phospho-IκBα, a subunit of NF-κBα that is representative of active NF-κBα. The results in **Figure 7A** demonstrate that activated NF-κBα was substantially expressed in MCF-10A cells treated with gp41, compared to the positive control (Pam3CSK4) and negative control (medium)-treated cells. In contrast, moderate expression of P-IκBα was observed in the MCF-10A cells treated with p17. However, in both the macrophages derived from THP-1 and BM cells, the three HIV-1 proteins greatly stimulated the production of active NF-κBα. In addition, translocation of the NF-κBα p65 subunit into the nuclei occurred in MCF-10A cells treated with Pam3CSK4 and gp41 (**Figure 7B**). p65 translocation was observed in a number of MCF-10A cells in the presence of p17 and p24. Compared to the medium control, treatment with Pam3CSK4 and each of the three HIV-1 proteins led to p65 translocation to the nuclei of THP-1 cells.

When TLR10 expression was knocked down using siRNA, NF-κBα activation in response to HIV-1 proteins was significantly reduced in THP-1 cells (**Figure 8**). The signaling activity induced by the ligation of TLR2 and TLR1 by the positive siRNA control was similar to the response induced by TLR10 activation by the three HIV-1 proteins (p17, p24, and gp41), suggesting that these proteins are involved in the activation of NF-κBα. Considering the possibility that endotoxin

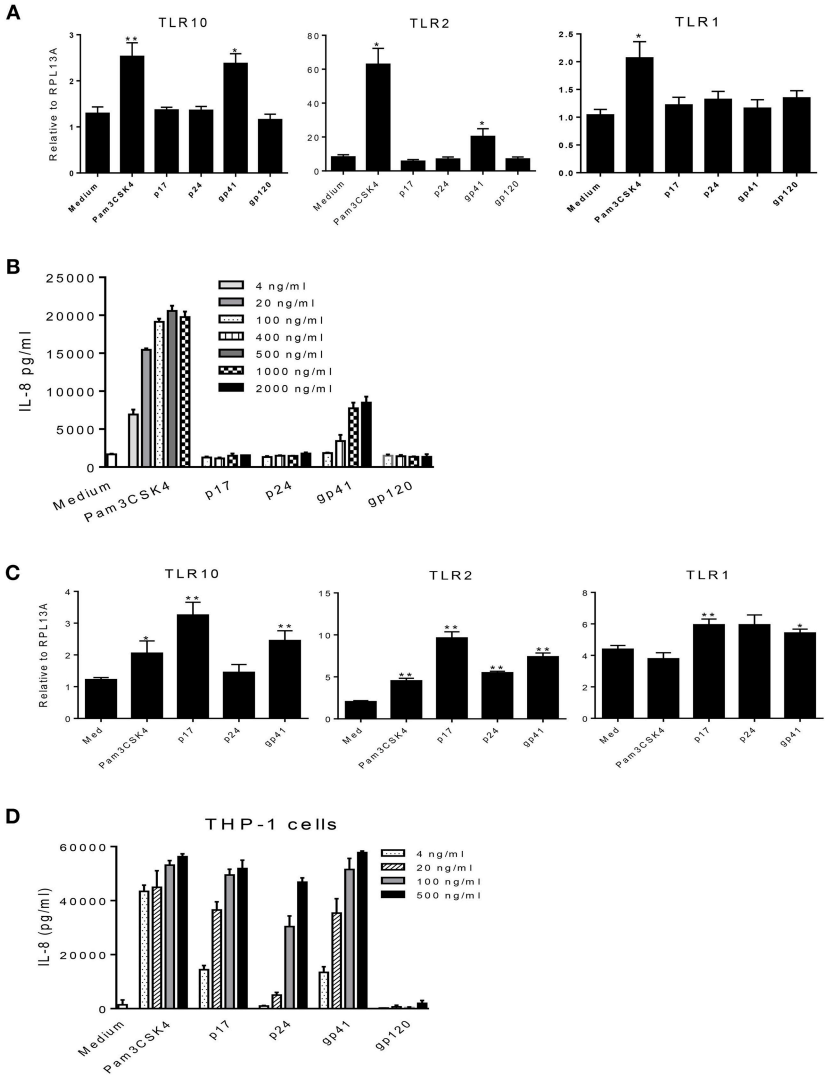

FIGURE 5 | Effects of HIV-1 proteins on TLR expression and cellular responses. **(A)** MCF-10A cells were treated with Pam3CSK4 and the HIV-1 structural proteins: p17, p24, gp41, and gp120. Cellular TLR10, TLR2, and TLR1 mRNAs were analyzed by qRT-PCR. **(B)** IL-8 production in cell culture supernatants in the presence of different concentrations of Pam3CSK4 and HIV-1 proteins were analyzed by ELISA. **(C)** The expression of TLR mRNAs analyzed by qRT-PCR in THP-1 cells treated with Pam3CSK4 and the HIV-1 structural proteins: p17, p24, and gp41. **(D)** IL-8 production in THP-1 cell culture supernatants in the presence of different concentrations of Pam3CSK4 and HIV-1 proteins was analyzed by ELISA. Data set is representative of three different experiments completed in triplicate. Statistic marks: $^{*}p < 0.05$, $^{**}p < 0.01$ for the Mann-Whitney *t*-tests, each group was compared to the medium-treated group (Medium).

was present in the HIV-1 products, we used TLR4 siRNA in the same experiment. The Western blot results clearly showed that knocking down TLR4 did not change the cellular response to p17 and gp41 in activating NF-κBα, which excluded endotoxin or LPS contamination in the two proteins. A 50% reduction in NF-κBα activation was observed in TLR4 siRNA transfected cells treated with Pam3CSK4 and p24, thus indicating cross-talk and a convergence between the different TLR signaling pathways.

DISCUSSION

To date, a total of 10 (1–10) human TLRs have been identified, which are known to play an important role in the innate immune sensing of invading pathogens (38, 39). Although the ligands for TLRs 1 through 9 are well-known, TLR10 has remained the only orphan receptor with no known ligand, despite being identified >17 years ago (4). To our knowledge, we are the first to report that TLR10 is involved in HIV-1 infection and most importantly, that gp41 acts as a ligand for TLR10 in human macrophages and MECs.

We initially attempted to identify and screen TLRs present in human BM and previously reported that soluble TLR2 (sTLR2) is present in human BM and significantly inhibits HIV-1 infection (15). Furthermore, we also showed that the HIV-1 structural proteins, p17, p24, and gp41, serve as PAMPs for TLR2, leading to the activation of the NF-κBα signaling pathway (16).

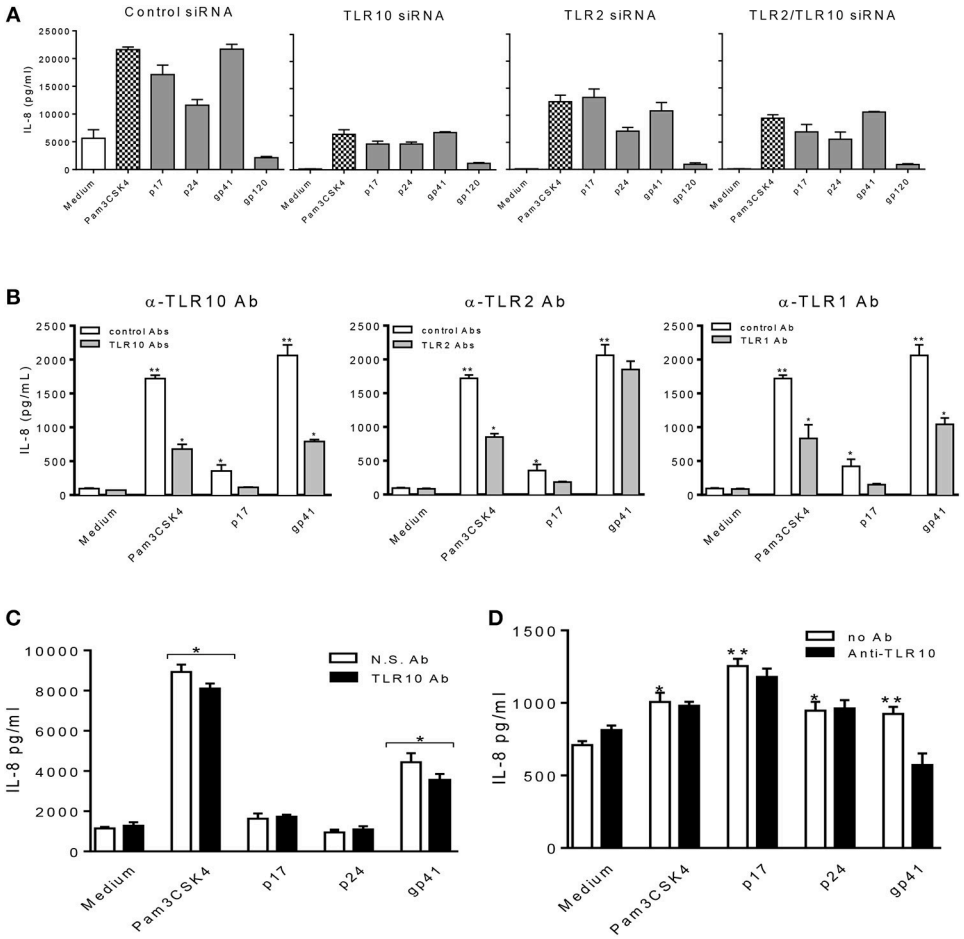

FIGURE 6 | HIV-1 proteins, p17 and gp41 elicit cellular responses through sensing TLR10, TLR2, and TLR1. IL-8 production stimulated by Pam3CSK4, p17, p24, and gp41 was greatly suppressed in THP-1 cells knocked-down of TLR10 with specific siRNA **(A)** and THP-1 cells neutralized with anti-TLR10 antibody **(B)**. **(C)** IL-8 stimulated by Pam3CSK4 and gp41 was reduced in MCF-10A cells neutralized with an anti-TLR10 antibody. **(D)** Primary BM cells displayed a significant decrease in IL-8 production induced by HIV-1 gp41 following neutralization with an anti-TLR10 antibody. Data set is representative of three different experiments completed in triplicate. Statistic marks: $^{*}p < 0.05$; $^{**}p < 0.01$ for Mann Whitney *t*-tests, with each group compared to the medium treated group (Medium).

Surprisingly, with the exception of TLR1 and TLR2, we found significantly higher levels of TLR10 (>100-fold) expression in BM samples collected from HIV-1 infected Nigerian women (**Figure 2**), thus indicating that TLR10 might play an important role in HIV-1 infection and pathogenesis. In addition, uninfected BM samples from Canadian women exhibited higher basal levels of TLR10 and TLR1 expression compared to uninfected Nigerian women. Although whether there is a significant difference in the level of these two TLRs in healthy populations remains unknown, it is tempting to speculate that the genetic differences present in these two populations might affect the outcome of HIV-1 infection.

TLR1, TLR6, and TLR10 share a common locus on chromosome 4p14 and are structurally similar to each another (40) and are thought to have arisen from several gene duplication events (41). Furthermore, it has been established that TLR10, TLR1, and TLR6 form a single cluster and provide an important first line of defense against infectious agents. Previous work related to TLR1, TLR2, TLR6, and TLR10 has failed to provide the agonist for TLR10 but suggests that the TLR10 ligand might be of a viral origin, leading to the activation of NF-κBα (40, 42). Our current study confirms that one ligand for TLR10 is indeed of viral origin, notably HIV-1 gp41.

TLR10 is known to possess point mutations in its TIR domain that play a critical role in its proper functioning (43). Furthermore, it has been shown that genetic variations in TLR10 can lead to various ailments, such as Crohn's disease (44) and asthma (45). Moreover, TLR10 has been shown to be involved in osteoarthritis (46), Crimean Congo hemorrhagic fever (47), *Listeria monocytogenes*, *Salmonella* Typhimurium (28), *Helicobacter pylori* (7), and influenza (2). Nevertheless, the involvement of TLR10 in various diseases paves the way for future exploratory studies.

Interestingly, recent data concerning early hominins, Neandertals, and Denisovans, who lived in Europe and Western Asia for over 200,000 years, likely interbred and

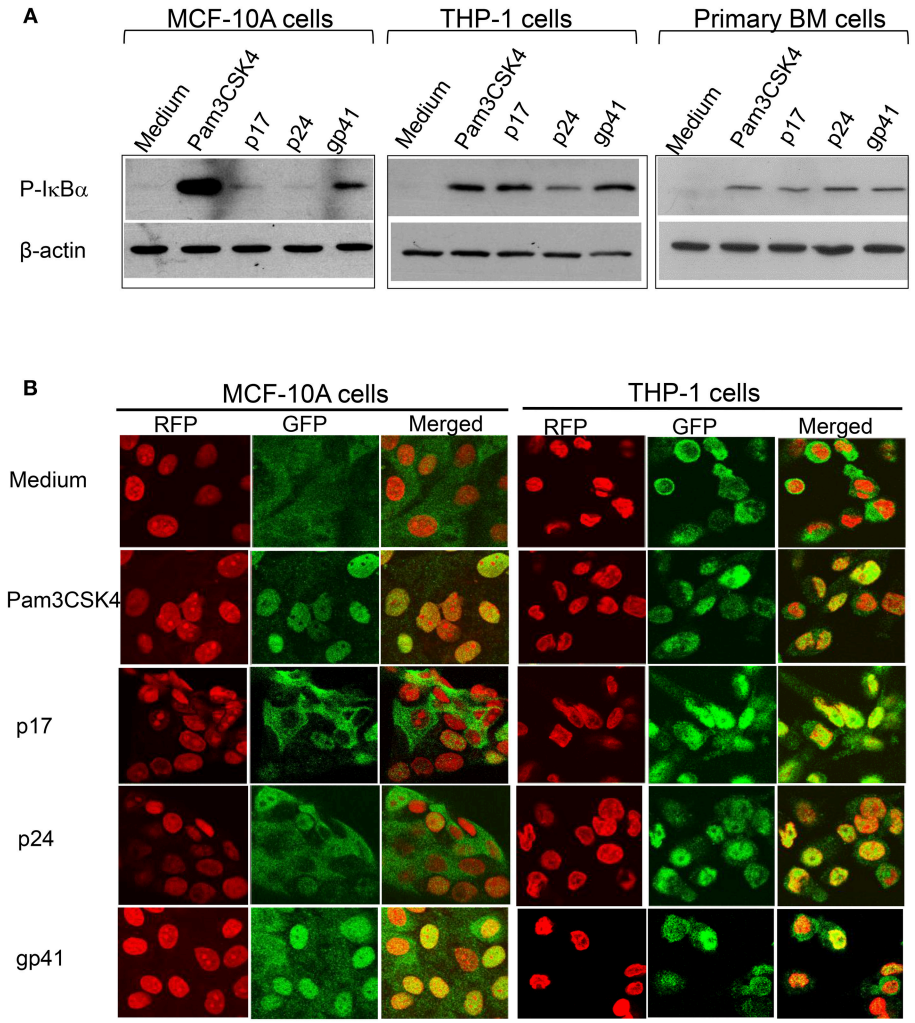

FIGURE 7 | HIV-1 proteins lead to NF-κBα activation **(A)** Western blot analysis of the cell lysates extracted from MCF-10A, THP-1, and primary BM cells treated with HIV-1 proteins and detected with an antibody against the active NF-κBα subunit, phospho(P)-IκBα, with anti β-actin used as the loading control on the same membranes **(B)** Confocal microscopy of HIV-treated MCF-10A and THP-1 cells fixed and stained with an anti- NF-κBα subunit p65 antibody and visualized with a second antibody, anti-rabbit-IgG-alexa488 (GFP; green), p65 was translocated upon activation into the nuclei (RFP; red with propidium iodide staining) displayed in yellow (Merged).

contributed advantageous genetic alleles to the immune systems of modern humans (48–50). Indeed, TLR genes, which are critical components of innate immunity, have also gained advantageous alleles through this mixing of the gene pool. Notably, adaptive introgression and local positive selection led to the significantly increased expression of the TLR6, TLR1, and TLR10 genes, which facilitated resistance to infectious diseases but may also be associated with increased hypersensitivity to non-pathogenic allergens.

Primary BM cells, MCF-10A MECs, and macrophages display significantly higher levels of TLR10 expression in response to HIV-1. In particular, gp41, not p17, and p24, was able to act as a ligand for TLR10. Since primary BM cells express TLR2, TLR1, and TLR10 (**Figures 1**, **2**); thus, it is plausible that these TLRs could form heterodimers.

Our data have shown that macrophages and MECs are human BM constituents that express TLR1, TLR2, and TLR10. Although gp41 was found to act as a ligand for both TLR2 (16) and TLR10 in the current study. Whether TLR2 and TLR10 interact and associate with each other in the context of an HIV-1 infection remains unclear and will be intriguing to investigate in future studies. However, since macrophages derived from THP-1 cells sensed gp41 in addition to p17 and p24, it is suggested that BM derived macrophages actively participates in HIV-1-induced innate immunity.

Although the induction of TLR10 by immune cells (e.g., B-cells, plasmacytoid dendritic cells, and macrophages) is well-reported (28, 40); the induction of TLR10 by non-immune cells (e.g., intestinal epithelial cells or MECs) raises the possibility of a

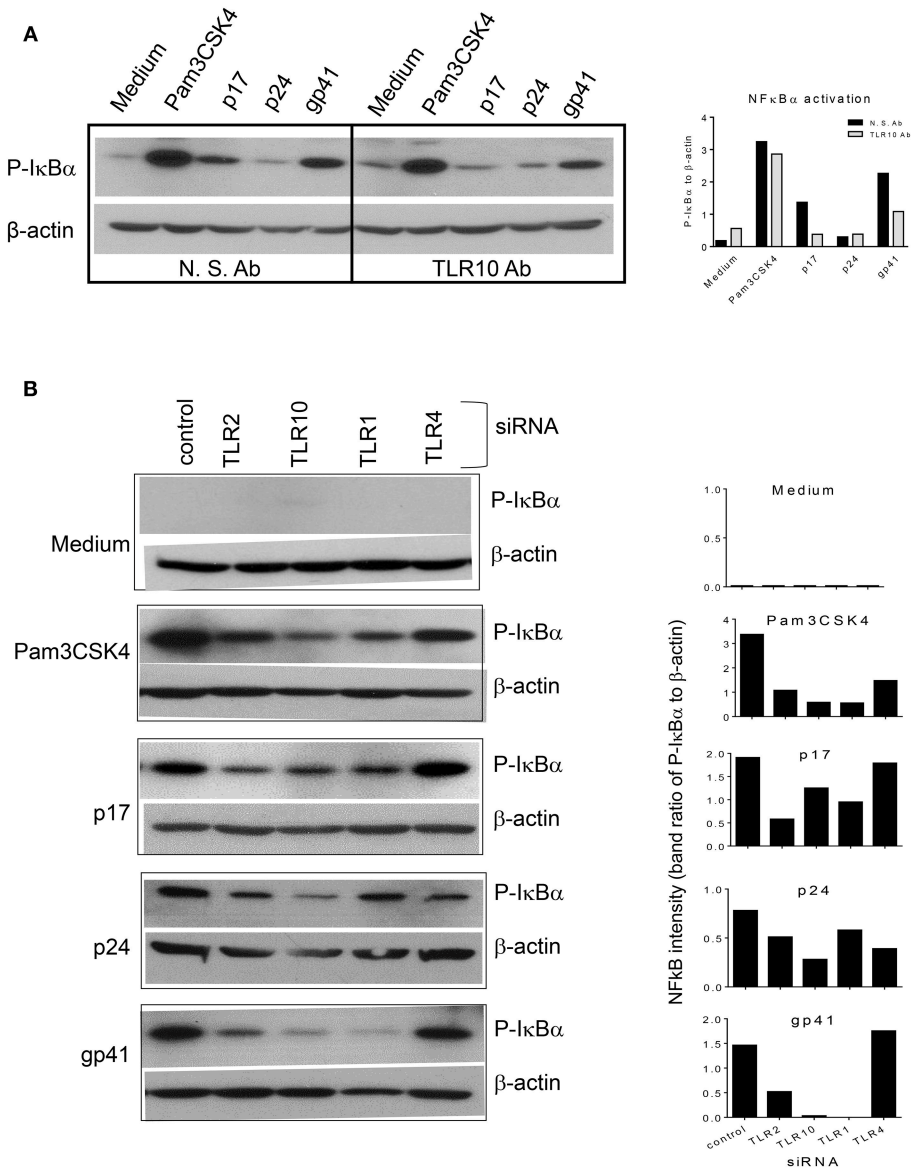

FIGURE 8 | siRNA mediated knockdown or antibody mediated blocking of TLR10 inhibits NF-κBα activation induced by HIV-1 proteins **(A)** anti-TLR10 antibody decreased gp41 induced P-IκBα by half in MCF-10A cells. **(B)** TLR10 siRNA ablated the induction of P-IκBα by gp41 in THP-1 cells.

conserved mechanism regarding TLR10 expression by epithelial cells (28).

We suggest that TLR10 and TLR1 both work cooperatively as the transfection of TRL10 and TLR1 alone or in combination significantly enhanced HIV-1 infection, indicating that TLR10 and TLR1 likely form heterodimers. This is evidenced by the observation that a depletion of TLR10 by a siRNA-mediated knockdown negatively impacted the proviral integration of HIV-1. Moreover, TLR10 knockdown led to significantly lower levels of IL-8 production in cells treated with gp41, p17, and p24. Furthermore, gp41, p17, and p24 were able to activate NF-κBα, which was readily blocked using an anti-TLR10 antibody or TLR10-specific siRNA-treated cells, suggesting that TLR10 signaling led to the activation of NF-κBα and ultimately the production of IL-8.

Importantly, the present study provides the first evidence that HIV-1 gp41 functions as a ligand for TLR10 in MCF-10A and THP-1 cells. Recently, double-stranded RNA (dsRNA) has been shown to act as a ligand for TLR10 (51). In addition, the same study demonstrated that TLR10 competes with TLR3 for binding to ligands in various endocytic pathways, ultimately leading to the induction of interferons. Similarly, synergy between TLR3 and TLR10 has been suggested in the context of an influenza virus infection. Although our current data demonstrates the involvement of TLR10 in HIV-1 infection, the existence of such

synergy between TLR10 and TLR3 in an HIV-1 infection cannot be dismissed and requires further future investigation.

Our data demonstrated that HIV-1 gp41 acts as a ligand for TLR10 and leads to the induction of IL-8 and NF-κBα activation. However, our observation is contradictory to some previous reports where TLR10 expression has been shown to suppress the cytokine responses (1, 52). These contradictions could be due to differences in cell-type use, ligand specificity or geographical location. Further, divergent roles of TLR10 have been suggested to be due to the mechanism of cross-talking between TLR10 and TLR3 (51) or perhaps the interaction of TLR10 with TLR2, TLR1 and TLR6 (1). Although, the exact mechanism is not known; we cannot exclude the possibility of spontaneous heterodimerization of TLR2 and TLR10 (1) due to HIV-1 gp41 which acts as a ligand for both TLR2 (16) and TLR10.

The present investigation demonstrated that TLR10 acts as an innate immune sensor for HIV-1 infection and leads to the induction of IL-8. Furthermore, we showed that blocking TLR10 with either an anti-TLR10 antibody or siRNA attenuates gp41-mediated NF-κBα activation (**Figure 8**). Interestingly, TLR1 depletion through siRNA knockdown also inhibited gp41-mediated NF-κB activation, suggesting that TLR1 and TLR10 might form a heterodimer. Recent evidence shows that TLR10 plays a key role in the innate immune response following an influenza infection (2). Specifically, it was found that silencing of the TLR10 gene impacted IL-8 production in human influenza virus-infected macrophages. Similarly, we observed that when TRL10 is silenced in HIV-1 infected macrophages, IL-8 production is severely impaired, thus raising the possibility that there is a conserved mechanism during HIV-1 and influenza virus infections in human macrophages.

Our studies have shown that human primary BM cells express significantly higher levels of TLR1, TLR2, and TLR10. Currently, the precise role of these TLRs in infants following BM ingestion remains unknown. However, in our other ongoing studies, we have identified some novel exosomal miRNAs in BM samples exclusive to HIV-1 infection present in mother's milk (data not shown) that could potentially play a protective role during MTCT of HIV-1 in conjunction with these TLRs.

Taken together, our data reveal for the first time that TLR10 is involved in HIV-1 infection. Furthermore, gp41 was found to act as a novel ligand for TLR10. We believe that the data shown in the present study describing an HIV-1 ligand for TLR10 will advance our current knowledge, as well as further our understanding of the role of TLR10 in innate immunity during HIV-1 infection.

MATERIALS AND METHODS

Human Subjects

HIV-1-uninfected (Hamilton, Ontario, Canada and Nigeria) and HIV-infected (Nigeria) women were recruited to participate in the present study. All HIV-infected women were in the chronic phase of infection as determined by at least two positive HIV-1 serological tests separated by at least 1 year. All women were sampled during voluntary "healthy" research visits as per the cohort protocol, and therefore, were not acutely ill at the time of assessment. Written as well as informed consent for the collection of demographics, behavioral data and biological samples were obtained from all study participants. Inclusion criteria included breastfeeding women who were HIV-uninfected and did not report complications *in utero* during their full-term pregnancies or intrapartum. Women were excluded if they had cesarean sections, their pregnancies were not full-term, or they were diagnosed with mastitis post-partum. Samples included in these analyses were obtained from women who were not taking medications other than vitamin supplements intra- or post-partum and did not receive an epidural intra-partum. Three mothers reported minor colic and one reported silent reflux in their infants. The study was approved by the institutional review boards of the University of Manitoba Hospital ethical review committee. All clinical investigations were conducted according to the principles of the Helsinki Declaration. The study was approved by the McMaster Research Ethics Board (REB Approval #08-176) and the CCI of Children's Hospital, Los Angeles.

Sample Acquisition and Preparation

Milk samples were self-collected into sterile tubes within the first week and at 1, 3, and 6 months post-partum, and immediately shipped on ice for processing in our laboratory. The samples were separated into lipid, supernatant, and cellular fractions and stored at −80°C and liquid nitrogen, respectively. BM supernatant fractions were used for Western blotting or were filter-sterilized (0.45 μm) for functional assays to avoid cellular contamination.

Cells and Reagents

THP-1 and primary BM cells were cultured in RMPI-1640 supplemented with 10% FBS, 2 mM L-glutamine, 10 mM HEPES, 1 mM Sodium Pyruvate, and 1% penicillin/streptomycin (Invitrogen). MCF-10A cells (American Type Culture Collection, Manassas, VA) were maintained in Dulbecco's modified Eagle's medium-F12 (DMEM/F12, Invitrogen) supplemented with 5% horse serum (Invitrogen), 100 ng/mL cholera toxin (Sigma), 10 μg/mL insulin (Sigma), 20 ng/mL recombinant human EGF (Peprotech), 0.5 μg/mL hydrocortisone (Sigma), and 1% penicillin/streptomycin (Invitrogen). The TZMbl cells were cultured in DMEM supplemented with 10% FBS and 1% (vol/vol) each of L-glutamine, penicillin, and streptomycin with and without 0.8 mg/mL geneticin (G418; Invitrogen, Burlington, ON, Canada), respectively, as described previously (16, 29). HIV-1 proteins included p17 (Virogen, Mississauga, ON, Canada), p24, and gp41 (Genway Biotech, Inc., San Diego, CA, USA). TLR ligands, ssRNA40 (Mobix, McMaster University), LPS, Pam3CSK4 (InvivoGen), and poly I:C (Sigma-Aldrich, Burlington, ON, Canada) were diluted in phosphate-buffered saline (PBS).

Quantitative Reverse-Transcriptase Real-Time Polymerase Chain Reaction

Total RNA was extracted from the cells using Trizol as per the manufacturer (Invitrogen, Carlsbad, California, USA) and treated with DNase I, DNA-free (Ambion, Austin, Texas, USA).

Reverse transcription (RT) reactions and quantitative real-time PCR (qRT-PCR) was performed as previously described (11).

Small Interfering RNA Knockdown

siRNA molecules targeting human TLR1 (Sigma-Aldrich, SASI_Hs01_00162170/AS), TLR2 (Sigma-Aldrich, SASI_Hs01_ 00081589/AS), TLR4 (Sigma-Aldrich, SASI_Hs01_00122250/AS), TLR10 (Sigma-Aldrich, SASI_Hs01_00099892), or non-targeting siRNA (Invitrogen, 129201 H07/129296 H05) were purchased and used as previously described (16). The cells were exposed to specific HIV-1 proteins, and the supernatants were collected to quantify the level of pro-inflammatory cytokine production as previously described (16).

Flow Cytometry

Flow cytometry analysis was performed as previously described (53). Briefly, 10 mL of fresh healthy human BM containing $\sim 5 \times 10^6$ cells collected within 3 months of lactation, was centrifuged at 2,000 × g at room temperature for 10 min, washed with PBS, and centrifuged two more times. The cells were first incubated with Live/Dead Fixable Aqua (ThermoFisher) at room temperature for 30 min and subsequently washed twice with PBS. Besides compensation and FMO controls, two sets of cells were immune-stained at room temperature for 30 min in 0.5% BSA-PBS containing a combination of conjugated antibodies (CD45-PerCP-Cy5.5 BD, CD14-V450 BD, MUC1-PE-Cy7 BioLegend, TLR2-APC R&D Systems, TLR10-PE BioLegend) and (CD45-PerCP-Cy5.5, CD14-V450, MUC1-PE-Cy7, TLR1-APC R&D Systems, TLR10-PE), respectively. The cells were washed twice with PBS and fixed with 1% PFA-PBS. The samples were run on a BD LSRFortessa and analyzed using FlowJo software.

Establishment of a Stable TLR10 Reporter Cell Line

The TLR10 expression plasmid, pIhT10G, was subcloned from pUNO1-hTLR10 (InvivoGen) into pIRES2-Green1 vector (Clontech), with a *Sac*I-*BamH*I fragment via PCR using Phusion DNA polymerase (New England Biolabs, USA). Transfection with 2.5 μg pIhT10G and 5 μL Lipofectamine 2,000 into TZMbl cells was performed in a six-well plate for 2 days. The cells were trypsinized and re-suspended in 0.2–1.4 mg/mL series of G418 geneticin (Thermo Fisher Scientific, MA, USA) containing growth medium in a 96-well plate, and cultured for at least 7 days, followed by repeating the selection for a total of three times in the same manner. The established cells were named TZMbl-10 and cultured in 0.2–0.4 mg/mL geneticin growth medium.

HIV-1 Infection and Integration

TZMbl and the derived TZMbl-2 and TZMbl-10 cells were transfected with plasmids, phT2G (16), phT10G, and pUNO1-hT1 (InvivoGen) expressing TLR10, TLR2, and TLR1, with PolyJet (SignaGen Rockville, MD, USA) in a 96-well plate for 24 h. The cells were infected with HIV-1 BAL 30-50 $TCID_{50}$/96-well plus 12 μg/mL DEAE-dextran for 45 h for HIV-1 infection. The proviral DNA analysis was performed by measuring the relative light units of luciferase activity for 8 h.

THP-1 cells grown in a 96-well plate were expanded in 8 mM PMA-growth medium for 3 days and PMA-free medium for another 2 days. The cells were then transfected with specific siRNAs using Lipofectamine RNAiMAX reagent (Thermo Fisher Scientific, MA, USA) for 2 days. The cells were infected with HIV-1 BAL 100 $TCID_{50}$/well plus 4 μg/mL polybrene overnight and washed with growth medium and cultured for a total of 7 days. HIV-1 integration was detected by the isolation of total cellular DNA using proteinase K digestion and phenol extraction, followed by PCR of the viral pol gene. The proviral DNA was normalized to the cellular 18S rRNA gene in a same sample.

IL-8 ELISA

IL-8 production from the cell culture was assessed via an EB ELISA in 20–100-fold dilution as per the manufacturer's instruction as described previously (16).

Stimulation of Primary BM Cells *in vitro* and Neutralization

Healthy BM was diluted 2-fold in PBS and the cells were isolated by centrifugation at 800 × g for 20 min. The lipid layer and fluid were removed, and the cell pellet was washed twice with PBS. The cells were resuspended in a 96-well plate at a density of 1.5×10^5 per well with RPMI-1640 medium and cultured overnight.

Since none of the available anti-TLR10 antibodies were able to efficiently neutralize TLR10 alone under our experimental conditions (data not shown), we used a cocktail of TLR10 antibodies from different sources comprising rabbit polyclonal sc-30198 (Santa Cruz Biotechnology, Santa Cruz, CA, USA), mouse monoclonal sc-293300 (Santa Cruz Biotechnology, Santa Cruz, CA, USA), mouse anti-human TLR10 H00081793-M01 (Novus Biologicals), and mouse monoclonal MA6619 (R&D Systems) compared to a cocktail control which consisted of rabbit and mouse isotype IgG controls (Santa Cruz Biotechnology, Santa Cruz, CA, USA).

Western Blot

The cells were washed with PBS and the lysates were prepared as previously described (16). Protein quantification was performed using a DC™ protein assay kit (Bio-Rad) and run on SDS-PAGE gels. The primary antibodies consisted of anti-TLR1, anti-TLR2 (R&D Systems), anti-TLR4 (Novus Biologicals), anti-TLR10 (Santa Cruz Biotechnology, Santa Cruz, CA, USA), phospho-IκBα #9246 (Cell Signaling), NF-κBα p65 sc-372 (Santa Cruz Biotechnology, Santa Cruz, CA, USA), and anti-β-actin antibodies. HRP-labeled goat anti-mouse IgG 1706516 (Bio-Rad) and HRP-labeled goat anti-rabbit IgG 1706515 (Bio-Rad) were used as secondary antibodies.

Confocal Microscopy

Immunofluorescence staining was performed as previously described (54). MCF-10A and THP1 cells grown on an eight-well BD Falcon culture slides (BD Biosciences) were either left untreated or treated with Pam3CSK4, or the HIV-1 proteins p17, p24, and gp41. The cells were fixed and immune-stained with NF-κBα p65 (1:500) to detect the nuclear translocation of NF-κBα p65. Corresponding Alexa Fluor 488 conjugated IgG (Molecular Probes, Eugene, OR, USA) was used as a secondary antibody. The images were acquired using an inverted laser-scanning confocal microscope (LSM 510, Zeiss, Oberkochen, Germany).

Statistical Analysis

The data were plotted and analyzed using Microsoft Excel, SPSS, and Prism 4.0 software and shown as Mean ± SEM (GraphPad Software, San Diego, California, USA). Non-parametric tests were used, including Mann-Whitney U-tests for unmatched comparisons, Wilcoxon paired *t*-tests for matched samples, and a Spearman's rank test for matched correlations.

DATA AVAILABILITY

All datasets generated for this study are included in the manuscript and/or the supplementary files.

AUTHOR CONTRIBUTIONS

BH, X-YD and MZ performed the experiments and wrote the manuscript. AA and SO performed clinical studies and collected the human samples. BH and KR conceived the idea. KR supervised the work, obtained the grant and wrote the manuscript.

ACKNOWLEDGMENTS

This work was supported by a grant from the Canadian Institute of Health Research (CIHR) as a part of the Canadian HIV-1 Vaccine Initiative (CHVI). We would like to thank the Canadian and Nigerian women who participated in our study.

SUPPLEMENTARY MATERIAL

The Supplementary Material for this article can be found online at: https://www.frontiersin.org/articles/10.3389/fimmu.2019.00482/full#supplementary-material

Supplementary Figure 1 | Confirmation of the siRNA mediated knockdown of TLR2, TLR10, TLR1, and TLR4 in THP-1 cells by Western blot. THP1 cells were either transfected with the specific siRNA targeting the respective TLRs or with a scrambled control. Lysates were prepared after 48 h and subjected to Western blot analysis using the indicated antibodies.

REFERENCES

1. Oosting M, Cheng S-C, Bolscher JM, Vestering-Stenger R, Plantinga TS, Verschueren IC, et al. Human TLR10 is an anti-inflammatory pattern-recognition receptor. *Proc Natl Acad Sci USA.* (2014) 111:E4478–84. doi: 10.1073/pnas.1410293111
2. Lee SMY, Kok K-H, Jaume M, Cheung TKW, Yip T-F, Lai JCC, et al. Toll-like receptor 10 is involved in induction of innate immune responses to influenza virus infection. *Proc Natl Acad Sci USA.* (2014) 111:3793–98. doi: 10.1073/pnas.1324266111
3. Guan Y, Ranoa DRE, Jiang S, Mutha SK, Li X, Baudry J, Tapping RI. Human TLRs 10 and 1 Share Common Mechanisms of Innate Immune Sensing but Not Signaling. *J Immunol.* (2010) 184:5094–103. doi: 10.4049/jimmunol.0901888
4. Chuang TH, Ulevitch RJ. Identification of hTLR10: a novel human toll-like receptor preferentially expressed in immune cells. *Biochim Biophys Acta.* (2001) 1518:157–61. doi: 10.1016/S0167-4781(00)00289-X
5. Hart KM, Murphy AJ, Barrett KT, Wira CR, Guyre PM, Pioli PA. Functional expression of pattern recognition receptors in tissues of the human female reproductive tract. *J Reprod Immunol.* (2009) 80:33–40. doi: 10.1016/j.jri.2008.12.004
6. Mohammed I, Abedin A, Tsintzas K, Abedin SA, Otri AM, Hopkinson A, et al. Increased expression of hepcidin and toll-like receptors 8 and 10 in viral keratitis. *Cornea.* (2011) 30:899–904. doi: 10.1097/ICO.0b013e31820126e5
7. Nagashima H, Iwatani S, Cruz M, Abreu JAJ, Uchida T, Mahachai V, et al. Toll-like receptor 10 in helicobacter pylori infection. *J Infect Dis.* (2015) 212:1666–76. doi: 10.1093/infdis/jiv270
8. Chougule P, Herlenius G, Hernandez NM, Patil PB, Xu B, Sumitran-Holgersson S. Isolation and characterization of human primary enterocytes from small intestine using a novel method. *Scand J Gastroenterol.* (2012) 47:1334–43. doi: 10.3109/00365521.2012.708940
9. Deeks SG. Immune dysfunction, inflammation, and accelerated aging in patients on antiretroviral therapy. *Top HIV Med.* (2008) 17:118–23. doi: 10.1109/ICASSP.2005.1416298
10. Lester RT, Yao XD, Ball TB, McKinnon LR, Omange WR, Kaul R, et al. HIV-1 RNA dysregulates the natural TLR response to subclinical endotoxemia in Kenyan female sex-workers. *PLoS ONE.* (2009) 4:e5644. doi: 10.1371/journal.pone.0005644
11. Lester RT, Yao XD, Ball TB, McKinnon LR, Kaul R, Wachihi C, ET AL. Toll-like receptor expression and responsiveness are increased in viraemic HIV-1 infection. *AIDS.* (2008) 22:685–94. doi: 10.1097/QAD.0b013e3282f4de35
12. Yao XD, Omange RW, Henrick BM, Lester RT, Kimani J, Ball TB, et al. Acting locally: innate mucosal immunity in resistance to HIV-1 infection in kenyan commercial sex workers. *Mucos Immun.* (2014) 7:268–79. doi: 10.1038/mi.2013.44
13. LeBouder E, Rey-Nores JE, Rushmere NK, Grigorov M, Lawn SD, Affolter M, et al. Soluble forms of Toll-Like Receptor (TLR)2 capable of modulating TLR2 signaling are present in human plasma and breast milk. *J Immunol.* (2003) 171:6680–9. doi: 10.4049/jimmunol.171.12.6680
14. Henrick BM, Nag K, Yao X-D, Drannik AG, Aldrovandi GM, Rosenthal KL. Milk matters: soluble Toll-Like Receptor 2 (sTLR2) in breast milk significantly inhibits HIV-1 infection and inflammation. *PLoS ONE.* (2012) 7:e40138. doi: 10.1371/journal.pone.0040138
15. Henrick BM, Yao XD, Drannik AG, Abimiku A, Rosenthal KL, INFANT Study Team. Soluble Toll-like receptor 2 is significantly elevated in HIV-1 infected breast milk and inhibits HIV-1 induced cellular activation, inflammation and infection. *AIDS.* (2014) 28:2023–32. doi: 10.1097/QAD.0000000000000381
16. Henrick BM, Yao XD, Rosenthal KL. HIV-1 structural proteins serve as PAMPs for TLR2 heterodimers significantly increasing infection and innate immune activation. *Front Immunol.* (2015) 6:426. doi: 10.3389/fimmu.2015.00426
17. Goldman AS. Human milk, leukocytes, and immunity. *J Pediatr.* (1977) 90:167–8. doi: 10.1016/S0022-3476(77)80805-6
18. Jain N, Mathur NB, Sharma VK, Dwarkadas AM. Cellular composition including lymphocyte subsets in preterm and full term human colostrum and milk. *Acta Paediatr Scand.* (1991) 80:395–9.
19. Michie CA, Tantscher E, Schall T, Rot A. Physiological secretion of chemokines in human breast milk. *Eur Cytokine Netw.* (1998) 9:123–9.
20. Dorosko SM, Connor RI. Primary human mammary epithelial cells endocytose HIV-1 and facilitate viral infection of CD4 $^+$ T lymphocytes. *J Virol.* (2010) 84:10533–42. doi: 10.1128/JVI.01263-10

21. Cacho NT, Lawrence RM. Innate immunity and breast milk. *Front Immunol.* (2017) 8:584. doi: 10.3389/fimmu.2017.00584
22. Satomi M, Shimizu M, Shinya E, Watari E, Owaki A, Hidaka C, et al. Transmission of macrophage-tropic HIV-1 by breast-milk macrophages via DC-SIGN. *J Infect Dis.* (2005) 191:174–81. doi: 10.1086/426829
23. Lohman-Payne B, Slyker JA, Moore S, Maleche-Obimbo E, Wamalwa DC, Richardson BA, et al. Breast milk cellular HIV-specific interferon gamma responses are associated with protection from peripartum HIV transmission. *AIDS.* (2012) 26:2007–16. doi: 10.1109/ICFHR.2014.121
24. Dalhatu I, Onotu D, Odafe S, Abiri O, Debem H, Agolory S, et al. Outcomes of Nigeria's HIV/AIDS treatment program for patients initiated on antiretroviral treatment between 2004-2012. *PLoS ONE.* (2016) 11:e0165528. doi: 10.1371/journal.pone.0165528
25. Sindhu S, Akhter N, Kochumon S, Thomas R, Wilson A, Shenouda S, et al. Increased expression of the innate immune receptor TLR10 in obesity and type-2 diabetes: association with ROS-mediated oxidative stress. *Cell Physiol Biochem.* (2018) 45:572–590. doi: 10.1159/000487034
26. Tsuchiya S, Yamabe M, Yamaguchi Y, Kobayashi Y, Konno T, Tada K. Establishment and characterization of a human acute monocytic leukemia cell line (THP-1). *Int J Cancer.* (1980) 26:171–6. doi: 10.1002/ijc.29102 60208
27. Bosshart H, Heinzelmann M. THP-1 cells as a model for human monocytes. *Ann Transl Med.* (2016) 4: 438. doi: 10.21037/atm.2016.08.53
28. Regan T, Nally K, Carmody R, Houston A, Shanahan F, MacSharry J, et al. Identification of TLR10 as a key mediator of the inflammatory response to listeria monocytogenes in intestinal epithelial cells and macrophages. *J Immunol.* (2013) 191:6084–92. doi: 10.4049/jimmunol.1203245
29. Nazli A, Dizzell S, Zahoor MA, Ferreira VH, Kafka J, Woods MW, et al. Interferon- β induced in female genital epithelium by HIV-1 glycoprotein 120 via toll-like-receptor 2 pathway acts to protect the mucosal barrier. *Cell Mol Immunol.* (2018) 16:178–94. doi: 10.1038/cmi.2017.168
30. Lalezari JP, Henry K, O'Hearn M, Montaner JSG, Piliero PJ, Trottier B, et al. Enfuvirtide, an HIV-1 fusion inhibitor, for drug-resistant HIV infection in North and South America. *N Engl J Med.* (2003) 348:2175–85. doi: 10.1056/NEJMoa035026
31. Ding X, Zhang X, Chong H, Zhu Y, Wei H, Wu X, et al. Enfuvirtide (T20)-based lipopeptide is a potent HIV-1 cell fusion inhibitor: implications for viral entry and inhibition. *J Virol.* (2017) 91:e00831-17. doi: 10.1128/JVI.00831-17
32. De Francesco MA, Baronio M, Fiorentini S, Signorini C, Bonfanti C, Poiesi C, et al. HIV-1 matrix protein p17 increases the production of proinflammatory cytokines and counteracts IL-4 activity by binding to a cellular receptor. *Proc Natl Acad Sci USA.* (2002) 99:9972–7. doi: 10.1073/pnas.142274699
33. De Francesco MA, Baronio M, Poiesi C. HIV-1 p17 matrix protein interacts with heparan sulfate side chain of CD44v3, syndecan-2, and syndecan-4 proteoglycans expressed on human activated CD4+ T cells affecting tumor necrosis factor α and interleukin 2 production. *J Biol Chem.* (2011) 286:19541–8. doi: 10.1074/jbc.M110.191270
34. De Francesco MA, Caruso A, Fallacara F, Canaris AD, Dima F, Poiesi C, et al. HIV p17 enhances lymphocyte proliferation and HIV-1 replication after binding to a human serum factor. *AIDS.* (1998) 12:245–52. doi: 10.1097/00002030-199803000-00001
35. Chirmule N, Pahwa S. Envelope glycoproteins of human immunodeficiency virus type 1: profound influences on immune functions. *Microbiol Rev.* (1996) 60:386–406.
36. Nazli A, Chan O, Dobson-Belaire WN, Ouellet M, Tremblay MJ, Gray-Owen SD, et al. Exposure to HIV-1 directly impairs mucosal epithelial barrier integrity allowing microbial translocation. *PLoS Pathog.* (2010) 6:e1000852. doi: 10.1371/journal.ppat.1000852
37. Caccuri F, Giagulli C, Bugatti A, Benetti A, Alessandri G, Ribatti D, et al. HIV-1 matrix protein p17 promotes angiogenesis via chemokine receptors CXCR1 and CXCR2. *Proc Natl Acad Sci USA.* (2012) 109:14580–5. doi: 10.1073/pnas.1206605109
38. Kawai T, Akira S. Antiviral signaling through pattern recognition receptors. *J Biochem.* (2007) 141:137–45. doi: 10.1093/jb/mvm032
39. Kawai T, Akira S. The role of pattern-recognition receptors in innate immunity: update on toll-like receptors. *Nat Immunol.* (2010) 11:373–84. doi: 10.1038/ni.1863
40. Hasan U, Chaffois C, Gaillard C, Saulnier V, Merck E, Tancredi S, et al. Human TLR10 is a functional receptor, expressed by B cellsand plasmacytoid dendritic cells, which activates gene transcription through MyD88. *J Immunol.* (2005) 174:2942–50. doi: 10.4049/jimmunol.174.5.2942
41. Mikacenic C, Reiner AP, Holden TD, Nickerson DA, Wurfel MM. Variation in the TLR10/TLR1/TLR6 locus is the major genetic determinant of interindividual difference in TLR1/2-mediated responses. *Genes Immun.* (2013) 14:52–7. doi: 10.1038/gene.2012.53
42. Loré K, Betts MR, Brenchley JM, Kuruppu J, Khojasteh S, Perfetto S, et al. Toll-like receptor ligands modulate dendritic cells to augment cytomegalovirus- and HIV-1-specific T cell responses 1. *J Immunol.* (2003) 171:4320–8. doi: 10.4049/jimmunol.171.8.4320
43. Hess NJ, Jiang S, Li X, Guan Y, Tapping RI. TLR10 is a B cell intrinsic suppressor of adaptive immune responses. *J Immunol.* (2017) 198:699–707. doi: 10.4049/jimmunol.1601335
44. Morgan AR, Lam WJ, Han DY, Fraser AG, Ferguson LR. Genetic variation within TLR10 is associated with Crohn's disease in a New Zealand population. *Hum Immunol.* (2012) 73:416–20. doi: 10.1016/j.humimm.2012.01.015
45. Lazarus R, Raby BA, Lange C, Silverman EK, Kwiatkowski DJ, Vercelli D, et al. TOLL-like receptor 10 genetic variation is associated with asthma in two independent samples. *Am J Respir Crit Care Med.* (2004) 170:594–600. doi: 10.1164/rccm.200404-491OC
46. Vrgoc G, Vrbanec J, Eftedal RK, Dembic PL, Balen S, Dembic Z, et al. Interleukin-17 and toll-like receptor 10 genetic polymorphisms and susceptibility to large joint osteoarthritis. *J Orthop Res.* (2018) 36:1684–93. doi: 10.1002/jor.23823
47. Kizildag S, Arslan S, Özbilüm N, Engin A, Bakir M. Effect of TLR10 (2322A/G, 720A/C, and 992T/A) polymorphisms on the pathogenesis of crimean congo hemorrhagic fever disease. *J Med Virol.* (2018) 90:19–25. doi: 10.1002/jmv.24924
48. Dannemann M, Andrés AM, Kelso J. Introgression of neandertal- and denisovan-like haplotypes contributes to adaptive variation in human toll-like receptors. *Am J Hum Genet.* (2016) 98:22–33. doi: 10.1016/j.ajhg.2015.11.015
49. Deschamps M, Laval G, Fagny M, Itan Y, Abel L, Casanova JL, et al. Genomic signatures of selective pressures and introgression from archaic hominins at human innate immunity genes. *Am J Hum Genet.* (2016) 98:5–21. doi: 10.1016/j.ajhg.2015.11.014
50. Laayouni H, Oosting M, Luisi P, Ioana M, Alonso S, Ricano-Ponce I, et al. Convergent evolution in european and rroma populations reveals pressure exerted by plague on toll-like receptors. *Proc Natl Acad Sci USA.* (2014) 111:2668–73. doi: 10.1073/pnas.1317723111
51. Lee SMY, Yip TF, Yan S, Jin DY, Wei HL, Guo RT, et al. Recognition of double-stranded RNA and regulation of interferon pathway by toll-like receptor 10. *Front Immunol.* (2018) 9:516. doi: 10.3389/fimmu.2018.00516
52. Jiang S, Li X, Hess NJ, Guan Y, Tapping RI. TLR10 is a negative regulator of both MyD88-dependent and-independent TLR signaling. *J Immunol.* (2016) 4:211. doi: 10.4049/jimmunol.1502599
53. Jiang JQ, Patrick A, Moss RB, Rosenthal KL. CD8+ T-cell-mediated cross-clade protection in the genital tract following intranasal immunization with inactivated human immunodeficiency virus antigen plus cpg oligodeoxynucleotides. *J Virol.* (2005) 79:393–400. doi: 10.1128/JVI.79.1.393-400.2005
54. Drannik AG, Nag K, Yao XD, Henrick BM, Ball TB, Plummer FA, et al. Anti-HIV-1 activity of elafin depends on its nuclear localization and altered innate immune activation in female genital epithelial cells. *PLoS ONE.* (2012) 7:e52738. doi: 10.1371/journal.pone.0052738

Conflict of Interest Statement: BH is an employee of Evolve Biosystems.

The remaining authors declare that the research was conducted in the absence of any commercial or financial relationships that could be construed as a potential conflict of interest.

frontiers in Immunology

REVIEW
published: 18 March 2019
doi: 10.3389/fimmu.2019.00465

Circulating LPS and (1→3)-β-D-Glucan: A Folie à Deux Contributing to HIV-Associated Immune Activation

Rayoun Ramendra[1,2,3], *Stéphane Isnard*[1,2], *Vikram Mehraj*[4], *Jun Chen*[1,2], *Yonglong Zhang*[5], *Malcolm Finkelman*[5] *and Jean-Pierre Routy*[1,2,6*]

[1] Chronic Viral Illness Service, McGill University Health Centre, Montreal, QC, Canada, [2] Infectious Diseases and Immunity in Global Health Program, Research Institute, McGill University Health Centre, Montreal, QC, Canada, [3] Department of Microbiology and Immunology, McGill University, Montreal, QC, Canada, [4] Centre de Recherche du Centre Hospitalier de l'Université de Montréal, Montreal, QC, Canada, [5] Associates of Cape Cod Inc., Falmouth, MA, United States, [6] Division of Hematology, McGill University Health Centre, Montreal, QC, Canada

Immune activation is the driving force behind the occurrence of AIDS and non-AIDS events, and is only partially reduced by antiretroviral therapy (ART). Soon after HIV infection, intestinal CD4+ T cells are depleted leading to epithelial gut damage and subsequent translocation of microbes and/or their products into systemic circulation. Bacteria and fungi are the two most abundant populations of the gut microbiome. Circulating lipopolysaccharide (LPS) and (1→3)-β-D-Glucan (βDG), major components of bacterial and fungal cell walls respectively, are measured as markers of microbial translocation in the context of compromised gut barriers. While LPS is a well-known inducer of innate immune activation, βDG is emerging as a significant source of monocyte and NK cell activation that contributes to immune dysfunction. Herein, we critically evaluated recent literature to untangle the respective roles of LPS and βDG in HIV-associated immune dysfunction. Furthermore, we appraised the relevance of LPS and βDG as biomarkers of disease progression and immune activation on ART. Understanding the consequences of elevated LPS and βDG on immune activation will provide insight into novel therapeutic strategies against the occurrence of AIDS and non-AIDS events.

Keywords: HIV, LPS, (1→3)-β-D-Glucan, immune activation, microbial translocation, antiretroviral therapy, non-AIDS events

OPEN ACCESS

Edited by:
Sara Gianella Weibel, University of California, San Diego, United States

Reviewed by:
Nicholas Funderburg, The Ohio State University, United States
Cristian Apetrei, University of Pittsburgh, United States

***Correspondence:**
Jean-Pierre Routy
jean-pierre.routy@mcgill.ca

Specialty section:
This article was submitted to Viral Immunology, a section of the journal Frontiers in Immunology

Received: *30 November 2018*
Accepted: *21 February 2019*
Published: *18 March 2019*

Citation:
Ramendra R, Isnard S, Mehraj V, Chen J, Zhang Y, Finkelman M and Routy J-P (2019) Circulating LPS and (1→3)-β-D-Glucan: A Folie à Deux Contributing to HIV-Associated Immune Activation. Front. Immunol. 10:465. doi: 10.3389/fimmu.2019.00465

INTRODUCTION

The gastrointestinal tract (GI) is a dynamic setting constantly in contact with nutrients, allergens, commensal microbes, and pathogens. As such, this milieu is equipped with a complex and well balanced system of physical and immunological barriers to allow the absorption of nutrients while preventing the translocation of microbes and their products (1). A physical barrier is formed by firmly linked intestinal epithelial cells (enterocytes) connected via tight junctions. These cells form villi to maximize the absorption of nutrients. The base of each villus forms crypts composed of intestinal stem cells and Paneth cells which secrete growth factors that promote intestinal stem cell proliferation, antimicrobial peptide secretion, and digestive enzyme production (2, 3). In the

upper regions of the villus, goblet cells contribute to the physical and chemical barriers by secreting a mucous layer that protects the gut epithelium from the microbiota (4). Patrolling leukocytes in the lamina propria constitute an immunological barrier that ensures any pathogens in the lamina propria are phagocytosed, cleared, and sent to the draining mesenteric lymph nodes (5).

HIV-infection is characterized by the depletion of gut CD4+ T cells, epithelial gut damage, and translocation of microbes and their products into systemic circulation (6). People living with HIV (PLWH) have damage to the gut epithelium which has been shown to precede immune activation in models of SIV-infected rhesus macaques (7, 8). As systemic immune activation is considered the driving force of CD4+ T cell depletion and development of acquired immunodeficiency syndrome (AIDS), it is important to understand the link between epithelial gut damage and systemic immune activation in PLWH.

In 2006, Brenchley et al. were the first to report that increased plasma levels of gram-negative bacterial cell wall antigen lipopolysaccharide (LPS) induces systemic immune activation in both PLWH and SIV-infected rhesus macaques (9). Estes et al. in 2010, demonstrated that elevated plasma levels of LPS in PLWH is a result of HIV-induced epithelial gut damage allowing for the translocation of microbial products from the gut microbiota into systemic circulation (10). Despite the success of antiretroviral therapy (ART), epithelial gut damage, microbial translocation, and to a lesser extent systemic immune activation are not reversed. In parallel, Cani et al. coined the term "metabolic endotoxemia" to describe the phenomenon of obese individuals with high plasma levels of LPS linked to reduced insulin sensitivity and increased risk of metabolic diseases (11). Furthermore, conserved parts of the LPS molecule act as a pathogen-associated molecular patterns (PAMPs) that have been associated *in vitro*, in animal models, and epidemiologically with increased innate immune activation, inflammation, and risk of developing non-AIDS events in ART-treated PLWH (9, 12).

Increasing awareness about the human gut microbiota reveals that it is a complex community of bacteria, fungi, archaea, viruses, and parasites influencing health and disease (13). However, studies regarding microbial translocation in PLWH have primarily focused on bacterial translocation. (1→3)-β-D-Glucan (βDG), a major component of most fungal cell walls, is commonly used as a biomarker for the diagnosis and management of invasive fungal infections (IFI) and has been recently used as a marker of fungal translocation in people without IFI (14). In 2012, Morris et al. were the first to show elevated plasma levels of βDG in PLWH (15). We and others have found that plasma levels of βDG are associated with epithelial gut damage, immune activation, inflammation, and risk of developing non-AIDS events (16–20). Like epithelial gut damage, plasma levels of βDG do not normalize despite long-term ART (20). These findings show converging evidence that like LPS, βDG also plays a significant role in chronic immune activation and development of non-AIDS events in PLWH (**Figure 1**).

Currently, persistence of systemic immune activation and development of non-AIDS events despite long-term ART represents one of the hurdles in caring for PLWH (21). Herein, we look to comprehensively review the existing English literature regarding the contribution of circulating LPS and βDG in systemic immune activation in PLWH. Understanding the consequences of LPS and βDG antigenemia will help with the development of therapeutic strategies against this "folie à deux."

GUT DAMAGE

In homeostatic conditions, the microbiota is contained within the gut by the mucous layer, epithelial barrier, and residential leukocytes (22–25).

HIV infection leads to early disruption of the gut epithelial barrier characterized by villous atrophy, crypt hyperplasia, increased gastrointestinal inflammation, and increased intestinal permeability (7, 26–28). Such damage is not completely restored despite long-term ART. Deterioration of the gastrointestinal landscape in PLWH and SIV-infected rhesus macaques has been shown to cause microbial translocation and resultant immune activation (9, 10, 29). Interestingly, SIV-infected sooty mangabeys, which do not progress to AIDS, present without disruption of the GI epithelial layer nor increased microbial translocation, and limited immune activation (30, 31). Thus, understanding the cause(s) and implications of epithelial gut damage in PLWH may help to understand the source(s) of systemic immune activation.

The precise mechanisms responsible for HIV-associated epithelial gut damage remain poorly understood and are now known to precede mucosal immune dysfunction (7). HIV gp120 and Tat proteins have been shown to have detrimental effects on intestinal epithelial cells (32–36). HIV induces inflammasome to produce IL-18, resulting in intestinal epithelial cell death and reduced expression of tight junction proteins, contributing to intestinal permeability and resultant microbial translocation (37, 38). Globally, HIV contributes to epithelial gut damage which is partially improved on ART (39, 40). Markers of epithelial gut damage such as soluble suppressor of tumorigenicity 2 (sST2) and intestinal fatty acid binding protein (I-FABP) have been reported to be elevated in inflammatory bowel diseases, graft vs. host disease, and HIV (41, 42).

As reported by Hensley-McBain et al., alterations to the intestinal epithelial structure precede mucosal immune dysfunction (7). Early mucosal damage in PLWH is partially explained by a substantially high expression of CCR5, a HIV co-receptor, on CD4+ T cells in the gut as compared to peripheral blood (43, 44). This is in line with findings that HIV is 10 times more likely to infect CD4+ T cells in the gut compared to peripheral blood (45). IL-17 producing cells, such as Th17 and Th22 CD4+ T cells, are known to homeostatically maintain the epithelial barrier (7). We and others have reported alterations of the Th17/Treg ratio in PLWH, owing to increased frequency of Tregs and decreased frequency of Th17 CD4+ T cells (46, 47). This in turn impairs the homeostatic response to prevent and restore epithelial gut damage in PLWH. HIV-associated gastrointestinal abnormalities have also been associated with changes in the composition of the gut microbiome (dysbiosis) and translocation of microbial products in PLWH.

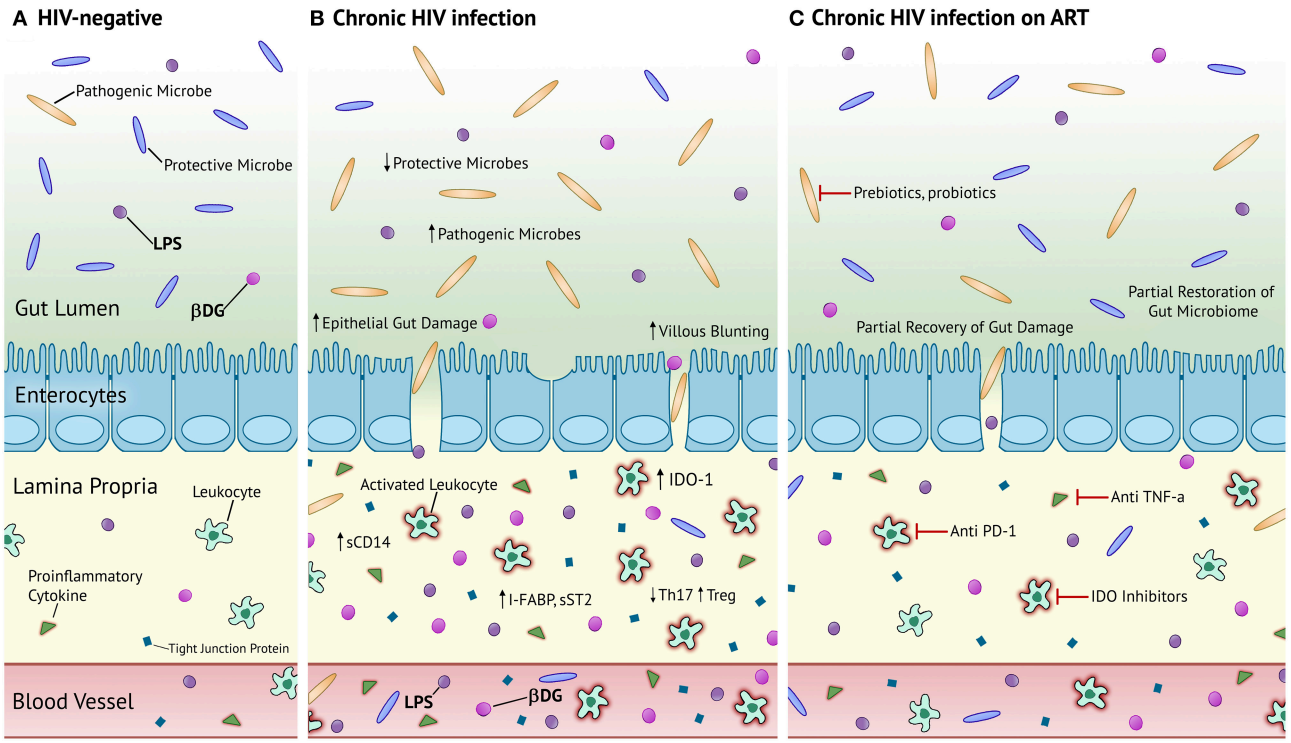

FIGURE 1 | Proposed mechanism of microbial translocation in chronic HIV-infection and chronic HIV-infection on ART compared to HIV- homeostasis. **(A)** Healthy, HIV-uninfected individuals have an abundance of protective microbes in the gut and tight junctions connecting enterocytes to prevent the translocation of gut microbes and their products. Patrolling leukocytes in the lamina propria are not activated and there is an almost negligible level of inflammation and epithelial damage. **(B)** PLWH in the chronic stage of infection have increased proportions of pathogenic microbes and decreased proportions of protective microbes in the gut. There is severe villous blunting, epithelial gut damage, and microbial translocation. Patrolling leukocytes are activated and secrete large quantities of pro-inflammatory cytokines. There is elevated circulation of markers of epithelial gut damage, microbial translocation, and inflammation. **(C)** PLWH on long-term ART have partially restored composition of the gut microbiota, epithelial gut damage, and reduced microbial translocation. Activated leukocytes and systemic inflammation persists. Prebiotics and probiotics are potential therapeutic strategies to fully recover the composition of the gut microbiota. Anti PD-1, anti TNF-α, and IDO inhibitors represent potential therapeutic strategies against persistent immune activation and inflammation. LPS, lipopolysaccharide; βDG, (1→3)-β-D-Glucan; sCD14, soluble cluster of differentiation 14; I-FABP, intestinal fatty acid binding protein; sST2, soluble suppressor of tumorigenicity 2; IDO-1, indoleamine-2,3-dioxygenase 1.

BACTERIAL AND FUNGAL TRANSLOCATION

In homeostatic conditions, microbial translocation is limited by physical and immunological barriers in the intestine (48). However, when the gut epithelium is damaged and the mucosal immune system is compromised, microbial products translocate out of the gut into systemic circulation via the lamina propria (49, 50). Microbial translocation has been implicated in several conditions including Crohn's disease, ulcerative colitis, graft-vs.-host disease, and HIV (40).

SIV-infected rhesus macaques were shown to have elevated plasma levels of LPS that could be partially reversed with antibiotics. Immunohistochemistry and immunofluorescence of gut biopsies demonstrated that such elevation was a result of bacterial translocation from the gut lumen into systemic circulation via the lamina propria (9, 10). Interestingly, SIV-infected African green monkeys, a natural host of SIV, receiving intravenous injection of LPS had increased viral replication, mucosal CD4+ T cell depletion, and systemic immune activation without inducing epithelial gut damage (51, 52). Altogether, this suggests that translocation of microbial products plays a major role in systemic immune activation and inflammation.

We and others have shown elevation of microbial products in the blood of PLWH (9, 15, 46). Most published studies measured microbial translocation using plasma levels of bacterial DNA fragments, LPS, LPS binding protein (LBP), soluble CD14 (sCD14), and EndoCab (50). Bacterial DNA fragments were quantified using 16S rDNA PCR. Most studies in PLWH use the Limulus Amebocyte Lysate (LAL) assay to measure plasma levels of LPS, a major component of the outer membrane of gram-negative bacteria. LPS binds to LBP, which transfers LPS onto monocytes/macrophages causing the release of soluble CD14 (sCD14) (53). EndoCab is a group of antibodies specific for the core of LPS that are produced by B cells in response to enteric gram-negative bacteria (54). LBP, sCD14, and EndoCab are commonly measured in plasma/serum using solid-phase enzyme-linked immunosorbent assay (ELISA)

as circulating biomarkers of LPS-induced innate immune activation (9, 39).

Most research on microbial translocation in PLWH has been focused on bacterial translocation (13). Morris et al. were the first to show elevation of circulating levels of fungal cell wall antigen, βDG, in PLWH (15). Hoenigl et al. have shown that plasma βDG is inversely correlated with the abundance of *Lactobacilli* in the distal gut (19). *Lactobacillus* is a protective genus of bacteria that is inversely associated with gut integrity and distal gut permeability. Furthermore, we have shown that plasma levels of βDG is strongly correlated with classical marker of epithelial gut damage, I-FABP, and markers of microbial translocation LPS and sCD14 (20) (**Table 1**). The origin of circulating βDG was first studied in murine models. As opposed to the human gut microbiome, there is no *Candida* in the murine gut. Mice fed with live or heat-inactivated *Candida* had elevated serum levels of βDG. Such elevation induced the production of pro-inflammatory cytokines IL-6 and TNF-α. Administration of Fluconazole, an anti-fungal small molecule, partially inhibited the elevation of serum βDG and systemic inflammation (55). Similar results were found in a murine model of lupus and sepsis (56, 57). As PLWH without invasive fungal infections are highly susceptible to increased proportions of fungal colonization and have high levels of epithelial gut damage, it is highly likely that elevated plasma levels of βDG in PLWH originates from the gut (14). Thus, there is a need to definitely determine whether elevated plasma levels of βDG in PLWH is a result of microbial translocation and involved in systemic immune activation.

MICROBIAL TRANSLOCATION AND SYSTEMIC IMMUNE ACTIVATION

Microbial products such as LPS and βDG represent potent PAMPs that trigger a significant immune response. Several studies have provided convincing evidence that elevated plasma levels of LPS induces immune activation in sepsis, Crohn's disease, ulcerative colitis, obesity, and HIV (9, 11, 58, 59).

LPS is captured by LBP and complexed with CD14, myeloid differentiation 2 protein, and Toll like receptor 4 (TLR4). The formation of this complex is crucial for the immune system to mount a response to LPS. Classical antigen presenting cells (APCs) recognize this complex using TLR4 and subsequently phagocytose LPS while shedding sCD14. B cells also express TLR4 to recognize different parts of the LPS core lipids and secrete EndoCAb to facilitate the phagocytosis of the antigen (60). LPS has been shown to induce the secretion of several pro-inflammatory cytokines including IL-6, IL-8, and TNF-α by APCs (61). Plasma levels of LPS correlated with plasma levels of IFN-α and frequency of activated CD4+ and CD8+ T cells in PLWH (9). Similarly, plasma levels of sCD14 correlated with plasma levels of IL-6 and C reactive protein in PLWH (62).

Meanwhile, βDG is predominantly recognized by complement receptor 3 (CR3), Dectin-1, NKp30, Ephrin type-A receptor 2 (EphA2), and Langerin. CR3 is a ubiquitous heterodimer receptor composed of CD11b and CD18. Recent findings have shown reduced expression of CR3 on both myeloid and plasmacytoid dendritic cells (DC) in PLWH. βDG-specific interactions with CR3 on DC have been shown to increase IL-6 and TNF-α production by activating the Syk-JNK-AP-1 pathway (63). Dectin-1 represents the most prominent myeloid cell receptor for βDG and is expressed on monocytes, macrophages, DCs, and neutrophils (63–65). We have shown that Dectin-1 expression on monocytes is reduced in PLWH and that such expression is inversely correlated with plasma levels of βDG but not LPS (20). βDG-specific binding to Dectin-1 leads to the production of pro-inflammatory cytokines IL-6, IL-8, and TNF-α by myeloid cells (66, 67). βDG is also specifically recognized by NK cells via NKp30, a functional activation receptor (68). In addition, we have shown that NKp30 expression is diminished in PLWH and inversely correlated with plasma levels of βDG but not LPS (20, 69). NKp30-specific binding has been shown to induce activation and the production of pro-inflammatory cytokines such as IL-1β and TNF-α (70, 71). EphA2 is a βDG-specific receptor expressed on epithelial cells, predominantly in the colon and small intestine, that has yet to be measured in PLWH (72). Interestingly, EphA2 has also been identified as a receptor for Kaposi Sarcoma associated herpes virus (also called HHV8), one of the most common HIV-associated co-infections (73). DCs play an important role in maintaining mucosal homeostasis. In the mucosa, they can be distinguished according to their expression of C-type lectins: Langerin [expressed by Langerhans cells (LCs)] and DC-SIGN (expressed by classical DCs). LCs reside in the epithelium of most mucosal surfaces and are thus one of the first APCs to encounter HIV as well as products of microbial translocation. Langerin has been shown to be an important receptor for βDG during *Candida* and *Saccharomyces* infections that has yet to be assessed in PLWH without IFI (74). βDG induces the secretion of pro-inflammatory cytokines IL-1β, IL-6, IL-8, IL-23, TNF-α, and chemokine CCL22 that has been shown to increase monocyte recruitment to the colon (66, 75, 76). Indeed, we and others have shown that elevated plasma levels of βDG is correlated with plasma levels of IL-6 and IL-8 in PLWH (15, 20).

Microbial translocation in PLWH is associated with Indoleamine-2,3-deoxygenase-1 (IDO-1) activity and HIV disease progression (77). IDO-1 is expressed in all myeloid cells and activated after PAMPs recognition to metabolize Tryptophan into Kynurenines (78). As such, IDO-1 activity is considered a marker of inflammation and immune activation. We and others have shown that IDO-1 activity is increased in PLWH and does not normalize with early ART. In PLWH, IDO-1 activity is associated with plasma levels of LPS and βDG, increased frequency of Tregs, epithelial gut damage, microbial translocation, immune activation, and HIV reservoir size (20, 46, 79, 80).

Persistent epithelial gut damage and elevated plasma levels of LPS and βDG, despite long-term ART, likely contribute to inflammation and chronic immune activation leading to the development of non-AIDS events in PLWH. In the ART-era, the development of non-AIDS events represents one of the challenges to caring for PLWH. Therefore, both LPS and βDG represent important therapeutic targets to reduce the risk of developing non-AIDS events.

TABLE 1 | Overview of studies associating elevation of plasma levels of βDG with immune activation and immune dysfunction in PLWH.

References (country)	Sample size	Study populations	Major findings
Morris et al. (15) (USA)	132	Chronic ART-treated PLWH; cross-sectional analysis	βDG was elevated in the plasma of PLWH and associated with plasma levels of IL-8, TNF-α, and frequency of CD38+ and HLA-DR+ CD8+ T cells. Elevated βDG was associated with cardiopulmonary dysfunction.
Hoenigl et al. (17) (USA)	41	Chronic ART-treated PLWH; cross-sectional analysis	Plasma level of βDG was positively associated with plasma levels of neopterin and IL-6.
Hoenigl et al. (19) (USA)	11	PLWH in early stage of infection, before and after ART; cross-sectional analysis	Elevated plasma levels of βDG was inversely correlated with abundance of *Lactobacillales* in the distal gut.
Hoenigl et al. (16) (USA)	21	Chronic ART-treated PLWH; cross-sectional analysis	βDG was elevated in the plasma and CSF of PLWH and positively associated with neurocognitive dysfunction.
Hoenigl et al. (18) (USA)	451	PLWH before and after ART; cross-sectional analysis	Multivariate analysis showed that pre-event plasma levels of βDG and LBP was independently associated with increased risk of non-AIDS events.
Mehraj et al. (20) (Canada)	146	PLWH in early and chronic stages, ART-treated and untreated; longitudinal and cross sectional analysis	Plasma levels of βDG was associated with plasma viral load, I-FABP, LPS, markers of IDO-1 metabolism, and frequency of Tregs. Expression of βDG-specific receptors, Dectin-1 and NKp30, was inversely correlated with plasma levels of βDG but not LPS. PLWH who initiated ART early had lower levels of plasma βDG and elevated βDG did not normalize despite long-term ART.

PLWH, People living with HIV; ART, Antiretroviral Therapy; βDG, (1→3)-β-D-Glucan; LPS, Lipopolysaccharide; LBP, LPS Binding Protein; I-FABP, Intestinal Fatty Acid Binding Protein (marker of epithelial gut damage).

MICROBIAL TRANSLOCATION, INFLAMMATION, AND NON-AIDS EVENTS

Despite the significant success of ART, PLWH still present with high rates of non-AIDS events that includes HIV-associated neurocognitive disorders (HANDs), cardiovascular diseases, renal failure, liver steatosis, and cancer (81, 82). Such non-AIDS events have been associated with epithelial gut damage, microbial translocation, and systemic immune activation (50). Hoenigl et al. have observed in a large cohort of ART-treated PLWH that in addition to soluble urokinase-type plasminogen receptor, plasma levels of βDG, and LBP represent two of the best predictors of increased risk of non-AIDS events (18).

Microbial Translocation and HAND

PLWH present with HANDs including asymptomatic neurocognitive impairment, mild neurocognitive disorder, and dementia (83, 84). Previous studies have found strong associations between plasma levels of sCD14, LPS, and βDG with neurocognitive dysfunction (16, 85). Moreover, ART-treated PLWH with severe neurocognitive dysfunction also presented with elevated sCD14 and βDG in their cerebrospinal fluid (CSF) (16). Supporting the concept of the gut-brain axis, increased microbial translocation likely plays a crucial role in the development of HANDs.

Microbial Translocation and Cardiovascular Diseases

A study with more than 27,000 participants showed that PLWH had a two-fold increased risk of developing acute myocardial infarction in every age group compared to matched control participants (86, 87). Elevated circulation of microbial products and resultant inflammation are associated with increased risk of heart disease (88). Plasma levels of LPS have been associated with known risk factors for cardiovascular diseases such as decreased insulin sensitivity and higher total cholesterol (11). Similarly, elevated plasma levels of βDG have also been associated with cardiopulmonary dysfunction (15).

CONCLUSIONS AND FUTURE DIRECTIONS

Due to the success of ART, the life expectancy and quality of life of PLWH has dramatically improved over the course of the last decade. While early initiation of ART is associated with lower reservoir size and reduced immune activation, PLWH on ART still suffer from unrecovered epithelial gut damage and chronic immune activation (89). It has been recently reported that epithelial gut damage precedes systemic immune activation in a SIV-infected rhesus macaque model (7). Like epithelial gut damage and systemic immune activation, markers of microbial translocation do not normalize despite long-term ART (20). Thus, understanding the mechanisms via which epithelial gut damage and resultant microbial translocation contribute to chronic immune activation is essential toward improving the prognosis of PLWH.

Circulating microbial polysaccharides LPS and βDG are elevated in PLWH (9, 15). Previous research on microbial translocation in PLWH and SIV-infected rhesus macaques has been primarily measured by plasma levels of LPS using the LAL assay. Of note, it has been initially found that LPS measured by the LAL assay also measures βDG (90). While it has been shown that increased plasma levels of LPS are a result of microbial translocation in PLWH, the source of circulating βDG remains to be clarified. Consumption of certain mushrooms,

oat fiber, and seaweed can also increase circulating levels of βDG (91). We and others have shown that plasma levels of βDG are positively associated with marker of epithelial gut damage I-FABP and inversely associated with the abundance of protective bacteria, *Lactobacillales*, in the distal gut (19, 20). Furthermore, murine models have shown that mice fed with heat-killed or live *Candida* have increased levels of circulating βDG after cecal ligation and puncture (55). Similarly, people with intestine disorders have increased plasma levels of βDG (56, 92, 93). Hence, there is converging evidence suggesting that elevated plasma levels of βDG in PLWH are a result of increased *Candida* or other fungal colonization, epithelial gut damage, and subsequent microbial translocation.

Both LPS and βDG have been associated with markers of systemic immune activation, inflammation, and the development of non-AIDS events. As such, the individual and potentially synergistic consequences of elevated plasma levels of LPS and βDG on systemic immune activation must be urgently addressed.

Understanding the respective mechanisms by which these two microbial polysaccharides contribute to chronic immune activation may lead to the development of novel therapeutic strategies against inflammation and the development of non-AIDS events in PLWH. Moreover, genetic factors may play a key role in determining the influence of these PAMPs on systemic immune activation. For example, people with CARD9 deficiencies have been shown to have increased susceptibility to fungal infections (94). Furthermore, Palesch et al. demonstrated that sooty mangabeys, a natural host of SIV, had a frameshift mutation in their TLR4 gene that was associated with a blunted response to TLR4 ligands *in vitro* (95). Thus, regular genetic variations in receptors for LPS and βDG may also play a pivotal role in determining the consequences of microbial translocation in PLWH.

In 2014, Kristoff et al. gave Sevelamer, a drug known to decrease circulating LPS (96), to SIV-infected pigtailed macaques. A single dose administration led to partially decreased HIV viral replication, decreased circulation of coagulation markers, and decreased immune activation/inflammation (52). However, when Sandler et al. gave Sevelamer to 36 ART-naïve PLWH, they did not observe a decrease in plasma levels of LPS (measured by LAL assay) nor markers of immune activation/inflammation (97). Future clinical trials should aim to reduce the burden of elevated circulation of products of both bacterial and fungal translocation. While therapeutic strategies targeting elevated circulation of PAMPs should be investigated, future studies should also look to target immune signaling molecules (such as TLR4 and Dectin-1) to reduce LPS and βDG induced systemic immune activation.

Overall, elevated plasma levels of LPS and βDG both play an important role in chronic immune activation in PLWH on long-term ART and may represent a "folie à deux" contributing to the development of non-AIDS events. To this end, gaining a comprehensive understanding of the origin and consequences of these circulating microbial polysaccharides is of critical importance to finding therapeutic strategies to restore mucosal homeostasis, and gut dysbiosis in PLWH.

AUTHOR CONTRIBUTIONS

RR made the first draft, constructed the figure and table, and made revisions to the final draft of the manuscript. RR and SI contributed significantly to conducting the literature review. VM, JC, YZ, and MF critically read and revised the manuscript. J-PR designed the review and critically revised the manuscript.

FUNDING

This study was supported by the Fonds de recherche du Québec—Santé (FRQ-S): Réseau SIDA/Maladies infectieuses and Thérapie cellulaire, the Canadian Institute of Health Research (CIHR grants MOP 103230 and 154051), the Vaccines & Immunotherapies Core of the CIHR Canadian HIV Trials Network (CTN): grant CTN 257, the Canadian Foundation for AIDS Research (CANFAR) grant 02-512, and the Canadian HIV Cure Enterprise Team Grant (HIG-133050) awarded by the CIHR in partnership with CANFAR. RR is an undergraduate student supported by the H. Grenville Smith Studentship, SI is a post-doctoral fellow supported by the William Turner research fellowship, J-PR is the holder of the Louis Lowenstein Chair in Hematology and Oncology at McGill University.

ACKNOWLEDGMENTS

The authors are grateful to study participants for their contribution. We thank Angie Massicotte and Josée Girouard for administrative assistance.

REFERENCES

1. Perez-Lopez A, Behnsen J, Nuccio SP, Raffatellu M. Mucosal immunity to pathogenic intestinal bacteria. *Nat Rev Immunol.* (2016) 16:135–48. doi: 10.1038/nri.2015.17
2. Ouellette AJ. Paneth cells and innate mucosal immunity. *Curr Opin Gastroenterol.* (2010) 26:547–53. doi: 10.1097/MOG.0b013e32833dccde
3. Bry L, Falk P, Huttner K, Ouellette A, Midtvedt T, Gordon JI. Paneth cell differentiation in the developing intestine of normal and transgenic mice. *Proc Natl Acad Sci USA.* (1994) 91:10335–9. doi: 10.1073/pnas.91.22.10335
4. Birchenough GM, Johansson ME, Gustafsson JK, Bergstrom JH, Hansson GC. New developments in goblet cell mucus secretion and function. *Mucosal Immunol.* (2015) 8:712–9. doi: 10.1038/mi.2015.32
5. Luissint AC, Parkos CA, Nusrat A. Inflammation and the intestinal barrier: leukocyte-epithelial cell interactions, cell junction remodeling, and mucosal repair. *Gastroenterology.* (2016) 151:616–32. doi: 10.1053/j.gastro.2016.07.008
6. Ghosn J, Taiwo B, Seedat S, Autran B, Katlama C. HIV. *Lancet.* (2018) 392:685–97. doi: 10.1016/S0140-6736(18)31311-4
7. Hensley-McBain T, Berard AR, Manuzak JA, Miller CJ, Zevin AS, Polacino P, et al. Intestinal damage precedes mucosal immune dysfunction in SIV infection. *Mucosal Immunol.* (2018) 11:1429–40. doi: 10.1038/s41385-018-0032-5
8. Brenchley JM, Douek DC. Microbial translocation across the GI tract. *Annu Rev Immunol.* (2012) 30:149–73. doi: 10.1146/annurev-immunol-020711-075001

9. Brenchley JM, Price DA, Schacker TW, Asher TE, Silvestri G, Rao S, et al. Microbial translocation is a cause of systemic immune activation in chronic HIV infection. *Nat Med.* (2006) 12:1365–71. doi: 10.1038/nm1511
10. Estes JD, Harris LD, Klatt NR, Tabb B, Pittaluga S, Paiardini M, et al. Damaged intestinal epithelial integrity linked to microbial translocation in pathogenic simian immunodeficiency virus infections. *PLoS Pathog.* (2010) 6:e1001052. doi: 10.1371/journal.ppat.1001052
11. Cani PD, Amar J, Iglesias MA, Poggi M, Knauf C, Bastelica D, et al. Metabolic endotoxemia initiates obesity and insulin resistance. *Diabetes.* (2007) 56:1761–72. doi: 10.2337/db06-1491
12. Baker JV, Peng G, Rapkin J, Abrams DI, Silverberg MJ, MacArthur RD, et al. Community programs for clinical research on, CD4+ count and risk of non-AIDS diseases following initial treatment for HIV infection. *AIDS.* (2008) 22:841–8. doi: 10.1097/QAD.0b013e3282f7cb76
13. Mirzaei MK, Maurice CF. Menage a trois in the human gut: interactions between host, bacteria and phages. *Nat Rev Microbiol.* (2017) 15:397–408. doi: 10.1038/nrmicro.2017.30
14. Farhour Z, Mehraj V, Chen J, Ramendra R, Lu H, Routy JP. Use of (1–>3)-beta-D-Glucan for diagnosis and management of invasive mycoses in HIV-infected patients. *Mycoses.* (2018) 61:718–22. doi: 10.1111/myc.12797
15. Morris A, Hillenbrand M, Finkelman M, George MP, Singh V, Kessinger C, et al. Serum (1–>3)-beta-D-glucan levels in HIV-infected individuals are associated with immunosuppression, inflammation, and cardiopulmonary function. *J Acquir Immune Defic Syndr.* (2012) 61:462–8. doi: 10.1097/QAI.0b013e318271799b
16. Hoenigl M, de Oliveira MF, Perez-Santiago J, Zhang Y, Morris S, McCutchan AJ, et al. (1–>3)-beta-D-glucan levels correlate with neurocognitive functioning in HIV-infected persons on suppressive antiretroviral therapy: a cohort study. *Medicine.* (2016) 95:e3162. doi: 10.1097/MD.0000000000003162
17. Hoenigl M, de Oliveira MF, Perez-Santiago J, Zhang Y, Woods SP, Finkelman M, et al. Correlation of (1–>3)-beta-D-glucan with other inflammation markers in chronically HIV infected persons on suppressive antiretroviral therapy. *GMS Infect Dis.* (2015) 3:Doc3. doi: 10.3205/id000018
18. Hoenigl M, Moser C, Funderburg N, Bosch R, Kantor A, Zhang Y, et al. Soluble urokinase plasminogen activator receptor (suPAR) is predictive of non-AIDS events during antiretroviral therapy-mediated viral suppression. *Clin Infect Dis.* (2018). doi: 10.1093/cid/ciy966. [Epub ahead of print].
19. Hoenigl M, Perez-Santiago J, Nakazawa M, de Oliveira MF, Zhang Y, Finkelman MA, et al. (1–>3)-beta-d-Glucan: a biomarker for microbial translocation in individuals with acute or early HIV infection? *Front Immunol.* (2016) 7:404. doi: 10.3389/fimmu.2016.00404
20. Mehraj V, Ramendra R, Isnard S, Dupuy FP, Ponte R, Chen J, et al. Circulating (1→3)-β-D-Glucan is associated with immune activation during HIV infection. *Clin Infect Dis.*
21. Deeks SG, Tracy R, Douek DC. Systemic effects of inflammation on health during chronic HIV infection. *Immunity.* (2013) 39:633–45. doi: 10.1016/j.immuni.2013.10.001
22. Nash AK, Auchtung TA, Wong MC, Smith DP, Gesell JR, Ross MC, et al. The gut mycobiome of the Human Microbiome Project healthy cohort. *Microbiome.* (2017) 5:15. doi: 10.1186/s40168-017-0373-4
23. Waldman AJ, Balskus EP. The human microbiota, infectious disease, and global health: challenges and opportunities. *ACS Infect Dis.* (2018) 4:14–26. doi: 10.1021/acsinfecdis.7b00232
24. Sheridan BS, Lefrancois L. Intraepithelial lymphocytes: to serve and protect. *Curr Gastroenterol Rep.* (2010) 12:513–21. doi: 10.1007/s11894-010-0148-6
25. Groschwitz KR, Hogan SP. Intestinal barrier function: molecular regulation and disease pathogenesis. *J Allergy Clin Immunol.* (2009) 124:3–20; quiz 21–2. doi: 10.1016/j.jaci.2009.05.038
26. Batman PA, Miller AR, Forster SM, Harris JR, Pinching AJ, Griffin GE. Jejunal enteropathy associated with human immunodeficiency virus infection: quantitative histology. *J Clin Pathol.* (1989) 42:275–81. doi: 10.1136/jcp.42.3.275
27. Batman PA, Kotler DP, Kapembwa MS, Booth D, Potten CS, Orenstein JM, et al. HIV enteropathy: crypt stem and transit cell hyperproliferation induces villous atrophy in HIV/Microsporidia-infected jejunal mucosa. *AIDS.* (2007) 21:433–9. doi: 10.1097/QAD.0b013e3280142ee8
28. Heise C, Dandekar S, Kumar P, Duplantier R, Donovan RM, Halsted CH. Human immunodeficiency virus infection of enterocytes and mononuclear cells in human jejunal mucosa. *Gastroenterology.* (1991) 100:1521–7. doi: 10.1016/0016-5085(91)90648-5
29. Klatt NR, Harris LD, Vinton CL, Sung H, Briant JA, Tabb B, et al. Compromised gastrointestinal integrity in pigtail macaques is associated with increased microbial translocation, immune activation, and IL-17 production in the absence of SIV infection. *Mucosal Immunol.* (2010) 3:387–98. doi: 10.1038/mi.2010.14
30. Milush JM, Mir KD, Sundaravaradan V, Gordon SN, Engram J, Cano CA, et al. Lack of clinical AIDS in SIV-infected sooty mangabeys with significant CD4+ T cell loss is associated with double-negative T cells. *J Clin Invest.* (2011) 121:1102–10. doi: 10.1172/JCI44876
31. Gordon SN, Klatt NR, Bosinger SE, Brenchley JM, Milush JM, Engram JC, et al. Severe depletion of mucosal CD4+ T cells in AIDS-free simian immunodeficiency virus-infected sooty mangabeys. *J Immunol.* (2007) 179:3026–34. doi: 10.4049/jimmunol.179.5.3026
32. Buccigrossi V, Laudiero G, Nicastro E, Miele E, Esposito F, Guarino A. The HIV-1 transactivator factor (Tat) induces enterocyte apoptosis through a redox-mediated mechanism. *PLoS ONE.* (2011) 6:e29436. doi: 10.1371/journal.pone.0029436
33. Canani RB, De Marco G, Passariello A, Buccigrossi V, Ruotolo S, Bracale I, et al. Inhibitory effect of HIV-1 Tat protein on the sodium-D-glucose symporter of human intestinal epithelial cells. *AIDS.* (2006) 20:5–10. doi: 10.1097/01.aids.0000198088.85572.68
34. Planes R, Ben Haij N, Leghmari K, Serrero M, BenMohamed L, Bahraoui E. HIV-1 Tat protein activates both the MyD88 and TRIF pathways to induce tumor necrosis factor alpha and interleukin-10 in human monocytes. *J Virol.* (2016) 90:5886–98. doi: 10.1128/JVI.00262-16
35. Maresca M, Mahfoud R, Garmy N, Kotler DP, Fantini J, Clayton F. The virotoxin model of HIV-1 enteropathy: involvement of GPR15/Bob and galactosylceramide in the cytopathic effects induced by HIV-1 gp120 in the HT-29-D4 intestinal cell line. *J Biomed Sci.* (2003) 10:156–66. doi: 10.1007/BF02256007
36. Clayton F, Kotler DP, Kuwada SK, Morgan T, Stepan C, Kuang J, et al. Gp120-induced Bob/GPR15 activation: a possible cause of human immunodeficiency virus enteropathy. *Am J Pathol.* (2001) 159:1933–9. doi: 10.1016/S0002-9440(10)63040-4
37. Allam O, Samarani S, Mehraj V, Jenabian MA, Tremblay C, Routy JP, et al. HIV induces production of IL-18 from intestinal epithelial cells that increases intestinal permeability and microbial translocation. *PLoS ONE.* (2018) 13:e0194185. doi: 10.1371/journal.pone.0194185
38. Nowarski R, Jackson R, Gagliani N, de Zoete MR, Palm NW, Bailis W, et al. Epithelial IL-18 equilibrium controls barrier function in colitis. *Cell.* (2015) 163:1444–56. doi: 10.1016/j.cell.2015.10.072
39. Mehraj V, Jenabian MA, Ponte R, Lebouche B, Costiniuk C, Thomas R, et al. Montreal primary Hiv infection, the plasma levels of soluble ST2 as a marker of gut mucosal damage in early HIV infection. *AIDS.* (2016) 30:1617–27. doi: 10.1097/QAD.0000000000001105
40. Ponte R, Mehraj V, Ghali P, Couedel-Courteille A, Cheynier R, Routy JP. Reversing gut damage in HIV infection: using non-human primate models to instruct clinical research. *EBioMedicine.* (2016) 4:40–9. doi: 10.1016/j.ebiom.2016.01.028
41. Mehraj V, Ponte R, Routy JP. The dynamic role of the IL-33/ST2 axis in chronic viral-infections: alarming and adjuvanting the immune response. *EBioMedicine.* (2016) 9:37–44. doi: 10.1016/j.ebiom.2016.06.047
42. Derikx JP, Luyer MD, Heineman E, Buurman WA. Non-invasive markers of gut wall integrity in health and disease. *World J Gastroenterol.* (2010) 16:5272–9. doi: 10.3748/wjg.v16.i42.5272
43. Brenchley JM, Schacker TW, Ruff LE, Price DA, Taylor JH, Beilman GJ, et al. CD4+ T cell depletion during all stages of HIV disease occurs predominantly in the gastrointestinal tract. *J Exp Med.* (2004) 200:749–59. doi: 10.1084/jem.20040874
44. Mehandru S, Poles MA, Tenner-Racz K, Horowitz A, Hurley A, Hogan C, et al. Primary HIV-1 infection is associated with preferential depletion of CD4+ T lymphocytes from effector sites in the gastrointestinal tract. *J Exp Med.* (2004) 200:761–70. doi: 10.1084/jem.20041196
45. Lim SG, Condez A, Lee CA, Johnson MA, Elia C, Poulter LW. Loss of mucosal CD4 lymphocytes is an early feature of HIV infection. *Clin Exp Immunol.* (1993) 92:448–54. doi: 10.1111/j.1365-2249.1993.tb03419.x

46. Jenabian MA, El-Far M, Vyboh K, Kema I, Costiniuk CT, Thomas R, et al. Montreal primary, and G slow progressor study, immunosuppressive tryptophan catabolism and gut mucosal dysfunction following early HIV infection. *J Infect Dis.* (2015) 212:355–66. doi: 10.1093/infdis/jiv037
47. Klatt NR, Estes JD, Sun X, Ortiz AM, Barber JS, Harris LD, et al. Loss of mucosal CD103+ DCs and IL-17+ and IL-22+ lymphocytes is associated with mucosal damage in SIV infection. *Mucosal Immunol.* (2012) 5:646–57. doi: 10.1038/mi.2012.38
48. Macpherson AJ, Smith K. Mesenteric lymph nodes at the center of immune anatomy. *J Exp Med.* (2006) 203:497–500. doi: 10.1084/jem.20060227
49. Brenchley JM, Douek DC. HIV infection and the gastrointestinal immune system. *Mucosal Immunol.* (2008) 1:23–30. doi: 10.1038/mi.2007.1
50. Marchetti G, Tincati C, Silvestri G. Microbial translocation in the pathogenesis of HIV infection and AIDS. *Clin Microbiol Rev.* (2013) 26:2–18. doi: 10.1128/CMR.00050-12
51. Pandrea I, Gaufin T, Brenchley JM, Gautam R, Monjure C, Gautam A, et al. Cutting edge: experimentally induced immune activation in natural hosts of simian immunodeficiency virus induces significant increases in viral replication and CD4+ T cell depletion. *J Immunol.* (2008) 181:6687–91. doi: 10.4049/jimmunol.181.10.6687
52. Kristoff J, Haret-Richter G, Ma D, Ribeiro RM, Xu C, Cornell E, et al. Early microbial translocation blockade reduces SIV-mediated inflammation and viral replication. *J Clin Invest.* (2014) 124:2802–6. doi: 10.1172/JCI75090
53. Triantafilou M, Triantafilou K. Lipopolysaccharide recognition: CD14, TLRs and the LPS-activation cluster. *Trends Immunol.* (2002) 23:301–4. doi: 10.1016/S1471-4906(02)02233-0
54. Barclay GR. Endogenous endotoxin-core antibody (EndoCAb) as a marker of endotoxin exposure and a prognostic indicator: a review. *Prog Clin Biol Res.* (1995) 392:263–72.
55. Panpetch W, Somboonna N, Bulan DE, Issara-Amphorn J, Finkelman M, Worasilchai N, et al. Oral administration of live- or heat-killed *Candida albicans* worsened cecal ligation and puncture sepsis in a murine model possibly due to an increased serum (1–>3)-beta-D-glucan. *PLoS ONE.* (2017) 12:e0181439. doi: 10.1371/journal.pone.0181439
56. Issara-Amphorn J, Surawut S, Worasilchai N, Thim-Uam A, Finkelman M, Chindamporn A, et al. The synergy of endotoxin and (1–>3)-beta-D-glucan, from gut translocation, worsens sepsis severity in a lupus model of Fc gamma receptor IIb-deficient mice. *J Innate Immun.* (2018) 10:189–201. doi: 10.1159/000486321
57. Leelahavanichkul A, Worasilchai N, Wannalerdsakun S, Jutivorakool K, Somparn P, Issara-Amphorn J, et al. Gastrointestinal leakage detected by serum (1–>3)-beta-D-glucan in mouse models and a pilot study in patients with sepsis. *Shock.* (2016) 46:506–18. doi: 10.1097/SHK.0000000000000645
58. Opal SM. Endotoxins and other sepsis triggers. *Contrib Nephrol.* (2010) 167:14–24. doi: 10.1159/000315915
59. Caradonna L, Amati L, Magrone T, Pellegrino NM, Jirillo E, Caccavo D. Enteric bacteria, lipopolysaccharides and related cytokines in inflammatory bowel disease: biological and clinical significance. *J Endotoxin Res.* (2000) 6:205–14. doi: 10.1177/09680519000060030101
60. Vaure C, Liu Y. A comparative review of toll-like receptor 4 expression and functionality in different animal species. *Front Immunol.* (2014) 5:316. doi: 10.3389/fimmu.2014.00316
61. Freudenberg MA, Tchaptchet S, Keck S, Fejer G, Huber M, Schutze N, et al. Lipopolysaccharide sensing an important factor in the innate immune response to Gram-negative bacterial infections: benefits and hazards of LPS hypersensitivity. *Immunobiology.* (2008) 213:193–203. doi: 10.1016/j.imbio.2007.11.008
62. Sandler NG, Wand H, Roque A, Law M, Nason MC, Nixon DE, et al. Plasma levels of soluble CD14 independently predict mortality in HIV infection. *J Infect Dis.* (2011) 203:780–90. doi: 10.1093/infdis/jiq118
63. Brown GD, Taylor PR, Reid DM, Willment JA, Williams DL, Martinez-Pomares L, et al. Dectin-1 is a major β-glucan receptor on macrophages. *J Exp Med.* (2002) 196:407–12. doi: 10.1084/jem.20020470
64. McDonald JU, Rosas M, Brown GD, Jones SA, Taylor PR. Differential dependencies of monocytes and neutrophils on dectin-1, dectin-2 and complement for the recognition of fungal particles in inflammation. *PLoS ONE.* (2012) 7:e45781. doi: 10.1371/journal.pone.0045781
65. Taylor PR, Brown GD, Reid DM, Willment JA, Martinez-Pomares L, Gordon S, et al. The B-glucan receptor, dectin-1, is predominantly expressed on the surface of cells of the monocyte/macrophage and neutrophil lineages. *J Immunol.* (2002) 169:3876–82. doi: 10.4049/jimmunol.169.7.3876
66. Elder MJ, Webster SJ, Chee R, Williams DL, Hill Gaston JS, Goodall JC. beta-glucan size controls dectin-1-mediated immune responses in human dendritic cells by regulating IL-1beta production. *Front Immunol.* (2017) 8:791. doi: 10.3389/fimmu.2017.00791
67. Hefter M, Lother J, Weiss E, Schmitt AL, Fliesser M, Einsele H, et al. Human primary myeloid dendritic cells interact with the opportunistic fungal pathogen *Aspergillus fumigatus* via the C-type lectin receptor Dectin-1. *Med Mycol.* (2017) 55:573–8. doi: 10.1093/mmy/myw105
68. Li SS, Kyei SK, Timm-McCann M, Ogbomo H, Jones GJ, Shi M, et al. The NK receptor NKp30 mediates direct fungal recognition and killing and is diminished in NK cells from HIV-infected patients. *Cell Host Microbe.* (2013) 14:387–97. doi: 10.1016/j.chom.2013.09.007
69. Tremblay-McLean A, Bruneau J, Lebouche B, Lisovsky I, Song R, Bernard NF. Expression profiles of ligands for activating natural killer cell receptors on HIV infected and uninfected CD4(+) T cells. *Viruses.* (2017) 9:295. doi: 10.3390/v9100295
70. Pandey R, DeStephan CM, Madge LA, May MJ, Orange JS. NKp30 ligation induces rapid activation of the canonical NF-kappaB pathway in NK cells. *J Immunol.* (2007) 179:7385–96. doi: 10.4049/jimmunol.179.11.7385
71. Lawrence T. The nuclear factor NF-kappaB pathway in inflammation. *Cold Spring Harb Perspect Biol.* (2009) 1:a001651. doi: 10.1101/cshperspect.a001651
72. Swidergall M, Solis NV, Lionakis MS, Filler SG. EphA2 is an epithelial cell pattern recognition receptor for fungal beta-glucans. *Nat Microbiol.* (2018) 3:53–61. doi: 10.1038/s41564-017-0059-5
73. Hahn AS, Desrosiers RC. Binding of the Kaposi's sarcoma-associated herpesvirus to the ephrin binding surface of the EphA2 receptor and its inhibition by a small molecule. *J Virol.* (2014) 88:8724–34. doi: 10.1128/JVI.01392-14
74. Legentil L, Paris F, Ballet C, Trouvelot S, Daire X, Vetvicka V, et al. Molecular interactions of beta-(1–>3)-glucans with their receptors. *Molecules.* (2015) 20:9745–66. doi: 10.3390/molecules20069745
75. Noss I, Doekes G, Thorne PS, Heederik DJ, Wouters IM. Comparison of the potency of a variety of beta-glucans to induce cytokine production in human whole blood. *Innate Immun.* (2013) 19:10–9. doi: 10.1177/1753425912447129
76. Sonnier DI, Bailey SR, Schuster RM, Gangidine MM, Lentsch AB, Pritts TA. Proinflammatory chemokines in the intestinal lumen contribute to intestinal dysfunction during endotoxemia. *Shock.* (2012) 37:63–9. doi: 10.1097/SHK.0b013e31823cbff1
77. Vujkovic-Cvijin I, Dunham RM, Iwai S, Maher MC, Albright RG, Broadhurst MJ, et al. Dysbiosis of the gut microbiota is associated with HIV disease progression and tryptophan catabolism. *Sci Transl Med.* (2013) 5:193ra91. doi: 10.1126/scitranslmed.3006438
78. Favre D, Mold J, Hunt PW, Kanwar B, Loke P, Seu L, et al. Tryptophan catabolism by indoleamine 2,3-dioxygenase 1 alters the balance of TH17 to regulatory T cells in HIV disease. *Sci Transl Med.* (2010) 2:32ra36. doi: 10.1126/scitranslmed.3000632
79. Jenabian MA, Patel M, Kema I, Kanagaratham C, Radzioch D, Thebault P, et al. Distinct tryptophan catabolism and Th17/Treg balance in HIV progressors and elite controllers. *PLoS ONE.* (2013) 8:e78146. doi: 10.1371/journal.pone.0078146
80. Chen J, Xun J, Yang J, Ji Y, Liu L, Qi T, et al. Plasma indoleamine 2,3-dioxygenase activity is associated with the size of HIV reservoir in patients receiving antiretroviral therapy. *Clin Infect Dis.* (2018) 10:676. doi: 10.1093/cid/ciy676
81. Kenneth Castro MDJ, Laurence Slutsker WWG, James Buehler PH, Harold Jaffe W, Ruth Berkelman MD. *1993 Revised Classification System 638 for HIV Infection and Expanded Surveillance Case Definition for AIDS Among Adolescents 639 and Adults*. Centre For Disease Control (1992).
82. Hsu DC, Sereti I, Ananworanich J. Serious Non-AIDS events: immunopathogenesis and interventional strategies. *AIDS Res Ther.* (2013) 10:29. doi: 10.1186/1742-6405-10-29
83. Clifford DB, Ances BM. HIV-associated neurocognitive disorder. *Lancet Infect Dis.* (2013) 13:976–86. doi: 10.1016/S1473-3099(13)70269-X

84. Ancuta P, Kamat A, Kunstman KJ, Kim EY, Autissier P, Wurcel A, et al. Microbial translocation is associated with increased monocyte activation and dementia in AIDS patients. *PLoS ONE.* (2008) 3:e2516. doi: 10.1371/journal.pone.0002516
85. Lyons JL, Uno H, Ancuta P, Kamat A, Moore DJ, Singer EJ, et al. Plasma sCD14 is a biomarker associated with impaired neurocognitive test performance in attention and learning domains in HIV infection. *J Acquir Immune Defic Syndr.* (2011) 57:371–9. doi: 10.1097/QAI.0b013e3182237e54
86. Justice AC, Dombrowski E, Conigliaro J, Fultz SL, Gibson D, Madenwald T, et al. Veterans aging cohort study (VACS): overview and description. *Med Care.* (2006) 44:S13–24. doi: 10.1097/01.mlr.0000223741.02074.66
87. Marconi VC, Duncan MS, So-Armah K, Re VL III, Lim JK, Butt AA, et al. Bilirubin is inversely associated with cardiovascular disease among HIV-positive and HIV-negative individuals in VACS (Veterans aging cohort study). *J Am Heart Assoc.* (2018) 7:7792. doi: 10.1161/JAHA.117.007792
88. Drosatos K, Lymperopoulos A, Kennel PJ, Pollak N, Schulze PC, Goldberg IJ. Pathophysiology of sepsis-related cardiac dysfunction: driven by inflammation, energy mismanagement, or both? *Curr Heart Fail Rep.* (2015) 12:130–40. doi: 10.1007/s11897-014-0247-z
89. Chen RRJ, Lu H, Routy JP. The early bird gets the worm: benefits and future directions with early antiretroviral therapy initiation in primary HIV infection. *Future Virol.* (2018) 13:11. doi: 10.2217/fvl-2018-0110
90. Wong J, Zhang Y, Patidar A, Vilar E, Finkelman M, Farrington K. Is endotoxemia in stable hemodialysis patients an artefact? Limitations of the limulus amebocyte lysate assay and role of (1–>3)-beta-D glucan. *PLoS ONE.* (2016) 11:e0164978. doi: 10.1371/journal.pone.0164978
91. Hashimoto N, Mori T, Hashida R, Sakurai M, Koda Y, Toyama T, et al. False-positive serum (1, 3)-beta-D-glucan elevation due to intake of seaweed in a hematopoietic stem cell transplant recipient. *Transpl Infect Dis.* (2017) 19. doi: 10.1111/tid.12653
92. Zainab Shahid NSK, Restrepo A, Haider S, Muzaffar J, Grazziutti M, Nucci M, et al. Elevated serum beta-D-glucan (BDG) as a marker for chemotherapy-induced mucosal barrier injury (MBI) in adults with hematologic malignancies: a retrospective analysis. In: *IDSA Annual Meeting.* Boston, MA (2011).
93. Ellis M, Al-Ramadi B, Finkelman M, Hedstrom U, Kristensen J, Ali-Zadeh H, et al. Assessment of the clinical utility of serial beta-D-glucan concentrations in patients with persistent neutropenic fever. *J Med Microbiol.* (2008) 57:287–95. doi: 10.1099/jmm.0.47479-0
94. Gavino C, Cotter A, Lichtenstein D, Lejtenyi D, Fortin C, Legault C, et al. CARD9 deficiency and spontaneous central nervous system candidiasis: complete clinical remission with GM-CSF therapy. *Clin Infect Dis.* (2014) 59:81–4. doi: 10.1093/cid/ciu215
95. Palesch D, Bosinger SE, Tharp GK, Vanderford TH, Paiardini M, Chahroudi A, et al. Sooty mangabey genome sequence provides insight into AIDS resistance in a natural SIV host. *Nature.* (2018) 553:77–81. doi: 10.1038/nature25140
96. Stinghen AE, Goncalves SM, Bucharles S, Branco FS, Gruber B, Hauser AB, et al. Sevelamer decreases systemic inflammation in parallel to a reduction in endotoxemia. *Blood Purif.* (2010) 29:352–6. doi: 10.1159/000302723
97. Sandler NG, Zhang X, Bosch RJ, Funderburg NT, Choi AI, Robinson JK, et al. Sevelamer does not decrease lipopolysaccharide or soluble CD14 levels but decreases soluble tissue factor, low-density lipoprotein (LDL) cholesterol, and oxidized LDL cholesterol levels in individuals with untreated HIV infection. *J Infect Dis.* (2014) 210:1549–54. doi: 10.1093/infdis/jiu305

Conflict of Interest Statement: MF and YZ are employees of Associates of Cape Cod, Inc., the manufacturers of Fungitell, the (1→3)-β-D-Glucan *in vitro* diagnostic kit.

The remaining authors declare that the research was conducted in the absence of any commercial or financial relationships that could be construed as a potential conflict of interest.

frontiers in Immunology

CLINICAL TRIAL
published: 09 April 2019
doi: 10.3389/fimmu.2019.00725

Poly-ICLC, a TLR3 Agonist, Induces Transient Innate Immune Responses in Patients With Treated HIV-Infection: A Randomized Double-Blinded Placebo Controlled Trial

Mansi Saxena[1], Rachel L. Sabado[1†], Melissa La Mar[2], Hiroshi Mohri[2], Andres M. Salazar[3], Hanqing Dong[1], Joel Correa Da Rosa[4], Martin Markowitz[2], Nina Bhardwaj[1‡] and Elizabeth Miller[1,4†‡]*

[1] Icahn School of Medicine at Mount Sinai, New York, NY, United States, [2] Aaron Diamond AIDS Research Center, Rockefeller University, New York, NY, United States, [3] Oncovir, Inc., Washington, DC, United States, [4] Laboratory of Investigative Dermatology, The Rockefeller University, New York, NY, United States

OPEN ACCESS

Edited by:
Sara Gianella Weibel, University of California, San Diego, United States

Reviewed by:
Jonathan Li, Brigham and Women's Hospital and Harvard Medical School, United States
Thomas Aagaard Rasmussen, Peter Doherty Institute for Infection and Immunity, Australia

****Correspondence:***
Nina Bhardwaj
nina.bhardwaj@mssm.edu

†Present Address:
Rachel L. Sabado, Genentech, South San Francisco, CA, United States
Elizabeth Miller, Regeneron Pharmaceuticals, Tarrytown, NY, United States

‡These authors share co-senior authorship

Specialty section:
This article was submitted to Vaccines and Molecular Therapeutics, a section of the journal Frontiers in Immunology

Received: *24 October 2018*
Accepted: *18 March 2019*
Published: *09 April 2019*

Citation:
Saxena M, Sabado RL, La Mar M, Mohri H, Salazar AM, Dong H, Correa Da Rosa J, Markowitz M, Bhardwaj N and Miller E (2019) Poly-ICLC, a TLR3 Agonist, Induces Transient Innate Immune Responses in Patients With Treated HIV-Infection: A Randomized Double-Blinded Placebo Controlled Trial. Front. Immunol. 10:725. doi: 10.3389/fimmu.2019.00725

Objective: Toll-like receptor-3 agonist Poly-ICLC has been known to activate immune cells and induce HIV replication in pre-clinical experiments. In this study we investigated if Poly-ICLC could be used for disrupting HIV latency while simultaneously enhancing innate immune responses.

Design: This was a randomized, placebo-controlled, double-blinded trial in aviremic, cART-treated HIV-infected subjects. Participants ($n = 15$) were randomized 3:1 to receive two consecutive daily doses of Poly-ICLC (1.4 mg subcutaneously) vs. placebo. Subjects were observed for adverse events, immune activation, and viral replication.

Methods: Besides primary outcomes of safety and tolerability, several longitudinal immune parameters were evaluated including immune cell phenotype and function via flowcytometry, ELISA, and transcriptional profiling. PCR assays for plasma HIV-1 RNA, $CD4^+$ T cell-associated HIV-1 RNA, and proviral DNA were performed to measure HIV reservoirs and latency.

Results: Poly-ICLC was overall safe and well-tolerated. Poly-ICLC-related adverse events were Grade 1/2, with the exception of one Grade 3 neutropenia which was short-lived. Mild Injection site reactions were observed in nearly all participants in the Poly-ICLC arm. Transcriptional analyses revealed upregulation of innate immune pathways in PBMCs following Poly-ICLC treatment, including strong interferon signaling accompanied by transient increases in circulating IP-10 (CXCL10) levels. These responses generally peaked by 24–48 h after the first injection and returned to baseline by day 8. $CD4^+$ T cell number and phenotype were unchanged, plasma viral control was maintained and no significant effect on HIV reservoirs was observed.

Conclusions: These finding suggest that Poly-ICLC could be safely used for inducing transient innate immune responses in treated HIV$^+$ subjects indicating promise as an adjuvant for HIV therapeutic vaccines.

Trial Registration: www.ClinicalTrials.gov, identifier: NCT02071095.

Keywords: HIV-1, vaccine, adjuvant, poly-ICLC, toll-like receptor ligand

INTRODUCTION

Innate immune dysregulation during HIV infection hinders the formation of anti-HIV adaptive immunity (1–6) resulting in rampant viral dissemination and progression to AIDS. Adherence to combination anti-retroviral therapy (cART) regimens controls viremia, restores CD4$^+$T cell counts and reverses immune dysfunction to a larg extent. However, cART fails to eradicate latent viral reservoirs, posing a major barrier to achieving sterilizing cure (7). Thus, safe and effective adjuvants that stimulate innate immune responses (8) and reactivate latent HIV, allowing for killing of infected cells, are likely to be a vital element of successful therapeutic immunization strategies in aviremic patients (9).

Pattern recognition receptors, such as Toll-like receptors (TLRs), are key activators of innate immunity. These germ line encoded receptors induce rapid inflammation in response to a wide range pathogen associated molecular patterns (PAMPs) (10). Of the 10 TLRs expressed in humans, TLRs 1,2,4,5,6, and 10 are expressed on the cell surface and recognize pathogenic cell membrane components such as lipoproteins, peptidoglycans, flagellin, etc. TLR 3, TLR 7/8, and TLR9 are intracellular receptors that respond to double stranded RNA, single stranded RNA and unmethylated DNA, respectively. TLR3 is expressed multiple cell types including myeloid dendritic cells (DCs), macrophages, Natural killer cells (NK cells), neuronal cells, fibroblasts, endothelial cells, mast cells, and epithelial cells (11). While TLR7 is also expressed on myeloid DCs, NK cells, macrophages, and mast cells, its expression is enriched in plasmacytoid DCs (pDCs), B cells and T cells (12). TLR9 expression pattern is similar to that of TLR7 as it is also primarily expressed in human memory B cells, NK cells, and pDCs (13). Once activated by their cognate ligands, the TLRs signal through the downstream receptors MyD88 (TLR1, 2, 4, 5, 6, 7, 8, 9) or TRIF (TLRs4 and 3) to initiate a complex signaling cascade that culminates in transcriptional induction of inflammatory genes (14).

TLR agonists are potent immune adjuvants. In general their primary adjuvant effects are orchestrated through activation of immune cells like Natural Killer (NK) cells and antigen presenting cells such as DCs (15). DC maturation, induced by TLR agonists, is marked by up regulation of MHC-I and MHC-II and induction of co-stimulatory markers such CD40, CD80, and CD86. TLR activation also leads to secretion of cytokines in immune cells, such as interleukin (IL) 12 secretion by DCs and interferon-gamma (IFNγ) secretion by NK cells. The cumulative net effect is the induction of T cell activation and other specific or general adaptive immune responses (16). Interestingly, TLR agonists have also been shown to reactivate latent HIV both *ex vivo* (17–19) and in patients (20, 21).

Polyinosinic-polycytidylic acid, and poly-L-lysine (Poly-ICLC) is a double stranded RNA complex that serves as a viral mimic recognized by endosomal receptor TLR3 and cytoplasmic sensors MDA-5 and DHX/DDX RNA helicases (22–24). Its adjuvant effects are multi-faceted, including activation of classical DCs to express high levels of IL-12 and type I IFN (16) to promote Th1 polarization (25). Studies in humanized mice models have validated the significance of Poly-IC as a potent adjuvant for driving DC-induced inflammation and activation of antigen specific cytotoxic T cells (26). Furthermore, Poly-IC has been reported to reverse viral latency in human microglial cells *in vitro* (27).

In clinical trials with healthy volunteers and cancer patients, Poly-ICLC has been found to be overall safe and immunogenic (28–33). Interestingly, Poly-IC has been reported to be more efficient than other TLR ligands at improving immunogenicity and inducing viral control when it is either administered alone (34) or in combination with other components (35–38).

A major challenge in using TLR ligands as therapy during HIV infection is the profound host immune dysfunction induced by the virus, including dampening of TLR responsiveness (6, 39, 40). While viremia suppression by cART has been reported to rescue DC activation (39); whether Poly-ICLC can be safely used as an adjuvant and a latency reversing agent in this setting remains to be determined.

Here we report the results of a randomized, placebo-controlled, double-blinded trial investigating the use of Poly-ICLC in HIV setting (NCT02071095). The primary end point of the study was to establish if Poly-ICLC is safe and well-tolerated in HIV-1-infected subjects on cART. The secondary end points were; (a) to determine whether Poly-ICLC disrupts viral latency in HIV-1-infected individuals on cART and (b) to confirm that Poly-ICLC enhances innate immune responses in HIV-infected subjects on cART, and that its immunostimulatory properties are transient in nature. The secondary endpoints include measuring innate immune activation (DC, NK Cells, soluble factors, and transcriptional responses), and measures of viral RNA and DNA. A special consideration for the use of an immunostimulant during HIV infection is the risk of inducing inappropriate immune activation resulting in increased number of cellular targets of infection. Therefore, multiple parameters of generalized immune activation and exhaustion were monitored as additional safety measures. While we did not observe any clear effects of Poly-ICLC in reversing HIV latency or on the size of viral reservoirs; we did determine that Poly-ICLC was safe and well-tolerated in the HIV-infected population studied.

Furthermore, Poly-ICLC lead to transient innate immune stimulation without undue generalized immune activation. These findings suggest that Poly-ICLC may enhance the formation of HIV-specific immune responses when administered with HIV therapeutic vaccines.

METHODS

Study Design and Eligibility

This was a randomized, placebo-controlled, double-blinded, trial in cART-suppressed subjects with HIV infection (NCT02071095). Participants ($N = 15$) were randomized 3:1 to receive 2 consecutive daily doses of Poly-ICLC (Hiltonol®, Oncovir) [1.4 mg subcutaneously (SQ)] vs. placebo (normal saline) (**Figure 1**) and followed for 48 weeks. Subjects were randomized into blocks of 4 4 8 4. In total 12 participants received Poly-ICLC and 3 participants received the placebo (**Figure 2**).

Eligible participants included non-pregnant, non-lactating men, and women aged 18–55 years with HIV-infection on cART. Further eligibility was determined based on documented plasma HIV-1 RNA suppression below 50 copies/ml for at least 48 weeks and $CD4^+$ T cells >500 cells/mm^3. Persons with co-morbidities including vascular disease, poorly controlled hypertension, diabetes, hyperlipidemia, renal disease, active hepatitis B/C co-infection, autoimmunity, or multi-drug resistant HIV were excluded. Subjects were recruited from the New York City area from Mount Sinai Hospital Clinics, Rockefeller University Recruitment Office and IRB-approved advertising.

Plasma HIV-1 RNA Levels

HIV-1 RNA levels in plasma were determined using the Roche COBAS AmpliPrep/COBAS TaqMan HIV-1 Assay, Version 2.0, which detects 10 to 20 $\times$ 10^6 copies per ml.

DC Enumeration and Activation

To enumerate and assess maturation of $CD11c^+$ DCs and pDCs, fresh peripheral blood mononuclear cells (PBMCs) were stained with Live/Dead Violet, HLA-DR PerCP-Cy5.5, CD123 PE-Cy7, Lin1 FITC, CD11c PE-CF594, CD40 APC, CD86 Alexa700, and CD83 PE. Fresh PBMCs, plated for 1 h, were treated with Golgi Plug (1:1,000) for 5 h and stained for surface expression of HLA-DR PerCP-Cy5.5, CD123 PE-Cy7, Lin1 FITC, CD11c PE-CF594, and Live/Dead Violet followed by intracellular cytokine staining with IFNα APC, IL-12 p40/70 PE, and TNFα Alexa700. For the control fluorescence minus one (FMO) wells, the corresponding antibody was omitted from the cocktail. Stained and fixed cells were acquired using BD Fortessa Cytometer.

NK Cell Enumeration and Activation

Fresh PBMCs were stained with Live/Dead Violet, CD3 PE-CF594, CD16 PerCP-Cy5.5, CD56 BV605, CD69 Alexa700, NKp44 APC, NKG2D PE-Cy7, TIM3 Alexa488, and KIR3DS1/DL1 PE. Stained and fixed cells were acquired using BD Fortessa Cytometer.

T Cell Phenotype

Thawed PBMCs were stained with CD4 FITC, CD8 Alexa700, HLA-DR PerCP-Cy5.5, CD38 APC, PD-1 BV605, CTLA-4 PE, CD3 PE-CF594, and Live/Dead Violet and acquired using BD Fortessa Cytometer.

ELISA

Presence of plasma IFNα (PBL Assay Science), IP-10 (R&D systems), sCD14 (R&D systems), TNFα (R&D systems), D-Dimer (Abcam), and C-Reactive Protein (CRP) (Abcam) was evaluated by ELISA per manufacturers protocol.

Transcriptional Responses

Transcriptional responses profiling 249 inflammation-related genes were evaluated in PBMCs at baseline and days 2, 4, and 8 in a subset of participants ($N = 12$) via NanoString Technologies including statistical analysis (nCounter® gene expression panel, human inflammation kit).

Quantification of Cell-Associated HIV-1 RNA and DNA in Peripheral $CD4^+$T Cells

Cell-associated HIV-1 proviral DNA was measured at baseline and week 4, and cell-associated HIV-1 RNA was measured at each visit through week 16 (baseline, days 2, 4, 8, week 4 and 16). $CD4^+$T cells were isolated from PBMCs using Dynabeads FlowComp Human CD4 Kit (Invitrogen). DNA and RNA isolation was performed with AllPrep DNA/RNA Mini Kit (Qiagen). Isolated RNA was treated with DNase I, Amplification Grade (Invitrogen) and purified with RNeasy Mini Kit (Qiagen). Real time PCR was performed with AmpliTaq Gold with Buffer A or AmpliTaq Gold DNA Polymerase with Buffer II and MgCl2 with ROX Reference Dye (Applied Biosystems) using the Stratagene Mx3000P QPCR System (Agilent Technologies). PCR reactions were performed in quadruplicate. Note that for each case an optimal primers/probe set was determined, which gave the highest amplification efficiency among three primer/probe sets tested. Accordingly two primer/probe sets were used, RF/RR/PB (41) for 9 participants and 6F/84R/HIV gag probe (42) for 6 participants.

Cell-associated RNA was primed with random hexamers and reverse transcribed with Superscript II (Invitrogen). PCR reagent mix containing primers, probe, and AmpliTaq Gold was added to each of RT product, and quantitative rtPCR was performed as described above in quadruplicate. No reverse transcriptase control was also included.

Statistical Methods

Comparisons among the treatment Arms on the proportions of related adverse events was made using Fisher's exact test. Immunologic and virologic parameters between and within treatment Arms were compared at each time points from baseline to post-administration of Poly-ICLC vs. placebo using a linear mixed effect model. Parameters between treatment arms were compared using analysis of covariance, with baseline values as a covariate, after a Box-Cox family variance stabilizing transformation.

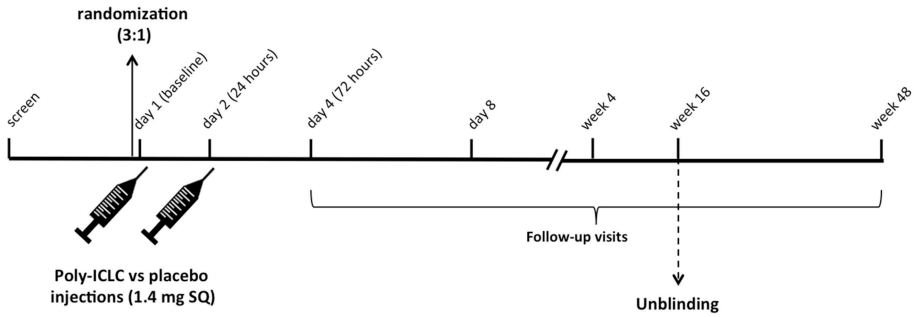

FIGURE 1 | Study Schema. Following screening, eligible subjects are randomized 3:1 to receive Poly-ICLC (1.4 mg SQ) vs. Placebo on days 1 and 2. Participants returned for follow up visits on days 4 and 8, weeks 4, 16, and 48. Unblinding of the study occurred after all subjects completed the week 16 follow up visit as specified by the protocol.

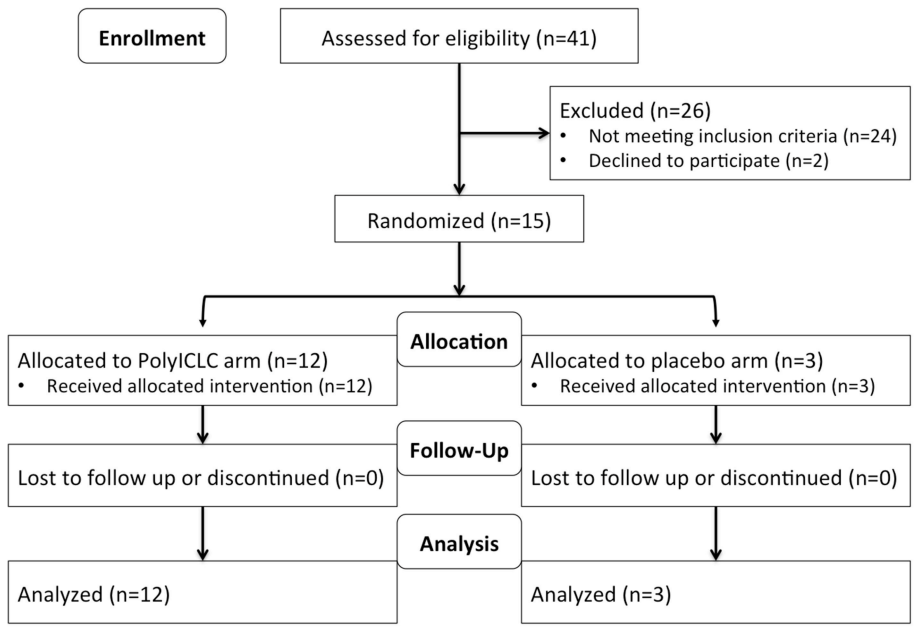

FIGURE 2 | Study flow diagram.

For primary end-point of safety, power of Fisher's Exact Test for difference between two proportions when sample sizes are $n1 = 12$ and $n2 = 3$ was determined (data not shown) and deemed appropriate. For the secondary endpoint, assuming a modest correlation between baseline and follow-up, maximum cellular associated HIV-1 RNA ($r = 0.32$), a sample size of 12 patients in the active arm and 3 patients in the control arm can detect a difference of $|2.23|$ standard deviations in cellular associated HIV-1 RNA maximum fold change between Poly-ICLC SQ and placebo with 2-sided $\alpha = 0.05$ and power = 92% (calculations from PASS version 12) (43). The assumptions used in this power calculation are consistent with the effect sizes, variability, and correlation over time for the primary outcome in work by Archin et al. (44). Considering the endpoints for cellular phenotype: the sample size provides 80% power at 5% of significance for detecting a minimum difference of $|1.95|$ standard deviations between the two study arms when using a two-sided unpaired t-test.

RESULTS

Participants and Demographic Details

Participants included 14 males and 1 transgender female with HIV infection. Participants hailed from diverse racial and ethnic backgrounds (40% white, 26.6% black or AA, 6.7% Native American, 6.7% Asian, and 20% multiple or unspecified race, with 46.6% Hispanic or Latino ethnicity). The median age was 39.73 years old (range 26–54), and median baseline $CD4^+$ T cell count was 619 cells/mm^3. A detailed description of baseline patient demographics across the two arms of the study can be found in **Table 1**.

TABLE 1 | Tabulated view of baseline patient demographics in each arm.

		Arm A: Poly:ICLC	Arm B: Placebo	Total
Number of participants		12	3	15
Age (years)	Continuous Mean (Standard Deviation)	41.1 (9.32)	34.33 (4.03)	39.73 (8.61)
Sex (Number)	Female	0	0	0
	Male	12	3	15
Ethnic Category (Number)	Hispanic or Latino	6	1	7
	Not Hispanic or Latino	6	2	8
Racial Categories (Number)	American Indian/Alaska Native	1	0	1
	Asian	1	0	1
	Native Hawaiian or Other Pacific Islander	0	0	0
	Black or African American	4 (1 Hispanic)	0	4
	White	4 (3 Hispanic)	2	6
	More than one race	1 (Hispanic)	0	1
	Unknown/ Unreported	1 (Hispanic)	1 (Hispanic)	2

TABLE 2 | Tabulated view of treatment related Adverse Events (AEs).

	Placebo ($n = 3$)			Poly:ICLC ($n = 12$)		
	Grade 1-2	Grade 3	Grade 4	Grade 1-2	Grade 3	Grade 4
GENERAL DISORDERS AND ADMINISTRATION SITE CONDITIONS						
Chills	0	0	0	3	0	0
Injection site reaction–erythema	0	0	0	5	0	0
Injection site reaction–pain	0	0	0	10	0	0
Fatigue	3	0	0	7	0	0
Fever	0	0	0	4	0	0
Malaise	1	0	0	2	0	0
NERVOUS SYSTEM DISORDERS						
Headache	2	0	0	1	0	0
MUSCULOSKELETAL AND CONNECTIVE TISSUE DISORDERS						
Myalgias	0	0	0	2	0	0
HEMATOLOGICAL						
Low neutrophils count	0	0	0	0	1	0

Safety and Tolerability

All study participants received both doses of Poly-ICLC or placebo as planned, and all subjects completed visits through week 48 (**Figure 2**). Overall, Poly-ICLC was safe and well-tolerated with only Grade 1/2 adverse events (AEs) attributed to the study agent, with the exception of one Grade 3 transient neutropenia without clinical sequelae. Injection site reactions (ISR) were the most frequent AE, all of which were Grade 1. Pain was the most common ISR, occurring at 66% of injection sites. Erythema was present at 33% of injection sites. Fever, generally low-grade, was also common (26.6%), lasting 24–48 h. Other frequently reported AEs include chills, myalgias, fatigue, malaise, and headache (**Table 2**). AEs deemed treatment-related were more common in the Poly-ICLC arm compared with the placebo arm ($P = 0.012$), as was injection site pain ($P = 0.022$). All subjects completed the protocol's dosing regimen, and there were no cases of discontinuation. Two serious adverse events (SAEs) occurred during the study which were deemed unrelated to Poly-ICLC, and both of these occurred in the placebo group.

There was no impact on subjects' $CD4^+$ T cell counts following Poly-ICLC injections. The median $CD4^+$ T cell count in the Poly-ICLC group increased from 604.5 cells/mm^3 at baseline to 698 cells/mm^3 and 656 cells/mm^3 at day 8 and week 16, respectively, but was not a statistically significant change (**Figure 3**).

All subjects maintained virologic control with plasma HIV-1 RNA remaining below the limit of detection (<20 copies/ml) throughout the study, with the exception of two discrete measurements of detectable HIV RNA, both in Poly-ICLC arm, with <200 copies/ml. One participant experienced a transient elevation in plasma HIV RNA to 110 copies/ml in the setting of a genital herpes simplex virus outbreak that occurred at their week 4 visit, and another participant was found to have a level of 190 copies/ml that occurred at their week 48 visit (data not shown).

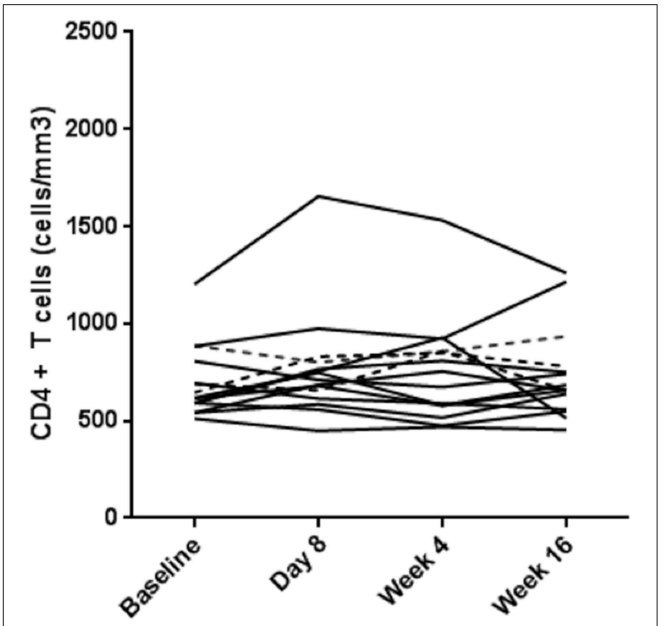

FIGURE 3 | No overall change in $CD4^+$ T cells counts in the treatment arm. $CD4^+$ T cell counts (cells/mm^3) for each subject are shown over the course of the study. Values for subjects in Arm A (Poly-ICLC) and Arm B (Placebo) are depicted by solid and dashed lines, respectively.

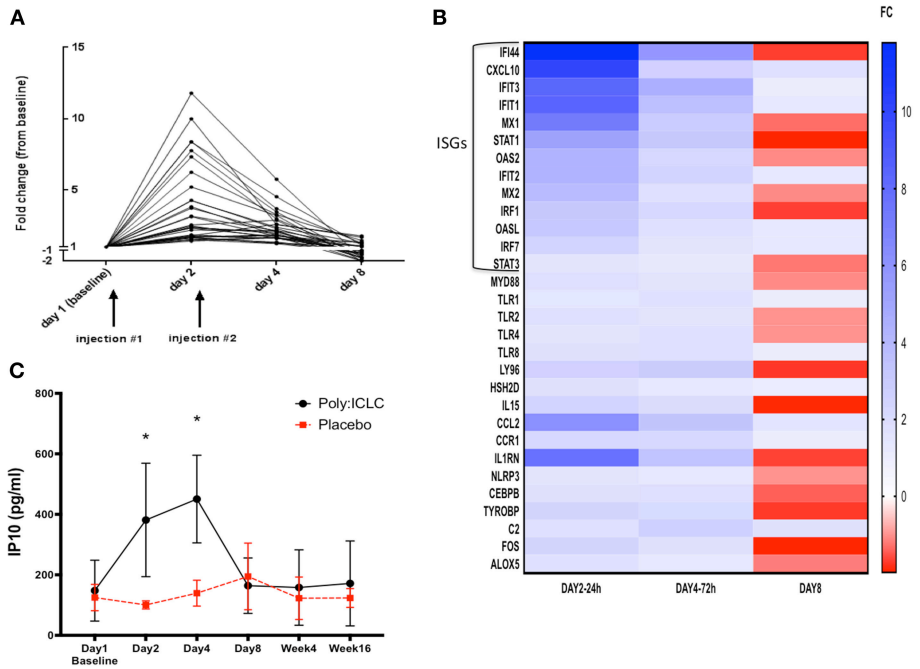

FIGURE 4 | Transient upregulation of pro-inflammatory genes in subjects who received Poly-ICLC, with strong induction of interferon pathway. Transcriptional responses were evaluated longitudinally in subjects' PBMCs using NanoString Technologies (nCounter® gene expression panel, human inflammation kit). **(A)** Fold change (FC) from baseline of significantly upregulated genes from subjects in Arm A (Poly-ICLC) are depicted graphically over time through day 8. Transient upregulation of several genes occurred ($N = 31$), generally peaking at 24 h and returning to baseline shortly thereafter. No significant changes were observed in subjects' PBMCs in Arm B (Placebo) (not shown). **(B)** Heat map of all significantly induced genes in Arm A (Poly-ICLC) represented as a FC over baseline. Most of the highly upregulated genes were found to be interferon-stimulated genes (ISGs) FDR < 1, FC ≥ ±1.5. **(C)** In concordance with strong upregulation of ISGs, plasma levels of IP-10 were transiently upregulated in subjects in Arm A Poly-ICLC ($N = 12$) vs. those in Arm B Placebo ($N = 3$). *$p < 0.001$.

Immune Responses From PBMCs

Transcriptional analyses of PBMCs revealed that multiple innate immune signatures were up regulated in subjects in the Poly-ICLC arm. These responses were transient and generally peaked at 24 h after injection (day 2) and returned to baseline by day 8 (**Figure 4A**). The interferon pathway was primarily induced, with strong up regulation of interferon-stimulated genes (ISGs) including Interferon Induced proteins with tetratricopeptide repeats (IFITs), interferon regulatory factors (IRFs), and 2′-5′ oligoadenylate synthase (OAS). Up regulation of genes associated with TLR pathways (MyD88, TLR1, TLR2, TLR4, TLR8, and Ly96) (45), T cell and NK cell activation [IL15 and Hematopoietic SH2 Domain Containing (HSH2D)] (46–48) inflammasome activation [NLR Family Pyrin Domain Containing 3 (NLRP3)] (49) and other inflammatory transcription factors, chemokines, and cytokines (FOS, CCL2, CCR1, etc.) was observed to a lesser extent (**Figure 4B** and **Supplemental Table 1**). In accordance with the strong up regulation of ISGs found on transcriptional analyses, transient increases in plasma IP-10 in the Poly-ICLC arm were observed on days 2 and 4 compared with baseline and subsequent time points ($p < 0.001$), while no changes were observed in the placebo arm (**Figure 4C**). Changes in levels of circulating IFNα and other inflammatory markers (IFNβ, TNFα, sCD14, D-dimer, and C reactive protein) were not detected following Poly-ICLC administration, though certain individuals did experience transient increases in D-dimer and CRP that quickly returned to baseline (**Supplemental Figure 1**).

T Cell Exhaustion

Immune activation on T cells was assessed by surface expression of HLA-DR and CD38. Programmed Cell Death 1 (PD-1) and Cytotoxic T-Lymphocyte Associated Protein 4 (CTLA-4) expression was used as an indicator of T cell exhaustion. Please note that PD1 and CTLA-4 maybe up regulated very early in activated T cells but in later stages are considered markers of exhaustion. Neither HLA-DR nor PD1 and CTLA-4 on $CD4^+$ and $CD8^+$ T cells was found to be overall changed from baseline following Poly-ICLC administration. However, CD38 was significantly upregulated on day 4 compared with baseline on $CD8^+$ T cells and normalized by day 8 ($P < 0.001$; **Figure 5**).

DC and NK Cell Activation

Many different subsets of DCs have been identified such as $CD141^+$ cDC1s, $CD1c^+$cDC2s, Langerhans cells, pDCs, and inflammatory DCs. We focused on analyzing the effect of Poly-ICLC on pDCs and mDCs (most similar to cDC2) as these two are the most abundant DC subsets in blood. DCs were identified by a lack of lineage marker expression (CD3, CD14, CD16, CD20, and CD56) and positive for HLA-DR (a heterodimeric MHC-II cell surface receptor). pDCs and mDCs were identified by

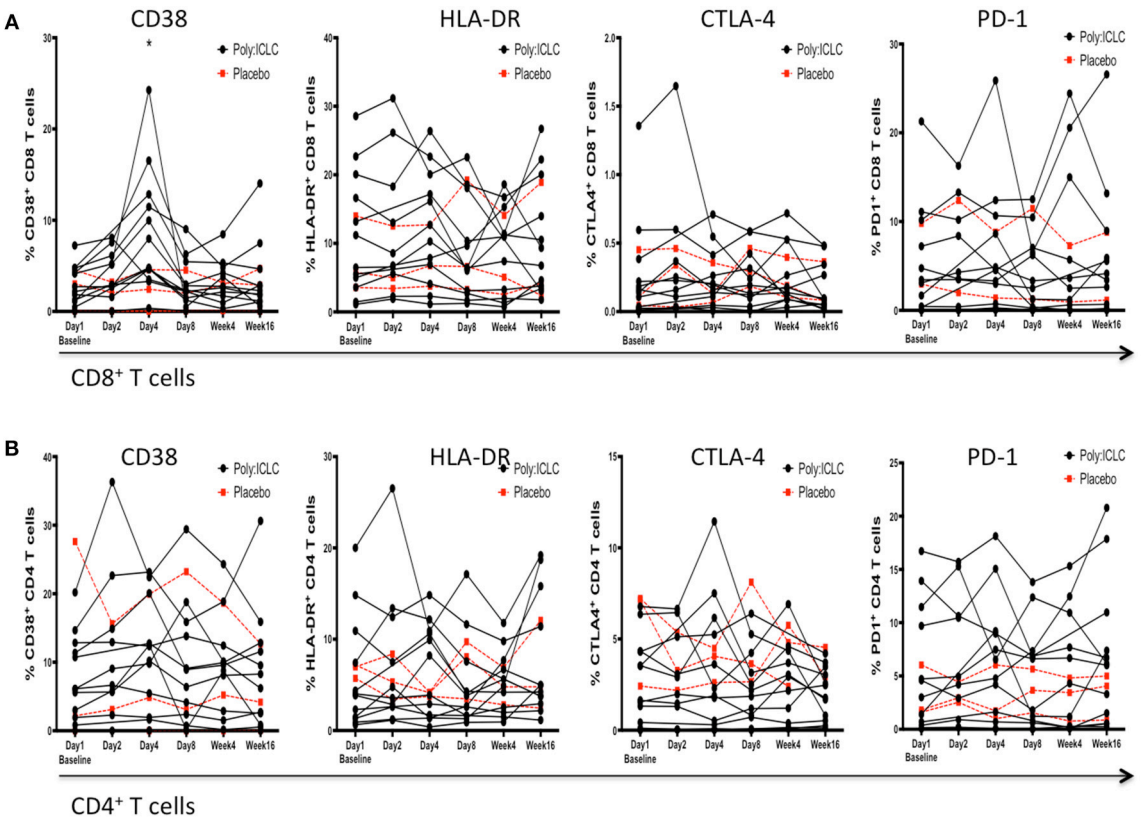

FIGURE 5 | Markers of immune activation and exhaustion on $CD4^+$ and $CD8^+$ T cells following Poly-ICLC administration. In order to monitor for the secondary induction of generalized immune activation following Poly-ICLC administration, surface expression of CD38, HLA-DR, PD-1, and CTLA-4 was evaluated at each time point via flowcytometry on subjects'; **(A)** $CD8^+$ T cells and **(B)** $CD4^+$ T cells. No longitudinal changes were found to be statistically significant following Poly-ICLC administration with the exception of transient upregulation of CD38 on $CD8^+$ T cells at Day 4. $^*p < 0.001$.

mutually exclusive expression of CD123 and CD11c, respectively (16, 50). NK cells were identified as being negative for CD3 and by co-expression of CD16 and CD56. $CD16^+CD56^{dim}$ NK cells are considered mature NK cells that are highly cytolytic and inflammatory while $CD16^{+/-}CD56^{bright}$ NK cells are highly proliferative and known for producing high levels of IFNγ upon stimulation. $CD16^+CD56^-$ NK cells have been previously described in healthy cord blood samples and chronic HIV donors (51, 52), however it is unclear if these are immature, dysfunctional NK cells or an artifact due to contamination from the myeloid fraction. There was no significant difference in percentage of pDCs and mDCs in circulation post Poly-ICLC treatment. The $CD56^{dim}$ NK cell subsets appeared to transiently decrease on day 2 compared with baseline but subsequently returned to baseline by day 8 ($P < 0.05$; **Figure 6**).

To determine the phenotype of circulating DCs expression of co-stimulatory cell surface proteins CD40, CD83, CD86, all of which are required for optimally engaging and activating T cells, was examined (8, 16). A unique array of activating and inhibitory receptors control NK cell effector functions by either recognizing the presence or absence of their ligands on target cells. For our study we analyzed the expression of two activating receptors, NKp44 and NKG2D and two inhibitory receptors, TIM3, and KIR3DS1/DL1 on circulating NK cells (53, 54). The activation status of both, DCs and NK cells, remained overall unchanged from baseline. There were also no changes in intracellular cytokine secretion of TNFα, IFNα, or IL-12 observed in DCs from baseline (not shown).

HIV-1 Latency and Reservoirs

$CD4^+$ T cell-associated HIV-1 RNA was measured to determine changes in HIV latency from baseline. Though certain individuals experienced increases in cell-associated HIV RNA following administration of Poly-ICLC at various time points, these were low in magnitude and overall was not a statistically significant finding (**Figure 7A**). Cell-associated HIV-1 proviral DNA was measured as an estimate of reservoir size at baseline and week 4, and there was no observed difference in this measure (**Figure 7B**).

DISCUSSION

The innate immune environment during vaccination plays a crucial role in the induction of strong and durable immunity. Here, we report multiple outcomes of the first study of Poly-ICLC, a TLR3 agonist, during treated HIV infection. In a

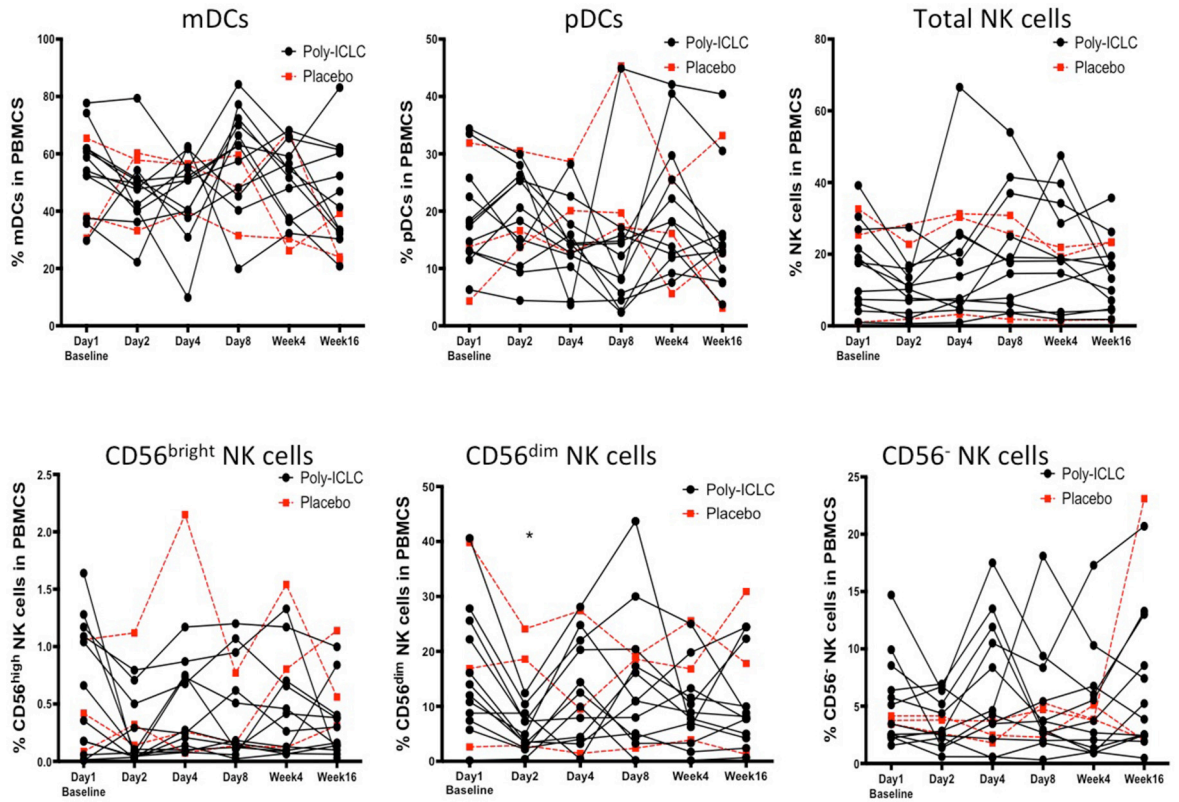

FIGURE 6 | No changes in DC and NK cell numbers and activation following Poly-ICLC treatment. DC and NK cell subsets were enumerated as described following Poly-ICLC vs. placebo. Percentage of mDCs, pDCs, total NK cells, CD56 bright, CD56 dim, and CD56 negative cells in PBMCs for each subject are shown over the course of the study as measured by flowcytometry. Values for subjects in Arm A (Poly-ICLC) and Arm B (Placebo) are depicted by solid and dashed lines, respectively. Though multiple NK cell subsets declined following Poly-ICLC, the only CD56 dim NK cells were found to be statistically significant. (*$p < 0.05$, FDR <1).

previous study of eight healthy volunteers who received a single dose of Poly-ICLC (1.6 mg SQ), majority of participants had reported moderate or severe ISRs, along with a high frequency of systemic AEs (31). However, in our study, Poly-ICLC was very well-tolerated in the HIV-infected population studied; with AEs primarily consisting of mild ISRs in nearly all subjects and less frequent fevers and other systemic symptoms. It is unclear as to why the AEs were relatively mild in our study. It has been suggested that there may be some Poly-ICLC lot variability in terms of reactogenicity on the other hand it is also possible that dampening of innate immune responses during HIV infection may be responsible for this outcome (6, 39, 40). Though favorable adjuvant tolerability during HIV infection is advantageous, it remains unclear what effect, if any, this may have on its potency when administered with a vaccine.

Nevertheless, we observed strong upregulation of numerous ISGs and increases in circulating levels of IP-10. These responses were transient, generally peaking by 24–48 h after injection and returning to baseline by day 8. In previous studies also, the transcriptional responses following Poly-ICLC, in healthy volunteers (31) and cancer patients (28), reported transient upregulation of ISGs with accompanying induction in other innate immune pathways but to a lesser extent. Similarly, in addition to ISGs, we detected transcriptional upregulation of other innate immune pathways but did not find associated significant increases in circulating pro-inflammatory cytokines beyond IP-10. It remains unclear if a lack of secreted inflammatory signature in our study was a result of a diminished effect of Poly-ICLC during HIV infection or due to low dosing over a short period of time.

Poly-ICLC administration also did not induce activation of circulating DCs and NK cells, as gleaned from flowcytometry analysis. However, local effects on tissue DCs and other innate immune cells were likely induced as evidenced by ISRs in the vast majority of individuals. Furthermore, we observed a transient decrease in circulating NK cells subsets ($CD56^{dim}$) following Poly-ICLC treatment, which may possibly reflect trafficking of this subset of NK cells to the tissues. In preclinical studies, Poly-ICLC has been shown to secondarily activate NK cells to enhance their cytotoxicity which may in turn augment the killing and elimination of latently infected cells alone (25, 55) or in combination with other TLR ligands (56).

Prior trials have primarily evaluated the formation of antigen-specific adaptive immune responses in patients administered with Poly-ICLC in combination with either tumor associated peptides or specific targeting antibodies (29, 30, 32, 57, 58), thus

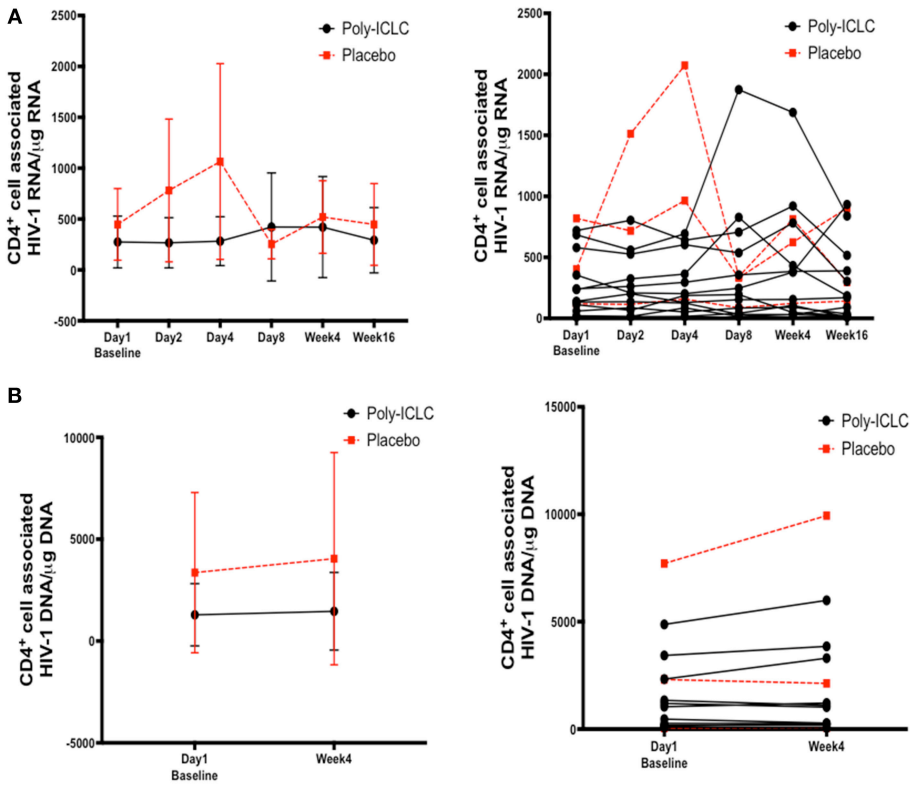

FIGURE 7 | Longitudinal assessment of cell associated HIV-1 RNA and DNA values show no significant changes overall following discrete dosing of Poly-ICLC. **(A)** Following RNA extraction from purified CD4$^+$ T cells at baseline and multiple time points following Poly-ICLC, rtPCR for HIV-1 RNA was performed in quadruplicate. Cell-associated HIV-1 RNA copy number is expressed as copy number per 1 μg of RNA in purified CD4$^+$ T cells. The left graph depicts pooled values from all participants in Arm A (Poly-ICLC) and Arm B (placebo), with the mean values and standard deviation. The right graph depicts this data as individual values over time for each participant in Arm A and Arm B. **(B)** Following DNA extraction from purified CD4$^+$ T cells at baseline and at week 4, rtPCR for HIV-1 DNA was performed in quadruplicate. Cell-associated HIV-1 DNA copy number is expressed as copy number per 1 μg of DNA in purified CD4$^+$ T cells. Left graph depicts pooled values from all participants in Arm A and Arm B. The right graph shows individual values for each participant in Arm A and Arm B. Values for subjects in Arm A (Poly-ICLC) and Arm B (Placebo) are depicted by solid and dashed lines, respectively.

making comparison to the current study of Poly-ICLC-alone difficult. Specially given our focus on induction of innate immune responses. In future trials, vaccination with Poly-ICLC combined with HIV related peptides will serve as the true test of its potential role as an adjuvant during HIV infection.

An ongoing safety concern associated with the use of novel adjuvants in HIV-infection is the potential for induction of generalized immune activation that could increase cellular targets of infection and contribute to immunopathogenesis. Therefore, in addition to monitoring viral parameters, we gauged levels of generalized immune activation and exhaustion on CD4$^+$ and CD8$^+$ T cells via flowcytometry and measured circulating markers of inflammation including D-dimer, CRP, sCD14. We did not find any upregulation in markers of immune activation on CD4$^+$ T cells that would lead to increased risk for infection. Similarly, markers of immune activation and exhaustion were not found to be significantly upregulated in plasma or on CD8$^+$ T cells except for a transient increase in CD38, a maker of T cell activation (59), expression on CD8$^+$ T cells on day 4 that returned to baseline by day 8. The elevated levels of CD38 on CD8$^+$ T cells in this study were likely a result of temporary increases in IFNs induced by Poly-ICLC (60). Given the fleeting nature of this upregulation, along with the stability of other surface markers including HLA-DR, PD-1, and CTLA-4, it is unlikely that deleterious effects on adaptive immune function are imparted overall.

TLR ligands may not only serve as vaccine adjuvants during HIV infection but may also impact viral latency (17–21). Indeed, TLR ligand driven activation of innate immune cells induces inflammatory cytokines, several of which are known to promote viral reactivation (61, 62). Here, we observed no overall effect within the Poly-ICLC-treated group on viral latency via measurement of CD4$^+$ T cell-associated HIV-1 RNA, despite increases detected in certain individuals following Poly-ICLC treatment that remains of unclear significance. Furthermore, there was no significant change in CD4$^+$ T cell-associated HIV-1 proviral DNA, suggesting that HIV reservoirs were largely unchanged following Poly-ICLC administration. Larger studies, possibly with more frequent dosing of poly-ICLC will be needed to assess whether this adjuvant will ultimately impact the HIV

reservoir. These findings are in contrast to preclinical studies with TLR ligands during HIV/Simian immunodeficiency virus (SIV) infection *in vivo* and *in vitro* (18, 21, 63). TLR9 agonist (MGN1703) has been shown to enhance HIV-1 transcription *in vitro* in PBMCs from aviremic donors (18). Moreover, recent preclinical studies of TLR7 agonists (GS-9620 and GS-980, Gilead) in SIV-infected non-human primates receiving cART, revealed transient increases in plasma SIV RNA levels and decreased viral reservoirs in PBMCs and lymph nodes (21). Additionally, viral load in two of the treated animals remained undetectable for more than 90 days after ART interruption (21).

There remains scant clinical data regarding the use of TLR ligands alone during HIV infection with the exception of a clinical trial that administered TLR9 agonist MGN-1703, twice weekly for 4 weeks, in cART suppressed patients (20). The study demonstrated a significant increase in plasma viremia in 6 out 15 patients along with increase in pDC, NK cell, and $CD8^+$ T cell activation and induction of plasma IFNα, TNFα, IFNγ during the course of the study. The differential findings in these studies with other TLR ligands vs. the current trial may be related to distinct effects of the TLR ligands themselves and to the dissimilar dosing strategies utilized. Though each of these TLR ligands (3, 7, 9) are involved in anti-viral immunity and known to stimulate type I IFN responses, TLRs 7 and 9 are expressed on pDC, as opposed to TLR3 which is expressed on mDC, perhaps accounting for divergent effects of these ligands on innate immunity in a vaccine context (64). Moreover, latency reversal effects of TLR7 ligands in SIV infection setting was not observed following the first two doses, but became evident after 3 more doses of the 10–19 received in total, indicating a net cumulative effect (21). It is possible that additional and/or higher doses of Poly-ICLC would have resulted in similar effects on viral latency. Given the early phase of this clinical trial with a primary emphasis on safety, such dosing regimens were not suitable. Exploration of increased or expanded dosing strategies and routes of administration in future studies will help clarify Poly-ICLC's effect on HIV latency.

There are several limitations to this study that must be considered, including relatively small sample size. This prevented the evaluation of multiple sub-group analyses, including the influence of individual ART regimens on immunologic and virologic parameters, which have been shown to alter TLR responsiveness *in vitro* (65). Other limitations include the overall homogeneity of the study population in terms of gender, though racially and ethnically diverse. Furthermore, due to strict study entry criteria designed to maximize safety, the exclusion of older individuals (>55 years) and common comorbidities such as cardiovascular disease and diabetes further limit the generalizability of the safety findings in the HIV-infected population as a whole. Additional studies that increase the diversity of the HIV-infected individuals included will help to bolster these safety findings.

In summary, the TLR3 ligand, Poly-ICLC, was safe and tolerable in the HIV-infected population studied and transiently stimulated innate immune responses without resulting in undue immune activation. Given the promising safety profile of PolyICLC in our trial, future studies may now be designed; enlisting a larger cohort, with a wider inclusion criteria, longer duration, and more frequent dosing to further optimize the potential use for PolyICLC as a latency reversal agent. Moreover, this study paves the way for HIV therapeutic vaccines trials that combine Poly-ICLC with HIV antigen vaccines to enhance adaptive immunity to ultimately reduce viral reservoirs.

ETHICS STATEMENT

This study was carried out in accordance with the good clinical practice (GCP), with written informed consent from all participants in accordance with the Declaration of Helsinki. The protocol was approved by Ethics Committees and IRBs at Icahn School of Medicine at Mount Sinai and Rockefeller University Hospital.

AUTHOR CONTRIBUTIONS

MS: critical data analysis, manuscript writing, reviewing, and editing. RS and EM: protocol immunologists. RS and HD: specimen handling and processing at Vaccine and Cell Therapy Laboratory at Icahn School of Medicine at Mount Sinai. HM: protocol virologist and manuscript review. ML: data and regulatory management. JC: biostatistician. AS: study design and reagents. MM: co-principal investigator, manuscript revision, and study design. NB and EM: co-principal investigators, senior authors, study design, data interpretation and manuscript writing and reviewing.

ACKNOWLEDGMENTS

This study was supported by funding from NIH/NIAID (R37 AI044628 to NB, R21 AI110736 to EM) and the Campbell Foundation to NB and EM. This research was also supported in part by grant # UL1 TR000043 from the National Center for Advancing Translational Sciences (NCATS, National Institutes of Health (NIH) Clinical and Translational Science Award (CTSA) program. NB is a member of the Parker Institute for Cancer Immunotherapy, which supports the Icahn School of Medicine at Mount Sinai, NY, Cancer Immunotherapy Program.

SUPPLEMENTARY MATERIAL

The Supplementary Material for this article can be found online at: https://www.frontiersin.org/articles/10.3389/fimmu.2019.00725/full#supplementary-material

Supplemental Figure 1 | No induction of soluble mediators of inflammation upon Poly-ICLC administration. Plasma levels of IFN alpha, IFN beta, TNF alpha, sCD14, D-dimer, and C-reactive protein (CRP) for each subject are shown as a mean with standard deviation over the course of the study as measured by ELISA. Values for subjects in Arm A (Poly-ICLC) and Arm B (Placebo) are depicted by solid (black) and dashed (red) lines, respectively. No longitudinal changes were found to be statistically significant following Poly-ICLC administration.

Supplemental Table 1 | Transient upregulation of pro-inflammatory genes in subjects whom received Poly-ICLC. Transcriptional responses were evaluated longitudinally in subjects' PBMCs using NanoString Technologies (nCounter® gene expression panel, human inflammation kit). Fold change (FC) from baseline of all significantly up regulated genes ($p < 0.05$, FDR < 1, FC ≥ +/−1.5) from subjects in Arm A (Poly-ICLC) are shown through day 8. No significant changes were observed in subjects' PBMCs in Arm B (Placebo) (not shown).

REFERENCES

1. Espindola MS, Soares LS, Galvao-Lima LJ, Zambuzi FA, Cacemiro MC, Brauer VS, et al. HIV infection: focus on the innate immune cells. *Immunol Res.* (2016) 64:1118–32. doi: 10.1007/s12026-016-8862-2
2. Miller E, Spadaccia M, Sabado R, Chertova E, Bess J, Trubey CM, et al. Autologous aldrithiol-2-inactivated HIV-1 combined with polyinosinic-polycytidylic acid-poly-L-lysine carboxymethylcellulose as a vaccine platform for therapeutic dendritic cell immunotherapy. *Vaccine.* (2015) 33:388–95. doi: 10.1016/j.vaccine.2014.10.054
3. Miller EA, Gopal R, Valdes V, Berger JS, Bhardwaj N, O'Brien MP. Soluble CD40 ligand contributes to dendritic cell-mediated T-cell dysfunction in HIV-1 infection. *AIDS.* (2015) 29:1287–96. doi: 10.1097/QAD.0000000000000698
4. Buisson S, Benlahrech A, Gazzard B, Gotch F, Kelleher P, Patterson S. Monocyte-derived dendritic cells from HIV type 1-infected individuals show reduced ability to stimulate T cells and have altered production of interleukin (IL)-12 and IL-10. *J Infect Dis.* (2009) 199:1862–71. doi: 10.1086/599122
5. Smed-Sorensen A, Lore K, Walther-Jallow L, Andersson J, Spetz AL. HIV-1-infected dendritic cells up-regulate cell surface markers but fail to produce IL-12 p70 in response to CD40 ligand stimulation. *Blood.* (2004) 104:2810–7. doi: 10.1182/blood-2003-07-2314
6. Frleta D, Ochoa CE, Kramer HB, Khan SA, Stacey AR, Borrow P, et al. HIV-1 infection-induced apoptotic microparticles inhibit human DCs via CD44. *J Clin Invest.* (2012) 122:4685–97. doi: 10.1172/JCI64439
7. Battistini A, Sgarbanti M. HIV-1 latency: an update of molecular mechanisms and therapeutic strategies. *Viruses.* (2014) 6:1715–58. doi: 10.3390/v6041715
8. Saxena M, Bhardwaj N. Turbocharging vaccines: emerging adjuvants for dendritic cell based therapeutic cancer vaccines. *Curr Opin Immunol.* (2017) 47:35–43. doi: 10.1016/j.coi.2017.06.003
9. Katlama C, Deeks SG, Autran B, Martinez-Picado J, van Lunzen J, Rouzioux C, et al. Barriers to a cure for HIV: new ways to target and eradicate HIV-1 reservoirs. *Lancet.* (2013) 381:2109–17. doi: 10.1016/S0140-6736(13)60104-X
10. Swaminathan G, Navas-Martin S, Martin-Garcia J. Interplay between microRNAs, Toll-like receptors, and HIV-1: potential implications in HIV-1 replication and chronic immune activation. *Discov Med.* (2014) 18:15–27.
11. Matsumoto M, Seya T. TLR3: interferon induction by double-stranded RNA including poly(I:C). *Adv Drug Deliv Rev.* (2008) 60:805–12. doi: 10.1016/j.addr.2007.11.005
12. Petes C, Odoardi N, Gee K. The toll for trafficking: toll-like receptor 7 delivery to the endosome. *Front Immunol.* (2017) 8:1075. doi: 10.3389/fimmu.2017.01075
13. Muller T, Hamm S, Bauer S. TLR9-mediated recognition of DNA. *Handb Exp Pharmacol* 2008:51–70. doi: 10.1007/978-3-540-72167-3_3
14. Satoh T, Akira S. Toll-like receptor signaling and its inducible proteins. *Microbiol Spectr.* (2016) 4. doi: 10.1128/microbiolspec.MCHD-0040-2016
15. Sivori S, Carlomagno S, Pesce S, Moretta A, Vitale M, Marcenaro E. TLR/NCR/KIR: which one to use and when? *Front Immunol.* (2014) 5:105. doi: 10.3389/fimmu.2014.00105
16. Saxena M, Bhardwaj N. Re-emergence of dendritic cell vaccines for cancer treatment. *Trends Cancer.* (2018) 4:119–37. doi: 10.1016/j.trecan.2017.12.007
17. Novis CL, Archin NM, Buzon MJ, Verdin E, Round JL, Lichterfeld M, et al. Reactivation of latent HIV-1 in central memory CD4(+) T cells through TLR-1/2 stimulation. *Retrovirology.* (2013) 10:119. doi: 10.1186/1742-4690-10-119
18. Offersen R, Nissen SK, Rasmussen TA, Ostergaard L, Denton PW, Sogaard OS, et al. A novel toll-like receptor 9 agonist, MGN1703, enhances hiv-1 transcription and nk cell-mediated inhibition of hiv-1-infected autologous CD4+ T cells. *J Virol.* (2016) 90:4441–53. doi: 10.1128/JVI.00222-16
19. Tsai A, Irrinki A, Kaur J, Cihlar T, Kukolj G, Sloan DD, et al. Toll-like receptor 7 agonist gs-9620 induces HIV expression and HIV-specific immunity in cells from HIV-infected individuals on suppressive antiretroviral therapy. *J Virol.* (2017) 91:e02166–16. doi: 10.1128/JVI.02166-16
20. Vibholm L, Schleimann MH, Hojen JF, Benfield T, Offersen R, Rasmussen K, et al. Short-course toll-like receptor 9 agonist treatment impacts innate immunity and plasma viremia in individuals with human immunodeficiency virus infection. *Clin Infect Dis.* (2017) 64:1686–95. doi: 10.1093/cid/cix201
21. Lim SY, Osuna CE, Hraber PT, Hesselgesser J, Gerold JM, Barnes TL, et al. TLR7 agonists induce transient viremia and reduce the viral reservoir in SIV-infected rhesus macaques on antiretroviral therapy. *Sci Transl Med.* (2018) 10:eaao4521. doi: 10.1126/scitranslmed.aao4521
22. Martins KA, Bavari S, Salazar AM. Vaccine adjuvant uses of poly-IC and derivatives. *Expert Rev Vaccines.* (2015) 14:447–59. doi: 10.1586/14760584.2015.966085
23. McCartney S, Vermi W, Gilfillan S, Cella M, Murphy TL, Schreiber RD, et al. Distinct and complementary functions of MDA5 and TLR3 in poly(I:C)-mediated activation of mouse NK cells. *J Exp Med.* (2009) 206:2967–76. doi: 10.1084/jem.20091181
24. Zhang Z, Kim T, Bao M, Facchinetti V, Jung SY, Ghaffari AA, et al. DDX1, DDX21, and DHX36 helicases form a complex with the adaptor molecule TRIF to sense dsRNA in dendritic cells. *Immunity.* (2011) 34:866–78. doi: 10.1016/j.immuni.2011.03.027
25. Longhi MP, Trumpfheller C, Idoyaga J, Caskey M, Matos I, Kluger C, et al. Dendritic cells require a systemic type I interferon response to mature and induce CD4+ Th1 immunity with poly IC as adjuvant. *J Exp Med.* (2009) 206:1589–602. doi: 10.1084/jem.20090247
26. Cheng L, Zhang Z, Li G, Li F, Wang L, Zhang L, et al. Human innate responses and adjuvant activity of TLR ligands in vivo in mice reconstituted with a human immune system. *Vaccine.* (2017) 35:6143–53. doi: 10.1016/j.vaccine.2017.09.052
27. Alvarez-Carbonell D, Garcia-Mesa Y, Milne S, Das B, Dobrowolski C, Rojas R, et al. Toll-like receptor 3 activation selectively reverses HIV latency in microglial cells. *Retrovirology.* (2017) 14:9. doi: 10.1186/s12977-017-0335-8
28. Kyi C, Roudko V, Sabado R, Saenger YM, Loging W, Mandeli J, et al. Therapeutic immune modulation against solid cancers with intratumoral poly-ICLC: a pilot trial. *Clin Cancer Res.* (2018) 24:4937–48. doi: 10.1158/1078-0432.CCR-17-1866
29. Liu H, Zha Y, Choudhury N, Malnassy G, Fulton N, Green M, et al. WT1 peptide vaccine in Montanide in contrast to poly ICLC, is able to induce WT1-specific immune response with TCR clonal enrichment in myeloid leukemia. *Exp Hematol Oncol.* (2018) 7:1. doi: 10.1186/s40164-018-0093-x
30. Griffiths EA, Srivastava P, Matsuzaki J, Brumberger Z, Wang ES, Kocent J, et al. NY-ESO-1 vaccination in combination with decitabine induces antigen-specific t-lymphocyte responses in patients with myelodysplastic syndrome. *Clin Cancer Res.* (2018) 24:1019–29. doi: 10.1158/1078-0432.CCR-17-1792
31. Caskey M, Lefebvre F, Filali-Mouhim A, Cameron MJ, Goulet JP, Haddad EK, et al. Synthetic double-stranded RNA induces innate immune responses similar to a live viral vaccine in humans. *J Exp Med.* (2011) 208:2357–66. doi: 10.1084/jem.20111171
32. Tsuji T, Sabbatini P, Jungbluth AA, Ritter E, Pan L, Ritter G, et al. Effect of Montanide and poly-ICLC adjuvant on human self/tumor antigen-specific CD4+ T cells in phase I overlapping long peptide vaccine trial. *Cancer Immunol Res.* (2013) 1:340–50. doi: 10.1158/2326-6066.CIR-13-0089
33. Salazar AM, Erlich RB, Mark A, Bhardwaj N, Herberman RB. Therapeutic in situ autovaccination against solid cancers with intratumoral poly-ICLC: case report, hypothesis, and clinical trial. *Cancer Immunol Res.* (2014) 2:720–4. doi: 10.1158/2326-6066.CIR-14-0024
34. Aravantinou M, Frank I, Hallor M, Singer R, Tharinger H, Kenney J, et al. PolyICLC exerts pro- and anti-HIV effects on the DC-T cell milieu *in vitro* and *in vivo*. *PLoS ONE.* (2016) 11:e0161730. doi: 10.1371/journal.pone.0161730
35. Vagenas P, Aravantinou M, Williams VG, Jasny E, Piatak M Jr, Lifson JD, et al. A tonsillar PolyICLC/AT-2 SIV therapeutic vaccine maintains low viremia following antiretroviral therapy cessation. *PLoS ONE.* (2010) 5:e12891. doi: 10.1371/journal.pone.0012891
36. Park H, Adamson L, Ha T, Mullen K, Hagen SI, Nogueron A, et al. Polyinosinic-polycytidylic acid is the most effective TLR adjuvant for SIV gag protein-induced T cell responses in nonhuman primates. *J Immunol.* (2013) 190:4103–15. doi: 10.4049/jimmunol.1202958
37. Zurawski G, Zurawski S, Flamar AL, Richert L, Wagner R, Tomaras GD, et al. Targeting HIV-1 Env gp140 to LOX-1 elicits immune responses in rhesus macaques. *PLoS ONE.* (2016) 11:e0153484. doi: 10.1371/journal.pone.0153484
38. Flynn BJ, Kastenmuller K, Wille-Reece U, Tomaras GD, Alam M, Lindsay RW, et al. Immunization with HIV Gag targeted to dendritic cells followed by recombinant New York vaccinia virus induces robust T-cell immunity

in nonhuman primates. *Proc Natl Acad Sci USA*. (2011) 108:7131–6. doi: 10.1073/pnas.1103869108
39. Miller EA, Spadaccia MR, O'Brien MP, Rolnitzky L, Sabado R, Manches O, et al. Plasma factors during chronic HIV-1 infection impair IL-12 secretion by myeloid dendritic cells via a virus-independent pathway. *J Acquir Immune Defic Syndr*. (2012) 61:535–44. doi: 10.1097/QAI.0b013e31826afbce
40. Miller EA, Spadaccia MR, Norton T, Demmler M, Gopal R, O'Brien M, et al. Attenuated Listeria monocytogenes vectors overcome suppressive plasma factors during HIV infection to stimulate myeloid dendritic cells to promote adaptive immunity and reactivation of latent virus. *AIDS Res Hum Retroviruses*. (2015) 31:127–36. doi: 10.1089/aid.2014.0138
41. Markowitz M, Evering TH, Garmon D, Caskey M, La Mar M, Rodriguez K, et al. A randomized open-label study of 3- versus 5-drug combination antiretroviral therapy in newly HIV-1-infected individuals. *J Acquir Immune Defic Syndr*. (2014) 66:140–7. doi: 10.1097/QAI.0000000000000111
42. Palmer S, Wiegand AP, Maldarelli F, Bazmi H, Mican JM, Polis M, et al. New real-time reverse transcriptase-initiated PCR assay with single-copy sensitivity for human immunodeficiency virus type 1 RNA in plasma. *J Clin Microbiol*. (2003) 41:4531–6. doi: 10.1128/JCM.41.10.4531-4536.2003
43. Hintze J. *P"ASS12. NCSS*. Kaysville, UT: LLC (2012). Available online at: www.ncss.com
44. Archin NM, Liberty AL, Kashuba AD, Choudhary SK, Kuruc JD, Crooks AM, et al. Administration of vorinostat disrupts HIV-1 latency in patients on antiretroviral therapy. *Nature*. (2012) 487:482–5. doi: 10.1038/nature11286
45. Chang JJ, Lacas A, Lindsay RJ, Doyle EH, Axten KL, Pereyra F, et al. Differential regulation of toll-like receptor pathways in acute and chronic HIV-1 infection. *AIDS*. (2012) 26:533–41. doi: 10.1097/QAD.0b013e32834f3167
46. Rautela J, Huntington ND. IL-15 signaling in NK cell cancer immunotherapy. *Curr Opin Immunol*. (2017) 44:1–6. doi: 10.1016/j.coi.2016.10.004
47. Shapiro MJ, Spruce L, Sundsbak R, Thapa P, Shapiro VS. Phosphorylation at serine 318 is not required for inhibition of T cell activation by ALX. *Biochem Biophys Res Commun*. (2010) 396:994–8. doi: 10.1016/j.bbrc.2010.05.043
48. Cornish GH, Sinclair LV, Cantrell DA. Differential regulation of T-cell growth by IL-2 and IL-15. *Blood*. (2006) 108:600–8. doi: 10.1182/blood-2005-12-4827
49. Saxena M, Yeretssian G. NOD-like receptors: master regulators of inflammation and cancer. *Front Immunol*. (2014) 5:327. doi: 10.3389/fimmu.2014.00327
50. Balan S, Arnold-Schrauf C, Abbas A, Couespel N, Savoret J, Imperatore F, et al. Large-scale human dendritic cell differentiation revealing notch-dependent lineage bifurcation and heterogeneity. *Cell Rep*. (2018) 24:1902–15.e1906. doi: 10.1016/j.celrep.2018.07.033
51. Milush JM, Lopez-Verges S, York VA, Deeks SG, Martin JN, Hecht FM, et al. CD56negCD16(+) NK cells are activated mature NK cells with impaired effector function during HIV-1 infection. *Retrovirology*. (2013) 10:158. doi: 10.1186/1742-4690-10-158
52. Jacobson A, Bell F, Lejarcegui N, Mitchell C, Frenkel L, Horton H. Healthy neonates possess a CD56-negative NK cell population with reduced anti-viral activity. *PLoS ONE*. (2013) 8:e67700. doi: 10.1371/journal.pone.0067700
53. da Silva IP, Gallois A, Jimenez-Baranda S, Khan S, Anderson AC, Kuchroo VK, et al. Reversal of NK-cell exhaustion in advanced melanoma by Tim-3 blockade. *Cancer Immunol Res*. (2014) 2:410–22. doi: 10.1158/2326-6066.CIR-13-0171
54. Gonzalez-Gugel E, Saxena M, Bhardwaj N. Modulation of innate immunity in the tumor microenvironment. *Cancer Immunol Immunother*. (2016) 65:1261–8. doi: 10.1007/s00262-016-1859-9
55. Akazawa T, Ebihara T, Okuno M, Okuda Y, Shingai M, Tsujimura K, et al. Antitumor NK activation induced by the Toll-like receptor 3-TICAM-1 (TRIF) pathway in myeloid dendritic cells. *Proc Natl Acad Sci USA*. (2007) 104:252–7. doi: 10.1073/pnas.0605978104
56. Nouri-Shirazi M, Tamjidi S, Nourishirazi E, Guinet E. TLR8 combined withTLR3 or TLR4 agonists enhances DC-NK driven effector Tc1 cells. *Immunol Lett*. (2018) 193:58–66. doi: 10.1016/j.imlet.2017.10.015
57. Dhodapkar MV, Sznol M, Zhao B, Wang D, Carvajal RD, Keohan ML, et al. Induction of antigen-specific immunity with a vaccine targeting NY-ESO-1 to the dendritic cell receptor DEC-205. *Sci Transl Med*. (2014) 6:232ra251. doi: 10.1126/scitranslmed.3008068
58. Okada H, Butterfield LH, Hamilton RL, Hoji A, Sakaki M, Ahn BJ, et al. Induction of robust type-I CD8+ T-cell responses in WHO grade 2 low-grade glioma patients receiving peptide-based vaccines in combination with poly-ICLC. *Clin Cancer Res*. (2015) 21:286–94. doi: 10.1158/1078-0432.CCR-14-1790
59. Quarona V, Zaccarello G, Chillemi A, Brunetti E, Singh VK, Ferrero E, et al. CD38 and CD157: a long journey from activation markers to multifunctional molecules. *Cytometry B Clin Cytom*. (2013) 84:207–17. doi: 10.1002/cyto.b.21092
60. Urban SL, Berg LJ, Welsh RM. Type 1 interferon licenses naive CD8 T cells to mediate anti-viral cytotoxicity. *Virology*. (2016) 493:52–9. doi: 10.1016/j.virol.2016.03.005
61. Castro-Gonzalez S, Colomer-Lluch M, Serra-Moreno R. Barriers for a HIV cure: the latent reservoir. *AIDS Res Hum Retroviruses*. (2018) 34:739–59. doi: 10.1089/aid.2018.0118
62. Kent SJ, Reece JC, Petravic J, Martyushev A, Kramski M, De Rose R, et al. The search for an HIV cure: tackling latent infection. *Lancet Infect Dis*. (2013) 13:614–21. doi: 10.1016/S1473-3099(13)70043-4
63. Jones RB, Mueller S, O'Connor R, Rimpel K, Sloan DD, Karel D, et al. A subset of latency-reversing agents expose HIV-infected resting CD4+ T-cells to recognition by cytotoxic T-lymphocytes. *PLoS Pathog*. (2016) 12:e1005545. doi: 10.1371/journal.ppat.1005545
64. Saxena M, Balan S, Roudko V, Bhardwaj N. Towards superior dendritic-cell vaccines for cancer therapy. *Nat Biomed Eng*. (2018) 2:341–6. doi: 10.1038/s41551-018-0250-x
65. Melchjorsen J, Risor MW, Sogaard OS, O'Loughlin KL, Chow S, Paludan SR, et al. Tenofovir selectively regulates production of inflammatory cytokines and shifts the IL-12/IL-10 balance in human primary cells. *J Acquir Immune Defic Syndr*. (2011) 57:265–75. doi: 10.1097/QAI.0b013e3182185276

Conflict of Interest Statement: NB has received research funds from Merck and is on the senior advisory board of Check Point Diagnostics, Curevac, Prime vax, Neon, and Tempest Therapeutics. EM is a current employee of Regeneron Pharmaceuticals, and serves on the Board of Trustees of Abzyme Research Foundation. AS is the CEO and Scientific Director of Oncovir, Inc. RS is a current employee of Genentech.

The remaining authors declare that the research was conducted in the absence of any commercial or financial relationships that could be construed as a potential conflict of interest.

frontiers in Immunology

ORIGINAL RESEARCH
published: 17 April 2019
doi: 10.3389/fimmu.2019.00814

Neuroanatomical Changes Underlying Vertical HIV Infection in Adolescents

Xiao Yu[1†], Lei Gao[1†], Haha Wang[1], Zhuang Yin[1], Jian Fang[1], Jing Chen[2], Qiang Li[3], Haibo Xu[1] and Xien Gui[3*]*

[1] Department of Radiology, Zhongnan Hospital of Wuhan University, Wuhan University, Wuhan, China, [2] Publicity Department, Zhongnan Hospital of Wuhan University, Wuhan University, Wuhan, China, [3] Training Centre of AIDS Prevention and Cure of Hubei Province, Zhongnan Hospital of Wuhan University, Wuhan University, Wuhan, China

Purpose: The aim of this study was to investigate how human immunodeficiency virus (HIV) affects brain development in adolescents, what are susceptible brain regions, and how these brain structural changes correlate with cognitive abilities.

Methods: We used structural magnetic resonance imaging to examine gray matter volume and cortical thickness in 16 HIV-infected children (mean age = 13.63 years) and 25 HIV-exposed uninfected children (mean age = 13.32 years), 12 of them were subjected to a 1-year repetitive magnetic resonance scan of the brain. Five neurocognitive tests were performed on each subject to assess cognitive performance in different areas.

Results: Cross-sectional studies showed that the gray matter volume of HIV-infected children was widely reduced (mainly in the bilateral frontal, temporal, and insular regions, and cerebellum). The changes in cortical thickness were mainly due to thinning of the right temporal lobe and thickening of the left occipital lobe. Longitudinal studies showed that the gray matter volume reduction of HIV-infected children after 1 year mainly occurs in the advanced functional area of the right prefrontal, parietal lobe and the motor area, cortical thinning of brain regions were sensorimotor cortex and the limbic system. The gray matter volume of the bilateral cerebellum was positively correlated with the performance of the Wisconsin Card Sorting Test, while the cortical thickness of the right dorsolateral prefrontal cortex was negatively correlated with this test.

Conclusion: This study found that HIV-infected pubertal children showed a delayed cortical maturation with atrophy. This abnormal pattern of cortical development may be the structural basis for cognitive impairment in HIV-infected children.

Keywords: AIDS, brain development, structural MRI, HIV exposure, children, mother-to-child transmission

OPEN ACCESS

Edited by:
Martin Hoenigl, University of California, San Diego, United States

Reviewed by:
Sarah Rowland-Jones, University of Oxford, United Kingdom
Michelli Faria De Oliveira, University of California, San Diego, United States

***Correspondence:**
Haibo Xu
xuhaibo1120@hotmail.com
Xien Gui
znact@126.com

[†]These authors have contributed equally to this work

Specialty section:
This article was submitted to Viral Immunology, a section of the journal Frontiers in Immunology

Received: *30 July 2018*
Accepted: *27 March 2019*
Published: *17 April 2019*

Citation:
Yu X, Gao L, Wang H, Yin Z, Fang J, Chen J, Li Q, Xu H and Gui X (2019) Neuroanatomical Changes Underlying Vertical HIV Infection in Adolescents. Front. Immunol. 10:814. doi: 10.3389/fimmu.2019.00814

INTRODUCTION

Acquired immune deficiency syndrome (AIDS)-related encephalopathy is one of the most serious complications of AIDS and is more common in children than in adults (1). At present, there are nearly 2 million children living with human immunodeficiency virus (HIV) in the world, almost all newly infected children are infected through mother-to-child transmission (2). Effective antiretroviral therapy (ART) can significantly reduce mortality and the incidence

of HIV encephalopathy (3). Although the children's HIV/AIDS has been transformed into chronic, controllable disease patterns, due to the HIV virus, antiretroviral drugs and a variety of environmental factors, a series of neuropsychological defects can still appear on HIV-infected (HIV+) children, sometimes even after the treatment has fully been accepted (4).

Currently, some studies have reported and summarized the neurocognitive impairment and behavioral abnormality in children infected with HIV. For example, language barriers, delayed motor development, poor school performance, etc., and some may even have psychological problems such as anxiety and depression (5, 6). Although highly active antiretroviral therapy can improve the cognitive function of HIV+ children in the long run (7), there are also studies showing that cognitive impairment will exist for a long time (8). It will affect their future learning, work performance and social practice, we need to focus on long-term outcomes of nervous system development to inform treatment options and guide early intervention treatment strategy to prevent deterioration of cognitive function.

The rapid development of neuroimaging has provided us with a powerful tool for studying brain development in children. Current structural magnetic resonance imaging (MRI) studies have observed some changes in brain structure in HIV+ children and adolescents, including subcortical volume, shape deformation (9), gyrification, and overall or regional gray matter volume (GMV) reduction (10, 11), but there are very few longitudinal research on cortical development. A longitudinal study observed persistent damage to human white matter development in HIV+ children, regardless of whether they received antiretroviral therapy or viral suppression at an early stage (12). Furthermore, many studies have used the emerging MRI technology to reveal the characteristics of brain structure, function and the influence of cognitive factors in children with HIV/AIDS, but the future impact of these developmental abnormalities are still unclear, brain regions vulnerable to HIV or antiretroviral drugs have also not been identified (13–15).

Some studies have shown that the developmental maturity of brain structure is consistent with the development of individual cognitive ability (16, 17). We hypothesized that HIV would have less influence on the development of brain regions related to primary functions such as sensory and motor domains, but have a greater impact on the development of brain regions related to advanced cognition such as decision-making and reasoning. We attempted to conduct cross-sectional and longitudinal studies through high-resolution structural MRI to observe which brain regions HIV may preferentially affect and to combine multiple domains of neuropsychological cognitive testing to observe the correlation between brain structural changes and cognitive ability.

Abbreviations: AIDS, acquired immune deficiency syndrome; HIV, human immunodeficiency virus; HIV+, HIV-infected; MRI, magnetic resonance imaging; GMV, gray matter volume; HEU, HIV-exposed uninfected; VBM, voxel-based morphometric; CT, cortical thickness; MNI, Montreal neurological institute; FWE, Family Wise Error; TFCE, threshold-free cluster enhancement; OFC, orbital frontal cortex.

MATERIALS AND METHODS

Subjects

We recruited 16 HIV+ adolescents (mean age ± SD, 13.63 ± 1.83 years; range, 11–17 years; mean CD4 count ± SD, 558.87 ± 199.89 cells/mm^3; range, 276–940), the viral load of them did not reach the lower limit of detection (<20 copies/ml). The presence of HIV+ children was confirmed by Western blot. We also recruited 25 age- and gender-matched HIV-Exposed Uninfected (HEU) subjects (mean age ± SD, 13.32 ± 1.62 years; range,11–17 years). All HIV+ adolescents were infected by mother-to-child transmission during pregnancy, childbirth or through breastfeeding. HEU subjects' fathers, mothers, or parents also suffered from HIV infections. The socioeconomic status, cultural background and ethnic background of the two communities were similar. Detailed population information and clinical measures are listed in **Table 1**. All subjects were enrolled from Training Centre of AIDS Prevention and Cure of Hubei Province. The inclusion criteria for HIV+ subjects included HIV acquisition during the fetal or neonatal period, currently treated with ART, and right-handed. For the control subjects, the inclusion criteria included confirmation of HIV negative status by ELISA and right-handedness.

Exclusion criteria for all subjects included those younger than 11 years of age or over 17 years of age, with acute medical illnesses, current or past medical or neurological diseases, psychiatric illnesses, mental retardation, current alcohol or drug abuse, HIV encephalopathy and opportunistic infections, MRI contraindications, claustrophobia, metabolic disorders or other brain diseases (not AIDS-related). We used the exclusion criteria, which included HIV-related encephalopathy to rule out space-occupying masses, other lesions or obvious cortical atrophy in the brain of HIV+ adolescents, so that we got the difference in anatomical gray matter covariance between the two groups. Only one individual in the HIV+ group was excluded because of age 7. For the control subjects, the exclusion criteria also included serious educational difficulties and a chronic medication other than asthma medication.

The study was approved by the Medical Ethics Committee of Zhongnan Hospital of Wuhan University, and a written and informed consent was made from all participants or their guardians in accordance with the Helsinki Declaration of 1975 (and as revised in 1983), following a complete description of the measurements. These methods were carried out in accordance with the approved guidelines and regulations.

Neuropsychological Tests

In order to more comprehensively assess the cognitive abilities of the subjects, we selected five tests based on the Frascati criteria (21). (1) Word Semantics Test: to examine written language comprehension, especially at the level of sentences. (2) Verbal Working Memory Test (present audio): comes from the digital memory span subtest of Wechsler Intelligence Scale. (3) Wisconsin Card Sorting Test: to examine executive control capabilities. (4) Picture Memory Test. (5) Indicate the Midpoint Test of the Line Segment: focus on sensory

TABLE 1 | Demographics and results of neuropsychological tests.

	HIV+ group	HEU group	*p*-value	Cohen' *d*(ES)	Power
Number of subjects (*n*)	16	25	–	–	–
Sex (male/female)	8/8	12/13	0.915	–	–
Age (years)	13.63 ± 1.83	13.32 ± 1.62	0.589	0.176	0.135
BMI (kg/m^2)	18.27 ± 2.66	18.29 ± 3.06	0.873	0.008	0.053
Education (years)	7.31 ± 2.20	7.16 ± 1.51	0.799	0.081	0.081
Ethnicity (Han/Tujia)	15/1	24/1	0.904	–	–
Longitudinal data (*n*)	5 (31.25%)	7 (28.0%)	–	–	–
Mother-to-child transmission	16 (100%)	25 (100%)	–	–	–
CD4 count (cells/mm^3)	558.87 ± 199.89	–	–	–	–
COGNITIVE DOMAIN					
Vocabulary/language (*n*)	4 (26.67%)	0 (0%)	0.17	–	–
Working memory/attention (*n*)	3 (23.08%)	0 (0%)	0.269	–	–
Executive/abstraction (*n*)	7 (46.67%)	0 (0%)	**0.015**	–	–
Memory/learning and recall (n)	1 (6.67%)	0 (0%)	0.733	–	–
Sensory perceptual/motor skills (*n*)	0 (0%)	0 (0%)	–	–	–

HIV+, HIV-infected; HEU, HIV-exposed uninfected; ES, effect size; BMI, Body Mass Index, Values are n (% of total) or mean ± standard-deviation. Cognitive results of individuals in HIV+ group failed to follow the normal distribution test, thus we used the rank sum test. Significance at P < 0.05.

perceptual and motor skills. We conducted all tests online using the professional "Multi-Dimensional Psychology" platform (http://www.dweipsy.com/lattice/). All these tests and MRI scans were carried out within a month of study enrollment for each participant.

MRI Acquisition

High-resolution T1-weighted structural MRI scans were acquired on the 3.0 T scanner (Siemens, Prisma, Germany), which was stationed at the Department of Radiology, the Zhongnan Hospital of Wuhan University, using a multi-echo magnetization prepared rapid gradient echo (MPRAGE) pulse sequence (repetition time = 5,000 ms, echo time = 2.88 ms, inversion time = 700 ms, flip angle = 4°, slice thickness = 1.00 mm, and matrix size = 256 × 256) that yielded 176 axial slices with an in-plane resolution of 1.0 × 1.0 mm. We visually inspected the cerebral microbleeds foci measured by susceptibility-weighted imaging (SWI), and white matter hyperintensity by T2- fluid-attenuated inversion recovery (FLAIR) images through all the subjects. We also excluded any subject that exhibited obvious gray and white matter lesion imaged by SWI and FLAIR.

Brain Morphometry Analysis

In this study, we analyzed two morphological brain measures, the gray matter volume [via voxel-based morphometric (VBM) analysis] and cortical thickness (CT) analysis. All data processing uses Statistical Parametric Mapping software (SPM12; Wellcome Department of Cognitive Neurology, London, UK; http://www.fl.ion.ucl.ac.uk/spm) and Computational Anatomy Toolbox (CAT12, http://dbm.neuro.uni-jena.de/vbm/) based on MATLAB (MathWorks, Natick, MA, USA). The data preprocessing mainly included: (1) experienced radiologists screen data with obvious abnormalities, excluding data with large artifacts and obvious lesions; (2) the original T1 images were manually reoriented to match the AC-PC plane, (3) segmented into gray matter, white matter, and cerebrospinal fluid using the standard unified segmented model (18, 19) in the CAT12, (4) nonlinearly normalized into standard Montreal Neurological Institute (MNI) space using a pediatric template for 12- to 18-year-old children from the Imaging Research Center at Cincinnati Children's Hospital Medical Center (CCHMC), (5) the normalized segmentations were then modulated to ensure that the relative volumes of gray matter were retained, (6) the modulated images were re-sampled to 1.5 × 1.5 × 1.5 mm^3 and smoothed with an 8 mm full-width at half-maximum (FWHM) Gaussian kernel, (7) to control for deviations, we included an additional quality check based on heterogeneity measurements of the sample as implemented in CAT; using the covariance of voxel-based data to identify the outliers who were two or more standard deviations outside of the GMV sample distributions, and one patient and one control were excluded based on this criterion, (8) finally, exclude voxels with a gray matter value <0.15 to eliminate the potential edge effects between the gray matter and white matter.

The CT was also computed by using the CAT12, all the parameters were set by default in the CAT12, except for the brain template using a pediatric template for 12- to 18-year-old children from the Imaging Research Center at Cincinnati Children's Hospital Medical Center (CCHMC) (https://irc.cchmc.org/software/pedbrain.php). Briefly, this automated method (20) allows for central surface reconstructions and CT measurement in one step, then the topological defects of cortical surface mesh were repaired by using a spherical harmonic method. Prior to the statistical analyses, the individual CT maps were smoothed by using a Gaussian filter with full-width at half-maximum of 15 mm.

For the longitudinal analysis of GMV and CT, we also used the CAT12 default parameters with the pediatric template and performed the analysis under the longitudinal analysis module to obtain subtle changes at the individual level between the two-time points (1 year before and after).

Statistical Analysis

For clinical and behavioral data, statistical analysis was conducted using IBM SPSS version 20 (IBM SPSS Inc., Chicago, IL, USA) and G*Power 3.1.9.3. The significance threshold was set to $p < 0.05$. For the brain morphological parameters (gray matter volume and cortical thickness), cross-sectional between-group comparisons were tested in SPM12 using independent two-sample *t*-tests, with age and gender as covariates, longitudinal comparisons were carried by flexible design 2 × 2 analysis of variance (ANOVA). The significance threshold was set to $p < 0.05$ with a cluster level Family Wise Error (FWE) correction and threshold-free cluster enhancement (TFCE) multiple comparison-corrected.

TABLE 2 | Between-group comparison on gray matter volume.

Contrast	Brain regions	Extent	*t*-value	MNI Coordinates		
				x	y	z
HIV + < HEU	Frontal_Inf_Tri_R	359	−4.7245	37.5	16.5	28.5
	Frontal_Inf_Oper_L	181	−3.8543	−48	12	13.5
	Temporal_Mid_R	158	−3.8214	45	−58.5	4.5
	Cerebelum_Crus1_L	334	−3.6533	−36	−69	−34.5
	Parietal_Inf_L	146	−3.5301	−27	−61.5	39
	Cerebelum_Crus1_R	378	−3.3279	39	−61.5	−37.5
	Cuneus_R	86	−3.2899	7.5	−81	18
	Insula_L	276	−3.251	−28.5	27	6
	Temporal_Pole_Sup_L	132	−3.1098	−51	6	−3
	Frontal_Mid_2_L	139	−3.0554	−31.5	19.5	60
	Frontal_Inf_Oper_L	124	−2.9471	−39	4.5	25.5
	Frontal_Sup_2_L	88	−2.9143	−18	33	39
	Insula_R	72	−2.9079	34.5	30	0
	Temporal_Sup_L	66	−2.7822	−52.5	−9	−3
	Angular_R	50	−2.7661	30	−60	40.5

HIV+, HIV-infected; HEU, HIV-exposed uninfected; MNI, Montreal Neurological Institute; L, left; R, right. All regions were corrected by FWE cluster level p < 0.05.

RESULTS

Demographics and Neuropsychological Tests

For demographic and clinical data, the HIV+ and HEU controls were comparable on age, gender, and education ($p > 0.05$, **Table 1**). For cognitive testing, the HIV+ group performed significantly worse in the Wisconsin card classification test (execution and abstraction functions) than their HEU controls ($p = 0.015$, **Table 1**). In addition, we also noted that 5 of the adolescents in the HIV+ group scored at least 2 items below the mean of the control group minus a standard deviation of one time, which can be diagnosed asymptomatic neurocognitive impairment according to Frascati criteria (21).

Between-Group Comparison on Gray Matter Volume

We first investigated the between-group differences on GMV by using VBM. This analysis revealed a significant reduction in the GMV across broad regions, including bilateral superior cerebellar, frontal, temporal, insular, angular regions, and right cuneus, in the HIV+ individuals, these results were corrected by FWE cluster level $p < 0.05$ (**Table 2**; **Figure 1**).

Between-Group Comparison on Cortical Thickness

We next reported the between-group differences on surface-based metrics of CT. Individuals with HIV showed significantly thicker cortices in left occipital (the middle and inferior gyri) and right olfactory sulcus, also, significantly thinner cortices in the temporal (the middle and the pole parts) and orbitofrontal regions. The results were corrected by FWE cluster level $p < 0.05$ (**Table 3**; **Figure 2**).

Longitudinal Changes in Gray Matter Volume

Based on the cross-sectional results, an important aim of this study is to investigate the longitudinal brain develop trajectory.

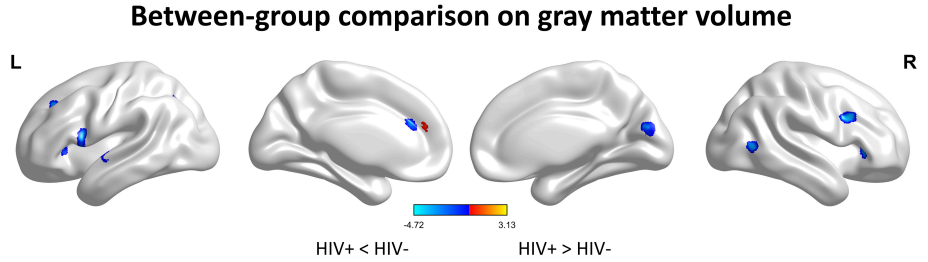

FIGURE 1 | Between-group comparison on gray matter volume (GMV). Clusters showing significantly (corrected $P < 0.05$) lower (blue) and higher (red) GMV in HIV+ children compared to controls. But the red region isn't successfully positioned in the template. This figure was rendered using BrainNet Viewer (http://www.nitrc.org/projects/bnv/).

Using a 2 × 2 ANOVA, we then contrasted the development patterns between the two groups.

For the GMV, generally, the HIV+ group showed changes in GMV over a wider range of brain regions and was dominated by a significant decrease in GMV after 1 year. These regions mainly included decreased GMV in the bilateral frontal, supplementary, parietal, and occipital regions; and increased GMV in the right inferior temporal, inferior occipital and orbital frontal cortex (OFC) regions (**Table 4**; **Figure 3A**).

TABLE 3 | Between-group comparison on cortical thickness.

Contrast	Cortical regions	Side	Size	*P*-value
HIV + > HEU	42% G_occipital_middle 24% S_oc_middle_and_Lunatus 21% G_and_S_occipital_inf 9% Pole_occipital 2% G_pariet_inf-Angular 2%S_oc_sup_and_transversal	L	611	0.00960
	100% G_cingul-Post-ventral	L	1	0.04800
	42% S_orbital_med-olfact 38% G_rectus 15%G_subcallosal	R	79	0.04260
HIV+<HEU	74% G_orbital 26%S_orbital_lateral	L	19	0.04740
	100% G_orbital	L	15	0.04640
	44% G_temporal_middle 32% Pole_temporal 12% S_temporal_inf 11% G_temp_sup-Lateral 1%S_temporal_sup	R	214	0.02880
	66% G_orbital 22% S_orbital_med-olfact 11% G_rectus 1%G_and_S_frontomargin	R	73	0.03380

HIV+, HIV-infected; HEU, HIV-exposed uninfected; L, left; R, right. All regions were corrected by FWE cluster level p <0.05.

TABLE 4 | Volume change of gray matter in HIV+ group after 1 year.

Contrast	Brain regions	Extent	*t*-value	MNI coordinates		
				x	y	z
Positive	Temporal_Inf_R	144	5.440	44	−56	−14
	Occipital_Inf_R	144	4.362	51	−75	−14
	OFCmed_R	134	5.293	21	27	−20
Negative	Frontal_Mid_2_L	306	−8.717	−30	54	6
	Occipital_Sup_R	292	−7.799	27	−69	42
	Supp_Motor_Area_R	2409	−7.215	5	15	50
	Frontal_Sup_Medial_R	2409	−6.253	6	38	51
	Parietal_Sup_R	172	−6.944	38	−50	56
	Precuneus_L	755	−6.851	−8	−47	63
	Paracentral_Lobule_R	755	−4.995	12	−35	48
	Parietal_Inf_L	315	−6.177	−44	−42	51
	Postcentral_L	315	−4.796	−53	−15	36
	Frontal_Sup_2_L	292	−5.973	−18	54	26
	Parietal_Inf_L	281	−5.877	−27	−69	42
	Frontal_Inf_Oper_L	296	−5.857	−50	8	15
	Postcentral_R	113	−5.798	56	−6	29
	Frontal_Sup_2_R	442	−5.697	24	54	27
	Frontal_Mid_2_R	442	−4.432	39	50	14
	Postcentral_R	286	−5.620	47	−35	54
	Cingulate_Post_L	96	−5.516	−6	−50	32
	Precuneus_R	95	−5.365	8	−50	51
	Frontal_Mid_2_L	154	−5.351	−30	47	21
	SupraMarginal_R	69	−5.146	65	−17	27
	Cerebelum_Crus1_L	50	−5.038	−45	−48	−41
	Supp_Motor_Area_R	335	−4.992	3	−11	62
	Frontal_Sup_2_R	81	−4.660	15	47	41
	Temporal_Sup_R	51	−4.435	56	−14	8
	Cerebelum_4_5_L	57	−4.291	−6	−47	−5
	Parietal_Inf_L	54	−4.237	−53	−44	36
	Frontal_Sup_2_L	50	−4.075	−18	42	44
	Precentral_L	71	−4.003	−38	0	60

HIV+, HIV-infected; MNI, Montreal Neurological Institute; L, left; R, right. All regions were corrected by FWE cluster level p < 0.05.

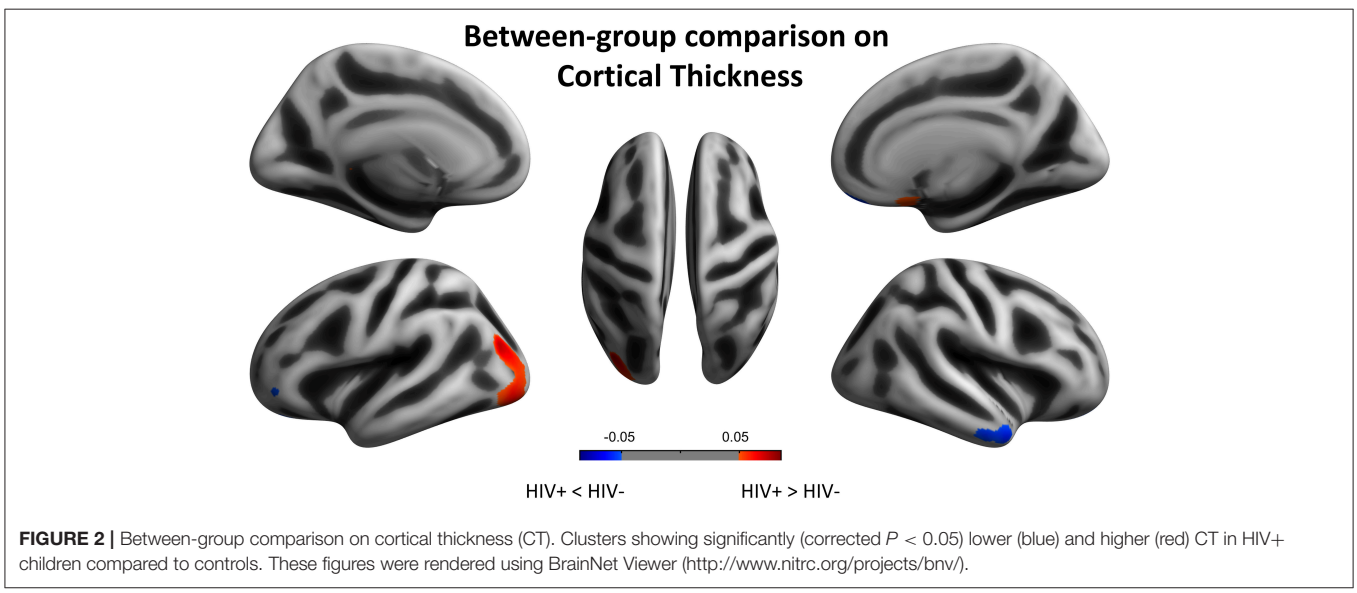

FIGURE 2 | Between-group comparison on cortical thickness (CT). Clusters showing significantly (corrected $P < 0.05$) lower (blue) and higher (red) CT in HIV+ children compared to controls. These figures were rendered using BrainNet Viewer (http://www.nitrc.org/projects/bnv/).

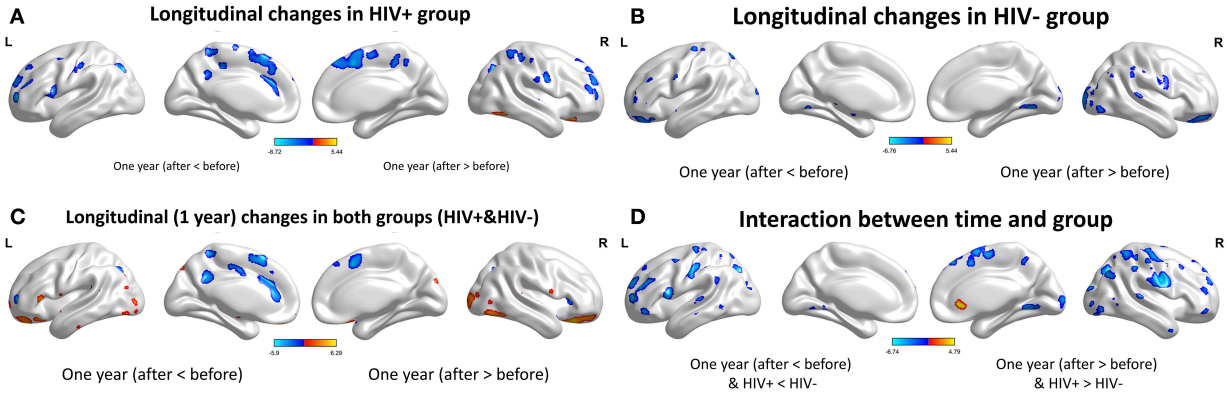

FIGURE 3 | Longitudinal changes on gray matter volume (GMV) after 1 year. Clusters showing significantly (corrected $P < 0.05$) lower (blue) and higher (red) GMV changes after 1 year. **(A)** Clusters showing many lower and few higher GMV regions in HIV+ group children. **(B)** Clusters only showing significantly lower GMV regions in HEU group children. **(C)** Put together the two groups for statistical analysis and showing significantly changes of GMV after 1 year. **(D)** In assessing the time and interactions between the two groups, clusters showing widely areas of GMV significantly reduced. These figures were rendered using BrainNet Viewer (http://www.nitrc.org/projects/bnv/).

The HEU group showed only areas with significantly reduced GMV after 1 year, mainly in the bilateral temporal lobe, left inferior frontal gyrus, right anterior OFC, and right parietal lobe (postcentral, angular, and superior parietal gyrus) and right occipital lobe, part of the basal ganglia nuclei (putamen, thalamus), bilateral cerebellum (**Table 5**; **Figure 3B**).

The two groups were put together for statistical analysis and showed that after 1 year, the GMV of multiple brain regions increased significantly, mainly including bilateral frontal lobes (the right OFC, the left inferior frontal cortex, the right precentral cortex, etc), and the right temporal lobe, bilateral upper cerebellar and parietal-occipital lobes, right amygdala, and thalamus; areas of markedly reduced GMV mainly include right medial OFC, left supplemental motor area, left cingulate gyrus, and temporal-occipital cortex (**Table 6**; **Figure 3C**). In assessing the time and interactions between the two groups, it was shown that the volume of gray matter in a wide area was significantly reduced, mainly including the bilateral parietal lobes (above gyrus, supramarginal gyrus, and precuneus), and bilateral multiple other lobes; significant gray matter volume increase only in the right cingulate anterior (**Table 7**; **Figure 3D**).

Longitudinal Changes on Cortical Thickness

For the cortical measures, the longitudinal results showed extensive cortical thinning in both the HIV+ and HEU groups after 1 year. In the HIV+ group, the bilateral cingulate gyrus, the postcentral gyrus, the parietal lobe and the left superior frontal gyrus, the calcarine, the angular gyrus, the precentral gyrus, the inferior frontal gyrus, the right paracentral lobes, the frontal pole, the central sulcus, and the inferior parietal lobule were displayed (**Table 8**; **Figure 4A**).

The HEU group showed significant cortical thinning mainly around the bilateral central sulcus and mainly in the frontal lobe, left occipital lobe and the right temporal lobe, significantly thickened cortex mainly in the left olfactory sulcus, orbital gyrus

TABLE 5 | Volume change of gray matter in HEU group after 1 year.

Contrast	Brain regions	Extent	*t*-value	MNI coordinates		
				x	y	z
Negative	Temporal_Pole_Sup_L	5516	−6.760	−60	8	−5
	Frontal_Inf_Oper_L	5516	−5.867	−54	20	32
	Postcentral_R	4111	−5.767	65	0	30
	Temporal_Pole_Mid_R	4111	−5.650	50	24	−27
	Temporal_Pole_Sup_R	4111	−5.417	62	11	−6
	OFCant_R	2130	−5.588	47	53	−14
	Precuneus_R	98	−5.308	2	−66	62
	Supp_Motor_Area_R	170	−5.105	9	2	75
	Angular_R	1266	−5.008	56	−68	35
	Parietal_Sup_R	1266	−4.506	35	−74	53
	Parietal_Sup_R	1266	−4.469	51	−39	59
	Frontal_Mid_2_R	357	−4.989	45	12	56
	Precentral_R	357	−3.925	42	−8	66
	Thalamus_R	413	−4.890	15	−20	5
	Lingual_L	1601	−4.130	−15	−66	−9
	Cerebelum_4_5_L	1601	−3.965	−11	−50	−23
	Occipital_Sup_R	1146	−4.669	23	−102	9
	Occipital_Mid_R	1146	−4.498	33	−90	26
	Occipital_Mid_R	1146	−4.086	39	−93	2
	Calcarine_L	123	−4.591	5	−98	0
	Temporal_Pole_Mid_L	269	−4.044	−20	15	−39
	Temporal_Sup_R	79	−4.429	66	−53	20
	Occipital_Inf_R	70	−4.388	44	−78	−9
	Thalamus_L	386	−4.288	−17	−27	2
	Putamen_R	940	−4.349	27	12	−8
	Putamen_R	940	−4.255	30	−5	11
	Precentral_L	306	−4.309	−30	−21	69
	Lingual_R	186	−4.254	15	−65	−6
	Temporal_Inf_L	72	−4.231	−69	−33	−20
	Cerebelum_4_5_R	553	−4.139	18	−45	−26
	Parietal_Inf_L	70	−4.125	−38	−63	51
	Occipital_Sup_L	77	−3.911	−18	−98	15

HEU, HIV-exposed uninfected; MNI, Montreal Neurological Institute; L, left; R, right. All regions were corrected by FWE cluster level $p < 0.05$.

TABLE 6 | Volume change of gray matter in HIV+ and HEU groups after 1 year.

Contrast	Brain regions	Extent	*t*-value	MNI coordinates		
				x	y	z
Positive	OFCpost_R	3035	5.829	23	23	−27
	Temporal_Inf_R	1626	4.445	56	−45	−29
	Cerebelum_6_R	1626	3.393	18	−62	−30
	Temporal_Pole_Sup_R	1996	5.278	57	18	−14
	Precentral_R	1996	4.207	66	5	18
	Temporal_Sup_R	1996	4.155	66	0	−5
	Occipital_Inf_R	630	5.100	50	−75	−12
	Temporal_Inf_R	630	4.142	45	−56	−14
	Occipital_Mid_L	2366	4.276	−33	−87	2
	Parietal_Sup_L	2366	4.011	−29	−72	57
	Frontal_Inf_Oper_L	1136	4.559	−54	20	33
	Frontal_Inf_Tri_L	1136	4.434	−59	26	6
	Frontal_Mid_2_L	1136	4.238	−48	50	6
	Amygdala_R	931	3.584	32	−5	−14
	Cerebelum_4_5_L	1443	4.258	−29	−27	−33
	Frontal_Sup_Medial_L	556	3.275	0	68	12
	Temporal_Sup_R	212	3.985	66	−51	23
	OFCant_L	197	3.831	−21	30	−18
	Occipital_Sup_R	463	3.819	26	−101	9
	Occipital_Inf_R	463	3.105	30	−87	−8
	Cerebelum_9_R	129	3.530	18	−41	−53
	Putamen_R	249	3.528	26	12	−8
	Parietal_Sup_L	58	3.528	−24	−57	74
	Postcentral_L	69	3.522	−36	−32	72
	Occipital_Mid_R	141	3.506	36	−89	24
	Frontal_Sup_Medial_L	114	3.476	−17	66	−2
	Parietal_Inf_R	54	3.438	42	−63	57
	Thalamus_L	74	3.286	−20	−27	0
Negative	Frontal_Mid_2_L	247	−5.901	−29	54	6
	Precuneus_L	100	−5.162	−8	−47	63
	Supp_Motor_Area_L	1270	−4.985	−6	20	56
	Cingulate_Mid_L	1270	−4.004	0	−2	39
	Cingulate_Mid_L	1270	−3.695	−11	−20	47
	Temporal_Sup_L	115	−4.479	−50	−42	18
	Cingulate_Post_L	248	−4.388	−6	−48	32
	Occipital_Mid_L	291	−4.161	−26	−62	38
	Cerebelum_8_R	57	−4.073	12	−69	−45
	Insula_R	63	−3.784	38	26	3
	Occipital_Sup_R	174	−3.739	26	−69	42
	Temporal_Sup_L	141	−3.438	−42	−15	−6
	Cerebelum_9_R	54	−3.395	2	−53	−56
	Temporal_Sup_R	51	−3.256	44	−8	−8
	OFCmed_R	3035	3.958	18	26	−24

HIV+, HIV-infected; HEU, HIV-exposed uninfected; MNI, Montreal Neurological Institute. All regions were corrected by FWE cluster level $p < 0.05$.

and the right inferior orbital sulcus and the right gyrus rectus (**Table 9**; **Figure 4B**).

The two groups were put together for statistical analysis, the areas of the cortical thickening were more obvious, mainly in the

TABLE 7 | Interactions between groups and time points of gray matter volume.

Contrast	Brain regions	Extent	*t*-value	MNI coordinates		
				x	y	z
Positive	Cingulate_Ant_R	100	4.936	5	27	−3
Negative	Occipital_Sup_R	676	−6.745	27	−69	44
	Frontal_Sup_2_L	2897	−6.375	−27	56	8
	Frontal_Mid_2_L	2897	−5.558	−44	41	29
	Frontal_Inf_Tri_L	2897	−4.869	−56	35	12
	SupraMarginal_R	4756	−6.233	65	−17	27
	Parietal_Sup_R	4756	−5.901	38	−50	56
	Postcentral_R	4756	−5.317	54	−26	56
	Vermis_10	221	−5.884	−2	−45	−38
	Parietal_Inf_L	84	−5.858	−44	−42	51
	Temporal_Pole_Sup_L	774	−5.560	−57	9	−6
	Frontal_Inf_Oper_L	774	−4.651	−51	9	15
	Occipital_Inf_R	213	−5.559	33	−83	−11
	Supp_Motor_Area_R	549	−5.552	9	2	75
	Parietal_Inf_L	428	−5.363	−51	−26	47
	Frontal_Sup_Medial_R	494	−5.327	9	38	56
	Cerebelum_4_5_L	902	−5.290	−6	−47	−5
	Lingual_L	902	−4.408	−15	−63	−12
	Cerebelum_Crus1_L	168	−5.261	−29	−80	−26
	OFCant_R	239	−5.039	45	51	−15
	Precuneus_R	420	−4.979	8	−50	51
	Precentral_L	436	−4.966	−41	0	62
	Frontal_Sup_Medial_L	131	−4.938	−6	54	44
	Supp_Motor_Area_R	124	−4.898	6	15	50
	Frontal_Sup_2_R	287	−4.855	27	59	24
	Angular_R	280	−4.850	53	−66	35
	Cerebelum_4_5_R	481	−4.829	9	−60	−5
	Frontal_Mid_2_R	241	−4.765	39	54	18
	Parietal_Inf_L	380	−4.732	−38	−62	53
	Precuneus_R	63	−4.695	3	−66	60
	Cerebelum_Crus2_R	443	−4.590	42	−78	−44
	Temporal_Mid_R	113	−4.542	65	−2	−21
	Temporal_Sup_L	171	−4.511	−65	−27	6
	SupraMarginal_L	355	−4.497	−59	−50	26
	Temporal_Sup_R	85	−4.447	65	−8	8
	Occipital_Sup_R	126	−4.441	24	−93	20
	Frontal_Sup_2_R	77	−4.410	23	12	68
	Temporal_Mid_R	402	−4.355	65	−42	9
	Temporal_Mid_R	335	−4.330	53	−66	8
	Parietal_Sup_L	66	−4.289	−21	−66	59
	Occipital_Mid_L	69	−4.262	−29	−87	21
	Precentral_L	182	−4.256	−27	−23	71
	Frontal_Sup_2_L	100	−4.254	−20	44	45
	Occipital_Mid_R	87	−4.246	38	−95	0
	Temporal_Pole_Mid_R	193	−4.211	51	9	−35
	Frontal_Sup_Medial_R	83	−4.103	11	69	2
	Temporal_Mid_L	80	−4.092	−60	−54	−5
	Thalamus_R	137	−3.943	17	−18	8
	Thalamus_L	214	−3.885	−6	−6	8
	Frontal_Inf_Tri_R	122	−3.882	53	38	17

Two groups = HIV-infected group and HIV-exposed uninfected group, MNI, Montreal Neurological Institute; L, left; R, right. All regions were corrected by FWE cluster level $p < 0.05$.

TABLE 8 | Cortical thickness change in HIV+ group after 1 year.

Contrast	Cortical regions	Side	Size	*P*-value
Positive	92% G_oc-temp_med-Parahip 8%S_collat_transv_ant	L	490	0.00287
	28% S_occipital_ant 22% S_temporal_inf 17% G_and_S_occipital_inf 13% S_temporal_sup 12% G_temporal_middle 4% G_occipital_middle 4%G_temporal_inf	R	1205	0.00032
	75% S_front_inf 25%G_front_middle	R	306	0.00029
Negative	56% G_front_sup 15% G_front_middle 8% G_and_S_frontomargin 6% G_and_S_cingul-Ant 5% G_and_S_transv_frontopol 4% S_orbital_lateral 3% S_front_sup 2% S_front_inf 1%S_front_middle	L	3546	0.00006
	66% S_calcarine 11% G_cingul-Post-ventral 8% S_parieto_occipital 8% G_oc-temp_med-Lingual 6%G_precuneus	L	2371	0.00000
	82% G_postcentral 8% S_postcentral 8% S_central 2%G_and_S_paracentral	L	851	0.00139
	48% G_pariet_inf-Angular 27% S_intrapariet_and_P_trans 19% G_pariet_inf-Supramar 7%S_postcentra	L	847	0.00000
	55% G_precentral 45%S_precentral-sup-part	L	671	0.00043
	77% S_front_inf 17% G_front_middle 5% G_front_inf-Opercular 2%G_front_inf-Triangul	L	482	0.00036
	51%G_cingul-Post-dorsal 36% S_cingul-Marginalis 12% G_and_S_cingul-Mid-Post 2% G_precuneus	L	335	0.00103
	56% S_intrapariet_and_P_trans 26% G_parietal_sup 18%S_postcentral	L	325	0.00095
	28% G_and_S_paracentral 26% G_front_sup 18% G_postcentral 17% S_central 10%G_precentral	R	2247	0.00085
	27% G_and_S_transv_frontopol 23% G_front_middle 21% G_front_sup 13% G_and_S_frontomargin 13% S_front_middle 2%G_and_S_cingul-Ant	R	1644	0.00000
	54% S_central 26% G_precentral 18%G_postcentral	R	1271	0.00173
	69% G_and_S_cingul-Mid-Post 31%G_front_sup	R	750	0.00070
	55% S_postcentral 40% S_interm_prim-Jensen 4%S_intrapariet_and_P_trans	R	688	0.00011
	83% S_subparietal 13% G_precuneus 4%G_cingul-Post-dorsal	R	581	0.00130
	100%S_intrapariet_and_P_trans	R	408	0.00006

HIV+, HIV-infected; L, left; R, right. All regions were corrected by FWE cluster level p <0.05.

bilateral middle occipital gyrus, the parietal lobe (angle gyrus), the frontal lobe (near the right inferior frontal gyrus) and the right middle temporal gyrus. Cortical thinning was mainly in the right frontal lobe (**Table 10**; **Figure 4C**). In the evaluation of the time and the interaction between the two groups, the cortical thinning in a wide area was shown, mainly around the bilateral central sulcus, the insular, the frontal lobe (mainly in the middle gyrus), the cingulate sulcus. Significant cortical thickening only showed in bilateral orbital gyrus and the right parahippocampal gyrus (**Table 11**; **Figure 4D**).

The Relationship Between Brain Morphological Metrics and Behavior

Finally, we analyzed the association between behavioral performance and brain morphological measures in HIV+ adolescents. Because there was a significant difference in Wisconsin Card Classification Test between the two groups, we performed a nonparametric correlation analysis on the Wisconsin Card Classification scores of the HIV+ group and the morphological measures with significant between-group differences on the cross-sectional analysis. For the GMV, the gray matter volume of the bilateral cerebellum in the HIV+ group was significantly positively correlated with the Wisconsin Card Classification Test score ($r = 0.681$, $p = 0.005$). For the CT, the cortical thickness of HIV+'s right rostral middle frontal ($r = -0.646$, $p = 0.009$) and right superior frontal gyri was significantly negatively correlated with the Wisconsin Card Classification Test score.

DISCUSSION

Cross-sectionally, we found a wide reduction in cortical volume and changes in cortical thickness with thinning of the right temporal lobe and thickening of the left occipital lobe in HIV+ individuals during adolescence. Longitudinally, the reduction in gray matter volume and thinning of the cortex in HIV+ individuals occurred mainly in different functional areas of the frontal and parietal lobe, which was significantly different from the pattern of their HEU controls.

Cross-sectionally, the alterations in the advanced cortices including the OFC and primary sensorimotor cortices as found

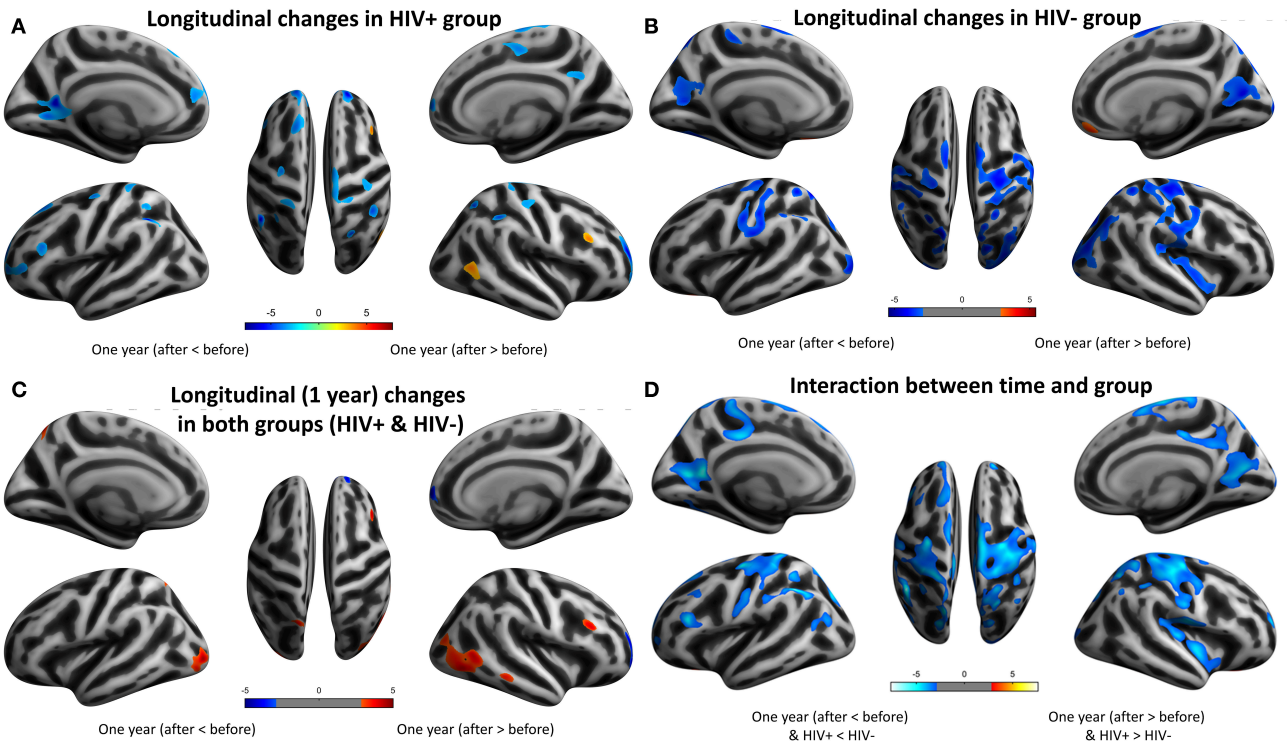

FIGURE 4 | Longitudinal changes on cortical thickness (CT) after 1 year. Clusters showing significantly (corrected $P < 0.05$) lower (blue) and higher (red) CT changes after 1 year. **(A)** Clusters showing lower and higher CT regions in HIV+ group children. **(B)** Clusters showing significantly lower and higher CT regions in HEU group children. **(C)** Put together the two groups for statistical analysis and showing significantly lower regions more obviously than higher regions of CT after 1 year. **(D)** In assessing the time and interactions between the two groups, clusters showing widely areas of CT significantly reduced.

here are generally consistent with our hypothesis and earlier reports (22, 23). The HIV virus can rapidly enter the central nervous system (CNS) and cause encephalitis within a few days after the exposure (24). In the early stages of the disease, HIV induces the CNS inflammatory T-cell response with vasculitis and leptomeningitis, directly damage oligodendrocytes, neurons, and white matter (25). The same process can be observed in the cerebral cortex of AIDS patients, thereby inducing neuronal apoptosis. Immunoreactive gliosis and neuronal loss can even cause diffuse poliodystrophy (26, 27). These pathological changes should explain why our GMV cross-sectional results only show a decrease in gray matter volume in multiple brain regions, mainly in the bilateral frontal, temporal, insular, and cerebellar cortical regions.

A major novelty of this study is the using of longitudinal structural brain data to examine brain development during early puberty after HIV exposure. Longitudinally, we found that the brain maturation in HIV-infected and non-HIV-infected children follows a general pattern, but unique changes have taken place in terms of developmental speed, spatial range, etc. The human brain decreases its gray matter in late childhood or adolescence in typical healthy development (28, 29). Our longitudinal VBM results also showed this trend, however, the GMV loss pattern of HIV+ children are significantly different from that of the controls over 1 year, the topographies of this loss including the right frontal, superior parietal, and sensorimotor regions. Changes in the OFC have been suggested with pronounced negative emotions (30). The difference in volume changes in the right OFC after 1 year suggests that this brain area may be one of the key brain areas affected by HIV. The OFC is an important limbic brain region responsible for emotion, decision making and reward evaluation, which collectively with basal ganglia, amygdala and the medial prefrontal cortex form an limbic-emotion circuit (31). It is generally believed that the functional imbalance of this circuit is related to the pathogenesis of obsessive-compulsive disorder (32, 33).

The neuroanatomical features are significantly controlled over genetic and environmental factors. GMV is a function of surface area and cortical thickness, the cortical surface area has been reported to more likely to be regulated by a genetic factor than the cortical thickness (34). A human study has shown that a decrease in synaptic density in healthy children between the ages of 2 and 16 years is accompanied by a slight decrease in neuronal density (35). We can consider that thinning of the cortex during adolescence represents the concurrent process of synapses, axons, dendritic pruning, and myelination. It plays an important role in improving the connectivity between brain networks and improving signal transmission efficiency. The thinning of association cortices is seen as a reliable marker of maturity in healthy children (36, 37). The difference in

TABLE 9 | Cortical thickness change in HEU group after 1 year.

Contrast	Cortical regions	Side	Size	*P*-value
Positive	51% S_orbital_med-olfact 34% G_orbital 11% S_orbital-H_Shaped 5%G_rectus	L	619	0.00013
	54% S_suborbital 32% G_rectus 13% G_and_S_cingul-Ant 2%G_front_sup	R	449	0.00073
Negative	41% G_postcentral 32% S_central 16% S_postcentral 7% G_pariet_inf-Supramar 3%G_and_S_subcentral	L	5583	0.00055
	68% G_parietal_sup 10% G_occipital_sup 8% G_precuneus 6% S_intrapariet_and_P_trans 5% S_oc_sup_and_transversal 3%G_and_S_paracentral	L	2688	0.00004
	53% S_parieto_occipital 24% S_calcarine 15% G_precuneus 6% G_cuneus 1%G_cingul-Post-dorsal	L	2637	0.00085
	43% G_occipital_middle 29% Pole_occipital 20% S_oc_middle_and_Lunatus 7% S_oc_sup_and_transversal 1%G_and_S_occipital_inf	L	2249	0.00049
	50% G_precentral 43% S_central 6%S_precentral-sup-part	L	1875	0.00086
	55% G_pariet_inf-Angular 31% G_pariet_inf-Supramar 10% S_postcentral 2% G_occipital_middle 2%S_oc_sup_and_transversal	L	1728	0.00169
	58%S_cingul-Marginalis 18%G_and_S_paracentral 15%G_and_S_cingul-Mid-Post 4% G_cingul-Post-dorsal 2% G_front_sup 2%G_precuneus	L	1657	0.00109
	100%G_front_sup	L	1163	0.00064
	53%G_oc-temp_lat-fusifor 32%S_oc-temp_med_and_Lingual 9% G_oc-temp_med-Lingual 6%S_collat_transv_post	L	853	0.00052
	100% G_parietal_sup	L	577	0.00044
	10%G_postcentral 9% S_central 9% G_precentral 6% G_parietal_sup 6% S_postcentral 5% G_pariet_inf-Supramar 5% G_occipital_middle 5% S_circular_insula_inf 5% Lat_Fis-post 5% Pole_occipital	R	29750	0.00024
	5% G_and_S_subcentral 5% G_front_sup 4% G_occipital_sup 4% G_pariet_inf-Angular 3% S_oc_sup_and_transversal 2% G_Ins_lg_and_S_cent_ins 2% G_temp_sup-Plan_tempo 2% S_oc_middle_and_Lunatus 2% G_precuneus 1% G_insular_short 1%G_temp_sup-G_T_transv			
	48% S_parieto_occipital 27% S_calcarine 21% G_cuneus 3%G_precuneus	R	2817	0.00030
	61% G_temp_sup-Lateral 24% G_temp_sup-G_T_transv 10% S_temporal_transverse 4%G_temp_sup-Plan_polar	R	522	0.00204
	100% G_and_S_paracentral	R	305	0.00246
	62% G_front_middle 38%S_front_inf	R	302	0.00156

HEU, HIV-exposed uninfected; L, left; R, right. All regions were corrected by FWE cluster level p <0.05.

cortical thickness between children with HIV and uninfected HEU children was predominantly in the association cortex with a few areas of excessive thinning, which may be the result of excessive synaptic pruning or abnormal plasticity. However, cross-sectional results are unavoidably affected by individual differences and groups. Our longitudinal study will overcome these limitations.

Neuroimaging has provided evidence of temporal hierarchy on typical brain development, with the primary cortices develop first and the association cortices continue to develop until the early three-decade of life. Sowell et al. mapped gray matter density in 176 typical development individuals aged 7 to 87 years and found that there was a significant non-linear decrease in gray matter density with age, especially on the lateral/dorsal frontal and parietal cortices. The primary sensorimotor regions, such as the visual, auditory, and the somatomotor cortices, begin to myelination at an early stage and exhibits a more linear developmental pattern, while the myelinization of the advanced functional cortex of the frontoparietal regions can continue into adulthood. In particular, the language cortex at the temporal cortex has the longest maturation process (16), and finally mature brain regions (frontal lobes) that involve advanced functions such as executive function and attention, but in this process not some brain regions are fully mature and other brain regions begin to develop (17). These studies indicate that the order of cortical maturation is consistent with the development of related cognitive abilities. Cortical thinning should occur first in the sensorimotor area, followed by the associated area, and finally in the more advanced cortical area. In our study, HIV+ children showed cortical maturation in multiple brain regions from primary to advanced functional regions after 1 year, but the brain regions involved were mostly sensory motor

TABLE 10 | Cortical thickness change in HIV+ and HEU groups after 1 year.

Contrast	Cortical regions	Side	Size	*P*-value
Positive	39% S_oc_middle_and_Lunatus 31% G_occipital_middle 15% Pole_occipital 14%G_and_S_occipital_inf	L	1687	0.00011
	66% G_parietal_sup 34%G_precuneus	L	820	0.00070
	32% G_occipital_middle 17% S_occipital_ant 12% S_oc_middle_and_Lunatus 12% G_and_S_occipital_inf 10% S_temporal_inf 9% G_temporal_middle 3% G_temporal_inf 3% S_temporal_sup 2%S_oc_sup_and_transversal	R	2912	0.00021
	99% G_pariet_inf-Angular	R	632	0.00253
	70% S_front_inf 30%G_front_middle	R	418	0.00023
	49% G_front_inf-Opercular 25% Lat_Fis-ant-Vertical 24% S_circular_insula_sup 1%G_front_inf-Triangul	R	361	0.00114
	100% G_temporal_middle	R	359	0.00096
Negative	44% G_and_S_transv_frontopol 26% G_and_S_frontomargin 23% G_front_middle 7%S_front_middle	R	764	0.00037
	59% G_front_sup 30% G_and_S_cingul-Ant 11%G_and_S_transv_frontopol	R	435	0.00011

HIV+, HIV-infected, HEU, HIV-exposed uninfected; L, left; R, right. All regions were corrected by FWE cluster level p <0.05.

TABLE 11 | Interactions between groups and time points of cortical thickness.

Contrast	Cortical regions	Side	Size	*P*-value
Positive	57% G_orbital 23% S_orbital_med-olfact 20%S_orbital-H_Shaped	L	261	0.00025
	52% G_orbital 34% S_orbital-H_Shaped 15%S_orbital_med-olfact	R	810	0.00156
	92% G_oc-temp_med-Parahip 8%S_oc-temp_med_and_Lingual	R	207	0.00184
Negative	13% G_postcentral 12% S_central 11% G_parietal_sup 9% S_calcarine 8% G_pariet_inf-Angular 8% S_parieto_occipital 8% G_pariet_inf-Supramar 7% G_precentral 4% S_postcentral 4% S_temporal_sup 3% G_precuneus 3% S_intrapariet_and_P_trans 2% S_precentral-sup-part 2% G_occipital_sup 2% G_and_S_paracentral 1%G_cuneus	L	18597	0.00000
	90% G_front_sup 6% G_front_middle 3%S_front_sup	L	3533	0.00038
	40% S_cingul-Marginalis 18% G_and_S_paracentral 12% G_and_S_cingul-Mid-Post 11% G_precuneus 9% S_subparietal 7% G_cingul-Post-dorsal 4%G_front_sup	L	3215	0.00014
	54% S_central 18% G_precentral 9% G_postcentral 6% S_precentral-inf-part 6% G_and_S_subcentral 4% S_precentral-sup-part 2%G_front_middle	L	2387	0.00066
	31% S_circular_insula_inf 25% S_circular_insula_sup 20% S_circular_insula_ant 15% G_insular_short 10%G_Ins_lg_and_S_cent_ins	L	1696	0.00139
	48% S_front_inf 25% G_front_inf-Opercular 19% G_front_middle 7%G_front_inf-Triangul	L	1067	0.00008
	42% G_front_middle 33% G_and_S_frontomargin 15% S_orbital_lateral 5% S_front_inf 3% S_front_middle 3%G_orbital	L	721	0.00088
	54% S_intrapariet_and_P_trans 33% G_parietal_sup 13%S_postcentral	L	669	0.00045

(Continued)

cortex and limbic systems. The range and extent of the HIV+ group's cortical maturation are significantly lower than that in HEU children. This pattern of high-function-associated cortical lagging development (especially in the left parietal lobe and bilateral occipital lobes) may be the basis for the manifestation of neurocognitive abnormalities and atypical brain development.

Cortical morphometry of neuroimaging has revealed atypical development in several brain diseases including schizophrenia and hyperactivity disorder, etc. (38). In a longitudinal study of children with schizophrenia, the developmental pattern of temporally and spatially thinning of the cerebral cortex was shown and was first detected in the parietal cortex associated with visual space and associative thinking. And this pattern of gray matter loss is related to the severity of mental symptoms (39). However, Shaw et al. showed that 223 children with attention-deficit/hyperactivity disorder (ADHD) showed that the age at which the peak cortical thickness was reached significantly later than that of normal children, especially in the prefrontal cortex. It indicates that there is a significant development delay in cortical maturation in children with ADHD (40). The different results of these studies suggest that changes in the basic maturation model of the cerebral cortex may be the basis of neurodevelopmental

TABLE 11 | Continued

Contrast	Cortical regions	Side	Size	*P*-value
	44% S_oc-temp_med_and_Lingual 37% G_oc-temp_lat-fusifor 19%G_oc-temp_med-Lingual	L	585	0.00234
	99% G_front_middle 1%S_front_sup	L	467	0.00177
	23% S_central 18% G_postcentral 16% G_precentral 13% G_front_sup 12% S_postcentral 8% G_and_S_paracentral 4% G_pariet_inf-Supramar 3% S_precentral-sup-part 1%G_and_S_cingul-Mid-Post	R	17427	0.00005
	26% S_circular_insula_inf 22% Lat_Fis-post 17% G_and_S_subcentral 8% G_Ins_lg_and_S_cent_ins 7% G_temp_sup-G_T_transv 6% G_insular_short 4% G_front_inf-Opercular 2% S_temporal_transverse 2% G_temp_sup-Lateral 2% S_circular_insula_ant 1%G_temp_sup-Plan_tempo	R	7725	0.00017
	27% S_subparietal 21% S_parieto_occipital 21% S_calcarine 9% G_precuneus 9% G_cuneus 5% G_cingul-Post-dorsal 4% S_cingul-Marginalis 2% G_oc-temp_med-Lingual 2%G_and_S_cingul-Mid-Post	R	5913	0.00019
	66% G_parietal_sup 20% S_intrapariet_and_P_trans 14% G_precuneus 1%S_postcentral	R	3429	0.00013
	49% Pole_occipital 17% G_occipital_middle 14% S_oc_sup_and_transversal 8% G_pariet_inf-Angular 6% G_occipital_sup 4% S_oc_middle_and_Lunatus 2%S_temporal_sup	R	2109	0.00176
	79% G_occipital_sup 8% S_oc_sup_and_transversal 5% G_cuneus 4% S_intrapariet_and_P_trans 3% G_parietal_sup 1%S_parieto_occipital	R	949	0.00037
	64% G_front_middle 28% S_front_middle 7% G_and_S_transv_frontopol 1%G_front_sup	R	408	0.00012
	61% G_oc-temp_lat-fusifor 39%S_oc-temp_med_and_Lingual	R	368	0.00124
	100%G_pariet_inf-Angular	R	362	0.00075
	80% G_front_middle 20%S_front_inf	R	226	0.00209

Two groups = HIV-infected group and HIV-exposed uninfected group; L, left; R, right. All regions were corrected by FWE cluster level p <0.05.

disorders. This process, together with social psychology and environmental factors, affects the development of individual cognitive abilities. The independent and interactive effects of these various factors may play an important role in brain structural changes and HIV-associated neurocognitive disorders in HIV+ patients. In the future, more in-depth clinical and basic research is needed to determine the pathophysiological mechanisms and potential therapeutic targets (41, 42).

Finally, we need to emphasize the role of white matter damage in the morphometric changes of HIV+. These cortical morphological changes found in this study may be partly due to the contribution of white matter damage. The axonal and myelin development of white matter has an important influence on the coordinated development of the gray matter. Recently, several studies have also pointed out that damage of the white matter structural connectivity that link the frontal, temporal, and occipital regions, as we reported, constitutes the basis of damage in HIV transmitted infection children, which suggests that the white matter damage may also be the basis for abnormal development of gray matter morphology in these population, but the relationship between them is still an open question, both for the typical development and HIV infected children. This relationship can be further analyzed and explored in future research (12, 43–45).

LIMITATIONS

There are several limitations in this study. Firstly, because the data of this type of population is extremely rare, the sample size is very small, even if this study is obtained by using an unique opportunity. Secondly, the results reported in this paper only involved 1-year follow-up, and further follow-up is needed to obtain a detailed description of their developmental trajectories, and relevant research is continuing. In addition, because the subjects in this study were from different regions of the country, it is not very easy to completely and accurately obtain their previous complications.

CONCLUSION

This cross-sectional and longitudinal study found that HIV-infected pubertal children showed a delayed cortical maturation (mainly in the left parietal lobe and bilateral occipital lobe) with atrophy (mainly occurs in the right frontal lobe, parietal lobe of the higher functional areas and multiple motor areas). This abnormal pattern of cortical development may be the structural basis for cognitive impairment in HIV+ children. Longer-term longitudinal studies are needed in the future to verify and improve this conclusion.

ETHICS STATEMENT

The study was approved by the Medical Ethics Committee of Zhongnan Hospital of Wuhan University, and a written and informed consent was made from all participants or their guardians in accordance with the Helsinki Declaration of 1975 (and as revised in 1983), following a complete description of the

measurements. These methods were carried out in accordance with the approved guidelines and regulations.

AUTHOR CONTRIBUTIONS

XY designed this study and wrote the paper, LG analyzed data, and contributed to writing of the paper. XY, HW, ZY, JF, JC, and QL performed experiments together. HX and XG guided the entire experimental process.

FUNDING

The author(s) disclosed receipt of the following financial support for the research, authorship, and/or publication of this article: This study has been supported by the National Natural Science Foundation of China (under Grant Nos. 81771819 and 81571734), National key research and development plan of China (Project 2017YFC0108803), Zhongnan Hospital of Wuhan University Science, Technology and Innovation Seed Fund (Projects cxpy2017048 and cxpy20160057), and the Fundamental Research Funds for the Central Universities (Projects 2042017kf0284 and 2016060605100525).

ACKNOWLEDGMENTS

We thank all the children and their parents for being willing to take part in this study.

REFERENCES

1. Tardieu M, Le Chenadec J, Persoz A, Meyer L, Blanche S, Mayaux MJ. HIV-1–related encephalopathy in infants compared with children and adults. *Neurology*. (2000) 54:1089–95. doi: 10.1212/WNL.54.5.1089
2. World Health Organization. *Global update on the Health Sector Response to HIV*, 2014, World Health Organization. (2014).
3. Patel K, Ming X, Williams PL, Robertson KR, Oleske JM, Seage GR, et al. Impact of HAART and CNS-penetrating antiretroviral regimens on HIV encephalopathy among perinatally infected children and adolescents. *AIDS*. (2009) 23:1893–901. doi: 10.1097/QAD.0b013e32832dc041
4. Cohen S, Ter Stege JA, Geurtsen GJ, Scherpbier HJ, Kuijpers TW, Reiss P, et al. Poorer cognitive performance in perinatally HIV-infected children versus healthy socioeconomically matched controls. *Clin Infect Dis*. (2015) 60:1111–9. doi: 10.1093/cid/ciu1144
5. Baillieu N, Potterton J. The extent of delay of language, motor, and cognitive development in HIV-positive infants. *J Neurol Phys Ther*. (2008) 32:118–21. doi: 10.1097/NPT.0b013e3181846232
6. Abubakar A. Infections of the Central Nervous System and Child Development in Sub-Saharan Africa. In: Abubakar A, van de Vijver FJR, editors. *Handbook of Applied Developmental Science in Sub-Saharan Africa*. Springer Science+Business Media LLC (2017). doi: 10.1007/978-1-4939-7328-6_7
7. Lindsey JC, Malee KM, Brouwers P, Hughes MD. Neurodevelopmental functioning in HIV-infected infants and young children before and after the introduction of protease inhibitor-based highly active antiretroviral therapy. *Pediatrics*. (2007) 119:681–93. doi: 10.1542/peds.2006-1145
8. Nozyce ML, Lee SS, Wiznia A, Nachman S, Mofenson LM, Smith ME, et al. A behavioral and cognitive profile of clinically stable HIV-infected children. *Pediatrics*. (2006) 117:763–70. doi: 10.1542/peds.2005-0451
9. Lewis-de Los Angeles CP, Alpert KI, Williams PL, Malee K, Huo Y, Csernansky JG, et al. Deformed subcortical structures are related to past HIV disease severity in youth with perinatally acquired HIV infection. *Pediatr Infect Dis Soc*. (2016) 5(Suppl. 1):S6–14. doi: 10.1093/jpids/piw051
10. Lewis-de Los Angeles CP, Williams PL, Huo Y, Wang SD, Uban KA, Herting MM, et al. Lower total and regional gray matter brain volumes in youth with perinatally-acquired HIV infection: associations with HIV disease severity, substance use, and cognition. *Brain Behav Immun*. (2017) 62:100–9. doi: 10.1016/j.bbi.2017.01.004
11. Nwosu EC, Robertson FC, Holmes MJ, Cotton MF, Dobbels E, Little F, et al. Altered brain morphometry in 7-year old HIV-infected children on early ART. *Metab Brain Dis*. (2018) 33:523–35. doi: 10.1007/s11011-017-0162-6
12. Jankiewicz M, Holmes MJ, Taylor PA, Cotton MF, Laughton B, van der Kouwe A, et al. White matter abnormalities in children with HIV infection and exposure. *Front Neuroanat*. (2017) 11:88. doi: 10.3389/fnana.2017.00088
13. Hoare J, Ransford GL, Phillips N, Amos T, Donald K, Stein DJ. Systematic review of neuroimaging studies in vertically transmitted HIV positive children and adolescents. *Metab Brain Dis*. (2014) 29:221–9. doi: 10.1007/s11011-013-9456-5
14. Thompson PM, Jahanshad N. Novel neuroimaging methods to understand how HIV affects the brain. *Curr HIV/AIDS Rep*. (2015) 12:289–98. doi: 10.1007/s11904-015-0268-6
15. Blokhuis C, Kootstra NA, Caan MW, Pajkrt D. Neurodevelopmental delay in pediatric HIV/AIDS: current perspectives. *Neurobehav HIV Med*. (2016) 7:1–13. doi: 10.2147/NBHIV.S68954
16. Sowell ER, Peterson BS, Thompson PM, Welcome SE, Henkenius AL, Toga AW. Mapping cortical change across the human life span. *Nat Neurosci*. (2003) 6:309–15. doi: 10.1038/nn1008
17. Gogtay N, Giedd JN, Lusk L, Hayashi KM, Greenstein D, Vaituzis AC, et al. Dynamic mapping of human cortical development during childhood through early adulthood. *Proc Natl Acad Sci USA*. (2004) 101:8174–9. doi: 10.1073/pnas.0402680101
18. Ashburner J, Friston K J. Unified segmentation. *Neuroimage*. (2005) 26:839–51. doi: 10.1016/j.neuroimage.2005.02.018
19. Tohka J, Zijdenbos A, Evans A. Fast and robust parameter estimation for statistical partial volume models in brain MRI. *Neuroimage*. (2004) 23:84–97. doi: 10.1016/j.neuroimage.2004.05.007
20. Dahnke R, Yotter RA, Gaser C. Cortical thickness and central surface estimation. *Neuroimage*. (2013) 65:336–48. doi: 10.1016/j.neuroimage.2012.09.050
21. Antinori A, Arendt G, Becker JT, Brew BJ, Byrd DA, Cherner M, et al. Updated research nosology for HIV-associated neurocognitive disorders. *Neurology*. (2007) 69:1789–99. doi: 10.1212/01.WNL.0000287431.88658.8b
22. Thompson PM, Dutton RA, Hayashi KM, Toga AW, Lopez OL, Aizenstein HJ, et al. Thinning of the cerebral cortex visualized in HIV/AIDS reflects CD4+ T lymphocyte decline. *Proc Natl Acad Sci USA*. (2005) 102:15647–52. doi: 10.1073/pnas.0502548102
23. Pfefferbaum A, Rogosa DA, Rosenbloom MJ, Chu W, Sassoon SA, Kemper CA, et al. Accelerated aging of selective brain structures in HIV infection: a controlled, longitudinal MRI study. *Neurobiol Aging*. (2014) 35:1755–68. doi: 10.1016/j.neurobiolaging.2014.01.008
24. Valcour V, Chalermchai T, Sailasuta N, Marovich M, Lerdlum S, Suttichom D, et al. Central nervous system viral invasion and inflammation during acute HIV infection. *J Infect Dis*. (2012) 206:275–82. doi: 10.1093/infdis/jis326
25. Gray F, Scaravilli F, Everall I, Chretien F, An S, Boche D, et al. Neuropathology of early HIV-1 infection. *Brain Pathol*. (1996) 6:1–15. doi: 10.1111/j.1750-3639.1996.tb00775.x
26. Soontornniyomkij V. *Neuropathology of HIV-1 Disease[M]*. New York, NY: Springer (2017). p. 143–208.
27. Ozdener H. Molecular mechanisms of HIV-1 associated neurodegeneration. *J Biosci*. (2005) 30:391–405. doi: 10.1007/BF02703676
28. Giedd JN, Blumenthal J, Jeffries NO, Castellanos FX, Liu H, Zijdenbos A, et al. Brain development during childhood and adolescence: a longitudinal MRI study. *Nat Neurosci*. (1999) 2:861–3. doi: 10.1038/13158

29. Lenroot RK, Gogtay N, Greenstein DK, Wells EM, Wallace GL, Clasen LS, et al. Sexual dimorphism of brain developmental trajectories during childhood and adolescence. *Neuroimage.* (2007) 36:1065–73. doi: 10.1016/j.neuroimage.2007.03.053
30. Miller EK, Cohen JD. An integrative theory of prefrontal cortex function. *Ann Rev Neurosci.* (2001) 24:167–202. doi: 10.1146/annurev.neuro.24.1.167
31. Krawczyk DC. Contributions of the prefrontal cortex to the neural basis of human decision making. *Neurosci Biobehav Rev.* (2002) 26:631–64 doi: 10.1016/S0149-7634(02)00021-0
32. Macmaster FP, O'Neill J, Rosenberg DR. Brain imaging in pediatric obsessive compulsive disorder. *J Am Acad Child Adolesc Psychiatry.* (2008) 47:1262–72. doi: 10.1097/CHI.0b013e318185d2be
33. Saxena S, Rauch SL. Functional neuroimaging and the neuroanatomy of obsessive-compulsive disorder. *Psychiatr Clinics North Am.* (2000) 23:563–86. doi: 10.1016/S0193-953X(05)70181-7
34. Winkler AM, Kochunov P, Blangero J, Almasy L, Zilles K, Fox PT, et al. Cortical thickness or gray matter volume? The importance of selecting the phenotype for imaging genetics studies. *Neuroimage.* (2010) 53:1135–46. doi: 10.1016/j.neuroimage.2009.12.028
35. Huttenlocher PR. Synaptic density in human frontal cortex - developmental changes and effects of aging. *Brain Res.* (1979) 163:195–205. doi: 10.1016/0006-8993(79)90349-4
36. Tau GZ, Peterson BS. Normal development of brain circuits. *Neuropsychopharmacology.* (2010) 35:147–68. doi: 10.1038/npp.2009.115
37. Giedd JN, Keshavan M, Paus T. Why do many psychiatric disorders emerge during adolescence? *Nat Rev Neurosci.* (2008) 9:947–57. doi: 10.1038/nrn2513
38. Kessler RC, Berglund P, Demler O, Jin R, Merikangas KR, Walters EE. Lifetime prevalence and age-of-onset distributions of DSM-IV disorders in the National Comorbidity Survey Replication. *Arch Gen Psychiatry.* (2005) 62:593–602. doi: 10.1001/archpsyc.62.6.593
39. Thompson PM, Vidal C, Giedd JN, Gochman P, Blumenthal J, Nicolson R, et al. Mapping adolescent brain change reveals dynamic wave of accelerated gray matter loss in very early-onset schizophrenia. *Proc Natl Acad Sci USA.* (2001) 98:11650–5. doi: 10.1073/pnas.201243998
40. Shaw P, Eckstrand K, Sharp W, Blumenthal J, Lerch JP, Greenstein D, et al. Attention-deficit/hyperactivity disorder is characterized by a delay in cortical maturation. *Proc Natl Acad Sci USA.* (2007) 104:19649–54. doi: 10.1073/pnas.0707741104
41. Thames AD, Kuhn TP, Mahmood Z, Bilder RM, Williamson TJ, Singer EJ, et al. Effects of social adversity and HIV on subcortical shape and neurocognitive function. *Brain Imag Behav.* (2018) 12:96–108. doi: 10.1007/s11682-017-9676-0
42. Womersley JS, Seedat S, Hemmings SMJ. Childhood maltreatment and HIV-associated neurocognitive disorders share similar pathophysiology: a potential sensitisation mechanism? *Metab Brain Dis.* (2017) 32:1717–33. doi: 10.1007/s11011-017-0062-9
43. Ackermann C, Andronikou S, Saleh MG, Laughton B, Alhamud AA, van der Kouwe A, et al. Early antiretroviral therapy in HIV-infected children is associated with diffuse white matter structural abnormality and corpus callosum sparing. *Am J Neuroradiol.* (2016) 37:2363–9. doi: 10.3174/ajnr.A4921
44. Fennema-Notestine C, Ellis RJ, Archibald SL, Jernigan TL, Letendre SL, Notestine RJ, et al. Increases in brain white matter abnormalities and subcortical gray matter are linked to CD4 recovery in HIV infection. *J Neurovirol.* (2013) 19:393–401. doi: 10.1007/s13365-013-0185-7
45. Zhu T, Zhong J, Hu R, Tivarus M, Ekholm S, Harezlak J, et al. Patterns of white matter injury in HIV infection after partial immune reconstitution: a DTI tract-based spatial statistics study. *J Neurovirol.* (2013) 19:10–23. doi: 10.1007/s13365-012-0135-9

Conflict of Interest Statement: The authors declare that the research was conducted in the absence of any commercial or financial relationships that could be construed as a potential conflict of interest.

Advantages of publishing in Frontiers

OPEN ACCESS
Articles are free to read for greatest visibility and readership

FAST PUBLICATION
Around 90 days from submission to decision

HIGH QUALITY PEER-REVIEW
Rigorous, collaborative, and constructive peer-review

TRANSPARENT PEER-REVIEW
Editors and reviewers acknowledged by name on published articles

Frontiers
Avenue du Tribunal-Fédéral 34
1005 Lausanne | Switzerland

Visit us: www.frontiersin.org
Contact us: info@frontiersin.org | +41 21 510 17 00

REPRODUCIBILITY OF RESEARCH
Support open data and methods to enhance research reproducibility

DIGITAL PUBLISHING
Articles designed for optimal readership across devices

FOLLOW US
@frontiersin

IMPACT METRICS
Advanced article metrics track visibility across digital media

EXTENSIVE PROMOTION
Marketing and promotion of impactful research

LOOP RESEARCH NETWORK
Our network increases your article's readership